Imperial College London

Department of Physics

Brane Tilings

and

Quiver Gauge Theories

Rak-Kyeong Seong

2013

Supervised by Professor Amihay Hanany

Submitted in part fulfilment of the requirements for the degree of
Doctor of Philosophy in Physics of Imperial College London
and the Diploma of Imperial College London

Declaration

I herewith certify that, to the best of my knowledge, all of the material in this dissertation which is not my own work has been properly acknowledged.

Rak-Kyeong Seong

Abstract

This work presents recent developments on brane tilings and their vacuum moduli spaces.

Brane tilings are bipartite periodic graphs on the torus and represent $4d$ $\mathcal{N} = 1$ supersymmetric worldvolume theories living on D3-branes probing Calabi-Yau 3-fold singularities. The graph and combinatorial properties of brane tilings make the set of supersymmetric quiver theories represented by them one of the largest and richest known so far. The aim of this work is to give a concise pedagogical introduction to brane tilings and a summary on recent exciting advancement on their classification, dualities and construction.

At first, particular focus is given on counting distinct Abelian orbifolds of the form $\mathbb{C}^3/\Gamma$. The presented counting of Abelian orbifolds of $\mathbb{C}^3$ and in more general of $\mathbb{C}^D$ gives a first insight on the rich combinatorial nature of brane tilings. Following the classification theme, the work proceeds with the identification of all brane tilings whose mesonic moduli spaces as toric Calabi-Yau 3-folds are represented by reflexive polygons. There are 16 of these special convex lattice polygons. It is shown that 30 brane tilings are associated with them. Some of these brane tilings are related by a correspondence known as toric duality.

The classification of brane tilings with reflexive toric diagrams led to the discovery of a new correspondence between brane tilings which we call specular duality. The new correspondence identifies brane tilings with the same master space – the combined mesonic and baryonic moduli space. As a by-product, the new correspondence paves the way for constructing brane tilings which are not confined to the torus but are on Riemann surfaces with arbitrary genus. We give the first classification of genus 2 brane tilings, illustrate the corresponding supersymmetric quiver theories and analyse their vacuum moduli spaces.

**

The author has published the following papers during his Ph.D.:

1. J. Davey, A. Hanany, and R.-K. Seong, *Counting Orbifolds*, *JHEP* **06** (2010) 010, [`arXiv:1002.3609`]

2. A. Hanany and R.-K. Seong, *Symmetries of Abelian Orbifolds*, *JHEP* **01** (2011) 027, [`arXiv:1009.3017`]

3. J. Davey, A. Hanany, and R.-K. Seong, *An Introduction to Counting Orbifolds*, *Fortsch. Phys.* **59** (2011) 677–682, [`arXiv:1102.0015`]

4. A. Hanany, V. Jejjala, S. Ramgoolam, and R.-K. Seong, *Calabi-Yau Orbifolds and Torus Coverings*, *JHEP* **09** (2011) 116, [`arXiv:1105.3471`]

5. A. Hanany and R.-K. Seong, *Brane Tilings and Reflexive Polygons*, *Fortsch.Phys.* **60** (2012) 695–803, [`arXiv:1201.2614`]

6. K. Hosomichi, R.-K. Seong, and S. Terashima, *Supersymmetric Gauge Theories on the Five-Sphere*, *Nucl.Phys.* **B865** (2012) 376–396, [`arXiv:1203.0371`]

7. A. Hanany and R.-K. Seong, *Brane Tilings and Specular Duality*, *JHEP* **1208** (2012) 107, [`arXiv:1206.2386`]

8. S. Franco, D. Galloni, and R.-K. Seong, *New Directions in Bipartite Field Theories*, `arXiv:1211.5139`

9. S. Cremonesi, A. Hanany, and R.-K. Seong, *Double Handled Brane Tilings*, `arXiv:1305.3607`

The following thesis is based on a subset of the publications above. The author has also written the following publications in condensed matter theory during his Ph.D.:

10. R.-K. Seong and D. D. Vvedensky, *Statistical thermodynamics and weighted topology of radial networks*, *ArXiv e-prints* (May, 2010) [`arXiv:1005.3019`]

11. R.-K. Seong, C. M. Salafia, and D. D. Vvedensky, *Statistical topology of radial networks: a case study of tree leaves*, *Philosophical Magazine* **92** (2012), no. 1-3 230–245, [`http://www.tandfonline.com/doi/pdf/10.1080/14786435.2011.614965`]

12. R.-K. Seong, P. Getreuer, Y. Li, T. Girardi, C. Salafia, and D. Vvedensky, *Statistical geometry and topology of the human placenta*, in *Advances in Applied Mathematics, Modeling, and Computational Science* (R. Melnik and I. S. Kotsireas, eds.), vol. 66 of *Fields Institute Communications*, pp. 187–208. Springer US, 2013

Acknowledgements

A word of thanks to family and friends for being with me during my journey as a Ph.D. student.

My journey as a Ph.D. student has been unbelievably exciting and rewarding. The people I have met have become my friends. I apologise that the following list is incomplete.

First of all, I would like to thank my supervisor and mentor Amihay Hanany who I have first met as an undergraduate student in autumn 2007. As his undergraduate student and as his Ph.D. student from autumn 2009, his guidance and patience have been invaluable assets in choosing the right path during my studies. His ability and taste to identify very interesting problems in string theory as well as his prophetic sight to sense the solution to challenging physical and mathematical problems have always amazed me. They made me to work even harder to reach his standard of excellence in research. I am very proud to have been his 12th Ph.D. student, and I will do my utmost to nourish the beacon of inquisitiveness and discovery which he has lit up for me. I also thank Valerie for her motherly understanding and care. Her French and Israeli cooking has always recharged my batteries. Lovely Elah has always been a delightful little friend who kept everything in perspective. Seeing her grow during my Ph.D. was like having a little sister who I always wished for.

I had a second mentor and supervisor during my Ph.D. studies at Imperial College London. I knew Dimitri V. Vvedensky since my second year as an undergraduate student and since his wonderful course in statistical mechanics I fell in love with theoretical condensed matter physics. I was fortunate to be given the freedom to work on projects in statistical mechanics and soft condensed matter physics with Dimitri Vvedensky. I am also grateful for the collaboration and support from Carolyn Salafia and Placenta Analytics during the course of my Ph.D..

I thank my collaborators for their teachings and share in enthusiasm for research. Vishnu Jejjala and Sanjaye Ramgoolam inspired me with their sense of innovation. Their refreshing perspective on brane tilings and other related problems is a trailblazing force for new exciting problems and future projects.

During my visit to the Yukawa Institute for Theoretical Physics at Kyoto University in early 2011, I have met Kazuo Hosomichi and Seiji Terashima. I consider both of

To my parents

Contents

List of Tables

List of Figures

1 Introduction and Outline

1.1 Motivation

The research presented in this work is mainly based on the publications in [1, 2, 3, 4, 5, 6, 7, 8] and has focused on various aspects of supersymmetric gauge theories in relation to quantum field theory and string theory.[1] They have attracted much interest both on the phenomenology as well as on the more formal side of string theory. One of the chief obligations of the theoretical particle physics and string theory community is to reconcile high-energy, supersymmetric and extra-dimensional theories to low-energy $4d$ gauge dynamics. This is especially important in light of a tour de force in string phenomenology to construct a framework for beyond-standard-model physics. The flow of data from the Large Hadron Collider (LHC) provides a powerful guidance for both experimentalists and theorists, and underscores the importance of the role string theory can play.

The beauty of studying supersymmetric gauge theories is that many of their properties can be analysed exactly and non-perturbatively. This provides an ideal environment in which one can study the dynamics of gauge theories [30, 31, 32], and a wide range of phenomena such as gauge theory phases and dualities [33, 31, 34, 35, 36, 37]. Most of these phenomena can be viewed from a string theory perspective. This can be done via the use of brane configurations and the AdS/CFT correspondence.

The gauge/gravity correspondence [38, 39, 40] has been the guiding beacon for much research and many advances in the field of theoretical high energy physics. This conjecture is a weak-strong coupling duality, in the sense that it connects the weak (strong) coupling regime of a gravity theory on AdS with the strong (weak) coupling limit of a CFT living on its boundary. This is what makes the correspondence, conjectured by Maldacena in 1997 [38], absolutely non-trivial and thoroughly invigorating: by studying the weak coupling limit of one side, one can learn a great deal on the strong coupling limit of the other side.

A very powerful way to construct interesting gauge theories is by probing Calabi-Yau singularities with D-branes [41, 42, 43]. Through this construction, a very deep connection between geometry and physics manifests itself, as different singularities give rise to different conformal field theories. This construction using D3-branes typically leads to

---

[1]For beautiful books and excellent reviews, the reader is referred to a personal selection [19, 20, 21, 22, 23, 24, 25, 26, 27, 28, 29].

theories with unitary gauge groups, bifundamental or adjoint matter and some superpotential. The matter content of the theories can be beautifully represented with a graph known as the quiver. The theory itself is referred to as a quiver theory [44]. A quiver and a superpotential contain all the information needed to construct the Lagrangian of the $4d$ $\mathcal{N} = 1$ supersymmetric gauge theory [45, 46, 47].

Recent fruitful interactions between mathematics and physics are related to super-symmetric quiver gauge theories in string theory. The space of solutions to the field equations – the moduli space of vacua – exhibits intricate structures which are of great interest for instance to algebraic geometry. Moduli spaces can be Calabi-Yau and toric, and tools from algebraic geometry and even number theory can be used to identify dualities and to test conformality of the supersymmetric theories.

A powerful tool to study the structure of the moduli space of vacua of a supersymmetric quiver gauge theory is to calculate the associated Hilbert series [48, 49, 50, 51, 52]. It is a partition function of holomorphic gauge invariant operators that play a central role in characterising the vacuum configuration of the theory. Not only does it carry information on the spectrum of operators, but also identifies whether the moduli space is Calabi-Yau or what its volume function and dimension are.

For $4d$ $\mathcal{N} = 1$ worldvolume theories of D3-brane at Calabi-Yau 3-fold singularities, the dual string theory background is $AdS_5 \times X_5$ where X_5 is a Sasaki-Einstein 5-manifold [45, 53, 42]. The field theory is superconformal [15, 54] and it can be represented by a periodic bipartite graph on a 2-torus. The graph is called a brane tiling [15, 55] and it has been used to classify supersymmetric gauge theories with toric Calabi-Yau moduli spaces and to study new gauge theory dualities.[2]

The recent progress in the study of brane tilings, also known as dimer models, is a classic example of the fruitful interaction between physics and mathematics. The subject has led to hundreds of papers in the past 7 years, fuelled by new developments in algebraic/differential geometry and gauge/string theories.

Brane tilings encode the matter content and superpotential of the supersymmetric quiver gauge theory. The underlying string theory brane construction [66, 67, 68, 15, 55] led to the term in the early physics literature. The name dimer more often used in mathematics, originates from the graph's similarity to a chemical compound consisting of two molecular components. Dimers have been much studied in early mathematics literature [66, 67, 69, 70].

Dimers and brane tilings have had an immense impact on mathematics and physics. The topics in string theory and high-energy physics related to brane tilings are[3]:

---

[2]For $3d$ $\mathcal{N} = 2$ worldvolume theories of M2-branes at 4-fold singularities [56, 57, 58, 59, 60, 61], the dual M-theory background is $AdS_4 \times X_7$ where X_7 is a Sasaki-Einstein 7-manifold [53, 42, 62, 63]. The brane tiling is modified to incorporate the Chern-Simons levels of the $3d$ theory [63, 64, 65]. These modified brane tilings are not the subject of this work and are mentioned here for completeness.

[3]Note that the references selected here are designed to give a taste of the topics and are far from complete.
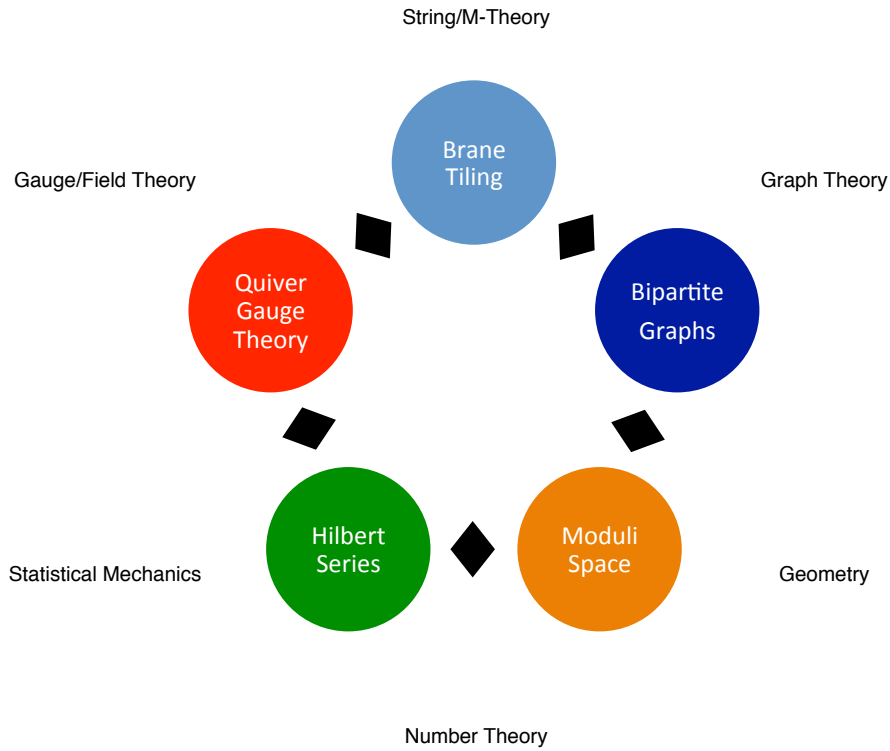
Figure 1.1: *Brane Tiling landscape of physics and mathematics.* Brane tilings bring together a plethora of subjects in physics and mathematics.

- AdS/CFT correspondence in $3 + 1d$ and $2 + 1d$: Calabi-Yau cones over Sasaki-Einstein 5-manifolds [45, 53, 42] and 7-manifolds [53, 42, 62, 63]

- Moduli spaces of supersymmetric gauge theories [71, 72, 73, 74, 75, 18, 52, 15, 55]

- Seiberg Duality in gauge theory [34, 35, 36, 37]

- Local constructions of MSSM and String Phenomenology [76]

- Crystal Melting and Wall-Crossing Phenomena [77, 78, 79]

- Integrable systems [80, 81]

- $\mathcal{N} = 4$ scattering amplitudes [82]

On the mathematics side, dimers have made a great impact in the following subjects:

- Mirror Symmetry [83]

- Graph Theory and Combinatorics [66, 67]

- Tropical Geometry [84]

- Calabi-Yau algebras [85, 86, 87]

- Number Theory: dessin d'enfant, finite fields [88]

These are promising topics for further investigation amongst mathematicians and physicists. Figure 1.1 shows schematically the different areas of mathematics and physics connected by brane tilings and their properties and the tools used to study them. The following sections aim to give a concise review on brane tilings. This work is written to be a helpful guide for the novice reader who wants to learn about the techniques and recent exciting developments on brane tilings.

1.2 Brane Tilings

The following section is a review on brane tilings [15, 55]. Brane tilings are graphical representations of the quiver and superpotential of a $3+1$ dimensional worldvolume theory living on a stack of D3-branes which probe a singular toric Calabi-Yau 3-fold. These theories are superconformal and are dual to Type IIB string theory in a $AdS_5 \times X_5$ background where X_5 is a Sasaki-Einstein 5-manifold [45, 42]. Sections §1.2.1 and §1.2.2 review quivers and superpotentials for brane tilings respectively. Section §1.2.3 gives the construction of periodic bipartite graphs on the 2-torus and how they are interpreted as brane tilings.

The following sections are based on the original papers [15, 55], reviews [89, 90] and extracts from [5, 7].

1.2.1 Quivers

Quiver $\mathcal{Q}$. The matter content of a supersymmetric gauge theory corresponding to a brane tiling is specified by a directed graph known as the **quiver** [44, 86, 91]. It consists of the following components:

- **Vertices** in $\mathcal{Q}$ correspond to $U(N_i)$ gauge groups with $i = 1, \ldots, G$.

- **Edges** in $\mathcal{Q}$ correspond to the matter fields X_{ij}. The matter fields are bifundamental and transform under the fundamental of $U(N_i)$ and antifundamental of $U(N_j)$, imposing a direction on the quiver edges, $i \to j$. The anomaly cancellation condition for the quiver gauge theory sets the number of incoming and outgoing edges on a quiver vertex to be equal.

- The **incidence matrix** $d_{G \times E}$ for E bifundamental matter fields encodes the quiver. Its entry for a gauge group $U(N_i)$ is -1 for X_{ij}, $+1$ for X_{ji}, and 0

otherwise. The matrix $d_{G \times E}$ has $G - 1$ independent rows which can be collected in a new matrix called $\Delta_{(G-1) \times e}$.

In general, the ranks of the $U(N_i)$ gauge groups are $N_i \geq 1$. For most parts of the following work on brane tilings, we consider the ranks of all gauge groups to be equal. If not explicitly stated otherwise, the quiver is considered to be Abelian where for all i, $N_i = 1$. For this case, we call the theory and its brane tiling Abelian.
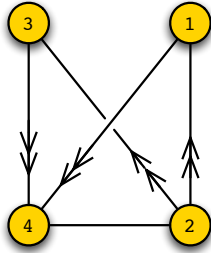
Figure 1.2: *The quiver for phase b of the Hirzebruch F_0 model.*

Example. Figure 1.2 shows the quiver diagram for phase b of the Hirzebruch F_0 model [92, 55, 15, 93]. The corresponding quiver incidence matrix is

$$
d = \left(\begin{array}{c|cccccccccccc}
 & X_{14}^1 & X_{14}^2 & X_{21}^1 & X_{21}^2 & X_{23}^1 & X_{23}^2 & X_{34}^1 & X_{34}^2 & X_{42}^1 & X_{42}^2 & X_{42}^3 & X_{42}^4 \\
\hline
U(N_1) & -1 & -1 & 1 & 1 & 0 & 0 & 0 & 0 & 0 & 0 & 0 & 0 \\
U(N_2) & 0 & 0 & -1 & -1 & -1 & -1 & 0 & 0 & 1 & 1 & 1 & 1 \\
U(N_3) & 0 & 0 & 0 & 0 & 1 & 1 & -1 & -1 & 0 & 0 & 0 & 0 \\
U(N_4) & 1 & 1 & 0 & 0 & 0 & 0 & 1 & 1 & -1 & -1 & -1 & -1
\end{array} \right) .
$$

$$(1.2.1)$$

We note that the columns of the incidence matrix are linearly dependent and hence the matrix can be reduced to a matrix Δ with 3 rows.

Anomaly Cancellation. For the most general case where the ranks of the $U(N_i)$ gauge groups in the quiver diagram are $N_i \geq 1$, the anomaly cancellation condition [54] can be written in terms of the quiver incidence matrix d as follows

$$
\sum_{a=(i,j)} d_{ia} N_j = 0 \; , \tag{1.2.2}
$$

where the sum goes over all arrows labelled by $a = (i, j)$ which are between nodes i and j. N_j is the rank of the $U(N_j)$ group represented by node j in the quiver.
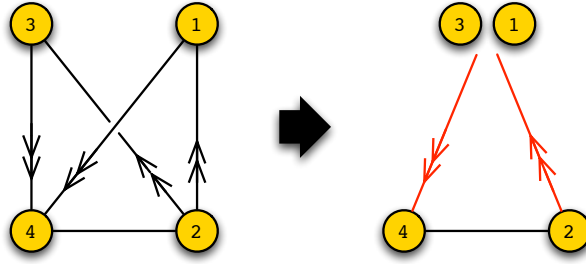
Figure 1.3: *Block quivers.* For the quiver for phase b of the Hirzebruch F_0 model vertices 1 and 3 share the same incidence information with no matter fields between them. They are combined into a block. All matter fields intersecting the block are colored red and are combined such that a red arrow represents all possible connections from and to all vertices within the block.

Block Quivers. If two or more quiver vertices share the same intersection number with other quiver vertices and have no matter fields between any two of them, then the quiver vertices can be grouped into a **block** [94, 95]. This property is illustrated in the example for phase b of the Hirzebruch F_0 model in Figure 1.3.

1.2.2 Toric Superpotentials

Toric Superpotential W. The superpotential for a brane tiling is a polynomial in quiver fields with the following conditions:

- **Gauge invariance.** Every term in W is a gauge invariant combination of quiver fields. In terms of the quiver diagram, every term in W corresponds to a closed directed loop in the quiver.

- **Bipartite.** The superpotential W has positive and negative terms. The number of positive terms is equal to the number of negative terms.

- **Toric.** Every quiver field appears twice in W, once in a positive term and once in a negative term. This ensures that the critical points $\partial_X W = 0$ in the superpotential, i.e. the F-terms, are relations between monomials. This **toric condition** ensures that the vacuum moduli space of the brane tiling is toric [14].

The superpotential W has an overall trace. For conciseness of notation, this trace is omitted in the following writing and the reader is reminded of this notational simplification.

Example. The superpotential for phase b of the Hirzebruch F_0 model whose quiver diagram is shown in Figure 1.2 is

$$
\begin{aligned}
W \;=\; & +X_{21}^1 X_{14}^1 X_{42}^1 + X_{21}^2 X_{14}^2 X_{42}^2 + X_{23}^1 X_{34}^2 X_{42}^3 + X_{23}^2 X_{34}^1 X_{42}^4 \\
& -X_{21}^1 X_{14}^2 X_{42}^3 - X_{21}^2 X_{14}^1 X_{42}^4 - X_{23}^1 X_{34}^1 X_{42}^2 - X_{23}^2 X_{34}^2 X_{42}^1 \ .
\end{aligned}
\tag{1.2.3}
$$

The superpotential is bipartite and toric. There are precisely 12 quadratic F-terms which equate single monomials. The first few F-terms are,

$$
\begin{aligned}
X_{42}^1 X_{21}^1 = X_{42}^4 X_{21}^2 \ , \ \ X_{42}^2 X_{21}^2 = X_{42}^3 X_{21}^1 \ , \\
X_{14}^1 X_{42}^1 = X_{14}^2 X_{42}^3 \ , \ \ X_{14}^2 X_{42}^2 = X_{14}^1 X_{42}^4 \ , \ \dots \ .
\end{aligned}
\tag{1.2.4}
$$

Mass terms. All terms in W are cubic or of higher degree. Quadratic terms relate to mass terms which are **integrated out**. The mass terms correspond to two bifundamental fields in the quiver with opposite gauge charges. A generic example is given by

$$
W = +X_{12}X_{21} - X_{12}P_{21}(X) - X_{21}P_{12}(X) + \dots \ ,
\tag{1.2.5}
$$

where X_{12}, X_{21} are the quiver fields contributing to the mass term and $P_{12}(X), P_{21}(X)$ are generic polynomials in quiver fields. The F-terms for fields X_{12}, X_{21} are

$$
X_{12} = P_{21}(X) \ , \ \ X_{21} = P_{12}(X) \ ,
\tag{1.2.6}
$$

which are used to give

$$
W = -P_{12}(X)P_{21}(X) + \dots \ .
\tag{1.2.7}
$$

Accordingly, quadratic mass terms are *irrelevant* for the construction of brane tiling superpotentials. In the brane tiling picture, integrating out mass terms corresponds to the removal of valence 2 nodes.

1.2.3 Bipartite Graphs and the Brane Tiling

Bipartite graphs have been studied extensively in mathematics[4] before they were first introduced by Hanany and Kennaway as brane tilings in string theory. In mathematics they have played an important role in representing Calabi-Yau geometry and algebras [85, 99].

---

[4]A selection of pioneering work by Kenyon and collaborators are [96, 97, 98].
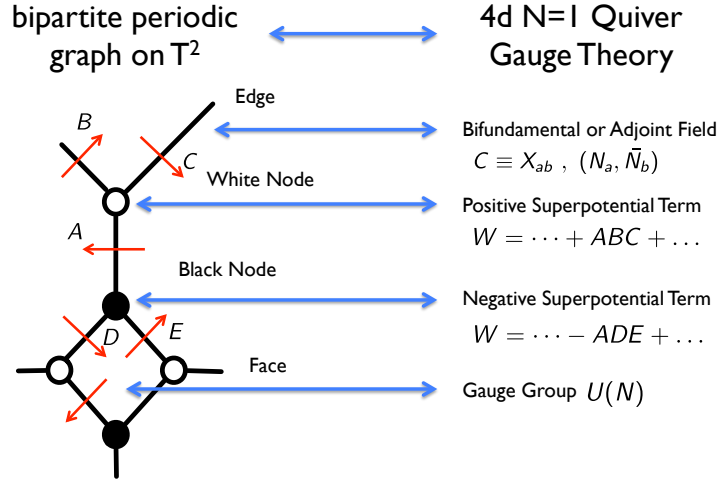
Figure 1.4: *Brane Tiling Dictionary.* A brane tiling consists of nodes, edges and faces which correspond respectively to superpotential terms, quiver fields and gauge groups.

Brane Tilings/Dimers. The superpotential and the quiver can be combined into a single representation. The representation is known as a brane tiling or dimer [15, 55, 100, 86]. It is a periodic bipartite graph on T^2 and has the following components:

- **White (resp. black) nodes** correspond to positive (negative) terms in the superpotential. They have a clockwise (anti-clockwise) orientation.

- **Edges** connect to nodes and correspond to the quiver fields in the superpotential. Going along the induced orientations around nodes, one can identify the matter fields associated to a specific superpotential term in the correct cyclic order.

- **Faces** correspond to $U(N_i)$ gauge groups. Every edge X_{ij} in the tiling has two neighbouring faces corresponding to $U(N_i)$ and $U(N_j)$. The quiver orientation of the bifundamental field X_{ij} is given by the orientation around the black and white nodes at the two ends of the corresponding tiling edge.

Figure 1.4 illustrates the brane tiling dictionary.

Example. Figure 1.5 shows the brane tiling and quiver diagram for the suspended pinch point (SPP) model [34, 101, 102]. The corresponding superpotential is

$$W \quad = \quad +X_{13}X_{31}X_{11} + X_{12}X_{23}X_{32}X_{21} - X_{12}X_{21}X_{11} - X_{13}X_{32}X_{23}X_{31} \ .$$

$$(1.2.8)$$

Fundamental Domain. The fundamental domain of the 2-torus T^2 on which the brane tiling is drawn is interpreted as a section of the periodic tiling which contains
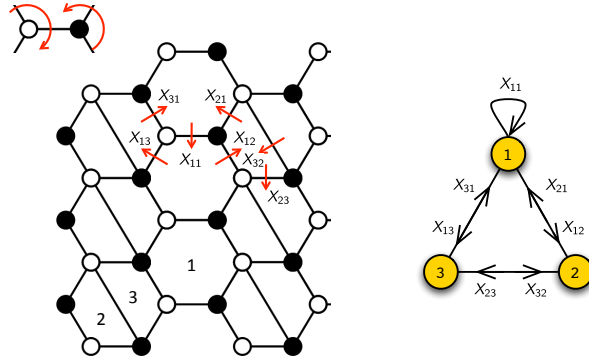
Figure 1.5: *Brane tiling and quiver for the suspended pinch point (SPP) model.* The quiver fields are labelled both in the brane tiling and quiver diagram. The field X_{11} between two equivalent faces in the brane tiling is an adjoint field.
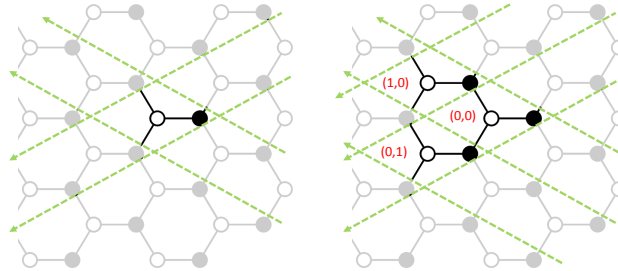
Figure 1.6: *Fundamental cell of the $\mathbb{C}^3$ brane tiling with heights.* By repeated pasting of the fundamental cell along the a- and b-cycles of the 2-torus, the periodic brane tiling is constructed. Each copy of the fundamental cell can be given a height (h_a, h_b) in relation to the reference fundamental cell $(0,0)$.

the quiver and superpotential information without repetition. Repeated pasting of the fundamental domain along the fundamental a- and b-cycles of the torus reproduces the complete periodic brane tiling. Figure 1.6 illustrates this process for the $\mathbb{C}^3$ brane tiling.

Every copy of the fundamental cell can be given a **height** (h_a, h_b) in relation to a reference copy of the cell, i.e. the origin. h_a and h_b count respectively how many copies of fundamental cells the cell with height (h_a, h_b) is away from the origin along the a- and b-cycles of the 2-torus.

Brane Construction [55, 90]. Brane tilings represent superconformal worldvolume theories living on a stack of D3-branes which probe a singular Calabi-Yau 3-fold. The singularity is conical and the base of the non-compact toric Calabi-Yau is a Sasaki-

4d *N=1* Superconformal Gauge Theory

Stack of D3-branes

CY3 cone

Sasaki-Einstein 5-base

worldvolume theory of a
stack of *N* D3 branes
probing singular CY

9+1d Type IIB on $AdS_5 \times X_5$
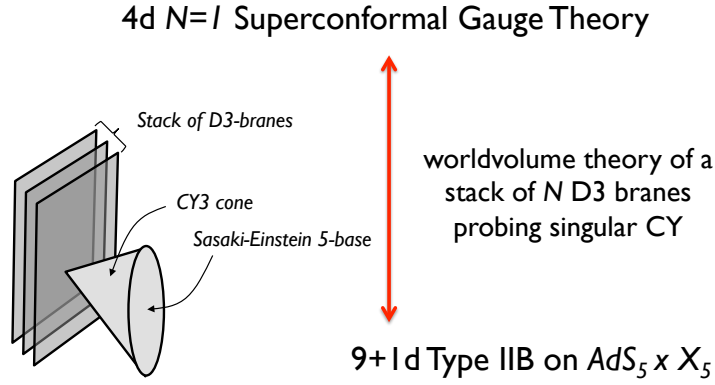
Figure 1.7: *AdS/CFT correspondence.* The superconformal gauge theory living on the probe D3-branes is dual to Type IIB string theory on $AdS_5 \times X_5$.

	0	1	2	3	4	5	6	7	8	9
D3	∘	∘	∘	∘						
CY3					∘	∘	∘	∘	∘	∘

Table 1.1: D3-branes probing the toric Calabi-Yau 3-fold.

Einstein 5-manifold X_5. The worldvolume theory is dual to Type IIB $9+1$ dimensional string theory in $AdS_5 \times X_5$ [45, 42]. The duality is illustrated schematically in Figure 1.7. Table 1.1 shows the brane configuration in $9+1$ dimensions.

Under T-duality, the D3-branes are mapped to D5-branes and the CY 3-fold is mapped to NS5-branes wrapping holomorphic curves. Let us illustrate the connection with a simple example. Given $\mathcal{N} = 4$ super-Yang-Mills theory with $\mathbb{C}^3$ which is dual to Type IIB string theory in $AdS_5 \times S^5$, we can introduce n_1 NS5-branes wrapping the 45-directions which give the orbifold $\mathbb{C}^3/\mathbb{Z}_{n_1}$. A further set of n_2 NS5-branes wrapping the 67-directions would give the orbifold $\mathbb{C}^3/\mathbb{Z}_{n_1} \times \mathbb{Z}_{n_2}$. The probe D3-branes dualise to D5-branes which are suspended between the set of NS5-branes and are wrapped along the 46-directions. The 46-directions are precisely where the D5- and NS5-branes intersect and relate to the 2-torus of the brane tiling picture. T-duality precisely acts on these torus directions. Table 1.2 shows the 5-brane configuration in 9+1 dimensions.

In general, the NS5-branes wrap a complex curve $f(x, y)$ where x, y are respectively

	0	1	2	3	4	5	6	7	8	9
m D5	∘	∘	∘	∘	∘		∘			
n_1 NS5	∘	∘	∘	∘	∘	∘				
n_2 NS5	∘	∘	∘	∘			∘	∘		

Table 1.2: 5-brane construction underlying a brane tiling on T^2 for $\mathbb{C}^3/\mathbb{Z}_{n_1} \times \mathbb{Z}_{n_2}$. The T^2 directions are 46.
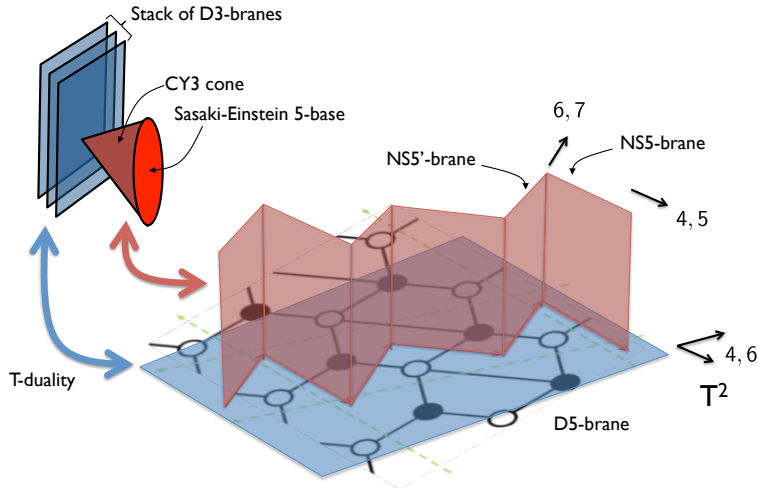
Figure 1.8: *Illustration of the 5-brane construction underlying a brane tiling on T^2.*

	0	1	2	3	4	5	6	7	8	9
D5	○	○	○	○	○		○			
NS5	○	○	○	○	—$f(x,y)$—					

Table 1.3: 5-brane construction underlying a brane tiling on T^2 for a general Calabi-Yau 3-fold. The T^2 directions are 46 and $f(x,y)$ is a complex curve in holomorphic coordinates x, y which respectively are given by the coordinates 45 and 67. The NS5-branes wrap $f(x,y)$.

holomorphic coordinates in 45 and 67. Accordingly, we can have any toric non-compact Calabi-Yau 3-fold beyond $\mathbb{C}^3$ and its Abelian orbifolds. The presence of NS5-branes also breaks the supersymmetry from $\mathcal{N} = 4$ to $\mathcal{N} = 1$. For the special case of the NS5-branes wrapping only a curve parameterised by a single holomorphic coordinate x, the supersymmetry is broken to just $\mathcal{N} = 2$. Note that this is a natural generalisation of brane interval [30] and brane box [68] constructions which can be considered as prototypical brane tilings.

1.3 Properties of the Bipartite Graph and Consistency

Brane tilings as periodic bipartite graphs on the 2-torus are computationally far more superior than a quiver and toric superpotential on their own. This is because as a graph, brane tilings posses many graphical properties that can be used as effective tools in the computation of physical quantities of the corresponding superconformal field theory. The following section gives a summary of the graphical properties of a brane tiling.
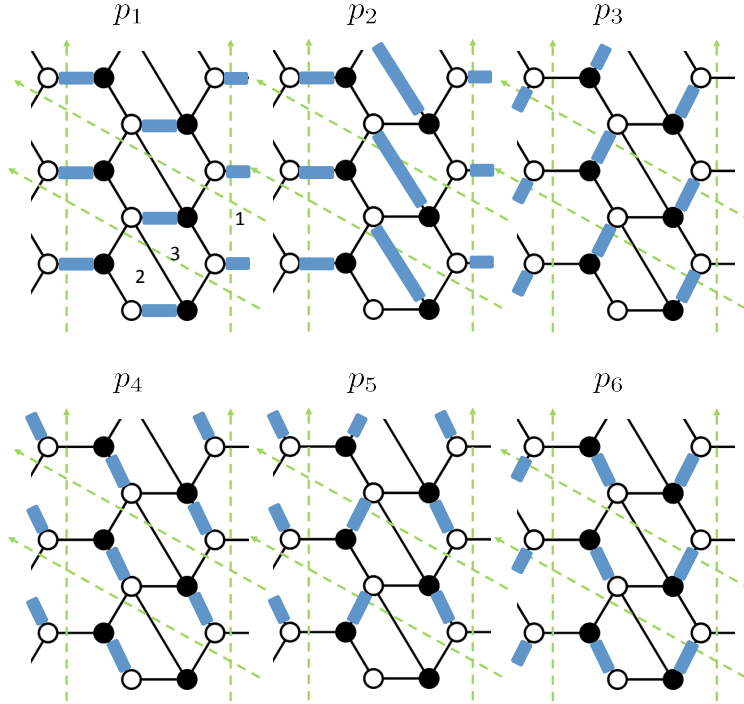
Figure 1.9: *Perfect matchings of the suspended pinch point (SPP) model.* The SPP brane tiling has in total 6 perfect matchings. The fundamental domain is highlighted in green.

1.3.1 Perfect Matchings

Perfect Matching [55, 103]. A perfect matching p_α is a set of bifundamental fields which connects to all nodes in the brane tiling precisely once. It corresponds to a point in the **toric diagram** [41, 42] of the Calabi-Yau 3-fold. A perfect matchings which relates to an **extremal (corner)** point of the toric diagram has non-zero IR $U(1)_R$ charge.[5] An **internal** as well as a non-extremal toric point on the perimeter of the toric diagram has zero R-charge. We call all points on the perimeter **external**, including extremal ones. The number of internal, external and extremal perfect matchings is denoted by n_i, n_e and n_p respectively. All perfect matchings are summarized in a matrix $P_{e\times c}$ [71], where e is the number of matter fields and c the number of perfect matchings. The perfect matching matrix $P_{e\times c}$ takes the form

$$P_{i\alpha} = \begin{cases} 1 & \text{if } X_i \in p_\alpha \\ 0 & \text{if } X_i \notin p_\alpha \end{cases}, \tag{1.3.9}$$

---

[5]A discussion on R-charges follows in section §1.5.2.

where $i = 1, \ldots, e$ and $\alpha = 1, \ldots, c$.

Example. Figure 1.9 shows the 6 perfect matchings of the SPP model. The corresponding perfect matching matrix is

$$
P = \left(
\begin{array}{c|cccccc}
 & p_1 & p_2 & p_3 & p_4 & p_5 & p_6 \\
\hline
X_{11} & 1 & 1 & 0 & 0 & 0 & 0 \\
X_{12} & 0 & 0 & 0 & 1 & 0 & 1 \\
X_{21} & 0 & 0 & 1 & 0 & 1 & 0 \\
X_{23} & 1 & 0 & 0 & 0 & 0 & 0 \\
X_{32} & 0 & 1 & 0 & 0 & 0 & 0 \\
X_{31} & 0 & 0 & 0 & 1 & 1 & 0 \\
X_{13} & 0 & 0 & 1 & 0 & 0 & 1 \\
\end{array}
\right) . \tag{1.3.10}
$$

Winding numbers of perfect matchings. A **winding number** w can be assigned to an oriented object that passes between two copies of the fundamental cell of a brane tiling with heights (h_a, h_b) and (k_a, k_b). The winding number is the difference in heights $(h_a - k_a, h_b - k_b)$ where the sign of the difference is determined by the orientation of the object.

Every edge in the brane tiling has an assigned orientation according to white and black nodes that connect to it. This orientation indicates the gauge charges carried by the corresponding quiver field. We can now define an **orthogonal orientation** which is by convention always along the edge from a white to a black node. Accordingly, every brane tiling edge X_i carries a winding number $w(X_i) = (h_a^i, h_b^i)$ under the orthogonal orientation. If an edge does not cross the boundary of a set fundamental domain, then it carries a trivial winding number $(0, 0)$.

Using the definition of winding numbers for tiling edges, the winding number of a perfect matching p_α is defined as

$$
w(p_\alpha) = \sum_{X_i \in p_\alpha} w(X_i) = \sum_{X_i \in p_\alpha} (h_a^i, h_b^i) . \tag{1.3.11}
$$

When the winding numbers of all perfect matchings of a brane tiling are taken as $\mathbb{Z}^2$ lattice coordinates of a set of points, the convex hull of the lattice points forms a polygon which is identified as the **toric diagram** of the toric Calabi-Yau 3-fold [55, 103].

Note that the choice of the fundamental cell is $GL(2, \mathbb{Z})$ invariant. Accordingly, winding numbers of perfect matchings and tiling edges can be $GL(2, \mathbb{Z})$ transformed without loss of information. In other words, the toric diagram is considered to be invariant under $GL(2, \mathbb{Z})$.

Example. Figure 1.10 shows the perfect matchings of the brane tiling of SPP with
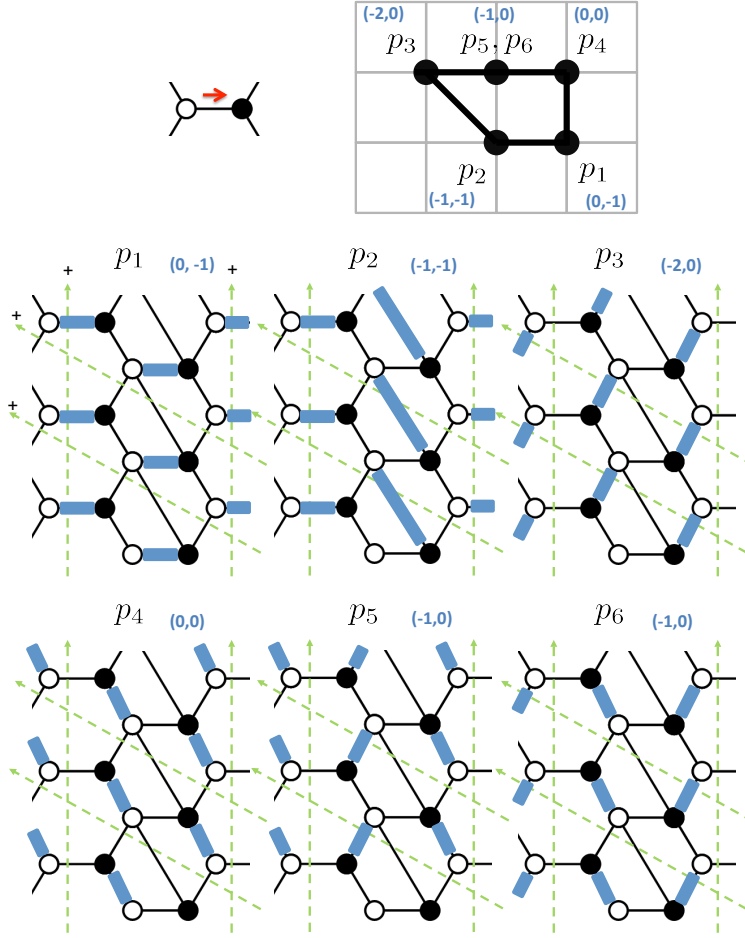
Figure 1.10: *Perfect matchings of the SPP model with the toric diagram from the perfect matching winding numbers.* The toric diagram of the non-compact Calabi-Yau 3-fold is the convex hull of the set of lattice points whose coordinates are given by the corresponding perfect matching winding numbers.

the corresponding winding numbers for the given perfect matchings. The set of lattice points which are obtained by taking the winding numbers as coordinates on $\mathbb{Z}^2$ give the toric diagram of SPP. The winding numbers are

$$w(p_1) = (0, -1) \ , \ w(p_2) = (-1, -1) \ , \ w(p_3) = (-2, 0) \ ,$$
$$w(p_4) = (0, 0) \ , \ w(p_5) = (-1, 0) \ , \ w(p_6) = (-1, 0) \ . \tag{1.3.12}$$

From the toric diagram we observe that the perfect matchings p_1, p_2, p_3, p_4 are extremal and the perfect matchings p_5, p_6 are external but not extremal. The two perfect matchings have the same winding number and correspond to the same toric point.

GLSM fields. The geometry of the toric Calabi-Yau 3-fold is encoded in the brane

44
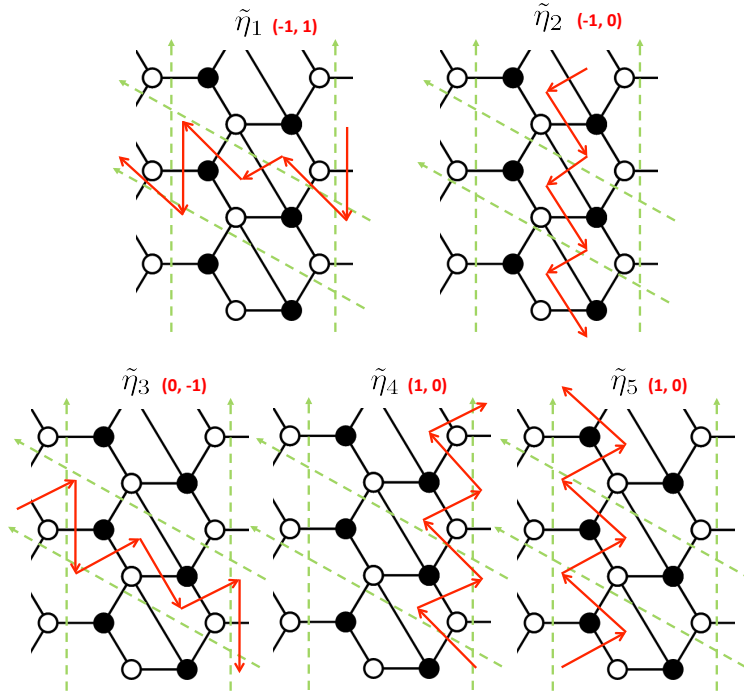
Figure 1.11: *The zig-zag paths of the SPP brane tiling with their winding numbers.* The winding number of every zig-zag path can be represented as vectors in the $\mathbb{Z}^2$ lattice. The resulting fan corresponds to the (p, q)-web diagram.

tiling as we have seen above. A new basis of fields is defined from the set of quiver fields in order to describe both F-term and D-term constraints of the supersymmetric gauge theory. The new fields are known as gauge linear sigma model (GLSM) fields [104] and precisely correspond to perfect matchings [15, 16, 89, 71] of the brane tiling.

1.3.2 Zig-Zag Paths

Zig-zag paths $\tilde{\eta}_i$ [105, 16]. A zig-zag path is a closed path along the edges on the brane tiling which alternates between white and black nodes. The path is such that it makes precisely one maximal clockwise turn around a white note and then a maximal anti-clockwise turn around the next black node before reaching the next edge and node in the sequence. A fundamental cell of a brane tiling has always a finite number of zig-zag paths. They correspond to the closed curves wrapped by the NS5-branes and the 46 torus cycles along which the NS5-branes intersect the D5-branes [106, 90].

(p, q)**-web diagrams [107, 108].** Every zig-zag path has a winding number in relation to a reference fundamental cell of the brane tiling. The winding numbers of the zig-zag paths of a brane tiling can be drawn as rays from the origin of a $\mathbb{Z}^2$ lattice. We call
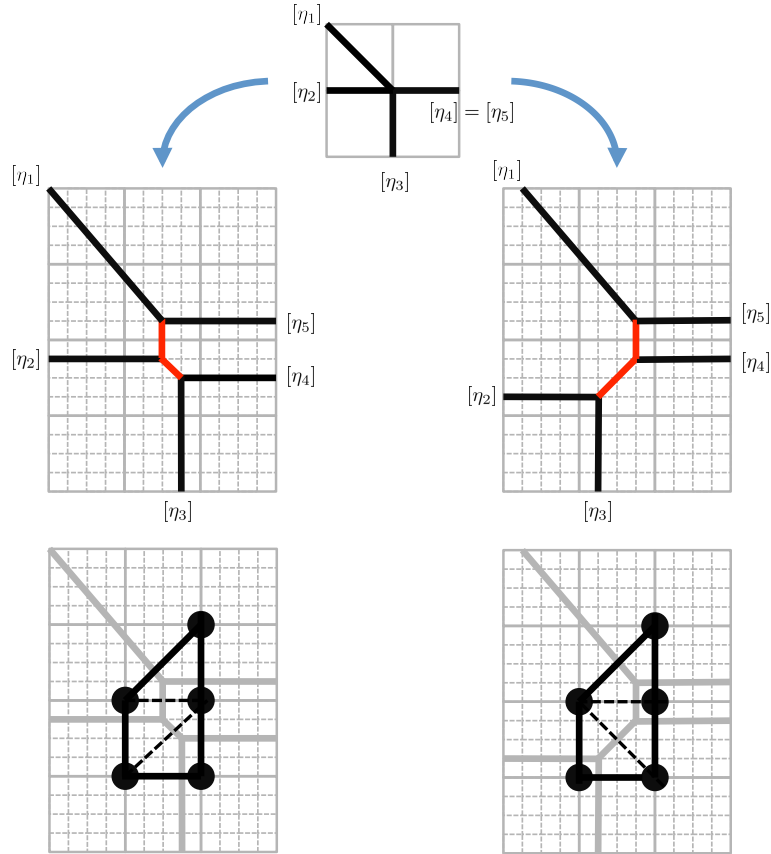
Figure 1.12: *The (p, q)-web of SPP and the corresponding triangulations of the toric diagram.* The winding numbers of the zig-zag paths give a reduced (p, q)-web diagram which can be extended such that the vertices of the web are all cubic. The dual of an extended (p, q)-web diagram is a triangulation of the toric diagram.

the resulting fan the **reduced** (p, q)**-web diagram**. The origin of this diagram is a N_{zz}-valent vertex where N_{zz} is the number of zig-zag paths.

The reduced (p, q)-web diagram can be extended by decomposing the N_{zz}-valent origin into 3-valent vertices. The dual of the resulting **extended** (p, q)**-web diagram** is precisely the toric diagram of the non-compact Calabi-Yau 3-fold. The different ways of decomposing the N_{zz}-valent origin of the reduced diagram correspond precisely to the different ways of triangulating the convex toric diagram.

Example. Figure 1.11 shows the 5 zig-zag paths of the SPP brane tiling and their corresponding winding numbers for the given reference fundamental domain. The winding

numbers of the zig-zag paths are

$$w(\tilde{\eta}_1) = (-1,1) \ , \ w(\tilde{\eta}_2) = (-1,0) \ , \ w(\tilde{\eta}_3) = (0,-1) \ , \ w(\tilde{\eta}_4) = (1,0) \ , \ w(\tilde{\eta}_5) = (1,0) \ .$$

$$(1.3.13)$$

The corresponding reduced (p,q)-web diagram is shown in Figure 1.12. We observe that the origin of the reduced web diagram is 5-valent. There are precisely two distinct ways of decomposing the 5-valent origin to 3-valent vertices. The two extended (p,q)-webs correspond to two distinct ways of triangulating the same toric diagram of SPP as shown in Figure 1.12.

1.3.3 Consistency
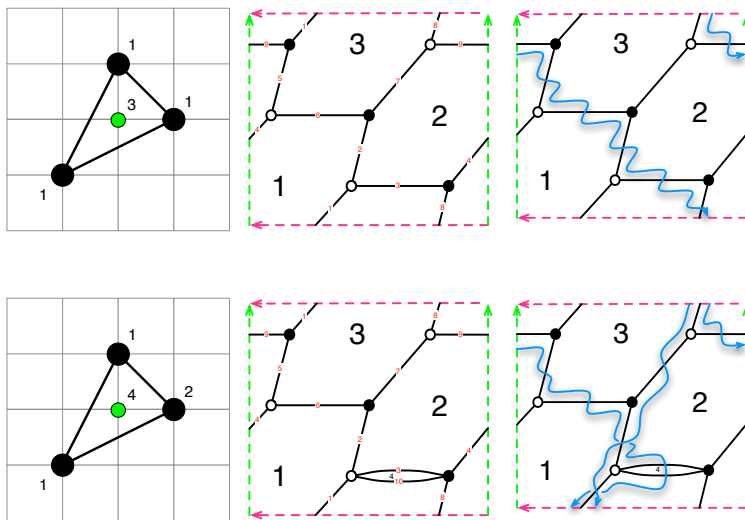
Figure 1.13: *Inconsistent dP_0 Model.* The top row shows the toric diagram of the dP_0 model [14, 15, 16, 17, 18] with the brane tiling and zig-zag path of the brane tiling going around the 2-torus. The bottom row shows an inconsistent toric diagram with an extremal toric point having a multiplicity greater than 1, and its corresponding double-bonded brane tiling with self-intersecting zig-zag path.

The notion of **consistency** of a brane tiling on the 2-torus was first discussed in [16]. Consistent torus brane tilings are expected to flow in the IR to a superconformal fixed point with a preferred $U(1)$ R-symmetry[6] which appears in the superconformal algebra and determines the scaling dimension of BPS operators. If the consistency conditions are not satisfied, one normally can expect zero superconformal R-charges to

---

[6]R-symmetry is discussed below in section §1.5.2.

be assigned to bifundamental fields under a-maximisation [109, 110, 111]. In this case, some dibaryon operators would violate the unitarity bound on the scaling dimension.

In order to discuss brane tiling consistency from a geometric and combinatorial point of view, we recall that the classical vacuum moduli space of the Abelian theory which we are considering with only $U(1)$ gauge groups is a toric Calabi-Yau 3-fold. As we have reviewed above, the Calabi-Yau 3-fold is represented by a convex lattice polygon known as the toric diagram. In terms of the toric diagram, **inconsistency** of the brane tiling and its corresponding supersymmetric gauge theory can be identified when

- Twice the area of the toric diagram is *not* the number of gauge groups in the brane tiling.

From a purely graphical point of view, a brane tiling is **consistent** if it has the following properties:

- No zig-zag paths self-intersect.

- No edges are 'multi-bonded' and hence no faces are 2-sided.

- No extremal toric point corresponds to more than one perfect matching of the toric diagram.

The above consistency conditions are illustrated in Figure 1.13.

1.4 Moduli Spaces

The following section reviews the vacuum moduli spaces of brane tilings. There are two moduli spaces of interest: the master space and the mesonic moduli space. Both are toric Calabi-Yau when all gauge groups of the brane tiling are $U(1)$, i.e. the supersymmetric quiver theory is Abelian. In particular, the mesonic moduli space is the probed toric Calabi-Yau 3-fold which was discussed previously. We first focus on the moduli spaces of Abelian brane tilings and on how they are characterised by a partition function of gauge invariant operators know as the Hilbert series. We then review the non-Abelian theories and their moduli spaces.

1.4.1 The Master Space

Master Space $\mathcal{F}^\flat$ **[71, 72, 73, 74, 75, 18].** The master space is the combined mesonic and baryonic moduli space. It is determined only by the F-term constraints of the supersymmetric gauge theory represented by a brane tiling. It has the following properties for the case of Abelian brane tilings where all gauge groups are $U(1)$:
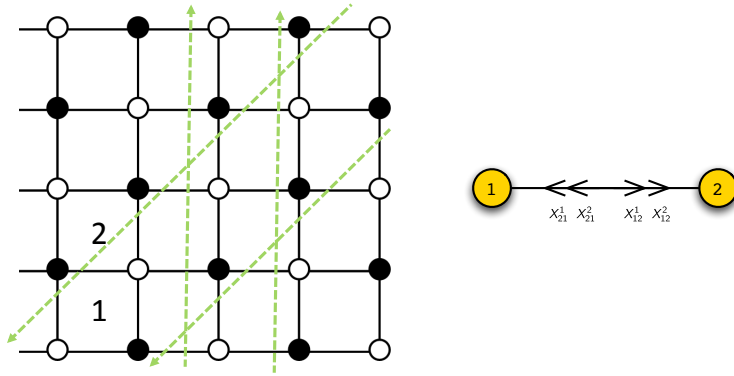
Figure 1.14: *The brane tiling and quiver diagram of the conifold theory.*

- The master space of the one D3-brane theory relates to the following quotient ring

$$\mathbb{C}^E[X_1, \ldots, X_E]/\mathcal{I}_{\partial W=0} \ , \tag{1.4.14}$$

where E is the number of bifundamental fields X_i. $\mathbb{C}^E[X_1, \ldots, X_E]$ is the complex ring over all bifundamental fields, and $\mathcal{I}_{\partial W=0}$ is the ideal formed by the F-terms.

- The master space in (1.4.14) is usually reducible into components. The largest irreducible component is known as the **coherent component** $^{\mathrm{Irr}}\mathcal{F}^\flat$ and is toric Calabi-Yau. All other smaller components are generally linear pieces of the form $\mathbb{C}^l$. In our discussion, we will concentrate on the coherent component of the master space and for simplicity use $\mathcal{F}^\flat$ and $^{\mathrm{Irr}}\mathcal{F}^\flat$ interchangeably for Abelian theories.

- The **dimension** of the master space $^{\mathrm{Irr}}\mathcal{F}^\flat$ is $G + 2$, where G is the number of gauge groups. For the Abelian theory, $^{\mathrm{Irr}}\mathcal{F}^\flat$ is toric Calabi-Yau.

Example. The conifold theory [45] has 2 gauge groups $U(N_1) \times U(N_2)$ with the quiver and brane tiling shown in Figure 1.14. The superpotential is as follows

$$W = +X_{12}^1 X_{21}^1 X_{12}^2 X_{21}^2 - X_{12}^1 X_{21}^2 X_{12}^2 X_{21}^1 \ . \tag{1.4.15}$$

For the Abelian theory with $N_1 = N_2 = 1$, the superpotential vanishes and there are no non-trivial F-terms. The master space $^{\mathrm{Irr}}\mathcal{F}^\flat$ is simply given by the ring formed by the bifundamental fields, in other words $^{\mathrm{Irr}}\mathcal{F}^\flat = \mathbb{C}^4$.

Non-Abelian case. We are interested in brane tilings in the IR limit where they flow to superconformal field theories. In the IR limit, the non-Abelian theory with G gauge groups $U(N_i)^G$ decomposes to $SU(N)^G \times U(1)^G$. This is because the $U(1)^G$ decouple in the IR. Only $SU(N)$ groups strongly couple in the IR. The remaining gauge symmetries

$SU(N)^G$ have to be quotiented out for the master space of the non-Abelian theory as follows,

$$\mathcal{F}^\flat_N = \mathcal{F}^\flat / SU(N)^G \ , \tag{1.4.16}$$

where $\mathcal{F}^\flat$ corresponds to the quotient ring formed by the F-terms $\partial W = 0$. The dimension of the master space is $3N + G - 1$.

Example. Let us take the $N_1 = N_2 = 2$ case for the conifold theory, with the bifundamental fields now being 2×2 matrices. For notational simplicity, we relabel the bifundamental fields as

$$A = X^1_{12} \ , \ \ B = X^2_{12} \ , \ \ C = X^1_{21} \ , \ \ D = X^2_{21} \ . \tag{1.4.17}$$

The superpotential is now non-vanishing,

$$W = +ABCD - ADCB \ , \tag{1.4.18}$$

and the F-terms $\partial_X W = 0$ are non-trivial. The F-terms form an ideal, and $\mathcal{F}^\flat$ is given by the quotient ring

$$\begin{aligned}
\mathbb{C}^{16}[A_{11}, A_{12}, A_{21}, A_{22}, \ldots, D_{21}, D_{22}] \\
/ \langle BCF - DCB, CDA - ADC, DAC - BAD, ABC - CBA \rangle \ .
\end{aligned} \tag{1.4.19}$$

The master space $\mathcal{F}^\flat_{N=2}$ is obtained by quotienting out the $SU(2)^2$ charges

$$\mathcal{F}^\flat_{N=2} = \mathcal{F}^\flat / SU(2)^2 \ . \tag{1.4.20}$$

1.4.2 The Mesonic Moduli Space

Mesonic Moduli Space $\mathcal{M}^{mes}$ [52, 5, 34]. The mesonic moduli space is a subspace of the master space. It is determined by both F- and D-term constraints. It has the following properties:

- In order to obtain the mesonic moduli space of the one D3-brane theory, the $U(1)^G$ charges have to be quotiented out. Note that an overall $U(1)$ decouples, giving in total only $U(1)^{G-1}$ independent charges that need to be taken into account. The

mesonic moduli space is therefore given by

$$\mathcal{M}^{mes} = {}^{\mathrm{Irr}}\mathcal{F}^{\flat}/U(1)^{G-1} \; . \tag{1.4.21}$$

- The mesonic moduli space for the Abelian theory is a toric Calabi-Yau 3-fold.

Non-Abelian case. We recall that the master space $\mathcal{F}^{\flat}$ is the space of mesonic and baryonic operators. In the IR limit the gauge symmetries $U(N)^G$ decompose to a weakly coupled part $U(1)^G$ which plays the role of the global baryonic symmetry and a strongly coupled non-Abelian part $SU(N)^G$ which is the remaining non-Abelian gauge symmetry. In the definition of the master space $\mathcal{F}^{\flat}_N$ for non-Abelian theories in (1.4.16), the gauge symmetry is quotiented out to remain with a space of baryonic and mesonic gauge invariant operators. In order to remain with a space of just mesonic gauge invariant operators, i.e. the mesonic moduli space, the baryonic symmetries $U(1)^G$ are quotiented out from the master space giving

$$\mathcal{M}^{mes}_N = \mathcal{F}^{\flat}_N/U(1)^{G-1} \; , \tag{1.4.22}$$

where an overall $U(1)$ decouples from $U(1)^G$. The dimension of the mesonic moduli space $\mathcal{M}^{mes}_N$ is $3N$.

From the point of view of a stack of N D3-branes probing a singular toric Calabi-Yau 3-fold, the mesonic moduli space of the worldvolume theory living on the stack can be interpreted simply from the mesonic moduli space that arises from a single probe D3-brane. The key point to consider is that the D3-branes in the stack are indistinguishable. Considering the $\mathbb{C}^3$ theory with a single gauge group $U(N)$ as a simple example, the Weyl group of $U(N)$ acts as a permutation group on the individual probe branes, i.e. on the individual Abelian copies of $\mathbb{C}^3$. Accordingly, the non-Abelian mesonic moduli space can be considered as the symmetric product $\mathrm{Sym}^N\mathbb{C}^3$. In general, the mesonic moduli space $\mathcal{M}^{mes}_N$ of a brane tiling with all gauge groups being $U(N)$ is the symmetric product

$$\mathcal{M}^{mes}_N = \mathrm{Sym}^N\mathcal{M}^{mes} = \frac{(\mathcal{M}^{mes})^N}{S_N} \; , \tag{1.4.23}$$

where $\mathcal{M}^{mes}$ is the mesonic moduli space of the corresponding brane tiling with only $U(1)$ gauge groups.

Example. Let us consider again the $N_1 = N_2 = 2$ conifold theory. The corresponding mesonic moduli space can be expressed as the quotient

$$\mathcal{M}^{mes}_{N=2} = \mathcal{F}^{\flat}_{N=2}/U(1). \tag{1.4.24}$$

As a symmetric product, the mesonic moduli space is

$$\mathcal{M}^{mes}_{N=2} = \mathrm{Sym}^2\mathcal{C} = \frac{(\mathcal{C})^2}{S_2} \ , \tag{1.4.25}$$

where $\mathcal{M}^{mes} = \mathcal{C}$ is the mesonic moduli space of the Abelian conifold theory.

1.4.3 The Hilbert Series

Hilbert series [48, 49, 50, 112, 51, 52, 113]. The Hilbert series is extensively used to characterise the moduli spaces of brane tilings and more generally of supersymmetric gauge theories. In algebraic geometry, it is associated to a multivariate graded polynomial ring or quotient ring. It is defined as

$$g(t; R) = \sum_{n-0}^{\infty} \dim(R_n) t^n \ , \tag{1.4.26}$$

where R is a ring with R_n being a component of R of degree $n \in \mathbb{N}$. The fugacity t counts the degree of the component.

One can introduce a multiple grading of the components of the ring R. For instance, the degree of the component $R_{\vec{n}}$ is $\vec{n} = (n_1, \dots, n_k)$ with the corresponding fugacities being $t_1, \dots, t_k$. Under this multi-grading, the corresponding Hilbert series of the ring would look like

$$g(t_1, \dots, t_k; R) = \sum_{n_1=0}^{\infty} \cdots \sum_{n_k=0}^{\infty} \dim(R_{\vec{n}}) t_1^{n_1} \dots t_k^{n_k} \ . \tag{1.4.27}$$

Example. Let us consider the ring $R = \mathbb{C}[a, b, c]$ over the complex field $\mathbb{C}$ and generated by a, b, c. The spectrum of the ring can be represented by the following sequence of monomials in a, b, c,

$$
\begin{aligned}
&1, a, b, c, \\
&a^2, ab, b^2, ac, bc, c^2, \\
&a^3, a^2 b, ab^2, b^3, a^2 c, abc, b^2 c, ac^2, bc^2, c^3, \dots \ .
\end{aligned}
\tag{1.4.28}
$$

Let now the grading of the ring be such that n_1, n_2, n_3 count the degrees in a, b, c respectively. As such, the Hilbert series is written as

$$g(t_1, t_2, t_3; \mathbb{C}^3) = \sum_{n_1=0}^{\infty} \sum_{n_2=0}^{\infty} \sum_{n_3=0}^{\infty} t_1^{n_1} t_2^{n_2} t^{n_3} = \frac{1}{(1 - t_1)(1 - t_2)(1 - t_3)} \ . \tag{1.4.29}$$
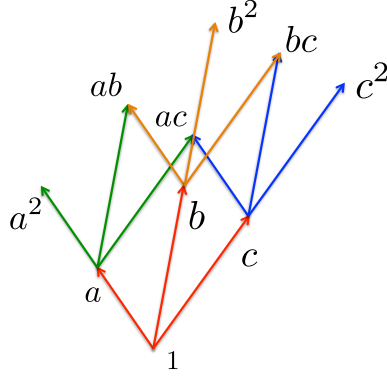
Figure 1.15: *The lattice structure of the spectrum of $\mathbb{C}[a,b,c]$.* The ring $\mathbb{C}[a,b,c]$ is generated by a,b,c. The elements of the spectrum of the ring can each be represented by a point in a lattice generated by 3 vectors corresponding to a,b,c.

The Hilbert series converges to a rational function. Effectively, the Hilbert series can also be considered as a partition function that counts points in a lattice generated by a,b,c. A schematic illustration of this lattice is given in Figure 1.15.

Hilbert series as rational functions. The Hilbert series as a rational function can be in two distinct forms. As such, the Hilbert series reveals information about the ring structure and for our purposes the moduli spaces $\mathcal{M}$ of brane tilings. In general, the Hilbert series as a rational function can be written as

$$g(t; \mathcal{M}) = \frac{P(t_i)}{Q(t_j)} \ . \tag{1.4.30}$$

The denominator is always factoriseable to take the form

$$Q(t_j) = \prod_j (1 - t_j^{n_j}) \ , \tag{1.4.31}$$

where the product runs over all generators and the n_j count the degree of each generator assigned to the fugacity t_j in this particular grading.

The numerator is a polynomial in the fugacities t_i. The polynomial is factoriseable if the space is a so called **complete intersection**. The factorisation takes the form

$$P(t_i) = \prod_i (1 - t_i^{m_i}) \ , \tag{1.4.32}$$

where the product runs over all first order relations formed by the generators $\mathcal{M}$. m_j counts the degrees of the relations for the particular grading.

For the case when the numerator is not factoriseable in the form shown in (1.4.32),

the space is known as a **non-complete intersection**. The interpretation is that the first order relations of the generators form relations among themselves, and by doing so form an infinite tower of relations among relations which are known as **syzygies**.

Finally, given the Hilbert series of a moduli space $\mathcal{M}$ in the form (1.4.30), when the numerator $P(t_i)$ is a palindromic polynomial, then $\mathcal{M}$ is Calabi-Yau [48].

Example. The ring can also be a quotient under an ideal. As such, the Hilbert series notices the changes to the components under the ideal. Let us take as an example the quotient ring

$$\mathbb{C}[a, b, c]/\langle a^2 - b \rangle \ , \tag{1.4.33}$$

where the ring is generated by a, b, c and the generators form the quadratic relation $a^2 = b$. As such the spectrum is modified to

$$\begin{aligned}
&1, a, b, c, \\
&ab, b^2, ac, bc, c^2, \\
&ab^2, b^3, abc, b^2c, ac^2, bc^2, c^3, \dots \ .
\end{aligned} \tag{1.4.34}$$

Using the grading where n_1, n_2, n_3 count the degrees in a, b, c respectively, the Hilbert series is

$$g(t_1, t_2, t_3; R) = \frac{1 - t_1^2}{(1 - t_1)(1 - t_2)(1 - t_3)} \ . \tag{1.4.35}$$

Plethystics. The **plethystic logarithm** of the Hilbert series encodes information about the generators of $\mathcal{M}$ and the relations formed by them. It is defined as

$$PL[g(t_i; \mathcal{M})] = \sum_{k=1}^{\infty} \frac{\mu(k)}{k} \log \left[g(t_i^k; \mathcal{M}) \right] \ , \tag{1.4.36}$$

where $\mu(k)$ is the Möbius function. If the expansion of the plethystic logarithm is finite, the space is a complete intersection generated by a finite number of generators subject to a finite number of relations. If the expansion is infinite, the moduli space is a non-complete intersection. The first positive terms of the expansion refer to generators of the moduli space.[7] All higher order terms refer to relations among generators and relations among relations, i.e. the syzygies.

The inverse function of the plethystic logarithm is the **plethystic exponential**. It

---

[7]The Groebner basis of a sequence of monomials, i.e. the spectrum of the ring, relates to the generators of the corresponding space.

is defined for a multivariate function $f(t_1, \ldots, t_n)$ as follows,

$$PE[f(t_1, \ldots, t_n)] = \exp\left[\sum_{k=1}^{\infty} \frac{f(t_1^k, \ldots, t_n^k)}{k}\right] \ . \tag{1.4.37}$$

Example. The mesonic moduli space of the Abelian conifold $\mathcal{C}$ theory is a complete intersection. Its Hilbert series, which we will compute explicitly later on, takes the form

$$g(t_i; \mathcal{C}) = \frac{1 - t_1 t_2 t_3 t_4}{(1 - t_1 t_3)(1 - t_2 t_3)(1 - t_1 t_4)(1 - t_2 t_4)} \ . \tag{1.4.38}$$

The plethystic logarithm is finite and is given by

$$PL[g(t_i; \mathcal{C})] = t_1 t_3 + t_2 t_3 + t_1 t_4 + t_2 t_4 - t_1 t_2 t_3 t_4 \ . \tag{1.4.39}$$

The first 4 positive terms in the plethystic logarithm correspond to 4 generators of the mesonic moduli space, which we label respectively as a, b, c, d. The first negative term indicates the degree of the relation formed by the generators. Using the degrees of the generators, we identify the relation as

$$ad = bc \ . \tag{1.4.40}$$

Accordingly, the conifold can be identified in terms of mesonic moduli space generators as being the following quotient ring,

$$\mathbb{C}[a, b, c, d]/\langle ad - bc \rangle \ . \tag{1.4.41}$$

Master space Hilbert series. The Hilbert series of the master space of Abelian brane tilings is precisely the Hilbert series of the quotient ring given in (1.4.14). An initial choice of the grading of the Hilbert series is such that $\vec{n} = (n_1, \ldots, n_E)$ counts the degree in the E quiver fields with fugacities $t_1, \ldots, t_E$. The algebraic geometry computer system *Macaulay2* [114] can be used to compute the Hilbert series in its rational form for any given quotient ring.

Example. The master space of the Abelian conifold theory is $^{\mathrm{Irr}}\mathcal{F}^{\flat} = \mathbb{C}^4$. The generators are the four quiver fields $X_{12}^1, X_{12}^2, X_{21}^1, X_{21}^2$. Using the grading where the fugacities t_1, t_2, t_3, t_4 count the degrees of the quiver fields $X_{12}^1, X_{12}^2, X_{21}^1, X_{21}^2$ respectively, the

Hilbert series can be written as

$$g(t_i; {}^{\mathrm{Irr}}\mathcal{F}^\flat) = \frac{1}{(1 - t_1)(1 - t_2)(1 - t_3)(1 - t_4)} \ . \tag{1.4.42}$$

For **non-Abelian** brane tiling theories, the grading of the Hilbert series of the quotient ring in (1.4.14) is such that n_i with fugacity t_i counts the degrees of the components of the quiver fields. In addition, one needs to introduce additional fugacities z_{km} which count the $SU(N)^G$ gauge charges of the quiver field components. The index $j = 1, \ldots, N^2 E$ where E is the number of quiver fields, $k = 1, \ldots, G$ is the index for the gauge groups, and $m = 1, \ldots, N - 1$ is the index for each $SU(N)$ gauge charge. The $SU(N)^G$ gauge symmetry can be summarized in a charge matrix with components Q_{jkm}. As such the Hilbert series of $\mathcal{F}^\flat$ of the non-Abelian theory would take the following general form

$$g(t_i, z_{km}; \mathcal{F}^\flat) = \frac{P(t_i, z_{km})}{\prod_{j,k}(1 - \prod_m z_{km}^{Q_{jkm}} t_j)} \ , \tag{1.4.43}$$

where $P(t_i, z_{km})$ is a polynomial in the fugacities.

In order to obtain the Hilbert series for gauge invariant operators of the master space, one needs to project the Hilbert series in (1.4.43) to the space of invariants under $SU(N)^G$ charges. This is achieved by the use of the **Molien integral formula** which gives the Hilbert series of $\mathcal{F}^\flat_N$ as follows,

$$g(t_i; \mathcal{F}^\flat_N) = \prod_{k,m} \oint_{|z_{km}|=1} \prod_i \mathrm{d}\mu_{SU(N_i)} \ g(t_i, z_{km}; \mathcal{F}^\flat) \ , \tag{1.4.44}$$

where $\mathrm{d}\mu_{SU(N)}$ is the Haar measure of $SU(N)$.[8]

Example. Let us consider again the $N_1 = N_2 = 2$ conifold theory. The $SU(2)^2$ gauge charges are summarized in Table 1.4. We use A, B, C, D for the quiver fields of the conifold theory, and $j = 1, \ldots, 16$, $k = 1, 2$ and $m = 1$. Accordingly, the Hilbert series of the master space can be written as

$$
\begin{aligned}
g(t_i = t; \mathcal{F}^\flat_{N=2}) \ &= \ \oint_{|z_1|=1} \oint_{|z_2|=1} \mathrm{d}z_1 \mathrm{d}z_2 \ \frac{(1 - z_1^2)(1 - z_2^2)}{z_1 z_2} \\
&\qquad \frac{P(t, z_1, z_2)}{(1 - z_1 z_2 t)^4 (1 - z_1 z_2^{-1} t)^4 (1 - z_1^{-1} z_2 t)^4 (1 - z_1^{-1} z_2^{-1} t)^4} \ ,
\end{aligned}
\tag{1.4.45}
$$

---

[8]For a general review on Haar measure, the reader is referred to [115].

	$SU(2)_1$	$SU(2)_2$	fugacities
A_{11}	-1	+1	$z_1^{-1} z_2 t_1$
A_{12}	-1	-1	$z_1^{-1} z_2^{-1} t_2$
A_{21}	+1	+1	$z_1 z_2 t_3$
A_{22}	+1	-1	$z_1 z_2^{-1} t_4$
B_{11}	+1	-1	$z_1 z_2^{-1} t_5$
B_{12}	+1	+1	$z_1 z_2 t_6$
B_{21}	-1	-1	$z_1^{-1} z_2^{-1} t_7$
B_{22}	-1	+1	$z_1^{-1} z_2 t_8$
$\vdots$	$\vdots$	$\vdots$	$\vdots$

Table 1.4: $SU(2)^2$ *gauge charge of the* $N = 2$ *conifold theory.* All components of the quiver fields carry $SU(2)^2$ gauge charges. The table shows the corresponding fugacity assignment. Note that the fields A, C and B, D carry the same gauge charges. In addition, the index m for fugacities z_{km} is ignored since we have $SU(2)$ gauge groups and we have always $m = 1$.

where the numerator $P(t, z_1, z_2)$ is a non-factoriseable polynomial. We have set for simplicity all the field component fugacities to $t_i = t$. The result of the Molien integral is

$$g(t_i = t; \mathcal{F}^\flat_{N=2}) \quad = \quad \frac{1 + 3t^2 + 6t^4}{(1 - t^2)^7} \ . \tag{1.4.46}$$

We note that the numerator is not palindromic and hence the master space of the $N = 2$ conifold theory is not Calabi-Yau as expected.

Mesonic Hilbert series. For the mesonic Hilbert series, one needs to take into account the $U(1)^{G-1}$ symmetries. For Abelian theories, these are the only symmetries that have to be taken into account for the grading of the quotient ring in (1.4.21). We introduce the fugacities w_k for the $U(1)^{G-1}$ charges, where $k = 1, \ldots, G - 1$ goes over the $G - 1$ $U(1)$ charges. The $U(1)^{G-1}$ charges can be summarized in a charge matrix Q_{jk}, where $j = 1, \ldots, E$ goes over the quiver fields. The Hilbert series of $^{\mathrm{Irr}}\mathcal{F}^\flat$ for the Abelian theory can be expressed as

$$g(t_i, w_k; {}^{\mathrm{Irr}}\mathcal{F}^\flat) = \frac{P(t_i, w_k)}{\prod_j (1 - \prod_k w_k^{Q_{jk}} t_j)} \ . \tag{1.4.47}$$

As for the master space Hilbert series, a grading n_i is used to count the degrees of the quiver field with fugacities t_i, where $i = 1, \ldots, E$. Since we are interested in invariants under $U(1)^{G-1}$, we make use of the Molien integral formula to obtain the Hilbert series

	$U(1)_1$	$U(1)_2$	fugacities
A	+1	-1	$w_1 w_2^{-1} t_1$
B	-1	+1	$w_1^{-1} w_2 t_2$
C	+1	-1	$w_1 w_2^{-1} t_3$
D	-1	+1	$w_1^{-1} w_2 t_4$

Table 1.5: $U(1)^2$ *charges on quiver fields for the Abelian conifold theory.* The $U(1)^2$ charges can be taken from the incidence information of arrows in the quiver diagram. Note that an overall $U(1)$ decouples, and only the charges counted by w_1 (or w_2) will affect the result of the Molien integral.

of mesonic moduli space $\mathcal{M}^{mes}$,

$$g(t_i; \mathcal{M}^{mes}) = \prod_k \oint_{|w_k|=1} \frac{\mathrm{d}w_k}{w_k} \, g(t_i, w_k; {}^{\mathrm{Irr}}\mathcal{F}^\flat) \,. \tag{1.4.48}$$

Example. For the Abelian conifold theory, the $U(1)^2$ charges on the 4 quiver fields are shown in Table 1.5. The master space ${}^{\mathrm{Irr}}\mathcal{F}^\flat$ Hilbert series with the $U(1)^2$ charge fugacities w_k is

$$g(t_i, w_k; {}^{\mathrm{Irr}}\mathcal{F}^\flat) = \frac{1}{(1 - w_1 t_1)(1 - w_1^{-1} t_2)(1 - w_1 t_3)(1 - w_1^{-1} t_4)} \,. \tag{1.4.49}$$

The Hilbert series of the mesonic moduli space $\mathcal{M}^{mes}$ is given by the Molien integral which is

$$g(t_i; \mathcal{M}^{mes}) = \oint_{|w_1|=1} \frac{\mathrm{d}w_1}{w_1} \, g(t_i, w_k; {}^{\mathrm{Irr}}\mathcal{F}^\flat) = \frac{1 - t_1 t_2 t_3 t_4}{(1 - t_1 t_2)(1 - t_1 t_4)(1 - t_3 t_2)(1 - t_3 t_4)} \,. \tag{1.4.50}$$

Given that the fugacities t_1, t_2, t_3, t_4 count respectively the degrees of the conifold quiver fields A, B, C, D, the generators of the mesonic moduli space can be expressed in terms of quiver fields by using the information provided by the Hilbert series in (1.4.50). They are

$$a = AB \,, \ b = AD \,, \ c = CB \,, \ d = CD \,. \tag{1.4.51}$$

The relation formed by the generators is $ad = bc$.

For the **non-Abelian** case, the Hilbert series of $\mathcal{F}^\flat$ needs to be refined under both fugacities w_k and z_{jk} which count $U(1)^{G-1}$ and $SU(N)^G$ charges respectively. In general, the Hilbert series is obtained by integrating out both the $U(1)^{G-1}$ and $SU(N)^G$ charges

	$U(1)_1$	$U(1)_2$	$SU(2)_1$	$SU(2)_2$	fugacities
A_{11}	-1	+1	-1	+1	$w_1^{-1}w_2z_1^{-1}z_2t_1$
A_{12}	-1	+1	-1	-1	$w_1^{-1}w_2z_1^{-1}z_2^{-1}t_2$
A_{21}	-1	+1	+1	+1	$w_1^{-1}w_2z_1z_2t_3$
A_{22}	-1	+1	+1	-1	$w_1^{-1}w_2z_1z_2^{-1}t_4$
B_{11}	+1	-1	+1	-1	$w_1w_2^{-1}z_1z_2^{-1}t_5$
B_{12}	+1	-1	+1	+1	$w_1w_2^{-1}z_1z_2t_6$
B_{21}	+1	-1	-1	-1	$w_1w_2^{-1}z_1^{-1}z_2^{-1}t_7$
B_{22}	+1	-1	-1	+1	$w_1w_2^{-1}z_1^{-1}z_2t_8$
⋮	⋮	⋮	⋮	⋮	⋮

Table 1.6: $U(1)^2$ and $SU(2)^2$ charges of the $N = 2$ conifold theory. Note that the components of A, C and B, D carry the same charges and therefore only the charges for the components of A, B are shown above.

as follows,

$$g(t_i; \mathcal{M}_N^{mes}) = \prod_{k,m} \oint_{|z_{km}|=1} \mathrm{d}\mu_{SU(N_k)} \prod_l \oint_{|w_l|=1} \frac{\mathrm{d}w_l}{w_l}\, g(t_i, z_{km}, w_l; \mathcal{F}^\flat)\,, \qquad (1.4.52)$$

where $g(t_i, z_{km}, w_l; \mathcal{F}^\flat)$ is the Hilbert series for $\mathcal{F}^\flat$ corresponding to the quotient ring in (1.4.14) with both $U(1)^{G-1}$ and $SU(N)^G$ charge fugacities.

Example. Let us consider again the $N_1 = N_2 = 2$ conifold theory. Table 1.6 shows the $U(1)^2 \times SU(2)^2$ charges on the components of the quiver fields A, B, C, D. The fugacity w_1 carries the independent $U(1)$ charge, and the fugacities z_1, z_2 carry the $SU(2)^2$ charges. The mesonic Hilbert series is given by the Molien integral

$$g(t_i = t; \mathcal{M}_{N=2}^{mes}) = \oint_{|w_1|=1} \oint_{|z_1|=1} \oint_{|z_2|=1} \frac{\mathrm{d}w_1}{w_1}\, \mathrm{d}z_1\mathrm{d}z_2 \frac{(1-z_1^2)(1-z_2^2)}{z_1z_2}$$

$$\times \frac{P(t, w_1, z_1, z_2)}{(1-w_1^{-1}z_1^{-1}z_2t)^2(1-w_1^{-1}z_1^{-1}z_2^{-1}t)^2(1-w_1^{-1}z_1z_2t)^2(1-w_1^{-1}z_1z_2^{-1}t)^2}$$

$$\times \frac{1}{(1-w_1z_1z_2^{-1}t)^2(1-w_1z_1z_2t)^2(1-w_1z_1^{-1}z_2^{-1}t)^2(1-w_1z_1^{-1}z_2t)^2}\,,$$

$$(1.4.53)$$

where the numerator in the integrand is a polynomial in the fugacities t, w_1, z_1, z_2. For simplicity, we have set all $t_i = t$. The result of the integration is

$$g(t_i = t; \mathcal{M}_{N=2}^{mes}) = \frac{1 + t^2 + 7t^4 + 3t^6 + 4t^8}{(1-t^2)^3(1-t^4)^3}\,. \qquad (1.4.54)$$

We note that the numerator of the mesonic Hilbert series for the $N = 2$ conifold theory is not palindromic. The mesonic moduli space is therefore not Calabi-Yau.

Hilbert series of symmetric products. The Hilbert series $g(t_i; \mathcal{M}_N)$ of the N-th symmetric product of a moduli space $\mathcal{M}$ can be obtained from the Hilbert series $g(t_i; \mathcal{M}_1)$ when $N = 1$. It is obtained by the use of the following generalised plethystic exponential formula,

$$
\begin{aligned}
PE[g(t_1, \ldots, t_n; \mathcal{M}_1)\, v] &= \exp\left[\sum_{k=1}^{\infty} \frac{g(t_1^k, \ldots, t_n^k; \mathcal{M}_1)}{k}\, v^k\right] \\
&= 1 + \sum_{m=1}^{\infty} g(t_1, \ldots, t_n; \mathcal{M}_m)\, v^m\ ,
\end{aligned}
\tag{1.4.55}
$$

where v is the fugacity of the degree of the symmetric product and the expansion in v gives as coefficients the Hilbert series of the symmetric products.

Example. We can now verify the mesonic Hilbert series of the $N_1 = N_2 = 2$ conifold theory in (1.4.54) by using the formula for symmetric product Hilbert series in (1.4.55). The mesonic Hilbert series of the $N_1 = N_2 = 1$ conifold theory is as we recall from (1.4.42)

$$
g(t; \mathcal{M}_1) = \frac{1 - t^4}{(1 - t^2)^4}\ ,
\tag{1.4.56}
$$

where we set all $t_i = t$ for simplicity. Using the formula in (1.4.55), we obtain

$$
\begin{aligned}
PE[g(t; \mathcal{M}_1)\, v] = 1 &+ \frac{1 - t^4}{(1 - t^2)^4}\, v + \frac{1 + t^2 + 7t^4 + 3t^6 + 4t^8}{(1 - t^2)^3 (1 - t^4)^3}\, v^2 \\
&+ \frac{1 + 7t^4 + 13t^6 + 18t^8 + 31t^{10} + 34t^{12} + 18t^{14} + 16t^{16} + 6t^{18}}{(1 - t^2)^4 (1 - t^4)^2 (1 - t^6)^3}\, v^3 + \ldots\ .
\end{aligned}
\tag{1.4.57}
$$

We observe that the mesonic Hilbert series for the $N_1 = N_2 = 2$ conifold theory is indeed the one computed in (1.4.54).

1.4.4 The Forward Algorithm

For Abelian brane tilings where all gauge groups are $U(1)$, we can make use of perfect matchings of the bipartite graph to identify the master and mesonic moduli spaces.

F- and D-term charges and the Forward Algorithm [34, 92, 14, 101, 15, 55, 103]. A new basis of fields can be defined from the set of quiver fields. The purpose of the new basis of fields is to describe both F-term and D-term constraints of the

supersymmetric gauge theory with a common setting. The new fields are known as gauge linear sigma model fields (GLSM) and are represented as perfect matchings in the brane tiling. They have the following properties:

- As reviewed in section §1.3.1, a **perfect matching** p_α is a set of bifundamental fields which connect to all nodes in the brane tiling precisely once. The perfect matchings correspond to extremal (corner), internal as well as all non-extremal toric points on the perimeter of the toric diagram. They are summarized in the perfect matching matrix $P_{E \times c}$ where E is the number of matter fields and c the number of perfect matchings.

- **F-terms** are encoded in the perfect matching matrix $P_{E \times c}$. The charges under the F-term constraints are given by the kernel,

$$Q_{F \ (c-G-2) \times c} = \ker (P_{E \times c}) . \tag{1.4.58}$$

- **D-terms** are of the form [104],

$$D_i = -e^2 \left(\sum_a d_{ia} |X_a|^2 - \zeta_i \right) , \tag{1.4.59}$$

where X_a is the matter field corresponding to the a-th column of the incidence matrix $d_{G \times E}$, i runs over the gauge groups in the quiver, e is the gauge coupling, and ζ_i is the Fayet-Iliopoulos (FI) parameter. The D-terms are encoded via the reduced quiver matrix $\Delta_{(G-1) \times E}$[9] and are related to the perfect matching matrix as follows,

$$\Delta_{(G-1) \times E} = Q_{D \ (G-1) \times c} . P^t_{c \times E} , \tag{1.4.60}$$

where the $Q_{D \ (G-1) \times c}$ matrix is the charge matrix under D-term constraints. Equivalently, in terms of an interim matrix $\tilde{Q}_{G \times c}$, which maps perfect matchings into their quiver charges, one has the relation

$$d_{G \times E} = \tilde{Q}_{G \times c} . P^t_{c \times E} . \tag{1.4.61}$$

Overall, the charge matrices Q_F and Q_D can be concatenated to form a $(c-3) \times c$ matrix,

$$Q_t = \begin{pmatrix} Q_F \\ Q_D \end{pmatrix} . \tag{1.4.62}$$

---

[9]Since the sum of rows in $d_{G \times E}$ vanishes, there are $G-1$ independent rows giving the reduced matrix $\Delta_{(G-1) \times E}$.

The kernel of the charge matrix,

$$G_t = \ker(Q_t) \ , \tag{1.4.63}$$

precisely encodes the coordinates of the **toric diagram** points with columns and hence perfect matchings and GLSM fields corresponding to points of the toric diagram.

The master space Hilbert series. As we have discussed above, the master space is the moduli space under F-term constraints, given by the quotient in (1.4.14). Since the F-terms are encoded in the charge matrix Q_F, the master space can be expressed as the following **symplectic quotient**,

$$^{\mathrm{Irr}}\mathcal{F}^{\flat} = \mathbb{C}^c // Q_F \ , \tag{1.4.64}$$

where now we use a basis of GLSM fields corresponding to perfect matchings of the brane tiling rather than quiver fields. The c GLSM fields form the space $\mathbb{C}^c$ known as the space of perfect matchings.

Given the symplectic quotient description of the master space, the corresponding Hilbert series can be expressed simply as the following Molien integral

$$g(t_\alpha; {}^{\mathrm{Irr}}\mathcal{F}^{\flat}) = \prod_{i=1}^{c-G-2} \oint_{|z_i|=1} \frac{\mathrm{d}z_i}{2\pi i z_i} \prod_{\alpha=1}^{c} \frac{1}{\left(1 - t_\alpha \prod_{j=1}^{c-G-2} z_j^{(Q_F)_{j\alpha}}\right)} \ , \tag{1.4.65}$$

where z_j are the fugacities for the Q_F charges and t_α are the fugacities for the perfect matchings p_α.

Mesonic Hilbert series. The mesonic moduli space is the space of invariants under F-term charges Q_F and D-term charges Q_D. The symplectic quotient

$$\mathcal{M}^{mes} = (\mathbb{C}^c // Q_F) // Q_D \ . \tag{1.4.66}$$

is the mesonic moduli space of the quiver gauge theory. The invariants under the symplectic quotient are mesonic gauge invariant operators. The mesonic Hilbert series is obtained via the Molien integral formula,

$$g(t_\alpha; \mathcal{M}^{mes}) = \prod_{i=1}^{c-3} \oint_{|z_i|=1} \frac{\mathrm{d}z_i}{2\pi i z_i} \prod_{\alpha=1}^{c} \frac{1}{\left(1 - t_\alpha \prod_{j=1}^{c-3} z_j^{(Q_t)_{j\alpha}}\right)} \ , \tag{1.4.67}$$

where c is the number of perfect matchings and Q_t is the total charge matrix in (1.4.62).

Example. Chapter §3 and §4 on brane tilings with reflexive polygons and chapter §5 on

brane tilings on Riemann surfaces use extensively the forward algorithm outlined above. The reader is referred to these chapters for a comprehensive collections of detailed examples.

1.4.5 The Fast Forward Algorithm

In section §1.3.1, we have reviewed how perfect matchings can have winding numbers (h_a, h_b) in relation to a reference fundamental cell of the brane tiling. Furthermore, section §1.3.2 discussed zig-zag paths and their winding numbers (h_a, h_b). They are used to identify the (p, q)-web diagram which is the dual of the toric diagram of a brane tiling. Winding numbers are essential tools for finding the toric diagram of the mesonic moduli space of an Abelian brane tiling.

In this section, we discuss a third method to obtain directly the toric diagram from a given brane tiling. The algorithm is known as the **fast forward algorithm** [55] and centres around an object known as the Kasteleyn matrix.

Kasteleyn Matrix [66, 67, 98, 15]. The Kasteleyn matrix K is the adjacency matrix of all unique edges in a given fundamental cell of a brane tiling. The matrix is a $N_w \times N_b$ matrix where N_w and N_b are the numbers of white and black nodes respectively in a given fundamental cell of the tiling. By the bipartite condition on the superpotential, $N_w = N_b$ and the Kasteleyn matrix is a square matrix. With the indices $i = 1, \ldots, N_w$ and $j = 1, \ldots, N_b$, the elements of the matrix are

$$K_{ij} = \sum_{X(i,j)} x^{h_a(X(i,j))} y^{h_b(X(i,j))} \ , \qquad (1.4.68)$$

where $X(i, j)$ is an edge between white node w_i and black node b_j in the brane tiling's fundamental cell. $(h_a(X(i,j)), h_b(X(i,j)))$ is the winding number of $X(i, j)$. The fugacities x and y count the winding number along the a- and b-cycles of the torus respectively.

The important property of the Kasteleyn matrix is that its permanent[10] satisfies the following identity,

$$\mathrm{perm}(K) = \sum_{p_\alpha} x^{h_a(p_\alpha)} y^{h_b(p_\alpha)} \ , \qquad (1.4.69)$$

which is a sum over all perfect matchings of the brane tiling weighted by their corresponding winding numbers (h_a, h_b) for a given fundamental cell. As such, given that the winding numbers of perfect matchings correspond to the lattice coordinates of toric points, the permanent of the Kasteleyn matrix gives the toric diagram of the brane tiling.

---

[10]The permanent of a matrix is the determinant of the matrix with all signs being positive.
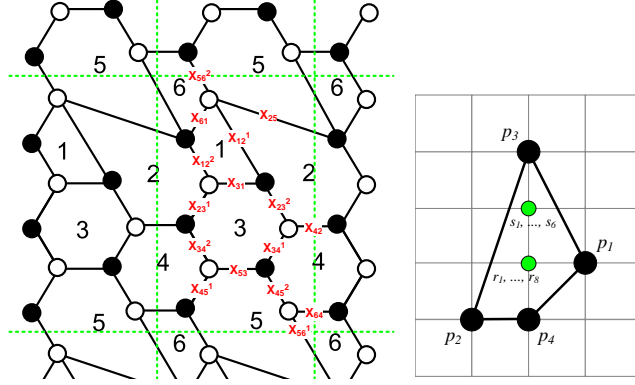
Figure 1.16: *The brane tiling and toric diagram of the $Y^{3,2}$ theory.*

Example. Let us consider an example from a famous class of brane tilings known as $Y^{p,q}$ models [116, 117, 118, 119, 120]. This class of theories is special because the corresponding metrics of the Sasaki-Einstein 5-manifolds are explicitly known. As an example, let us consider the brane tiling of the $Y^{3,2}$ theory which is shown in Figure 1.16. The fundamental cell for the given brane tiling in Figure 1.16 gives the following Kasteleyn matrix

$$
K = \left(
\begin{array}{c|ccccc}
 & b_1 & b_2 & b_3 & b_4 & b_5 \\
\hline
w_1 & 1+y & 1 & 0 & 0 & \frac{1}{x} \\
w_2 & 1 & 1 & 1 & 0 & 0 \\
w_3 & 0 & 1 & y & 1 & 0 \\
w_4 & 0 & 0 & 1 & 1 & 1 \\
w_5 & xy & 0 & 0 & 1 & y
\end{array}
\right) .
\tag{1.4.70}
$$

The corresponding permanent is given by

$$
\mathrm{perm}(K) \;=\; 1 + xy + \frac{1}{x} + 8y + 6y^2 + y^3 \;.
\tag{1.4.71}
$$

We observe that two terms have coefficients greater than 1, corresponding to multiple perfect matchings associated to the same toric point. The corresponding toric diagram is shown in Figure 1.16.

1.5 Symmetries

In the sections above, we have discussed the computation of Hilbert series and by doing so have mentioned symmetries of supersymmetric gauge theories given by brane tilings. The following section elaborates on mesonic and baryonic symmetries as well as the R-symmetry of brane tilings. The computation of charges under these symmetries is reviewed. We will review the symmetries in the context of Abelian theories where all gauge groups of the brane tiling are $U(1)$.

1.5.1 Mesonic and Baryonic Symmetries

Master space symmetries. The master space exhibits the following symmetries:

- The **mesonic symmetry** is $U(1)^3$ or an enhancement with rank 3. An enhancement is indicated by extremal perfect matchings which carry the same Q_F charges. The mesonic symmetry contains the $U(1)_R$ symmetry and the flavor symmetries. It derives from the isometry of the toric Calabi-Yau 3-fold.

- The **baryonic symmetry** is $U(1)^{G-1}$ or an enhancement with rank $G-1$. An enhancement is indicated by non-extremal perfect matchings which carry the same Q_F charges. It contains both anomalous and non-anomalous symmetries which have decoupling gauge dynamics in the IR. Non-Abelian extensions of these symmetries are known as **hidden symmetries** [71, 72, 18].

Let I and E denote respectively the number of internal and external points in the toric diagram.[11] They are used to define the following quantities:

- The number of **anomalous** $U(1)$ baryonic symmetries or the total rank of enhanced **hidden** baryonic symmetries is given by $2I$.

- The number of **non-anomalous** baryonic $U(1)$'s is $E-3$.

- The total number of baryonic symmetries is as stated above $G-1$. Accordingly,

$$G - 1 = 2I + E - 3 \implies A = \frac{G}{2} = I + \frac{E}{2} - 1 \tag{1.5.72}$$

which is **Pick's theorem** generalised to toric diagrams. The unit square area A of a toric diagram is scaled by a factor of 2 in order to relate it to the number of gauge groups G.

---

[11]Note: Points in the toric diagram can carry multiplicities according to the number of perfect matchings associated to them. I and E is a counting that ignores multiplicities.

Perfect matchings carry charges under the mesonic and baryonic symmetries. The choices of assigning charges on perfect matchings are under certain basic constraints which are reviewed at the end of this section.

Mesonic symmetry. The mesonic moduli space of a given Abelian brane tiling on T^2 is a non-compact toric Calabi-Yau 3-fold. The mesonic symmetry of the quiver gauge theory has rank 3 and hence takes one of the following forms,

- $U(1) \times U(1) \times U(1)$

- $SU(2) \times U(1) \times U(1)$

- $SU(2) \times SU(2) \times U(1)$

- $SU(3) \times U(1)$,

where the R-symmetry is a subgroup. For $\mathcal{N} = 2$ and $\mathcal{N} = 1$, the R-symmetry is respectively $SU(2) \times U(1)$ and $U(1)$.

The above global symmetries derive from the isometry group of the Calabi-Yau 3-fold. The enhancement of a $U(1)$ flavor to $SU(2)$ or $SU(3)$ is indicated by columns in the total charge matrix Q_t which carry the same charge and correspond to external perfect matchings.

Mesonic and baryonic charges on perfect matchings. The perfect matchings carry $G + 2$ charges which relate to the 3 mesonic and $G - 1$ baryonic symmetries. Each perfect matching is assigned a $G + 2$ dimensional charge vector, and the choice of its components is arbitrary up to the following constraints:

- All $G + 2$ dimensional charge vectors are linearly independent to each other.

- The sum of all charge vectors is $(0, \ldots, 0, 2)$ where the non-zero component 2 is the total $U(1)_R$-charge.

Note that if two charge vectors are linearly dependent, information about the algebraic structure of the moduli space is lost. For the purpose of studying specular duality in chapter §4, the following additional constraints are introduced without loosing track of the algebraic structure of the master space:

- For a pair of dual brane tilings, the charge vectors can be chosen such that a swap between internal and external perfect matchings equates to a swap of mesonic flavour and anomalous or hidden baryonic symmetry charges.

- If the $U(1)_R$-charges are irrational or otherwise incompatible between two specular dual brane tilings, one can find a set of orthogonal replacement charges without loosing information on the algebraic structure of the master space. This modification corresponds to a mix of the R-symmetry with the remaining global symmetry.

1.5.2 Computation of R-charges

R-charge constraints on the brane tiling. The $U(1)_R$ symmetry of the superconformal field theory sets the following constraints on the brane tiling,

- The R-charge of the superpotential W of a brane tiling is $R(W) = 2$. Accordingly, the total R-charge around a node in the brane tiling is

$$\sum_{X_j \in \text{node}_i} R(X_j) = 2 \ . \tag{1.5.73}$$

  The sum over all nodes in the brane tiling gives

$$\sum_{i=1}^{V} \sum_{X_j \in \text{node}_i} R(X_j) = 2V \ , \tag{1.5.74}$$

  where V is the number of distinct nodes in the brane tiling.

- Given that the quiver gauge theories corresponding to brane tiling are superconformal, the beta functions for every coupling in the theories are required to vanish. For the non-Abelian case, the numerator of the $SU(N)$ NSVZ beta function [121, 54] takes the following form

$$\beta_i = N_i + \sum_{X_{ii}} N_i(R(X_{ii}) - 1) + \frac{1}{2} \sum_{\substack{X_{ij} \\ i \neq j}} N_j(R(X_{ij}) - 1) \ , \tag{1.5.75}$$

  where X_{ii} is an adjoint quiver field and X_{ij} is a bifundamental quiver field. For the Abelian case where all $N_i = 1$, the above expression in conjunction with the requirement $\beta_i = 0$ leads to the following constraint on the brane tiling,

$$2 + \sum_{X_j \in \text{face}_i} (R(X_j) - 1) = 0 \ , \tag{1.5.76}$$

  where the sum is over all edges X_j adjacent to the i-th face in the brane tiling.

The R-charge constraints on the brane tiling can be represented pictorially by an **isoradial embedding** [16] of the bipartite graph.

Volume of the Sasaki-Einstein Manifold and R-charges. An interesting property of the Hilbert series is that its leading pole in the limit where the fugacities go to 1 gives the complex dimension of the moduli space of the corresponding gauge theory. Furthermore, the mesonic Hilbert series contains information about the volume of $\mathcal{M}^{mes}$. Let the Hilbert series $g(t_\alpha; \mathcal{M}^{mes})$ be fully refined such that there is a fugacity t_α for each GLSM field p_α. By introducing parameters μ and r_α, which in statistical

mechanics correspond to the Boltzmann constant k_B and energy state E_α respectively, the fugacities in the Hilbert series counting GLSM fields can be re-expressed as,

$$t_\alpha = e^{-\mu r_\alpha} \ . \tag{1.5.77}$$

A natural interpretation of the expression above is that the set of fugacities, and hence the set of parameters $\{r_\alpha\}$, form a c-dimensional polyhedral cone on a lattice $\mathbb{Z}^c$, where μ measures the lattice spacing. As discussed in [122], in the limit of a small lattice spacing, $\mu \to 0$, the volume of the cone approximates increasingly better the volume of the Sasaki-Einstein manifold. This process can be interpreted as taking the Riemann integral over the fully refined Hilbert series, such that the volume of the Sasaki-Einstein manifold H is given by[12]:

$$\mathrm{Vol}(r_\alpha; H) = \frac{8\pi^3}{27} \lim_{\mu \to 0} \mu^3 g(e^{-\mu r_\alpha}; \mathcal{M}^{mes} = \mathcal{C}(H)) \ . \tag{1.5.78}$$

In converse, the Hilbert series can be expanded in μ, where the leading order is related to the volume of the Sasaki-Einstein base,

$$g(e^{-\mu r_\alpha}; \mathcal{M}^{mes} = \mathcal{C}(H)) \ \sim \ \frac{\mathrm{Vol}(r_\alpha; H)}{\mu^3} + \dots \ . \tag{1.5.79}$$

In the limit where the volume $\mathrm{vol}(r_\alpha; H)$ is at its minimum, the parameters r_α form a vector known as the Reeb vector $\vec{r}$, with $\sum_\alpha r_\alpha = 2$.

In order to determine the R-charges specific to the GLSM fields p_α, one recalls that the GLSM fields and the corresponding points of the toric diagram are associated with divisors D_α of the Calabi-Yau.[13] The Hilbert series associated with the **divisor** D_α of $\mathcal{M}$ is given by the following modified form of the Molien-Weyl integral,

$$
\begin{aligned}
g^{D_\alpha}(t_\alpha; \mathcal{M}^{mes}) &= \prod_{i=1}^{c-3} \oint_{|z_i|=1} \frac{\mathrm{d}z_i}{2\pi i z_i} \left(t_\alpha \prod_{k=1}^{c-3} z_k^{(Q_t)_{k\alpha}} \right)^{-1} g(\{t_\alpha, z_i\}; \mathbb{C}^c) \\
&= \prod_{i=1}^{c-3} \oint_{|z_i|=1} \frac{\mathrm{d}z_i}{2\pi i z_i} \prod_{\beta=1}^{c} \frac{\left(t_\alpha \prod_{k=1}^{c-3} z_k^{(Q_t)_{k\alpha}} \right)^{-1}}{1 - t_\beta \prod_{j=1}^{c-3} z_j^{(Q_t)_{j\beta}}} \ .
\end{aligned}
\tag{1.5.80}
$$

Under an analogous limit to the one in (1.5.78), one obtains the volume of the base of the Calabi-Yau divisor D_α.

---

[12]The factor $\frac{8}{27}\pi^3$ is for normalisation purposes. In these units the volume of the five-sphere is exactly π^3.

[13]Only the extremal toric points and the corresponding GLSM fields whose corresponding CY divisors D_α have a base with non-zero volume are of interest. The non-vanishing volume of the base of the divisors is related to a non-zero R-charge of the corresponding GLSM field.

The R-charge R_α of the perfect matching p_α associated to the divisor D_α is given by the following normalised μ-expansion of the Hilbert series of the divisor,

$$\frac{g^{D_\alpha}(e^{-\mu r_i}; \mathcal{M}^{mes})}{g(e^{-\mu r_i}; \mathcal{M}^{mes})} \sim 1 + \mu R_\alpha + \dots , \tag{1.5.81}$$

where the Reeb vector elements $\vec{r} = (r_1, \dots, r_c)$ take the values at the minimum of the volume of the base of $\mathcal{M}^{mes}$, $\text{Vol}(r_\alpha; H)$, as previously determined. Accordingly, the R-charge associated to the GLSM field p_α can be expressed as the limit,

$$R_\alpha = \lim_{\mu \to 0} \frac{1}{\mu} \left[\frac{g^{D_\alpha}(e^{-\mu r_i}; \mathcal{M}^{mes})}{g(e^{-\mu r_i}; \mathcal{M}^{mes})} - 1 \right] . \tag{1.5.82}$$

Furthermore, the requirement that the theory is superconformal imposes the constraint

$$\sum_\alpha R_\alpha = 2 . \tag{1.5.83}$$

R-charges via a-maximisation. There is a second method of computing R-charges of perfect matchings and quiver fields which is known as a-maximisation [110, 13]. The procedure makes use of the toric diagram to write down a cubic a-function which when maximised leads to the R-charges of the perfect matchings. It is shown that a-maximisation is equivalent to volume minimisation [110, 123].

1.5.3 The refined Hilbert Series

In the sections above on Hilbert series, we have seen two types of fugacities which relate to the grading of the ring. These two types of **refinement** are

- **Quiver field refinement.** There is a set of fugacities t_i each counting the degree of a quiver field X_i. We have encountered this refinement so far in the computation of the Hilbert series for the master space and for Hilbert series of moduli spaces of non-Abelian brane tilings.

- **Perfect matching refinement.** GLSM fields represented by perfect matchings p_α of the brane tiling are assigned fugacities t_α. These fugacities count the degrees in perfect matchings which in turn relate to the quiver fields of the brane tiling. One can introduce multiple fugacities p_α and for instance s_α where respectively the fugacities count extremal and non-extremal perfect matchings of the brane tiling.[14] We have encountered this refinement for the computation of the Hilbert

---

[14]This distinction is done in chapters §3 and §4.

	$SU(2)_{z_1}$	$SU(2)_{z_2}$	$U(1)_b$	$U(1)_R$	fugacities
$A = X_{12}^1 = p_1$	+1	0	+1	1/2	$t_1 = z_1 b t^{1/2}$
$B = X_{21}^1 = p_2$	0	+1	-1	1/2	$t_2 = z_2 b^{-1} t^{1/2}$
$C = X_{12}^2 = p_3$	-1	0	+1	1/2	$t_3 = z_1^{-1} b t^{1/2}$
$D = X_{21}^2 = p_4$	0	-1	-1	1/2	$t_4 = z_2^{-1} b^{-1} t^{1/2}$

Table 1.7: *Mesonic and baryonic symmetries of the Abelian conifold theory.* The fugacities z_1, z_2 count charges under the flavor symmetries $SU(2)_{z_1} \times SU(2)_{z_2}$ and the fugacity t relates to the $U(1)_R$ charges.

series for moduli spaces of Abelian brane tilings.

Given the above choices of refinement, one is always able to introduce a new set of fugacities orthogonal to the original set. A natural choice is a **refinement under the mesonic flavour and baryonic symmetries** of the brane tiling.

Let us consider the mesonic moduli space and an initial set of perfect matching fugacities. An illustrative example would be a theory with the mesonic symmetry being $SU(3) \times U(1)_R$. We introduce fugacities z_1, z_2 for the $SU(3)$ and t for the $U(1)_R$ charges. As such, the perfect matching fugacities can be changed as follows

$$t_\alpha = z_1^{Q_{\alpha 1}^{SU(3)}} z_2^{Q_{\alpha 2}^{SU(3)}} t^{Q_{\alpha 1}^{U(1)_R}} \ , \tag{1.5.84}$$

where $Q_\alpha = (Q_{\alpha 1}^{SU(3)}, Q_{\alpha 2}^{SU(3)}, Q_{\alpha 1}^{U(1)_R})$ is a full charge matrix of the mesonic symmetries of the brane tiling.

Given that $SU(3)$ is a global flavor symmetry of the mesonic moduli space, the fugacities z_1, z_2 are expected to form in the Hilbert series characters of irreducible representations of $SU(3)$. We use highest weight notation for characters of irreducible representation. For instance, the fundamental, antifundamental and adjoint representations of $SU(3)$ are respectively given by

$$[1,0]_{SU(3)} = z_1 + \frac{z_2}{z_1} + \frac{1}{z_2} \ , \ \ [0,1]_{SU(3)} = \frac{1}{z_1} + \frac{z_1}{z_2} + z_2 \ ,$$
$$[1,1]_{SU(3)} = [1,0]_{SU(3)}[0,1]_{SU(3)} - 1 = z_1 z_2 + \frac{z_1^2}{z_2} + \frac{z_2^2}{z_1} + 2 + \frac{z_1}{z_2^2} + \frac{z_2}{z_1^2} + \frac{1}{z_1 z_2} \ \ .$$
$$\tag{1.5.85}$$

Example. Let us consider the Abelian conifold theory with $U(1)^2$ gauge groups. Every bifundamental field on its own is a perfect matching of the brane tiling of the Abelian conifold theory. Accordingly, the perfect matching matrix P is an identity matrix. Therefore the Q_F charge matrix is empty and as we know the master space is $\mathbb{C}^4$ with the corresponding Hilbert series in (1.4.42).

The global flavour symmetry of the theory is $SU(2)_{z_1} \times SU(2)_{z_2}$ with a $U(1)_R$ symmetry. The charges under these symmetries on perfect matchings are summarized in Table 1.7. We note that the quartic superpotential of the conifold carries R-charge 2, and every bifundamental carries a R-charge $R(X) = 1/2$. We use the following fugacity map to indicate the symmetries in Table 1.7 for the mesonic Hilbert series,

$$(t_1, t_2, t_3, t_4) = (z_1 b t^{1/2}, z_2 b^{-1} t^{1/2}, z_1^{-1} b t^{1/2}, z_2^{-1} b^{-1} t^{1/2}) \ . \tag{1.5.86}$$

Applied on the mesonic Hilbert series of the conifold theory given in (1.4.50), the following newly refined mesonic Hilbert series is obtained

$$g(z_i, t; \mathcal{M}^{mes}) = \frac{1 - t^2}{(1 - z_1 z_2 t)(1 - z_1 z_2^{-1} t)(1 - z_1^{-1} z_2 t)(1 - z_1^{-1} z_2^{-1} t)} \ . \tag{1.5.87}$$

Note that the baryonic symmetry is only an isometry of the master space and not the mesonic moduli space. Accordingly, the mesonic Hilbert series above under the new charge refinement is independent of the baryonic charge fugacity b. When expanded, the mesonic Hilbert series in (1.5.87) can be expressed in terms of characters of irreducible representations of the global flavour symmetry $SU(2) \times SU(2)$ as follows

$$g(z_i, t; \mathcal{M}^{mes}) = \sum_{n=0}^{\infty} [n; n] t^n \ , \tag{1.5.88}$$

where $[n; n] = [n]_{SU(2)_{z_1}} [n]_{SU(2)_{z_2}}$ are the characters of the irreducible representations of $SU(2)_{z_1} \times SU(2)_{z_1}$.

For more examples of global charge refined mesonic Hilbert series and also master space Hilbert series with refinement under baryonic symmetries, the reader is referred to chapters §3 and §4.

1.6 Higgsing and Toric Duality

An important advantage of using brane tilings as representations of supersymmetric quiver gauge theories is that properties of the bipartite graph can be used as tools to better understand physical phenomena. In mathematics, graph or so called quiver mutations have been studied extensively [124, 125] and their interpretation in the context of brane tilings and supersymmetric quiver gauge theories has been intriguing and fruitful. The following section reviews two such graph mutations which are interpreted as a Higgs mechanism and toric (Seiberg) duality. The hope is to set a stage for new mutations of brane tilings, such as specular duality discussed in chapter §4.

1.6.1 Higgsing and Unhiggsing

The **Higgs mechanism** has a natural interpretation in the brane tiling picture [101]. By giving a non-zero vacuum expectation value (VEV) to a gauge field in brane tiling I, and integrating out resulting quadratic mass terms in the superpotential as explained above, one obtains a new brane tiling II whose mesonic moduli space is a different toric Calabi-Yau 3-fold to the one of brane tiling I. Giving a VEV to a bifundamental field X_{ij} results in the removal of the corresponding edge in the brane tiling picture. This results in an effective merger between two adjacent faces, analogous of combining two gauge groups into one.

Let us consider the example of the $\mathbb{C}^3/\mathbb{Z}_2 \times \mathbb{Z}_2$ orbifold theory with orbifold action $((0,1,1)(1,0,1))$. The corresponding brane tiling and toric diagram are shown in Figure 1.17, and the superpotential is

$$
\begin{aligned}
W_I \quad = \quad & +X_{42}X_{23}X_{34} + X_{31}X_{14}X_{43} + X_{24}X_{41}X_{12} + X_{13}X_{32}X_{21} \\
& -X_{42}X_{21}X_{14} - X_{31}X_{12}X_{23} - X_{24}X_{43}X_{32} - X_{13}X_{34}X_{41} \; . \quad (1.6.89)
\end{aligned}
$$

By giving the bifundamental field X_{14} a VEV, such that $\langle X_{14}\rangle = 1$, the superpotential becomes,

$$
\begin{aligned}
W_{I\prime} \quad = \quad & +X_{42}X_{23}X_{34} + \underline{X_{31}X_{43}} + X_{24}X_{41}X_{12} + X_{13}X_{32}X_{21} \\
& -\underline{X_{42}X_{21}} - X_{31}X_{12}X_{23} - X_{24}X_{43}X_{32} - X_{13}X_{34}X_{41} \; , \quad (1.6.90)
\end{aligned}
$$

which in turn, by integrating out the above underlined quadratic mass terms, becomes

$$
W_{II} = +X_{13}X_{32}X_{23}X_{31} + X_{12}X_{21}X_{11} - X_{12}X_{23}X_{32}X_{21} - X_{13}X_{31}X_{11} \; . \quad (1.6.91)
$$

Theory II with the above superpotential and brane tiling shown in Figure 1.17 corresponds to the suspended pinch point (SPP) theory. Thus one has, by giving a VEV to a field in theory I, blown down a toric point in $\mathbb{C}^3/\mathbb{Z}_2 \times \mathbb{Z}_2$ to give the SPP model. Figure 1.17 shows the perfect matchings and their field content for each toric point of the toric diagrams of $\mathbb{C}^3/\mathbb{Z}_2 \times \mathbb{Z}_2$ and SPP.

1.6.2 Toric Duality

Two $3+1$ dimensional worldvolume theories are called **toric (Seiberg) dual** [33, 34, 35, 36, 92, 14, 37] if in the UV they have different Lagrangians with a different field content and superpotential, but flow to the same universality class in the IR.
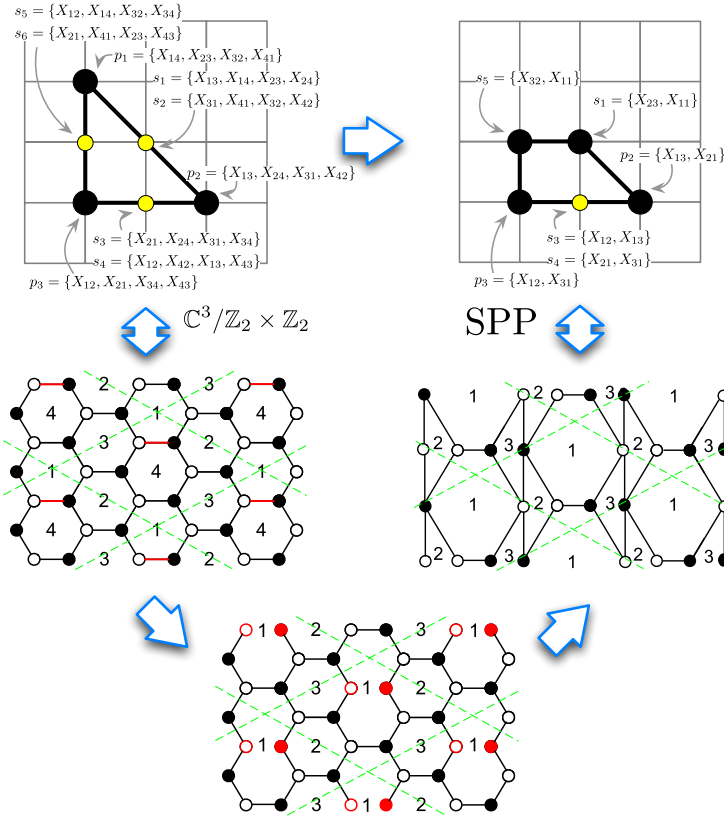
Figure 1.17: *Higgs mechanism.* By giving a non-zero vacuum expectation value to the bifundamental field X_{14} of the $\mathbb{C}^3/\mathbb{Z}_2 \times \mathbb{Z}_2$ orbifold theory, one obtains the suspended pinch point (SPP) theory. The bifundamental field X_{14} is represented by a red edge in the brane tiling. By setting $\langle X_{14} \rangle = 1$, one obtains quadratic mass terms represented by red nodes in the second brane tiling, which are integrated out to give the third SPP tiling. The nodes of the corresponding toric diagrams are labelled with perfect matching variables and the corresponding sets of bifundamental fields. The Higgsing procedure corresponds to a blow down from $\mathbb{C}^3/\mathbb{Z}_2 \times \mathbb{Z}_2$ to the cone over the Suspended Pinch Point.

The mesonic moduli spaces of toric (Seiberg) dual theories are toric Calabi-Yau 3-folds which are identical. The corresponding toric diagrams are $GL(2, \mathbb{Z})$ equivalent, however multiplicities of internal toric points and hence GLSM fields with zero R-charge can differ.

The relationship between two toric (Seiberg) dual theories is best illustrated with an example using brane tilings. Dualizing on a given gauge group has a natural interpretation in the brane tiling picture. Let us consider the Hirzebruch F_0 model. The
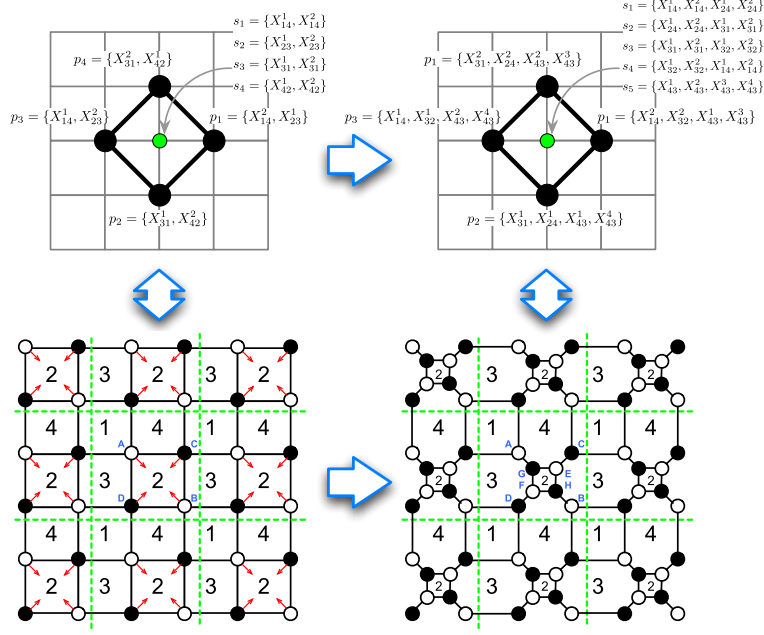
Figure 1.18: The toric (Seiberg) duality action on the brane tiling of the zeroth Hirzebruch surface F_0 model with corresponding toric diagrams. The points in the toric diagram correspond to GLSM fields which are presented as perfect matchings or sets of bifundamental fields in the brane tiling picture.

corresponding gauge theory has a superpotential of the form

$$W_I = + \underbrace{X_{14}^1 X_{42}^1 X_{23}^1 X_{31}^1}_{A} + \underbrace{X_{14}^2 X_{42}^2 X_{23}^2 X_{31}^2}_{B} - \underbrace{X_{14}^2 X_{42}^1 X_{23}^2 X_{31}^1}_{C} - \underbrace{X_{14}^1 X_{42}^2 X_{23}^1 X_{31}^2}_{D},$$
(1.6.92)

whose corresponding brane tiling and toric diagram are shown in the first column of Figure 1.18. The terms are labelled A to D and the corresponding brane tiling nodes are indicated in Figure 1.18. By dualizing on the gauge group labelled 2, the superpotential becomes

$$
\begin{aligned}
W_{II} \;=\; & + \underbrace{X_{14}^1 X_{43}^1 X_{31}^1}_{A} + \underbrace{X_{14}^2 X_{43}^2 X_{31}^2}_{B} - \underbrace{X_{14}^2 X_{43}^3 X_{31}^1}_{C} - \underbrace{X_{14}^1 X_{43}^4 X_{31}^2}_{D} \\
& + \underbrace{X_{14}^1 X_{43}^3 X_{31}^2}_{E} + \underbrace{X_{14}^2 X_{43}^4 X_{31}^1}_{F} - \underbrace{X_{14}^1 X_{43}^1 X_{31}^1}_{G} - \underbrace{X_{14}^2 X_{43}^2 X_{31}^2}_{H}
\end{aligned}
$$
(1.6.93)

and the corresponding new brane tiling and quiver are shown in the second column of Figure 1.18. One observes that under toric (Seiberg) duality, the number of gauge groups G remains constant, the number of bifundamental fields E and the number of superpotential terms both increase each by 4.

The change in the number of bifundamental fields and superpotential terms corresponds to the change in the number of GLSM fields corresponding to internal points of the corresponding toric diagram. The area of the toric diagram corresponding to the number of gauge groups G remains constant. The two toric diagrams and brane tilings in Figure 1.18 with the corresponding superpotentials given in (1.6.92) and (1.6.93) are called **phases** of the F_0 model.

The duality action often leads to superpotentials with quadratic mass terms. Quadratic mass terms relate to massive fields which become non-dynamical in the IR. The removal of quadratic mass terms and the corresponding deformation of the brane tiling have been discussed in section §1.2.2.

The claim is that the combination of toric duality procedures, integrating out mass terms, and Higgs mechanisms on the $\mathbb{C}^3/\mathbb{Z}_4 \times \mathbb{Z}_4$ orbifold theory with orbifold action $((1,0,3)(0,1,3))$ results in all possible quiver gauge theories whose mesonic moduli space is toric Calabi-Yau and has a toric diagram which is a reflexive polygon on $\mathbb{Z}^2$.[15] This is further discussed in chapter §3.

1.7 Outline

Chapter §2 is designed to give an overview of the rich combinatorial structure of brane tilings. Abelian orbifolds of $\mathbb{C}^3$ and $\mathbb{C}^D$ in higher dimensions D are taken as prime examples of the combinatorial challenge when dealing with brane tilings. Based on [2] with parts from [1, 3, 4], we describe various counting techniques for distinct Abelian orbifolds of the form $\mathbb{C}^D/\Gamma$. A particular emphasis is put on Polya's Enumeration Theorem and invariance of Abelian orbifolds under elements of the permutation group S_D. The counting of distinct Abelian orbifolds with the use of techniques from number theory sets the stage for the later use of Hilbert series as partition functions for gauge invariant operators.

Chapter §3 elaborates further on the problem of classification of brane tilings by focusing on supersymmetric quiver theories whose mesonic moduli space as a toric Calabi-Yau 3-fold is represented by a particular geometric object known as a reflexive polygon. There are in total 16 reflexive polygons and it is shown that precisely 30 brane tilings have a reflexive polygon as their toric diagram. Based on [5], this chapter illustrates the computation of mesonic Hilbert series and their refinement under global symmetries. Moreover, it illustrates that the lattice of mesonic moduli space generators provided by the global charges of the Abelian theories is dual to the reflexive toric diagram of the Calabi-Yau 3-fold. Intriguingly, we discover a new correspondence between brane tilings

---

[15]See appendix §A.4 for the full $\mathbb{C}^3/\mathbb{Z}_4 \times \mathbb{Z}_4$ orbifold theory.

from the classification which we call specular duality.

Chapter §4 is based on [7] and describes specular duality which has been discovered in the context of brane tilings with reflexive toric diagrams. Specular duality is a correspondence between two Abelian brane tilings which have the same master space. Moreover, the two corresponding brane tilings have mesonic and baryonic symmetries which are swapped under the duality map analogous to a swap of external and internal perfect matchings. By explicit computations of the master space Hilbert series refined under both mesonic and baryonic symmetries, the correspondence is verified. The actual mutation of the brane tiling involved in specular duality, which is known as the untwisting map, is identified as a pathway to generate brane tilings beyond the 2-torus. In fact, a prototypical class of brane tilings on higher genus Riemann surfaces is provided at the end of the chapter with the corresponding quiver diagrams.

Chapter §5 discusses a new class of brane tilings defined on genus 2 Riemann surfaces. A complete classification of such brane tilings up to 8 quiver fields and 4 superpotential terms is provided. Using the standard forward algorithm, the mesonic moduli spaces of the Abelian field theories are identified and the corresponding Hilbert series are computed. Based on [9], this chapter provides a pioneering analysis of brane tilings on higher genus Riemann surfaces.

Chapter §6 summarises the results in this work and provides an overview of new directions on the study of brane tilings. We conclude with a summary of ongoing projects.

2 Brane Tilings and Abelian Orbifolds

The following chapter covers a study on Abelian orbifolds of $\mathbb{C}^3$ and in general $\mathbb{C}^D$. Abelian orbifolds of toric Calabi-Yau 3-folds play an important role in studying brane tilings. This is because for every Abelian orbifold of a toric Calabi-Yau 3-fold, one expects to find at least one corresponding brane tiling whose mesonic moduli space is the orbifold itself. Given that $\mathbb{C}^3$ is the first Calabi-Yau 3-fold to consider, it is natural to study first Abelian orbifolds of $\mathbb{C}^3$ in the context of brane tilings.

An important challenge facing us from the onset is due to the infinite number of Abelian orbifolds of $\mathbb{C}^3$ or any other toric Calabi-Yau 3-fold. The challenge is to identify and to classify the distinct Abelian orbifolds of a given toric Calabi-Yau 3-fold and to know how many there are for a given order of the finite Abelian quotienting group. The studies in [126, 1] use the parameterisation of Abelian orbifolds of $\mathbb{C}^3$ to count and write a partition function for the number of distinct Abelian orbifolds for arbitrary orders of the quotienting group. In the following chapter, based on [2], we elaborate on the counting technique using Polya's Enumeration Theorem. With particular emphasis on Abelian orbifolds of the form $\mathbb{C}^3/\Gamma$ up to $\mathbb{C}^6/\Gamma$, a counting is presented which highlights Abelian orbifolds that are invariant under cycles of the permutation group S_D. The resulting multiplicative sequences, which are controlled by their values on primes and pure powers of primes, are used to calculate the counting of distinct Abelian orbifolds of the form $\mathbb{C}^D/\Gamma$ for prime orders of Γ in any dimension D.

The chapter illustrates well the combinatorial richness of brane tilings and gives an introduction to the problem of counting by using partition functions. Both subjects will play a more important role in the following chapters of this work. This chapter is an edited version of [2] with parts from [1, 3, 4]. These are parts of research work in collaboration with John Davey, Amihay Hanany, Vishnu Jejjala and Sanjaye Ramgoolam.

2.1 Introduction

Advances in enumerating and counting distinct Abelian orbifolds [126, 1] have uncovered rich structures in the vast family of quiver gauge theories. In the past, quiver gauge theories [44, 127, 41] as worldvolume theories of D3-branes probing toric non-compact Calabi-Yau (CY) singularities [45, 53] have been fruitfully studied [15, 55, 90, 17, 16,

100, 89]. Brane tilings were instrumental in relating worldvolume gauge theories of D3-branes with probed toric non-compact Calabi-Yau geometries. Trailblazing examples of study were the Abelian orbifolds of $\mathbb{C}^3$ [128, 129, 130, 131, 132, 43, 133, 134]. A guiding principle has been the fact that an infinite sub-class of $(3+1)$-dimensional worldvolume gauge theories have moduli spaces which are Abelian orbifolds of the form $\mathbb{C}^3/\Gamma$ with Γ being an Abelian subgroup of $SU(3)$. The moduli spaces are toric, and for Abelian orbifolds of $\mathbb{C}^3$ the toric diagrams are always elegantly triangles. Accordingly, from the geometrical perspective, two distinct Abelian orbifolds of $\mathbb{C}^3$ have toric triangles which are not related under a $GL(2,\mathbb{Z})$ transformation. A thought-provoking example is the Abelian orbifold of the form $\mathbb{C}^3/\mathbb{Z}_{30}$ with action $(2, 3, 25)$ whose toric triangle cannot be $GL(2,\mathbb{Z})$ equivalent to an orbifold with an action of the unnecessarily restrictive but commonly used form $(1, a, -1 - a)$. This and many other untouched orbifolds lead to the problem of classifying and counting distinct Abelian orbifolds of $\mathbb{C}^3$ which has been solved in the pioneering work in [1] and [126].

How about higher dimensional Abelian orbifolds of $\mathbb{C}^D$? The most recent break-throughs which led towards studies on Calabi-Yau four-folds as orbifold backgrounds have been the works on ABJM theory [56, 57, 58, 59, 59, 60]. These prompted an upgrade of brane tilings to accommodate the worldvolume gauge theories of M2-branes which probe toric non-compact CY 4-folds. The worldvolume gauge theories of probe M2 branes are $\mathcal{N} = 2$ $(2 + 1)$-dimensional quiver Chern-Simons theories [62, 63, 135]. The theories' Chern-Simons levels are represented in a modified brane tiling [64, 136, 137, 138] which obviates the use of the initially proposed brane crystal constructions [139, 140]. The special connection to our work has been the observation that an infinite sub-class of $(2 + 1)$-dimensional M2-brane worldvolume gauge theories have moduli spaces which are Abelian orbifolds of the form $\mathbb{C}^4/\Gamma$ with Γ being an Abelian subgroup of $SU(4)$. As for the CY3 case, the moduli spaces are toric, and the associated toric diagrams elegantly turn out to be always tetrahedra [64, 141]. Again, from a geometrical perspective two distinct Abelian orbifolds of $\mathbb{C}^4$ have toric tetrahedra which are not related under a $GL(3,\mathbb{Z})$ transformation. Accordingly, not surprisingly we encounter from this special example of Chern-Simons gauge theories the familiar problem of enumerating and counting distinct Abelian orbifolds of $\mathbb{C}^4$ [126, 1].

By continuation, we expect that higher dimensional Abelian orbifolds of the form $\mathbb{C}^D/\Gamma$ with Γ being an Abelian subgroup of $SU(D)$ have toric diagrams which are $(D-1)$-dimensional simplices embedded in $\mathbb{Z}^{D-1}$. An efficient method of testing $GL(D-1,\mathbb{Z})$ equivalence between toric simplices has been outlined in detail in [1].

In the following we argue that discrete symmetries of an Abelian orbifold of $\mathbb{C}^D$ can be observed directly through its toric diagram using the same method used to test $GL(D - 1,\mathbb{Z})$ equivalence between toric simplices. Discrete symmetries have played an integral role in specifying the global symmetries of the gauge theory in $3 + 1$ dimensions
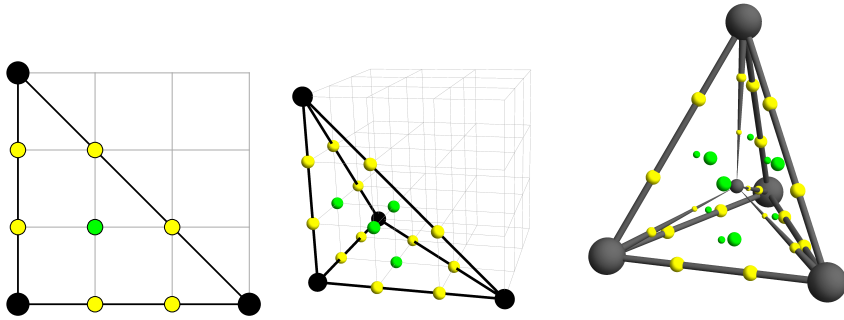
Figure 2.1: The toric diagrams for the Abelian orbifolds of the form $\mathbb{C}^3/\mathbb{Z}_3\times\mathbb{Z}_3$, $\mathbb{C}^4/\mathbb{Z}_3\times\mathbb{Z}_3\times\mathbb{Z}_3$ and $\mathbb{C}^5/\mathbb{Z}_3\times\mathbb{Z}_3\times\mathbb{Z}_3\times\mathbb{Z}_3$ respectively. The 4-dimensional toric diagram of $\mathbb{C}^5/\mathbb{Z}_3\times\mathbb{Z}_3\times\mathbb{Z}_3\times\mathbb{Z}_3$ has been projected into 3-space. $\mathbb{Z}^D$ lattice points on 1-simplices and 2-simplices are colored yellow and green respectively, whereas the defining vertex points are in black.

in the past [35, 14], and so far, they have been identified only through the quiver or superpotential of the gauge theory. The method we present in this work to 'measure' symmetries directly from the toric diagram of a given Abelian orbifold of $\mathbb{C}^D$ is a novel approach whose unexpected by-product through Polya's Enumeration Theorem is the counting of distinct Abelian orbifolds of $\mathbb{C}^D$ – something which we believe has never been done before.

We identify and count explicitly Abelian orbifolds of $\mathbb{C}^3$ to $\mathbb{C}^6$ which are invariant under cycles of the permutation group S_D. This produces multiplicative sequences, each corresponding to a cycle in the Cycle Index of the permutation group S_D. Multiplicativity states that the sequence values at co-prime orders n_1 and n_2 give as a product the sequence value at order $n_1 n_2$. Accordingly, we put emphasis on orbifolds of the form $\mathbb{C}^D/\Gamma$ with the order of Γ being a prime number. From this perspective, we propose a novel generalisation of sequences which count distinct Abelian orbifolds of $\mathbb{C}^D$ and Abelian orbifolds which are invariant under cycles of the permutation group S_D. Such a generalisation enables us to probe and quantify the rich geometrical structure of Abelian orbifolds of $\mathbb{C}^D$ in any dimension D.

The chapter is divided into the following sections:

- Section §2.2 gives a short summary of how to identify distinct Abelian orbifolds of $\mathbb{C}^D$ and toric diagrams which are invariant under cycles of the symmetric group S_D.

- Section §2.3 presents the results of counting for the orbifolds of $\mathbb{C}^3$, $\mathbb{C}^4$, $\mathbb{C}^5$ and $\mathbb{C}^6$, and reviews how these results can be encoded in terms of partition functions for the special cases of $\mathbb{C}^3/\Gamma_N$ and $\mathbb{C}^4/\Gamma_N$.

- Section §2.4 presents the role of values on prime indices of sequences which count orbifolds that are invariant under cycles of S_D, and discusses how the values on prime indices affect the derivation of partition functions. We explicitly derive the partition function counting distinct $\mathbb{C}^5/\Gamma$.

- Section §2.5 outlines generalisations for partition functions which count orbifolds that are invariant under certain cycles of S_D. In addition, a complete generalisation is presented for sequences which count distinct Abelian orbifolds of the form $\mathbb{C}^D/\Gamma$ and their symmetries where the order of Γ is prime.

Notation and Nomenclature. A list of the most common notation and nomenclature used in this chapter is presented below. The reader will be introduced to them in more detail in the main text.

- A cycle g of the permutation group S_D is denoted by g^α to emphasise its correspondence to a conjugacy class H_α of S_D. A conjugacy class $H_\alpha \subset S_D$ is labeled by a cycle index variable x^α.

- Given a sequence $\mathbf{g}$ with elements $\mathbf{g}_n = \mathbf{g}(n)$ denoted by integer indices $n \in \mathbb{Z}^+$, we write a partition function of the sequence as $g(t) = \sum_n \mathbf{g}_n t^n$.

- Given a sequence $\mathbf{g}$, the new sequence formed by picking elements $\mathbf{g}_p$ on prime indices p is called a *prime index sequence* of $\mathbf{g}$.

2.2 Background and Methods

2.2.1 Introduction to Abelian Orbifolds

Let $\mathbb{C}^3$ be parameterised by z_1, z_2, z_3. We consider quotients of the form $\mathbb{C}^3/\Gamma_N$ with discrete Abelian $\Gamma_N \subset SU(3)$ and of order $N \in \mathbb{Z}^+$. In general, we consider orbifolds with $\Gamma_N = \mathbb{Z}_{n_1} \times \mathbb{Z}_{n_2}$ and order $n_1 n_2 = N \in \mathbb{Z}^+$. Without loss of generality, it is assumed that $n_1 \geq n_2$.

Let an irreducible representation of $\Gamma_N = \mathbb{Z}_{n_1} \times \mathbb{Z}_{n_2}$ be called $R_{(n_1,n_2)}$ with elements $\omega^{(\{a_i\},\{b_i\})}$, $i = 1, \ldots, 3$ and $|R_{(n_1,n_2)}| = N$. The elements of the representation $\omega^{(\{a_i\},\{b_i\})} \in R_{(n_1,n_2)}$ are of the form

$$\omega^{(\{a_i\},\{b_i\})} = \text{diag}\begin{pmatrix} e^{\frac{i2\pi a_1}{n_1}} \\ e^{\frac{i2\pi a_2}{n_1}} \\ e^{\frac{i2\pi a_3}{n_1}} \end{pmatrix} \text{diag}\begin{pmatrix} e^{\frac{i2\pi b_1}{n_2}} \\ e^{\frac{i2\pi b_2}{n_2}} \\ e^{\frac{i2\pi b_3}{n_2}} \end{pmatrix} = \text{diag}\begin{pmatrix} e^{i2\pi(\frac{a_1}{n_1}+\frac{b_1}{n_2})} \\ e^{i2\pi(\frac{a_2}{n_1}+\frac{b_2}{n_2})} \\ e^{i2\pi(\frac{a_3}{n_1}+\frac{b_3}{n_2})} \end{pmatrix}, \quad (2.2.1)$$

with $(a_1 + a_2 + a_3) \bmod n_1 = 0$ and $(b_1 + b_2 + b_3) \bmod n_2 = 0$. The zero sum conditions are a manifestation of the Calabi-Yau condition on the orbifold $\mathbb{C}^3/\Gamma_N$ and the det $= 1$

property of $SU(3)$. We introduce notation such that (2.2.1) can be expressed as

$$\omega^{(\{a_i\},\{b_i\})} = \omega^{(a_1,a_2,a_3)}\omega^{(b_1,b_2,b_3)} = \omega^{((a_1,a_2,a_3),(b_1,b_2,b_3))} . \qquad (2.2.2)$$

For the element $\omega^{(\{a_i\},\{b_i\})} \in R_{(n_1,n_2)}$ to be also a generator of the representation, it has to fulfil $\gcd(n_1,\{a_i\}) = 1$ and $\gcd(n_2,\{b_i\}) = 1$. In addition, the identity element of the representation is defined as $(\omega^{(\{a_i\},\{b_i\})})^N = 1$. The Calabi-Yau condition also results in $\det(\omega^{(\{a_i\},\{b_i\})}) = 1$.

The generator $\omega^{(\{a_i\},\{b_i\})}$ of the representation $R_{(n_1,n_2)}$ acts on the coordinates of $\mathbb{C}^3$ as

$$\omega^{(\{a_i\},\{b_i\})} \; : \; z_i \; \mapsto \; \omega^{(\{a_i\},\{b_i\})} z_i \; = \; z_i \, e^{i2\pi(\frac{a_i}{n_1}+\frac{b_i}{n_2})} . \qquad (2.2.3)$$

The dual to the generator $\omega^{(\{a_i\},\{b_i\})}$ of the representation $R_{(n_1,n_2)}$ is now the 2×3 matrix orbifold action $((a_1,a_2,a_3),(b_1,b_2,b_3))$ generating the representation $\tilde{R}_{(n_1,n_2)}$ with $\gcd(n_1,\{a_i\}) = 1$ and $\gcd(n_2,\{b_i\}) = 1$. For $\gcd(n_1,\{a_i\}) \neq 1$ and $\gcd(n_2,\{b_i\}) \neq 1$, $((a_1,a_2,a_3),(b_1,b_2,b_3))$ is not an orbifold action of $\mathbb{C}^3/\Gamma_{n_1 n_2}$.

Let the set of all generators of representations $\{\tilde{R}_{(n_1,n_2)}\}$ of Γ_N orbifold groups of order $N = n_1 n_2$ be called $\mathcal{A}_N = \{A_k\}$ with $k = 1, \ldots, |\mathcal{A}_N|$. This set is defined as

$$\mathcal{A}_{N=n_1 n_2} \; = \; \left\{ \begin{pmatrix} (a_1,a_2,a_3) \\ (b_1,b_2,b_3) \end{pmatrix} \; \middle| \; \begin{array}{c} (a_1+a_2+a_3) \bmod n_1 = 0 \; , \\ (b_1+b_2+b_3) \bmod n_2 = 0 \; , \\ \gcd(n_1,\{a_i\}) = 1 \; , \; \gcd(n_2,\{b_i\}) = 1 \end{array} \right\} . \qquad (2.2.4)$$

As for $\mathbb{C}^2$ orbifolds, the set of orbifold actions $\mathcal{A}_N$ does not consist of distinct inequivalent orbifold actions. The set of orbifold actions $\mathcal{A}_N$ at a given order $N = n_1 n_2$ can be re-expressed as the union of all orbifold action equivalence classes $[A_k]$. If two orbifold actions $A_l \in [A_k]$ and $A_m \in [A_k]$ are of the same equivalence class $[A_k]$ and are both generators of representations $\tilde{R}_{(n_1,n_2)}(A_l)$ and $\tilde{R}_{(\tilde{n}_1,\tilde{n}_2)}(A_k)$ respectively with $N = n_1 n_2 = \tilde{n}_1 \tilde{n}_2$, then the two representations of Γ_N are equivalent $\tilde{R}_{(n_1,n_2)}(A_l) \sim \tilde{R}_{(\tilde{n}_1,\tilde{n}_2)}(A_k)$ up to a permutation of the complex coordinates of $\mathbb{C}^3$.

It is of use to consider an orbifold action in terms of its components. An orbifold action A_k in $\mathbb{C}^3$ consists of two components corresponding to the two rows in the 2×3 orbifold action matrix $A_k = ((a_1,a_2,a_3),(b_1,b_2,b_3))$. We denote the two components as $A_k^{(n_1)} = (a_1,a_2,a_3)$ and $A_k^{(n_2)} = (b_1,b_2,b_3)$ such that the action can be written as $A_k = (A_k^{(n_1)}, A_k^{(n_2)})$. The dual operator has the corresponding notation $\omega^{(\{a_i\},\{b_i\})} = (\omega^{(a_1,a_2,a_3)}, \omega^{(b_1,b_2,b_3)})$.

For the case when $n_2 = 1$ with $n_1 > n_2$, the orbifold action and its dual are of the form $A_k = (A_k^{(n_1)},(0,0,0))$ and $\omega^{(\{a_i\},\{b_i\})} = (\omega^{(a_1,a_2,a_3)},1)$ respectively. In this case, it is beneficial to talk about the *effective* component $A_k^{(n_1)}$ of the orbifold action instead of the orbifold action A_k itself. In the context of representations, for $\gcd(n_1,\{a_i\}) = 1$, the component $A_k^{(n_1)}$ is the generator of the representation $\tilde{R}_{n_1}$ of the group $\Gamma_{N=n_1} = \mathbb{Z}_{n_1}$

with $n_2 = 1$.

2.2.2 Abelian Orbifolds as Brane Tilings

Equivalence of two orbifold actions can be illustrated in the setting of brane tilings. In the context of brane boxes and brane configurations, this has been illustrated in [68, 142, 143].

We recall, the worldvolume gauge theories that arise when a collection of D-branes probe a non-compact toric Calabi-Yau (CY) singularity, the CY 3-fold, are quiver gauge theories. In 10-dimensional Type IIB String Theory, the configuration of the probe D3-branes on the cone over the CY 3-fold is T-dualised to a configuration of D5-branes suspended between NS5-branes. The resulting so called brane box configurations of NS5 and D5-branes, their corresponding T-dual configuration of D3-branes probing a non-compact Calabi-Yau singularity, and the $(3 + 1)$-dimensional D-brane worldvolume gauge theories have a combined description in the form of a brane tiling [143, 55].

The configuration of n_1 NS5-branes and n_2 NS5$'$-branes, the $n_1 \times n_2$ brane box configuration, is T-dual to the orbifold $\mathbb{C}^3/\mathbb{Z}_{n_1} \times \mathbb{Z}_{n_2}$. The orbifold action can be considered as a labelling of distinct $n_1 \times n_2$ brane box configurations. Accordingly, under the brane tiling description of brane box configurations, two inequivalent orbifold actions correspond to two distinct brane tilings.

Brane Tiling Dictionary for Abelian Orbifolds. The order of the orbifold, $N = n_1 n_2$, is the number of faces in the fundamental domain of the tiling corresponding to the gauge groups $U(1)^N$ of the $(3 + 1)$-dimensional worldvolume gauge theory. Faces in the tiling for $\mathbb{C}^3$ orbifolds are hexagonal such that the tiling has 3 symmetry axes corresponding to 3 fundamental directions

$$\{v_i^1, v_i^2, v_i^3\} \tag{2.2.5}$$

crossing at a face F_i in the tiling, with $i = 1, \ldots, N$, as shown in Figure 2.2. Note that the directions $\{v_i^1, v_i^2, v_i^3\}$ at a given face F_i are isomorphic to the complex coordinates $\{z_1, z_2, z_3\}$ of $\mathbb{C}^3$,

$$B \; : \; \{z_1, z_2, z_3\} \;\; \rightarrow \;\; \{v_i^1, v_i^2, v_i^3\} \; . \tag{2.2.6}$$

Moreover, these correspond to the generators σ for a convex polyhedral cone [144] as shown in the discussion on toric geometry in Section §2.2.4.

To represent the action A_k in the brane tiling setup of the orbifold action $\mathbb{C}^3/\mathbb{Z}_{n_1} \times \mathbb{Z}_{n_2}$, it is useful to specify the face labels F_i as a pair of two positive integer numbers $\mathsf{F}_i = (f_{i1}, f_{i2})$ with $f_{ij} \in \mathbb{N}_0$. Then the orbifold action can be visualized as acting on the face
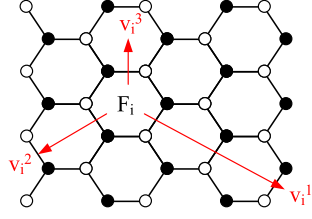
Figure 2.2: The fundamental directions v_i^1, v_i^2, v_i^3 at a given face F_i in the brane tiling of $\mathbb{C}^3$.

labels of the tiling in a chosen direction v_i^m,

$$A_k^m = \begin{pmatrix} a_m \\ b_m \end{pmatrix} \; : \; \mathsf{F}_i = (f_{i1}, f_{i2}) \; \mapsto \; ((f_{i1} + a_m) \bmod n_1, (f_{i2} + b_m) \bmod n_2) \;, \quad (2.2.7)$$

where A_k^m is a column of the orbifold action matrix A_k such that $A_k = (A_k^1, A_k^2, A_k^3)^\top$.

As an example, the orbifold used in Section §2.1, $\mathbb{C}^3/\mathbb{Z}_3 \times \mathbb{Z}_2$ with action $A_2 = ((1,0,2),(0,1,1))$ has a brane tiling as shown in Figure 2.3 with an arbitrarily chosen reference face $\mathsf{F}_1 = (f_{11}, f_{12}) = (0,0)$ that has 3 direct neighbours along the fundamental directions $\{v_1^1, v_1^2, v_1^3\}$. These direct neighbours share with F_1 a unique edge in the tiling and have labels given by

$$\begin{aligned}
A_1^1 &: & (0,0) &\mapsto (1,0) \\
A_1^2 &: & (0,0) &\mapsto (0,1) \\
A_1^3 &: & (0,0) &\mapsto (2,1) \;.
\end{aligned} \qquad (2.2.8)$$

The entire brane tiling structure can be constructed by finding recursively the face labels of neighbouring faces of all faces $\{\mathsf{F}_i\}$ in the brane tiling.

Equivalence of Brane Tilings. It is now instructive to see how the brane tiling conveys equivalence between orbifold actions. For example, the brane tiling for the orbifold action $A_1 = ((1,2,3),(0,0,0))$ of $\mathbb{C}^3/\mathbb{Z}_6$ can be drawn as shown in Figure 2.4.

For any brane tiling with face labels $\mathsf{F}_i = (f_{i1}, f_{i2})$, there is a consistent relabeling of faces ρ such that

$$\rho \; : \; \mathsf{F}_i = (f_{i1}, f_{i2}) \; \mapsto \; \bar{f}_l \in \mathbb{N}_0 \;, \qquad (2.2.9)$$

where $l = 1, \ldots, N$ and $\bar{f}_l \neq \bar{f}_k$ if $l \neq k$. For the tiling corresponding to $A_1 = ((1,2,3),(0,0,0))$ with faces $\{\mathsf{F}_i^{A_2}\}$, a straightforward relabelling choice is

$$\rho^{A_1} \; : \; (f_{i1}{}^{A_1}, f_{i2}{}^{A_1}) \; \mapsto \; \bar{f}_l = f_{i1}{}^{A_1} \qquad (2.2.10)$$
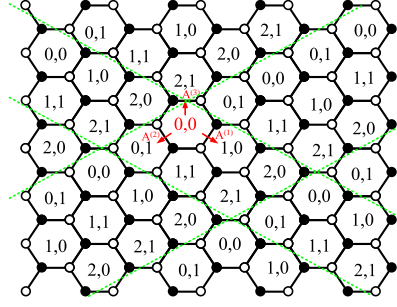
Figure 2.3: The brane tiling for the orbifold $\mathbb{C}^3/\mathbb{Z}_3 \times \mathbb{Z}_2$ with action $A_2 = ((1,0,2),(0,1,1))$.
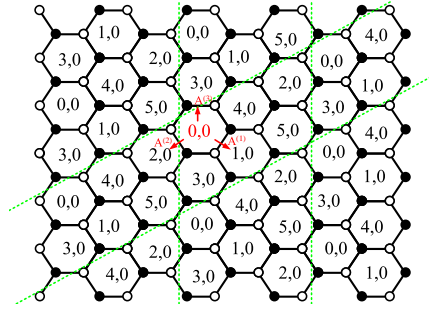
Figure 2.4: The brane tiling for the orbifold $\mathbb{C}^3/\mathbb{Z}_6$ with action $A_1 = ((1,2,3),(0,0,0))$.

since $f_{i2} = 0 \; \forall i$. It can be now shown that there is a consistent relabelling ρ^{A_2} such that it maps the face labels $\{\mathsf{F}_i{}^{A_2}\}$ of the tiling for A_2 in the following way,

$$\rho^{A_2} \; : \; \{\mathsf{F}_i{}^{A_2}\} = \{(f_{i1}{}^{A_2}, f_{i2}{}^{A_2})\} \;\rightarrow\; \{\bar{f}_l\} = \rho^{A_1}(\{\mathsf{F}_i{}^{A_1}\}) \,, \qquad (2.2.11)$$

where ρ^{A_2} is the map on the face labels of the A_2 action tiling as shown in (2.2.10).

In fact, in general if the relation in (2.2.11) holds for two brane tilings of orbifold actions $A_1 \in \tilde{R}_{(n_1,n_2)}$ and $A_2 \in \tilde{R}_{(n'_1,n'_2)}$ with $n_1 n_2 = n'_1 n'_2 = N$, then $A_1 \sim A_2$. For the above two example actions A_1 and A_2, the relabelling map on $\{\mathsf{F}_i{}^{A_2}\}$ can be chosen as

$$
\begin{aligned}
\rho^{A_2} \; : \; (0,0) &\;\mapsto\; 0 = \rho^{A_1}((0,0)) \\
(1,0) &\;\mapsto\; 1 = \rho^{A_1}((4,0)) \\
(2,0) &\;\mapsto\; 2 = \rho^{A_1}((2,0)) \\
(0,1) &\;\mapsto\; 3 = \rho^{A_1}((3,0)) \\
(1,1) &\;\mapsto\; 4 = \rho^{A_1}((1,0)) \\
(2,1) &\;\mapsto\; 5 = \rho^{A_1}((5,0)) \qquad (2.2.12)
\end{aligned}
$$

verifying that $A_1 \sim A_2$ where $A_1 \in \tilde{R}_{(6,1)}$ and $A_2 \in \tilde{R}_{(3,2)}$. Accordingly, we have shown
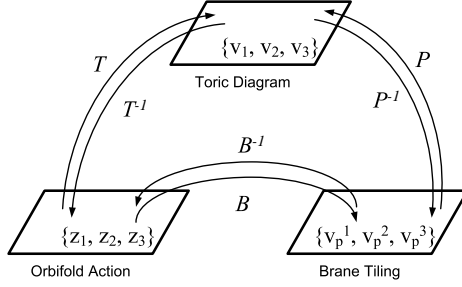
Figure 2.5: The correspondence between barycentric coordinates of the toric triangle, coordinates of the hexagonal brane tiling and the complex coordinates of $\mathbb{C}^3$ as first illustrated in [1].

that $A_1 \sim A_2$ in the context of brane tilings verifying the result in Section §2.1.

Another correspondence can be identified between equivalent brane tilings and orbifold actions that are equivalent up to a permutation of the complex coordinates of $\mathbb{C}^3$, $\{z_1, z_2, z_3\}$. By the correspondence between the coordinates $\{z_1, z_2, z_3\}$ and the fundamental directions $\{v_i^1, v_i^2, v_i^3\}$ of a face F_i in the tiling, orbifold equivalence up to a permutation of coordinates corresponds to tiling equivalence due to permutations of $\{v_i^1, v_i^2, v_i^3\}$ that are interpreted as reflections or rotations around a face F_i in the tiling. Accordingly, orbifold action equivalence can be identified as a *symmetry* on the brane tiling.

2.2.3 Toric Diagrams and Barycentric Coordinates

More generally, two orbifolds of $\mathbb{C}^D$ are distinct if there is no $GL(D-1, \mathbb{Z})$ transformation which maps between the corresponding toric diagrams. We give here a short summary of the method which tests this condition efficiently.

Toric Diagrams and Barycentric Coordinates. Non-compact toric CY singularities are represented by toric diagrams. For Abelian orbifolds of the form $\mathbb{C}^2/\Gamma_N$, the toric diagrams are lines in $\mathbb{Z}^1$ with length N. For Abelian orbifolds of the form $\mathbb{C}^3/\Gamma_N$, the toric diagrams are triangles embedded in $\mathbb{Z}^2$ with area N. For Abelian orbifolds of the form $\mathbb{C}^4/\Gamma_N$, the toric diagrams are tetrahedra embedded in $\mathbb{Z}^3$ with volume N. By continuation, Abelian orbifolds of the form $\mathbb{C}^D/\Gamma_N$ have toric diagrams as $(D-1)$-simplices, henceforth denoted by σ^{D-1}, which are embedded in $\mathbb{Z}^{D-1}$ with hyper-volume N.

Every lattice point w_k on and enclosed by the boundary of σ^{D-1} ($w_k \in \sigma^{D-1}$) divides
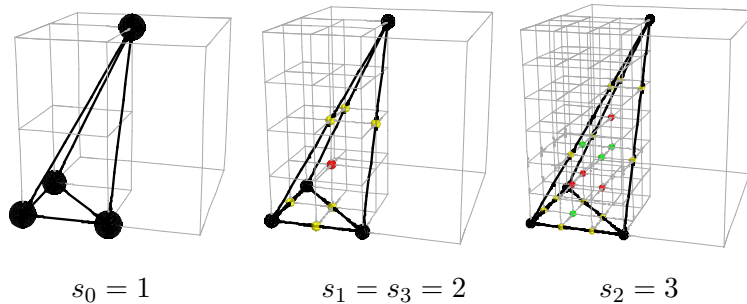
$$s_0 = 1 \qquad\qquad s_1 = s_3 = 2 \qquad\qquad s_2 = 3$$

Figure 2.6: Toric tetrahedra corresponding to $\mathbb{C}^4/\mathbb{Z}_2$ with orbifold action $A = ((1,1,1,1),(0,0,0,0),(0,0,0,0))$ and scalings $s_0 = 1$, $s_1 = s_3 = 2$ and $s_2 = 3$ respectively. Lattice points on edges (I_0), lattice points on faces (I_1) and internal lattice points (I_3) are colored yellow, green and red respectively.

σ^{D-1} into D sub-simplices of dimension $D-1$ or less. These sub-simplices have $(D-1)$-dimensional hyper-volumes with values $\lambda_{k1}, \lambda_{k2}, \ldots, \lambda_{kD}$. Accordingly, the lattice point $w_k \in \sigma^{D-1}$ can be given in terms of **barycentric coordinates** of the form

$$w_k = \frac{1}{N}(\lambda_{k1}, \lambda_{k2}, \ldots, \lambda_{ki}, \ldots, \lambda_{kD}) , \tag{2.2.13}$$

where the barycentric coordinate axes are labeled by $i = 1, \ldots, D$ and N is the $(D-1)$-dimensional hyper-volume of the simplex σ^{D-1}.

It has been proposed in [1] that the barycentric coordinates defined on toric simplices of $\mathbb{C}^D/\Gamma$ correspond to complex coordinates on $\mathbb{C}^D$ as well as for $D = 3$ the zig-zag-paths on the hexagonal brane tiling of $\mathbb{C}^3$. The correspondence is illustrated in Figure 2.5.

The Topological Character and Scaling. The topological character of a given toric simplex σ^{D-1} is defined as the set of barycentric coordinates for all $w_k \in I(\sigma^{D-1})$. $I(\sigma^{D-1})$ is the set of relevant lattice points of σ^{D-1}, and is defined as

$$I(\sigma^{D-1}) = \bigcup_{d=0}^{D-1} I_d(f_s(\sigma^{d-1})) . \tag{2.2.14}$$

Here, $I_d(\sigma^{D-1})$ is the set of defining lattice points of all d-dimensional sub-simplices contained in σ^{D-1}. Accordingly, $I_0(\sigma^{D-1})$ is the set of D corner points of σ^{D-1} (Figure 2.6). $f_{s_d}(\sigma^{D-1})$ is a scaled simplex σ^{D-1} such that $I_d(f_{s_d}(\sigma^{D-1})) \neq \emptyset$ with s_d being the scaling coefficient. In (2.2.14) we use an overall scaling coefficient $s = \max(s_1, \ldots, s_{D-1})$.

Example. Let us take the example shown in Figure 2.6 for the orbifold of the form $\mathbb{C}^4/\mathbb{Z}_2$. Here, I_0 is the set of the four corner points of the toric tetrahedron which are 'visible' with scaling $s_0 = 1$. The internal (red) points and points on edges (yellow)

86
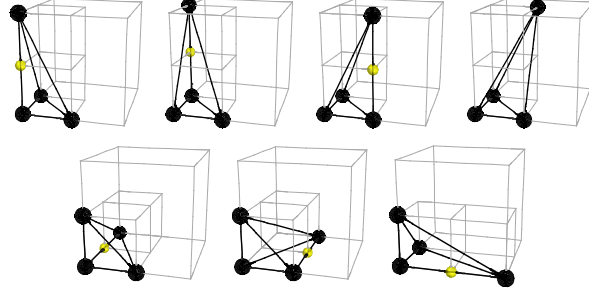
Figure 2.7: The Hermite Normal Forms $D(2)$ for $\mathbb{C}^4/\Gamma_2$.

forming the sets I_1 and I_3 respectively are visible only with scaling $s_1 = s_3 = 2$. Finally, lattice points on faces of the tetrahedron (green) forming the set I_3 are visible only with an overall scaling $s_3 = 3$. In order to collect all topologically significant lattice points in the overall set I, we scale the toric tetrahedron of $\mathbb{C}^4/\mathbb{Z}_2$ to $\max(s_0, s_1, s_2, s_3) = 3$.

Overall, the **topological character** of a toric simplex σ^{D-1} is defined as

$$\tau = \left\{ \frac{1}{N} (\lambda_{k1}, \lambda_{k2}, \ldots, \lambda_{ki}, \ldots, \lambda_{kD}) \;\Big|\; w_k \in I(\sigma^{D-1}) \right\}, \qquad (2.2.15)$$

where w_k is the barycentric coordinate defined in (2.2.13) of a point in the set $I(\sigma^{D-1})$ defined in (2.2.14).

Observation 2.2.1. *Two toric simplices of $\mathbb{C}^D/\Gamma_N$ that are related under a $GL(D-1, \mathbb{Z})$ transformation, and hence are equivalent, have equal topological characters up to a permutation of the barycentric coordinate axes labeled by $i = 1, \ldots, D$.*

2.2.4 Hermite Normal Forms and Symmetries

Hermite Normal Forms. The Hermite Normal Form (HNF) is an upper diagonal square matrix of size $D - 1$ with non-negative integer entries. It takes the form

$$M = \begin{pmatrix} m_{11} & m_{12} & \ldots & m_{1j} & \ldots & m_{1(D-1)} \\ 0 & m_{22} & \ldots & m_{2j} & \ldots & m_{2(D-1)} \\ 0 & 0 & & m_{3j} & & m_{3(D-1)} \\ \vdots & \vdots & & \vdots & & \vdots \\ 0 & 0 & & m_{(j-1)j} & & m_{(j-1)(D-1)} \\ 0 & 0 & & m_{jj} & & m_{j(D-1)} \\ 0 & 0 & & 0 & & m_{(j+1)(D-1)} \\ \vdots & \vdots & & \vdots & & \vdots \\ 0 & 0 & \ldots & 0 & \ldots & m_{(D-1)(D-1)} \end{pmatrix}, \qquad (2.2.16)$$

87

where $\det M = \prod_{j=1}^{D-1} m_{jj} = N$ and the off diagonal entries are restricted by the condition $0 \le m_{jk} < m_{jj}$ with $m_{jk} \in \mathbb{N}_0$. For each such matrix one can construct a toric diagram with hyper-volume N by multiplying the matrix on the Cartesian basis in D dimensions, $\{(1, 0, \ldots, 0), (0, 1, 0, \ldots, 0), \ldots, (0, \ldots, 0, 1)\}$. The set of all toric diagrams will henceforth be called the set of HNF's.

All HNF's of order N and given dimension D form a set $D(N)$. Denoting the permutation group of order D by S_D,[1] one observes that every permutation $g \in S_D$ forms an automorphism of $D(N)$,

$$ g \; : \; D(N) \; \overset{\cong}{\to} \; D(N) \; . \tag{2.2.17} $$

Observation 2.2.2. *Under all $g \in S_D$, $D(N)$ is partitioned into $\mathbf{g}^D(N)$ subsets where each subset $[\sigma^{D-1}]$ corresponds to a distinct Abelian orbifold of the form $\mathbb{C}^D/\Gamma_N$.*

A consequence of the above observation is the following:

Observation 2.2.3. *A subset $[\sigma^{D-1}] \in D(N)$ which corresponds to a distinct orbifold of the form $\mathbb{C}^D/\Gamma_N$ is mapped onto itself under all $g \in S_D$.*

Example. Let us consider an example with orbifolds of the form $\mathbb{C}^4/\Gamma_2$. The corresponding set of all possible HNF matrices $D(2)$ is given by

$$ \left\{ \begin{pmatrix} 1 & 0 & 0 \\ 0 & 1 & 0 \\ 0 & 0 & 2 \end{pmatrix}, \begin{pmatrix} 1 & 0 & 0 \\ 0 & 1 & 1 \\ 0 & 0 & 2 \end{pmatrix}, \begin{pmatrix} 1 & 0 & 1 \\ 0 & 1 & 0 \\ 0 & 0 & 2 \end{pmatrix}, \begin{pmatrix} 1 & 0 & 1 \\ 0 & 1 & 1 \\ 0 & 0 & 2 \end{pmatrix}, \begin{pmatrix} 1 & 0 & 0 \\ 0 & 2 & 0 \\ 0 & 0 & 1 \end{pmatrix}, \begin{pmatrix} 1 & 1 & 0 \\ 0 & 2 & 0 \\ 0 & 0 & 1 \end{pmatrix}, \begin{pmatrix} 2 & 0 & 0 \\ 0 & 1 & 0 \\ 0 & 0 & 1 \end{pmatrix} \right\} \; . $$

The corresponding toric tetrahedra are shown respectively in Figure 2.7.

Orbifold Symmetries. Let C_g be a transformation on the topological character τ of a toric simplex σ^{D-1} where $g \in S_D$. C_g is defined as the g-permutation of the barycentric coordinate axes which define τ. If for a given transformation C_g the topological character τ of σ^{D-1} is invariant, then we call C_g and the corresponding cycle $g \in S_D$ a **symmetry** of σ^{D-1}.
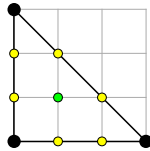
Figure 2.8: The toric diagram of $\mathbb{C}^3/\mathbb{Z}_3 \times \mathbb{Z}_3$.

Example. Let us consider 4 elements of the topological character of the orbifold of the form $\mathbb{C}^3/\mathbb{Z}_3 \times \mathbb{Z}_3$ with the toric triangle shown in Figure 2.8. The 4 elements correspond

---

[1]Elements of a permutation group are written in cyclic form. For example, $S_3 = \{(1)(2)(3), (1\ 2)(3), (1)(2\ 3), (1\ 3)(2), (1\ 2\ 3), (1\ 3\ 2)\}$.

to the barycentric coordinates of the 3 corner points and the green internal point, and are

$$\tau = \{(0, 0, 1), (0, 1, 0), (1, 0, 0), (1/3, 1/3, 1/3), \dots\} \ .$$

By transforming under $C_{(1\ 2\ 3)}$ which is a cyclic permutation of all 3 barycentric coordinate axes, we see that the elements which correspond to the corner points are permuted whilst the element corresponding to the internal point is mapped onto itself. Accordingly, we note that under $C_{(1\ 2\ 3)}$, from considering just the first 4 elements, τ is invariant under the cycle $(1\ 2\ 3) \in S_3$.

2.2.5 Counting Orbifold Symmetries

$$Z_{S_4} = \tfrac{1}{24} \left(x_1^4 + 6x_1^2 x_2 + 3x_2^2 + 8x_1 x_3 + 6x_4 \right)$$

(1 2)	(1 2)(3 4)	(1 2 3)	(1 2 3 4)
(1 3)	(1 3)(2 4)	(1 2 4)	(1 2 4 3)
(1 4)	(1 4)(2 3)	(1 3 2)	(1 3 2 4)
(2 3)		(1 3 4)	(1 3 4 2)
(2 4)		(1 4 2)	(1 4 2 3)
(3 4)		(1 4 3)	(1 4 3 2)
		(2 3 4)	
		(2 4 3)	

Figure 2.9: The cycle index of S_4 and the S_4 cycles corresponding to terms of the cycle index.

The Cycle Index of S_D. The cycle index Z_{S_D} of a permutation group S_D is a polynomial in D variables where every monomial term corresponds to a conjugacy class of S_D. The coefficient of a monomial term is the ratio between the number of elements in the corresponding conjugacy class and the total number of elements in S_D.

Let a cycle $g \in S_D$ be denoted as $g = \{\gamma^i\}$ where $i = 1, \dots, |g| = M$. Each subcycle $\gamma^i \in g$ permutes $n_i = |\gamma_i|$ elements at positions $\{m_1^i, \dots, m_{n_i}^i\}$. Furthermore, let $\alpha = 1, \dots, N_H$ be the index over conjugacy classes H_α of S_D.

Using this notation, the cycle index of S_D is given by

$$Z_{S_D} = \frac{1}{|S_D|} \sum_{\alpha=1}^{N_H} \left(|H_\alpha| \prod_{i=1}^{M} x_{n_i(g_\alpha)} \right) \ , \tag{2.2.18}$$

The cycle index of S_D can be found recursively using

$$Z_{S_D} = \frac{1}{D} \sum_{r=1}^{D} x_r \, Z_{S_{D-r}} \ , \tag{2.2.19}$$

D	Orbifold	Cycle Index
1	$\mathbb{C}$	$Z_{S_1} = x_1$
2	$\mathbb{C}^2/\Gamma_N$	$Z_{S_2} = \frac{1}{2}\left(x_1^2 + x_2\right)$
3	$\mathbb{C}^3/\Gamma_N$	$Z_{S_3} = \frac{1}{6}\left(x_1^3 + 3x_1 x_2 + 2x_3\right)$
4	$\mathbb{C}^4/\Gamma_N$	$Z_{S_4} = \frac{1}{24}\left(x_1^4 + 6x_1^2 x_2 + 3x_2^2 + 8x_1 x_3 + 6x_4\right)$
5	$\mathbb{C}^5/\Gamma_N$	$Z_{S_5} = \frac{1}{120}\left(x_1^5 + 10x_1^3 x_2 + 15x_1 x_2^2 + 20x_1^2 x_3 + 20x_2 x_3 + 30x_1 x_4 + 24x_5\right)$
6	$\mathbb{C}^6/\Gamma_N$	$Z_{S_6} = \frac{1}{720}(x_1^6 + 15x_1^4 x_2 + 45x_1^2 x_2^2 + 15x_2^3 + 40x_1^3 x_3 + 120x_1 x_2 x_3 + 40x_3^2$ $+ 90x_1^2 x_4 + 90x_2 x_4 + 144x_1 x_5 + 120x_6)$
7	$\mathbb{C}^7/\Gamma_N$	$Z_{S_7} = \frac{1}{5040}(x_1^7 + 21x_1^5 x_2 + 105x_1^3 x_2^2 + 105x_1 x_2^3 + 70x_1^4 x_3 + 420x_1^2 x_2 x_3$ $+ 210x_2^2 x_3 + 280x_1 x_3^2 + 210x_1^3 x_4 + 630x_1 x_2 x_4 + 420x_3 x_4$ $+ 504x_1^2 x_5 + 504x_2 x_5 + 840x_1 x_6 + 720x_7)$
8	$\mathbb{C}^8/\Gamma_N$	$Z_{S_8} = \frac{1}{40320}(x_1^8 + 28x_1^6 x_2 + 210x_1^4 x_2^2 + 420x_1^2 x_2^3 + 105x_2^4 + 112x_1^5 x_3$ $+ 1120x_1^3 x_2 x_3 + 1680x_1 x_2^2 x_3 + 1120x_1^2 x_3^2 + 1120x_2 x_3^2$ $+ 420x_1^4 x_4 + 2520x_1^2 x_2 x_4 + 1260x_2^2 x_4 + 3360x_1 x_3 x_4 + 1260x_4^2$ $+ 1344x_1^3 x_5 + 4032x_1 x_2 x_5 + 2688x_3 x_5 + 3360x_1^2 x_6 + 3360x_2 x_6$ $+ 5760x_1 x_7 + 5040x_8)$
9	$\mathbb{C}^9/\Gamma_N$	$Z_{S_9} = \frac{1}{362880}(x_1^9 + 36x_1^7 x_2 + 378x_1^5 x_2^2 + 1260x_1^3 x_2^3 + 945x_1 x_2^4$ $+ 168x_1^6 x_3 + 2520x_1^4 x_2 x_3 + 7560x_1^2 x_2^2 x_3 + 2520x_2^3 x_3$ $+ 3360x_1^3 x_3^2 + 10080x_1 x_2 x_3^2 + 2240x_3^3 + 756x_1^5 x_4 + 7560x_1^3 x_2 x_4$ $+ 11340x_1 x_2^2 x_4 + 15120x_1^2 x_3 x_4 + 15120x_2 x_3 x_4 + 11340x_1 x_4^2$ $+ 3024x_1^4 x_5 + 18144x_1^2 x_2 x_5 + 9072x_2^2 x_5 + 24192x_1 x_3 x_5$ $+ 18144x_4 x_5 + 10080x_1^3 x_6 + 30240x_1 x_2 x_6 + 20160x_3 x_6$ $+ 25920x_1^2 x_7 + 25920x_2 x_7 + 45360x_1 x_8 + 40320x_9)$

Table 2.1: The first nine cycle indices of S_D and the corresponding Abelian orbifolds.

where $Z_{S_0} = 1$. The first 9 cycle indices are shown in Table 2.1.

Polya's Enumeration Theorem. We recall that the set of HNF's $D(N)$ is invariant under all $g \in S_D$ and is partitioned into $\mathbf{g}^{(D)}(N)$ subsets under observation §2.2.2. Each subset corresponds to a distinct Abelian orbifold of the form $\mathbb{C}^{(D)}/\Gamma_N$ and hence $\mathbf{g}^D(N)$ counts the number of distinct Abelian orbifolds of the form $\mathbb{C}^D/\Gamma_N$ at order N.

A single HNF of $D(N)$ is invariant under $g \in S_D$ if C_g is a symmetry of the corresponding toric simplex σ^{D-1}. Let $\mathbf{g}_{x^\alpha}(N)$ be the number of g^α-symmetric HNF's in $D(N)$ where $g^\alpha \in H_\alpha$. x^α is a label of the α-term in the cycle index of S_D, and the corresponding conjugacy class H_α.

Under **Polya's Enumeration Theorem**, $Z_{S_D} = \mathbf{g}^{(D)}(N)$ if we insert for every monomial factor x^α in Z_{S_D} the count $\mathbf{g}_{x^\alpha}(N)$ such that $x^\alpha = \mathbf{g}_{x^\alpha}(N)$. We recall that $\mathbf{g}^{(D)}(N)$ is the number of distinct toric simplices σ^{D-1} of hyper-volume N and equivalently the number of distinct Abelian orbifolds of the form $\mathbb{C}^D/\Gamma_N$.

For the first three dimensions, the cycle indices are re-written as

$$Z_{S_1} = x_1 \quad \Rightarrow \quad \mathbf{g}^{(D=1)}(N) = \mathbf{g}_{x_1}(N)$$

$$Z_{S_2} = \frac{1}{2}\left(x_1^2 + x_2\right) \quad \Rightarrow \quad \mathbf{g}^{(D=2)}(N) = \frac{1}{2}\left(\mathbf{g}_{x_1^2}(N) + \mathbf{g}_{x_2}(N)\right)$$

$$Z_{S_3} = \frac{1}{6}\left(x_1^3 + 3x_1 x_2 + 2x_3\right) \quad \Rightarrow \quad \mathbf{g}^{(D=3)}(N) =$$
$$\frac{1}{6}\left(\mathbf{g}_{x_1^3}(N) + 3\mathbf{g}_{x_1 x_2}(N) + 2\mathbf{g}_{x_3}(N)\right) .$$

$$(2.2.20)$$

The Counting Algorithm. In summary, the following algorithm is used to count distinct orbifolds of the form $\mathbb{C}^D/\Gamma_N$ and HNF's symmetric under cycles of S_D:
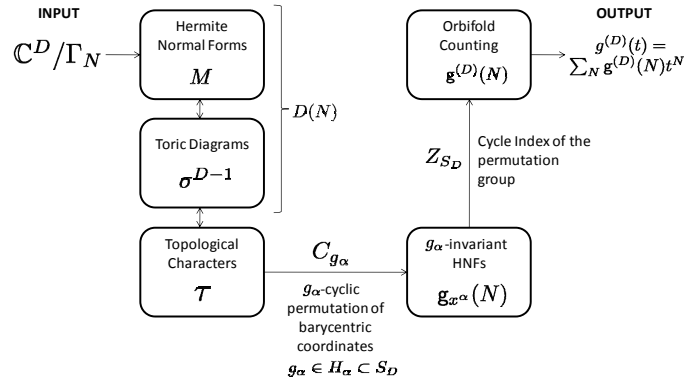
The input of the algorithm is the dimension D and the order N of orbifolds of the form $\mathbb{C}^D/\Gamma_N$ where $\Gamma_N \subset SU(D)$. The output is the counting $\mathbf{g}^{(D)}(N)$ of distinct Abelian orbifolds of $\mathbb{C}^D$. A by-product is the counting $\mathbf{g}_{x^\alpha}(N)$ of HNF's which are invariant under the cycle $g_\alpha \in H_\alpha \subset S_D$ where H_α is a conjugacy class of S_D.

2.3 The Symmetries of Abelian Orbifolds of $\mathbb{C}^3$, $\mathbb{C}^4$, $\mathbb{C}^5$ and $\mathbb{C}^6$

2.3.1 Counting Symmetric Orbifolds

Our explicit counting is presented in Table 2.2 for $\mathbb{C}^3/\Gamma_N$, in Table 2.3 for $\mathbb{C}^4/\Gamma_N$, in Table 2.4 and Table 2.5 for $\mathbb{C}^5/\Gamma_N$ and in Table 2.6 for $\mathbb{C}^6/\Gamma_N$.

The orbifold counting confirms the results presented in [1]. The sequences $\mathbf{g}_{x^\alpha}$ which count g^α-symmetric HNF's of $\mathbb{C}^3/\Gamma_N$ and $\mathbb{C}^4/\Gamma_N$ also match the results in [126]. Accordingly, the counting method presented above gives a geometrical interpretation to the sequences in [126].

2.3.2 Partition Functions

Let an infinite sequence $\mathbf{g}$ be expressed as a partition function $g(t) = \sum_{n=1}^{\infty} \mathbf{g}(n)t^n$. The partition functions $g^{(D)}(t) = \sum_{N=1}^{\infty} \mathbf{g}^{(D)}(N)t^N$ for sequences of $\mathbb{C}^3/\Gamma_N$ and $\mathbb{C}^4/\Gamma_N$ are presented in [126, 1], and are summarized below.[2]

---

[2]Note: We use $g(t)$ for partition functions and $\mathbf{g}(N)$ for an element of a sequence.

Partition Functions for $\mathbb{C}^3/\Gamma_N$. The partition functions for the sequences that count g^α-symmetric HNF's which correspond to Abelian orbifolds of $\mathbb{C}^3$ can be presented in terms of rational functions $f(t)$. A partition function $g(t)$ is expressed as $g(t) = \sum_{k=1}^{\infty} f(t^k)$. The rational functions for the symmetries of $\mathbb{C}^3/\Gamma_N$ are

$$f_{x_1^3}(t) = \frac{(1-t^6)}{(1-t)(1-t^2)(1-t^3)} - 1 \ , \quad f_{x_1 x_2}(t) = \frac{(1+t^3)}{(1-t)(1+t^2)} - 1 \ ,$$

$$f_{x_3}(t) = \frac{(1-t^2)^2}{(1-t)(1-t^3)} - 1 \ , \tag{2.3.21}$$

such that the partition function for distinct $\mathbb{C}^3/\Gamma_N$ is

$$
\begin{aligned}
g^{(D=3)}(t) &= \sum_{k=1}^{\infty} f^{(D=3)}(t^k) \\
&= \frac{1}{6} \sum_{k=1}^{\infty} \left(f_{x_1^3}(t^k) + 3 f_{x_1 x_2}(t^k) + 2 f_{x_3}(t^k) \right) \ .
\end{aligned} \tag{2.3.22}
$$

The rational function for $g^{(D=3)}(t)$ is

$$f^{(D=3)}(t) = \frac{1}{(1-t)(1+t^2)(1-t^3)} - 1 \ . \tag{2.3.23}$$

We note that the sequences which are generated in (2.3.21) can be expressed as Dirichlet Series and in terms of Riemann zeta functions as shown in [126].

Partition Functions for $\mathbb{C}^4/\Gamma_N$. The rational functions for the symmetries of $\mathbb{C}^4/\Gamma_N$ are

$$
\begin{aligned}
f_{x_1^4}(t) &= \sum_{n,m=1}^{\infty} n m^2 t^{mn} \ , \\
f_{x_1^2 x_2}(t) &= \sum_{n,m=1}^{\infty} m \left(t^{mn} - t^{2mn} + 4 t^{4mn} \right) \ , \\
f_{x_2^2}(t) &= \sum_{n,m=1}^{\infty} m \left(t^{mn} - t^{2mn} + 4 t^{4mn} \right) \ , \\
f_{x_1 x_3}(t) &= \frac{1}{2} \left[\sum_{n,m=-\infty}^{\infty} t^{n^2+4m^2} - 1 \right] \\
f_{x_4}(t) &= \frac{1}{2} \left[\sum_{n,m=-\infty}^{\infty} t^{n^2+mn+7m^2} - 1 \right] \ .
\end{aligned} \tag{2.3.24}
$$

These can also be expressed as Dirichlet Series and in terms of Riemann zeta functions.

$\mathbb{C}^3/\Gamma_N$									
N	1	2	3	4	5	6	7	8	9	10
$\mathbf{g}_{x_1^3}$	1	3	4	7	6	12	8	15	13	18
$\mathbf{g}_{x_1x_2}$	1	1	2	3	2	2	2	5	3	2
$\mathbf{g}_{x_3}$	1	0	1	1	0	0	2	0	1	0
$g^{(D=3)}$	1	1	2	3	2	3	3	5	4	4
N	11	12	13	14	15	16	17	18	19	20
$\mathbf{g}_{x_1^3}$	12	28	14	24	24	31	18	39	20	42
$\mathbf{g}_{x_1x_2}$	2	6	2	2	4	7	2	3	2	6
$\mathbf{g}_{x_3}$	0	1	2	0	0	1	0	0	2	0
$g^{(D=3)}$	3	8	4	5	6	9	4	8	5	10
N	21	22	23	24	25	26	27	28	29	30
$\mathbf{g}_{x_1^3}$	32	36	24	60	31	42	40	56	30	72
$\mathbf{g}_{x_1x_2}$	4	2	2	10	3	2	4	6	2	4
$\mathbf{g}_{x_3}$	2	0	0	0	1	0	1	2	0	0
$g^{(D=3)}$	8	7	5	15	7	8	9	13	6	14
N	31	32	33	34	35	36	37	38	39	40
$\mathbf{g}_{x_1^3}$	32	63	48	54	48	91	38	60	56	90
$\mathbf{g}_{x_1x_2}$	2	9	4	2	4	9	2	2	4	10
$\mathbf{g}_{x_3}$	2	0	0	0	0	1	2	0	2	0
$g^{(D=3)}$	7	15	10	10	10	20	8	11	12	20
N	41	42	43	44	45	46	47	48	49	50
$\mathbf{g}_{x_1^3}$	42	96	44	84	78	72	48	124	57	93
$\mathbf{g}_{x_1x_2}$	2	4	2	6	6	2	2	14	3	3,
g_{x_3}	0	0	2	0	0	0	0	1	3	0
$g^{(D=3)}$	8	18	9	17	16	13	9	28	12	17
N	51	52	53	54	55	56	57	58	59	60
$\mathbf{g}_{x_1^3}$	72	98	54	120	72	120	80	90	60	168
$\mathbf{g}_{x_1x_2}$	4	6	2	4	4	10	4	2	2	12
$\mathbf{g}_{x_3}$	0	2	0	0	0	0	2	0	0	0
$g^{(D=3)}$	14	20	10	22	14	25	16	16	11	34

Table 2.2: The symmetry count for $\mathbb{C}^3/\Gamma_N$ with cycle index Z_{S_3}.

The partition function for distinct Abelian orbifolds of $\mathbb{C}^4$ is

$$g^{(D=4)}(t) \;=\; \frac{1}{24}\sum_{k=1}^{\infty}\Big(f_{x_1^4}(t^k) + 6f_{x_1^3x_2}(t^k) + 3f_{x_2^2}(t^k) + 8f_{x_1x_3}(t^k) + 6f_{x_4}(t^k)\Big)\;.$$

(2.3.25)

2.4 Prime Index Sequences and Series Convolutions

2.4.1 Series Convolutions

Sequences that count g^{α}-symmetric HNF's which correspond to Abelian orbifolds of $\mathbb{C}^D$ can be expressed in terms of sequence convolutions. A sequence $\mathbf{g} = \{\mathbf{g}(1), \mathbf{g}(2), \mathbf{g}(3), \dots\}$ is related to its corresponding partition function by $g(t) = \sum_{n=1}^{\infty}\mathbf{g}(n)t^n$.

$\mathbb{C}^4/\Gamma_N$									
N	1	2	3	4	5	6	7	8	9	10
$\mathsf{g}_{x_1^4}$	1	7	13	35	31	91	57	155	130	217
$\mathsf{g}_{x_1^2 x_2}$	1	3	5	11	7	15	9	31	18	21
$\mathsf{g}_{x_2^2}$	1	3	5	11	7	15	9	31	18	21
$\mathsf{g}_{x_1 x_3}$	1	1	1	2	1	1	3	2	4	1
g_{x_4}	1	1	1	3	3	1	1	5	2	3
$g^{(D=4)}$	1	2	3	7	5	10	7	20	14	18
N	11	12	13	14	15	16	17	18	19	20
$\mathsf{g}_{x_1^4}$	133	455	183	399	403	651	307	910	381	1085
$\mathsf{g}_{x_1^2 x_2}$	13	55	15	27	35	75	19	54	21	77
$\mathsf{g}_{x_2^2}$	13	55	15	27	35	75	19	54	21	77
$\mathsf{g}_{x_1 x_3}$	1	2	3	3	1	3	1	4	3	2
g_{x_4}	1	3	3	1	3	7	3	2	1	9
$g^{(D=4)}$	11	41	15	28	31	58	21	60	25	77
N	21	22	23	24	25	26	27	28	29	30
$\mathsf{g}_{x_1^4}$	741	931	553	2015	806	1281	1210	1995	871	2821
$\mathsf{g}_{x_1^2 x_2}$	45	39	25	155	38	45	58	99	31	105
$\mathsf{g}_{x_2^2}$	45	39	25	155	38	45	58	99	31	105
$\mathsf{g}_{x_1 x_3}$	3	1	1	2	2	3	7	6	1	1
g_{x_4}	1	1	1	5	6	3	2	3	3	3
$g^{(D=4)}$	49	54	33	144	50	72	75	123	49	158
N	31	32	33	34	35	36	37	38	39	40
$\mathsf{g}_{x_1^4}$	993	2667	1729	2149	1767	4550	1407	2667	2379	4805
$\mathsf{g}_{x_1^2 x_2}$	33	167	65	57	63	198	39	63	75	217
$\mathsf{g}_{x_2^2}$	33	167	65	57	63	198	39	63	75	217
$\mathsf{g}_{x_1 x_3}$	3	3	1	1	3	8	3	3	3	2
g_{x_4}	1	9	1	3	3	6	3	1	3	15
$g^{(D=4)}$	55	177	97	112	99	268	75	136	129	286
N	41	42	43	44	45	46	47	48	49	50
$\mathsf{g}_{x_1^4}$	1723	5187	1893	4655	4030	3871	2257	8463	2850	5642
$\mathsf{g}_{x_1^2 x_2}$	43	135	45	143	126	75	49	375	66	114
$\mathsf{g}_{x_2^2}$	43	135	45	143	126	75	49	375	66	114
$\mathsf{g}_{x_1 x_3}$	1	3	3	2	4	1	1	3	6	2
g_{x_4}	3	1	1	3	6	1	1	7	2	6
$g^{(D=4)}$	89	268	97	249	218	190	113	496	146	280

Table 2.3: The symmetry count for $\mathbb{C}^4/\Gamma_N$ with cycle index Z_{S_4}.

Partition Functions and Sequence Convolutions. As outlined in [126] and [145], given a sequence $\mathsf{q} = \mathsf{r} * \mathsf{s}$ generated by a convolution of the sequences r and s, the partition function for the sequence q, $q(t)$, is expressed as,

$$q(t) \;=\; \sum_{m,k=1}^{\infty} \mathsf{r}(m)\mathsf{s}(k)t^{mk} \;=\; \sum_{m=1}^{\infty} \mathsf{r}(m)s(t^m) \;=\; \sum_{m=1}^{\infty} \mathsf{s}(m)r(t^m)\;, \qquad (2.4.26)$$

where $r(t)$ and $s(t)$ are the partition functions of the sequences r and s respectively. We invert (2.4.26) as follows

$$r(t) \;=\; \sum_{m=1}^{\infty} q(t^k)\mathsf{s}(k)\mu(k)\;, \qquad (2.4.27)$$

where $\mu(n)$ is the Möbius function. It is expected that the above inversion is valid for

	$\mathbb{C}^5/\Gamma_N$									
N	1	2	3	4	5	6	7	8	9	10
$\mathsf{g}_{x_1^5}$	1	15	40	155	156	600	400	1395	1210	2340
$\mathsf{g}_{x_1^3 x_2}$	1	7	14	43	32	98	58	219	144	224
$\mathsf{g}_{x_1 x_2^2}$	1	3	8	19	12	24	16	75	42	36
$\mathsf{g}_{x_1^2 x_3}$	1	3	4	8	6	12	10	18	22	18
$\mathsf{g}_{x_2 x_3}$	1	1	2	4	2	2	4	6	6	2
$\mathsf{g}_{x_1 x_4}$	1	1	2	3	4	2	2	7	4	4
g_{x_5}	1	0	0	0	1	0	0	0	0	0
$g^{(D=5)}$	1	2	4	10	8	19	13	45	33	47
N	11	12	13	14	15	16	17	18	19	20
$\mathsf{g}_{x_1^5}$	1464	6200	2380	6000	6240	11811	5220	18150	7240	24180
$\mathsf{g}_{x_1^3 x_2}$	134	602	184	406	448	995	308	1008	382	1376
$\mathsf{g}_{x_1 x_2^2}$	24	152	28	48	96	251	36	126	40	228
$\mathsf{g}_{x_1^2 x_3}$	12	32	16	30	24	39	18	66	22	48
$\mathsf{g}_{x_2 x_3}$	2	8	4	4	4	11	2	6	4	8
$\mathsf{g}_{x_1 x_4}$	2	6	4	2	8	19	4	4	2	12
g_{x_5}	4	0	0	0	0	1	0	0	0	0
$g^{(D=5)}$	30	129	43	96	108	226	78	264	102	357
N	21	22	23	24	25	26	27	28	29	30
$\mathsf{g}_{x_1^5}$	16000	21960	12720	55800	20306	35700	33880	62000	25260	93600
$\mathsf{g}_{x_1^3 x_2}$	812	938	554	3066	838	1288	1354	2494	872	3136
$\mathsf{g}_{x_1 x_2^2}$	128	72	48	600	98	84	184	304	60	288
$\mathsf{g}_{x_1^2 x_3}$	40	36	24	72	32	48	85	80	30	72
$\mathsf{g}_{x_2 x_3}$	8	2	2	12	4	4	13	16	2	4
$\mathsf{g}_{x_1 x_4}$	4	2	2	14	10	4	6	6	4	8
g_{x_5}	0	0	0	0	1	0	0	0	0	0
$g^{(D=5)}$	226	277	163	813	260	425	436	780	297	1092
N	31	32	33	34	35	36	37	38	39	40
$\mathsf{g}_{x_1^5}$	30784	97155	58560	78300	62400	187550	52060	108600	95200	217620
$\mathsf{g}_{x_1^3 x_2}$	994	4251	1876	2156	1856	6192	1408	2674	2576	7008
$\mathsf{g}_{x_1 x_2^2}$	64	747	192	108	192	798	76	120	224	900
$\mathsf{g}_{x_1^2 x_3}$	34	81	48	54	60	176	40	66	64	108
$\mathsf{g}_{x_2 x_3}$	4	15	4	2	8	24	4	4	8	12
$\mathsf{g}_{x_1 x_4}$	2	31	4	4	8	12	4	2	8	28
g_{x_5}	4	0	0	0	0	0	0	0	0	0
$g^{(D=5)}$	355	1281	678	856	712	2202	569	1155	1050	2537

Table 2.4: The symmetry count for $\mathbb{C}^5/\Gamma_N$ with cycle index Z_{S_5} (**Part 1/2**).

particular sequences r and s which are discussed and used below.

Multiplicative Sequences. As first noted in [126], the sequences g_{x^α} in Tables 2.2-2.6 which count g^α-symmetric HNF's are *multiplicative*. Multiplicativity of g_{x^α} says that given two integers q_1 and q_2 with $\gcd(q_1, q_2) = 1$, we have

$$\mathsf{g}_{x^\alpha}(q_1)\mathsf{g}_{x^\alpha}(q_2) = \mathsf{g}_{x^\alpha}(q_1 q_2) \ . \tag{2.4.28}$$

This property can be seen from the counting of orbifold symmetries and is related to the convolution property in (2.4.26).

Standard Sequences. Convolution preserves multiplicativity, and therefore it is useful

	$\mathbb{C}^5/\Gamma_N$									
N	41	42	43	44	45	46	47	48	49	50
$\mathbf{g}_{x_1^5}$	70644	240000	81400	226920	188760	190800	106080	472440	140050	304590
$\mathbf{g}_{x_1^3 x_2}$	1724	5684	1894	5762	4608	3878	2258	13930	2908	5866
$\mathbf{g}_{x_1 x_2^2}$	84	384	88	456	504	144	96	2008	178	294
$\mathbf{g}_{x_1^2 x_3}$	42	120	46	96	132	72	48	156	76	96
$\mathbf{g}_{x_2 x_3}$	2	8	4	8	12	2	2	22	10	4
$\mathbf{g}_{x_1 x_4}$	4	4	2	6	16	2	2	38	4	10
$\mathbf{g}_{x_5}$	4	0	0	0	0	0	0	0	0	0
$g^{(D=5)}$	752	2544	856	2447	2048	1944	1093	5388	1447	3083
N	51	52	53	54	55	56	57	58	59	60
$\mathbf{g}_{x_1^5}$	208800	368900	151740	508200	228384	558000	289600	378900	208920	967200
$\mathbf{g}_{x_1^3 x_2}$	4312	7912	2864	9478	4288	12702	5348	6104	3542	19264
$\mathbf{g}_{x_1 x_2^2}$	288	532	108	552	288	1200	320	180	120	1824
$\mathbf{g}_{x_1^2 x_3}$	72	128	54	255	72	180	88	90	60	192
$\mathbf{g}_{x_2 x_3}$	4	16	2	13	4	24	8	2	2	16
$\mathbf{g}_{x_1 x_4}$	8	12	4	6	8	14	4	4	2	24
$\mathbf{g}_{x_5}$	0	0	0	0	4	0	0	0	0	0
$g^{(D=5)}$	2150	3827	1527	5140	2312	5896	2916	3705	2062	9934
N	61	62	63	64	65	66	67	68	69	70
$\mathbf{g}_{x_1^5}$	230764	461760	484000	788035	371280	878400	305320	809100	508800	936000
$\mathbf{g}_{x_1^3 x_2}$	3784	6958	8352	17587	5888	13132	4558	13244	7756	12992
$\mathbf{g}_{x_1 x_2^2}$	124	192	672	2043	336	576	136	684	384	576
$\mathbf{g}_{x_1^2 x_3}$	64	102	220	166	96	144	70	144	96	180
$\mathbf{g}_{x_2 x_3}$	4	4	24	22	8	4	4	8	4	8
$\mathbf{g}_{x_1 x_4}$	4	2	8	51	16	4	2	12	4	8
$\mathbf{g}_{x_5}$	4	0	0	0	0	0	0	0	0	0
$g^{(D=5)}$	2267	4470	4856	8332	3684	8512	2954	7960	4952	8988
N	71	72	73	74	75	76	77	78	79	80
$\mathbf{g}_{x_1^5}$	363024	1687950	394420	780900	812240	1122200	585600	1428000	499360	1842516
$\mathbf{g}_{x_1^3 x_2}$	5114	31536	5404	9856	11732	16426	7772	18032	6322	31840
$\mathbf{g}_{x_1 x_2^2}$	144	3150	148	228	784	760	384	672	160	3012
$\mathbf{g}_{x_1^2 x_3}$	72	396	76	120	128	176	120	192	82	234
$\mathbf{g}_{x_2 x_3}$	2	36	4	4	8	16	8	8	4	22
$\mathbf{g}_{x_1 x_4}$	2	28	4	4	20	6	4	8	2	76
$\mathbf{g}_{x_5}$	4	0	0	0	0	0	0	0	0	1
$g^{(D=5)}$	3483	17167	3770	7379	7872	10849	5598	13522	4723	18446

Table 2.5: The symmetry count for $\mathbb{C}^5/\Gamma_N$ with cycle index Z_{S_5} (**Part 2/2**).

to discuss basic multiplicative sequences.

- The unit sequence:

$$\mathsf{u} = \{1, 1, 1, \dots\} \;\Leftrightarrow\; u(t) = \sum_{n=1}^{\infty} t^n = t + t^2 + t^3 + \dots \tag{2.4.29}$$

- The natural number sequence:

$$\mathsf{N} = \{1, 2, 3, \dots\} \;\Leftrightarrow\; N(t) = \sum_{n=1}^{\infty} n t^n = t + 2t^2 + 3t^3 + \dots \tag{2.4.30}$$

$\mathbb{C}^6/\Gamma_N$										
N	1	2	3	4	5	6	7	8	9	10
$g_{x_1^6}$	1	31	121	651	781	3751	2801	11811	11011	24211
$g_{x_1^4 x_2}$	1	15	41	171	157	615	401	1651	1251	2355
$g_{x_1^2 x_2^2}$	1	7	17	59	37	119	65	371	195	259
$g_{x_2^3}$	1	7	17	59	37	119	65	371	195	259
$g_{x_1^3 x_3}$	1	7	13	36	31	91	59	162	157	217
$g_{x_1 x_2 x_3}$	1	3	5	12	7	15	11	34	27	21
$g_{x_1^2 x_4}$	1	3	5	11	9	15	9	35	19	27
$g_{x_2 x_4}$	1	3	5	11	9	15	9	35	19	27
$g_{x_3^2}$	1	1	4	6	1	4	17	6	22	1
$g_{x_1 x_5}$	1	1	1	1	1	1	1	1	1	1
g_{x_6}	1	1	2	2	1	2	5	2	6	1
$g^{(D=6)}$	1	3	6	17	13	40	27	106	78	127
N	11	12	13	14	15	16	17	18	19	20
$g_{x_1^6}$	16105	78771	30941	86831	94501	200787	88741	341341	137561	508431
$g_{x_1^4 x_2}$	1465	7011	2381	6015	6437	14547	5221	18765	7241	26847
$g_{x_1^2 x_2^2}$	145	1003	197	455	629	1987	325	1365	401	2183
$g_{x_2^3}$	145	1003	197	455	629	1987	325	1365	401	2183
$g_{x_1^3 x_3}$	133	468	185	413	403	687	307	1099	383	1116
$g_{x_1 x_2 x_3}$	13	60	17	33	35	87	19	81	23	84
$g_{x_1^2 x_4}$	13	55	17	27	45	115	21	57	21	99
$g_{x_2 x_4}$	13	55	17	27	45	115	21	57	21	99
$g_{x_3^2}$	1	24	29	17	4	27	1	22	41	6
$g_{x_1 x_5}$	5	1	1	1	1	2	1	1	1	1
g_{x_6}	1	4	5	5	2	7	1	6	5	2
$g^{(D=6)}$	79	391	129	321	358	832	285	1070	409	1549

Table 2.6: The symmetry count for $\mathbb{C}^6/\Gamma_N$ with cycle index Z_{S_6}.

- Powers of the natural number sequence:

$$\mathsf{N}^d = \{1^d, 2^d, 3^d, \dots\} \;\Leftrightarrow\; N^d(t) = \sum_{n=1}^{\infty} n^d t^n = t + 2^d t^2 + 3^d t^3 + \dots \;, \quad (2.4.31)$$

where $\mathsf{N}^0 = \mathsf{u}$.

- The Dirichlet character $\chi_{k,m}$ of modulo k and index m is defined under the conditions

$$
\begin{aligned}
\chi_{k,m}(1) &= 1 \\
\chi_{k,m}(a) &= \chi_{k,m}(a+k) \\
\chi_{k,m}(a)\chi_{k,m}(b) &= \chi_{k,m}(ab) \\
\chi_{k,m}(a) &= 0 \text{ if } \gcd(k,a) \neq 1 \;.
\end{aligned}
\quad (2.4.32)
$$

Under these conditions there are several solutions which are parameterized by m.

The Dirichlet characters up to modulo 10 used in this chapter are

$$\chi_{1,1} = \mathsf{u} \qquad\qquad\qquad\qquad \chi_{8,1} = \{1, 0, 1, 0, 1, 0, 1, 0, \dots\}$$
$$\chi_{2,1} = \{1, 0, \dots\} \qquad\qquad\qquad \chi_{8,2} = \{1, 0, 1, 0, -1, 0, -1, 0, \dots\}$$
$$\chi_{3,1} = \{1, 1, 0, \dots\} \qquad\qquad\qquad \chi_{8,3} = \{1, 0, -1, 0, 1, 0, -1, 0, \dots\}$$
$$\chi_{3,2} = \{1, -1, 0, \dots\} \qquad\qquad\quad\; \chi_{8,4} = \{1, 0, -1, 0, -1, 0, 1, 0, \dots\}$$
$$\chi_{4,1} = \{1, 0, 1, 0, \dots\} \qquad\qquad\quad \chi_{9,1} = \{1, 1, 0, 1, 1, 0, 1, 1, 0, \dots\}$$
$$\chi_{4,2} = \{1, 0, -1, 0, \dots\} \qquad\qquad\; \chi_{9,2} = \{1, \omega, 0, \omega^2, -\omega^2, 0, -\omega, -1, 0, \dots\}$$
$$\chi_{5,1} = \{1, 1, 1, 1, 0, \dots\} \qquad\qquad \chi_{9,3} = \{1, \omega^2, 0, -\omega, -\omega, 0, \omega^2, 1, 0, \dots\}$$
$$\chi_{5,2} = \{1, i, -i, -1, 0, \dots\} \qquad\quad\; \chi_{9,4} = \{1, -1, 0, 1, -1, 0, 1, -1, 0, \dots\}$$
$$\chi_{5,3} = \{1, -1, -1, 1, 0, \dots\} \qquad\;\, \chi_{9,5} = \{1, -\omega, 0, \omega^2, \omega^2, 0, -\omega, 1, 0, \dots\}$$
$$\chi_{5,4} = \{1, -i, i, -1, 0, \dots\} \qquad\quad \chi_{9,6} = \{1, -\omega^2, 0, -\omega, \omega, 0, \omega^2, -1, 0, \dots\}$$
$$\chi_{6,1} = \{1, 0, 0, 0, 1, 0 \dots\} \qquad\quad \chi_{10,1} = \{1, 0, 1, 0, 0, 0, 1, 0, 1, 0, \dots\}$$
$$\chi_{6,2} = \{1, 0, 0, 0, -1, 0 \dots\} \qquad\; \chi_{10,2} = \{1, 0, i, 0, 0, 0, -i, 0, -1, 0, \dots\}$$
$$\chi_{7,1} = \{1, 1, 1, 1, 1, 1, 0 \dots\} \qquad \chi_{10,3} = \{1, 0, -1, 0, 0, 0, -1, 0, 1, 0, \dots\}$$
$$\chi_{7,2} = \{1, -\omega, \omega^2, \omega^2, -\omega, 1, 0 \dots\} \quad \chi_{10,4} = \{1, 0, -i, 0, 0, 0, i, 0, -1, 0, \dots\}$$
$$\chi_{7,3} = \{1, \omega^2, \omega, -\omega, -\omega^2, -1, 0 \dots\}$$
$$\chi_{7,4} = \{1, 1, -1, 1, -1, -1, 0 \dots\}$$
$$\chi_{7,5} = \{1, -\omega, -\omega^2, \omega^2, \omega, -1, 0 \dots\}$$
$$\chi_{7,6} = \{1, \omega^2, -\omega, -\omega, \omega^2, 1, 0 \dots\}$$

where the first elements given above are the periods of the infinite sequences, and $\omega = \exp \frac{i\pi}{3}$.

The number of distinct Dirichlet characters of period k is given by the Euler totient function $\varphi(k)$. It is defined as the number of integers less than or equal to k which are co-prime to k. For primes p, the totient function takes the values

$$\varphi(p) = p - 1 \ . \tag{2.4.33}$$

Moreover, the direct sum of all distinct Dirichlet characters of period k is given by

$$\sum_{m=1}^{\varphi(k)} \chi_{k,m}(n) = \varphi(k) \ \delta_{n, 1 \bmod k} + \delta_{kn} \ . \tag{2.4.34}$$

The totient function φ is related to the natural number sequence N under

$$\varphi * \mathsf{u} = \mathsf{N} \Leftrightarrow \varphi = \mu * \mathsf{N} \ . \tag{2.4.35}$$

With N being a multiplicative sequence, both the Euler totient function $\varphi(n)$ and Möbius function $\mu(n)$ are multiplicative.

A direct product of any of the above multiplicative sequences,

$$\mathsf{AB} = \{\mathsf{A}(1)\mathsf{B}(1), \mathsf{A}(2)\mathsf{B}(2), \mathsf{A}(3)\mathsf{B}(3), \dots\} \Leftrightarrow \mathsf{AB}(n) = \mathsf{A}(n)\mathsf{B}(n) \ , \tag{2.4.36}$$

is a multiplicative sequence as well. An example is the direct product of $\chi_{3,2}$ and N

$\mathbb{C}^3/\Gamma_N$															
$N=p$	2	3	5	7	11	13	17	19	23	29	31	37	41	43	47	53
$\mathsf{g}_{x_1^3}$	3	4	6	8	12	14	18	20	24	30	32	38	42	44	48	54
$\mathsf{g}_{x_1x_2}$	1	2	2	2	2	2	2	2	2	2	2	2	2	2	2	2
g_{x_3}	0	1	0	2	0	2	0	2	0	0	2	2	0	2	0	0

$\mathbb{C}^4/\Gamma_N$															
$N=p$	2	3	5	7	11	13	17	19	23	29	31	37	41	43	47	53
$\mathsf{g}_{x_1^4}$	7	13	31	57	133	183	307	381	553	871	993	1407	1723	1893	2257	2863
$\mathsf{g}_{x_1^2x_2}$	3	5	7	9	13	15	19	21	25	31	33	39	43	45	49	55
$\mathsf{g}_{x_2^2}$	3	5	7	9	13	15	19	21	25	31	33	39	43	45	49	55
$\mathsf{g}_{x_1x_3}$	1	1	1	3	1	3	1	3	1	1	3	3	1	3	1	1
g_{x_4}	1	1	3	1	1	3	3	1	1	3	1	3	3	1	1	3

$\mathbb{C}^5/\Gamma_N$															
$N=p$	2	3	5	7	11	13	17	19	23	29	31	37	41	43	47	53
$\mathsf{g}_{x_1^5}$	15	40	156	400	1464	2380	5220	7240	12720	25260	30784	52060	70644	81400	106080	151740
$\mathsf{g}_{x_1^3x_2}$	7	14	32	58	134	184	308	382	554	872	994	1408	1724	1894	2258	2864
$\mathsf{g}_{x_1x_2^2}$	3	8	12	16	24	28	36	40	48	60	64	76	84	88	96	108
$\mathsf{g}_{x_1^2x_3}$	3	4	6	10	12	16	18	22	24	30	34	40	42	46	48	54
$\mathsf{g}_{x_2x_3}$	1	2	2	4	2	4	2	4	2	2	4	4	2	4	2	2
$\mathsf{g}_{x_1x_4}$	1	2	4	2	2	4	4	2	2	4	2	4	4	2	2	4
g_{x_5}	0	0	1	0	4	0	0	0	0	0	4	0	4	0	0	0

Table 2.7: Sequences of $\mathbb{C}^3/\Gamma_N$, $\mathbb{C}^4/\Gamma_N$ and $\mathbb{C}^5/\Gamma_N$ for prime N.

which gives

$$\mathsf{N}_{\chi_{3,2}} = \{1, -2, 0, 4, -5, 0, 7, -8, 0, \dots\} \, . \tag{2.4.37}$$

Furthermore, the direct product of two Dirichlet characters is another Dirichlet character.

2.4.2 Functions on Primes for Prime Index Sequences

Multiplicative sequences are determined by their values at indices which are prime numbers or pure powers of prime. The values on prime indices of sequences in Table 2.2 to Table 2.6 for orbifolds of $\mathbb{C}^3$ to $\mathbb{C}^6$ are shown in Table 2.7 and Table 2.8.

It is of interest to find for a given sequence $\mathsf{g}_{x^\alpha}(p)$ in Table 2.7 and Table 2.8 a function on primes p, $P_{\mathsf{g}_{x^\alpha}}(p)$, which takes the values $P_{\mathsf{g}_{x^\alpha}}(p) = \mathsf{g}_{x^\alpha}(p)$.

Observation 2.4.4. *For every sequence g_{x^α} which counts HNF's symmetric under the cycle $g^\alpha \in H_\alpha \subset S_D$, there is a well defined function $P_{\mathsf{g}_{x^\alpha}}(p)$ over primes p that takes the values $P_{\mathsf{g}_{x^\alpha}}(p) = \mathsf{g}_{x^\alpha}(p)$.*

The function on primes for the sequences of the Abelian orbifolds of $\mathbb{C}^3$ are as follows:

$$P_{\mathbf{g}_{x_1^3}}(p) \;=\; 1+p \tag{2.4.38}$$

$$P_{\mathbf{g}_{x_1 x_2}}(p) \;=\; \begin{cases} 1 & \text{if } p = 2 \\ 2 & \text{if } p \neq 2 \end{cases} \tag{2.4.39}$$

$$P_{\mathbf{g}_{x_3}}(p) \;=\; \begin{cases} 2 & \text{if } p = 1 \mod 3 \\ 0 & \text{if } p = 2 \mod 3 \\ 1 & \text{if } p = 3 \end{cases} . \tag{2.4.40}$$

For the case of Abelian orbifolds of $\mathbb{C}^4$, the functions on primes are of the form

$$P_{\mathbf{g}_{x_1^4}}(p) \;=\; 1+p+p^2 \tag{2.4.41}$$

$$P_{\mathbf{g}_{x_1^2 x_2}}(p) = P_{\mathbf{g}_{x_2^2}}(p) \;=\; \begin{cases} 3 & \text{if } p = 2 \\ p+2 & \text{if } p \neq 2 \end{cases} \tag{2.4.42}$$

$$P_{\mathbf{g}_{x_1 x_3}}(p) \;=\; \begin{cases} 3 & \text{if } p = 1 \mod 3 \\ 1 & \text{if } p = 2 \mod 3 \\ 1 & \text{if } p = 3 \end{cases} \tag{2.4.43}$$

$$P_{\mathbf{g}_{x_4}}(p) \;=\; \begin{cases} 3 & \text{if } p = 1 \mod 4 \\ 1 & \text{if } p = 2 \mod 4 \\ 1 & \text{if } p = 3 \mod 4 \end{cases} . \tag{2.4.44}$$

	$\mathbb{C}^6/\Gamma_N$															
$N=p$	2	3	5	7	11	13	17	19	23	29	31	37	41	43	47	53
$\mathbf{g}_{x_1^6}$	31	121	781	2801	16105	30941	88741	137561	292561	732541	954305	1926221	2896405	3500201	4985761	8042221
$\mathbf{g}_{x_1^4 x_2}$	15	41	157	401	1465	2381	5221	7241	12721	25261	30785	52061	70645	81401	106081	151741
$\mathbf{g}_{x_1^2 x_2^2}$	7	17	37	65	145	197	325	401	577	901	1025	1445	1765	1937	2305	2917
$\mathbf{g}_{x_2^3}$	7	17	37	65	145	197	325	401	577	901	1025	1445	1765	1937	2305	2917
$\mathbf{g}_{x_1^3 x_3}$	7	13	31	59	133	185	307	383	553	871	995	1409	1723	1895	2257	2863
$\mathbf{g}_{x_1 x_2 x_3}$	3	5	7	11	13	17	19	23	25	31	35	41	43	47	49	55
$\mathbf{g}_{x_1^2 x_4}$	3	5	9	9	13	17	21	21	25	33	33	41	45	45	49	57
$\mathbf{g}_{x_2 x_4}$	3	5	9	9	13	17	21	21	25	33	33	41	45	45	49	57
$\mathbf{g}_{x_3^2}$	1	4	1	17	1	29	1	41	1	1	65	77	1	89	1	1
$\mathbf{g}_{x_1 x_5}$	1	1	1	1	5	1	1	1	1	1	5	1	5	1	1	1
$\mathbf{g}_{x_6}$	1	2	1	5	1	5	1	5	1	1	5	5	1	5	1	1

Table 2.8: Sequences of $\mathbb{C}^6/\Gamma_N$ for prime N.

For the case of Abelian orbifolds of $\mathbb{C}^5$, the functions on primes are of the form

$$P_{\mathbf{g}_{x_1^5}}(p) \;=\; 1 + p + p^2 + p^3 \tag{2.4.45}$$

$$P_{\mathbf{g}_{x_1^3 x_2}}(p) \;=\; \begin{cases} 7 & \text{if } p = 2 \\ p^2 + p + 2 & \text{if } p \neq 2 \end{cases} \tag{2.4.46}$$

$$P_{\mathbf{g}_{x_1 x_2^2}}(p) \;=\; \begin{cases} 3 & \text{if } p = 2 \\ 2p + 2 & \text{if } p \neq 2 \end{cases} \tag{2.4.47}$$

$$P_{\mathbf{g}_{x_1^2 x_3}}(p) \;=\; \begin{cases} p + 3 & \text{if } p = 1 \mod 3 \\ p + 1 & \text{if } p = 2 \mod 3 \\ 4 & \text{if } p = 3 \end{cases} \tag{2.4.48}$$

$$P_{\mathbf{g}_{x_2 x_3}}(p) \;=\; \begin{cases} 4 & \text{if } p = 1 \mod 3 \\ 2 & \text{if } p = 2 \mod 3 \\ 1 & \text{if } p = 2 \\ 2 & \text{if } p = 3 \end{cases} \tag{2.4.49}$$

$$P_{\mathbf{g}_{x_1 x_4}}(p) \;=\; \begin{cases} 4 & \text{if } p = 1 \mod 4 \\ 1 & \text{if } p = 2 \mod 4 \\ 2 & \text{if } p = 3 \mod 4 \end{cases} \tag{2.4.50}$$

$$P_{\mathbf{g}_{x_5}}(p) \;=\; \begin{cases} 4 & \text{if } p = 1 \mod 5 \\ 0 & \text{if } p = 2, 3, 4 \mod 5 \\ 1 & \text{if } p = 5 \end{cases} . \tag{2.4.51}$$

For the case of Abelian orbifolds of $\mathbb{C}^6$, the functions on primes are of the form

$$P_{\mathsf{g}_{x_1^6}}(p) = 1 + p + p^2 + p^3 + p^4 \tag{2.4.52}$$

$$P_{\mathsf{g}_{x_1^4 x_2}}(p) = \begin{cases} 15 & \text{if } p = 2 \\ p^3 + p^2 + p + 2 & \text{if } p \neq 2 \end{cases} \tag{2.4.53}$$

$$P_{\mathsf{g}_{x_1^2 x_2^2}}(p) = P_{\mathsf{g}_{x_2^3}}(p) = \begin{cases} 7 & \text{if } p = 2 \\ p^2 + 2p + 2 & \text{if } p \neq 2 \end{cases} \tag{2.4.54}$$

$$P_{\mathsf{g}_{x_1^3 x_3}}(p) = \begin{cases} p^2 + p + 3 & \text{if } p = 1 \mod 3 \\ p^2 + p + 1 & \text{if } p = 2 \mod 3 \\ 13 & \text{if } p = 3 \end{cases} \tag{2.4.55}$$

$$P_{\mathsf{g}_{x_1 x_2 x_3}}(p) = \begin{cases} p + 4 & \text{if } p = 1 \mod 3 \\ p + 2 & \text{if } p = 2 \mod 3 \\ 3 & \text{if } p = 2 \\ 5 & \text{if } p = 3 \end{cases} \tag{2.4.56}$$

$$P_{\mathsf{g}_{x_1^2 x_4}}(p) = P_{\mathsf{g}_{x_2 x_4}}(p) = \begin{cases} p + 4 & \text{if } p = 1 \mod 4 \\ p + 2 & \text{if } p = 3 \mod 4 \\ 3 & \text{if } p = 2 \end{cases} \tag{2.4.57}$$

$$P_{\mathsf{g}_{x_3^2}}(p) = \begin{cases} 2p + 3 & \text{if } p = 1 \mod 3 \\ 1 & \text{if } p = 2 \mod 3 \\ 4 & \text{if } p = 3 \end{cases} \tag{2.4.58}$$

$$P_{\mathsf{g}_{x_1 x_5}}(p) = \begin{cases} 5 & \text{if } p = 1 \mod 5 \\ 1 & \text{if } p = 2, 3, 4 \mod 5 \\ 1 & \text{if } p = 5 \end{cases} \tag{2.4.59}$$

$$P_{\mathsf{g}_{x_6}}(p) = \begin{cases} 5 & \text{if } p = 1 \mod 6 \\ 1 & \text{if } p = 2 \mod 6 \\ 2 & \text{if } p = 3 \mod 6 \\ 1 & \text{if } p = 5 \mod 6 \end{cases} . \tag{2.4.60}$$

2.4.3 Series Convolutions from Functions on Primes

The infinite sequences $\mathsf{u} = \{1, 1, 1 \ldots\}$ and $\mathsf{N} = \{1, 2, 3, \ldots\}$ have functions on primes $P_{\mathsf{u}}(p) = 1$ and $P_{\mathsf{N}}(p) = p$ respectively. If we now convolute the two infinite sequences to obtain $\mathsf{u} * \mathsf{N} = \{1, 3, 4, 7, 6, 12, 8, \ldots\}$, the corresponding function on primes turns out to be $P_{\mathsf{u} * \mathsf{N}}(p) = P_{\mathsf{u}}(p) + P_{\mathsf{N}}(p) = 1 + p$.

Observation 2.4.5. *Multiplicativity turns into additivity on prime indices. One can*
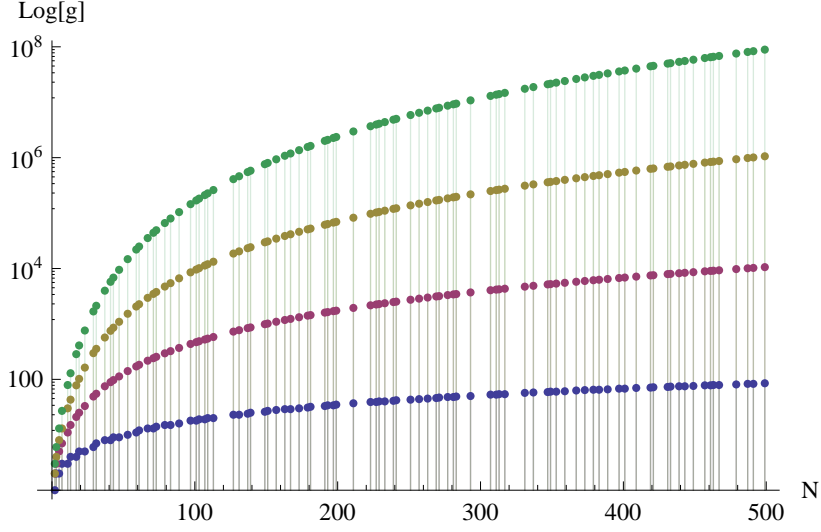
Figure 2.10: The number of distinct orbifolds of $\mathbb{C}^3$ (blue), $\mathbb{C}^4$ (red), $\mathbb{C}^5$ (yellow) and $\mathbb{C}^6$ (green) respectively for prime N.

translate between a convolution and a function on primes with

$$\mathsf{g} = *_{i=1}^{A} \mathsf{N}^{d_i} \ *_{j=1}^{B} \mathsf{N}^{d_j} \chi_{k_j,m_j} \ * \mathsf{C} \ \Leftrightarrow \ P_{\mathsf{g}}(p) = \sum_{i=1}^{A} p^{d_i} + \sum_{j=1}^{B} p^{d_j} \chi_{k_j,m_j}(p) + \mathsf{C}_p \quad (2.4.61)$$

where d_i is a non-negative integer. C can be any finite or infinite sequence with elements on prime indices denoted by C_p.

The aim is to keep C well-defined under the right combinations of N^d and $\chi_{k,m}$ in the convolution in (2.4.61).

Example x_3. An example is the sequence g_{x_3} that counts x_3-symmetric HNF's which correspond to the Abelian orbifolds of $\mathbb{C}^3$. The sequence has a function of period 3 on primes and is given in (2.4.40). The function on primes can be written in terms of the values on prime indices of basic multiplicative sequences as follows,

$$
\begin{aligned}
P_{\mathsf{g}_{x_3}}(p) &= 1 + \chi_{3,2}(p) \\
&= \chi_{3,1}(p) + \chi_{3,2}(p) \quad\quad\quad (2.4.62)
\end{aligned}
$$

When considering the entire sequence with values on non-prime indices, the convolu-

tions take the form

$$
\begin{aligned}
\mathsf{g}_{x_3} &= \mathsf{u} * \chi_{3,2} \\
&= \chi_{3,1} * \chi_{3,2} * \left(\sum_{a=0}^{\infty} t^{3^a} \right) ,
\end{aligned}
\tag{2.4.63}
$$

where $\mathsf{C} = 1$ and $\mathsf{C} = \sum_{a=0}^{\infty} t^{3^a}$ respectively. As desired, C is a well-defined partition function for both choices in (2.4.63).

Under this scheme, sequences which count orbifolds that are invariant under cycles of S_D can be re-written in terms of convolutions of the form (2.4.61). Table 2.9 and Table 2.10 show choices of sequence convolutions for the orbifolds of $\mathbb{C}^2$ to $\mathbb{C}^5$. Convolutions for the sequences for the Abelian orbifolds of $\mathbb{C}^3$ and $\mathbb{C}^4$ have been first presented in [126]. We present here the convolutions for the Abelian orbifolds of $\mathbb{C}^5$.

In the section below, some generalisations are given for sequences on all indices. The reason why not all sequences on all indices can be generalised is that some sequences require finite term corrections on power of prime indices. This can be seen for sequences $\mathsf{g}_{x_1 x_2^2}$ and $\mathsf{g}_{x_1 x_4}$ in Table 2.9 and Table 2.10. However, a complete set of generalisations for the sequences on prime indices can be given. Using the cycle index of S_D, this set of generalisations lead to the counting of distinct Abelian orbifolds of the form $\mathbb{C}^d/\Gamma$ with any prime order of Γ and any dimension D.

2.5 Generalisations for Orbifold Symmetries of Abelian Orbifolds of $\mathbb{C}^D$

Having discussed the explicit counting of distinct Abelian orbifolds of $\mathbb{C}^D$, [2] has made explicit predictions for a general formula for the counting. In this chapter, we summarise the predicted counting on prime indices and compare them with the experimental counting. For a detailed account of the predictions, the reader is referred to [2].

2.5.1 Generalisations for Symmetry Sequences with only Prime Indices

Let us restrict ourselves to elements on prime indices of sequences that count g^{α}-symmetric HNF's which correspond to orbifolds of $\mathbb{C}^D$. The functions on primes which reproduce sequence elements on prime indices are fully generalizable to any orbifold dimension D. We observe in this section patterns of functions on primes and derive generalisations.

$\mathbb{C}^2/\Gamma_N$	
x_1^2	u
x_2	u

$\mathbb{C}^3/\Gamma_N$	
x_1^3	u $*$ N
$x_1 x_2$	u $*$ u $* (t - t^2 + 2t^4)$
x_3	u $* \chi_{3,2}$

$\mathbb{C}^4/\Gamma_N$	
x_1^4	u $*$ N $*$ N^2
$x_1^2 x_2$	u $*$ u $*$ N $* (t - t^2 + 4t^4)$
x_2^2	u $*$ u $*$ N $* (t - t^2 + 4t^4)$
$x_1 x_3$	u $*$ u $* \chi_{3,2} * (t - t^3 + 3t^9)$
x_4	u $*$ u $* \chi_{4,2} * (t - t^2 + 2t^4)$

$\mathbb{C}^5/\Gamma_N$	
x_1^5	u $*$ N $*$ N^2 $*$ N^3
$x_1^3 x_2$	u $*$ u $*$ N $*$ N^2 $* (t - t^2 + 8t^4)$
$x_1 x_2^2$	u $*$ u $*$ N $*$ N $* (t - 3t^2 + 14t^4 - 12t^8 + 16t^{16})$
$x_1^2 x_3$	u $*$ u $*$ N $* \chi_{3,2} * (t - t^3 + 9t^9)$
$x_2 x_3$	u $*$ u $*$ u $* \chi_{3,2} * (t - t^2 + 2t^4) * (t - t^3 + 3t^9)$
$x_1 x_4$	u $*$ u $*$ u $* \chi_{4,2} * (t - 2t^2 + 3t^4 + 6t^{16} - 8t^{32} + 8t^{64})$
x_5	u $* \chi_{5,2} * \chi_{5,3} * \chi_{5,4}$

Table 2.9: Summary of the first choice of convolutions for orbifolds of $\mathbb{C}^2$, $\mathbb{C}^3$, $\mathbb{C}^4$ and $\mathbb{C}^5$.

The first sequence which we consider is g_{x_a} where $a \in \mathbb{Z}^+$. This sequence counts HNF's which are invariant under the cycle $(12\ldots a) \in S_a$. The HNF's are dual to abelian orbifolds of $\mathbb{C}^a$. On prime indices, the elements of the sequence are derived by the following function on primes:

Proposition 2.5.6. *Given the sequence g_{x_a} where $a \in \mathbb{Z}^+$, the corresponding function on primes is*

$$P_{\mathsf{g}_{x_a}}(p) \;=\; \sum_{m=1}^{\varphi(a)} \chi_{a,m}(p) \;+\; \sum_{\substack{k|a \\ 1<k<a}} \sum_{m=1}^{\varphi(k)} \chi_{k,m}(p) \;+\; \sum_{\substack{k|a \\ k=prime}} \delta_{pk} \qquad (2.5.64)$$

$$\;=\; \varphi(a)\,\delta_{p,1 \bmod a} \;+\; \sum_{\substack{k|a \\ 1<k<a}} \varphi(k)\,\delta_{p,1 \bmod k} \;+\; \sum_{\substack{k|a \\ k=prime}} \delta_{pk} \;, \qquad (2.5.65)$$

$\mathbb{C}^2/\Gamma_N$	
x_1^2	u
x_2	$\chi_{2,1} * \left(\sum_{a=0}^{\infty} t^{2^a}\right)$

$\mathbb{C}^3/\Gamma_N$	
x_1^3	$\mathsf{u} * \mathsf{N}$
$x_1 x_2$	$\mathsf{u} * \chi_{2,1} * \left(t + 2\sum_{a=0}^{\infty} t^{2^{(a+2)}}\right)$
x_3	$\chi_{3,1} * \chi_{3,2} * \left(\sum_{a=0}^{\infty} t^{3^a}\right)$

$\mathbb{C}^4/\Gamma_N$	
x_1^4	$\mathsf{u} * \mathsf{N} * \mathsf{N}^2$
$x_1^2 x_2$	$\mathsf{u} * \mathsf{N} * \chi_{2,1} * \left(t + 4\sum_{a=0}^{\infty} t^{2^{(a+2)}}\right)$
x_2^2	$\mathsf{u} * \mathsf{N} * \chi_{2,1} * \left(t + 4\sum_{a=0}^{\infty} t^{2^{(a+2)}}\right)$
$x_1 x_3$	$\mathsf{u} * \chi_{3,1} * \chi_{3,2} * \left(t + 3\sum_{a=0}^{\infty} t^{3^{(a+2)}}\right)$
x_4	$\mathsf{u} * \chi_{4,1} * \chi_{4,2} * \left(t + 2\sum_{a=0}^{\infty} t^{2^{(a+2)}}\right)$

$\mathbb{C}^5/\Gamma_N$	
x_1^5	$\mathsf{u} * \mathsf{N} * \mathsf{N}^2 * \mathsf{N}^3$
$x_1^3 x_2$	$\mathsf{u} * \mathsf{N} * \mathsf{N}^2 * \chi_{2,1} * \left(t + 8\sum_{a=0}^{\infty} t^{2^{(a+2)}}\right)$
$x_1 x_2^2$	$\mathsf{u} * \mathsf{N} * \mathsf{N} * \chi_{2,1} * \left(t + 16\sum_{a=0}^{\infty} t^{2^{(a+2)}} - 2t^2 - 4t^4 - 16t^8\right)$
$x_1^2 x_3$	$\mathsf{u} * \mathsf{N} * \chi_{3,1} * \chi_{3,2} * \left(t + 9\sum_{a=0}^{\infty} t^{3^{(a+2)}}\right)$
$x_2 x_3$	$\mathsf{u} * \chi_{2,1} * \chi_{3,1} * \chi_{3,2} * \left(t + 2\sum_{a=0}^{\infty} t^{2^{(a+2)}}\right) * \left(t + 3\sum_{a=0}^{\infty} t^{3^{(a+2)}}\right)$
$x_1 x_4$	$\mathsf{u} * \mathsf{u} * \chi_{4,1} * \chi_{4,2} * \left(t + 8\sum_{a=0}^{\infty} t^{2^{(a+2)}} - t^2 - 6t^4 - 6t^8 - 8t^{32}\right)$
x_5	$\chi_{5,1} * \chi_{5,2} * \chi_{5,3} * \chi_{5,4} * \left(\sum_{a=0}^{\infty} t^{5^a}\right)$

Table 2.10: Summary of the second choice of convolutions for orbifolds of $\mathbb{C}^2$, $\mathbb{C}^3$, $\mathbb{C}^4$ and $\mathbb{C}^5$.

where $\varphi(k)$ is the Euler totient function which is the number of distinct Dirichlet characters of periodicity k. The simplification in (2.5.64) comes from the property in (2.4.34).

Example. From explicit counting we have

$$
\begin{aligned}
P_{\mathsf{g}_{x_2}}(p) &= \chi_{2,1}(p) + \delta_{p2} \\
&= \delta_{p,1 \bmod 2} + \delta_{p2} \\
P_{\mathsf{g}_{x_3}}(p) &= \chi_{3,1}(p) + \chi_{3,2}(p) + \delta_{p3} \\
&= 2\delta_{p,1 \bmod 3} + \delta_{p3}
\end{aligned}
$$

$\mathbb{C}^2/\Gamma_N$	
x^α	$P_{\mathsf{g}_{x^\alpha}}(p)$
x_1^2	1
x_2	$\delta_{p,1 \bmod 2} + \delta_{p2}$

$\mathbb{C}^3/\Gamma_N$	
x^α	$P_{\mathsf{g}_{x^\alpha}}(p)$
x_1^3	$1 + p$
$x_1 x_2$	$1 + \delta_{p,1 \bmod 2}$
x_3	$2\delta_{p,1 \bmod 3} + \delta_{p3}$

$\mathbb{C}^4/\Gamma_N$	
x^α	$P_{\mathsf{g}_{x^\alpha}}(p)$
x_1^4	$1 + p + p^2$
$x_1^2 x_2$	$1 + p + \delta_{p,1 \bmod 2}$
x_2^2	$1 + (1+p)\delta_{p,1 \bmod 2} + 2\delta_{p2}$
$x_1 x_3$	$1 + 2\delta_{p,1 \bmod 3}$
x_4	$\delta_{p,1 \bmod 2} + 2\delta_{p,1 \bmod 4} + \delta_{p2}$

$\mathbb{C}^5/\Gamma_N$	
x^α	$P_{\mathsf{g}_{x^\alpha}}(p)$
x_1^5	$1 + p + p^2 + p^3$
$x_1^3 x_2$	$1 + p + p^2 + \delta_{p,1 \bmod 2}$
$x_1 x_2^2$	$1 + p + (1+p)\delta_{p,1 \bmod 2}$
$x_1^2 x_3$	$1 + p + 2\delta_{p,1 \bmod 3}$
$x_2 x_3$	$1 + \delta_{p,1 \bmod 2} + 2\delta_{p,1 \bmod 3}$
$x_1 x_4$	$1 + \delta_{p,1 \bmod 2} + 2\delta_{p,1 \bmod 4}$
x_5	$4\delta_{p,1 \bmod 5} + \delta_{p5}$

Table 2.11: Derived functions on primes for symmetries of orbifolds of the form $\mathbb{C}^2/\Gamma_N$, $\mathbb{C}^3/\Gamma_N$, $\mathbb{C}^4/\Gamma_N$ and $\mathbb{C}^5/\Gamma_N$ where N is prime.

$$
\begin{aligned}
P_{\mathsf{g}_{x_4}}(p) &= \chi_{2,1}(p) + \chi_{4,1}(p) + \chi_{4,2}(p) + \delta_{p2} \\
&= \delta_{p,1 \bmod 2} + 2\delta_{p,1 \bmod 4} + \delta_{p2} \\
P_{\mathsf{g}_{x_5}}(p) &= \chi_{5,1}(p) + \chi_{5,2}(p) + \chi_{5,3}(p) + \chi_{5,4}(p) + \delta_{p5} \\
&= 4\delta_{p,1 \bmod 5} + \delta_{p5} \\
P_{\mathsf{g}_{x_6}}(p) &= \chi_{2,1}(p) + \chi_{3,1}(p) + \chi_{3,2}(p) + \chi_{6,1}(p) + \chi_{6,2}(p) + \delta_{p,2} + \delta_{p,3} \\
&= \delta_{p,1 \bmod 2} + 2\delta_{p,1 \bmod 3} + 2\delta_{p,1 \bmod 6} + \delta_{p2} + \delta_{p3} \ .
\end{aligned}
\tag{2.5.66}
$$

The above functions reproduce the prime index elements of the sequences which have been obtained by explicit counting for the orbifolds of $\mathbb{C}^2$ to $\mathbb{C}^6$ (Table 2.2 to Table 2.6).

	$\mathbb{C}^6/\Gamma_N$
x^α	$P_{\mathrm{g}_{\mathrm{x}^\alpha}}(p)$
x_1^6	$1 + p + p^2 + p^3 + p^4$
$x_1^4 x_2$	$1 + p + p^2 + p^3 + \delta_{p,1 \bmod 2}$
$x_1^2 x_2^2$	$1 + p + p^2 + (1+p)\delta_{p,1 \bmod 2}$
x_2^3	$1 + p + (1+p+p^2)\delta_{p,1 \bmod 2} + 4\delta_{p2}$
$x_1^3 x_3$	$1 + p + p^2 + 2\delta_{p,1 \bmod 3}$
$x_1 x_2 x_3$	$1 + p + \delta_{p,1 \bmod 2} + 2\delta_{p,1 \bmod 3}$
$x_1^2 x_4$	$1 + p + \delta_{p,1 \bmod 2} + 2\delta_{p,1 \bmod 4}$
$x_2 x_4$	$1 + (1+p)\delta_{p,1 \bmod 2} + 2\delta_{p,1 \bmod 4} + 2\delta_{p2}$
x_3^2	$1 + 2(1+p)\delta_{p,1 \bmod 3} + 3\delta_{p3}$
$x_1 x_5$	$1 + 4\delta_{p,1 \bmod 5}$
x_6	$\delta_{p,1 \bmod 2} + 2\delta_{p,1 \bmod 3} + 2\delta_{p,1 \bmod 6} + \delta_{p2} + \delta_{p3}$

	$\mathbb{C}^7/\Gamma_N$
x^α	$P_{\mathrm{g}_{\mathrm{x}^\alpha}}(p)$
x_1^7	$1 + p + p^2 + p^3 + p^4 + p^5$
$x_1^5 x_2$	$1 + p + p^2 + p^3 + p^4 + \delta_{p,1 \bmod 2}$
$x_1^3 x_2^2$	$1 + p + p^2 + p^3 + (1+p)\delta_{p,1 \bmod 2}$
$x_1 x_2^3$	$1 + p + p^2 + (1+p+p^2)\delta_{p,1 \bmod 2}$
$x_1^4 x_3$	$1 + p + p^2 + p^3 + 2\delta_{p,1 \bmod 3}$
$x_1^2 x_2 x_3$	$1 + p + p^2 + \delta_{p,1 \bmod 2} + 2\delta_{p,1 \bmod 3}$
$x_2^2 x_3$	$1 + p + (1+p)\delta_{p,1 \bmod 2} + 2\delta_{p,1 \bmod 3}$
$x_1 x_3^2$	$1 + p + 2(1+p)\delta_{p,1 \bmod 3}$
$x_1^3 x_4$	$1 + p + p^2 + \delta_{p,1 \bmod 2} + 2\delta_{p,1 \bmod 4}$
$x_1 x_2 x_4$	$1 + p + (1+p)\delta_{p,1 \bmod 2} + 2\delta_{p,1 \bmod 4}$
$x_3 x_4$	$1 + \delta_{p,1 \bmod 2} + 2\delta_{p,1 \bmod 3} + 2\delta_{p,1 \bmod 4}$
$x_1^2 x_5$	$1 + p + 4\delta_{p,1 \bmod 5}$
$x_2 x_5$	$1 + \delta_{p,1 \bmod 2} + 4\delta_{p,1 \bmod 5}$
$x_1 x_6$	$1 + \delta_{p,1 \bmod 2} + 2\delta_{p,1 \bmod 3} + 2\delta_{p,1 \bmod 6}$
x_7	$6\delta_{p,1 \bmod 7} + \delta_{p7}$

Table 2.12: Derived functions on primes for symmetries of orbifolds of the form $\mathbb{C}^6/\Gamma_N$ and $\mathbb{C}^7/\Gamma_N$ where N is prime.

We recall that in Section §2.2.5, we mentioned that an element $g^\alpha \in S_D$ consists of M disjoint cycles γ^i of length $n_i = |\gamma^i|$. The general form of x^α which corresponds to a conjugacy class $H_\alpha \subset S_D$ and a term in the cycle index of S_D is

$$x^\alpha = \prod_{i=1}^{M} x_{n_i} \ . \tag{2.5.67}$$

	$\mathbb{C}^8/\Gamma_N$
x^α	$P_{\mathsf{g}_{x^\alpha}}(p)$
x_1^8	$1 + p + p^2 + p^3 + p^4 + p^5 + p^6$
$x_1^6 x_2$	$1 + p + p^2 + p^3 + p^4 + p^5 + \delta_{p,1 \bmod 2}$
$x_1^4 x_2^2$	$1 + p + p^2 + p^3 + p^4 + (1 + p)\delta_{p,1 \bmod 2}$
$x_1^2 x_2^3$	$1 + p + p^2 + p^3 + (1 + p + p^2)\delta_{p,1 \bmod 2}$
x_2^4	$1 + p + p^2 + (1 + p + p^2 + p^3)\delta_{p,1 \bmod 2} + 8\delta_{p2}$
$x_1^5 x_3$	$1 + p + p^2 + p^3 + p^4 + 2\delta_{p,1 \bmod 3}$
$x_1^3 x_2 x_3$	$1 + p + p^2 + p^3 + \delta_{p,1 \bmod 2} + 2\delta_{p,1 \bmod 3}$
$x_1 x_2^2 x_3$	$1 + p + p^2 + (1 + p)\delta_{p,1 \bmod 2} + 2\delta_{p,1 \bmod 3}$
$x_1^2 x_3^2$	$1 + p + p^2 + 2(1 + p)\delta_{p,1 \bmod 3}$
$x_2 x_3^2$	$1 + p + \delta_{p,1 \bmod 2} + 2(1 + p)\delta_{p,1 \bmod 3}$
$x_1^4 x_4$	$1 + p + p^2 + p^3 + \delta_{p,1 \bmod 2} + 2\delta_{p,1 \bmod 4}$
$x_1^2 x_2 x_4$	$1 + p + p^2 + (1 + p)\delta_{p,1 \bmod 2} + 2\delta_{p,1 \bmod 4}$
$x_2^2 x_4$	$1 + p + (1 + p + p^2)\delta_{p,1 \bmod 2} + 2\delta_{p,1 \bmod 4} + 4\delta_{p2}$
$x_1 x_3 x_4$	$1 + p + \delta_{p,1 \bmod 2} + 2\delta_{p,1 \bmod 3} + 2\delta_{p,1 \bmod 4}$
x_4^2	$1 + (1 + p)\delta_{p,1 \bmod 2} + 2(1 + p)\delta_{p,1 \bmod 4} + 2\delta_{p2}$
$x_1^3 x_5$	$1 + p + p^2 + 4\delta_{p,1 \bmod 5}$
$x_1 x_2 x_5$	$1 + p + \delta_{p,1 \bmod 2} + 4\delta_{p,1 \bmod 5}$
$x_3 x_5$	$1 + 2\delta_{p,1 \bmod 3} + 4\delta_{p,1 \bmod 5}$
$x_1^2 x_6$	$1 + p + \delta_{p,1 \bmod 2} + 2\delta_{p,1 \bmod 3} + 2\delta_{p,1 \bmod 6}$
$x_2 x_6$	$1 + (1 + p)\delta_{p,1 \bmod 2} + 2\delta_{p,1 \bmod 3} + 2\delta_{p,1 \bmod 6} + 2\delta_{p2}$
$x_1 x_7$	$1 + 6\delta_{p,1 \bmod 7}$
x_8	$\delta_{p,1 \bmod 2} + 2\delta_{p,1 \bmod 4} + 4\delta_{p,1 \bmod 8} + \delta_{p2}$

Table 2.13: Derived functions on primes for symmetries of orbifolds of the form $\mathbb{C}^8/\Gamma_N$ where N is prime.

We call M the partition number of the symmetry cycle. The dimension D of the corresponding orbifold of $\mathbb{C}^D$ is given by $\sum_{k=1}^{M} n_k = D$. For example, the partition number of the following cycles are,

$$M(x_2^3) = 3 \ , \ \ M(x_1^2 x_2 x_3) = 4 \ , \ \ M(x_2^2 x_4) = 3 \ . \tag{2.5.68}$$

Using the definition of the partition number, let us define an additional quantity which will be of use in our generalisation.

Definition 2.5.7. *Given the cycle g^α of the conjugacy class x^α with corresponding partition number $M(x^\alpha)$, let the number of divisions by m of the cycle g^α be defined as*

$$Q_m(x^\alpha) = \sum_{i=1}^{M(x^\alpha)} \sum_{m \mid n_i} 1 \ , \tag{2.5.69}$$

$\mathbb{C}^9/\Gamma_N$	
x^α	$P_{\mathbf{g}_{x^\alpha}}(p)$
x_1^9	$1 + p + p^2 + p^3 + p^4 + p^5 + p^6 + p^7$
$x_1^7 x_2$	$1 + p + p^2 + p^3 + p^4 + p^5 + p^6 + \delta_{p,1 \bmod 2}$
$x_1^5 x_2^2$	$1 + p + p^2 + p^3 + p^4 + p^5 + (1+p)\delta_{p,1 \bmod 2}$
$x_1^3 x_2^3$	$1 + p + p^2 + p^3 + p^4 + (1 + p + p^2)\delta_{p,1 \bmod 2}$
$x_1 x_2^4$	$1 + p + p^2 + p^3 + (1 + p + p^2 + p^3)\delta_{p,1 \bmod 2}$
$x_1^6 x_3$	$1 + p + p^2 + p^3 + p^4 + p^5 + 2\delta_{p,1 \bmod 3}$
$x_1^4 x_2 x_3$	$1 + p + p^2 + p^3 + p^4 + \delta_{p,1 \bmod 2} + 2\delta_{p,1 \bmod 3}$
$x_1^2 x_2^2 x_3$	$1 + p + p^2 + p^3 + (1+p)\delta_{p,1 \bmod 2} + 2\delta_{p,1 \bmod 3}$
$x_2^3 x_3$	$1 + p + p^2 + (1 + p + p^2)\delta_{p,1 \bmod 2} + 2\delta_{p,1 \bmod 3}$
$x_1^3 x_3^2$	$1 + p + p^2 + p^3 + 2(1+p)\delta_{p,1 \bmod 3}$
$x_1 x_2 x_3^2$	$1 + p + p^2 + \delta_{p,1 \bmod 2} + 2(1+p)\delta_{p,1 \bmod 3}$
x_3^3	$1 + p + 2(1 + p + p^2)\delta_{p,1 \bmod 3} + 9\delta_{p3}$
$x_1^5 x_4$	$1 + p + p^2 + p^3 + p^4 + \delta_{p,1 \bmod 2} + 2\delta_{p,1 \bmod 4}$
$x_1^3 x_2 x_4$	$1 + p + p^2 + p^3 + (1+p)\delta_{p,1 \bmod 2} + 2\delta_{p,1 \bmod 4}$
$x_1 x_2^2 x_4$	$1 + p + p^2 + (1 + p + p^2)\delta_{p,1 \bmod 2} + 2\delta_{p,1 \bmod 4}$
$x_1^2 x_3 x_4$	$1 + p + p^2 + \delta_{p,1 \bmod 2} + 2\delta_{p,1 \bmod 3} + 2\delta_{p,1 \bmod 4}$
$x_2 x_3 x_4$	$1 + p + (1+p)\delta_{p,1 \bmod 2} + 2\delta_{p,1 \bmod 3} + 2\delta_{p,1 \bmod 4}$
$x_1 x_4^2$	$1 + p + (1+p)\delta_{p,1 \bmod 2} + 2(1+p)\delta_{p,1 \bmod 4}$
$x_1^4 x_5$	$1 + p + p^2 + p^3 + 4\delta_{p,1 \bmod 5}$
$x_1^2 x_2 x_5$	$1 + p + p^2 + \delta_{p,1 \bmod 2} + 4\delta_{p,1 \bmod 5}$
$x_2^2 x_5$	$1 + p + (1+p)\delta_{p,1 \bmod 2} + 4\delta_{p,1 \bmod 5}$
$x_1 x_3 x_5$	$1 + p + 2\delta_{p,1 \bmod 3} + 4\delta_{p,1 \bmod 5}$
$x_4 x_5$	$1 + \delta_{p,1 \bmod 2} + 2\delta_{p,1 \bmod 4} + 4\delta_{p,1 \bmod 5}$
$x_1^3 x_6$	$1 + p + p^2 + \delta_{p,1 \bmod 2} + 2\delta_{p,1 \bmod 3} + 2\delta_{p,1 \bmod 6}$
$x_1 x_2 x_6$	$1 + p + (1+p)\delta_{p,1 \bmod 2} + 2\delta_{p,1 \bmod 3} + 2\delta_{p,1 \bmod 6}$
$x_3 x_6$	$1 + \delta_{p,1 \bmod 2} + 2(1+p)\delta_{p,1 \bmod 3} + 2\delta_{p,1 \bmod 6} + 3\delta_{p3}$
$x_1^2 x_7$	$1 + p + 6\delta_{p,1 \bmod 7}$
$x_2 x_7$	$1 + \delta_{p,1 \bmod 2} + 6\delta_{p,1 \bmod 7}$
$x_1 x_8$	$1 + \delta_{p,1 \bmod 2} + 2\delta_{p,1 \bmod 4} + 4\delta_{p,1 \bmod 8}$
x_9	$2\delta_{p,1 \bmod 3} + 6\delta_{p,1 \bmod 9} + \delta_{p3}$

Table 2.14: Derived functions on primes for symmetries of orbifolds of the form $\mathbb{C}^9/\Gamma_N$ where N is prime.

where the dimension of the orbifold is given by $D = \sum_{k=1}^{M(x^\alpha)} n_k$. The number of divisions by 1 is by definition the number of partitions of the cycle g^α,

$$Q_1(x^\alpha) = M(x^\alpha) . \tag{2.5.70}$$

Accordingly, we derive the number of division by 2, 3 and 4 respectively for a cycle

of the conjugacy class $x_2 x_4$ as

$$Q_2(x_2 x_4) = 2 \ , \ Q_3(x_2 x_4) = 0 \ , \ Q_4(x_2 x_4) = 1 \ . \tag{2.5.71}$$

Other examples are $x_2^2 x_3$ and x_2^3 with

$$Q_2(x_2^2 x_3) = 2 \ , \ Q_3(x_2^2 x_3) = 1 \ , \ Q_4(x_2^2 x_3) = 0 \ ,$$
$$Q_2(x_2^3) = 3 \ , \ Q_3(x_2^3) = 0 \ , \ Q_4(x_2^3) = 0 \ . \tag{2.5.72}$$

Let us consider now the most general sequence $\mathbf{g}_{x^\alpha}$ which counts HNF's that are invariant under the cycle $g^\alpha \in S_D$ where g^α is in the conjugacy class denoted by the cycle index variable x^α. The elements of this sequence at prime indices are obtained from the function on primes $P_{x^\alpha}(p)$ which we generalise as follows:

Proposition 2.5.8. *Given the cycle g^α with partition number $M(x^\alpha) > 1$, the corresponding function on primes has the form*

$$P_{x^\alpha}(p) \ = \ \sum_{d=1}^{M(x^\alpha)-1} p^{d-1} + \sum_{d=2}^{D} \sum_{q=1}^{Q_d(x^\alpha)} \sum_{m=1}^{\varphi(d)} p^{q-1} \chi_{d,m}(p) \ + \sum_{\substack{s|D \\ s=prime \\ Q_s(x^\alpha)=M(x^\alpha) \\ x_1 \notin x^\alpha}}^{D} s^{Q_s(x^\alpha)-1} \delta_{ps}$$

$$\tag{2.5.73}$$

$$= \ \sum_{d=1}^{M(x^\alpha)-1} p^{d-1} + \sum_{d=2}^{D} \sum_{q=1}^{Q_d(x^\alpha)} p^{q-1} \varphi(d) \ \delta_{p,1 \bmod d} \ + \sum_{\substack{s|D \\ s=prime \\ Q_s(x^\alpha)=M(x^\alpha) \\ x_1 \notin x^\alpha}}^{D} s^{Q_s(x^\alpha)-1} \delta_{ps} \ ,$$

$$\tag{2.5.74}$$

where $\varphi(d)$ is the Euler totient function.

Examples and Derivations. According to the above propositions, we are able to derive the functions on primes which correspond to any cycle $g^\alpha \in S_D$. Tables 2.11, 2.12, 2.13 and 2.14 present the derived functions on primes for the orbifolds of $\mathbb{C}^2$ to $\mathbb{C}^9$. The functions on primes reproduce the sequence elements on prime indices presented in Table 2.2 to Table 2.6 for the orbifolds of $\mathbb{C}^3$ to $\mathbb{C}^6$. The derived functions for the orbifolds of $\mathbb{C}^7$ to $\mathbb{C}^9$ have not been verified by an explicit counting.

We recall that these sequences count HNF's which are invariant under cycles of conjugacy classes of the permutation group S_D. The HNF's are dual to abelian orbifolds of $\mathbb{C}^D$ where Table 2.9 and Table 2.10 present the results for dimensions $D = 2, 3, 4, 5$. Using the cycle index of the permutation group S_D, the sequences which count g^α-

invariant HNF's are combined to count distinct abelian orbifolds of $\mathbb{C}^D$.

Sequence Predictions for higher dimensional orbifolds. Using the observations in Section §2.5.1 and the cycle indices in Table 2.1, we are able to derive the prime index sequences which count distinct orbifolds of the form $\mathbb{C}^D/\Gamma_p = \mathbb{C}^D/\mathbb{Z}_p$. The counting for distinct Abelian orbifolds of the form $\mathbb{C}^7/\Gamma_p$, $\mathbb{C}^8/\Gamma_p$ and $\mathbb{C}^9/\Gamma_p$ are presented in Table 2.15, Table 2.16 and Table 2.17 respectively. *Explicit counting which matches with the predictions is marked by a $*$ in Table 2.15, Table 2.16 and Table 2.17.*

The large N limit. Figure 2.11 shows a logarithmic plot of the prime index sequences which count distinct orbifolds of the form $\mathbb{C}^3/\Gamma_p$ to $\mathbb{C}^9/\Gamma_p$. In the limit $p \to \infty$, the logarithmic difference between consecutive sequences becomes

$$\lim_{p \to \infty} \log \left(\frac{\mathsf{g}^{(D)}(p)}{\mathsf{g}^{(D-1)}(p)} \right) = \log \left(\frac{p}{D} \right) . \tag{2.5.75}$$

This confirms the asymptotic behaviour analysis from [126].
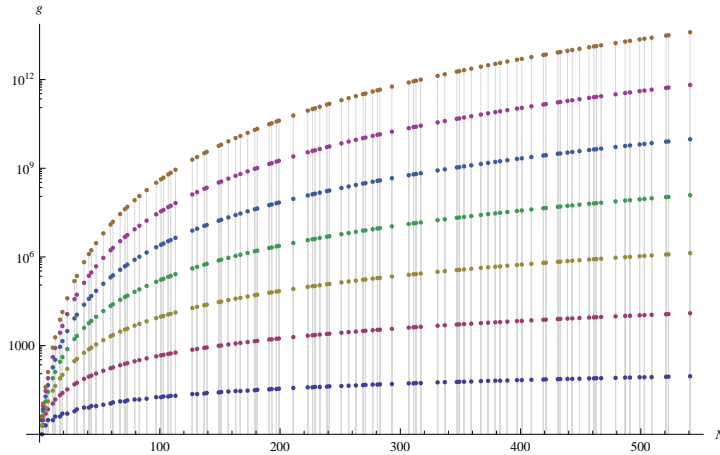
Figure 2.11: The orbifold counting for $\mathbb{C}^3/\Gamma_N$ to $\mathbb{C}^9/\Gamma_N$ with prime N. The ordering of the sequences reflects the dimension of the orbifolds, with logarithmic differences between consecutive sequences approaching $log(p/D)$ at $p \to \infty$.

2.6 Discussions and Prospects

By studying the worldvolume gauge theories of probe D3-branes and M2-branes, various toric singularities were identified and classified [136, 137, 17]. An open subset of the infinitely many probed toric singularities have been the Abelian orbifolds of $\mathbb{C}^3$ and $\mathbb{C}^4$,

					$\mathbb{C}^7/\Gamma_N$					
N	2*	3*	5*	7*	11	13	17	19	23	29
x_1^7	63*	364*	3906*	19608*	177156	402234	1508598	2613660	6728904	21243690
$x_1^5 x_2$	31*	122*	782*	2802*	16106	30942	88742	137562	292562	732542
$x_1^3 x_2^2$	15*	44*	162*	408*	1476	2394	5238	7260	12744	25290
$x_1 x_2^3$	7*	26*	62*	114*	266	366	614	762	1106	1742
$x_1^4 x_3$	15*	40*	156*	402*	1464	2382	5220	7242	12720	25260
$x_1^2 x_2 x_3$	7*	14*	32*	60*	134	186	308	384	554	872
$x_2^2 x_3$	3*	8*	12*	18*	24	30	36	42	48	60
$x_1 x_3^2$	3*	4*	6*	24*	12	42	18	60	24	30
$x_1^3 x_4$	7*	14*	34*	58*	134	186	310	382	554	874
$x_1 x_2 x_4$	3*	8*	14*	16*	24	30	38	40	48	62
$x_3 x_4$	1*	2*	4*	4*	2	6	4	4	2	4
$x_1^2 x_5$	3*	4*	6*	8*	16	14	18	20	24	30
$x_2 x_5$	1*	2*	2*	2*	6	2	2	2	2	2
$x_1 x_6$	1*	2*	2*	6*	2	6	2	6	2	2
x_7	0*	0*	0*	1*	0	0	0	0	0	6
$g^{(D=7)}$	3*	7*	19*	46*	183	333	912	1421	3101	8307
N	31	37	41	43	47	53	59	61	67	71
x_1^7	29583456	71270178	118752606	150508644	234330768	426237714	727250580	858672906	1370581548	1830004056
$x_1^5 x_2$	954306	1926222	2896406	3500202	4985762	8042222	12326282	14076606	20456442	25774706
$x_1^3 x_2^2$	30816	52098	70686	81444	106128	151794	208980	230826	305388	363096
$x_1 x_2^3$	1986	2814	3446	3786	4514	5726	7082	7566	9114	10226
$x_1^4 x_3$	30786	52062	70644	81402	106080	151740	208920	230766	305322	363024
$x_1^2 x_2 x_3$	996	1410	1724	1896	2258	2864	3542	3786	4560	5114
$x_2^2 x_3$	66	78	84	90	96	108	120	126	138	144
$x_1 x_3^2$	96	114	42	132	48	54	60	186	204	72
$x_1^3 x_4$	994	1410	1726	1894	2258	2866	3542	3786	4558	5114
$x_1 x_2 x_4$	64	78	86	88	96	110	120	126	136	144
$x_3 x_4$	4	6	4	4	2	4	2	6	4	2
$x_1^2 x_5$	36	38	46	44	48	54	60	66	68	76
$x_2 x_5$	6	2	6	2	2	2	2	6	2	6
$x_1 x_6$	6	6	2	6	2	2	2	6	6	2
x_7	0	0	0	6	0	0	0	0	0	6
$g^{(D=7)}$	11103	24235	38394	47619	71353	123855	203531	237709	368581	483987

Table 2.15: The derived symmetry count for the orbifolds of the form $\mathbb{C}^7/\Gamma_N$ with prime N. *The values on indices marked by a * have been verified by explicit counting.*
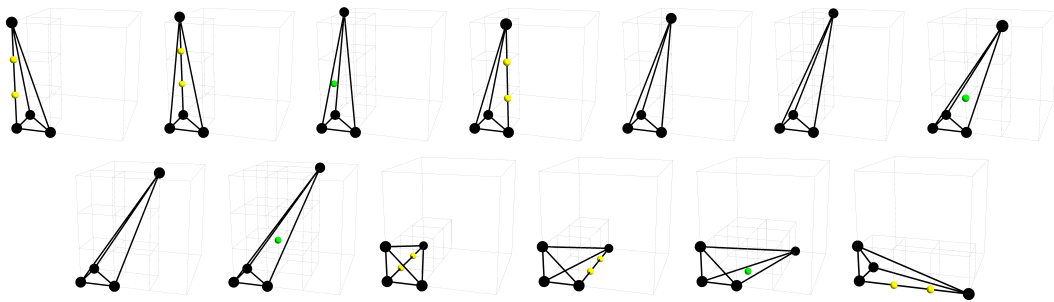
Figure 2.12: The Hermite Normal Form toric tetrahedra of the orbifolds of the form $\mathbb{C}^4/\Gamma_3$. Lattice points on faces are colored green and lattice points on edges are colored yellow.

	$\mathbb{C}^8/\Gamma_N$									
N	2	3	5	7	11	13	17	19	23	29
x_1^8	127	1093	19531	137257	1948717	5229043	25646167	49659541	154764793	616067011
$x_1^6 x_2$	63	365	3907	19609	177157	402235	1508599	2613661	6728905	21243691
$x_1^4 x_2^2$	31	125	787	2809	16117	30955	88759	137581	292585	732571
$x_1^2 x_2^3$	15	53	187	457	1597	2563	5527	7621	13273	26131
x_2^4	15	53	187	457	1597	2563	5527	7621	13273	26131
$x_1^5 x_3$	31	121	781	2803	16105	30943	88741	137563	292561	732541
$x_1^3 x_2 x_3$	15	41	157	403	1465	2383	5221	7243	12721	25261
$x_1 x_2^2 x_3$	7	17	37	67	145	199	325	403	577	901
$x_1^2 x_3^2$	7	13	31	73	133	211	307	421	553	871
$x_2 x_3^2$	3	5	7	25	13	43	19	61	25	31
$x_1^4 x_4$	15	41	159	401	1465	2383	5223	7241	12721	25263
$x_1^2 x_2 x_4$	7	17	39	65	145	199	327	401	577	903
$x_2^2 x_4$	7	17	39	65	145	199	327	401	577	903
$x_1 x_3 x_4$	3	5	9	11	13	19	21	23	25	33
x_4^2	3	5	19	9	13	43	55	21	25	91
$x_1^3 x_5$	7	13	31	57	137	183	307	381	553	871
$x_1 x_2 x_5$	3	5	7	9	17	15	19	21	25	31
$x_3 x_5$	1	1	1	3	5	3	1	3	1	1
$x_1^2 x_6$	3	5	7	13	13	19	19	25	25	31
$x_2 x_6$	3	5	7	13	13	19	19	25	25	31
$x_1 x_7$	1	1	1	1	1	1	1	1	1	7
x_8	1	1	3	1	1	3	7	1	1	3
$g^{(D=8)}$	4	9	29	79	411	829	2737	4611	11629	37379

Table 2.16: The derived symmetry count for the orbifolds of the form $\mathbb{C}^8/\Gamma_N$ with prime N.

and initial work on identifying associated quiver gauge theories [141] led to the work on counting distinct Abelian orbifold theories and singularities [126, 1].

In this chapter we have shown that it is possible to predict the number of distinct Abelian orbifolds of the form $\mathbb{C}^D/\Gamma$ for any dimension D where the order of the Abelian group Γ is a square-free product of primes. We have seen that an integral part of the computation are the discrete symmetries of the Abelian orbifolds of $\mathbb{C}^D$ which are Abelian subgroups of the permutation group S_D.

Such discrete symmetries appeared in previous work [35, 14] as 'nodal' quiver symmetries in the context of $3+1$ dimensional quiver gauge theories. We have shown in this chapter that such discrete symmetries can be identified directly from the toric diagram of the probed singularity for the Abelian orbifolds of $\mathbb{C}^D$.

There are several open questions which await us from here. Firstly, although we are able to predict the number of distinct Abelian orbifolds of the form $\mathbb{C}^D/\Gamma$ where the order of Γ is a square free product of primes, we are not able to do so for orders which are powers of prime. A solution to this problem would give us a truly complete picture of the infinite family of Abelian orbifolds of $\mathbb{C}^D$.

Secondly, we have restricted ourselves to distinct Abelian orbifolds of $\mathbb{C}^D$. In [126], Abelian orbifolds of the conifold $\mathcal{C}$ and L_{aba} theories have been counted explicitly. In principle, we are not restricted to these toric singularities and are able to count distinct

					$\mathbb{C}^9/\Gamma_N$					
N	2	3	5	7	11	13	17	19	23	29
x_1^9	255	3280	97656	960800	21435888	67977560	435984840	943531280	3559590240	17865943320
$x_1^7 x_2$	127	1094	19532	137258	1948718	5229044	25646168	49659542	154764794	616067012
$x_1^5 x_2^2$	63	368	3912	19616	177168	402248	1508616	2613680	6728928	21243720
$x_1^3 x_2^3$	31	134	812	2858	16238	31124	89048	137942	293114	733412
$x_1 x_2^4$	15	80	312	800	2928	4760	10440	14480	25440	50520
$x_1^6 x_3$	63	364	3906	19610	177156	402236	1508598	2613662	6728904	21243690
$x_1^4 x_2 x_3$	31	122	782	2804	16106	30944	88742	137564	292562	732542
$x_1^2 x_2^2 x_3$	15	44	162	410	1476	2396	5238	7262	12744	25290
$x_2^3 x_3$	7	26	62	116	368	368	614	764	1106	1742
$x_1^3 x_3^2$	15	40	156	416	1464	2408	5220	7280	12720	25260
$x_1 x_2 x_3^2$	7	14	32	74	134	212	308	422	554	872
x_3^3	3	13	6	122	12	380	18	782	24	30
$x_1^5 x_4$	31	122	784	2802	16106	30944	88744	137562	292562	732544
$x_1^3 x_2 x_4$	15	44	164	408	1476	2396	5240	7260	12744	25292
$x_1 x_2^2 x_4$	7	26	64	114	266	368	616	762	1106	1744
$x_1^2 x_3 x_4$	7	14	34	60	134	188	310	384	554	874
$x_2 x_3 x_4$	3	8	14	18	24	32	38	42	48	62
$x_1 x_4^2$	3	8	24	16	24	56	72	40	48	120
$x_1^4 x_5$	15	40	156	400	1468	2380	5220	7240	12720	25260
$x_1^2 x_2 x_5$	7	14	32	58	138	184	308	382	554	872
$x_2^2 x_5$	3	8	12	16	28	28	36	40	48	60
$x_1 x_3 x_5$	3	4	6	10	16	16	18	22	24	30
$x_4 x_5$	1	2	4	2	6	4	4	2	2	4
$x_1^3 x_6$	7	14	32	62	134	188	308	386	554	872
$x_1 x_2 x_6$	3	8	12	20	24	32	36	44	48	60
$x_3 x_6$	1	5	2	20	2	32	2	44	2	2
$x_1^2 x_7$	3	4	6	8	12	14	18	20	24	36
$x_2 x_7$	1	2	2	2	2	2	2	2	2	8
$x_1 x_8$	1	2	4	2	2	4	8	2	2	4
x_9	0	1	0	2	0	2	0	8	0	0
$g^{(D=9)}$	4	11	40	128	853	1909	7544	13754	39904	153319

Table 2.17: The derived symmetry count for the orbifolds of the form $\mathbb{C}^9/\Gamma_N$ with prime N.

Abelian orbifolds of any toric singularity using the techniques described in this chapter. From our observation that the number of distinct Abelian orbifolds relies on the discrete symmetries of the toric singularity, we can reverse the relationship and ask whether two toric singularities have the same discrete symmetries if the number of distinct ways of orbifolding these singularities are the same.

In fact, an unpublished work in collaboration with Amihay Hanany [146] is introducing a paramterisation of orbifold actions of Abelian orbifolds of the conifold and the suspended pinch point (SPP). The proposed parameterisation directly translates to the corresponding brane tiling and can be used to count distinct Abelian orbifolds in the same way as it is the case for $\mathbb{C}^3/\Gamma$. Figure 2.13 and Figure 2.14 show respectively for Abelian orbifolds of the form $\mathcal{C}/\Gamma$ and SPP/Γ the toric diagram and the corresponding proposed orbifold action.

We finally believe that further study of symmetries of Abelian orbifolds of various toric singularities can give new valuable insights into underlying structures of the corresponding quiver gauge theories.
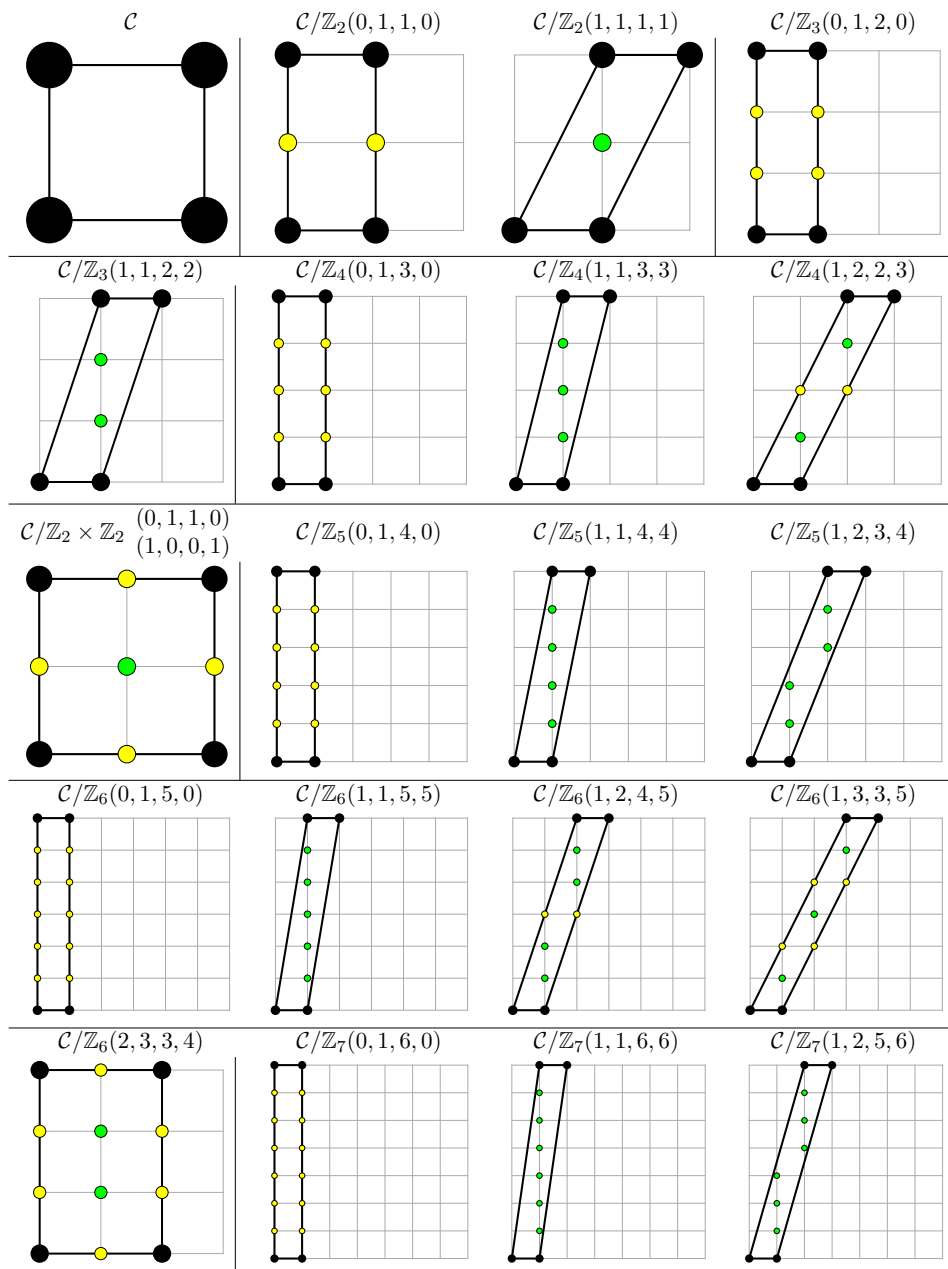
Figure 2.13: Toric diagrams corresponding to distinct Abelian orbifolds of the form $\mathcal{C}/\Gamma_n$ and the corresponding Abelian orbifold actions.
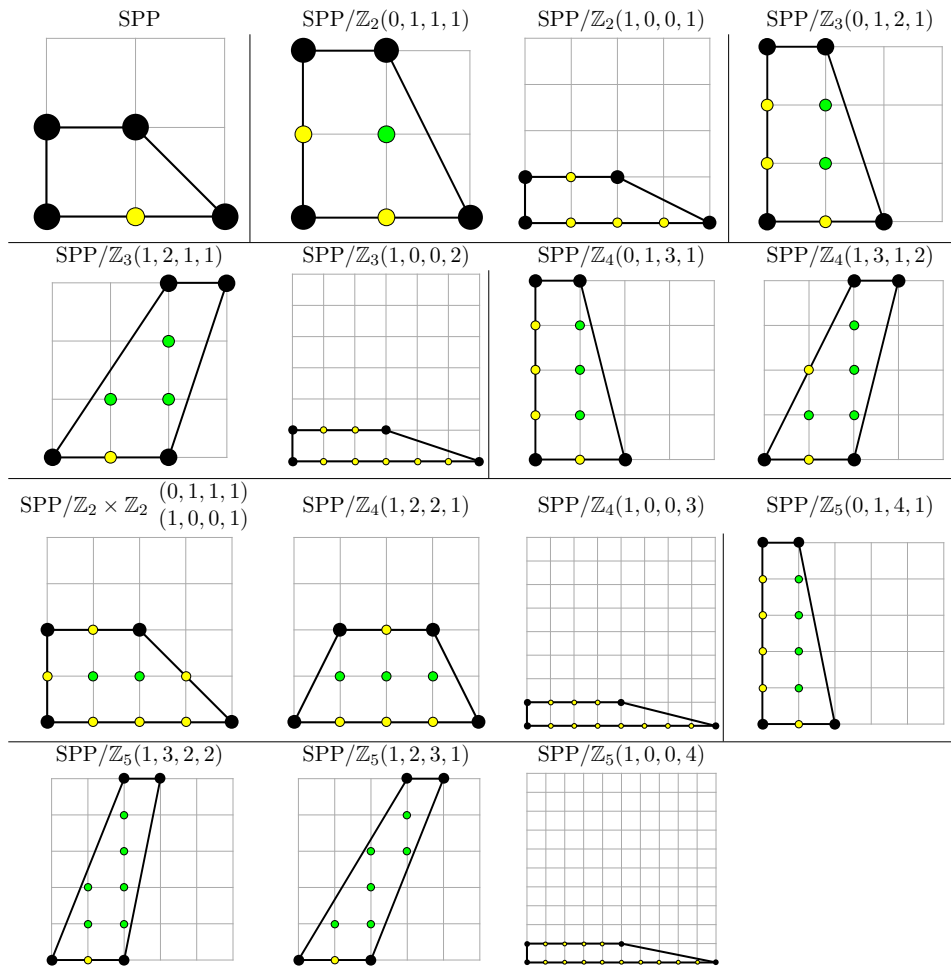
Figure 2.14: Toric diagrams corresponding to distinct Abelian orbifolds of the form SPP/Γ_n and the corresponding orbifold actions.

#	Orbifold	Orbifold Action	I_0 (Corners)	$\mathbf{g}_{x_1^3}$	$\mathbf{g}_{x_1 x_1^2}$	$\mathbf{g}_{x_3}$
(1.1)	$\mathbb{C}^3/\mathbb{Z}_1$	$\begin{pmatrix} (0,0,0) \\ (0,0,0) \end{pmatrix}$	$\{(0,0),(1,0),(0,1)\}$	1	1	1
			Total	1	1	1
(2.1)	$\mathbb{C}^3/\mathbb{Z}_2$	$\begin{pmatrix} (0,1,1) \\ (0,0,0) \end{pmatrix}$	$\{(0,0),(1,0),(0,2)\}$	3	1	0
			Total	3	1	1
(3.1)	$\mathbb{C}^3/\mathbb{Z}_3$	$\begin{pmatrix} (0,1,2) \\ (0,0,0) \end{pmatrix}$	$\{(0,0),(1,0),(0,3)\}$	3	1	0
(3.2)	$\mathbb{C}^3/\mathbb{Z}_3$	$\begin{pmatrix} (1,1,1) \\ (0,0,0) \end{pmatrix}$	$\{(0,0),(1,0),(2,3)\}$	1	1	1
			Total	4	2	1
(4.1)	$\mathbb{C}^3/\mathbb{Z}_4$	$\begin{pmatrix} (0,1,3) \\ (0,0,0) \end{pmatrix}$	$\{(0,0),(1,0),(0,4)\}$	3	1	0
(4.2)	$\mathbb{C}^3/\mathbb{Z}_4$	$\begin{pmatrix} (1,1,2) \\ (0,0,0) \end{pmatrix}$	$\{(0,0),(1,0),(2,4)\}$	3	1	0
(4.3)	$\mathbb{C}^3/\mathbb{Z}_2 \times \mathbb{Z}_2$	$\begin{pmatrix} (1,0,1) \\ (0,1,1) \end{pmatrix}$	$\{(0,0),(2,0),(0,2)\}$	1	1	1
			Total	7	3	1
(5.1)	$\mathbb{C}^3/\mathbb{Z}_5$	$\begin{pmatrix} (0,1,4) \\ (0,0,0) \end{pmatrix}$	$\{(0,0),(1,0),(0,5)\}$	3	1	0
(5.2)	$\mathbb{C}^3/\mathbb{Z}_5$	$\begin{pmatrix} (1,1,3) \\ (0,0,0) \end{pmatrix}$	$\{(0,0),(1,0),(2,5)\}$	3	1	0
			Total	6	2	0
(6.1)	$\mathbb{C}^3/\mathbb{Z}_6$	$\begin{pmatrix} (0,1,5) \\ (0,0,0) \end{pmatrix}$	$\{(0,0),(1,0),(0,6)\}$	3	1	0
(6.2)	$\mathbb{C}^3/\mathbb{Z}_6$	$\begin{pmatrix} (1,1,4) \\ (0,0,0) \end{pmatrix}$	$\{(0,0),(1,0),(2,6)\}$	3	1	0
(6.3)	$\mathbb{C}^3/\mathbb{Z}_6$	$\begin{pmatrix} (1,2,3) \\ (0,0,0) \end{pmatrix}$	$\{(0,0),(1,0),(3,6)\}$	6	0	0
			Total	12	2	0
(7.1)	$\mathbb{C}^3/\mathbb{Z}_7$	$\begin{pmatrix} (0,1,6) \\ (0,0,0) \end{pmatrix}$	$\{(0,0),(1,0),(0,7)\}$	3	1	0
(7.2)	$\mathbb{C}^3/\mathbb{Z}_7$	$\begin{pmatrix} (1,1,5) \\ (0,0,0) \end{pmatrix}$	$\{(0,0),(1,0),(2,7)\}$	3	1	0
(7.3)	$\mathbb{C}^3/\mathbb{Z}_7$	$\begin{pmatrix} (1,2,4) \\ (0,0,0) \end{pmatrix}$	$\{(0,0),(1,0),(3,7)\}$	2	0	2
			Total	8	2	2
(8.1)	$\mathbb{C}^3/\mathbb{Z}_8$	$\begin{pmatrix} (0,1,7) \\ (0,0,0) \end{pmatrix}$	$\{(0,0),(1,0),(0,8)\}$	3	1	0
(8.2)	$\mathbb{C}^3/\mathbb{Z}_8$	$\begin{pmatrix} (1,1,6) \\ (0,0,0) \end{pmatrix}$	$\{(0,0),(1,0),(2,8)\}$	3	1	0
(8.3)	$\mathbb{C}^3/\mathbb{Z}_8$	$\begin{pmatrix} (1,2,5) \\ (0,0,0) \end{pmatrix}$	$\{(0,0),(1,0),(3,8)\}$	3	1	0
(8.4)	$\mathbb{C}^3/\mathbb{Z}_8$	$\begin{pmatrix} (1,3,4) \\ (0,0,0) \end{pmatrix}$	$\{(0,0),(1,0),(4,8)\}$	3	1	0
(8.5)	$\mathbb{C}^3/\mathbb{Z}_4 \times \mathbb{Z}_2$	$\begin{pmatrix} (1,0,3) \\ (0,1,1) \end{pmatrix}$	$\{(0,0),(2,0),(0,4)\}$	3	1	0
			Total	15	5	0

Table 2.18: The symmetry counting of distinct Abelian orbifolds $\mathbb{C}^3$ with corresponding orbifold actions and toric triangles given in terms of I_0 (corner points in Cartesian coordinates).

#	Orbifold	Orbifold Action	I_0 (Corners)	$\mathbf{g}_{x_1^4}$	$\mathbf{g}_{x_1^2 x_2}$	$\mathbf{g}_{x_2^2}$	$\mathbf{g}_{x_1 x_3}$	$\mathbf{g}_{x_4}$
(1.1)	$\mathbb{C}^4/\mathbb{Z}_1$	$\begin{pmatrix} (0,0,0,0) \\ (0,0,0,0) \\ (0,0,0,0) \end{pmatrix}$	$\left\{\begin{array}{c} (0,0,0) \\ (1,0,0) \\ (0,1,0) \\ (0,0,1) \end{array}\right\}$	1	1	1	1	1
			Total	1	1	1	1	1
(2.1)	$\mathbb{C}^4/\mathbb{Z}_2$	$\begin{pmatrix} (0,0,1,1) \\ (0,0,0,0) \\ (0,0,0,0) \end{pmatrix}$	$\left\{\begin{array}{c} (0,0,0) \\ (1,0,0) \\ (0,1,0) \\ (0,0,2) \end{array}\right\}$	6	2	2	0	0
(2.2)	$\mathbb{C}^4/\mathbb{Z}_2$	$\begin{pmatrix} (1,1,1,1) \\ (0,0,0,0) \\ (0,0,0,0) \end{pmatrix}$	$\left\{\begin{array}{c} (0,0,0) \\ (1,0,0) \\ (0,1,0) \\ (1,1,2) \end{array}\right\}$	1	1	1	1	1
			Total	7	3	3	1	1
(3.1)	$\mathbb{C}^4/\mathbb{Z}_3$	$\begin{pmatrix} (0,0,1,2) \\ (0,0,0,0) \\ (0,0,0,0) \end{pmatrix}$	$\left\{\begin{array}{c} (0,0,0) \\ (1,0,0) \\ (0,1,0) \\ (0,0,3) \end{array}\right\}$	6	2	2	0	0
(3.2)	$\mathbb{C}^4/\mathbb{Z}_3$	$\begin{pmatrix} (0,1,1,1) \\ (0,0,0,0) \\ (0,0,0,0) \end{pmatrix}$	$\left\{\begin{array}{c} (0,0,0) \\ (1,0,0) \\ (0,1,0) \\ (0,2,3) \end{array}\right\}$	4	2	0	1	0
(3.3)	$\mathbb{C}^4/\mathbb{Z}_3$	$\begin{pmatrix} (1,1,2,2) \\ (0,0,0,0) \\ (0,0,0,0) \end{pmatrix}$	$\left\{\begin{array}{c} (0,0,0) \\ (1,0,0) \\ (0,1,0) \\ (1,1,3) \end{array}\right\}$	3	1	3	0	1
			Total	13	5	5	1	1

Table 2.19: The symmetry counting of distinct Abelian orbifolds of $\mathbb{C}^4$ with corresponding orbifold actions and toric tetrahedra given in terms of I_0 (corner points in Cartesian coordinates) **(Part 1/2)**.

#	Orbifold	Orbifold Action	I_0 (Corners)	$\mathsf{g}_{x_1^4}$	$\mathsf{g}_{x_1^2 x_2}$	$\mathsf{g}_{x_2^2}$	$\mathsf{g}_{x_1 x_3}$	g_{x_4}
(4.1)	$\mathbb{C}^4/\mathbb{Z}_4$	$\begin{pmatrix} (0,0,1,3) \\ (0,0,0,0) \\ (0,0,0,0) \end{pmatrix}$	$\left\{\begin{array}{l}(0,0,0)\\(1,0,0)\\(0,1,0)\\(0,0,4)\end{array}\right\}$	6	2	2	0	0
(4.2)	$\mathbb{C}^4/\mathbb{Z}_4$	$\begin{pmatrix} (0,1,1,2) \\ (0,0,0,0) \\ (0,0,0,0) \end{pmatrix}$	$\left\{\begin{array}{l}(0,0,0)\\(1,0,0)\\(0,1,0)\\(0,2,4)\end{array}\right\}$	12	2	0	0	0
(4.3)	$\mathbb{C}^4/\mathbb{Z}_4$	$\begin{pmatrix} (1,1,3,3) \\ (0,0,0,0) \\ (0,0,0,0) \end{pmatrix}$	$\left\{\begin{array}{l}(0,0,0)\\(1,0,0)\\(0,1,0)\\(1,1,4)\end{array}\right\}$	3	1	3	0	1
(4.4)	$\mathbb{C}^4/\mathbb{Z}_4$	$\begin{pmatrix} (1,2,2,3) \\ (0,0,0,0) \\ (0,0,0,0) \end{pmatrix}$	$\left\{\begin{array}{l}(0,0,0)\\(1,0,0)\\(0,1,0)\\(1,2,4)\end{array}\right\}$	6	2	2	0	0
(4.5)	$\mathbb{C}^4/\mathbb{Z}_4$	$\begin{pmatrix} (1,1,1,1) \\ (0,0,0,0) \\ (0,0,0,0) \end{pmatrix}$	$\left\{\begin{array}{l}(0,0,0)\\(1,0,0)\\(0,1,0)\\(3,3,4)\end{array}\right\}$	1	1	1	1	1
(4.6)	$\mathbb{C}^4/\mathbb{Z}_2 \times \mathbb{Z}_2$	$\begin{pmatrix} (0,1,0,1) \\ (0,0,1,1) \\ (0,0,0,0) \end{pmatrix}$	$\left\{\begin{array}{l}(0,0,0)\\(1,0,0)\\(0,2,0)\\(0,0,2)\end{array}\right\}$	4	2	0	1	0
(4.7)	$\mathbb{C}^4/\mathbb{Z}_2 \times \mathbb{Z}_2$	$\begin{pmatrix} (0,0,1,1) \\ (1,1,1,1) \\ (0,0,0,0) \end{pmatrix}$	$\left\{\begin{array}{l}(0,0,0)\\(1,0,0)\\(0,2,0)\\(1,0,2)\end{array}\right\}$	3	1	3	0	1
			Total	35	11	11	2	3

Table 2.20: The symmetry counting of distinct Abelian orbifolds of $\mathbb{C}^4$ with corresponding orbifold actions and toric tetrahedra given in terms of I_0 (corner points in Cartesian coordinates) **(Part 2/2)**.

3 Brane Tilings and Reflexive Polygons

The previous chapter discussed the work on Abelian orbifold counting using techniques from combinatorics and number theory. The problem of counting orbifolds can be considered as part of the more fundamental challenge of brane tiling classification. Given that every consistent brane tiling refers to a $3 + 1$ dimensional $\mathcal{N} = 1$ supersymmetric quiver theory with a toric Calabi-Yau mesonic moduli space, one can formulate the problem of classifying all possible such theories for a fixed number of gauge groups, quiver fields and superpotential terms. A pioneering work along this line of thought has been [17] in which such a classification of brane tilings was first attempted.

The following chapter illustrates a fundamentally different approach to the problem of brane tiling classification. It is important to recall that more than one brane tiling can have the same mesonic moduli space and hence can be associated to the same toric Calabi-Yau 3-fold. It seems therefore more efficient to fix first parameters of the moduli space geometry and to identify the associated brane tilings.

The following chapter gives a classification of a particular set of brane tilings. The set is defined such that the mesonic moduli space has a toric diagram which is a reflexive polygon. There exist only 16 reflexive polygons which have attracted much interest both in mathematics and physics. We find that there are in total 30 brane tilings which are associated to the 16 reflexive polygons, some of the brane tilings being toric dual to each other. Through the Hilbert series, we compute the mesonic generators of the moduli spaces and show that the lattice of generators is the dual reflexive polygon of the original toric diagram. As such, we show that duality between reflexive polygons is analogous to the correspondence between the toric diagram of brane tilings and their lattice of mesonic generators, and vice versa.

The chapter is an edited version of [5]. The published work is a collaboration with Amihay Hanany.

3.1 Introduction

The study of $\mathcal{N} = 1$ supersymmetric gauge theories living on D-branes probing singular non-compact Calabi-Yau 3-folds has been an immensely active and fruitful endeavour in string theory. As we have seen before, the matter content of the 4 dimensional

worldvolume theories is encoded in a graph known as the *quiver* [44].[1] An interesting subset of these theories possess mesonic moduli spaces which are toric and are associated to convex lattice polygons. We have encountered these polygons above as *toric diagrams* [147] of the Calabi-Yau singularity.

In the last two decades, a particular type of polytope caught the attention in string theory in the context of *mirror symmetry* [148, 149, 150, 151, 152, 153, 154]. This polytope is known as a *reflexive polytope*.

A reflexive polytope is a convex lattice polytope which possesses a single internal lattice point.[2] For a long time, del Pezzo surfaces [34, 92, 101, 14, 155] and more generally Fano varieties [156, 157, 158, 159, 160, 161, 162, 163, 164, 165, 166] have been associated to a range of reflexive polytopes.

When Type II superstring theory is compactified on a Calabi-Yau 3-fold, its world-sheet theory is a $\mathcal{N} = (2, 2)$ superconformal field theory. By swapping the Hodge numbers h_{11} and h_{12} associated to the Calabi-Yau 3-fold, one obtains another Calabi-Yau 3-fold. If one flips the signs of the U(1) R-charges of the left and right moving components of the theory's superalgebra, one obtains another superconformal field theory which is the one compactified on the "mirror" of the original Calabi-Yau 3-fold.

Reflexive polytopes have played an important role in studying the relationship between mirror paired Calabi-Yau manifolds and the corresponding superconformal field theories. The reflexive polytopes are used for constructing Calabi-Yau manifolds as hypersurfaces in toric varieties. The underlying property of reflexive polytopes is that they have a polar dual partner which in turn is reflexive and relates to the mirror Calabi-Yau manifold. This property led to a systematic study of mirror paired Calabi-Yau manifolds. The resulting classification [167, 168, 169, 170, 171, 172] found connections to for instance heterotic string compactifications [173, 174, 175] or to F-theory backgrounds [176, 177, 178, 179].

In the following work, reflexive polygons are used to study mesonic moduli spaces of 4d supersymmetric quiver gauge theories dual to Type IIB string theory on $\text{AdS}_5 \times X_5$ where X_5 is a Sasaki-Einstein 5-manifold. There are 16 distinct reflexive polygons and the corresponding theories are worldvolume theories of D3-branes probing Calabi-Yau 3-fold singularities. The mesonic moduli spaces are toric Calabi-Yau 3-folds and the reflexive polygons are the corresponding toric diagrams.

The aim of the following work is to identify all 4d supersymmetric quiver gauge theories whose moduli space is represented by a reflexive polygon. In order to do so, extensive use is made of *brane tilings* [15, 55][3] on T^2.

Every consistent brane tiling relates to a consistent quiver gauge theory. Starting from the brane tiling for the orbifold of the form $\mathbb{C}^3/\mathbb{Z}_4 \times \mathbb{Z}_4$ with orbifold action

---

[1] For more mathematical reviews on quivers see for example [86, 91].

[2] From Latin *reflexus*, Medieval Latin *reflexivus*, meaning to be turned back or reflected.

[3] For applications of brane tilings see for example [100, 16, 180, 89, 90].

$(1, 0, 3)(0, 1, 3)$ [126, 1, 2, 3, 4], one applies the *Higgs mechanism* [101] and uses *Seiberg duality* [34, 92, 14, 33, 36, 181, 182] on brane tilings in order to find that there exist exactly 30 quiver gauge theories corresponding to the 16 reflexive polygons. Seiberg duality, also known as toric duality in this context, relates theories with different matter content and superpotential to the same mesonic moduli space.

In order to have a complete classification of the mesonic moduli spaces, the moduli space generators for all 30 quiver gauge theories are found by computing the *Hilbert series* [50, 112, 51, 52, 113]. As we have reviewed above, the Hilbert series encodes information about the moduli space generators. They are identified using a method known as *plethystics* [183]. The lattice of generators formed by the mesonic charges is the dual reflexive polygon for the 16 toric diagrams. It is shown that this is the case for all 30 quiver gauge theories.

The complete classification of $4d \, \mathcal{N} = 1$ supersymmetric gauge theories corresponding to the 16 reflexive polygons leads to new observations. The most important observation is that of a new correspondence between brane tilings which we name *specular duality*. It relates brane tilings with different mesonic moduli spaces under a swap of external and internal points of the toric diagram. Specular duality partitions the set of 30 quiver gauge theories in dual pairs and illustrates interesting physics at work. An illustration of this new duality is given at the concluding section, and it is of great interest to explore it further in future work.

The chapter is structured as follows. In section §3.2, the concepts and motivations behind studying reflexive polygons are reviewed. The section also reviews the lattice of mesonic generators which is a key ingredient of the discussion. Sections §3.3 to §3.18 summarize the 30 quiver gauge theories associated to reflexive polygons, and illustrate the duality between the toric diagram and generator lattices. In section §3.19, the trees illustrating the relationships between toric (Seiberg) dual brane tiling models corresponding to the same reflexive polygon are presented.

3.2 Background and Motivation

3.2.1 Reflexive Polytopes

Mirror Symmetry. Reflexive polytopes have been introduced in string theory in the context of mirror symmetry [148, 149, 150, 151, 152, 153, 154]. A way to study mirror symmetry is to consider Type II superstring theory compactified on a Calabi-Yau 3-fold. Its string worldsheet theory is a $\mathcal{N} = (2, 2)$ superconformal field theory. It contains a superalgebra with left and right moving components. When one flips the signs of the $U(1)$ R-symmetry charges of the left and right moving components, the Calabi-Yau transitions to a different Calabi-Yau manifold with its Hodge numbers h_{11} and h_{12}

d	Number of Polytopes
1	1
2	16
3	4319
4	473800776

Table 3.1: Number of reflexive lattice polytopes in dimension $d \leq 4$. The number of polytopes forms a sequence which has the identifier A090045 on OEIS.

being interchanged.

The understanding of mirror symmetry in the context of compactified superstring theory led to a search of mirror paired Calabi-Yau manifolds. Batyrev-Borisov [150, 152] laid the foundations for industrialising the search for mirror paired Calabi-Yau manifolds by formulating the construction of Calabi-Yau manifolds as hypersurfaces in toric varieties represented by reflexive polytopes. These reflexive polytopes are on a lattice with the dual polytope and hence corresponding mirror Calabi-Yau manifold being identified by a straightforward geometrical transformation.

Let the following summary review the notion of a reflexive polytope and the concept of its dual:

- A **reflexive polytope** is a convex polytope with points in a lattice $\mathbb{Z}^d$ and the origin $(0, \ldots, 0)$ being the unique interior point of the polytope.

- A **dual (polar) polytope** exists for every reflexive polytope. The dual of polytope Δ, Δ°, is another lattice polytope with points

$$\Delta^\circ = \{ v^\circ \in \mathbb{Z}^d \mid \langle v^\circ, v \rangle \geq -1 \ \forall v \in \Delta \} \tag{3.2.1}$$

  The dual of every reflexive polygon is another reflexive polygon. A reflexive polygon can be self-dual, $\Delta = \Delta^\circ$.

- A **classification of reflexive polytopes** [168, 169, 170] is available for the dimensions $d \leq 4$ with the number of reflexive polytopes given in Table 3.1. It is unknown how many exist for higher dimensions.

D-branes on Calabi-Yau. Next to the study of mirror symmetry, reflexive polytopes are playing an interesting role in a different context in string theory. Witten described in 1993 an $\mathcal{N} = (2, 2)$ supersymmetric field theory with $U(1)$ gauge groups [104] in the language of what is today known as gauge linear sigma models (GLSM). He illustrated how the Fayet-Iliopoulos parameter of the $\mathcal{N} = (2, 2)$ supersymmetric field theory interpolates between the Landau-Ginzburg and Calabi-Yau phases of the theory. The large parameter limit leads to the space of classical vacua as toric Calabi-Yau spaces determined by the D- and F-terms of the supersymmetric field theory. The formulation
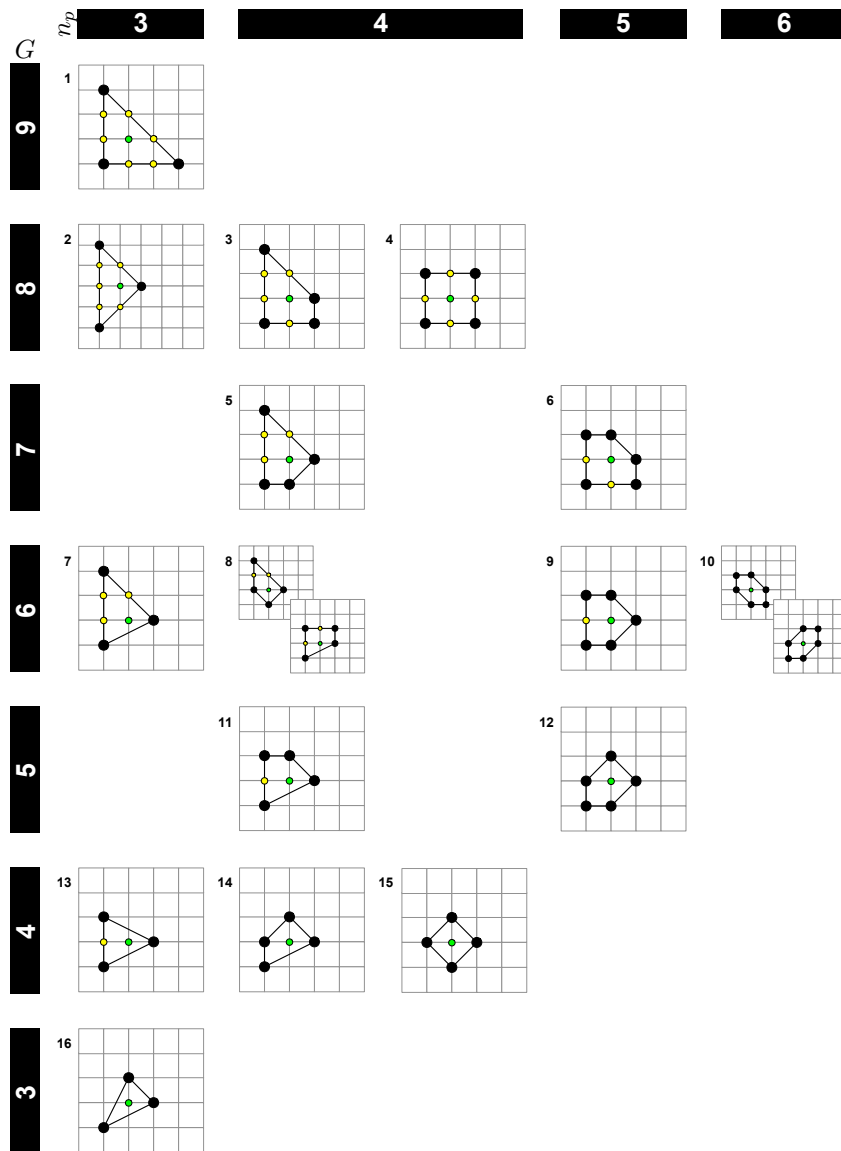
Figure 3.1: *The 16 reflexive polygons.* The polygons have been $GL(2, \mathbb{Z})$ adjusted to reflect the duality under (3.2.1). The green internal points are the origins. G is the area of the polygon with the smallest lattice triangle having normalized area 1, and n_G is the number of extremal points which are in black. The 4 polygons with $G = 6$ are self-dual. The paired polygons in 8 and 10 are $GL(2, \mathbb{Z})$ equivalent and are each others dual polygon.

of GLSM is going to be used in the context of D-brane gauge theories in this chapter even though the FI terms will not play a crucial role during the discussion.

Let the focus be on worldvolume theories living on a stack of D3-branes probing Calabi-Yau 3-fold singularities. The gravity dual of these theories is Type IIB string theory on the background $AdS_5 \times X_5$ where X_5 is a Sasaki-Einstein 5-manifold. The

worldvolume theories are $4d$ $\mathcal{N} = 1$ supersymmetric quiver gauge theories whose space of vacua being toric Calabi-Yau 3-fold are described by lattice polygons on $\mathbb{Z}^2$ known as the toric diagrams.

A restriction that the toric diagrams are reflexive polygons is introduced for the purpose of the study. A motivation for introducing the restriction is the fact that there are only a finite number 16 of these reflexive polygons. The natural question to ask, and the question which is fully answered in the following discussion, is which supersymmetric quiver gauge theories exist whose space of vacua correspond to the 16 reflexive polygons.

There are useful properties of the quiver gauge theories which are considered in this chapter and have been reviewed above. These properties provide the essential tools for finding all quiver gauge theories corresponding to reflexive polygons and have been summarized below:

- The **Higgs Mechanism** [101] in the context of quiver gauge theories has a natural interpretation in terms of the geometrical blow down, i.e. 'higgsing', or blow up, i.e. 'un-higgsing', of the toric variety corresponding to the gauge theory vacuum moduli space. All 16 reflexive polygons and the corresponding toric varieties can be related by the geometrical blow downs starting from the Abelian orbifold of the form $\mathbb{C}^3/\mathbb{Z}_4 \times \mathbb{Z}_4$ with orbifold action $(1, 0, 3)(0, 1, 3)$ [126, 1, 2, 3, 4].

- **Toric (Seiberg) Duality** [34, 92, 14, 33, 36, 181, 182] in the context of quiver gauge theories relates theories with the same vacuum moduli space. In other words, two toric dual theories relate to the same reflexive polygon. Consequently, a single toric variety can be the vacuum moduli space of multiple quiver gauge theories. Such dual quiver gauge theories are known as *toric phases* of the moduli space. More generally, Seiberg duality relates an infinite number of quiver gauge theories by allowing the ranks of gauge groups in the theory to be greater than one. In the following discussion based on brane tilings, only $U(1)$ gauge groups are taken. The search for brane tilings corresponding to the 16 reflexive polygons uses toric duality in order to identify all toric phases. It turns out that there are 30 brane tiling theories corresponding to the 16 reflexive polygons.

Many of the quiver gauge theories related to reflexive polygons have been studied in the past. A selection of the available literature is given in Table 3.2. With the following work, a complete classification of all 30 quiver gauge theories related to reflexive polygons in Witten's language of **GLSM fields** is provided for the first time. GLSM fields relate the points of the toric diagram with the matter fields of the quiver gauge theory. The F-term and D-term constraint charges on the GLSM fields are used to obtain the **mesonic Hilbert series**. The mesonic Hilbert series encodes the moduli space **generators**.

Model #	Model Name	Quiver & W (Brane Tiling)	Toric Data	Mesonic HS	Generators & Generator Lattice
1	$\mathbb{C}^3/\mathbb{Z}_3 \times \mathbb{Z}_3 \ (1,0,2)(0,1,2)$	[15, 181]			
2	$\mathbb{C}^3/\mathbb{Z}_4 \times \mathbb{Z}_2 \ (1,0,3)(0,1,1)$	[15]			
3	$L_{1,3,1}/\mathbb{Z}_2 \ (0,1,1,1)$	[100, 110]	[110]		
4	PdP$_5$, $\mathcal{C}/\mathbb{Z}_2 \ (1,0,0,1)(0,1,1,0)$	[101, 15, 55, 71]	[101, 55, 71]		
5	PdP$_{4b}$				
6	PdP$_{4a}$	[101, 71, 184]	[101, 71, 184]	[50]	
7	PdP$_{3a}$, $\mathbb{C}^3/\mathbb{Z}_6 \ (1,2,3)$	[15, 181]	[15]		
8	PdP$_{3c}$, SPP$/\mathbb{Z}_2 \ (0,1,1,1)$	[101, 181, 93]	[101, 93]		
9	PdP$_{3b}$	[101, 181, 93]	[101, 93]		
10	dP$_3$	[101, 14, 55, 181, 93, 71, 73]	[92, 101, 55, 71, 93, 73]	[50]	
11	PdP$_2$	[101, 93]	[101, 93]		
12	dP$_2$	[14, 55, 71, 93, 13, 73, 185, 17]	[92, 55, 71, 93, 73, 185]	[50]	[185]
13	$Y^{2,2}$, $\mathbb{C}^3/\mathbb{Z}_4 \ (1,1,2)$	[15, 55]	[102]	[50]	[118, 119]
14	$Y^{2,1}$, dP$_1$	[14, 55, 71, 93, 13, 17]	[92, 71, 93, 102]	[50, 52]	[118, 119]
15	$\mathbb{F}_0$, $Y^{2,0}$, $\mathcal{C}/\mathbb{Z}_2 \ (1,1,1,1)$	[92, 55, 15, 17, 93, 71, 73, 75]	[92, 71, 93, 73, 102, 75]	[50]	[118, 119]
16	dP$_0$, $\mathbb{C}^3/\mathbb{Z}_3 \ (1,1,1)$	[14, 15, 16, 17, 18]	[92, 101, 18]	[50, 52, 18]	

Table 3.2: A selection of the literature on quiver gauge theories corresponding to reflexive polygons.

An intriguing property of theories corresponding to reflexive polygons, which is exemplified in the work below, is as follows:

The global charges on moduli space generators form a lattice polygon on $\mathbb{Z}^2$ which is reflexive and which is precisely the dual polygon of the toric diagram.

The two sections below provide a review of the physical concepts involved in order to proceed with the complete classification of quiver gauge theories corresponding to reflexive polygons.

3.2.2 The Brane Tiling and the Forward Algorithm

The worldvolume theory of a stack of n D3-branes probing singular non-compact Calabi-Yau 3-folds is a $3 + 1$ dimensional $\mathcal{N} = 1$ supersymmetric gauge theory. The corresponding Lagrangian is specified by the theory's gauge groups, matter content and superpotential.

The probed Calabi-Yau 3-fold is toric, and is the mesonic moduli space of the worldvolume theory. It is of great interest to associate to each worldvolume theory the corresponding mesonic moduli space. The **forward algorithm** [34, 106] translates the gauge theory information into toric data. This algorithm is used extensively for this work and the reader is referred to the review in section §1.4.4.

3.2.3 Hilbert Series and Lattice of Generators

The generating function of mesonic gauge invariant operators (GIOs) is known as the **mesonic Hilbert series** [50, 112, 51, 52, 113]. The Hilbert series encodes the generators of the associated moduli space. These are essential for a complete classification of the mesonic moduli spaces of brane tilings corresponding to reflexive polygons. The moduli
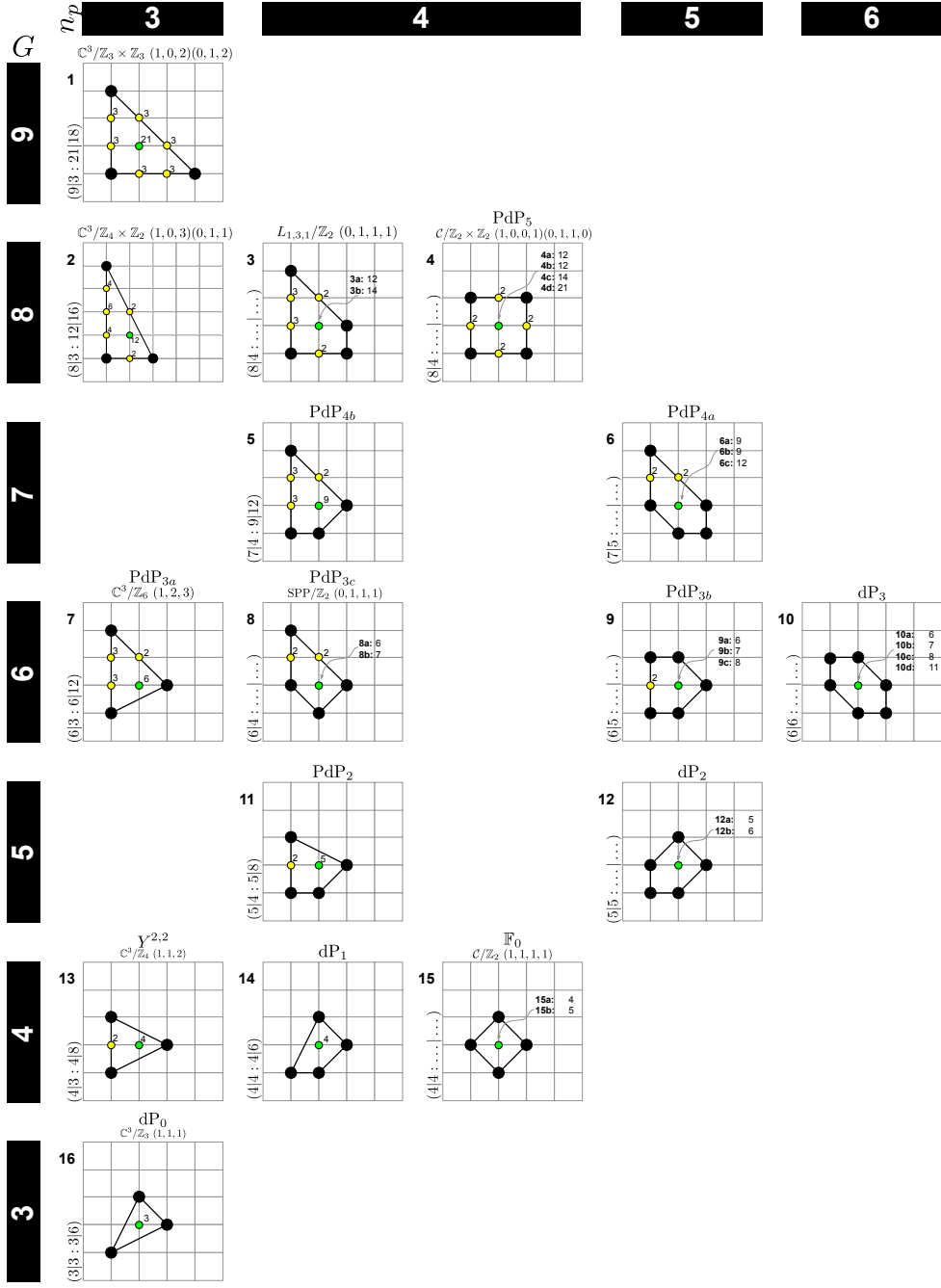
Figure 3.2: *Reflexive Toric Diagrams.* The figure shows the 16 reflexive toric diagrams which correspond to 30 brane tilings. Each polygon is labelled by $(G|n_p : n_i|n_W)$, where G is the number of $U(N)$ gauge groups, n_p is the number of extremal perfect matchings, n_i is the number of internal perfect matchings, and n_W is the number of superpotential terms. A reflexive polygon can correspond to multiple brane tilings by toric duality.

space generators can be extracted from the Hilbert series using a method known as **plethystics**. These carry charges under the **mesonic symmetry**. The charges on a $\mathbb{Z}_2$ lattice form a convex polygon which is the dual polygon of the toric diagram.

For a comprehensive review of the mesonic Hilbert series and plethystics for brane tilings, the reader is encouraged to go to the comprehensive review in section §1.4.3. In order to understand a fundamental ingredient – the lattice of mesonic generators – for the following study of brane tilings related to reflexive polygons, let us revisit the mesonic symmetry of brane tilings.

Mesonic Symmetry. The mesonic moduli space of a given brane tiling is a non-compact toric Calabi-Yau 3-fold. The mesonic symmetry of the associated quiver gauge theory takes one of the following forms,

- $U(1)_{f_1} \times U(1)_{f_2} \times U(1)_R$

- $SU(2)_x \times U(1)_f \times U(1)_R$

- $SU(2)_{x_1} \times SU(2)_{x_2} \times U(1)_R$

- $SU(3)_{x_1,x_2} \times U(1)_R$,

where the lower case indices denote fugacities of the gauge group with the exemption of the R-symmetry group $U(1)_R$. The fugacity associated to the $U(1)_R$ charge is t. For a review on how to calculate R-charges, the reader is referred to section §1.5.2.

The above global symmetries derive from the isometry group of the Calabi-Yau 3-fold. The enhancement of a $U(1)$ flavour to $SU(2)$ or $SU(3)$ is indicated by repeated columns in the total charge matrix Q_t.

Lattice of Generators. The lattice of generators is determined by the mesonic charges carried by the generators of the mesonic moduli space. Ignoring the $U(1)_R$ factor, the remaining flavour symmetries have ranks which sum up to 2. Hence, there are always 2 fugacities which count flavour charges. The pair of flavour charges carried by each generator is taken as coordinates of a point on the plane. The convex hull of the collection of points corresponding to the collection of moduli space generators forms a convex polygon. This is known as the lattice of generators.

For a non-vanishing convex polygon on $\mathbb{Z}^2$, the flavour charges are subject to the following constraints:

- The pairs of flavour charges carried by all n_p extremal perfect matchings form a pair of n_p-dimensional charge vectors. For a non-trivial choice of flavour charges, the charge vectors are linearly independent.

- The elements of the n_p-dimensional charge vectors sum up to zero.

- The charges on GLSM fields are scaled such that the charges on mesonic moduli space generators take integer values and the lattice of generators is on $\mathbb{Z}^2$.

The lattice of generators subject to the constraints above still exhibits a remaining $GL(2,\mathbb{Z})$ degree of freedom. Moreover, each generator also carries a R-charge which plays the role of a third coordinate for each point in the lattice of generators. In order to remove these remaining degrees of freedom, one makes use of a particular property of generator lattices introduced below.

Duality between Generator Lattices and Toric Diagrams.

The lattice of generators of a brane tiling is
the dual of the toric diagram.

The duality between *reflexive* polygons follows (3.2.1). Hence, for reflexive polygons as toric diagrams, the lattice of generators is another reflexive polygon in $\mathbb{Z}^2$. Accordingly, the remaining $GL(2,\mathbb{Z})$ degree of freedom on the lattice of generators can be removed by making the duality for reflexive polygons exact as defined in (3.2.1). In addition, for reflexive polygons the lattice of generators always lies on $\mathbb{Z}^2$.

When the lattice of generators is considered as a toric diagram of a new brane tiling, the duality between reflexive polygons manifestly relates between two quiver gauge theories with toric moduli spaces. In terms of the number of $U(n)$ gauge groups G and the number of GLSM fields with non-zero R-charge n_p, the duality map takes the form

$$
\begin{array}{ccl}
\text{Model A} & \leftrightarrow & \text{Model B} \\
G & \leftrightarrow & 12 - G \\
n_p & \leftrightarrow & n_p
\end{array}
\tag{3.2.2}
$$

as illustrated in Figure 3.2.

In the following sections, all 30 quiver gauge theories with their brane tilings corresponding to the 16 reflexive polygons are classified. All 30 quiver gauge theories are obtained by higgsing and toric (Seiberg) dualizing the theory related to the Abelian orbifold of the form $\mathbb{C}^3/\mathbb{Z}_4 \times \mathbb{Z}_4$ with orbifold action $(1,0,3)(0,1,3)$. The details for the *parent* theory for all reflexive polygon theories are given in appendix §A.4.

Figure 3.3: The quiver, toric diagram, and brane tiling of Model 1. The red arrows in the quiver indicate all possible connections between blocks of nodes.

3.3 Model 1: $\mathbb{C}^3/\mathbb{Z}_3 \times \mathbb{Z}_3$ $(1,0,2)(0,1,2)$

The superpotential is

$$
\begin{aligned}
W \;=\; & +X_{15}X_{56}X_{61} + X_{29}X_{91}X_{12} + X_{31}X_{18}X_{83} + X_{42}X_{23}X_{34} + X_{53}X_{37}X_{75} \\
& +X_{67}X_{72}X_{26} + X_{78}X_{89}X_{97} + X_{86}X_{64}X_{48} + X_{94}X_{45}X_{59} \\
& -X_{15}X_{59}X_{91} - X_{29}X_{97}X_{72} - X_{31}X_{12}X_{23} - X_{42}X_{26}X_{64} - X_{53}X_{34}X_{45} \\
& -X_{67}X_{75}X_{56} - X_{78}X_{83}X_{37} - X_{86}X_{61}X_{18} - X_{94}X_{48}X_{89} \; .
\end{aligned}
\tag{3.3.3}
$$

The perfect matching matrix is

$$
\tag{3.3.4}
$$

	$U(1)_{f_1}$	$U(1)_{f_2}$	$U(1)_R$	fugacity
p_1	1/3	0	2/3	t_1
p_2	-1/3	-1/3	2/3	t_2
p_3	0	1/3	2/3	t_3

Table 3.3: The GLSM fields corresponding to extremal points of the toric diagram with their mesonic charges (Model 1).

The F-term charge matrix $Q_F = \ker(P)$ is

$$Q_F = \begin{pmatrix} & & & & & & & & & & & & & & & & & & & & & & & & & & & & & & & & & & & & & \\ \end{pmatrix} \quad (3.3.5)$$

The D-term charge matrix is

$$Q_D = \begin{pmatrix} & & & & & & & & & & & & & & & & & & & & & & & & & & & & & & & & & & & & & \\ \end{pmatrix} \quad (3.3.6)$$

The total charge matrix Q_t exhibits no repeated columns. Accordingly, the global symmetry group is $U(1)_{f_1} \times U(1)_{f_2} \times U(1)_R$. Following the discussion on flavour symmetry and R-charges in section §3.2.3, the charges on GLSM fields with non-zero R-charges are chosen as shown in Table 3.3.

Products of non-extremal perfect matchings are labelled by a single variable as follows,

$$q = q_1 q_2 q_3 \ , \quad r = r_1 r_2 r_3 \ , \quad u = u_1 u_2 u_3 \ , \quad v = v_1 v_2 v_3 \ ,$$

$$w = w_1 w_2 w_3 \ , \quad x = x_1 x_2 x_3 \ , \quad s = \prod_{m=1}^{21} s_m \ . \quad (3.3.7)$$

The fugacities t_α count extremal perfect matchings corresponding to GLSM fields with non-zero R-charge. The fugacity of the form y_q counts the product of non-extremal perfect matchings q above.

The mesonic Hilbert series of Model 1 is calculated using the Molien integral formula in (1.4.67). It is

$$
\begin{aligned}
&g_1(t_\alpha, y_q, y_r, y_u, y_v, y_w, y_x, y_s; \mathcal{M}_1^{mes}) = \\
&\frac{1 - y_q^3 y_r^3 y_u^3 y_v^3 y_w^3 y_x^3 y_s^3 \ t_1^3 t_2^3 t_3^3}{(1 - y_q^2 y_r y_v^2 y_w y_s \ t_1^3)(1 - y_q y_u y_w^2 y_x^2 y_s \ t_2^3)(1 - y_r^2 y_u^2 y_v y_x y_s \ t_3^3)} \\
&\times \frac{1}{1 - y_q y_r y_u y_v y_w y_x y_s \ t_1 t_2 t_3} \ .
\end{aligned}
$$

(3.3.8)

The plethystic logarithm of the mesonic Hilbert series is

$$
\begin{aligned}
PL[g_1(t_\alpha, y_q, y_r, y_u, y_v, y_w, y_x, y_s; \mathcal{M}_1^{mes})] &= y_q y_r y_u y_v y_w y_x y_s \ t_1 t_2 t_3 + y_q^2 y_r y_v^2 y_w y_s \ t_1^3 \\
&+ y_r^2 y_u^2 y_v y_x y_s \ t_3^3 + y_q y_u y_w^2 y_x^2 y_s \ t_2^3 - y_q^3 y_r^3 y_u^3 y_v^3 y_w^3 y_x^3 y_s^3 \ t_1^3 t_2^3 t_3^3 \ .
\end{aligned}
$$

(3.3.9)

The finite plethystic logarithm indicates that the mesonic moduli space is a complete intersection.

In terms of the fugacity map

$$
f_1 = \frac{y_q y_v \ t_1^2}{y_u y_x \ t_2 t_3} \ , \quad f_2 = \frac{y_r y_u \ t_3^2}{y_q y_w \ t_1 t_2} \ , \quad t = y_q^{1/3} y_r^{1/3} y_u^{1/3} y_v^{1/3} y_w^{1/3} y_x^{1/3} y_s^{1/3} \ t_1^{1/3} t_2^{1/3} t_3^{1/3}
$$

(3.3.10)

where f_1, f_2 and t are the fugacities counting the mesonic charges, the above plethystic logarithm becomes

$$
PL[g_1(t, f_1, f_2; \mathcal{M}_1^{mes})] = \left(1 + f_1 + f_2 + \frac{1}{f_1 f_2}\right) t^3 - t^9
$$

(3.3.11)

The above plethystics logarithm identifies both the moduli space generators and the mesonic charges carried by them. The generators and the corresponding mesonic charges are summarized in Table 3.4. The generators can be presented on a charge lattice. It is a convex polygon as shown in Table 3.4 and is the dual reflexive polygon of the toric diagram of Model 16.

The relation formed among the generators is as follows,

$$
A_1 A_2 A_3 = B^3 \ .
$$

(3.3.12)

With the following fugacity map

$$
\begin{aligned}
T_1 &= f_1^{1/3} \ t = y_q^{2/3} y_r^{1/3} y_v^{2/3} y_w^{1/3} y_s^{1/3} t_1 \ , \\
T_2 &= f_1^{-1/3} f_2^{-1/3} \ t = y_q^{1/3} y_u^{1/3} y_w^{2/3} y_x^{2/3} y_s^{1/3} t_2 \ , \\
T_3 &= f_2^{1/3} \ t = y_r^{2/3} y_u^{2/3} y_v^{1/3} y_x^{1/3} y_s^{1/3} t_3 \ ,
\end{aligned}
$$

(3.3.13)

Generator	$U(1)_{f_1}$	$U(1)_{f_2}$
$A_1 = p_1^3\ q^2\ r\ v^2\ w\ s$	1	0
$A_2 = p_2^3\ q\ u\ w^2\ x^2\ s$	-1	-1
$A_3 = p_3^3\ r^2\ u^2\ v\ x\ s$	0	1
$B = p_1 p_2 p_3\ q\ r\ u\ v\ w\ x\ s$	0	0
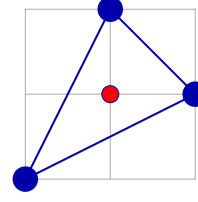
Table 3.4: The generators and lattice of generators of the mesonic moduli space of Model 1 in terms of GLSM fields with the corresponding flavor charges.

Generator	$U(1)_{f_1}$	$U(1)_{f_2}$
$X_{18}X_{89}X_{91} = X_{23}X_{37}X_{72} = X_{45}X_{56}X_{64}$	1	0
$X_{15}X_{53}X_{31} = X_{29}X_{94}X_{42} = X_{67}X_{78}X_{86}$	-1	-1
$X_{12}X_{26}X_{61} = X_{34}X_{48}X_{83} = X_{59}X_{97}X_{75}$	0	1
$X_{12}X_{23}X_{31} = X_{12}X_{29}X_{91} = X_{15}X_{56}X_{61} = X_{15}X_{59}X_{91} = X_{18}X_{83}X_{31} = X_{18}X_{86}X_{61} = X_{23}X_{34}X_{42} = X_{26}X_{64}X_{42} = X_{26}X_{67}X_{72}$	0	0
$= X_{29}X_{97}X_{72} = X_{34}X_{45}X_{53} = X_{37}X_{75}X_{53} = X_{37}X_{78}X_{83} = X_{45}X_{59}X_{94} = X_{48}X_{86}X_{64} = X_{48}X_{89}X_{94} = X_{56}X_{67}X_{75} = X_{78}X_{89}X_{97}$		

Table 3.5: The generators in terms of bifundamental fields (Model 1).

the mesonic Hilbert series becomes

$$g_1(T_1, T_2, T_3; \mathcal{M}_1^{mes}) = \frac{1 - T_1^3 T_2^3 T_3^3}{(1 - T_1^3)(1 - T_2^3)(1 - T_3^3)(1 - T_1 T_2 T_3)} \qquad (3.3.14)$$

with the plethystic logarithm being

$$PL[g_1(T_1, T_2, T_3; \mathcal{M}_1^{mes})] = T_1 T_2 T_3 + T_1^3 + T_3^3 + T_2^3 - T_1^3 T_2^3 T_3^3 \ . \qquad (3.3.15)$$

The above refinement of the Hilbert series exemplifies the conical structure of the toric Calabi-Yau space.

3.4 Model 2: $\mathbb{C}^3/\mathbb{Z}_4 \times \mathbb{Z}_2\ (1, 0, 3)(0, 1, 1)$

The superpotential is

$$\begin{aligned}
W \ = \ & +X_{17}X_{72}X_{21} + X_{28}X_{81}X_{12} + X_{31}X_{14}X_{43} + X_{42}X_{23}X_{34} \\
& +X_{53}X_{36}X_{65} + X_{64}X_{45}X_{56} + X_{75}X_{58}X_{87} + X_{86}X_{67}X_{78} \\
& -X_{17}X_{78}X_{81} - X_{28}X_{87}X_{72} - X_{31}X_{12}X_{23} - X_{42}X_{21}X_{14} \\
& -X_{53}X_{34}X_{45} - X_{64}X_{43}X_{36} - X_{75}X_{56}X_{67} - X_{86}X_{65}X_{58} \ . \qquad (3.4.16)
\end{aligned}$$

The perfect matching matrix is

$$P = $$

	p_1	p_2	p_3	q_1	q_2	r_1	r_2	u_1	u_2	u_3	u_4	v_1	v_2	v_3	v_4	w_1	w_2	w_3	w_4	w_5	w_6	s_1	s_2	s_3	s_4	s_5	s_6	s_7	s_8	s_9	s_{10}	s_{11}	s_{12}
X_{67}	1	0	0	1	0	0	0	1	1	1	0	1	0	0	0	1	0	1	1	0	0	1	0	0	0	1	1	0	0	0	0	0	0
X_{45}	1	0	0	1	0	0	0	1	1	0	1	0	1	0	0	1	0	0	0	1	1	1	0	0	0	0	1	1	0	0	0	0	0
X_{58}	1	0	0	0	1	0	0	1	1	1	0	1	0	0	0	1	0	1	1	0	0	0	1	0	0	0	0	0	0	1	1	0	0
X_{36}	1	0	0	0	1	0	0	1	1	0	1	0	1	0	0	1	0	0	0	1	1	0	1	0	0	0	0	0	0	0	0	1	1
X_{23}	1	0	0	1	0	0	0	1	0	1	1	0	0	0	1	0	1	1	0	1	0	0	0	0	1	0	1	0	1	0	0	0	0
X_{81}	1	0	0	1	0	0	0	0	1	1	1	0	0	0	1	0	1	0	1	0	1	0	0	1	0	1	0	0	0	0	0	0	1
X_{14}	1	0	0	0	1	0	0	1	0	1	1	0	0	1	0	0	1	1	0	1	0	0	0	0	1	0	1	0	0	0	0	1	0
X_{72}	1	0	0	0	1	0	0	0	1	1	1	0	0	0	1	0	1	0	1	0	1	0	0	0	1	0	0	0	1	0	1	0	0
X_{28}	0	1	0	1	0	0	0	0	1	0	0	1	1	1	0	1	0	1	0	1	0	1	0	0	0	0	1	0	1	0	0	0	0
X_{31}	0	1	0	0	0	1	0	0	1	0	0	1	1	1	0	1	0	0	1	0	1	0	1	0	0	1	0	0	0	0	0	0	1
X_{17}	0	1	0	0	0	0	1	1	0	0	0	1	1	1	0	1	0	1	0	1	0	1	0	0	0	1	0	0	0	0	0	1	0
X_{42}	0	1	0	0	0	0	1	0	1	0	0	1	1	0	1	1	0	0	1	0	1	1	0	0	0	0	0	1	0	1	0	0	0
X_{64}	0	1	0	0	0	1	0	0	0	1	0	1	0	1	1	0	1	1	1	0	0	0	0	0	1	1	1	0	0	0	0	0	0
X_{75}	0	1	0	0	0	1	0	0	0	0	1	0	1	1	1	0	1	0	0	1	1	0	0	1	0	0	1	1	0	0	0	0	0
X_{53}	0	1	0	0	0	0	1	0	0	1	0	1	0	1	1	0	1	1	1	0	0	0	0	1	0	0	0	0	0	1	1	0	0
X_{86}	0	1	0	0	0	0	1	0	0	0	1	0	1	1	1	0	1	0	0	1	1	0	0	1	0	0	0	0	0	0	0	1	1
X_{65}	0	0	1	1	0	1	0	0	0	0	0	0	0	0	0	0	0	0	0	0	0	1	0	0	1	1	1	1	1	0	0	0	0
X_{21}	0	0	1	1	0	1	0	0	0	0	0	0	0	0	0	0	0	0	0	0	0	0	1	1	0	1	0	1	0	1	0	0	1
X_{43}	0	0	1	1	0	0	1	0	0	0	0	0	0	0	0	0	0	0	0	0	0	1	0	1	0	0	0	1	1	1	1	0	0
X_{87}	0	0	1	1	0	0	1	0	0	0	0	0	0	0	0	0	0	0	0	0	0	1	0	1	0	1	1	0	0	0	0	1	1
X_{78}	0	0	1	0	1	1	0	0	0	0	0	0	0	0	0	0	0	0	0	0	0	0	1	0	1	0	0	1	1	1	1	0	0
X_{34}	0	0	1	0	1	1	0	0	0	0	0	0	0	0	0	0	0	0	0	0	0	0	1	0	1	1	1	1	0	0	0	1	1
X_{12}	0	0	1	0	1	0	1	0	0	0	0	0	0	0	0	0	0	0	0	0	0	1	0	0	1	0	1	0	1	0	1	1	0
X_{56}	0	0	1	0	1	0	1	0	0	0	0	0	0	0	0	0	0	0	0	0	0	0	1	1	0	0	0	0	1	1	1	1	1

$$(3.4.17)$$

The F-term charge matrix $Q_F = \ker(P)$ is

$$Q_F = $$

p_1	p_2	p_3	q_1	q_2	r_1	r_2	u_1	u_2	u_3	u_4	v_1	v_2	v_3	v_4	w_1	w_2	w_3	w_4	w_5	w_6	s_1	s_2	s_3	s_4	s_5	s_6	s_7	s_8	s_9	s_{10}	s_{11}	s_{12}
1	1	0	0	0	0	0	-1	0	0	0	0	0	0	-1	0	0	0	0	0	0	0	0	0	0	0	0	0	0	0	0	0	0
1	1	0	0	0	0	0	0	-1	0	0	0	0	-1	0	0	0	0	0	0	0	0	0	0	0	0	0	0	0	0	0	0	0
1	1	0	0	0	0	0	0	0	-1	0	0	-1	0	0	0	0	0	0	0	0	0	0	0	0	0	0	0	0	0	0	0	0
1	0	1	-1	-1	0	0	0	0	0	0	0	0	0	0	0	0	0	0	0	0	0	0	0	0	0	0	0	0	0	0	0	0
1	0	0	-1	0	0	0	0	-1	0	0	0	0	0	0	0	0	0	0	0	0	1	0	0	0	0	0	0	0	0	0	-1	1
1	0	0	-1	0	0	0	0	0	-1	0	0	0	0	0	0	0	0	0	0	0	0	-1	0	0	1	0	0	0	1	0	0	0
1	0	0	0	0	1	0	-1	0	0	0	0	0	0	0	0	0	0	0	0	0	0	0	0	-1	-1	1	0	0	0	0	0	0
1	0	0	0	0	0	0	-1	0	0	-1	0	0	0	0	0	0	0	1	0	0	0	0	0	0	0	0	0	0	0	0	0	0
1	0	0	0	0	0	0	0	-1	0	-1	0	0	0	0	0	0	0	0	1	0	0	0	0	0	0	0	0	0	0	0	0	0
1	0	0	0	0	0	0	0	0	-1	-1	0	0	0	0	0	1	0	0	0	0	0	0	0	0	0	0	0	0	0	0	0	0
1	0	0	0	0	0	0	-1	-1	0	0	0	0	0	0	1	0	0	0	0	0	0	0	0	0	0	0	0	0	0	0	0	0
1	0	0	0	0	0	0	-1	0	-1	0	0	0	0	0	0	0	1	0	0	0	0	0	0	0	0	0	0	0	0	0	0	0
1	0	0	0	0	0	0	0	-1	-1	0	0	0	0	0	0	0	0	1	0	0	0	0	0	0	0	0	0	0	0	0	0	0
1	0	0	0	0	0	0	0	0	-1	0	1	0	0	0	-1	0	0	0	0	0	0	0	0	0	0	0	0	0	0	0	0	0
1	0	0	0	0	0	0	0	0	0	-1	0	1	0	0	-1	0	0	0	0	0	0	0	0	0	0	0	0	0	0	0	0	0
0	1	1	0	0	-1	-1	0	0	0	0	0	0	0	0	0	0	0	0	0	0	0	0	0	0	0	0	0	0	0	0	0	0
0	0	1	-1	0	-1	0	0	0	0	0	0	0	0	0	0	0	0	1	0	0	0	0	0	0	1	0	0	0	0	0	-1	0
0	0	1	0	0	0	0	0	0	0	0	0	0	0	0	1	0	0	0	0	0	-1	-1	0	0	0	0	0	0	0	0	0	0
0	0	1	0	0	0	0	0	0	0	0	0	0	0	0	0	0	0	1	0	0	0	0	0	0	-1	0	0	0	-1	0	0	0
0	0	0	1	0	1	0	0	0	0	0	0	0	0	0	0	0	0	0	0	0	0	0	0	-1	0	-1	0	0	0	0	0	0
0	0	0	1	0	0	1	0	0	0	0	0	0	0	0	0	0	0	0	0	0	-1	0	-1	0	0	0	0	0	0	0	0	0
0	0	0	0	0	0	0	0	0	0	0	0	0	0	0	0	0	0	0	0	0	1	0	0	1	0	-1	0	-1	0	0	0	0
0	0	0	0	0	0	0	0	0	0	0	0	0	0	0	0	0	0	0	0	0	0	0	0	0	1	-1	0	0	0	1	-1	

$$(3.4.18)$$

	$U(1)_{f_1}$	$U(1)_{f_2}$	$U(1)_R$	fugacity
p_1	-1/4	1/4	2/3	t_1
p_2	-1/4	-1/4	2/3	t_2
p_3	1/2	0	2/3	t_3

Table 3.6: The GLSM fields corresponding to extremal points of the toric diagram with their mesonic charges (Model 2).

The D-term charge matrix is

$$
Q_D = \begin{pmatrix}
p_1 & p_2 & p_3 & q_1 & q_2 & r_1 & r_2 & u_1 & u_2 & u_3 & u_4 & v_1 & v_2 & v_3 & v_4 & w_1 & w_2 & w_3 & w_4 & w_5 & w_6 & s_1 & s_2 & s_3 & s_4 & s_5 & s_6 & s_7 & s_8 & s_9 & s_{10} & s_{11} & s_{12} \\
0 & 0 & 0 & 0 & 0 & 0 & 0 & 0 & 0 & 0 & 0 & 0 & 0 & 0 & 0 & 0 & 0 & 0 & 0 & 0 & 0 & 0 & 1 & -1 & 0 & 0 & 0 & 0 & 0 & 0 & 0 & 0 & 0 \\
0 & 0 & 0 & 0 & 0 & 0 & 0 & 0 & 0 & 0 & 0 & 0 & 0 & 0 & 0 & 0 & 0 & 0 & 0 & 0 & 0 & 0 & 0 & 1 & -1 & 0 & 0 & 0 & 0 & 0 & 0 & 0 & 0 \\
0 & 0 & 0 & 0 & 0 & 0 & 0 & 0 & 0 & 0 & 0 & 0 & 0 & 0 & 0 & 0 & 0 & 0 & 0 & 0 & 0 & 0 & 0 & 0 & 1 & -1 & 0 & 0 & 0 & 0 & 0 & 0 & 0 \\
0 & 0 & 0 & 0 & 0 & 0 & 0 & 0 & 0 & 0 & 0 & 0 & 0 & 0 & 0 & 0 & 0 & 0 & 0 & 0 & 0 & 0 & 0 & 0 & 0 & 1 & -1 & 0 & 0 & 0 & 0 & 0 & 0 \\
0 & 0 & 0 & 0 & 0 & 0 & 0 & 0 & 0 & 0 & 0 & 0 & 0 & 0 & 0 & 0 & 0 & 0 & 0 & 0 & 0 & 0 & 0 & 0 & 0 & 0 & 1 & -1 & 0 & 0 & 0 & 0 & 0 \\
0 & 0 & 0 & 0 & 0 & 0 & 0 & 0 & 0 & 0 & 0 & 0 & 0 & 0 & 0 & 0 & 0 & 0 & 0 & 0 & 0 & 0 & 0 & 0 & 0 & 0 & 0 & 1 & -1 & 0 & 0 & 0 & 0 \\
0 & 0 & 0 & 0 & 0 & 0 & 0 & 0 & 0 & 0 & 0 & 0 & 0 & 0 & 0 & 0 & 0 & 0 & 0 & 0 & 0 & 0 & 0 & 0 & 0 & 0 & 0 & 0 & 1 & -1 & 0 & 0 & 0 \\
\end{pmatrix} .
$$
(3.4.19)

The total charge matrix Q_t does not exhibit repeated columns. Accordingly, the global symmetry is $U(1)_{f_1} \times U(1)_{f_2} \times U(1)_R$. Following the discussion in §3.2.3, the flavour and R-charges on the extremal prefect matchings are found as shown in Table 3.6.

Products of non-extremal perfect matchings are set to be associated with a single variable as follows,

$$
q = q_1 q_2 \; , \; r = r_1 r_2 \; , \; u = u_1 u_2 u_3 u_4 \; , \; v = v_1 v_2 v_3 v_4 \; ,
$$
$$
w = w_1 w_2 w_3 w_4 w_5 w_6 \; , \; s = \prod_{m=1}^{12} s_m \; .
$$
(3.4.20)

The fugacities t_α counts extremal perfect matchings p_α with non-zero R-charge. The fugacity y_q counts the product of non-extremal perfect matchings q above.

The mesonic Hilbert series of Model 2 is calculated using the Molien integral formula in (1.4.67). It is

$$
g_1(t_\alpha, y_q, y_r, y_u, y_v, y_w, y_s; \mathcal{M}_2^{mes}) =
$$
$$
(1 - y_q^2 y_r^2 y_u^4 y_v^4 y_w^4 y_s^2 \; t_1^4 t_2^4)(1 - y_q^2 y_r^2 y_u^2 y_v^2 y_w^2 y_s^2 \; t_1^2 t_2^2 t_3^2)
$$
$$
\times \frac{1}{(1 - y_q^2 y_u^3 y_v y_w^2 y_s \; t_1^4)(1 - y_r^2 y_u y_v^3 y_w^2 y_s \; t_2^4)(1 - y_q y_r y_s \; t_3^2)}
$$
$$
\times \frac{1}{(1 - y_q y_r y_u^2 y_v^2 y_w^2 y_s \; t_1^2 t_2^2)(1 - y_q y_r y_u y_v y_w y_s \; t_1 t_2 t_3)} \; .
$$
(3.4.21)

Generator	$U(1)_{f_1}$	$U(1)_{f_2}$
$A_1 = p_3^2\ q\ r\ s$	1	0
$A_2 = p_1 p_2 p_3\ q\ r\ uv\ w\ s$	0	0
$A_3 = p_1^2 p_2^2\ q\ r\ u^2 v^2\ w^2\ s$	-1	0
$B_1 = p_1^4\ q^2\ u^3 v\ w^2\ s$	-1	1
$B_2 = p_2^4\ r^2\ uv^3\ w^2\ s$	-1	-1
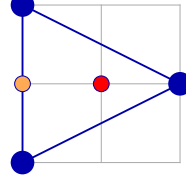
Table 3.7: The generators and lattice of generators of the mesonic moduli space of Model 2 in terms of GLSM fields with the corresponding flavor charges.

Generator	$U(1)_{f_1}$	$U(1)_{f_2}$
$X_{12}X_{21} = X_{34}X_{43} = X_{56}X_{65} = X_{78}X_{87}$	1	0
$X_{12}X_{23}X_{31} = X_{12}X_{28}X_{81} = X_{14}X_{42}X_{21} = X_{14}X_{43}X_{31} = X_{17}X_{72}X_{21} = X_{17}X_{78}X_{81} = X_{23}X_{34}X_{42} = X_{28}X_{87}X_{72} = X_{34}X_{45}X_{53}$ $= X_{36}X_{64}X_{43} = X_{36}X_{65}X_{53} = X_{45}X_{56}X_{64} = X_{56}X_{67}X_{75} = X_{58}X_{86}X_{65} = X_{58}X_{87}X_{75} = X_{67}X_{78}X_{86}$	0	0
$X_{14}X_{42}X_{23}X_{31} = X_{14}X_{42}X_{28}X_{81} = X_{14}X_{45}X_{53}X_{31} = X_{17}X_{72}X_{23}X_{31} = X_{17}X_{72}X_{28}X_{81} = X_{17}X_{75}X_{58}X_{81} = X_{23}X_{36}X_{64}X_{42}$ $= X_{28}X_{86}X_{67}X_{72} = X_{36}X_{64}X_{45}X_{53} = X_{36}X_{67}X_{75}X_{53} = X_{45}X_{58}X_{86}X_{64} = X_{58}X_{86}X_{67}X_{75}$	-1	0
$X_{14}X_{45}X_{58}X_{81} = X_{23}X_{36}X_{67}X_{72}$	-1	1
$X_{17}X_{75}X_{53}X_{31} = X_{28}X_{86}X_{64}X_{42}$	-1	-1

Table 3.8: The generators in terms of bifundamental fields (Model 2).

The plethystic logarithm of the mesonic Hilbert series is

$$
\begin{aligned}
PL[g_1(t_\alpha, y_q, y_r, y_u, y_v, y_w, y_s; \mathcal{M}_2^{mes})] &= y_q y_r y_s\ t_3^2 + y_q y_r y_u y_v y_w y_s\ t_1 t_2 t_3 \\
&+ y_q y_r y_u^2 y_v^2 y_w^2 y_s\ t_1^2 t_2^2 + y_q^2 y_u^3 y_v y_w^2 y_s\ t_1^4 + y_r^2 y_u y_v^3 y_w^2 y_s\ t_2^4 \\
&- y_q^2 y_r^2 y_u^2 y_v^2 y_w^2 y_s^2\ t_1^2 t_2^2 t_3^2 - y_q^2 y_r^2 y_u^4 y_v^4 y_w^4 y_s^2\ t_1^4 t_2^4\ .
\end{aligned}
\tag{3.4.22}
$$

The finite plethystic logarithm indicates that the mesonic moduli space is a complete intersection.

With the fugacity map

$$
\begin{aligned}
f_1 &= y_q^{1/3} y_r^{1/3} y_u^{-2/3} y_v^{-2/3} y_w^{-2/3} y_s^{-2/3} t_1^{-2/3} t_2^{-2/3} t_3^{4/3}\ , \\
f_2 &= y_q y_r^{-1} y_u y_v^{-1}\ t_1^2 t_2^{-2}\ , \\
t &= y_q^{1/3} y_r^{1/3} y_u^{1/3} y_v^{1/3} y_w^{1/3} y_s^{1/3} t_1^{1/3} t_2^{1/3} t_3^{1/3}\ ,
\end{aligned}
\tag{3.4.23}
$$

where f_1, f_2 and t are the mesonic charge fugacities, the plethystic logarithm becomes

$$
PL[g_1(t, f_1, f_2; \mathcal{M}_2^{mes})] = f_1 t^2 + t^3 + \frac{1}{f_1}\left(1 + f_2 + \frac{1}{f_2}\right) t^4 - t^6 - \frac{1}{f_1^2} t^8\ .
\tag{3.4.24}
$$

From the above plethystic logarithm, one can identify the moduli space generators as well as their mesonic charges. They are shown in Table 3.7. The charge lattice of generators in Table 3.7 is the dual reflexive polygon of the toric diagram of Model 2. The two relations formed by the generators are

$$
A_1 A_3 = A_2^2\ ,\ \ B_1 B_2 = A_3^2\ .
\tag{3.4.25}
$$
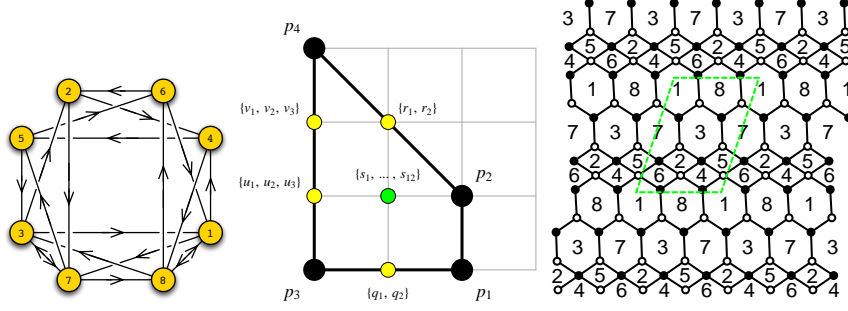
Figure 3.5: The quiver, toric diagram, and brane tiling of Model 3a.

With the fugacity map

$$
\begin{aligned}
T_1 &= f_1^{-1/4} f_2^{1/4} \ t = y_q^{1/2} y_u^{3/4} y_v^{1/4} y_w^{1/2} y_s^{1/4} \ t_1 \ , \\
T_2 &= f_1^{-1/4} f_2^{-1/4} \ t = y_r^{1/2} y_u^{1/4} y_v^{3/4} y_w^{1/2} y_s^{1/4} \ t_2 \ , \\
T_3 &= f_1^{1/2} \ t = y_q^{1/2} y_r^{1/2} y_s^{1/2} \ t_3 \ ,
\end{aligned}
\tag{3.4.26}
$$

the mesonic Hilbert series takes the form

$$
g_1(T_1, T_2, T_3; \mathcal{M}_2^{mes}) = \frac{(1 - T_1^4 T_2^4)(1 - T_1^2 T_2^2 T_3^2)}{(1 - T_1^4)(1 - T_2^4)(1 - T_3^2)(1 - T_1^2 T_2^2)(1 - T_1 T_2 T_3)} \ , \tag{3.4.27}
$$

with the plethystic logarithm being

$$
PL[g_1(T_1, T_2, T_3; \mathcal{M}_2^{mes})] = T_3^2 + T_1 T_2 T_3 + T_1^2 T_2^2 + T_1^4 + T_2^4 - T_1^2 T_2^2 T_3^2 - T_1^4 T_2^4 \ . \tag{3.4.28}
$$

The above refinement of the mesonic Hilbert series emphasises the conical structure of the toric Calabi-Yau space.

3.5 Model 3: $L_{1,3,1}/\mathbb{Z}_2$ $(0,1,1,1)$

3.5.1 Model 3 Phase a

The superpotential is

$$
\begin{aligned}
W \ = \ &+ X_{31} X_{18} X_{83} + X_{32} X_{27} X_{73} + X_{53} X_{37} X_{75} + X_{78} X_{81} X_{17} \\
&- X_{14} X_{48} X_{81} - X_{31} X_{17} X_{73} - X_{78} X_{83} X_{37} - X_{86} X_{61} X_{18} \\
&+ X_{14} X_{45} X_{56} X_{61} + X_{62} X_{24} X_{48} X_{86} - X_{32} X_{24} X_{45} X_{53} - X_{62} X_{27} X_{75} X_{56} \ .
\end{aligned}
\tag{3.5.29}
$$

The perfect matching matrix is

$$P =$$

	p_1	p_2	p_3	p_4	q_1	q_2	r_1	r_2	u_1	u_2	u_3	v_1	v_2	v_3	s_1	s_2	s_3	s_4	s_5	s_6	s_7	s_8	s_9	s_{10}	s_{11}	s_{12}
X_{81}	1	1	0	0	1	0	1	0	0	0	0	0	0	0	1	0	1	0	1	1	1	1	0	0	0	0
X_{73}	1	1	0	0	1	0	0	1	0	0	0	0	0	0	1	0	1	0	0	0	1	0	1	1	0	1
X_{37}	1	1	0	0	0	1	1	0	0	0	0	0	0	0	0	1	0	1	1	1	0	1	0	0	1	0
X_{18}	1	1	0	0	0	1	0	1	0	0	0	0	0	0	0	1	0	1	0	0	0	0	1	1	1	1
X_{24}	1	0	0	0	1	0	0	0	0	0	0	0	0	0	0	0	0	0	1	0	0	0	0	1	1	0
X_{56}	1	0	0	0	0	1	0	0	0	0	0	0	0	0	1	0	0	0	0	0	0	1	1	0	0	0
X_{45}	0	1	0	0	0	0	1	0	0	0	0	0	0	0	0	1	1	0	0	0	0	0	0	0	0	1
X_{62}	0	1	0	0	0	0	0	1	0	0	0	0	0	0	0	0	0	1	0	1	1	0	0	0	0	0
X_{83}	0	0	1	0	1	0	0	0	1	1	0	0	1	0	1	0	1	0	0	0	1	0	0	0	0	0
X_{61}	0	0	1	0	1	0	0	0	1	0	1	0	0	1	0	0	0	0	1	1	1	0	0	0	0	0
X_{17}	0	0	1	0	0	1	0	0	1	1	0	0	1	0	0	1	0	1	0	0	0	0	0	0	1	0
X_{48}	0	0	1	0	0	1	0	0	1	0	1	0	0	1	0	1	0	0	0	0	0	0	1	0	0	1
X_{75}	0	0	1	0	1	0	0	0	0	1	1	1	0	0	0	0	1	0	0	0	0	0	0	1	0	1
X_{32}	0	0	1	0	0	1	0	0	0	1	1	1	0	0	0	0	0	1	0	1	0	1	0	0	0	0
X_{27}	0	0	0	1	0	0	1	0	1	0	0	0	1	1	0	1	0	0	1	0	0	0	0	0	1	0
X_{86}	0	0	0	1	0	0	1	0	0	1	0	1	1	0	1	0	1	0	0	0	0	1	0	0	0	0
X_{53}	0	0	0	1	0	0	0	1	1	0	0	0	1	1	1	0	0	0	0	1	0	1	0	0	0	0
X_{14}	0	0	0	1	0	0	0	1	0	1	0	1	1	0	0	0	0	1	0	0	0	0	0	1	1	0
X_{31}	0	0	0	1	0	0	1	0	0	0	1	1	0	1	0	0	0	0	1	1	0	1	0	0	0	0
X_{78}	0	0	0	1	0	0	0	1	0	0	1	1	0	1	0	0	0	0	0	0	0	1	1	0	1	

(3.5.30)

The F-term charge matrix $Q_F = \ker(P)$ is

$$Q_F =$$

p_1	p_2	p_3	p_4	q_1	q_2	r_1	r_2	u_1	u_2	u_3	v_1	v_2	v_3	s_1	s_2	s_3	s_4	s_5	s_6	s_7	s_8	s_9	s_{10}	s_{11}	s_{12}
1	0	1	0	-1	-1	0	0	0	0	0	0	0	0	0	0	0	0	0	0	0	0	0	0	0	0
0	1	0	1	0	0	-1	-1	0	0	0	0	0	0	0	0	0	0	0	0	0	0	0	0	0	0
1	0	0	1	0	0	-1	0	0	0	0	0	0	0	-1	0	1	0	0	0	0	0	0	-1	0	0
0	1	1	0	-1	0	0	0	0	0	0	0	0	0	0	-1	0	0	1	-1	0	0	0	0	0	0
1	0	0	0	0	0	0	0	0	0	0	0	1	0	-1	0	0	0	0	0	0	0	0	0	-1	0
0	1	0	0	0	0	0	0	1	0	0	0	0	0	0	-1	0	0	0	0	-1	0	0	0	0	0
1	0	0	0	0	0	1	0	1	0	0	0	0	0	-1	-1	0	0	-1	0	0	0	0	0	0	0
0	1	0	0	0	0	0	0	0	1	0	0	0	0	0	0	-1	-1	0	0	0	0	0	0	0	0
0	0	1	1	0	0	0	0	-1	0	0	-1	0	0	0	0	0	0	0	0	0	0	0	0	0	0
0	0	1	1	0	0	0	0	0	-1	0	0	0	-1	0	0	0	0	0	0	0	0	0	0	0	0
0	0	1	0	0	0	0	0	-1	-1	0	0	1	0	0	0	0	0	0	0	0	0	0	0	0	0
0	0	1	0	0	0	0	0	0	-1	-1	1	0	0	0	0	0	0	0	0	0	0	0	0	0	0
0	0	1	0	-1	0	0	0	0	-1	0	0	0	0	1	0	0	0	0	0	0	0	0	-1	1	0
0	0	0	0	1	0	1	0	0	0	0	0	0	0	0	0	-1	0	-1	0	0	0	0	0	0	0
0	0	0	0	0	1	1	0	0	0	0	0	0	0	0	-1	0	0	0	0	-1	0	0	0	0	0
0	0	0	0	0	0	0	0	0	0	0	0	0	0	1	0	-1	0	0	0	0	-1	0	0	0	1

(3.5.31)

The D-term charge matrix is

$$Q_D =$$

p_1	p_2	p_3	p_4	q_1	q_2	r_1	r_2	u_1	u_2	u_3	v_1	v_2	v_3	s_1	s_2	s_3	s_4	s_5	s_6	s_7	s_8	s_9	s_{10}	s_{11}	s_{12}
0	0	0	0	0	0	0	0	0	0	0	0	0	0	0	0	0	0	1	-1	0	0	0	0	0	0
0	0	0	0	0	0	0	0	0	0	0	0	0	0	0	0	0	0	0	1	-1	0	0	0	0	0
0	0	0	0	0	0	0	0	0	0	0	0	0	0	0	0	0	0	0	0	1	-1	0	0	0	0
0	0	0	0	0	0	0	0	0	0	0	0	0	0	0	0	0	0	0	0	0	1	-1	0	0	0
0	0	0	0	0	0	0	0	0	0	0	0	0	0	0	0	0	0	0	0	0	0	1	-1	0	0
0	0	0	0	0	0	0	0	0	0	0	0	0	0	0	0	0	0	0	0	0	0	0	1	-1	0
0	0	0	0	0	0	0	0	0	0	0	0	0	0	0	0	0	0	0	0	0	0	0	0	1	-1

(3.5.32)

The total charge matrix does not exhibit repeated columns. Accordingly, the global symmetry is $U(1)_{f_1} \times U(1)_{f_2} \times U(1)_R$. Following the discussion in §3.2.3, the mesonic charges on the extremal perfect matchings are found as shown in Table 3.9.

Products of non-extremal perfect matchings are associated to a single variable as

	$U(1)_{f_1}$	$U(1)_{f_2}$	$U(1)_R$	fugacity
p_1	1/2	1/2	$R_1 = \frac{1}{6}\left(5 - \sqrt{7}\right)$	t_1
p_2	0	-1/2	$R_1 = \frac{1}{6}\left(5 - \sqrt{7}\right)$	t_2
p_3	-1/2	-1/2	$R_2 = \frac{1}{6}\left(1 + \sqrt{7}\right)$	t_3
p_4	0	1/2	$R_2 = \frac{1}{6}\left(1 + \sqrt{7}\right)$	t_4

Table 3.9: The GLSM fields corresponding to extremal points of the toric diagram with their mesonic charges (Model 3a). The R-charges are obtained using a-maximization.

follows

$$q = q_1 q_2 \ , \ \ r = r_1 r_2 \ , \ \ u = u_1 u_2 u_3 \ , \ \ v = v_1 v_2 v_3 \ , \ \ s = \prod_{m=1}^{12} s_m \ . \qquad (3.5.33)$$

The fugacity t_α counts extremal perfect matchings. The fugacity y_q counts the product of non-extremal perfect matchings q above.

The mesonic Hilbert series of Model 3a is calculated using the Molien integral formula in (1.4.67). It is

$$g_1(t_\alpha, y_q, y_r, y_u, y_v, y_s; \mathcal{M}_{3a}^{mes}) = (1 - y_q^2 y_r^2 y_u^2 y_v^2 y_s^2 \ t_1^2 t_2^2 t_3^2 t_4^2)(1 - y_q^2 y_r^2 y_u^3 y_v^3 y_s^2 \ t_1 t_2 t_3^3 t_4^3)$$
$$\times \frac{1}{(1 - y_q y_r y_s \ t_1^2 t_2^2)(1 - y_q^2 y_u^2 y_v y_s \ t_1 t_3^3)(1 - y_q y_r y_u^2 y_v^2 y_s \ t_3^2 t_4^2)}$$
$$\times \frac{1}{(1 - y_r^2 y_u y_v^2 y_s \ t_2 t_4^3)(1 - y_q y_r y_u y_v y_s \ t_1 t_2 t_3 t_4)} \ . $$

$$(3.5.34)$$

The plethystic logarithm of the mesonic Hilbert series is

$$PL[g_1(t_\alpha, y_q, y_r, y_u, y_v, y_s; \mathcal{M}_{3a}^{mes})] = y_q y_r y_s \ t_1^2 t_2^2 + y_q y_r y_u y_v y_s \ t_1 t_2 t_3 t_4 + y_q^2 y_u^2 y_v y_s \ t_1 t_3^3$$
$$+ y_r^2 y_u y_v^2 y_s \ t_2 t_4^3 + y_q y_r y_u^2 y_v^2 y_s \ t_3^2 t_4^2 - y_q^2 y_r^2 y_u^2 y_v^2 y_s^2 \ t_1^2 t_2^2 t_3^2 t_4^2 - y_q^2 y_r^2 y_u^3 y_v^3 y_s^2 \ t_1 t_2 t_3^3 t_4^3 \ .$$

$$(3.5.35)$$

The finite plethystic logarithm indicates that the mesonic moduli space is a complete intersection.

Generator	$U(1)_{f_1}$	$U(1)_{f_2}$
$A_1 = p_1^2 p_2^2 \ q \ r \ s$	1	0
$A_2 = p_3^2 p_4^2 \ q \ r \ u^2 v^2 \ s$	-1	0
$B = p_1 p_2 p_3 p_4 \ q \ r \ uv \ s$	0	0
$C_1 = p_1 p_3^3 \ q^2 \ u^2 v \ s$	-1	-1
$C_2 = p_2 p_4^3 \ r^2 \ uv^2 \ s$	0	1
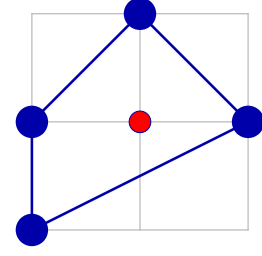
Table 3.10: The generators and lattice of generators of the mesonic moduli space of Model 3a in terms of GLSM fields with the corresponding flavor charges.

Generator	$U(1)_{f_1}$	$U(1)_{f_2}$
$X_{24}X_{45}X_{56}X_{62} = X_{18}X_{81} = X_{37}X_{73}$	1	0
$X_{14}X_{48}X_{83}X_{31} = X_{14}X_{48}X_{86}X_{61} = X_{17}X_{75}X_{53}X_{31} = X_{17}X_{78}X_{83}X_{31}$ $= X_{17}X_{78}X_{86}X_{61} = X_{27}X_{75}X_{53}X_{32} = X_{27}X_{78}X_{83}X_{32}$	-1	0
$X_{14}X_{45}X_{56}X_{61} = X_{24}X_{45}X_{53}X_{32} = X_{24}X_{48}X_{86}X_{62} = X_{27}X_{75}X_{56}X_{62} = X_{14}X_{48}X_{81}$ $= X_{17}X_{73}X_{31} = X_{17}X_{78}X_{81} = X_{18}X_{83}X_{31} = X_{18}X_{86}X_{61} = X_{27}X_{73}X_{32} = X_{37}X_{75}X_{53} = X_{37}X_{78}X_{83}$	0	0
$X_{17}X_{75}X_{56}X_{61} = X_{24}X_{48}X_{83}X_{32}$	-1	-1
$X_{14}X_{45}X_{53}X_{31} = X_{27}X_{78}X_{86}X_{62}$	0	1

Table 3.11: The generators in terms of bifundamental fields (Model 3a).

Consider the fugacity map

$$
\begin{aligned}
f_1 &= \frac{1}{y_u y_v} \ , \\
f_2 &= \frac{y_r y_v \ t_2^{1/2} t_4^{3/2}}{y_q \ t_1^{1/2} t_3^{3/2}} \ , \\
\tilde{t}_1 &= y_q^{1/4} y_r^{1/4} y_u^{1/4} y_v^{1/4} y_s^{1/4} \ t_1^{1/2} t_2^{1/2} \ , \\
\tilde{t}_2 &= y_q^{1/4} y_r^{1/4} y_u^{1/4} y_v^{1/4} y_s^{1/4} \ t_3^{1/2} t_4^{1/2} \ ,
\end{aligned}
\tag{3.5.36}
$$

where f_1 and f_2 are the flavor fugacities, and $\tilde{t}_1$ and $\tilde{t}_2$ are the fugacities for the R-charges R_1 and R_2 in Table 3.9 respectively. Under the above fugacity map, the plethystic logarithm becomes

$$
PL[g_1(t_\alpha, f_1, f_2; \mathcal{M}_{3a}^{mes})] = f_1 \tilde{t}_1^4 + \tilde{t}_1^2 \tilde{t}_2^2 + \left(\frac{1}{f_1 f_2} + f_2 \right) \tilde{t}_1 \tilde{t}_2^3 + \frac{\tilde{t}_2^4}{f_1} - \tilde{t}_1^4 \tilde{t}_2^4 - \frac{\tilde{t}_1^2 \tilde{t}_2^6}{f_1} \ .
\tag{3.5.37}
$$

The above plethystic logarithm indicates both the moduli space generators as well as their mesonic charges. They are summarized in Table 3.10. The generators can be presented on a charge lattice. The convex polygon formed by the generators in Table 3.10 is the dual reflexive polygon of the toric diagram of Model 3a. The generators satisfy the following relations

$$
A_1 A_2 = B^2 \ , \quad A_2 B = C_1 C_2 \ .
\tag{3.5.38}
$$

Figure 3.6: The quiver, toric diagram, and brane tiling of Model 3b. The red arrows in the quiver indicate all possible connections between blocks of nodes.

The mesonic Hilbert series and the plethystic logarithm can be re-expressed in terms of the following 3 fugacities,

$$T_1 = \frac{f_2}{\tilde{t}_1^3 \tilde{t}_2} = \frac{t_4}{y_q^2 y_u y_s \ t_1^2 t_2 t_3^2} \ ,$$

$$T_2 = \frac{1}{f_1 f_2} \ \tilde{t}_1 \tilde{t}_2^3 = y_q^2 y_u^2 y_v y_s \ t_1 t_3^3 \ , \quad T_3 = f_1 \ \tilde{t}_1^4 = y_q y_r y_s \ t_1^2 t_2^2 \ , \tag{3.5.39}$$

such that

$$g_1(T_1, T_2, T_3; \mathcal{M}_{3a}^{mes}) = \frac{(1 - T_1^2 T_2^2 T_3^2)(1 - T_1^3 T_2^3 T_3^2)}{(1 - T_3)(1 - T_2)(1 - T_1^2 T_2^2 T_3)(1 - T_1^3 T_2^2 T_3^2)(1 - T_1 T_2 T_3)} \tag{3.5.40}$$

and

$$
\begin{aligned}
PL[g_1(T_1, T_2, T_3; \mathcal{M}_{3a}^{mes})] \quad = \quad & T_3 + T_1 T_2 T_3 + T_2 + T_1^2 T_2^2 T_3 + T_1^3 T_2^2 T_3^2 \\
& - T_1^2 T_2^2 T_3^2 - T_1^3 T_2^3 T_3^2 \ .
\end{aligned} \tag{3.5.41}
$$

The above refinement of the mesonic Hilbert series and the plethystic logarithm illustrates the conical structure of the toric Calalbi-Yau 3-fold.

3.5.2 Model 3 Phase b

The superpotential is

$$
\begin{aligned}
W \quad = \quad & + X_{31} X_{18} X_{83} + X_{42} X_{23} X_{34} + X_{53} X_{37} X_{75} + X_{67} X_{72} X_{26} \\
& - X_{14} X_{48} X_{81} - X_{42} X_{26} X_{64} - X_{53} X_{34} X_{45} - X_{67} X_{75} X_{56} \\
& + X_{78} X_{81} X_{17} + X_{86} X_{64} X_{48} + X_{14} X_{45} X_{56} X_{61} \\
& - X_{78} X_{83} X_{37} - X_{86} X_{61} X_{18} - X_{17} X_{72} X_{23} X_{31} \ .
\end{aligned} \tag{3.5.42}
$$

The perfect matching matrix is

$$P =$$

	p_1	p_2	p_3	p_4	q_1	q_2	r_1	r_2	u_1	u_2	u_3	v_1	v_2	v_3	s_1	s_2	s_3	s_4	s_5	s_6	s_7	s_8	s_9	s_{10}	s_{11}	s_{12}	s_{13}	s_{14}
X_{37}	1	1	0	0	1	0	1	0	0	0	0	0	0	0	1	1	1	1	0	0	0	0	0	0	0	0	0	0
X_{18}	1	1	0	0	0	1	1	0	0	0	0	0	0	0	1	0	1	0	1	0	1	1	1	1	0	0	0	0
X_{81}	1	1	0	0	1	0	0	1	0	0	0	0	0	0	0	1	0	1	0	1	0	0	0	0	1	1	1	1
X_{64}	1	1	0	0	0	1	0	1	0	0	0	0	0	0	1	1	0	0	1	1	0	0	0	0	0	0	0	0
X_{67}	1	0	1	0	1	1	0	0	0	0	1	0	1	1	1	1	1	0	0	1	0	0	0	0	0	0	0	0
X_{34}	0	1	0	1	0	0	1	1	1	1	0	1	0	0	1	1	0	1	1	0	0	0	0	0	0	0	0	0
X_{45}	1	0	0	0	1	0	0	0	0	0	0	0	0	0	0	0	1	0	0	0	1	1	0	0	1	1	0	0
X_{23}	1	0	0	0	0	1	0	0	0	0	0	0	0	0	0	0	0	0	1	1	0	1	0	1	0	1	0	1
X_{56}	0	1	0	0	0	0	1	0	0	0	0	0	0	0	0	0	0	1	0	0	0	0	1	1	0	0	1	1
X_{72}	0	1	0	0	0	0	0	1	0	0	0	0	0	0	0	0	0	0	1	0	0	1	0	1	0	1	0	1
X_{86}	0	0	1	0	1	0	0	0	1	0	0	1	1	0	0	0	0	1	0	0	0	0	0	0	1	1	1	1
X_{31}	0	0	1	0	1	0	0	0	0	1	0	1	0	1	0	1	0	1	0	0	0	0	0	0	0	0	0	0
X_{14}	0	0	1	0	0	1	0	0	1	0	0	1	1	0	1	0	0	0	1	0	0	0	0	0	0	0	0	0
X_{78}	0	0	1	0	0	1	0	0	0	1	0	1	0	1	0	0	0	0	1	0	1	1	1	1	0	0	0	0
X_{42}	0	0	1	0	1	0	1	0	0	1	0	0	1	1	0	0	1	0	0	0	1	0	1	0	1	0	1	0
X_{53}	0	0	1	0	0	1	0	0	0	0	1	0	1	1	0	0	0	0	1	0	1	0	1	1	0	0	1	1
X_{17}	0	0	0	1	0	0	1	0	1	0	1	0	1	0	1	0	1	0	0	0	0	0	0	0	0	0	0	0
X_{48}	0	0	0	1	0	0	1	0	0	1	1	0	0	1	0	0	1	0	0	0	1	1	1	1	0	0	0	0
X_{83}	0	0	0	1	0	0	0	1	1	0	1	0	1	0	0	0	0	0	0	1	0	0	0	0	1	1	1	1
X_{61}	0	0	0	1	0	0	0	1	0	1	1	0	0	1	0	1	0	0	0	1	0	0	0	0	0	0	0	0
X_{26}	0	0	0	1	0	0	1	0	1	1	0	1	0	0	0	0	0	1	0	0	1	0	1	0	1	0	1	0
X_{75}	0	0	0	1	0	0	0	1	1	1	0	1	0	0	0	0	0	0	1	0	1	1	0	0	1	1	0	0

$$(3.5.43)$$

The F-term charge matrix $Q_F = \ker(P)$ is

$$Q_F =$$

p_1	p_2	p_3	p_4	q_1	q_2	r_1	r_2	u_1	u_2	u_3	v_1	v_2	v_3	s_1	s_2	s_3	s_4	s_5	s_6	s_7	s_8	s_9	s_{10}	s_{11}	s_{12}	s_{13}	s_{14}
1	0	1	0	-1	-1	0	0	0	0	0	0	0	0	0	0	0	0	0	0	0	0	0	0	0	0	0	0
0	1	0	1	0	0	-1	-1	0	0	0	0	0	0	0	0	0	0	0	0	0	0	0	0	0	0	0	0
1	0	0	0	0	0	0	0	1	0	0	0	0	0	-1	0	0	0	0	0	0	0	0	0	-1	0	0	0
1	0	0	0	0	0	0	0	0	1	0	0	0	0	0	-1	0	0	0	0	-1	0	0	0	0	0	0	0
0	1	0	0	0	0	0	0	0	0	0	0	1	0	-1	0	0	0	0	0	0	0	0	0	0	0	0	-1
0	1	0	0	0	0	0	0	0	0	0	0	0	1	0	-1	0	0	0	0	0	0	-1	0	0	0	0	0
0	1	0	0	0	0	-1	0	0	1	0	0	0	0	1	-1	0	0	-1	0	0	0	0	0	0	0	0	0
0	0	1	1	0	0	0	0	-1	0	0	0	0	-1	0	0	0	0	0	0	0	0	0	0	0	0	0	0
0	0	1	1	0	0	0	0	0	-1	0	0	-1	0	0	0	0	0	0	0	0	0	0	0	0	0	0	0
0	0	0	1	0	0	0	0	-1	0	-1	0	1	0	0	0	0	0	0	0	0	0	0	0	0	0	0	0
0	0	0	1	1	0	0	0	-1	0	0	0	0	0	1	-1	-1	0	0	0	0	0	0	0	0	0	0	0
0	0	0	1	0	0	0	0	-1	-1	0	1	0	0	0	0	0	0	0	0	0	0	0	0	0	0	0	0
0	0	0	1	1	0	0	0	-1	0	0	0	0	0	0	-1	0	0	1	0	0	-1	0	0	0	0	0	0
0	0	0	1	0	1	0	0	0	-1	0	0	0	0	-1	1	0	0	0	-1	0	0	0	0	0	0	0	0
0	0	0	1	0	0	-1	0	-1	0	0	0	0	0	1	-1	0	1	0	0	0	0	0	0	0	0	0	0
0	0	0	0	1	0	0	1	0	0	0	0	0	0	0	-1	0	0	0	0	0	0	0	0	-1	0	0	0
0	0	0	0	0	1	1	0	0	0	0	0	0	0	-1	0	0	0	0	0	0	0	-1	0	0	0	0	0
0	0	0	0	0	0	0	0	0	0	0	0	0	0	0	1	0	-1	0	-1	0	0	0	0	0	0	1	0

$$(3.5.44)$$

The D-term charge matrix is

$$Q_D =$$

p_1	p_2	p_3	p_4	q_1	q_2	r_1	r_2	u_1	u_2	u_3	v_1	v_2	v_3	s_1	s_2	s_3	s_4	s_5	s_6	s_7	s_8	s_9	s_{10}	s_{11}	s_{12}	s_{13}	s_{14}
0	0	0	0	0	0	0	0	0	0	0	0	0	0	0	1	-1	0	0	0	0	0	0	0	0	0	0	0
0	0	0	0	0	0	0	0	0	0	0	0	0	0	0	0	1	-1	0	0	0	0	0	0	0	0	0	0
0	0	0	0	0	0	0	0	0	0	0	0	0	0	0	0	0	1	-1	0	0	0	0	0	0	0	0	0
0	0	0	0	0	0	0	0	0	0	0	0	0	0	0	0	0	0	1	-1	0	0	0	0	0	0	0	0
0	0	0	0	0	0	0	0	0	0	0	0	0	0	0	0	0	0	0	1	-1	0	0	0	0	0	0	0
0	0	0	0	0	0	0	0	0	0	0	0	0	0	0	0	0	0	0	0	1	-1	0	0	0	0	0	0
0	0	0	0	0	0	0	0	0	0	0	0	0	0	0	0	0	0	0	0	0	1	-1	0	0	0	0	0

$$(3.5.45)$$

The total charge matrix does not exhibit repeated columns. Accordingly, the global symmetry is $U(1)_{f_1} \times U(1)_{f_2} \times U(1)_R$. The mesonic charges on the GLSM fields with non-zero R-charges are the same as for Model 3a and are shown in Table 3.9.

Products of non-extremal perfect matchings are expressed in terms of single variables

Generator	$U(1)_{f_1}$	$U(1)_{f_2}$
$X_{18}X_{81} = X_{23}X_{37}X_{72} = X_{45}X_{56}X_{64}$	1	0
$X_{14}X_{42}X_{26}X_{61} = X_{14}X_{48}X_{83}X_{31} = X_{14}X_{48}X_{86}X_{61} = X_{17}X_{75}X_{53}X_{31} = X_{17}X_{78}X_{83}X_{31} = X_{17}X_{78}X_{86}X_{61}$	-1	0
$X_{14}X_{45}X_{56}X_{61} = X_{17}X_{72}X_{23}X_{31} = X_{14}X_{48}X_{81} = X_{17}X_{78}X_{81} = X_{18}X_{83}X_{31} = X_{18}X_{86}X_{61} = X_{23}X_{34}X_{42}$ $= X_{26}X_{64}X_{42} = X_{26}X_{67}X_{72} = X_{34}X_{45}X_{53} = X_{37}X_{75}X_{53} = X_{37}X_{78}X_{83} = X_{48}X_{86}X_{64} = X_{56}X_{67}X_{75}$	0	0
$X_{34}X_{48}X_{83} = X_{17}X_{72}X_{26}X_{61} = X_{17}X_{75}X_{56}X_{61}$	-1	-1
$X_{67}X_{78}X_{86} = X_{14}X_{42}X_{23}X_{31} = X_{14}X_{45}X_{53}X_{31}$	0	1

Table 3.12: The generators in terms of bifundamental fields (Model 3b).
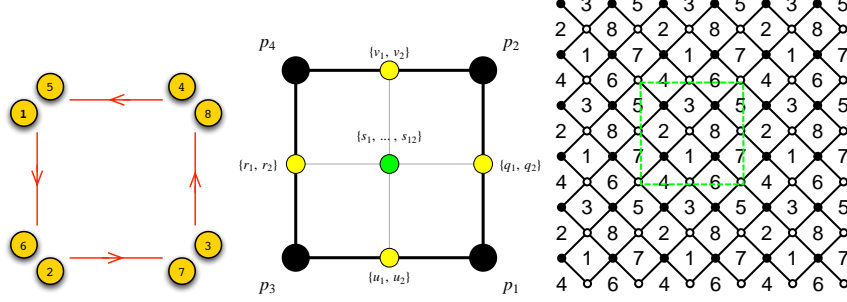
Figure 3.7: The quiver, toric diagram, and brane tiling of Model 4a. The red arrows in the quiver indicate all possible connections between blocks of nodes.

as follows

$$q = q_1q_2 \ , \ r = r_1r_2 \ , \ u = u_1u_2u_3 \ , \ v = v_1v_2v_3 \ , \ s = \prod_{m=1}^{14} s_m \ . \qquad (3.5.46)$$

The fugacity t_α counts GLSM fields corresponding to extremal perfect matchings p_α. The fugacity y_q for instance counts the product of non-extremal perfect matchings q shown above.

The refined mesonic Hilbert series and the corresponding plethystic logarithm are found using the Molien integral formula in (1.4.67). The Hilbert series is found to be the same as the one for Model 3a given in (3.5.34), (3.5.35) and (3.5.37). Accordingly, the mesonic moduli spaces of Model 3a and 3b are the same, with the corresponding quiver gauge theories being toric (Seiberg) duals.

The generators in terms of all perfect matchings of Model 3b are given in Table 3.10 with the corresponding mesonic symmetry charges. The corresponding mesonic generators in terms of quiver fields are given in Table 3.12. The mesonic moduli space is a complete intersection, and the generators satisfy the relation in (3.5.38).

3.6 Model 4: $\mathcal{C}/\mathbb{Z}_2 \times \mathbb{Z}_2$ $(1,0,0,1)(0,1,1,0)$, $\mathbf{PdP_5}$

3.6.1 Model 4 Phase a

The superpotential is

$$
\begin{aligned}
W \;=\; & +X_{23}X_{38}X_{81}X_{12} + X_{41}X_{16}X_{63}X_{34} + X_{67}X_{74}X_{45}X_{56} + X_{85}X_{52}X_{27}X_{78} \\
& -X_{27}X_{74}X_{41}X_{12} - X_{45}X_{52}X_{23}X_{34} - X_{63}X_{38}X_{85}X_{56} - X_{81}X_{16}X_{67}X_{78}
\end{aligned}
\tag{3.6.47}
$$

The perfect matching matrix is

$$
P = \left(\begin{array}{c|cccc|cc|cc|cc|cc|cccccccccccc}
 & p_1 & p_2 & p_3 & p_4 & q_1 & q_2 & r_1 & r_2 & u_1 & u_2 & v_1 & v_2 & s_1 & s_2 & s_3 & s_4 & s_5 & s_6 & s_7 & s_8 & s_9 & s_{10} & s_{11} & s_{12} \\
\hline
X_{23} & 1 & 0 & 0 & 0 & 1 & 0 & 0 & 0 & 1 & 0 & 0 & 0 & 1 & 1 & 1 & 0 & 0 & 0 & 0 & 0 & 0 & 0 & 0 & 0 \\
X_{41} & 1 & 0 & 0 & 0 & 1 & 0 & 0 & 0 & 0 & 1 & 0 & 0 & 0 & 0 & 0 & 1 & 1 & 1 & 0 & 0 & 0 & 0 & 0 & 0 \\
X_{85} & 1 & 0 & 0 & 0 & 0 & 1 & 0 & 0 & 1 & 0 & 0 & 0 & 0 & 0 & 0 & 1 & 0 & 0 & 1 & 1 & 0 & 0 & 0 & 0 \\
X_{67} & 1 & 0 & 0 & 0 & 0 & 1 & 0 & 0 & 0 & 1 & 0 & 0 & 1 & 0 & 0 & 0 & 0 & 0 & 0 & 0 & 1 & 1 & 0 & 0 \\
X_{56} & 0 & 1 & 0 & 0 & 1 & 0 & 0 & 0 & 0 & 0 & 1 & 0 & 0 & 1 & 0 & 0 & 1 & 0 & 0 & 0 & 0 & 0 & 1 & 0 \\
X_{78} & 0 & 1 & 0 & 0 & 1 & 0 & 0 & 0 & 0 & 0 & 0 & 1 & 0 & 0 & 1 & 0 & 0 & 1 & 0 & 0 & 0 & 0 & 0 & 1 \\
X_{34} & 0 & 1 & 0 & 0 & 0 & 1 & 0 & 0 & 0 & 0 & 1 & 0 & 0 & 0 & 0 & 0 & 0 & 0 & 1 & 0 & 1 & 0 & 0 & 1 \\
X_{12} & 0 & 1 & 0 & 0 & 0 & 1 & 0 & 0 & 0 & 0 & 0 & 1 & 0 & 0 & 0 & 0 & 0 & 0 & 0 & 1 & 0 & 1 & 1 & 0 \\
X_{74} & 0 & 0 & 1 & 0 & 0 & 0 & 1 & 0 & 1 & 0 & 0 & 0 & 0 & 0 & 1 & 0 & 0 & 0 & 1 & 0 & 0 & 0 & 0 & 1 \\
X_{52} & 0 & 0 & 1 & 0 & 0 & 0 & 1 & 0 & 0 & 1 & 0 & 0 & 0 & 0 & 0 & 0 & 1 & 0 & 0 & 0 & 0 & 1 & 1 & 0 \\
X_{16} & 0 & 0 & 1 & 0 & 0 & 0 & 0 & 1 & 1 & 0 & 0 & 0 & 0 & 1 & 0 & 0 & 0 & 0 & 0 & 1 & 0 & 0 & 1 & 0 \\
X_{38} & 0 & 0 & 1 & 0 & 0 & 0 & 0 & 1 & 0 & 1 & 0 & 0 & 0 & 0 & 0 & 0 & 0 & 1 & 0 & 0 & 1 & 0 & 0 & 1 \\
X_{81} & 0 & 0 & 0 & 1 & 0 & 0 & 1 & 0 & 0 & 0 & 1 & 0 & 0 & 0 & 0 & 1 & 1 & 0 & 1 & 0 & 0 & 0 & 0 & 0 \\
X_{63} & 0 & 0 & 0 & 1 & 0 & 0 & 1 & 0 & 0 & 0 & 0 & 1 & 1 & 0 & 1 & 0 & 0 & 0 & 0 & 0 & 0 & 1 & 0 & 0 \\
X_{27} & 0 & 0 & 0 & 1 & 0 & 0 & 0 & 1 & 0 & 0 & 1 & 0 & 1 & 1 & 0 & 0 & 0 & 0 & 0 & 1 & 0 & 0 & 0 & 0 \\
X_{45} & 0 & 0 & 0 & 1 & 0 & 0 & 0 & 1 & 0 & 0 & 0 & 1 & 0 & 0 & 0 & 1 & 0 & 1 & 0 & 1 & 0 & 0 & 0 & 0
\end{array}\right).
\tag{3.6.48}
$$

The F-term charge matrix $Q_F = \ker(P)$ is

$$
Q_F = \left(\begin{array}{cccc|cc|cc|cc|cc|cccccccccccc}
p_1 & p_2 & p_3 & p_4 & q_1 & q_2 & r_1 & r_2 & u_1 & u_2 & v_1 & v_2 & s_1 & s_2 & s_3 & s_4 & s_5 & s_6 & s_7 & s_8 & s_9 & s_{10} & s_{11} & s_{12} \\
\hline
1 & 1 & 0 & 0 & -1 & -1 & 0 & 0 & 0 & 0 & 0 & 0 & 0 & 0 & 0 & 0 & 0 & 0 & 0 & 0 & 0 & 0 & 0 & 0 \\
0 & 0 & 1 & 1 & 0 & 0 & -1 & -1 & 0 & 0 & 0 & 0 & 0 & 0 & 0 & 0 & 0 & 0 & 0 & 0 & 0 & 0 & 0 & 0 \\
1 & 0 & 1 & 0 & 0 & 0 & 0 & 0 & -1 & -1 & 0 & 0 & 0 & 0 & 0 & 0 & 0 & 0 & 0 & 0 & 0 & 0 & 0 & 0 \\
0 & 1 & 0 & 1 & 0 & 0 & 0 & 0 & 0 & 0 & -1 & -1 & 0 & 0 & 0 & 0 & 0 & 0 & 0 & 0 & 0 & 0 & 0 & 0 \\
1 & 0 & 0 & 0 & 0 & 0 & 1 & 0 & 0 & 0 & 1 & 0 & -1 & 0 & 0 & 0 & -1 & 0 & -1 & 0 & 0 & 0 & 0 & 0 \\
1 & 0 & 0 & 0 & 0 & 0 & 0 & 1 & 0 & 0 & 1 & 0 & 0 & -1 & 0 & -1 & 0 & 0 & 0 & 0 & -1 & 0 & 0 & 0 \\
1 & 0 & 0 & 0 & 0 & 0 & 0 & 1 & 0 & 0 & 1 & 0 & 0 & -1 & 0 & 0 & 0 & -1 & -1 & 0 & -1 & 0 & 0 & 1 \\
1 & 0 & 0 & 1 & 0 & 0 & 0 & 0 & 0 & 0 & 0 & 0 & -1 & 0 & 0 & -1 & 0 & 0 & 0 & 0 & 0 & 0 & 0 & 0 \\
0 & 0 & 1 & 1 & 0 & 1 & -1 & 0 & 0 & 0 & 0 & 0 & 0 & 0 & 0 & 0 & 0 & 0 & 0 & -1 & -1 & 0 & 0 & 0 \\
0 & 0 & 0 & 0 & 1 & 0 & 0 & 1 & 0 & 0 & 0 & 0 & 0 & -1 & 0 & 0 & 0 & -1 & 0 & 0 & 0 & 0 & 0 & 0 \\
0 & 0 & 0 & 0 & 0 & 1 & 1 & 0 & 0 & 0 & 0 & 0 & 0 & 0 & 0 & 0 & 0 & 0 & -1 & 0 & 0 & -1 & 0 & 0 \\
0 & 0 & 0 & 0 & 0 & 0 & 0 & 0 & 1 & 0 & 1 & 0 & 0 & -1 & 0 & 0 & 0 & -1 & 0 & 0 & 0 & 0 & 0 & 0 \\
0 & 0 & 0 & 0 & 0 & 0 & 0 & 0 & 0 & 0 & 0 & 0 & 1 & -1 & 0 & 0 & 0 & 0 & 0 & 0 & 0 & -1 & 1 & 0 \\
0 & 0 & 0 & 0 & 0 & 0 & 0 & 0 & 0 & 0 & 0 & 0 & 1 & 0 & -1 & 0 & 0 & 0 & 0 & 0 & -1 & 0 & 0 & 1
\end{array}\right).
\tag{3.6.49}
$$

145

	$U(1)_{f_1}$	$U(1)_{f_2}$	$U(1)_R$	fugacity
p_1	1/4	-1/4	1/2	t_1
p_2	1/4	1/4	1/2	t_2
p_3	-1/4	-1/4	1/2	t_3
p_4	-1/4	1/4	1/2	t_4

Table 3.13: The GLSM fields corresponding to extremal points of the toric diagram with their mesonic charges (Model 4a).

The D-term charge matrix is

$$
Q_D = \left(\begin{array}{cccc|cc|cc|cc|cc|cccccccccccc}
p_1 & p_2 & p_3 & p_4 & q_1 & q_2 & r_1 & r_2 & u_1 & u_2 & v_1 & v_2 & s_1 & s_2 & s_3 & s_4 & s_5 & s_6 & s_7 & s_8 & s_9 & s_{10} & s_{11} & s_{12} \\
0 & 0 & 0 & 0 & 0 & 0 & 0 & 0 & 0 & 0 & 0 & 0 & 0 & 0 & 1 & -1 & 0 & 0 & 0 & 0 & 0 & 0 & 0 & 0 \\
0 & 0 & 0 & 0 & 0 & 0 & 0 & 0 & 0 & 0 & 0 & 0 & 0 & 0 & 0 & 1 & -1 & 0 & 0 & 0 & 0 & 0 & 0 & 0 \\
0 & 0 & 0 & 0 & 0 & 0 & 0 & 0 & 0 & 0 & 0 & 0 & 0 & 0 & 0 & 0 & 1 & -1 & 0 & 0 & 0 & 0 & 0 & 0 \\
0 & 0 & 0 & 0 & 0 & 0 & 0 & 0 & 0 & 0 & 0 & 0 & 0 & 0 & 0 & 0 & 0 & 1 & -1 & 0 & 0 & 0 & 0 & 0 \\
0 & 0 & 0 & 0 & 0 & 0 & 0 & 0 & 0 & 0 & 0 & 0 & 0 & 0 & 0 & 0 & 0 & 0 & 1 & -1 & 0 & 0 & 0 & 0 \\
0 & 0 & 0 & 0 & 0 & 0 & 0 & 0 & 0 & 0 & 0 & 0 & 0 & 0 & 0 & 0 & 0 & 0 & 0 & 1 & -1 & 0 & 0 & 0 \\
0 & 0 & 0 & 0 & 0 & 0 & 0 & 0 & 0 & 0 & 0 & 0 & 0 & 0 & 0 & 0 & 0 & 0 & 0 & 0 & 1 & -1 & 0 & 0
\end{array} \right) .
$$

$$(3.6.50)$$

The total charge matrix Q_t does not exhibit repeated columns. Accordingly, the global symmetry is $U(1)_{f_1} \times U(1)_{f_2} \times U(1)_R$. The mesonic charges on the extremal perfect matchings are found following the discussion in §3.2.3. They are shown in Table 3.13.

Products of GLSM fields corresponding to non-extremal perfect matchings are called by single variables as follows

$$
q = q_1 q_2 \ , \ \ r = r_1 r_2 \ , \ \ u = u_1 u_2 \ , \ \ v = v_1 v_2 \ , \ \ s = \prod_{m=1}^{12} s_m \ .
$$

$$(3.6.51)$$

The fugacity t_α counts extremal perfect matchings p_α. The fugacity y_q for instance corresponds to the product of non-extremal perfect matchings q shown above.

The refined mesonic Hilbert series of Model 4a is calculated using the Molien integral formula in (1.4.67). It is

$$
g_1(t_\alpha, y_q, y_r, y_u, y_v, y_s; \mathcal{M}_{4a}^{mes}) = (1 - y_q^2 y_r^2 y_u^2 y_v^2 y_s^2 \ t_1^2 t_2^2 t_3^2 t_4^2)^2
$$
$$
\times \frac{1}{(1 - y_q^2 y_u y_v y_s \ t_1^2 t_2^2)(1 - y_q y_r y_u^2 y_s \ t_1^2 t_3^2)(1 - y_q y_r y_v^2 y_s \ t_2^2 t_4^2)}
$$
$$
\times \frac{1}{(1 - y_r^2 y_u y_v y_s \ t_3^2 t_4^2)(1 - y_q y_r y_u y_v y_s \ t_1 t_2 t_3 t_4)} \ .
$$

$$(3.6.52)$$

Generator	$U(1)_{f_1}$	$U(1)_{f_2}$
$A_1 = p_1^2 p_3^2\ q\ r\ u^2\ s$	0	-1
$A_2 = p_2^2 p_4^2\ q\ r\ v^2\ s$	0	1
$B_1 = p_1^2 p_2^2\ q^2\ u\ v\ s$	1	0
$B_2 = p_3^2 p_4^2\ r^2\ u\ v\ s$	-1	0
$C = p_1 p_2 p_3 p_4\ q\ r\ u\ v\ s$	0	0
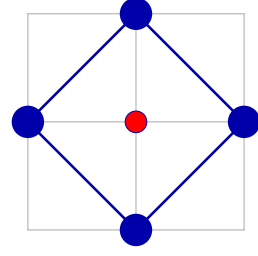
Table 3.14: The generators and lattice of generators of the mesonic moduli space of Model 4a in terms of GLSM fields with the corresponding flavor charges.

The plethystic logarithm of the mesonic Hilbert series is

$$PL[g_1(t_\alpha, y_q, y_r, y_u, y_v, y_s; \mathcal{M}_{4a}^{mes})] = y_q y_r y_u y_v y_s\ t_1 t_2 t_3 t_4 + y_q^2 y_u y_v y_s\ t_1^2 t_2^2$$
$$+ y_r^2 y_u y_v y_s\ t_3^2 t_4^2 + y_q y_r y_v^2 y_s\ t_2^2 t_4^2 + y_q y_r y_u^2 y_s\ t_1^2 t_3^2 - 2\ y_q^2 y_r^2 y_u^2 y_v^2 y_s^2\ t_1^2 t_2^2 t_3^2 t_4^2\ .$$

$$(3.6.53)$$

The finite plethystic logarithm indicates that the mesonic moduli space is a complete intersection.

With the fugacity map

$$f_1 = \frac{y_q\ t_1 t_2}{y_r\ t_3 t_4}\ ,\quad f_2 = \frac{y_v\ t_2 t_4}{y_u\ t_1 t_3}\ ,\quad t = y_q^{1/4} y_r^{1/4} y_u^{1/4} y_v^{1/4} y_s^{1/4}\ t_1^{1/4} t_2^{1/4} t_3^{1/4} t_4^{1/4}\ ,\qquad (3.6.54)$$

where the fugacities f_1, f_2 and t count mesonic charges, the Hilbert series becomes

$$g_1(t, f_1, f_2; \mathcal{M}_{4a}^{mes}) = \frac{(1 - t^8)^2}{(1 - t^4)(1 - \frac{1}{f_1} t^4)(1 - f_1 t^4)(1 - \frac{1}{f_2} t^4)(1 - f_2 t^4)}\ .\qquad (3.6.55)$$

The corresponding plethystic logarithm is

$$PL[g_1(t, f_1, f_2; \mathcal{M}_{4a}^{mes})] = \left(1 + f_1 + \frac{1}{f_1} + f_2 + \frac{1}{f_2}\right) t^4 - 2t^8\ .\qquad (3.6.56)$$

The above plethystic logarithm identifies the moduli space generators with their mesonic charges. They are summarized in Table 3.14. The charge lattice of generators in Table 3.14 is the dual reflexive polygon of the toric diagram of Model 4a. The generators satisfy the following relations

$$A_1 A_2 = B_1 B_2 = C^2\ .\qquad (3.6.57)$$

147

Generator	$U(1)_{f_1}$	$U(1)_{f_2}$
$X_{16}X_{67}X_{74}X_{41} = X_{23}X_{38}X_{85}X_{52}$	0	-1
$X_{12}X_{23}X_{34}X_{41} = X_{56}X_{67}X_{78}X_{85}$	1	0
$X_{12}X_{23}X_{38}X_{81} = X_{12}X_{27}X_{74}X_{41} = X_{16}X_{63}X_{34}X_{41} = X_{16}X_{67}X_{78}X_{81} = X_{23}X_{34}X_{45}X_{52} = X_{27}X_{78}X_{85}X_{52} = X_{38}X_{85}X_{56}X_{63} = X_{45}X_{56}X_{67}X_{74}$	0	0
$X_{16}X_{63}X_{38}X_{81} = X_{27}X_{74}X_{45}X_{52}$	-1	0
$X_{12}X_{27}X_{78}X_{81} = X_{34}X_{45}X_{56}X_{63}$	0	1

Table 3.15: The generators in terms of bifundamental fields (Model 4a).
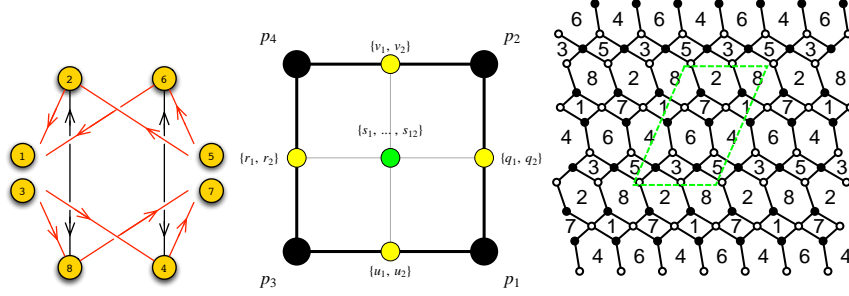
Figure 3.8: The quiver, toric diagram, and brane tiling of Model 4b. The red arrows in the quiver indicate all possible connections between blocks of nodes.

The fugacities

$$
T_1 = \frac{y_r^2 y_u^2 y_s\, t_1 t_3^3 t_4}{t_2} = \frac{t^4}{f_1 f_2} \; , \; T_2 = \frac{y_q\, t_1 t_2}{y_r\, t_3 t_4} = f_1 \; , \; T_3 = \frac{y_v\, t_2 t_4}{y_u\, t_1 t_3} = f_2 \; ,
$$

(3.6.58)

can be introduced to rewrite the Hilbert series and plethystic logarithm as

$$
g_1(T_1, T_2, T_3; \mathcal{M}_{4a}^{mes}) = \frac{(1 - T_1^2 T_2^2 T_3^2)^2}{(1 - T_1 T_2 T_3)(1 - T_1 T_3)(1 - T_1 T_2^2 T_3)(1 - T_1 T_2)(1 - T_1 T_2 T_3^2)}
$$

(3.6.59)

and

$$
PL[g_1(T_1, T_2, T_3; \mathcal{M}_{4a}^{mes})] = T_1 T_2 T_3 + T_1 T_2^2 T_3 + T_1 T_3 + T_1 T_2 T_3^2 + T_1 T_2 - T_1^2 T_2^2 T_3^2
$$

(3.6.60)

such that powers of the fugacities in the expressions are positive. This illustrates the cone structure of the variety.

3.6.2 Model 4 Phase b

The superpotential is

$$
\begin{aligned}
W \;=\; & +X_{23}X_{38}X_{82} + X_{45}X_{56}X_{64} + X_{63}X_{34}X_{46} + X_{85}X_{52}X_{28} \\
& +X_{21}X_{14}X_{47}X_{72} + X_{61}X_{18}X_{87}X_{76} \\
& -X_{21}X_{18}X_{82} - X_{47}X_{76}X_{64} - X_{87}X_{72}X_{28} - X_{61}X_{14}X_{46} \\
& -X_{45}X_{52}X_{23}X_{34} - X_{63}X_{38}X_{85}X_{56}
\end{aligned}
\tag{3.6.61}
$$

The perfect matching matrix is

$$ P = $$

	p_1	p_2	p_3	p_4	q_1	q_2	r_1	r_2	u_1	u_2	v_1	v_2	s_1	s_2	s_3	s_4	s_5	s_6	s_7	s_8	s_9	s_{10}	s_{11}	s_{12}
X_{61}	1	0	0	0	1	0	0	0	1	0	0	0	1	0	1	0	1	0	0	0	0	0	0	0
X_{47}	1	0	0	0	1	0	0	0	0	1	0	0	0	1	0	1	0	1	0	0	0	0	0	0
X_{34}	1	0	0	0	0	1	0	0	1	0	0	0	1	0	0	0	0	0	1	0	1	0	0	0
X_{56}	1	0	0	0	0	1	0	0	0	1	0	0	0	1	0	0	0	0	1	0	1	0	0	0
X_{63}	0	1	0	0	1	0	0	0	0	0	1	0	0	0	1	0	1	0	0	0	0	0	1	0
X_{45}	0	1	0	0	1	0	0	0	0	0	0	1	0	0	0	1	0	1	0	0	0	0	0	1
X_{14}	0	1	0	0	0	1	0	0	0	0	1	0	0	0	0	0	0	0	1	0	1	0	1	0
X_{76}	0	1	0	0	0	1	0	0	0	0	0	1	0	0	0	0	0	0	0	1	0	1	0	1
X_{85}	0	0	1	0	0	0	1	0	1	0	0	0	0	0	0	0	0	1	0	0	1	0	0	1
X_{23}	0	0	1	0	0	0	1	0	0	1	0	0	0	0	0	0	1	0	0	0	0	1	1	0
X_{72}	0	0	1	0	0	0	0	1	1	0	0	0	0	0	1	0	0	0	0	1	0	0	0	1
X_{18}	0	0	1	0	0	0	0	1	0	1	0	0	0	0	0	1	0	0	1	0	0	0	1	0
X_{87}	0	0	0	1	0	0	1	0	0	0	1	0	0	1	0	0	0	1	0	0	1	0	0	0
X_{21}	0	0	0	1	0	0	1	0	0	0	0	1	1	0	0	0	1	0	0	0	0	1	0	0
X_{52}	0	0	0	1	0	0	0	1	0	0	1	0	0	1	1	0	0	0	0	1	0	0	0	0
X_{38}	0	0	0	1	0	0	0	1	0	0	0	1	1	0	0	1	0	0	1	0	0	0	0	0
X_{82}	1	1	0	0	1	1	0	0	1	0	1	0	0	1	1	0	0	1	0	1	1	0	0	1
X_{28}	1	1	0	0	1	1	0	0	0	1	0	1	1	0	0	1	1	0	1	0	0	1	1	0
X_{64}	0	0	1	1	0	0	1	1	1	0	1	0	1	0	1	0	1	0	1	0	1	0	1	0
X_{46}	0	0	1	1	0	0	1	1	0	1	0	1	0	1	0	1	0	1	0	1	0	1	0	1

$$\tag{3.6.62}$$

The F-term charge matrix $Q_F = \ker(P)$ is

$$ Q_F = $$

p_1	p_2	p_3	p_4	q_1	q_2	r_1	r_2	u_1	u_2	v_1	v_2	s_1	s_2	s_3	s_4	s_5	s_6	s_7	s_8	s_9	s_{10}	s_{11}	s_{12}
1	1	0	0	-1	-1	0	0	0	0	0	0	0	0	0	0	0	0	0	0	0	0	0	0
0	0	1	1	0	0	-1	-1	0	0	0	0	0	0	0	0	0	0	0	0	0	0	0	0
1	0	1	0	0	0	0	0	-1	-1	0	0	0	0	0	0	0	0	0	0	0	0	0	0
0	1	0	1	0	0	0	0	0	0	-1	-1	0	0	0	0	0	0	0	0	0	0	0	0
1	0	0	1	0	0	0	0	0	0	0	0	-1	-1	0	0	0	0	0	0	0	0	0	0
0	0	0	0	1	0	0	1	0	0	0	0	0	0	-1	-1	0	0	0	0	0	0	0	0
0	0	0	0	1	0	1	0	0	0	0	0	0	0	0	0	-1	-1	0	0	0	0	0	0
0	0	0	0	0	0	0	0	1	0	1	0	0	0	-1	0	0	0	0	-1	0	0	0	0
0	0	0	0	0	0	0	0	1	0	0	1	-1	0	0	0	0	0	0	0	0	0	0	-1
0	0	1	0	0	0	-1	0	0	0	1	0	0	0	-1	0	1	0	0	0	0	0	-1	0
0	0	1	0	0	0	0	0	-1	0	0	0	1	0	-1	0	0	0	-1	0	0	0	0	0
0	0	0	1	0	1	0	0	0	0	-1	0	-1	0	1	0	0	0	0	-1	0	0	0	0
0	0	0	1	0	0	-1	0	1	0	0	0	-1	0	-1	0	1	0	0	0	0	0	0	0
0	0	0	0	0	0	0	0	0	0	0	0	0	0	1	0	-1	0	0	-1	0	1	0	0

$$\tag{3.6.63}$$

Generator	$U(1)_{f_1}$	$U(1)_{f_2}$
$X_{56}X_{18}X_{85}X_{61} = X_{23}X_{34}X_{47}X_{72}$	0	-1
$X_{28}X_{82} = X_{14}X_{45}X_{56}X_{61} = X_{14}X_{47}X_{76}X_{61} = X_{34}X_{45}X_{56}X_{63} = X_{34}X_{47}X_{76}X_{63}$	1	0
$X_{21}X_{14}X_{47}X_{72} = X_{61}X_{18}X_{87}X_{76} = X_{23}X_{34}X_{45}X_{52} = X_{56}X_{38}X_{85}X_{63} = X_{14}X_{46}X_{61} = X_{21}X_{18}X_{82}$ $= X_{23}X_{38}X_{82} = X_{52}X_{28}X_{85} = X_{72}X_{28}X_{87} = X_{34}X_{46}X_{63} = X_{45}X_{56}X_{64} = X_{64}X_{47}X_{76}$	0	0
$X_{46}X_{64} = X_{21}X_{18}X_{85}X_{52} = X_{21}X_{18}X_{87}X_{72} = X_{23}X_{38}X_{85}X_{52} = X_{23}X_{38}X_{87}X_{72}$	-1	0
$X_{21}X_{14}X_{45}X_{52} = X_{63}X_{38}X_{87}X_{76}$	0	1

Table 3.16: The generators in terms of bifundamental fields (Model 4b).

The D-term charge matrix is

$$
Q_D = \left(
\begin{array}{cccc|cc|cc|cc|cc|cccccccccccc}
p_1 & p_2 & p_3 & p_4 & q_1 & q_2 & r_1 & r_2 & u_1 & u_2 & v_1 & v_2 & s_1 & s_2 & s_3 & s_4 & s_5 & s_6 & s_7 & s_8 & s_9 & s_{10} & s_{11} & s_{12} \\
0 & 0 & 0 & 0 & 0 & 0 & 0 & 0 & 0 & 0 & 0 & 0 & 0 & 0 & 0 & 0 & 1 & -1 & 0 & 0 & 0 & 0 & 0 & 0 \\
0 & 0 & 0 & 0 & 0 & 0 & 0 & 0 & 0 & 0 & 0 & 0 & 0 & 0 & 0 & 0 & 0 & 1 & -1 & 0 & 0 & 0 & 0 & 0 \\
0 & 0 & 0 & 0 & 0 & 0 & 0 & 0 & 0 & 0 & 0 & 0 & 0 & 0 & 0 & 0 & 0 & 0 & 1 & -1 & 0 & 0 & 0 & 0 \\
0 & 0 & 0 & 0 & 0 & 0 & 0 & 0 & 0 & 0 & 0 & 0 & 0 & 0 & 0 & 0 & 0 & 0 & 0 & 1 & -1 & 0 & 0 & 0 \\
0 & 0 & 0 & 0 & 0 & 0 & 0 & 0 & 0 & 0 & 0 & 0 & 0 & 0 & 0 & 0 & 0 & 0 & 0 & 0 & 1 & -1 & 0 & 0 \\
0 & 0 & 0 & 0 & 0 & 0 & 0 & 0 & 0 & 0 & 0 & 0 & 0 & 0 & 0 & 0 & 0 & 0 & 0 & 0 & 0 & 1 & -1 & 0 \\
0 & 0 & 0 & 0 & 0 & 0 & 0 & 0 & 0 & 0 & 0 & 0 & 0 & 0 & 0 & 0 & 0 & 0 & 0 & 0 & 0 & 0 & 1 & -1
\end{array}
\right) . \qquad (3.6.64)
$$

The total charge matrix Q_t does not have repeated columns. Accordingly, the global symmetry is $U(1)_{f_1} \times U(1)_{f_2} \times U(1)_R$. This is the same global symmetry as for Model 4a, and the same mesonic charges on extremal perfect matchings are assigned as for Model 4a, as shown in Table 3.13.

Let products of non-extremal perfect matchings be associated to a single variable as follows

$$
q = q_1 q_2 \ , \ r = r_1 r_2 \ , \ u = u_1 u_2 \ , \ v = v_1 v_2 \ , \ s = \prod_{m=1}^{12} s_m \ . \qquad (3.6.65)
$$

The extremal perfect matchings p_α are counted by t_α. The fugacity of the form y_q counts the non-extremal perfect matching product q above.

The refined mesonic Hilbert series is calculated using the Molien integral formula in (1.4.67). The Hilbert series and the corresponding plethystic logarithm turn out to be the same as for Model 4a. The mesonic Hilbert series and the refined plethystic logarithms are given in (3.6.52), (3.6.53) and (3.6.56). Accordingly, the mesonic moduli spaces of Model 4a and 4b are the same, with the corresponding quiver gauge theories being toric dual.

The generators in terms of perfect matchings of Model 4b are given in Table 3.14 with the correspoding mesonic symmetry charges. The corresponding generators in terms of quiver fields are shown in Table 3.16. The mesonic moduli space is a complete intersection, with the generators satisfying the relations in (3.6.57).
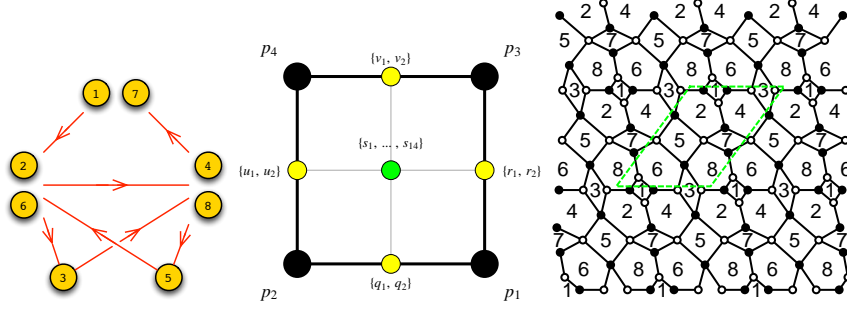
Figure 3.9: The quiver, toric diagram, and brane tiling of Model 4c. The red arrows in the quiver indicate all possible connections between blocks of nodes.

3.6.3 Model 4 Phase c

The superpotential is

$$
\begin{aligned}
W \;=\; &+X_{21}X_{14}X_{42} + X_{23}X_{38}X_{82} + X_{61}X_{18}X_{86} + X_{63}X_{34}X_{46} \\
&+X_{67}X_{74}X_{45}X_{56} + X_{85}X_{52}X_{27}X_{78} \\
&-X_{21}X_{18}X_{82} - X_{27}X_{74}X_{42} - X_{61}X_{14}X_{46} - X_{67}X_{78}X_{86} \\
&-X_{45}X_{52}X_{23}X_{34} - X_{63}X_{38}X_{85}X_{56}
\end{aligned}
\tag{3.6.66}
$$

The perfect matching matrix is

$$P =$$

	p_1	p_2	p_3	p_4	q_1	q_2	r_1	r_2	u_1	u_2	v_1	v_2	s_1	s_2	s_3	s_4	s_5	s_6	s_7	s_8	s_9	s_{10}	s_{11}	s_{12}	s_{13}	s_{14}
X_{61}	1	0	0	0	1	0	1	0	0	0	0	0	0	0	1	1	1	0	1	0	0	0	0	0	1	0
X_{78}	1	0	0	0	1	0	0	1	0	0	0	0	0	0	0	0	1	1	0	0	1	0	1	0	1	0
X_{34}	1	0	0	0	0	1	1	0	0	0	0	0	0	0	1	0	0	1	0	0	0	1	0	1	1	0
X_{56}	1	0	0	0	0	1	0	1	0	0	0	0	1	0	0	0	0	0	0	1	0	0	0	0	0	0
X_{45}	0	1	0	0	1	0	0	0	1	0	0	0	0	1	0	0	0	0	0	0	0	1	0	0	0	0
X_{63}	0	1	0	0	1	0	0	0	0	1	0	0	0	0	1	1	0	1	0	1	0	0	0	0	0	1
X_{27}	0	1	0	0	0	1	0	0	1	0	0	0	0	0	1	1	0	0	0	1	0	1	0	0	0	1
X_{14}	0	1	0	0	0	1	0	0	0	1	0	0	0	0	0	0	0	1	0	0	1	1	0	1	0	1
X_{67}	0	0	1	0	0	0	1	0	0	0	1	0	0	0	1	1	0	0	1	0	0	1	0	0	0	1
X_{85}	0	0	1	0	0	0	1	0	0	0	0	1	0	1	0	0	0	0	0	0	0	0	0	1	0	0
X_{18}	0	0	1	0	0	0	0	1	0	0	1	0	0	0	0	0	1	0	0	1	1	1	0	0	0	1
X_{23}	0	0	1	0	0	0	0	1	0	0	0	1	0	0	0	1	1	0	0	1	1	0	0	0	0	1
X_{38}	0	0	0	1	0	0	0	0	1	0	1	0	0	0	1	0	0	1	0	0	0	1	1	0	1	0
X_{21}	0	0	0	1	0	0	0	0	1	0	0	1	0	0	1	1	1	0	0	1	0	0	0	0	1	0
X_{52}	0	0	0	1	0	0	0	0	0	1	1	0	1	0	0	0	0	0	1	0	0	0	0	0	0	0
X_{74}	0	0	0	1	0	0	0	0	0	1	0	1	0	0	0	0	1	1	0	0	1	0	0	1	1	0
X_{82}	1	1	0	0	1	1	1	0	0	1	0	0	1	1	0	0	0	0	1	0	0	0	0	1	0	0
X_{42}	1	0	1	0	1	0	1	1	0	0	1	0	1	1	0	0	0	0	1	0	0	1	0	0	0	0
X_{86}	0	1	0	1	0	1	0	0	1	1	0	1	1	1	0	0	0	0	0	1	0	0	0	1	0	0
X_{46}	0	0	1	1	0	0	0	1	1	0	1	1	1	1	0	0	0	0	0	1	0	0	1	0	0	0

$$\tag{3.6.67}$$

The F-term charge matrix $Q_F = \ker(P)$ is

$$
Q_F = \left(
\begin{array}{cccc|cc|cc|cc|cc|cccccccccccccc}
p_1 & p_2 & p_3 & p_4 & q_1 & q_2 & r_1 & r_2 & u_1 & u_2 & v_1 & v_2 & s_1 & s_2 & s_3 & s_4 & s_5 & s_6 & s_7 & s_8 & s_9 & s_{10} & s_{11} & s_{12} & s_{13} & s_{14} \\
\hline
1 & 1 & 0 & 0 & -1 & -1 & 0 & 0 & 0 & 0 & 0 & 0 & 0 & 0 & 0 & 0 & 0 & 0 & 0 & 0 & 0 & 0 & 0 & 0 & 0 & 0 \\
1 & 0 & 1 & 0 & 0 & 0 & -1 & -1 & 0 & 0 & 0 & 0 & 0 & 0 & 0 & 0 & 0 & 0 & 0 & 0 & 0 & 0 & 0 & 0 & 0 & 0 \\
0 & 1 & 0 & 1 & 0 & 0 & 0 & 0 & -1 & -1 & 0 & 0 & 0 & 0 & 0 & 0 & 0 & 0 & 0 & 0 & 0 & 0 & 0 & 0 & 0 & 0 \\
0 & 0 & 1 & 1 & 0 & 0 & 0 & 0 & 0 & 0 & -1 & -1 & 0 & 0 & 0 & 0 & 0 & 0 & 0 & 0 & 0 & 0 & 0 & 0 & 0 & 0 \\
1 & 0 & 0 & 1 & 0 & 0 & 0 & 0 & 0 & 0 & 0 & 0 & -1 & 0 & 0 & 0 & 0 & 0 & 0 & 0 & 0 & 0 & 0 & 0 & -1 & 0 \\
0 & 1 & 1 & 0 & 0 & 0 & 0 & 0 & 0 & 0 & 0 & 0 & 0 & -1 & 0 & 0 & 0 & 0 & 0 & 0 & 0 & 0 & 0 & 0 & 0 & -1 \\
1 & 0 & 0 & 0 & -1 & 0 & 0 & -1 & 0 & 0 & 0 & 0 & 0 & 0 & 0 & 0 & 0 & -1 & 0 & 0 & 1 & 0 & 1 & 0 & 0 & 0 \\
1 & 0 & 0 & 0 & -1 & 0 & -1 & 0 & 0 & 0 & 0 & 0 & 0 & 1 & 0 & 1 & 0 & 0 & 0 & -1 & 0 & 0 & 0 & 0 & 0 & 0 \\
0 & 0 & 1 & 0 & 1 & 0 & -1 & 0 & 0 & 0 & 0 & 0 & 0 & -1 & 0 & 0 & 0 & 0 & 0 & 0 & -1 & 0 & 0 & 1 & 0 & 0 \\
0 & 0 & 1 & 0 & 0 & 0 & 0 & 0 & 1 & 0 & -1 & 0 & 1 & -1 & 0 & 0 & 0 & 0 & 0 & -1 & 0 & 0 & 0 & 0 & 0 & 0 \\
0 & 0 & 0 & 0 & 1 & 0 & 0 & 0 & 0 & 0 & 1 & 0 & 0 & 0 & 0 & 0 & 0 & 0 & -1 & 0 & 0 & 0 & -1 & 0 & 0 & 0 \\
0 & 0 & 0 & 0 & 1 & 0 & 0 & 0 & 0 & 0 & 0 & 1 & 0 & -1 & 0 & 0 & -1 & 0 & 0 & 0 & 0 & 0 & 0 & 0 & 0 & 0 \\
0 & 0 & 0 & 0 & 0 & 1 & 0 & 0 & 0 & 0 & 1 & 0 & -1 & 0 & 0 & 0 & 0 & 0 & 0 & 0 & 0 & -1 & 0 & 0 & 0 & 0 \\
0 & 0 & 0 & 0 & 0 & 0 & 1 & 0 & 1 & 0 & 0 & 0 & 0 & -1 & -1 & 0 & 0 & 0 & 0 & 0 & 0 & 0 & 0 & 0 & 0 & 0 \\
0 & 0 & 0 & 0 & 0 & 0 & 0 & 1 & 0 & 1 & 0 & 0 & -1 & 0 & 0 & 0 & 0 & 0 & 0 & 0 & -1 & 0 & 0 & 0 & 0 & 0 \\
0 & 0 & 0 & 0 & 0 & 0 & 0 & 0 & 0 & 0 & 0 & 0 & 1 & 0 & 0 & 1 & 0 & 0 & -1 & -1 & 0 & 0 & 0 & 0 & 0 & 0 \\
\end{array}
\right). \tag{3.6.68}
$$

The D-term charge matrix is

$$
Q_D = \left(
\begin{array}{cccc|cc|cc|cc|cc|cccccccccccccc}
p_1 & p_2 & p_3 & p_4 & q_1 & q_2 & r_1 & r_2 & u_1 & u_2 & v_1 & v_2 & s_1 & s_2 & s_3 & s_4 & s_5 & s_6 & s_7 & s_8 & s_9 & s_{10} & s_{11} & s_{12} & s_{13} & s_{14} \\
\hline
0 & 0 & 0 & 0 & 0 & 0 & 0 & 0 & 0 & 0 & 0 & 0 & 0 & 0 & 0 & 0 & 0 & 0 & 1 & -1 & 0 & 0 & 0 & 0 & 0 & 0 \\
0 & 0 & 0 & 0 & 0 & 0 & 0 & 0 & 0 & 0 & 0 & 0 & 0 & 0 & 0 & 0 & 0 & 0 & 0 & 1 & -1 & 0 & 0 & 0 & 0 & 0 \\
0 & 0 & 0 & 0 & 0 & 0 & 0 & 0 & 0 & 0 & 0 & 0 & 0 & 0 & 0 & 0 & 0 & 0 & 0 & 0 & 1 & -1 & 0 & 0 & 0 & 0 \\
0 & 0 & 0 & 0 & 0 & 0 & 0 & 0 & 0 & 0 & 0 & 0 & 0 & 0 & 0 & 0 & 0 & 0 & 0 & 0 & 0 & 1 & -1 & 0 & 0 & 0 \\
0 & 0 & 0 & 0 & 0 & 0 & 0 & 0 & 0 & 0 & 0 & 0 & 0 & 0 & 0 & 0 & 0 & 0 & 0 & 0 & 0 & 0 & 1 & -1 & 0 & 0 \\
0 & 0 & 0 & 0 & 0 & 0 & 0 & 0 & 0 & 0 & 0 & 0 & 0 & 0 & 0 & 0 & 0 & 0 & 0 & 0 & 0 & 0 & 0 & 1 & -1 & 0 \\
0 & 0 & 0 & 0 & 0 & 0 & 0 & 0 & 0 & 0 & 0 & 0 & 0 & 0 & 0 & 0 & 0 & 0 & 0 & 0 & 0 & 0 & 0 & 0 & 1 & -1 \\
\end{array}
\right). \tag{3.6.69}
$$

The global symmetry is $U(1)_{f_1} \times U(1)_{f_2} \times U(1)_R$. The global symmetry charge assignment on the GLSM fields with non-zero R-charges is the same as for Model 4a and is shown Table 3.13.

Products of non-extremal perfect matchings are labelled in terms of single variables as follows

$$
q = q_1 q_2 \;,\;\; r = r_1 r_2 \;,\;\; u = u_1 u_2 \;,\;\; v = v_1 v_2 \;,\;\; s = \prod_{m=1}^{14} s_m \;. \tag{3.6.70}
$$

The fugacity which counts GLSM fields corresponding to extremal perfect matchings p_α is t_α. A product non-extremal perfect matchings, for instance q, is assigned a fugacity of the form y_q.

The mesonic Hilbert series and plethystic logarithm for Model 4c is the same form as for Model 4a. They are given respectively in (3.6.52), (3.6.53) and (3.6.56). Accordingly, the mesonic moduli space of Model 4c is the same as for Model 4a. In other words they are toric (Seiberg) duals.

The generators in terms of the perfect matching variables of Model 4c are given in Table 3.14 with their mesonic charges. The generators in terms of quiver fields are given in Table 3.17. The mesonic moduli space is a complete intersection and the generators satisfy the relations given in (3.6.57).

Generator	$U(1)_{f_1}$	$U(1)_{f_2}$
$X_{27}X_{78}X_{82} = X_{14}X_{45}X_{56}X_{61} = X_{34}X_{45}X_{56}X_{63}$	0	-1
$X_{23}X_{34}X_{42} = X_{56}X_{18}X_{85}X_{61} = X_{56}X_{67}X_{78}X_{85}$	1	0
$X_{23}X_{34}X_{45}X_{52} = X_{52}X_{27}X_{78}X_{85} = X_{56}X_{38}X_{85}X_{63} = X_{45}X_{56}X_{67}X_{74} = X_{21}X_{14}X_{42} = X_{14}X_{46}X_{61}$ $= X_{21}X_{18}X_{82} = X_{61}X_{18}X_{86} = X_{23}X_{38}X_{82} = X_{42}X_{27}X_{74} = X_{34}X_{46}X_{63} = X_{67}X_{78}X_{86}$	0	0
$X_{63}X_{38}X_{86} = X_{21}X_{14}X_{45}X_{52} = X_{45}X_{27}X_{74}X_{52}$	-1	0
$X_{46}X_{67}X_{74} = X_{21}X_{18}X_{85}X_{52} = X_{23}X_{38}X_{85}X_{52}$	0	1

Table 3.17: The generators in terms of bifundamental fields (Model 4c).
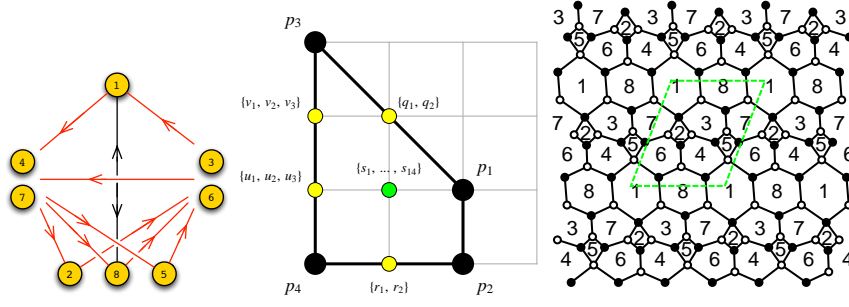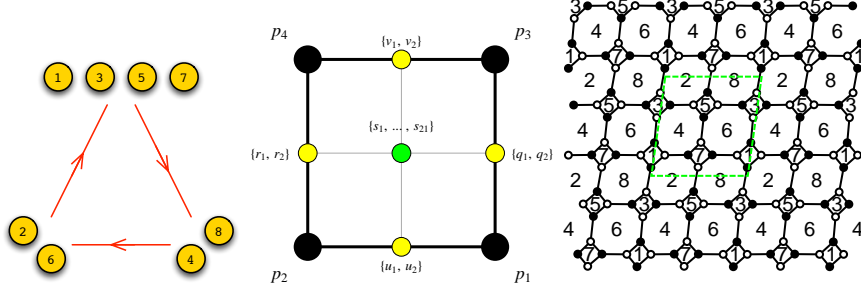

Figure 3.10: The quiver, toric diagram, and brane tiling of Model 4d. The red arrows in the quiver indicate all possible connections between blocks of nodes.

3.6.4 Model 4 Phase d

The superpotential is

$$
\begin{aligned}
W \; = \; & +X_{21}X_{14}X_{42}^1 + X_{23}X_{38}X_{82}^1 + X_{25}X_{54}X_{42}^2 + X_{27}X_{78}X_{82}^2 \\
& +X_{61}X_{18}X_{86}^1 + X_{63}X_{34}X_{46}^1 + X_{65}X_{58}X_{86}^2 + X_{67}X_{74}X_{46}^2 \\
& -X_{21}X_{18}X_{82}^1 - X_{23}X_{34}X_{42}^2 - X_{25}X_{58}X_{82}^2 - X_{27}X_{74}X_{42}^1 \\
& -X_{61}X_{14}X_{46}^1 - X_{63}X_{38}X_{86}^2 - X_{65}X_{54}X_{46}^2 - X_{67}X_{78}X_{86}^1
\end{aligned}
\tag{3.6.71}
$$

The perfect matching matrix is

$$\tag{3.6.72}$$

The F-term charge matrix $Q_F = \ker(P)$ is

$$
Q_F = \left(
\begin{array}{cccc|cc|cc|cc|cc|ccccccccccccccccccccc}
 & p_1 & p_2 & p_3 & p_4 & q_1 & q_2 & r_1 & r_2 & u_1 & u_2 & v_1 & v_2 & s_1 & s_2 & s_3 & s_4 & s_5 & s_6 & s_7 & s_8 & s_9 & s_{10} & s_{11} & s_{12} & s_{13} & s_{14} & s_{15} & s_{16} & s_{17} & s_{18} & s_{19} & s_{20} & s_{21}
\end{array}
\right)
$$

(see matrix in equation (3.6.73))

$$ \tag{3.6.73} $$

The D-term charge matrix is

$$
Q_D = \left(
\begin{array}{cccc|cc|cc|cc|cc|ccccccccccccccccccccc}
 p_1 & p_2 & p_3 & p_4 & q_1 & q_2 & r_1 & r_2 & u_1 & u_2 & v_1 & v_2 & s_1 & s_2 & s_3 & s_4 & s_5 & s_6 & s_7 & s_8 & s_9 & s_{10} & s_{11} & s_{12} & s_{13} & s_{14} & s_{15} & s_{16} & s_{17} & s_{18} & s_{19} & s_{20} & s_{21} \\
 0 & 0 & 0 & 0 & 0 & 0 & 0 & 0 & 0 & 0 & 0 & 0 & 0 & 0 & 0 & 0 & 0 & 0 & 0 & 0 & 0 & 0 & 1 & -1 & 0 & 0 & 0 & 0 & 0 & 0 & 0 & 0 & 0 \\
 0 & 0 & 0 & 0 & 0 & 0 & 0 & 0 & 0 & 0 & 0 & 0 & 0 & 0 & 0 & 0 & 0 & 0 & 0 & 0 & 0 & 0 & 0 & 1 & -1 & 0 & 0 & 0 & 0 & 0 & 0 & 0 & 0 \\
 0 & 0 & 0 & 0 & 0 & 0 & 0 & 0 & 0 & 0 & 0 & 0 & 0 & 0 & 0 & 0 & 0 & 0 & 0 & 0 & 0 & 0 & 0 & 0 & 1 & -1 & 0 & 0 & 0 & 0 & 0 & 0 & 0 \\
 0 & 0 & 0 & 0 & 0 & 0 & 0 & 0 & 0 & 0 & 0 & 0 & 0 & 0 & 0 & 0 & 0 & 0 & 0 & 0 & 0 & 0 & 0 & 0 & 0 & 1 & -1 & 0 & 0 & 0 & 0 & 0 & 0 \\
 0 & 0 & 0 & 0 & 0 & 0 & 0 & 0 & 0 & 0 & 0 & 0 & 0 & 0 & 0 & 0 & 0 & 0 & 0 & 0 & 0 & 0 & 0 & 0 & 0 & 0 & 1 & -1 & 0 & 0 & 0 & 0 & 0 \\
 0 & 0 & 0 & 0 & 0 & 0 & 0 & 0 & 0 & 0 & 0 & 0 & 0 & 0 & 0 & 0 & 0 & 0 & 0 & 0 & 0 & 0 & 0 & 0 & 0 & 0 & 0 & 1 & -1 & 0 & 0 & 0 & 0 \\
 0 & 0 & 0 & 0 & 0 & 0 & 0 & 0 & 0 & 0 & 0 & 0 & 0 & 0 & 0 & 0 & 0 & 0 & 0 & 0 & 0 & 0 & 0 & 0 & 0 & 0 & 0 & 0 & 1 & -1 & 0 & 0 & 0 \\
\end{array}
\right)
$$

$$ \tag{3.6.74} $$

The global symmetry is $U(1)_{f_1} \times U(1)_{f_2} \times U(1)_R$. The global symmetry charge assignment on perfect matchings with non-zero R-charge is the same as for Model 4a and is shown in Table 3.13.

Products of non-extremal perfect matchings are expressed in terms of single variables as follows

$$
q = q_1 q_2 \ , \quad r = r_1 r_2 \ , \quad u = u_1 u_2 \ , \quad v = v_1 v_2 \ , \quad s = \prod_{m=1}^{21} s_m \ . \tag{3.6.75}
$$

The fugacity which counts extremal perfect matchings is t_α. A product of non-extremal perfect matchings such as q is assigned a fugacity of the form y_q.

The mesonic Hilbert series and the plethystic logarithm are the same as for Model 4a. The mesonic Hilbert series and the refined plethystic logarithms are given in (3.6.52), (3.6.53) and (3.6.56) respectively.

The mesonic moduli space generators in terms of perfect matching variables of Model 4d are given in Table 3.14. In terms of quiver fields, the generators with their mesonic charges are shown in Table 3.18. The mesonic moduli space is a complete intersection and the generators satisfy the relations in (3.6.57).

Generator	$U(1)_{f_1}$	$U(1)_{f_2}$
$X_{21}X_{14}X_{42}^2 = X_{42}^2 X_{27}X_{74} = X_{63}X_{38}X_{86}^1 = X_{65}X_{58}X_{86}^1$	0	-1
$X_{14}X_{46}^2 X_{61} = X_{25}X_{58}X_{82}^1 = X_{27}X_{78}X_{82}^1 = X_{34}X_{46}^2 X_{63}$	1	0
$X_{21}X_{14}X_{42}^1 = X_{14}X_{61}^1 X_{61} = X_{21}X_{18}X_{82}^1 = X_{61}X_{18}X_{86}^1 = X_{23}X_{34}X_{42}^2 = X_{23}X_{38}X_{82}^1$ $= X_{42}^2 X_{25}X_{54} = X_{25}X_{58}X_{82}^2 = X_{42}^1 X_{27}X_{74} = X_{27}X_{78}X_{82}^2 = X_{34}X_{46}^1 X_{63} = X_{63}X_{38}X_{86}^2$ $= X_{54}X_{46}^2 X_{65} = X_{46}^2 X_{67}X_{74} = X_{65}X_{58}X_{86}^2 = X_{67}X_{78}X_{86}^1$	0	0
$X_{21}X_{18}X_{82}^2 = X_{23}X_{38}X_{82}^2 = X_{54}X_{46}^1 X_{65} = X_{46}^1 X_{67}X_{74}$	-1	0
$X_{61}X_{18}X_{86}^2 = X_{23}X_{34}X_{42}^1 = X_{42}^1 X_{25}X_{54} = X_{67}X_{78}X_{86}^2$	0	1

Table 3.18: The generators in terms of bifundamental fields (Model 4d).
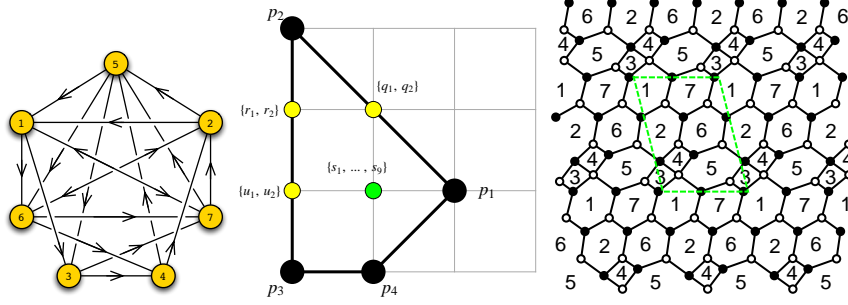
Figure 3.11: The quiver, toric diagram, and brane tiling of Model 5.

3.7 Model 5: PdP_{4b}

The superpotential is

$$
\begin{aligned}
W = \ & +X_{21}X_{17}X_{72} + X_{42}X_{26}X_{64} + X_{56}X_{62}X_{25} + X_{67}X_{71}X_{16} + X_{75}X_{53}X_{37} \\
& +X_{13}X_{34}X_{45}X_{51} - X_{13}X_{37}X_{71} - X_{16}X_{62}X_{21} - X_{56}X_{64}X_{45} \\
& -X_{67}X_{72}X_{26} - X_{75}X_{51}X_{17} - X_{25}X_{53}X_{34}X_{42}
\end{aligned}
\tag{3.7.76}
$$

The perfect matching matrix is

$$
P = \left(
\begin{array}{c|cccc|cc|ccc|ccc|ccccccccc}
 & p_1 & p_2 & p_3 & p_4 & q_1 & q_2 & r_1 & r_2 & r_3 & u_1 & u_2 & u_3 & s_1 & s_2 & s_3 & s_4 & s_5 & s_6 & s_7 & s_8 & s_9 \\
\hline
X_{45} & 1 & 0 & 0 & 0 & 1 & 0 & 0 & 0 & 0 & 0 & 0 & 0 & 1 & 1 & 0 & 0 & 0 & 0 & 1 & 0 & 0 \\
X_{53} & 1 & 0 & 0 & 0 & 0 & 1 & 0 & 0 & 0 & 0 & 0 & 0 & 0 & 0 & 1 & 1 & 0 & 0 & 0 & 1 & 0 \\
X_{26} & 1 & 0 & 0 & 1 & 1 & 0 & 0 & 0 & 0 & 0 & 0 & 0 & 0 & 0 & 1 & 0 & 1 & 0 & 1 & 1 & 0 \\
X_{17} & 1 & 0 & 0 & 0 & 1 & 0 & 0 & 0 & 0 & 0 & 0 & 0 & 1 & 0 & 1 & 1 & 1 & 0 & 0 & 0 & 1 \\
X_{62} & 1 & 0 & 0 & 0 & 0 & 1 & 0 & 0 & 0 & 0 & 0 & 0 & 1 & 1 & 0 & 1 & 0 & 1 & 0 & 0 & 1 \\
X_{71} & 1 & 0 & 0 & 1 & 0 & 1 & 0 & 0 & 0 & 0 & 0 & 0 & 0 & 1 & 0 & 0 & 0 & 1 & 1 & 1 & 0 \\
X_{25} & 0 & 1 & 0 & 0 & 0 & 1 & 0 & 1 & 0 & 1 & 0 & 0 & 0 & 0 & 0 & 0 & 0 & 0 & 1 & 0 & 0 \\
X_{75} & 0 & 0 & 1 & 1 & 0 & 0 & 1 & 0 & 0 & 1 & 1 & 0 & 0 & 1 & 0 & 0 & 0 & 1 & 1 & 0 & 0 \\
X_{51} & 0 & 1 & 0 & 0 & 0 & 1 & 0 & 1 & 1 & 0 & 0 & 1 & 0 & 0 & 0 & 0 & 0 & 0 & 0 & 1 & 0 \\
X_{56} & 0 & 0 & 1 & 1 & 0 & 0 & 0 & 1 & 0 & 1 & 0 & 1 & 0 & 0 & 1 & 0 & 1 & 0 & 0 & 1 & 0 \\
X_{37} & 0 & 1 & 0 & 0 & 1 & 0 & 0 & 1 & 1 & 0 & 0 & 1 & 1 & 0 & 0 & 0 & 1 & 0 & 0 & 0 & 1 \\
X_{42} & 0 & 0 & 1 & 0 & 0 & 0 & 0 & 1 & 0 & 1 & 0 & 1 & 1 & 1 & 0 & 0 & 0 & 0 & 0 & 0 & 0 \\
X_{64} & 0 & 1 & 0 & 0 & 0 & 1 & 1 & 0 & 1 & 0 & 1 & 0 & 0 & 0 & 0 & 1 & 0 & 1 & 0 & 0 & 1 \\
X_{13} & 0 & 0 & 1 & 0 & 0 & 0 & 1 & 0 & 0 & 1 & 1 & 0 & 0 & 0 & 1 & 1 & 0 & 0 & 0 & 0 & 0 \\
X_{16} & 0 & 1 & 0 & 0 & 1 & 0 & 1 & 1 & 0 & 1 & 0 & 0 & 0 & 0 & 1 & 0 & 1 & 0 & 0 & 0 & 0 \\
X_{72} & 0 & 1 & 0 & 0 & 0 & 1 & 1 & 1 & 0 & 1 & 0 & 0 & 0 & 1 & 0 & 0 & 0 & 1 & 0 & 0 & 0 \\
X_{21} & 0 & 0 & 1 & 1 & 0 & 0 & 0 & 0 & 1 & 0 & 1 & 1 & 0 & 0 & 0 & 0 & 0 & 0 & 1 & 1 & 0 \\
X_{67} & 0 & 0 & 1 & 0 & 0 & 0 & 0 & 0 & 1 & 0 & 1 & 1 & 1 & 0 & 0 & 1 & 0 & 0 & 0 & 0 & 1 \\
X_{34} & 0 & 0 & 0 & 1 & 0 & 0 & 0 & 0 & 0 & 0 & 0 & 0 & 0 & 0 & 0 & 0 & 1 & 1 & 0 & 0 & 1 \\
\end{array}
\right).
\tag{3.7.77}
$$

	$U(1)_{f_1}$	$U(1)_{f_2}$	$U(1)_R$	fugacity
p_1	0	-1/2	$R_1 \simeq 0.577$	t_1
p_2	0	1/2	$R_2 \simeq 0.640$	t_2
p_3	-1	-1	$R_3 \simeq 0.539$	t_3
p_4	1	1	$R_4 \simeq 0.243$	t_4

Table 3.19: The GLSM fields corresponding to extremal points of the toric diagram with their mesonic charges (Model 5).

The F-term charge matrix $Q_F = \ker(P)$ is

$$
Q_F = \left(\begin{array}{cccc|cc|ccc|ccc|ccccccccc}
p_1 & p_2 & p_3 & p_4 & q_1 & q_2 & r_1 & r_2 & r_3 & u_1 & u_2 & u_3 & s_1 & s_2 & s_3 & s_4 & s_5 & s_6 & s_7 & s_8 & s_9 \\
1 & 1 & 0 & 0 & -1 & -1 & 0 & 0 & 0 & 0 & 0 & 0 & 0 & 0 & 0 & 0 & 0 & 0 & 0 & 0 & 0 \\
1 & 0 & 0 & 0 & 0 & 0 & 0 & 0 & 0 & 1 & 0 & 0 & 0 & -1 & -1 & 0 & 0 & 0 & 0 & 0 & 0 \\
1 & 0 & 0 & 0 & 0 & 0 & 0 & 0 & 0 & 0 & 0 & 1 & -1 & 0 & 0 & 0 & 0 & 0 & 0 & -1 & 0 \\
1 & 0 & 0 & 0 & -1 & 0 & 1 & 0 & 0 & 0 & 0 & 0 & 1 & -1 & 0 & -1 & 0 & 0 & 0 & 0 & 0 \\
0 & 1 & 0 & 0 & -1 & 0 & 0 & -1 & 0 & 0 & 0 & 0 & 0 & 1 & 0 & 0 & 1 & -1 & 0 & 0 & 0 \\
0 & 1 & 0 & 0 & 0 & 0 & -1 & -1 & 0 & 1 & 0 & 0 & 0 & 0 & 0 & 0 & 0 & 0 & 0 & 0 & 0 \\
0 & 1 & 0 & 0 & 0 & 0 & -1 & 0 & -1 & 0 & 1 & 0 & 0 & 0 & 0 & 0 & 0 & 0 & 0 & 0 & 0 \\
0 & 1 & 1 & 0 & 0 & 0 & -1 & 0 & 0 & 0 & 0 & -1 & 0 & 0 & 0 & 0 & 0 & 0 & 0 & 0 & 0 \\
0 & 1 & 1 & 0 & 0 & 0 & 0 & -1 & 0 & 0 & -1 & 0 & 0 & 0 & 0 & 0 & 0 & 0 & 0 & 0 & 0 \\
0 & 0 & 1 & -1 & 1 & 0 & -1 & 0 & 0 & 0 & 0 & 0 & -1 & 0 & 0 & 0 & 0 & 1 & 0 & 0 & 0 \\
0 & 0 & 0 & 0 & 1 & 0 & -1 & 0 & 0 & 0 & 1 & 0 & -1 & 1 & 0 & 0 & 0 & 0 & -1 & 0 & 0 \\
0 & 0 & 0 & 0 & 0 & 0 & 0 & 0 & 0 & 0 & 0 & 0 & 1 & -1 & 0 & 0 & 0 & 1 & 0 & 0 & -1
\end{array}\right). \tag{3.7.78}
$$

The D-term charge matrix is

$$
Q_D = \left(\begin{array}{cccc|cc|ccc|ccc|ccccccccc}
p_1 & p_2 & p_3 & p_4 & q_1 & q_2 & r_1 & r_2 & r_3 & u_1 & u_2 & u_3 & s_1 & s_2 & s_3 & s_4 & s_5 & s_6 & s_7 & s_8 & s_9 \\
0 & 0 & 0 & 0 & 0 & 0 & 0 & 0 & 0 & 0 & 0 & 0 & 0 & 0 & 1 & -1 & 0 & 0 & 0 & 0 & 0 \\
0 & 0 & 0 & 0 & 0 & 0 & 0 & 0 & 0 & 0 & 0 & 0 & 0 & 0 & 0 & 1 & -1 & 0 & 0 & 0 & 0 \\
0 & 0 & 0 & 0 & 0 & 0 & 0 & 0 & 0 & 0 & 0 & 0 & 0 & 0 & 0 & 0 & 1 & -1 & 0 & 0 & 0 \\
0 & 0 & 0 & 0 & 0 & 0 & 0 & 0 & 0 & 0 & 0 & 0 & 0 & 0 & 0 & 0 & 0 & 1 & -1 & 0 & 0 \\
0 & 0 & 0 & 0 & 0 & 0 & 0 & 0 & 0 & 0 & 0 & 0 & 0 & 0 & 0 & 0 & 0 & 0 & 1 & -1 & 0 \\
0 & 0 & 0 & 0 & 0 & 0 & 0 & 0 & 0 & 0 & 0 & 0 & 0 & 0 & 0 & 0 & 0 & 0 & 0 & 1 & -1
\end{array}\right) \tag{3.7.79}
$$

The total charge matrix Q_t does not have repeated columns. Accordingly, the global symmetry is $U(1)_{f_1} \times U(1)_{f_2} \times U(1)_R$. Following the discussion in §3.2.3, the flavour and R-charges on GLSM fields corresponding to extremal points in the toric diagram in Figure 3.11 are found. They are shown in Table 3.19.

Fine-tuning R-charges. The exact R-charges can be expressed in terms of roots of the following polynomials

$$
\begin{aligned}
0 &= 75 + 110x - 684x^2 + 162x^3 + 81x^4 \\
0 &= -1124565 + 2218649x_0 - 1141683x_0^2 - 16497x_0^3 \\
&\quad + (746100 - 259716x_0 + 4428x_0^2 - 64476x_0^3)y \\
&\quad + (775170 + 520182x_0 - 390258x_0^2 - 70470x_0^3)y^2 \\
&\quad + (14580 + 100764x_0 + 164268x_0^2 + 26244x_0^3)y^3 \\
&\quad + (-110565 - 26487x_0 - 19683x_0^2 - 6561x_0^3)y^4 \\
&\quad + 38880y^5 \ ,
\end{aligned} \tag{3.7.80}
$$

where the roots satisfy the bounds $0 \leq 1 - x_0 \leq \frac{2}{3}$ and $0 \leq 1 - y_0 \leq \frac{2}{3}$. The exact R-charges are

$$
\begin{aligned}
R_1 &= \frac{1}{8989575077760}(-443015521905 + 10382230129225x_0 - 1861588105479x_0^2 \\
&\quad -1223569555569x_0^3 + 788576007420y_0 + 7322446656900x_0y_0 - 1514870485020x_0^2y_0 \\
&\quad -803839472100x_0^3y_0 + 105890430210y_0^2 - 45532791090x_0y_0^2 + 616773772782x_0^2y_0^2 \\
&\quad +132554296962x_0^3y_0^2 - 87638359380y_0^3 - 829308203820x_0y_0^3 + 57898633140x_0^2y_0^3 \\
&\quad +57715867980x_0^3y_0^3 + 9044838615y_0^4 + 354606896385x_0y_0^4 - 66414222351x_0^2y_0^4 \\
&\quad -37556288361x_0^3y_0^4)
\end{aligned}
$$

$$
R_2 = y_0 \ , \quad R_3 = x_0 \ , \tag{3.7.81}
$$

$$
\begin{aligned}
R_4 &= \frac{1}{2763024913642025714519166800855040 0}(443015521905 - 10382230129225x_0 \\
&\quad +1861588105479x_0^2 + 1223569555569x_0^3 - 788576007420y_0 - 7322446656900x_0y_0 \\
&\quad +1514870485020x_0^2y_0 + 803839472100x_0^3y_0 - 105890430210y_0^2 + 45532791090x_0y_0^2 \\
&\quad -616773772782x_0^2y_0^2 - 132554296962x_0^3y_0^2 + 87638359380y_0^3 + 829308203820x_0y_0^3 \\
&\quad -57898633140x_0^2y_0^3 - 57715867980x_0^3y_0^3 - 9044838615y_0^4 - 354606896385x_0y_0^4 \\
&\quad +66414222351x_0^2y_0^4 + 37556288361x_0^3y_0^4) \ (3435680922231398676675 - \\
&\quad 1087593430938330485873 1x_0 + 2208889158465224949597x_0^2 \\
&\quad +1149691223996073074763x_0^3 + 1308961575315964402860y_0 \\
&\quad -5303703543601718636316x_0y_0 + 1007391627507047358708x_0^2y_0 \\
&\quad +5777678033465820551 64x_0^3y_0 - 41445446612526178750y_0^2 \\
&\quad +324345443167855962702x_0y_0^2 - 26748023766096050137 8x_0^2y_0^2 \\
&\quad -83757129586072681230x_0^3y_0^2 - 143402222077829778740y_0^3 \\
&\quad +581897049297268121604x_0y_0^3 - 736697373094359931 32x_0^2y_0^3 \\
&\quad -538608345646998873 96x_0^3y_0^3 + 46554904501591527955y_0^4 \\
&\quad -286145797904951411547x_0y_0^4 + 58286941395335651277x_0^2y_0^4 \\
&\quad +31675092179803827579x_0^3y_0^4) \ . \tag{3.7.82}
\end{aligned}
$$

Products of non-extremal perfect matchings are expressed in terms of single variables as follows

$$
q = q_1q_2 \ , \quad r = r_1r_2 \ , \quad u = u_1u_2 \ , \quad s = \prod_{m=1}^{9} s_m \ . \tag{3.7.83}
$$

The fugacity which counts extremal perfect matchings is t_α. The fugacity of the form

y_q counts the product of non-extremal perfect matchings q.

The mesonic Hilbert series of Model 5 is found using the Molien integral formula in (1.4.67). It is

$$g_1(t_\alpha, y_q, y_r, y_u, y_s; \mathcal{M}_5^{mes}) = (1 + y_q y_r y_u y_s \ t_1 t_2 t_3 t_4 + y_q y_r^2 y_u^2 y_s \ t_2^2 t_3^2 t_4$$
$$- y_q^3 y_r^3 y_u^2 y_s^2 \ t_1^2 t_2^4 t_3 t_4 - y_q^3 y_r^4 y_u^3 y_s^2 \ t_1 t_2^5 t_3^2 t_4 - y_q^4 y_r^5 y_u^4 y_s^3 \ t_1^2 t_2^6 t_3^3 t_4^2)$$
$$\times \frac{1}{(1 - y_q^2 y_r^2 y_u y_s \ t_1 t_2^3)(1 - y_q^2 y_r^3 y_u^2 y_s \ t_2^4 t_3)(1 - y_q y_s \ t_1^2 t_4)(1 - y_r y_u^2 y_s \ t_3^3 t_4^2)} \ .$$
(3.7.84)

The plethystic logarithm of the mesonic Hilbert series is

$$PL[g_1(t_\alpha, y_q, y_r, y_u, y_s; \mathcal{M}_5^{mes})] = y_q y_r y_u y_s \ t_1 t_2 t_3 t_4 + y_q y_s \ t_1^2 t_4 + y_q^2 y_r^2 y_u y_s \ t_1 t_2^3$$
$$+ y_r y_u^2 y_s \ t_3^3 t_4^2 + y_q y_r^2 y_u^2 y_s \ t_2^2 t_3^2 t_4 + y_q^2 y_r^3 y_u^2 y_s \ t_2^4 t_3 - y_q^2 y_r^2 y_u^2 y_s^2 \ t_1^2 t_2^2 t_3^2 t_4^2$$
$$- y_q^3 y_r^3 y_u^2 y_s^2 \ t_1^2 t_2^4 t_3 t_4 - y_q^2 y_r^3 y_u^3 y_s^2 \ t_1 t_2^3 t_3^3 t_4^2 - y_q^3 y_r^4 y_u^3 y_s^2 \ t_1 t_2^5 t_3^2 t_4 - y_q^2 y_r^4 y_u^4 y_s^2 \ t_2^4 t_3^4 t_4^2$$
$$+ y_q^4 y_r^4 y_u^3 y_s^3 \ t_1^3 t_2^5 t_3^2 t_4^2 + \dots \ .$$
(3.7.85)

Consider the following fugacity map

$$f_1 = \frac{1}{y_u y_r} \ , \ f_2 = \frac{1}{y_u y_s} \ ,$$
$$\tilde{t}_1 = y_q^{1/2} y_r^{1/2} y_u^{1/2} y_s^{1/2} t_1 \ , \ \tilde{t}_2 = y_q^{1/2} y_r^{1/2} y_u^{1/2} y_s^{1/2} t_2 \ ,$$
$$\tilde{t}_3 = t_3 \ , \ \tilde{t}_4 = t_4 \ ,$$
(3.7.86)

where f_1 and f_2 are the fugacities for the flavor charges, and $\tilde{t}_i$ is the fugacity for the R-charge R_i in table Table 3.19. In terms of the fugacity map above, the plethystic logarithm becomes

$$PL[g_1(\tilde{t}_\alpha, f_1, f_2; \mathcal{M}_5^{mes})] = \tilde{t}_1 \tilde{t}_2 \tilde{t}_3 \tilde{t}_4 + f_1 \tilde{t}_1^2 \tilde{t}_4 + f_2 \tilde{t}_1 \tilde{t}_2^3 + \frac{1}{f_1 f_2} \tilde{t}_3^3 \tilde{t}_4^2 + \frac{1}{f_1} \tilde{t}_2^2 \tilde{t}_3^2 \tilde{t}_4 + \frac{f_2}{f_1} \tilde{t}_2^4 \tilde{t}_3$$
$$- \tilde{t}_1^2 \tilde{t}_2^2 \tilde{t}_3^2 \tilde{t}_4^2 - f_2 \tilde{t}_1^2 \tilde{t}_2^4 \tilde{t}_3 \tilde{t}_4 - \frac{1}{f_1} \tilde{t}_1 \tilde{t}_2^3 \tilde{t}_3^3 \tilde{t}_4^2 + \dots \ .$$
(3.7.87)

The above plethystic logarithm exhibits the moduli space generators with their mesonic charges.

The generators can be presented as points on a $\mathbb{Z}^2$ with the $U(1)_{f_1} \times U(1)_{f_2}$ charges giving the lattice coordinates. The convex polygon formed by the generators on the lattice in Table 3.20 is the dual reflexive polygon of the toric diagram of Model 5.

The Hilbert series and the plethystic logarithm can be re-expressed in terms of just

Generator	$U(1)_{f_1}$	$U(1)_{f_2}$
$p_1^2 p_4\ q\ s$	1	0
$p_1 p_2 p_3 p_4\ q\ r\ u\ s$	0	0
$p_1 p_2^3\ q^2\ r^2\ u\ s$	0	1
$p_3^3 p_4^2\ r\ u^2\ s$	-1	-1
$p_2^2 p_3^2 p_4\ q\ r^2\ u^2\ s$	-1	0
$p_2^4 p_3\ q^2\ r^3\ u^2\ s$	-1	1
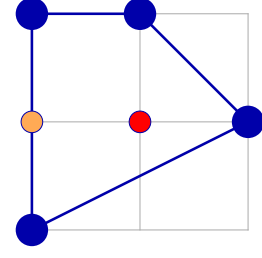
Table 3.20: The generators and lattice of generators of the mesonic moduli space of Model 5 in terms of GLSM fields with the corresponding flavor charges.

Generator	$U(1)_{f_1}$	$U(1)_{f_2}$
$X_{34}X_{45}X_{53} = X_{17}X_{71} = X_{26}X_{62}$	1	0
$X_{13}X_{34}X_{45}X_{51} = X_{25}X_{53}X_{34}X_{42} = X_{13}X_{37}X_{71} = X_{16}X_{62}X_{21} = X_{16}X_{67}X_{71} = X_{17}X_{72}X_{21}$ $= X_{17}X_{75}X_{51} = X_{25}X_{56}X_{62} = X_{26}X_{64}X_{42} = X_{26}X_{67}X_{72} = X_{37}X_{75}X_{53} = X_{45}X_{56}X_{64}$	0	0
$X_{16}X_{62}X_{25}X_{51} = X_{16}X_{64}X_{45}X_{51} = X_{17}X_{72}X_{25}X_{51} = X_{25}X_{53}X_{37}X_{72}$	0	1
$X_{56}X_{67}X_{75} = X_{13}X_{34}X_{42}X_{21}$	-1	-1
$X_{13}X_{34}X_{42}X_{25}X_{51} = X_{13}X_{37}X_{72}X_{21} = X_{13}X_{37}X_{75}X_{51} = X_{16}X_{64}X_{42}X_{21}$ $= X_{16}X_{67}X_{72}X_{21} = X_{16}X_{67}X_{75}X_{51} = X_{25}X_{56}X_{64}X_{42} = X_{25}X_{56}X_{67}X_{72}$	-1	0
$X_{13}X_{37}X_{72}X_{25}X_{51} = X_{16}X_{64}X_{42}X_{25}X_{51} = X_{16}X_{67}X_{72}X_{25}X_{51}$	-1	1

Table 3.21: The generators in terms of bifundamental fields (Model 5).

3 fugacities

$$
\begin{aligned}
T_1 &= \frac{\tilde{t}_3}{f_1 f_2\ \tilde{t}_1^2 \tilde{t}_2^2} = \frac{t_3}{y_q^2 y_r y_s\ t_1^2 t_2^2}\ , \\
T_2 &= f_2\ \tilde{t}_1 \tilde{t}_2^3 = y_q^2 y_r^2 y_u y_s\ t_1 t_2^3\ , \\
T_3 &= f_1\ \tilde{t}_1^2 \tilde{t}_4 = y_q y_s\ t_1^2 t_4\ ,
\end{aligned}
\tag{3.7.88}
$$

such that

$$
g_1(T_1, T_2, T_3; \mathcal{M}_5^{mes}) = \frac{1 + T_1 T_2 T_3 + T_1^2 T_2^2 T_3 - T_1 T_2^2 T_3 - T_1^2 T_2^3 T_3 - T_1^3 T_2^4 T_3^2}{(1 - T_2)(1 - T_1 T_2^2)(1 - T_3)(1 - T_1^3 T_2^2 T_3^2)}
\tag{3.7.89}
$$

and

$$
\begin{aligned}
PL[g_1(T_1, T_2, T_3; \mathcal{M}_5^{mes})] &= T_1 T_2 T_3 + T_3 + T_2 + T_1^3 T_2^2 T_3^2 + T_1 T_2^2 + T_1^2 T_2^2 T_3 \\
&\quad - T_1 T_2^2 T_3 - T_1^2 T_2^2 T_3^2 - T_1^2 T_2^3 T_3 - T_1^3 T_2^3 T_3^2 - T_1^4 T_2^4 T_3^2 + T_1^2 T_2^3 T_3^2 + T_1^3 T_2^4 T_3^2 \\
&\quad + T_1^4 T_2^4 T_3^3 + T_1^4 T_2^5 T_3^2 + T_1^5 T_2^5 T_3^3 - T_1^3 T_2^4 T_3^3 \dots\ .
\end{aligned}
\tag{3.7.90}
$$

The above mesonic Hilbert series and plethystic logarithm illustrates the conical structure of the toric Calalbi-Yau 3-fold.
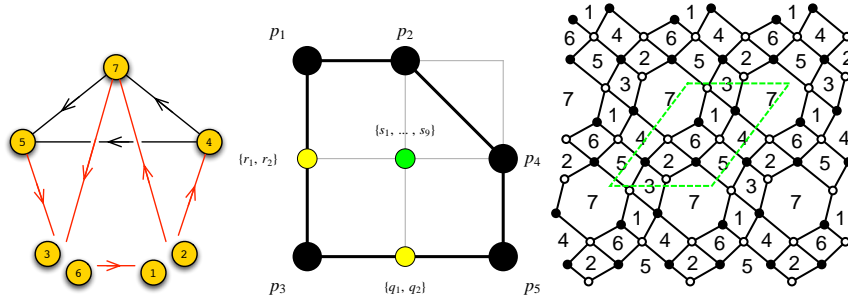
Figure 3.12: The quiver, toric diagram and brane tiling of Model 6a. The red arrows in the quiver indicate all possible connections between blocks of nodes.

3.8 Model 6: PdP$_{4a}$

3.8.1 Model 6 Phase a

The superpotential is

$$
\begin{aligned}
W \;=\; & +X_{32}X_{27}X_{73} + X_{14}X_{45}X_{56}X_{61} + X_{31}X_{17}X_{75}X_{53} + X_{62}X_{24}X_{47}X_{76} \\
& -X_{76}X_{61}X_{17} - X_{31}X_{14}X_{47}X_{73} - X_{32}X_{24}X_{45}X_{53} - X_{62}X_{27}X_{75}X_{56}
\end{aligned}
$$

(3.8.91)

The perfect matching matrix is

$$
P = \left(
\begin{array}{c|ccccc|cc|cc|ccccccccc}
 & p_1 & p_2 & p_3 & p_4 & p_5 & q_1 & q_2 & r_1 & r_2 & s_1 & s_2 & s_3 & s_4 & s_5 & s_6 & s_7 & s_8 & s_9 \\
\hline
X_{17} & 1 & 1 & 0 & 0 & 0 & 0 & 0 & 1 & 0 & 1 & 0 & 1 & 0 & 1 & 0 & 0 & 0 & 0 \\
X_{73} & 1 & 1 & 0 & 0 & 0 & 0 & 0 & 0 & 1 & 0 & 1 & 0 & 1 & 0 & 1 & 0 & 0 & 0 \\
X_{56} & 1 & 0 & 0 & 0 & 0 & 0 & 0 & 1 & 0 & 0 & 1 & 0 & 0 & 0 & 0 & 1 & 0 & 0 \\
X_{24} & 1 & 0 & 0 & 0 & 0 & 0 & 0 & 0 & 1 & 1 & 0 & 0 & 0 & 0 & 0 & 0 & 1 & 0 \\
X_{45} & 0 & 1 & 0 & 1 & 0 & 0 & 0 & 0 & 0 & 0 & 0 & 1 & 0 & 0 & 1 & 0 & 0 & 0 \\
X_{62} & 0 & 1 & 0 & 0 & 0 & 0 & 0 & 0 & 0 & 0 & 0 & 0 & 1 & 1 & 0 & 0 & 0 & 1 \\
X_{32} & 0 & 0 & 1 & 0 & 0 & 1 & 0 & 1 & 0 & 0 & 0 & 0 & 0 & 1 & 0 & 1 & 0 & 1 \\
X_{75} & 0 & 0 & 1 & 0 & 0 & 1 & 0 & 0 & 1 & 0 & 0 & 0 & 0 & 0 & 1 & 0 & 0 & 0 \\
X_{47} & 0 & 0 & 1 & 0 & 0 & 0 & 1 & 1 & 0 & 0 & 0 & 1 & 0 & 0 & 0 & 0 & 0 & 0 \\
X_{61} & 0 & 0 & 1 & 0 & 0 & 0 & 1 & 0 & 1 & 0 & 0 & 0 & 1 & 0 & 0 & 0 & 1 & 1 \\
X_{76} & 0 & 0 & 0 & 1 & 1 & 1 & 0 & 0 & 0 & 0 & 1 & 0 & 0 & 0 & 1 & 1 & 0 & 0 \\
X_{27} & 0 & 0 & 0 & 1 & 1 & 0 & 1 & 0 & 0 & 1 & 0 & 1 & 0 & 0 & 0 & 0 & 1 & 0 \\
X_{31} & 0 & 0 & 0 & 1 & 0 & 0 & 0 & 0 & 0 & 0 & 0 & 0 & 0 & 0 & 0 & 1 & 1 & 1 \\
X_{14} & 0 & 0 & 0 & 0 & 1 & 1 & 0 & 0 & 0 & 1 & 0 & 0 & 0 & 1 & 0 & 0 & 0 & 0 \\
X_{53} & 0 & 0 & 0 & 0 & 1 & 0 & 1 & 0 & 0 & 0 & 1 & 0 & 1 & 0 & 0 & 0 & 0 & 0 \\
\end{array}
\right).
$$

(3.8.92)

	$U(1)_{f_1}$	$U(1)_{f_2}$	$U(1)_R$	fugacity
p_1	-1	0	$R_1 \simeq 0.427$	t_1
p_2	1	0	$R_2 \simeq 0.298$	t_2
p_3	0	0	$R_3 \simeq 0.550$	t_3
p_4	0	1	$R_2 \simeq 0.298$	t_4
p_5	0	-1	$R_1 \simeq 0.427$	t_5

Table 3.22: The GLSM fields corresponding to extremal points of the toric diagram with their mesonic charges (Model 6a).

The F-term charge matrix $Q_F = \ker(P)$ is

$$
Q_F = \left(
\begin{array}{ccccc|cc|cc|ccccccccc}
p_1 & p_2 & p_3 & p_4 & p_5 & q_1 & q_2 & r_1 & r_2 & s_1 & s_2 & s_3 & s_4 & s_5 & s_6 & s_7 & s_8 & s_9 \\
\hline
0 & 0 & 1 & 0 & 1 & -1 & -1 & 0 & 0 & 0 & 0 & 0 & 0 & 0 & 0 & 0 & 0 & 0 \\
1 & 0 & 1 & 0 & 0 & 0 & 0 & -1 & -1 & 0 & 0 & 0 & 0 & 0 & 0 & 0 & 0 & 0 \\
1 & 0 & 0 & 0 & 1 & 0 & 0 & 0 & 0 & -1 & -1 & 0 & 0 & 0 & 0 & 0 & 0 & 0 \\
0 & 1 & 0 & 0 & 0 & 0 & 1 & 0 & 0 & 0 & 0 & -1 & -1 & 0 & 0 & 0 & 0 & 0 \\
0 & 1 & 0 & 0 & 0 & 1 & 0 & 0 & 0 & 0 & 0 & 0 & 0 & -1 & -1 & 0 & 0 & 0 \\
0 & 0 & 0 & 1 & 0 & 0 & 0 & 1 & 0 & 0 & 0 & -1 & 0 & 0 & 0 & -1 & 0 & 0 \\
0 & 0 & 0 & 1 & 0 & 0 & 0 & 0 & 1 & 0 & 0 & 0 & 0 & 0 & -1 & 0 & -1 & 0 \\
0 & 0 & 0 & 0 & 1 & 0 & -1 & 1 & 0 & -1 & 0 & 0 & 0 & 0 & 0 & -1 & 1 & 0 \\
0 & 0 & 0 & 0 & 0 & 0 & 0 & 0 & 0 & 1 & 0 & 0 & 0 & -1 & 0 & 0 & -1 & 1
\end{array}
\right) .
\tag{3.8.93}
$$

The D-term charge matrix is

$$
Q_D = \left(
\begin{array}{ccccc|cc|cc|ccccccccc}
p_1 & p_2 & p_3 & p_4 & p_5 & q_1 & q_2 & r_1 & r_2 & s_1 & s_2 & s_3 & s_4 & s_5 & s_6 & s_7 & s_8 & s_9 \\
\hline
0 & 0 & 0 & 0 & 0 & 0 & 0 & 0 & 0 & 0 & 0 & 1 & -1 & 0 & 0 & 0 & 0 & 0 \\
0 & 0 & 0 & 0 & 0 & 0 & 0 & 0 & 0 & 0 & 0 & 0 & 1 & -1 & 0 & 0 & 0 & 0 \\
0 & 0 & 0 & 0 & 0 & 0 & 0 & 0 & 0 & 0 & 0 & 0 & 0 & 1 & -1 & 0 & 0 & 0 \\
0 & 0 & 0 & 0 & 0 & 0 & 0 & 0 & 0 & 0 & 0 & 0 & 0 & 0 & 1 & -1 & 0 & 0 \\
0 & 0 & 0 & 0 & 0 & 0 & 0 & 0 & 0 & 0 & 0 & 0 & 0 & 0 & 0 & 1 & -1 & 0 \\
0 & 0 & 0 & 0 & 0 & 0 & 0 & 0 & 0 & 0 & 0 & 0 & 0 & 0 & 0 & 0 & 1 & -1
\end{array}
\right) .
\tag{3.8.94}
$$

The total charge matrix Q_t does not exhibit repeated columns. Accordingly, the global symmetry is $U(1)_{f_1} \times U(1)_{f_2} \times U(1)_R$. The mesonic charges on the GLSM fields corresponding to extremal points in the toric diagram in Figure 3.12 are found following the discussion in §3.2.3. They are presented in Table 3.22.

Fine-tuning R-charges. The exact R-charges on extremal perfect matchings can be expressed in terms of a root x_0 of the following polynomial

$$
0 = 289 - 695x + 331x^2 + 3x^3 ,
\tag{3.8.95}
$$

where the root of interest lies in the range $0 \leq 1 - x_0 \leq \frac{2}{3}$. The exact R-charges are

$$R_1 = R_5 = x_0 \ ,$$

$$
\begin{aligned}
R_2 = R_4 = &\frac{1}{2497416307960655824746468547906174933430973669888}(1791039188638478428147683691212722044339352504896 \\
&- 14898979385812450997203995618175138834683612621776 x_0 + 9465606277116561007612744735839203666371878276840 x_0^2 \\
&+ 8171632306068776293575876125737079492808889002 3074 x_0^3 - 10662275916980187263135080855654891328467257996 4562 x_0^4 \\
&- 22312936155603381509800509872608673629726066365173 x_0^5 + 4762528868015187354760510267495372040181430194 3043 x_0^6 \\
&+ 17436573584263377204018474073188553946245197817747 x_0^7 - 10640233660391309102082256624734477840137858566189 x_0^8 \\
&- 5762098668974680244859599181817775913551620378815 x_0^9 + 42017893035471743309404992594592751017973 8217313 x_0^{10} \\
&+ 7212825052981360329273982686349741119531180244 91 x_0^{11} + 846916317102495296446954749046668918672055 65263 x_0^{12} \\
&- 28845127177680312829862811387042101533046922792 x_0^{13} - 5936715130045788144646704656470430250253226360 x_0^{14} \\
&- 98568203174737761263257326460337456059549812 x_0^{15} - 4278361125883159493660637122162650710849 00 x_0^{16})
\end{aligned}
$$

$$
\begin{aligned}
R_3 = &\frac{1}{162164293596963665649085313948683843212137836604660555443821244188609125275748366817763000746246144} \times \\
&(11692294617320807663196027080653718484358393208189527262867661744855787547208697913805484870299 93472 \\
&+ 211180778264971290234686689177114661495550847435083609777692608446996489161070763569563200559556608 x_0 \\
&- 80459112603546548938444825974208855190483057568577580925249244974281309459738076069606442366472 2176 x_0^2 \\
&+ 7868186882915851426335876977581680670251639520854407669554513212398555158000171156489937456815968256 x_0^3 \\
&+ 1061412415136716326837022119308869488382612389978875078709377550354824411184572440342496757041597952 x_0^4 \\
&- 1653502269547432808110213130155065398558657253926330204747817424734038646912023554904414840355605600 x_0^5 \\
&- 1803409805355686010966266040602399537481777012614017830538582946961232414356541894961178034998651796 x_0^6 \\
&- 549776367467559089730992163878433891954155708840766662975198907329834783154666201068238731372409 68 x_0^7 \\
&+ 15672058008122196253179486809850384291434387064888629503746417904547452584660052893046108951981657 28 x_0^8 \\
&+ 143372141123223427893722579570981599815299873016608292988946609826131841127293292913140425912965 3584 x_0^9 \\
&- 6136882330931619036640793227475316505163955291657344172904274083192180668079316628784041862317038 21 x_0^{10} \\
&- 111329359093379310642227053776163913335738086439537494201648209333162655868499870321712814024965 074 x_0^{11} \\
&- 10204191865252901868459492073510337651746233315941831589294920411409019664759595680785042841245 7223 x_0^{12} \\
&+ 423971220164725630883036801237262772103566877143219787938265323979123862245114383980033760835726 68 x_0^{13} \\
&+ 180759001526368976093293859900166369755100685781123847882792925416526429014249267867672715988158 11 x_0^{14} \\
&- 640764096127088788849150828315571184154634070722519763037036773102752130682680966574160797466136 30 x_0^{15} \\
&- 6551504819136579714820873890716651117283500144325459851304645267888406140527648899700282075382087 9 x_0^{16} \\
&- 6673543248212741805371881957906917086875901203329952658459597394917113521671659599449171717221560 x_0^{17}
\end{aligned}
$$

162

$$+9783618126417420629286524671582244856923708960297834037315293570385351437452828996816592454899857 x_0^{18}$$

$$+37435969981897046762180969239164515423873511202458999481670983223762520764404776489976816429325578 x_0^{19}$$

$$-275998133977857656048993198548594390031696954517741623737712596072996328801012600935299966017093 x_0^{20}$$

$$-476041152324864443368732013757192469363702044100009981148537231549870724895965447800279556079204 x_0^{21}$$

$$-856092768411646596113754207670971923135383442150512155012876797645663813283235144075041426504194 x_0^{22}$$

$$+1736756218281380840704019663440980233984061044275370082133820797625435430996110590672837549597 4 x_0^{23}$$

$$+881543794927554297285227144050115836057253481762294476766080205104483905989081785303812093547 5 x_0^{24}$$

$$+81085911723111772038103560964401442242693898780482881797653680703957865774365148440284178808 0 x_0^{25}$$

$$-19205307290965232821054500357008003762177313861097915381237493680723848108366363053533396450 40 x_0^{26}$$

$$-536547465916963306855684181739332349934774148635831117395010981027151389082337797671568704 80 x_0^{27}$$

$$-4633797214013132583423895629091032185087243889634863057878937498434947801893349846356567080 x_0^{28}$$

$$-1252888490757713861363139507690945073375815948541871969696840844835338178928215289399961 60 x_0^{29}$$

$$-1502297452596476410349719722105724798487349802028494174267727244065661237915976256430480 x_0^{30}$$

$$-841889100321404520539211676832304188428177227649543520598402143968437354127971229200 0 x_0^{31}$$

$$-180798415114252405052986121862480887985654540988732106456532930478692381618004500000 00 x_0^{32}) \ . \qquad (3.8.96)$$

Products of non-extremal perfect matchings are expressed in terms of single variables as follows

$$q = q_1 q_2 \ , \ \ r = r_1 r_2 \ , \ \ s = \prod_{m=1}^{9} s_m \ . \qquad (3.8.97)$$

Extremal perfect matchings are counted by the fugacity t_α. The fugacity y_q is assigned to the product of non-extremal perfect matchings q above.

The refined mesonic Hilbert series of Model 6a is

$$g_1(t_\alpha, y_q, y_r, y_s; \mathcal{M}_{6a}^{mes}) = (1 + y_q y_r y_s \ t_1 t_2 t_3 t_4 t_5 - y_q^2 y_r^3 y_s^2 \ t_1^3 t_2^2 t_3^3 t_4 t_5 - y_q^3 y_r^3 y_s^2 \ t_1^2 t_2 t_3^4 t_4 t_5^2$$
$$- y_q^2 y_r^2 y_s^2 \ t_1^2 t_2^2 t_3^2 t_4^2 t_5^2 - y_q^3 y_r^2 y_s^2 \ t_1 t_2 t_3^3 t_4^2 t_5^3 + y_q^4 y_r^4 y_s^3 \ t_1^3 t_2^2 t_3^5 t_4^2 t_5^3 + y_q^5 y_r^5 y_s^4 \ t_1^4 t_2^3 t_3^6 t_4^3 t_5^4)$$
$$\times \frac{1}{(1 - y_q y_r^2 y_s \ t_1^2 t_2 t_3^2)(1 - y_r y_s \ t_1^2 t_2^2 t_4)(1 - y_q^2 y_r^2 y_s \ t_1 t_3^3 t_5)}$$
$$\times \frac{1}{(1 - y_q^2 y_r y_s \ t_3^2 t_4 t_5^2)(1 - y_q y_s \ t_2 t_4^2 t_5^2)} \ .$$

$$(3.8.98)$$

Generator	$U(1)_{f_1}$	$U(1)_{f_2}$
$p_2 p_4^2 p_5^2 \; q \; s$	1	0
$p_1^2 p_2^2 p_4 \; r \; s$	0	1
$p_1 p_2 p_3 p_4 p_5 \; q \; r \; s$	0	0
$p_3^2 p_4 p_5^2 \; q^2 \; r \; s$	0	-1
$p_1^2 p_2 p_3^2 \; q \; r^2 \; s$	-1	0
$p_1 p_3^3 p_5 \; q^2 \; r^2 \; s$	-1	-1
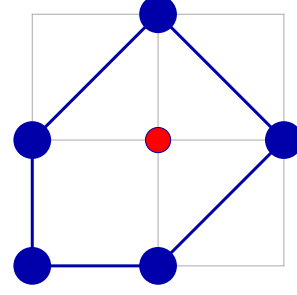
Table 3.23: The generators and lattice of generators of the mesonic moduli space of Model 6a in terms of GLSM fields with the corresponding flavor charges.

The plethystic logarithm of the mesonic Hilbert series is

$$
\begin{aligned}
PL[g_1(t_\alpha, y_q, y_r, y_s; \mathcal{M}_{6a}^{mes})] ={}& y_q y_s \; t_2 t_4^2 t_5^2 + y_r y_s \; t_1^2 t_2^2 t_4 + y_q y_r y_s \; t_1 t_2 t_3 t_4 t_5 \\
& + y_q y_r^2 y_s \; t_1^2 t_2 t_3^2 + y_q^2 y_r y_s \; t_3^2 t_4 t_5^2 + y_q^2 y_r^2 y_s \; t_1 t_3^3 t_5 - 2 \; y_q^2 y_r^2 y_s^2 \; t_1^2 t_2^2 t_3^2 t_4^2 t_5^2 \\
& - y_q^3 y_r^3 y_s^2 \; t_1^2 t_2 t_3^4 t_4 t_5^2 + \dots \; .
\end{aligned}
\tag{3.8.99}
$$

Consider the following fugacity map

$$
f_1 = \frac{1}{y_r \; t_1^2 t_2^2 t_4} \;,\quad f_2 = \frac{1}{y_q \; t_2 t_4^2 t_5^2} \;,\quad \tilde{t}_1 = y_q^{1/2} y_r^{1/2} y_s^{1/2} \; t_1 t_5 \;,\quad \tilde{t}_2 = t_2 t_4 \;,\quad \tilde{t}_3 = \frac{t_3}{t_1 t_2 t_4 t_5} \;,
\tag{3.8.100}
$$

where f_1 and f_2 are the flavour charge fugacities, and $\tilde{t}_i$ is the fugacity for the R-charge R_i in Table 3.22.

In terms of the fugacity map above, the plethystic logarithm becomes

$$
\begin{aligned}
PL[g_1(\tilde{t}_\alpha, f_1, f_2; \mathcal{M}_{6a}^{mes})] ={}& (f_1 + f_2) \, \tilde{t}_1^2 \tilde{t}_2^3 + \tilde{t}_1^2 \tilde{t}_2^2 \tilde{t}_3 + \left(\frac{1}{f_1} + \frac{1}{f_2} \right) \tilde{t}_1^2 \tilde{t}_2 \tilde{t}_3^2 + \frac{1}{f_1 f_2} \tilde{t}_1^2 \tilde{t}_3^3 \\
& - 2 \tilde{t}_1^4 \tilde{t}_2^4 \tilde{t}_3^2 - \frac{1}{f_1 f_2} \tilde{t}_1^4 \tilde{t}_2^2 \tilde{t}_3^4 + \dots \; .
\end{aligned}
\tag{3.8.101}
$$

The above plethystic logarithm exhibits the moduli space generators with the corresponding mesonic charges. They are summarized in Table 3.23. The generators can be presented on a charge lattice. The convex polygon formed by the generators in Table 3.23 is the dual reflexive polygon of the toric diagram of Model 6a.

The mesonic Hilbert series and plethystic logarithm can be re-expressed in terms of just 3 fugacities

$$
T_1 = \frac{f_1}{f_2 \; \tilde{t}_1^2 \tilde{t}_2^2 \tilde{t}_3} = \frac{t_5}{y_r^2 y_s \; t_1^3 t_2^2 t_3} \;,\quad T_2 = \frac{\tilde{t}_1^2 \tilde{t}_2 \tilde{t}_3^2}{f_1} = y_q y_r^2 y_s \; t_1^2 t_2 t_3^2 \;,
$$
$$
T_3 = f_2 \; \tilde{t}_1^2 \tilde{t}_2^3 = y_r y_s \; t_1^2 t_2^2 t_4 \;,
\tag{3.8.102}
$$

164

Generator	$U(1)_{f_1}$	$U(1)_{f_2}$
$X_{27}X_{76}X_{62} = X_{14}X_{45}X_{53}X_{31}$	1	0
$X_{17}X_{73}X_{31} = X_{24}X_{45}X_{56}X_{62}$	0	1
$X_{17}X_{76}X_{61} = X_{27}X_{73}X_{32} = X_{14}X_{47}X_{73}X_{31} = X_{14}X_{45}X_{56}X_{61}$	0	0
$= X_{17}X_{75}X_{53}X_{31} = X_{24}X_{45}X_{53}X_{32} = X_{24}X_{47}X_{76}X_{62} = X_{27}X_{75}X_{56}X_{62}$		
$X_{14}X_{47}X_{75}X_{53}X_{31} = X_{14}X_{47}X_{76}X_{61} = X_{27}X_{75}X_{53}X_{32}$	0	-1
$X_{24}X_{47}X_{75}X_{56}X_{62} = X_{17}X_{75}X_{56}X_{61} = X_{24}X_{47}X_{73}X_{32}$	-1	0
$X_{14}X_{47}X_{75}X_{56}X_{61} = X_{24}X_{47}X_{75}X_{53}X_{32}$	-1	-1

Table 3.24: The generators in terms of bifundamental fields (Model 6a).
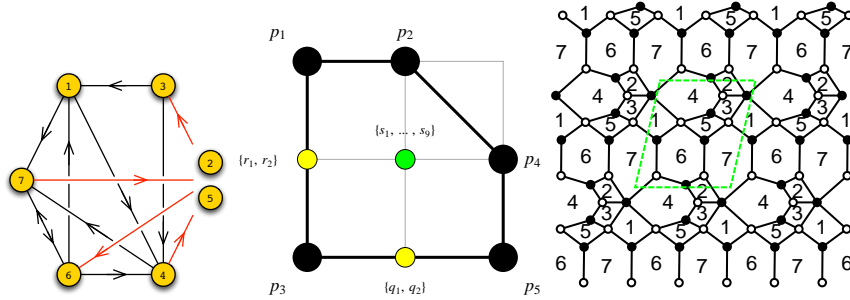
Figure 3.13: The quiver, toric diagram, and brane tiling of Model 6b. The red arrows in the quiver indicate all possible connections between blocks of nodes.

such that

$$g_1(T_1, T_2, T_3; \mathcal{M}_{6a}^{mes}) =$$
$$\frac{1 + T_1T_2T_3 - T_1T_2^2T_3 - T_1^2T_3^3T_3 - T_1^2T_2^2T_3^2 - T_1^3T_2^3T_3^2 + T_1^3T_2^4T_3^2 + T_1^4T_2^5T_3^3}{(1 - T_2)(1 - T_3)(1 - T_1T_2^2)(1 - T_1^2T_2^2T_3)(1 - T_1^2T_2T_3^2)}$$

(3.8.103)

and

$$PL[g_1(T_1, T_2, T_3; \mathcal{M}_{6a}^{mes})] = T_1^2T_2T_3^2 + T_3 + T_1T_2T_3 + T_2 + T_1^2T_2^2T_3 + T_1T_2^2$$
$$- 2T_1^2T_2^2T_3^2 - T_1^2T_2^3T_3 + \dots .$$

(3.8.104)

The Hilbert series and plethystic logarithm above illustrate the conical structure of the toric Calabi-Yau 3-fold.

3.8.2 Model 6 Phase b

The superpotential is

$$
\begin{aligned}
W \;=\; &+X_{42}X_{23}X_{34} + X_{67}X_{72}X_{26} + X_{76}X_{64}X_{47} + X_{14}X_{45}X_{56}X_{61} + X_{31}X_{17}X_{75}X_{53} \\
&-X_{67}X_{75}X_{56} - X_{76}X_{61}X_{17} - X_{42}X_{26}X_{64} - X_{53}X_{34}X_{45} - X_{14}X_{47}X_{72}X_{23}X_{31}
\end{aligned}
\tag{3.8.105}
$$

The perfect matching matrix is

$$
P =
\left(
\begin{array}{c|ccccc|cc|cc|ccccccccc}
 & p_1 & p_2 & p_3 & p_4 & p_5 & q_1 & q_2 & r_1 & r_2 & s_1 & s_2 & s_3 & s_4 & s_5 & s_6 & s_7 & s_8 & s_9 \\
\hline
X_{67} & 1 & 1 & 0 & 1 & 0 & 0 & 0 & 1 & 0 & 1 & 0 & 0 & 0 & 1 & 1 & 1 & 0 & 0 \\
X_{76} & 1 & 1 & 0 & 0 & 0 & 0 & 0 & 0 & 1 & 0 & 1 & 1 & 1 & 0 & 0 & 0 & 1 & 1 \\
X_{42} & 1 & 1 & 0 & 0 & 0 & 0 & 0 & 1 & 0 & 1 & 1 & 0 & 1 & 0 & 0 & 0 & 0 & 0 \\
X_{14} & 1 & 0 & 0 & 0 & 0 & 0 & 0 & 0 & 1 & 0 & 0 & 0 & 0 & 1 & 0 & 0 & 0 & 0 \\
X_{53} & 1 & 0 & 0 & 0 & 0 & 0 & 0 & 1 & 0 & 0 & 1 & 0 & 0 & 0 & 1 & 0 & 1 & 0 \\
X_{31} & 0 & 1 & 0 & 0 & 0 & 0 & 0 & 0 & 0 & 0 & 0 & 0 & 0 & 0 & 0 & 1 & 0 & 1 \\
X_{45} & 0 & 1 & 0 & 1 & 0 & 0 & 0 & 0 & 0 & 1 & 0 & 1 & 1 & 0 & 0 & 0 & 0 & 0 \\
X_{34} & 0 & 0 & 1 & 0 & 1 & 1 & 1 & 0 & 1 & 0 & 0 & 0 & 0 & 1 & 0 & 1 & 0 & 1 \\
X_{17} & 0 & 0 & 0 & 1 & 1 & 1 & 0 & 0 & 0 & 1 & 0 & 0 & 0 & 1 & 0 & 0 & 0 & 0 \\
X_{64} & 0 & 0 & 0 & 1 & 1 & 0 & 1 & 0 & 0 & 0 & 0 & 0 & 0 & 1 & 1 & 1 & 0 & 0 \\
X_{72} & 0 & 0 & 0 & 0 & 1 & 0 & 1 & 0 & 0 & 0 & 1 & 0 & 1 & 0 & 0 & 0 & 0 & 0 \\
X_{23} & 0 & 0 & 0 & 1 & 0 & 0 & 0 & 0 & 0 & 0 & 0 & 1 & 0 & 0 & 1 & 0 & 1 & 0 \\
X_{56} & 0 & 0 & 0 & 0 & 1 & 1 & 0 & 0 & 0 & 0 & 1 & 0 & 0 & 0 & 0 & 0 & 1 & 1 \\
X_{26} & 0 & 0 & 1 & 0 & 0 & 1 & 0 & 0 & 1 & 0 & 0 & 1 & 0 & 0 & 0 & 0 & 1 & 1 \\
X_{47} & 0 & 0 & 1 & 0 & 0 & 1 & 0 & 1 & 0 & 1 & 0 & 0 & 0 & 0 & 0 & 0 & 0 & 0 \\
X_{75} & 0 & 0 & 1 & 0 & 0 & 0 & 1 & 0 & 1 & 0 & 0 & 1 & 1 & 0 & 0 & 0 & 0 & 0 \\
X_{61} & 0 & 0 & 1 & 0 & 0 & 0 & 1 & 1 & 0 & 0 & 0 & 0 & 0 & 0 & 1 & 1 & 0 & 0 \\
\end{array}
\right).
\tag{3.8.106}
$$

The F-term charge matrix $Q_F = \ker(P)$ is

$$
Q_F =
\left(
\begin{array}{ccccc|cc|cc|ccccccccc}
p_1 & p_2 & p_3 & p_4 & p_5 & q_1 & q_2 & r_1 & r_2 & s_1 & s_2 & s_3 & s_4 & s_5 & s_6 & s_7 & s_8 & s_9 \\
\hline
1 & 0 & 1 & 0 & 0 & 0 & 0 & -1 & -1 & 0 & 0 & 0 & 0 & 0 & 0 & 0 & 0 & 0 \\
1 & 0 & 0 & 0 & 1 & 0 & 0 & 0 & 0 & 0 & -1 & 0 & 0 & -1 & 0 & 0 & 0 & 0 \\
0 & 1 & 0 & 0 & 0 & 1 & 0 & 0 & 0 & -1 & 0 & 0 & 0 & 0 & 0 & 0 & 0 & -1 \\
0 & 1 & 0 & 0 & 0 & 0 & 1 & 0 & 0 & 0 & 0 & 0 & -1 & 0 & 0 & -1 & 0 & 0 \\
0 & 0 & 1 & 1 & 0 & -1 & 0 & 0 & 0 & 0 & 1 & 0 & -1 & 0 & -1 & 0 & 0 & 0 \\
0 & 0 & 1 & 0 & 1 & -1 & -1 & 0 & 0 & 0 & 0 & 0 & 0 & 0 & 0 & 0 & 0 & 0 \\
0 & 0 & 0 & 1 & 0 & 0 & 0 & 1 & 0 & -1 & 0 & 0 & 0 & 0 & -1 & 0 & 0 & 0 \\
0 & 0 & 0 & 1 & -1 & 1 & 0 & 0 & 0 & -1 & 1 & 0 & 0 & 0 & 0 & 0 & -1 & 0 \\
0 & 0 & 0 & 0 & 0 & 0 & 0 & 0 & 0 & 0 & 1 & 1 & -1 & 0 & 0 & 0 & -1 & 0 \\
\end{array}
\right).
\tag{3.8.107}
$$

The D-term charge matrix is

$$
Q_D =
\left(
\begin{array}{ccccc|cc|cc|ccccccccc}
p_1 & p_2 & p_3 & p_4 & p_5 & q_1 & q_2 & r_1 & r_2 & s_1 & s_2 & s_3 & s_4 & s_5 & s_6 & s_7 & s_8 & s_9 \\
\hline
0 & 0 & 0 & 0 & 0 & 0 & 0 & 0 & 0 & 1 & -1 & 0 & 0 & 0 & 0 & 0 & 0 & 0 \\
0 & 0 & 0 & 0 & 0 & 0 & 0 & 0 & 0 & 0 & 1 & -1 & 0 & 0 & 0 & 0 & 0 & 0 \\
0 & 0 & 0 & 0 & 0 & 0 & 0 & 0 & 0 & 0 & 0 & 1 & -1 & 0 & 0 & 0 & 0 & 0 \\
0 & 0 & 0 & 0 & 0 & 0 & 0 & 0 & 0 & 0 & 0 & 0 & 1 & -1 & 0 & 0 & 0 & 0 \\
0 & 0 & 0 & 0 & 0 & 0 & 0 & 0 & 0 & 0 & 0 & 0 & 0 & 1 & -1 & 0 & 0 & 0 \\
0 & 0 & 0 & 0 & 0 & 0 & 0 & 0 & 0 & 0 & 0 & 0 & 0 & 0 & 1 & -1 & 0 & 0 \\
\end{array}
\right).
\tag{3.8.108}
$$

The global symmetry of Model 6b has the form $U(1)_{f_1} \times U(1)_{f_2} \times U(1)_R$. The charges under the global symmetry on the extremal perfect matchings p_α are the same as for

Generator	$U(1)_{f_1}$	$U(1)_{f_2}$
$X_{45}X_{56}X_{64} = X_{17}X_{72}X_{23}X_{31}$	0	1
$X_{67}X_{76} = X_{14}X_{42}X_{23}X_{31} = X_{14}X_{45}X_{53}X_{31}$	1	0
$X_{14}X_{47}X_{72}X_{23}X_{31} = X_{14}X_{45}X_{56}X_{61} = X_{17}X_{75}X_{53}X_{31} = X_{17}X_{76}X_{61} = X_{23}X_{34}X_{42}$ $= X_{26}X_{64}X_{42} = X_{26}X_{67}X_{72} = X_{34}X_{45}X_{53} = X_{47}X_{76}X_{64} = X_{56}X_{67}X_{75}$	0	0
$X_{17}X_{72}X_{26}X_{61} = X_{17}X_{75}X_{56}X_{61} = X_{23}X_{34}X_{47}X_{72} = X_{26}X_{64}X_{47}X_{72} = X_{47}X_{75}X_{56}X_{64}$	-1	0
$X_{14}X_{47}X_{75}X_{53}X_{31} = X_{14}X_{42}X_{26}X_{61} = X_{14}X_{47}X_{76}X_{61}$	0	-1
$X_{34}X_{47}X_{75}X_{53} = X_{14}X_{47}X_{72}X_{26}X_{61} = X_{14}X_{47}X_{75}X_{56}X_{61}$	-1	-1

Table 3.25: The generators in terms of bifundamental fields (Model 6b).
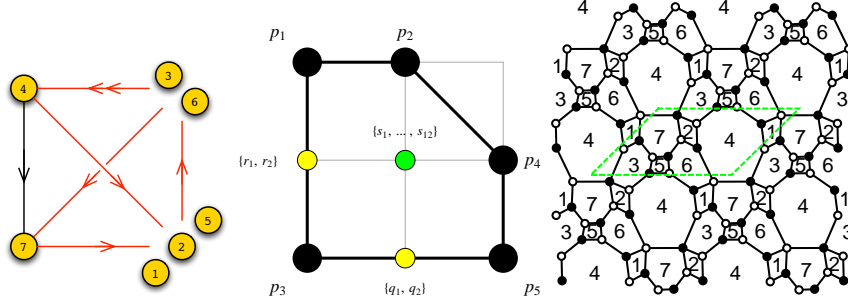
Figure 3.14: The quiver, toric diagram, and brane tiling of Model 6c. The red arrows in the quiver indicate all possible connections between blocks of nodes.

Model 6a. They are shown in Table 3.22.

Product of non-extremal perfect matchings are expressed in terms of single variables as follows

$$q = q_1 q_2 \ , \ \ r = r_1 r_2 \ , \ \ s = \prod_{m=1}^{9} s_m \ . \tag{3.8.109}$$

The fugacity counting extremal perfect matchings p_α is t_α. The fugacity y_q counts the product of non-extremal perfect matchings q.

The refined mesonic Hilbert series of Model 6b is identical to the mesonic Hilbert series for Model 6a. The mesonic Hilbert series and the corresponding plethystic logarithm is shown in (3.8.98) and (3.8.99) respectively. The mesonic Hilbert series for Model 6a and 6b are identical and are not complete intersections.

The generators in terms of perfect matchings of Model 6b are shown in Table 3.23. The charge lattice of generators forms a reflexive polygon which is the dual of the toric diagram. The generators in terms of quiver fields of Model 6b are shown in Table 3.25.

3.8.3 Model 6 Phase c

The superpotential is

$$
\begin{aligned}
W \quad = \quad & +X_{41}X_{13}X_{34}^2 + X_{42}X_{23}X_{34}^1 + X_{45}X_{56}X_{64}^2 + X_{67}X_{72}X_{26} + X_{75}X_{53}X_{37} \\
& +X_{47}X_{71}X_{16}X_{64}^1 - X_{41}X_{16}X_{64}^2 - X_{42}X_{26}X_{64}^1 - X_{45}X_{53}X_{34}^1 \\
& -X_{67}X_{75}X_{56} - X_{71}X_{13}X_{37} - X_{47}X_{72}X_{23}X_{34}^2
\end{aligned}
\tag{3.8.110}
$$

The perfect matching matrix is

$$
P =
\left(
\begin{array}{c|ccccc|cc|cc|cccccccccccc}
 & p_1 & p_2 & p_3 & p_4 & p_5 & q_1 & q_2 & r_1 & r_2 & s_1 & s_2 & s_3 & s_4 & s_5 & s_6 & s_7 & s_8 & s_9 & s_{10} & s_{11} & s_{12} \\
\hline
X_{37} & 1 & 1 & 0 & 1 & 0 & 0 & 0 & 0 & 1 & 1 & 1 & 0 & 1 & 0 & 0 & 0 & 0 & 0 & 0 & 0 & 0 \\
X_{64}^1 & 1 & 1 & 0 & 0 & 0 & 0 & 0 & 1 & 0 & 1 & 0 & 1 & 0 & 0 & 0 & 0 & 0 & 0 & 0 & 0 & 0 \\
X_{41} & 1 & 1 & 0 & 0 & 0 & 0 & 0 & 0 & 1 & 0 & 1 & 0 & 0 & 1 & 0 & 1 & 0 & 1 & 0 & 1 & 0 \\
X_{34}^1 & 1 & 0 & 1 & 0 & 0 & 1 & 0 & 1 & 1 & 1 & 0 & 0 & 1 & 0 & 0 & 0 & 0 & 0 & 0 & 0 & 0 \\
X_{72} & 1 & 0 & 0 & 0 & 0 & 0 & 0 & 1 & 0 & 0 & 0 & 0 & 0 & 1 & 1 & 0 & 0 & 1 & 1 & 0 & 0 \\
X_{56} & 1 & 0 & 0 & 0 & 0 & 0 & 0 & 0 & 1 & 0 & 0 & 0 & 1 & 0 & 0 & 0 & 0 & 1 & 1 & 1 & 1 \\
X_{67} & 0 & 1 & 0 & 1 & 1 & 0 & 1 & 0 & 0 & 1 & 1 & 1 & 0 & 0 & 0 & 0 & 0 & 0 & 0 & 0 & 0 \\
X_{45} & 0 & 1 & 0 & 1 & 0 & 0 & 0 & 0 & 0 & 0 & 1 & 0 & 0 & 1 & 1 & 1 & 1 & 0 & 0 & 0 & 0 \\
X_{23} & 0 & 1 & 0 & 0 & 0 & 0 & 0 & 0 & 0 & 0 & 0 & 1 & 0 & 0 & 1 & 1 & 0 & 0 & 1 & 1 \\
X_{64}^2 & 0 & 0 & 1 & 0 & 1 & 1 & 1 & 1 & 0 & 1 & 0 & 1 & 0 & 0 & 0 & 0 & 0 & 0 & 0 & 0 & 0 \\
X_{75} & 0 & 0 & 1 & 0 & 0 & 1 & 0 & 1 & 0 & 0 & 0 & 0 & 0 & 1 & 1 & 1 & 1 & 0 & 0 & 0 & 0 \\
X_{26} & 0 & 0 & 1 & 0 & 0 & 1 & 0 & 0 & 1 & 0 & 0 & 0 & 1 & 0 & 0 & 1 & 1 & 0 & 0 & 1 & 1 \\
X_{13} & 0 & 0 & 1 & 0 & 0 & 0 & 1 & 1 & 0 & 0 & 0 & 1 & 0 & 0 & 1 & 0 & 1 & 0 & 1 & 0 & 1 \\
X_{47} & 0 & 0 & 1 & 0 & 0 & 0 & 1 & 0 & 1 & 0 & 1 & 0 & 0 & 0 & 0 & 0 & 0 & 0 & 0 & 0 & 0 \\
X_{34}^2 & 0 & 0 & 0 & 1 & 1 & 1 & 0 & 0 & 0 & 1 & 0 & 0 & 1 & 0 & 0 & 0 & 0 & 0 & 0 & 0 & 0 \\
X_{42} & 0 & 0 & 0 & 1 & 1 & 0 & 1 & 0 & 0 & 0 & 1 & 0 & 0 & 1 & 1 & 0 & 0 & 1 & 1 & 0 & 0 \\
X_{16} & 0 & 0 & 0 & 1 & 0 & 0 & 0 & 0 & 0 & 0 & 0 & 0 & 1 & 0 & 1 & 0 & 1 & 0 & 1 & 0 & 1 \\
X_{71} & 0 & 0 & 0 & 0 & 1 & 1 & 0 & 0 & 0 & 0 & 0 & 0 & 0 & 1 & 0 & 1 & 0 & 1 & 0 & 1 & 0 \\
X_{53} & 0 & 0 & 0 & 0 & 1 & 0 & 1 & 0 & 0 & 0 & 0 & 1 & 0 & 0 & 0 & 0 & 0 & 1 & 1 & 1 & 1 \\
\end{array}
\right).
\tag{3.8.111}
$$

The F-term charge matrix $Q_F = \ker(P)$ is

$$
Q_F =
\left(
\begin{array}{ccccc|cc|cc|cccccccccccc}
p_1 & p_2 & p_3 & p_4 & p_5 & q_1 & q_2 & r_1 & r_2 & s_1 & s_2 & s_3 & s_4 & s_5 & s_6 & s_7 & s_8 & s_9 & s_{10} & s_{11} & s_{12} \\
\hline
1 & 0 & 0 & 1 & 0 & 0 & 1 & 0 & 0 & -1 & -1 & 0 & 0 & 0 & 0 & 0 & 0 & 0 & -1 & 0 & 0 \\
1 & 0 & 0 & 0 & 1 & 0 & 0 & 0 & 0 & -1 & 0 & 0 & 0 & 0 & 0 & 0 & 0 & -1 & 0 & 0 & 0 \\
0 & 1 & 0 & 0 & 0 & 1 & 0 & 0 & 0 & -1 & 0 & 0 & 0 & 0 & 0 & -1 & 0 & 0 & 0 & 0 & 0 \\
0 & 1 & 0 & 0 & 0 & 0 & 1 & 0 & 0 & 0 & -1 & -1 & 0 & 0 & 0 & 0 & 0 & 0 & 0 & 0 & 0 \\
0 & 0 & 1 & 0 & 0 & -1 & 0 & -1 & 0 & 1 & -1 & 0 & 0 & 1 & 0 & 0 & 0 & 0 & 0 & 0 & 0 \\
0 & 0 & 0 & 1 & 0 & 0 & 0 & 1 & 0 & -1 & 0 & 0 & 0 & 0 & 0 & 0 & -1 & 0 & -1 & 0 & 1 \\
0 & 0 & 0 & 1 & 0 & 0 & 0 & 1 & 0 & -1 & 0 & 0 & 0 & 0 & 0 & -1 & 0 & 0 & -1 & 1 & 0 \\
0 & 0 & 0 & 1 & 0 & 0 & 0 & 0 & 1 & 0 & -1 & 0 & -1 & 0 & 0 & 0 & 0 & 0 & 0 & 0 & 0 \\
0 & 0 & 0 & 1 & 0 & -1 & 0 & 0 & 1 & 0 & -1 & 0 & 0 & 1 & 0 & 0 & 0 & -1 & 0 & 0 & 0 \\
0 & 0 & 0 & 0 & 1 & 0 & -1 & 1 & 0 & -1 & 1 & 0 & 0 & -1 & 0 & 0 & 0 & 0 & 0 & 0 & 0 \\
0 & 0 & 0 & 0 & 0 & 0 & 0 & 1 & -1 & -1 & 1 & 0 & 1 & 0 & -1 & 0 & 0 & 0 & 0 & 0 & 0 \\
0 & 0 & 0 & 0 & 0 & 0 & 0 & 0 & 0 & 0 & 0 & 0 & 0 & -1 & 0 & 1 & 0 & 0 & 1 & 0 & -1 \\
\end{array}
\right).
\tag{3.8.112}
$$

The D-term charge matrix is

$$
Q_D =
\left(
\begin{array}{ccccc|cc|cc|cccccccccccc}
p_1 & p_2 & p_3 & p_4 & p_5 & q_1 & q_2 & r_1 & r_2 & s_1 & s_2 & s_3 & s_4 & s_5 & s_6 & s_7 & s_8 & s_9 & s_{10} & s_{11} & s_{12} \\
\hline
0 & 0 & 0 & 0 & 0 & 0 & 0 & 0 & 0 & 1 & -1 & 0 & 0 & 0 & 0 & 0 & 0 & 0 & 0 & 0 & 0 \\
0 & 0 & 0 & 0 & 0 & 0 & 0 & 0 & 0 & 0 & 1 & -1 & 0 & 0 & 0 & 0 & 0 & 0 & 0 & 0 & 0 \\
0 & 0 & 0 & 0 & 0 & 0 & 0 & 0 & 0 & 0 & 0 & 1 & -1 & 0 & 0 & 0 & 0 & 0 & 0 & 0 & 0 \\
0 & 0 & 0 & 0 & 0 & 0 & 0 & 0 & 0 & 0 & 0 & 0 & 1 & -1 & 0 & 0 & 0 & 0 & 0 & 0 & 0 \\
0 & 0 & 0 & 0 & 0 & 0 & 0 & 0 & 0 & 0 & 0 & 0 & 0 & 1 & -1 & 0 & 0 & 0 & 0 & 0 & 0 \\
0 & 0 & 0 & 0 & 0 & 0 & 0 & 0 & 0 & 0 & 0 & 0 & 0 & 0 & 1 & -1 & 0 & 0 & 0 & 0 & 0 \\
\end{array}
\right).
\tag{3.8.113}
$$

The global symmetry of Model 6c is $U(1)_{f_1} \times U(1)_{f_2} \times U(1)_R$. The global symmetry

Generator	$U(1)_{f_1}$	$U(1)_{f_2}$
$X_{16}X_{67}X_{71} = X_{23}X_{34}^2 X_{42} = X_{34}^2 X_{45} X_{53}$	1	0
$X_{41}X_{16}X_{64}^1 = X_{23}X_{37}X_{72} = X_{45}X_{56}X_{64}^1$	0	1
$X_{47}X_{71}X_{16}X_{64}^1 = X_{23}X_{34}^2 X_{47}X_{72} = X_{13}X_{34}^2 X_{41} = X_{13}X_{37}X_{71} = X_{41}X_{16}X_{64}^2 = X_{23}X_{34}^1 X_{42}$ $= X_{42}X_{26}X_{64}^1 = X_{26}X_{67}X_{72} = X_{34}^1 X_{45}X_{53} = X_{53}X_{37}X_{75} = X_{45}X_{56}X_{64}^2 = X_{56}X_{67}X_{75}$	0	0
$X_{42}X_{26}X_{64}^2 = X_{13}X_{34}^2 X_{47}X_{71} = X_{47}X_{71}X_{16}X_{64}^2 = X_{34}^2 X_{47}X_{75}X_{53}$	0	-1
$X_{13}X_{34}^1 X_{41} = X_{23}X_{34}^1 X_{47}X_{72} = X_{47}X_{72}X_{26}X_{64}^1 = X_{56}X_{47}X_{75}X_{64}^1$	-1	0
$X_{13}X_{34}^1 X_{47}X_{71} = X_{47}X_{72}X_{26}X_{64}^2 = X_{34}^1 X_{47}X_{75}X_{53} = X_{56}X_{47}X_{75}X_{64}^2$	-1	-1

Table 3.26: The generators in terms of bifundamental fields (Model 6c).
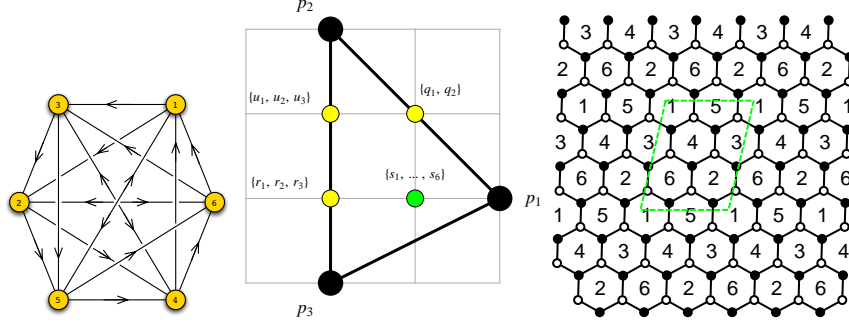
Figure 3.15: The quiver, toric diagram, and brane tiling of Model 7.

is the same as for Model 6a and 6b. The charges on the extremal perfect matchings are shown in Table 3.22.

Products of non-extremal perfect matchings are chosen to be associated to a single variable as shown below

$$q = q_1 q_2 \ , \ r = r_1 r_2 \ , \ s = \prod_{m=1}^{12} s_m \ . \tag{3.8.114}$$

Extremal perfect matchings are counted by the fugacity t_α. Products of non-extremal perfect matchings such as q are counted by fugacities of the form y_q.

The refined mesonic Hilbert series of Model 6c computed using the Molien integral formula is identical to the mesonic Hilbert series of Model 6a and 6b in (3.8.98). Accordingly, the plethystic logarithm are identical as well and hence the mesonic moduli space is a non-complete intersection.

The moduli space generators in terms of perfect matchings of Model 6c are shown in Table 3.23. The lattice of generators is a reflexive polygon and is the dual of the toric diagram. The generators in terms of quiver fields of Model 6c are shown in Table 3.26.

3.9 Model 7: $\mathbb{C}^3/\mathbb{Z}_6\ (1,2,3)$, $\mathbf{PdP}_{3a}$

The superpotential is

$$
\begin{aligned}
W \;=\; & +X_{12}X_{26}X_{61} + X_{63}X_{34}X_{46} + X_{24}X_{43}X_{32} + X_{35}X_{51}X_{13} + X_{41}X_{15}X_{54} \\
& +X_{56}X_{62}X_{25} - X_{12}X_{25}X_{51} - X_{63}X_{32}X_{26} - X_{24}X_{46}X_{62} - X_{35}X_{54}X_{43} \\
& -X_{41}X_{13}X_{34} - X_{56}X_{61}X_{15}
\end{aligned}
\tag{3.9.115}
$$

The perfect matching matrix is

$$
P =
\begin{pmatrix}
& p_1 & p_2 & p_3 & q_1 & q_2 & r_1 & r_2 & r_3 & u_1 & u_2 & u_3 & s_1 & s_2 & s_3 & s_4 & s_5 & s_6 \\
X_{26} & 1 & 0 & 0 & 1 & 0 & 0 & 0 & 0 & 0 & 0 & 0 & 1 & 0 & 0 & 1 & 1 & 0 \\
X_{62} & 1 & 0 & 0 & 0 & 1 & 0 & 0 & 0 & 0 & 0 & 0 & 0 & 1 & 1 & 0 & 0 & 1 \\
X_{15} & 1 & 0 & 0 & 1 & 0 & 0 & 0 & 0 & 0 & 0 & 0 & 0 & 1 & 1 & 0 & 1 & 0 \\
X_{51} & 1 & 0 & 0 & 0 & 1 & 0 & 0 & 0 & 0 & 0 & 0 & 1 & 0 & 0 & 1 & 0 & 1 \\
X_{43} & 1 & 0 & 0 & 1 & 0 & 0 & 0 & 0 & 0 & 0 & 0 & 1 & 0 & 1 & 0 & 0 & 1 \\
X_{34} & 1 & 0 & 0 & 0 & 1 & 0 & 0 & 0 & 0 & 0 & 0 & 0 & 1 & 0 & 1 & 1 & 0 \\
X_{46} & 0 & 1 & 0 & 1 & 0 & 1 & 0 & 0 & 1 & 1 & 0 & 1 & 0 & 0 & 0 & 0 & 0 \\
X_{32} & 0 & 1 & 0 & 0 & 1 & 1 & 0 & 0 & 1 & 1 & 0 & 0 & 1 & 0 & 0 & 0 & 0 \\
X_{13} & 0 & 1 & 0 & 1 & 0 & 0 & 1 & 0 & 1 & 0 & 1 & 0 & 0 & 1 & 0 & 0 & 0 \\
X_{54} & 0 & 1 & 0 & 0 & 1 & 0 & 1 & 0 & 1 & 0 & 1 & 0 & 0 & 0 & 1 & 0 & 0 \\
X_{25} & 0 & 1 & 0 & 1 & 0 & 0 & 0 & 1 & 0 & 1 & 1 & 0 & 0 & 0 & 0 & 1 & 0 \\
X_{61} & 0 & 1 & 0 & 0 & 1 & 0 & 0 & 1 & 0 & 1 & 1 & 0 & 0 & 0 & 0 & 0 & 1 \\
X_{56} & 0 & 0 & 1 & 0 & 0 & 1 & 1 & 0 & 1 & 0 & 0 & 1 & 0 & 0 & 1 & 0 & 0 \\
X_{12} & 0 & 0 & 1 & 0 & 0 & 1 & 1 & 0 & 1 & 0 & 0 & 0 & 1 & 1 & 0 & 0 & 0 \\
X_{41} & 0 & 0 & 1 & 0 & 0 & 1 & 0 & 1 & 0 & 1 & 0 & 1 & 0 & 0 & 0 & 0 & 1 \\
X_{35} & 0 & 0 & 1 & 0 & 0 & 1 & 0 & 1 & 0 & 1 & 0 & 0 & 1 & 0 & 0 & 1 & 0 \\
X_{24} & 0 & 0 & 1 & 0 & 0 & 0 & 1 & 1 & 0 & 0 & 1 & 0 & 0 & 0 & 1 & 1 & 0 \\
X_{63} & 0 & 0 & 1 & 0 & 0 & 0 & 1 & 1 & 0 & 0 & 1 & 0 & 0 & 1 & 0 & 0 & 1 \\
\end{pmatrix}.
\tag{3.9.116}
$$

The F-term charge matrix $Q_F = \ker{(P)}$ is

$$
Q_F =
\begin{pmatrix}
p_1 & p_2 & p_3 & q_1 & q_2 & r_1 & r_2 & r_3 & u_1 & u_2 & u_3 & s_1 & s_2 & s_3 & s_4 & s_5 & s_6 \\
1 & 1 & 0 & -1 & -1 & 0 & 0 & 0 & 0 & 0 & 0 & 0 & 0 & 0 & 0 & 0 & 0 \\
1 & 0 & 0 & 0 & 0 & 1 & 0 & 0 & 0 & 0 & 0 & -1 & -1 & 0 & 0 & 0 & 0 \\
1 & 0 & 0 & 0 & 0 & 0 & 1 & 0 & 0 & 0 & 0 & 0 & 0 & -1 & -1 & 0 & 0 \\
1 & 0 & 0 & 0 & 0 & 0 & 0 & 1 & 0 & 0 & 0 & 0 & 0 & 0 & 0 & -1 & -1 \\
1 & 0 & 0 & 0 & -1 & 0 & 0 & 0 & 1 & 0 & 0 & -1 & 0 & -1 & 0 & 0 & 1 \\
0 & 1 & 1 & 0 & 0 & -1 & 0 & 0 & 0 & 0 & -1 & 0 & 0 & 0 & 0 & 0 & 0 \\
0 & 1 & 1 & 0 & 0 & 0 & -1 & 0 & 0 & -1 & 0 & 0 & 0 & 0 & 0 & 0 & 0 \\
0 & 1 & 1 & 0 & 0 & 0 & 0 & -1 & -1 & 0 & 0 & 0 & 0 & 0 & 0 & 0 & 0 \\
0 & 0 & 1 & 0 & 0 & -1 & -1 & 0 & 1 & 0 & 0 & 0 & 0 & 0 & 0 & 0 & 0 \\
\end{pmatrix}.
\tag{3.9.117}
$$

The D-term charge matrix is

$$
Q_D =
\begin{pmatrix}
p_1 & p_2 & p_3 & q_1 & q_2 & r_1 & r_2 & r_3 & u_1 & u_2 & u_3 & s_1 & s_2 & s_3 & s_4 & s_5 & s_6 \\
0 & 0 & 0 & 0 & 0 & 0 & 0 & 0 & 0 & 0 & 0 & 1 & -1 & 0 & 0 & 0 & 0 \\
0 & 0 & 0 & 0 & 0 & 0 & 0 & 0 & 0 & 0 & 0 & 0 & 1 & -1 & 0 & 0 & 0 \\
0 & 0 & 0 & 0 & 0 & 0 & 0 & 0 & 0 & 0 & 0 & 0 & 0 & 1 & -1 & 0 & 0 \\
0 & 0 & 0 & 0 & 0 & 0 & 0 & 0 & 0 & 0 & 0 & 0 & 0 & 0 & 1 & -1 & 0 \\
0 & 0 & 0 & 0 & 0 & 0 & 0 & 0 & 0 & 0 & 0 & 0 & 0 & 0 & 0 & 1 & -1 \\
\end{pmatrix}.
\tag{3.9.118}
$$

The total charge matrix Q_t does not exhibit repeated columns. Accordingly, the global symmetry is $U(1)_{f_1} \times U(1)_{f_2} \times U(1)_R$. The flavour and R-charges on the GLSM fields corresponding to extremal points in the toric diagram in Figure 3.15 are found as

	$U(1)_{f_1}$	$U(1)_{f_2}$	$U(1)_R$	fugacity
p_1	1/2	0	2/3	t_1
p_2	-1/6	1/3	2/3	t_2
p_3	-1/3	-1/3	2/3	t_3

Table 3.27: The GLSM fields corresponding to extremal points of the toric diagram with their mesonic charges (Model 7).

shown in Table 3.27 following the discussion in §3.2.3.

Products of non-extremal perfect matchings are expressed in terms of single variables as follows

$$q = q_1 q_2 \ , \ r = r_1 r_2 r_3 \ , \ u = u_1 u_2 u_3 \ , \ s = \prod_{m=1}^{6} s_m \ . \tag{3.9.119}$$

Extremal perfect matchings are counted by the fugacity t_α. Products of non-extremal perfect matchings such as q are counted by fugacities of the form y_q.

The mesonic Hilbert series of Model 7 is

$$g_1(t_\alpha, y_q, y_r, y_u, y_s; \mathcal{M}_7^{mes}) =$$
$$\frac{1 + y_q^2 y_r y_u^2 y_s \ t_1 t_2^3 + y_q y_r y_u y_s \ t_1 t_2 t_3 + y_q^2 y_r^2 y_u^3 y_s \ t_2^4 t_3 + y_q y_r^2 y_u^2 y_s \ t_2^2 t_3^2 + y_q^3 y_r^3 y_u^4 y_s^2 \ t_1 t_2^5 t_3^2}{(1 - y_q y_s \ t_1^2)(1 - y_q^3 y_r^2 y_u^4 y_s \ t_2^6)(1 - y_r^2 y_u y_s \ t_3^3)} \ . \tag{3.9.120}$$

The plethystic logarithm of the mesonic Hilbert series is

$$PL[g_1(t_\alpha, y_q, y_r, y_u, y_s; \mathcal{M}_7^{mes})] = y_q y_s \ t_1^2 + y_q y_r y_u y_s \ t_1 t_2 t_3 + y_r^2 y_u y_s \ t_3^3$$
$$+ y_q y_r^2 y_u^2 y_s \ t_2^2 t_3^2 + y_q^2 y_r y_u^2 y_s \ t_1 t_2^3 + y_q^2 y_r^2 y_u^3 y_s \ t_2^4 t_3 - y_q^2 y_r^2 y_u^2 y_s^2 \ t_1^2 t_2^2 t_3^2$$
$$+ y_q^3 y_r^2 y_u^4 y_s \ t_2^6 - y_q^2 y_r^3 y_u^3 y_s^2 \ t_1 t_2^3 t_3^3 - y_q^3 y_r^2 y_u^3 y_s^2 \ t_1^2 t_2^4 t_3 + \dots \ . \tag{3.9.121}$$

With the following fugacity map

$$\begin{aligned}
f_1 &= y_q^{1/3} y_r^{-2/3} y_u^{-2/3} y s^{1/3} \ t_1^{4/3} t_2^{-2/3} t_3^{-2/3} \ , \\
f_2 &= y_q^{2/3} y_r^{-1/3} y_u^{2/3} y_s^{-1/3} \ t_1^{-1/3} t_2^{5/3} t_3^{-4/3} \ , \\
t &= y_q^{1/3} y_r^{1/3} y_u^{1/3} y_s^{1/3} t_1^{1/3} t_2^{1/3} t_3^{1/3} \ , \tag{3.9.122}
\end{aligned}$$

where the fugacities f_1, f_2 and t count the mesonic symmetry charges. Under the

171

| Generator	$U(1)_{f_1}$	$U(1)_{f_2}$
$p_1^2\, q\, s$	1	0
$p_1 p_2 p_3\, q\, r\, u\, s$	0	0
$p_1 p_2^3\, q^2\, r\, u^2\, s$	0	1
$p_3^3\, r^2\, u\, s$	-1	-1
$p_2^2 p_3^2\, q\, r^2\, u^2\, s$	-1	0
$p_2^4 p_3\, q^2\, r^2\, u^3\, s$	-1	1
$p_2^6\, q^3\, r^2\, u^4\, s$	-1	2
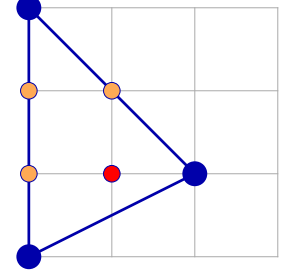
Table 3.28: The generators and lattice of generators of the mesonic moduli space of Model 7 in terms of GLSM fields with the corresponding flavor charges.

Generator	$U(1)_{f_1}$	$U(1)_{f_2}$
$X_{15}X_{51} = X_{26}X_{62} = X_{34}X_{43}$	1	0
$X_{12}X_{25}X_{51} = X_{12}X_{26}X_{61} = X_{13}X_{34}X_{41} = X_{13}X_{35}X_{51} = X_{15}X_{54}X_{41} = X_{15}X_{56}X_{61}$ $= X_{24}X_{43}X_{32} = X_{24}X_{46}X_{62} = X_{25}X_{56}X_{62} = X_{26}X_{63}X_{32} = X_{34}X_{46}X_{63} = X_{35}X_{54}X_{43}$	0	0
$X_{13}X_{32}X_{25}X_{51} = X_{13}X_{32}X_{26}X_{61} = X_{13}X_{34}X_{46}X_{61} = X_{15}X_{54}X_{46}X_{61} = X_{25}X_{54}X_{43}X_{32} = X_{25}X_{54}X_{46}X_{62}$	0	1
$X_{12}X_{24}X_{41} = X_{35}X_{56}X_{63}$	-1	-1
$X_{12}X_{24}X_{46}X_{61} = X_{12}X_{25}X_{54}X_{41} = X_{12}X_{25}X_{56}X_{61} = X_{13}X_{32}X_{24}X_{41} = X_{13}X_{35}X_{54}X_{41}$ $= X_{13}X_{35}X_{56}X_{61} = X_{24}X_{46}X_{63}X_{32} = X_{25}X_{56}X_{63}X_{32} = X_{35}X_{54}X_{46}X_{63}$	-1	0
$X_{12}X_{25}X_{54}X_{46}X_{61} = X_{13}X_{32}X_{24}X_{46}X_{61} = X_{13}X_{32}X_{25}X_{54}X_{41}$ $= X_{13}X_{32}X_{25}X_{56}X_{61} = X_{13}X_{35}X_{54}X_{46}X_{61} = X_{25}X_{54}X_{46}X_{63}X_{32}$	-1	1
$X_{13}X_{32}X_{25}X_{54}X_{46}X_{61}$	-1	2

Table 3.29: The generators in terms of bifundamental fields (Model 7).

fugacity map above, the above plethystic logarithm becomes

$$
PL[g_1(t, f_1, f_2; \mathcal{M}_7^{mes})] = f_1 t^2 + \left(1 + \frac{1}{f_1 f_2}\right) t^3 + \left(\frac{1}{f_1} + f_2\right) t^4 + \frac{f_2}{f_1} t^5 - t^6 + \frac{f_2^2}{f_1} t^6
$$
$$
- \left(\frac{1}{f_1} + f_2\right) t^7 + \dots .
$$

(3.9.123)

The plethystic logarithm above exhibits the moduli space generators with their mesonic charges. They are summarized in Table 3.28. The mesonic generators can be presented on a charge lattice. The convex polygon formed by the generators in Table 3.28 is the dual reflexive polygon of the toric diagram of Model 7. For the case of Model 7, the toric diagram is self-dual, and the charge lattice of the generators forms again the toric diagram of Model 7.
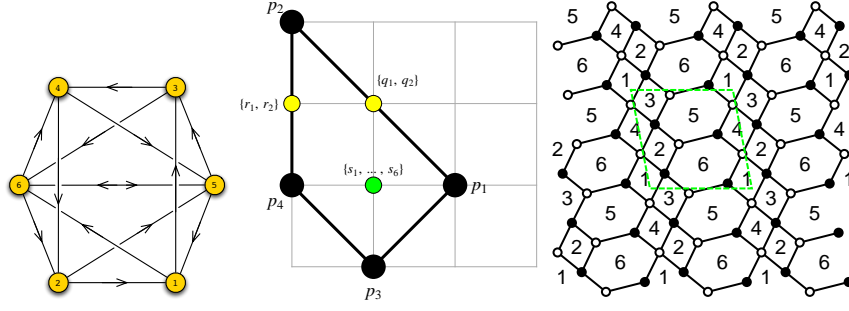
Figure 3.16: The quiver, toric diagram, and brane tiling of Model 8a.

With the fugacity map

$$
\begin{aligned}
T_1 &= f_1^{1/2}\, t = y_q^{1/2} y_s^{1/2}\, t_1\ , \\
T_2 &= \frac{f_2^{1/3}\, t}{f_1^{1/6}} = y_q^{1/2} y_r^{1/3} y_u^{2/3} y_s^{1/6}\, t_2\ , \\
T_3 &= \frac{t}{f_1^{1/3} f_2^{1/3}} = y_r^{2/3} y_u^{1/3} y_s^{1/3}\, t_3
\end{aligned}
\tag{3.9.124}
$$

the mesonic Hilbert series becomes

$$
g_1(T_1, T_2, T_3; \mathcal{M}_7^{mes}) = \frac{1 + T_1 T_2^3 + T_1 T_2 T_3 + T_2^4 T_3 + T_2^2 T_3^2 + T_1 T_2^5 T_3^2}{(1 - T_1^2)(1 - T_2^6)(1 - T_3^2)}
\tag{3.9.125}
$$

with the plethystic logarithm being

$$
\begin{aligned}
PL[g_1(T_1, T_2, T_3; \mathcal{M}_7^{mes})] = {}& T_1^2 + T_1 T_2 T_3 + T_3^3 + T_2 T_3 + T_1 T_2^3 \\
& + T_2^4 T_3 - T_1^2 T_2^2 T_3^2 + T_2^6 - T_1 T_2^3 T_3^3 - T_1^2 T_2^4 T_3 + \dots
\end{aligned}
\tag{3.9.126}
$$

The above Hilbert series and plethystic logarithm illustrate the conical structure of the toric Calabi-Yau 3-fold.

3.10 Model 8: $\mathbf{SPP}/\mathbb{Z}_2$ $(0, 1, 1, 1)$, $\mathbf{PdP}_{3c}$

3.10.1 Model 8 Phase a

The superpotential is

$$
\begin{aligned}
W = {}& + X_{56} X_{62} X_{25} + X_{65} X_{53} X_{36} + X_{13} X_{34} X_{45} X_{51} + X_{21} X_{16} X_{64} X_{42} \\
& - X_{56} X_{64} X_{45} - X_{65} X_{51} X_{16} - X_{13} X_{36} X_{62} X_{21} - X_{25} X_{53} X_{34} X_{42}\ .
\end{aligned}
\tag{3.10.127}
$$

173

	$U(1)_{f_1}$	$U(1)_{f_2}$	$U(1)_R$	fugacity
p_1	1	0	$R_1 = 1/\sqrt{3}$	t_1
p_2	-1/2	1/2	$R_1 = 1/\sqrt{3}$	t_2
p_3	-1	0	$R_2 = 1 - 1/\sqrt{3}$	t_3
p_4	1/2	-1/2	$R_2 = 1 - 1/\sqrt{3}$	t_4

Table 3.30: The GLSM fields corresponding to extremal points of the toric diagram with their mesonic charges (Model 8a). The R-charges are obtained using a-maximization.

The perfect matching matrix is

$$
P = \begin{pmatrix}
 & p_1 & p_2 & p_3 & p_4 & q_1 & q_2 & r_1 & r_2 & s_1 & s_2 & s_3 & s_4 & s_5 & s_6 \\
X_{16} & 1 & 0 & 0 & 0 & 1 & 0 & 0 & 0 & 0 & 1 & 1 & 0 & 0 & 0 \\
X_{45} & 1 & 0 & 0 & 0 & 1 & 0 & 0 & 0 & 0 & 0 & 0 & 0 & 1 & 1 \\
X_{62} & 1 & 0 & 0 & 0 & 0 & 1 & 0 & 0 & 1 & 0 & 0 & 0 & 0 & 1 \\
X_{53} & 1 & 0 & 0 & 0 & 0 & 1 & 0 & 0 & 0 & 0 & 1 & 1 & 0 & 0 \\
X_{36} & 0 & 1 & 0 & 0 & 1 & 0 & 1 & 0 & 0 & 1 & 0 & 0 & 0 & 0 \\
X_{25} & 0 & 1 & 0 & 0 & 1 & 0 & 0 & 1 & 0 & 0 & 0 & 0 & 1 & 0 \\
X_{51} & 0 & 1 & 0 & 0 & 0 & 1 & 1 & 0 & 0 & 0 & 0 & 1 & 0 & 0 \\
X_{64} & 0 & 1 & 0 & 0 & 0 & 1 & 0 & 1 & 1 & 0 & 0 & 0 & 0 & 0 \\
X_{56} & 0 & 0 & 1 & 1 & 0 & 0 & 1 & 0 & 0 & 1 & 1 & 1 & 0 & 0 \\
X_{65} & 0 & 0 & 1 & 1 & 0 & 0 & 0 & 1 & 1 & 0 & 0 & 0 & 1 & 1 \\
X_{34} & 0 & 0 & 1 & 0 & 0 & 0 & 0 & 0 & 1 & 1 & 0 & 0 & 0 & 0 \\
X_{21} & 0 & 0 & 1 & 0 & 0 & 0 & 0 & 0 & 0 & 0 & 0 & 1 & 1 & 0 \\
X_{42} & 0 & 0 & 0 & 1 & 0 & 0 & 1 & 0 & 0 & 0 & 0 & 0 & 0 & 1 \\
X_{13} & 0 & 0 & 0 & 1 & 0 & 0 & 0 & 1 & 0 & 0 & 1 & 0 & 0 & 0
\end{pmatrix}. \tag{3.10.128}
$$

The F-term charge matrix $Q_F = \ker(P)$ is

$$
Q_F = \begin{pmatrix}
p_1 & p_2 & p_3 & p_4 & q_1 & q_2 & r_1 & r_2 & s_1 & s_2 & s_3 & s_4 & s_5 & s_6 \\
1 & 1 & 0 & 0 & -1 & -1 & 0 & 0 & 0 & 0 & 0 & 0 & 0 & 0 \\
1 & 0 & 0 & 0 & -1 & 0 & 0 & 1 & -1 & 1 & -1 & 0 & 0 & 0 \\
0 & 1 & 0 & 0 & -1 & 0 & -1 & 0 & -1 & 1 & 0 & 0 & 0 & 1 \\
0 & 1 & 0 & 1 & 0 & 0 & -1 & -1 & 0 & 0 & 0 & 0 & 0 & 0 \\
0 & 0 & 1 & 0 & 1 & 0 & 0 & 0 & 0 & -1 & 0 & 0 & -1 & 0 \\
0 & 0 & 1 & 0 & 0 & 1 & 0 & 0 & -1 & 0 & 0 & -1 & 0 & 0
\end{pmatrix}. \tag{3.10.129}
$$

The D-term charge matrix is

$$
Q_D = \begin{pmatrix}
p_1 & p_2 & p_3 & p_4 & q_1 & q_2 & r_1 & r_2 & s_1 & s_2 & s_3 & s_4 & s_5 & s_6 \\
0 & 0 & 0 & 0 & 0 & 0 & 0 & 0 & 1 & -1 & 0 & 0 & 0 & 0 \\
0 & 0 & 0 & 0 & 0 & 0 & 0 & 0 & 0 & 1 & -1 & 0 & 0 & 0 \\
0 & 0 & 0 & 0 & 0 & 0 & 0 & 0 & 0 & 0 & 1 & -1 & 0 & 0 \\
0 & 0 & 0 & 0 & 0 & 0 & 0 & 0 & 0 & 0 & 0 & 1 & -1 & 0 \\
0 & 0 & 0 & 0 & 0 & 0 & 0 & 0 & 0 & 0 & 0 & 0 & 1 & -1
\end{pmatrix}. \tag{3.10.130}
$$

The total charge matrix Q_t does not have repeated columns. Accordingly, the global symmetry is $U(1)_{f_1} \times U(1)_{f_2} \times U(1)_R$. The mesonic charges on the GLSM fields corresponding to extremal points in the toric diagram in Figure 3.16 are presented in Table 3.30. The charges have been found using the constraints discussed in §3.2.3.

Products of non-extremal perfect matchings are labelled in terms of single variables as follows

$$q = q_1 q_2 \ , \ r = r_1 r_2 \ , \ s = \prod_{m=1}^{6} s_m \ . \tag{3.10.131}$$

The fugacity which counts extremal perfect matchings p_α is t_α. A product of non-extremal perfect matchings such as q above is associated to the fugacity of the form y_q.

The mesonic Hilbert series of Model 8a is calculated using the Molien integral formula in (1.4.67). It is

$$\begin{aligned}
g_1(t_\alpha, y_q, y_r, y_s; \mathcal{M}_{8a}^{mes}) = &(1 + y_q^2 y_r^2 y_s \ t_1 t_2^3 t_4 + y_q y_r y_s \ t_1 t_2 t_3 t_4 - y_q^3 y_r^2 y_s^2 \ t_1^3 t_2^3 t_3 t_4 \\
&+ y_q y_r^2 y_s \ t_2^2 t_3 t_4^2 - y_q^3 y_r^3 y_s^2 \ t_1^2 t_2^4 t_3 t_4^2 - y_q^2 y_r^2 y_s^2 \ t_1^2 t_2^2 t_3^2 t_4^2 - y_q^4 y_r^4 y_s^3 \ t_1^3 t_2^5 t_3^2 t_4^3) \\
&\times \frac{1}{(1 - y_q^2 y_r y_s \ t_1^2 t_2^2)(1 - y_q y_s \ t_1^2 t_3)(1 - y_q^2 y_r^3 y_s \ t_2^4 t_4^2)(1 - y_r y_s \ t_3^2 t_4^2)} \tag{3.10.132}
\end{aligned}$$

The plethystic logarithm of the mesonic Hilbert series is

$$\begin{aligned}
PL[g_1(t_\alpha, y_q, y_r, y_s; \mathcal{M}_{8a}^{mes})] = &y_q^2 y_r y_s \ t_1^2 t_2^2 + y_q y_s \ t_1^2 t_3 + y_q^2 y_r^2 y_s \ t_1 t_2^3 t_4 + y_q y_r y_s \ t_1 t_2 t_3 t_4 \\
&+ y_q^2 y_r^3 y_s \ t_2^4 t_4^2 - y_q^3 y_r^2 y_s^2 \ t_1^3 t_2^3 t_3 t_4 - y_q^4 y_r^4 y_s^2 \ t_1^2 t_2^6 t_4^2 + y_q y_r^2 y_s \ t_2^2 t_3 t_4^2 - 2 \ y_q^3 y_r^3 y_s^2 \ t_1^2 t_2^4 t_3 t_4^2 \\
&+ \dots \ . \tag{3.10.133}
\end{aligned}$$

Consider the following fugacity map

$$f_1 = \frac{t_1 t_3^{1/2}}{y_r \ t_2 t_4^{1/2}} \ , \ f_2 = \frac{t_2 t_4^{1/2}}{y_s \ t_1 t_3^{1/2}} \ , \ \tilde{t}_1 = y_q^{1/2} y_r^{1/2} y_s^{1/2} \ t_1^{1/2} t_2^{1/2} \ , \ \tilde{t}_2 = t_3^{1/2} t_4^{1/2} \tag{3.10.134}$$

where the fugacities f_1 and f_2 count flavour charges, and the fugacities $\tilde{t}_1$ and $\tilde{t}_2$ count R-charges R_1 and R_2 in Table 3.30 respectively. Under the fugacity map above, the plethystic logarithm becomes

$$\begin{aligned}
PL[g_1(\tilde{t}_\alpha, f_1, f_2; \mathcal{M}_{8a}^{mes})] = &f_1 f_2 \tilde{t}_1^4 + f_1 \tilde{t}_1^4 \tilde{t}_2 + f_2 \tilde{t}_1^4 \tilde{t}_2 + \tilde{t}_1^2 \tilde{t}_2^2 + \frac{f_2}{f_1} \tilde{t}_1^4 \tilde{t}_2^2 - f_1 f_2 \tilde{t}_1^6 \tilde{t}_2^2 \\
&- f_2^2 \tilde{t}_1^8 \tilde{t}_2^2 + \frac{1}{f_1} \tilde{t}_1^2 \tilde{t}_2^3 - 2 f_2 \tilde{t}_1^6 \tilde{t}_2^3 \dots \ . \tag{3.10.135}
\end{aligned}$$

The above plethystic logarithm exhibits the moduli space generators with their corresponding mesonic charges. They are summarized in Table 3.31. The generators can be presented on a charge lattice. The convex polygon formed by the generators in Table 3.31 is the dual reflexive polygon of the toric diagram of Model 8a. For the case of Model 8a, the toric diagram is self-dual, and the charge lattice of the generators forms again the toric diagram of Model 8a.

Generator	$U(1)_{f_1}$	$U(1)_{f_2}$
$p_1^2 p_3 \, q \, s$	1	0
$p_3^2 p_4^2 \, r \, s$	-1	-1
$p_1 p_2 p_3 p_4 \, q \, r \, s$	0	0
$p_1^2 p_2^2 \, q^2 \, r \, s$	1	1
$p_2^2 p_3 p_4^2 \, q \, r^2 \, s$	-1	0
$p_1 p_2^3 p_4 \, q^2 \, r^2 \, s$	0	1
$p_2^4 p_4^2 \, q^2 \, r^3 \, s$	-1	1

Table 3.31: The generators and lattice of generators of the mesonic moduli space of Model 8a in terms of GLSM fields with the corresponding flavor charges.

Generator	$U(1)_{f_1}$	$U(1)_{f_2}$
$X_{16}X_{62}X_{21} = X_{34}X_{45}X_{53}$	1	0
$X_{56}X_{65} = X_{13}X_{34}X_{42}X_{21}$	-1	-1
$X_{16}X_{65}X_{51} = X_{25}X_{56}X_{62} = X_{36}X_{65}X_{53} = X_{45}X_{56}X_{64}$	0	0
$= X_{13}X_{36}X_{62}X_{21} = X_{13}X_{34}X_{45}X_{51} = X_{16}X_{64}X_{42}X_{21} = X_{25}X_{53}X_{34}X_{42}$		
$X_{16}X_{62}X_{25}X_{51} = X_{16}X_{64}X_{45}X_{51} = X_{25}X_{53}X_{36}X_{62} = X_{36}X_{64}X_{45}X_{53}$	1	1
$X_{13}X_{36}X_{65}X_{51} = X_{25}X_{56}X_{64}X_{42} = X_{13}X_{36}X_{64}X_{42}X_{21} = X_{13}X_{34}X_{42}X_{25}X_{51}$	-1	0
$X_{13}X_{36}X_{62}X_{25}X_{51} = X_{13}X_{36}X_{64}X_{45}X_{51} = X_{16}X_{64}X_{42}X_{25}X_{51} = X_{25}X_{53}X_{36}X_{64}X_{42}$	0	1
$X_{13}X_{36}X_{64}X_{42}X_{25}X_{51}$	-1	1

Table 3.32: The generators in terms of bifundamental fields (Model 8a).

The mesonic Hilbert series and the plethystic logarithm can be re-expressed in terms of just 3 fugacities

$$T_1 = \frac{\tilde{t}_2}{f_1^2 f_2 \, \tilde{t}_1^4} = \frac{t_4}{y_q^2 y_s \, t_1^3 t_2} \;,\; T_2 = f_1 f_2 \, \tilde{t}_1^4 = y_q^2 y_r y_s \, t_1^2 t_2^2 \;,\; T_3 = f_1 \, \tilde{t}_1^2 \tilde{t}_2 = y_q y_s \, t_1^2 t_3 \;,$$

(3.10.136)

such that

$$g_1(T_1, T_2, T_3; \mathcal{M}_{8a}^{mes}) =$$
$$\frac{1 + T_1 T_2^2 + T_1 T_2 T_3 - T_1 T_2^2 T_3 + T_1^2 T_2^2 T_3 - T_1^2 T_2^3 T_3 - T_1^2 T_2^2 T_3^2 - T_1^3 T_2^4 T_3^2}{(1 - T_2)(1 - T_3)(1 - T_1^2 T_2^3)(1 - T_1^2 T_2 T_3^2)}$$

(3.10.137)

and

$$PL[g_1(T_1, T_2, T_3; \mathcal{M}_{8a}^{mes})] = T_2 + T_3 + T_1 T_2^2 + T_1 T_2 T_3 + T_1^2 T_2^3 - T_1 T_2^2 T_3 - T_1^2 T_2^4$$
$$+ T_1^2 T_2^2 T_3 - 2 T_1^2 T_2^3 T_3 + \dots \;.$$

(3.10.138)

The above Hilbert series and plethystic logarithm in terms of just three fugacities with positive powers illustrate the conical structure of the toric Calabi-Yau 3-fold.
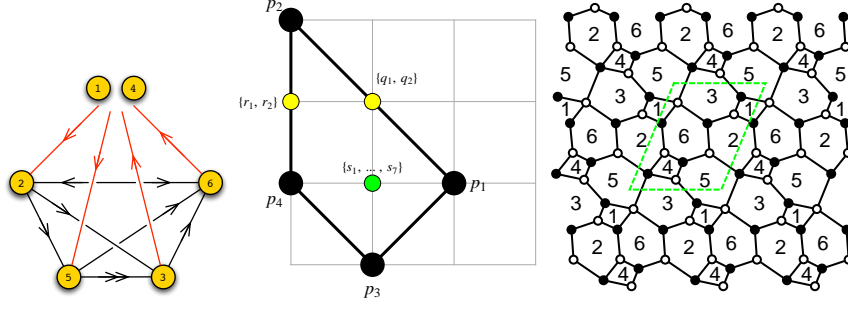
Figure 3.17: The quiver, toric diagram, and brane tiling of Model 8b. The red arrows in the quiver indicate all possible connections between blocks of nodes.

3.10.2 Model 8 Phase b

The superpotential is

$$
\begin{aligned}
W \;=\; & +X_{31}X_{12}X_{23} + X_{56}X_{62}X_{25} + X_{64}X_{42}X_{26} + X_{61}X_{15}X_{53}^{1}X_{36} + X_{34}X_{45}X_{53}^{2} \\
& -X_{31}X_{15}X_{53}^{2} - X_{36}X_{62}X_{23} - X_{56}X_{64}X_{45} - X_{61}X_{12}X_{26} - X_{25}X_{53}^{1}X_{34}X_{42} \;.
\end{aligned}
\tag{3.10.139}
$$

The perfect matching matrix is

$$
P = \left(
\begin{array}{c|cccc|cc|cc|ccccccc}
 & p_1 & p_2 & p_3 & p_4 & q_1 & q_2 & r_1 & r_2 & s_1 & s_2 & s_3 & s_4 & s_5 & s_6 & s_7 \\
\hline
X_{56} & 1 & 1 & 0 & 0 & 0 & 0 & 1 & 0 & 0 & 0 & 1 & 1 & 0 & 0 & 0 \\
X_{23} & 1 & 1 & 0 & 0 & 0 & 0 & 0 & 1 & 1 & 0 & 0 & 1 & 0 & 0 & 0 \\
X_{26} & 1 & 0 & 1 & 0 & 0 & 1 & 0 & 0 & 1 & 0 & 1 & 1 & 0 & 0 & 0 \\
X_{15} & 1 & 0 & 0 & 0 & 0 & 0 & 0 & 0 & 1 & 0 & 0 & 0 & 1 & 0 & 1 \\
X_{34} & 1 & 0 & 0 & 0 & 0 & 0 & 0 & 0 & 0 & 1 & 1 & 0 & 0 & 0 & 1 \\
X_{53}^{2} & 0 & 1 & 0 & 1 & 1 & 0 & 1 & 1 & 0 & 0 & 0 & 1 & 0 & 0 & 0 \\
X_{42} & 0 & 1 & 0 & 0 & 0 & 0 & 1 & 0 & 0 & 0 & 0 & 0 & 1 & 1 & 0 \\
X_{61} & 0 & 1 & 0 & 0 & 0 & 0 & 0 & 1 & 0 & 1 & 0 & 0 & 0 & 1 & 0 \\
X_{62} & 0 & 0 & 1 & 0 & 1 & 0 & 0 & 0 & 0 & 1 & 0 & 0 & 1 & 1 & 1 \\
X_{53}^{1} & 0 & 0 & 1 & 0 & 1 & 0 & 0 & 0 & 0 & 0 & 0 & 1 & 0 & 0 & 0 \\
X_{45} & 0 & 0 & 1 & 0 & 0 & 1 & 0 & 0 & 1 & 0 & 0 & 0 & 1 & 1 & 0 \\
X_{31} & 0 & 0 & 1 & 0 & 0 & 1 & 0 & 0 & 0 & 1 & 1 & 0 & 0 & 1 & 0 \\
X_{12} & 0 & 0 & 0 & 1 & 1 & 0 & 1 & 0 & 0 & 0 & 0 & 0 & 1 & 0 & 1 \\
X_{64} & 0 & 0 & 0 & 1 & 1 & 0 & 0 & 1 & 0 & 1 & 0 & 0 & 0 & 0 & 1 \\
X_{36} & 0 & 0 & 0 & 1 & 0 & 1 & 1 & 0 & 0 & 0 & 1 & 0 & 0 & 0 & 0 \\
X_{25} & 0 & 0 & 0 & 1 & 0 & 1 & 0 & 1 & 1 & 0 & 0 & 0 & 0 & 0 & 0 \\
\end{array}
\right) .
\tag{3.10.140}
$$

The F-term charge matrix $Q_F = \ker(P)$ is

$$Q_F = \begin{pmatrix} p_1 & p_2 & p_3 & p_4 & q_1 & q_2 & r_1 & r_2 & s_1 & s_2 & s_3 & s_4 & s_5 & s_6 & s_7 \\ \hline 1 & 1 & 1 & 1 & 0 & 0 & -1 & 0 & 0 & -1 & 0 & 0 & -1 & -1 & 0 \\ 1 & 1 & 0 & 0 & -1 & -1 & 0 & 0 & 0 & 0 & 0 & 0 & 0 & 0 & 0 \\ 0 & 1 & 1 & 0 & 0 & 0 & -1 & 0 & 1 & 0 & -1 & 0 & 0 & -1 & 0 \\ 0 & 0 & 1 & 0 & 1 & 0 & 0 & 0 & 0 & 0 & 0 & 0 & 0 & -1 & -1 \\ 0 & 0 & 0 & 1 & 1 & 0 & -1 & 0 & 0 & -1 & 1 & 0 & 0 & -1 & 0 \\ 0 & 0 & 0 & 1 & 1 & 0 & -1 & 0 & 1 & 0 & 0 & -1 & 0 & -1 & 0 \\ 0 & 0 & 0 & 1 & 1 & 0 & 0 & -1 & -1 & 0 & 1 & 0 & 0 & 0 & -1 \end{pmatrix} . \tag{3.10.141}$$

The D-term charge matrix is

$$Q_D = \begin{pmatrix} p_1 & p_2 & p_3 & p_4 & q_1 & q_2 & r_1 & r_2 & s_1 & s_2 & s_3 & s_4 & s_5 & s_6 & s_7 \\ \hline 0 & 0 & 0 & 0 & 0 & 0 & 0 & 0 & 0 & 1 & -1 & 0 & 0 & 0 & 0 \\ 0 & 0 & 0 & 0 & 0 & 0 & 0 & 0 & 0 & 0 & 1 & -1 & 0 & 0 & 0 \\ 0 & 0 & 0 & 0 & 0 & 0 & 0 & 0 & 0 & 0 & 0 & 1 & -1 & 0 & 0 \\ 0 & 0 & 0 & 0 & 0 & 0 & 0 & 0 & 0 & 0 & 0 & 0 & 1 & -1 & 0 \\ 0 & 0 & 0 & 0 & 0 & 0 & 0 & 0 & 0 & 0 & 0 & 0 & 0 & 1 & -1 \end{pmatrix} . \tag{3.10.142}$$

The total charge matrix Q_t does not have repeated columns. Accordingly, the global symmetry is $U(1)_{f_1} \times U(1)_{f_2} \times U(1)_R$. The flavour and R-charges on the GLSM fields corresponding to extremal points in the toric diagram are the same as in Model 8a, and are given in Table 3.30.

Products of non-extremal perfect matchings are expressed as

$$q = q_1 q_2 \ , \ \ r = r_1 r_2 \ , \ \ s = \prod_{m=1}^{7} s_m \ . \tag{3.10.143}$$

The extremal perfect matchings are counted by t_α. Products of non-extremal perfect matchings such as q are associated to a fugacity of the form y_q.

The mesonic Hilbert series and the plethystic logarithm are identical to the ones for Model 8a and are given in (3.10.132) and (3.10.133) respectively. As a result, the mesonic moduli spaces for Models 8a and 8b are the same.

The generators of the mesonic moduli space in terms of all perfect matchings of Model 8b are shown in Table 3.31. In terms of Model 8b quiver fields, the generators are shown in Table 3.33. From the plethystic logarithm in (3.10.133) one observes that the mesonic moduli space is not a complete intersection.

Generator	$U(1)_{f_1}$	$U(1)_{f_2}$
$X_{26}X_{62} = X_{15}X_{53}^1 X_{31} = X_{34}X_{45}X_{53}^1$	1	0
$X_{15}X_{56}X_{61} = X_{23}X_{34}X_{42}$	-1	-1
$X_{15}X_{53}^1 X_{36}X_{61} = X_{25}X_{53}^1 X_{34}X_{42} = X_{12}X_{23}X_{31} = X_{12}X_{26}X_{61} = X_{15}X_{53}^2 X_{31}$	0	0
$= X_{23}X_{36}X_{62} = X_{25}X_{56}X_{62} = X_{26}X_{64}X_{42} = X_{34}X_{45}X_{53}^2 = X_{45}X_{56}X_{64}$		
$X_{12}X_{25}X_{53}^1 X_{31} = X_{25}X_{53}^1 X_{36}X_{62} = X_{36}X_{64}X_{45}X_{53}^1$	1	1
$X_{12}X_{23}X_{36}X_{61} = X_{12}X_{25}X_{56}X_{61} = X_{15}X_{53}^2 X_{36}X_{61}$	-1	0
$= X_{23}X_{36}X_{64}X_{42} = X_{25}X_{53}^2 X_{34}X_{42} = X_{25}X_{56}X_{64}X_{42}$		
$X_{12}X_{25}X_{53}^1 X_{36}X_{61} = X_{25}X_{53}^1 X_{36}X_{64}X_{42} = X_{12}X_{25}X_{53}^2 X_{31} = X_{25}X_{53}^2 X_{36}X_{62} = X_{36}X_{64}X_{45}X_{53}^2$	0	1
$X_{12}X_{25}X_{53}^2 X_{36}X_{61} = X_{25}X_{53}^2 X_{36}X_{64}X_{42}$	-1	1

Table 3.33: The generators in terms of bifundamental fields (Model 8b).
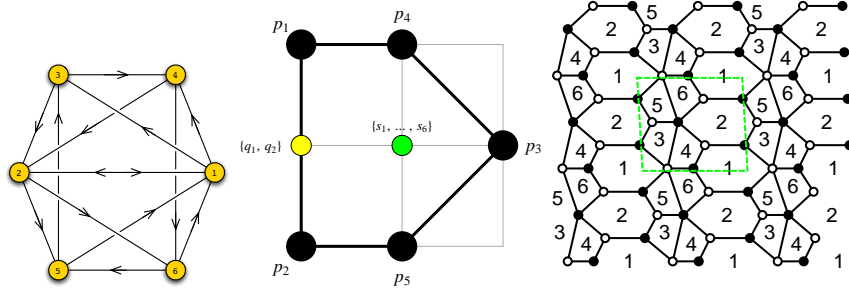
Figure 3.18: The quiver, toric diagram, and brane tiling of Model 9a.

3.11 Model 9: PdP$_{3b}$

3.11.1 Model 9 Phase a

The superpotential is

$$
\begin{aligned}
W \quad = \quad & +X_{12}X_{26}X_{61} + X_{25}X_{53}X_{32} + X_{42}X_{21}X_{14} + X_{13}X_{34}X_{46}X_{65}X_{51} \\
& -X_{13}X_{32}X_{21} - X_{25}X_{51}X_{12} - X_{46}X_{61}X_{14} - X_{26}X_{65}X_{53}X_{34}X_{42} \ .
\end{aligned}
$$

$$(3.11.144)$$

	$U(1)_{f_1}$	$U(1)_{f_2}$	$U(1)_R$	fugacity
p_1	-2/5	1/2	$R_1 = 2\left(-2 + \sqrt{5}\right)$	t_1
p_2	-1/5	-1/2	$R_1 = 2\left(-2 + \sqrt{5}\right)$	t_2
p_3	2/5	0	$R_1 = 2\left(-2 + \sqrt{5}\right)$	t_3
p_4	1/5	0	$R_2 = 7 - 3\sqrt{5}$	t_4
p_5	0	0	$R_2 = 7 - 3\sqrt{5}$	t_5

Table 3.34: The GLSM fields corresponding to extremal points of the toric diagram with their mesonic charges (Model 9a). The R-charges are obtained using a-maximization.

The perfect matching matrix is

$$
P = \left(
\begin{array}{c|ccccc|cc|cccccc}
 & p_1 & p_2 & p_3 & p_4 & p_5 & q_1 & q_2 & s_1 & s_2 & s_3 & s_4 & s_5 & s_6 \\
\hline
X_{26} & 1 & 0 & 0 & 0 & 0 & 1 & 0 & 1 & 0 & 0 & 0 & 0 & 0 \\
X_{51} & 1 & 0 & 0 & 0 & 0 & 0 & 1 & 0 & 1 & 0 & 0 & 0 & 0 \\
X_{13} & 0 & 1 & 0 & 0 & 0 & 1 & 0 & 0 & 0 & 1 & 0 & 0 & 0 \\
X_{42} & 0 & 1 & 0 & 0 & 0 & 0 & 1 & 0 & 0 & 0 & 1 & 0 & 0 \\
X_{46} & 0 & 0 & 1 & 0 & 0 & 0 & 0 & 1 & 0 & 0 & 1 & 0 & 0 \\
X_{53} & 0 & 0 & 1 & 0 & 0 & 0 & 0 & 0 & 1 & 1 & 0 & 0 & 0 \\
X_{14} & 1 & 0 & 0 & 1 & 0 & 1 & 0 & 0 & 0 & 1 & 0 & 1 & 0 \\
X_{32} & 1 & 0 & 0 & 1 & 0 & 0 & 1 & 0 & 0 & 0 & 1 & 1 & 0 \\
X_{25} & 0 & 1 & 0 & 0 & 1 & 1 & 0 & 1 & 0 & 0 & 0 & 0 & 1 \\
X_{61} & 0 & 1 & 0 & 0 & 1 & 0 & 1 & 0 & 1 & 0 & 0 & 0 & 1 \\
X_{12} & 0 & 0 & 1 & 1 & 0 & 0 & 0 & 0 & 0 & 1 & 1 & 1 & 0 \\
X_{21} & 0 & 0 & 1 & 0 & 1 & 0 & 0 & 1 & 1 & 0 & 0 & 0 & 1 \\
X_{65} & 0 & 0 & 0 & 1 & 0 & 0 & 0 & 0 & 0 & 0 & 0 & 0 & 1 \\
X_{34} & 0 & 0 & 0 & 0 & 1 & 0 & 0 & 0 & 0 & 0 & 0 & 1 & 0 \\
\end{array}
\right).
\tag{3.11.145}
$$

The F-term charge matrix $Q_F = \ker(P)$ is

$$
Q_F = \left(
\begin{array}{ccccc|cc|cccccc}
p_1 & p_2 & p_3 & p_4 & p_5 & q_1 & q_2 & s_1 & s_2 & s_3 & s_4 & s_5 & s_6 \\
\hline
1 & 1 & 0 & 0 & 0 & -1 & -1 & 0 & 0 & 0 & 0 & 0 & 0 \\
0 & 0 & 0 & 1 & 1 & 0 & 0 & 0 & 0 & 0 & 0 & -1 & -1 \\
1 & 0 & 1 & 0 & 1 & 0 & 0 & -1 & -1 & 0 & 0 & -1 & 0 \\
0 & 0 & 1 & 0 & 0 & 1 & 0 & -1 & 0 & -1 & 0 & 0 & 0 \\
0 & 0 & 1 & 0 & 0 & 0 & 1 & 0 & -1 & 0 & -1 & 0 & 0 \\
\end{array}
\right).
\tag{3.11.146}
$$

The D-term charge matrix is

$$
Q_D = \left(
\begin{array}{ccccc|cc|cccccc}
p_1 & p_2 & p_3 & p_4 & p_5 & q_1 & q_2 & s_1 & s_2 & s_3 & s_4 & s_5 & s_6 \\
\hline
0 & 0 & 0 & 0 & 0 & 0 & 0 & 1 & -1 & 0 & 0 & 0 & 0 \\
0 & 0 & 0 & 0 & 0 & 0 & 0 & 0 & 1 & -1 & 0 & 0 & 0 \\
0 & 0 & 0 & 0 & 0 & 0 & 0 & 0 & 0 & 1 & -1 & 0 & 0 \\
0 & 0 & 0 & 0 & 0 & 0 & 0 & 0 & 0 & 0 & 1 & -1 & 0 \\
0 & 0 & 0 & 0 & 0 & 0 & 0 & 0 & 0 & 0 & 0 & 1 & -1 \\
\end{array}
\right).
\tag{3.11.147}
$$

The total charge matrix does not exhibit repeated columns. Accordingly, the global symmetry is $U(1)_{f_1} \times U(1)_{f_2} \times U(1)_R$. Following the discussion in §3.2.3, the mesonic charges on extremal perfect matchings are found. They are shown in Table 3.34.

Products of non-extremal perfect matchings are expressed as

$$q = q_1 q_2 \ , \quad s = \prod_{m=1}^{6} s_m \ . \tag{3.11.148}$$

Extremal perfect matchings are counted by t_α. Products of non-extremal perfect matchings such as q are counted by a fugacity of the form y_q.

The mesonic Hilbert series of Model 9a is found using the Molien integral formula in (3.2.3). It is

$$g_1(t_\alpha, y_q, y_s; \mathcal{M}_{9a}^{mes}) =$$
$$\frac{P(t_\alpha)}{(1 - y_q^2 y_s \ t_1^3 t_2 t_4^2)(1 - y_q y_s \ t_1^2 t_3 t_4^2)(1 - y_s \ t_3^2 t_4 t_5)(1 - y_q^2 y_s \ t_1 t_2^3 t_5^2)(1 - y_q y_s \ t_2^2 t_3 t_5^2)} \ . \tag{3.11.149}$$

The numerator is given by the polynomial

$$
\begin{aligned}
P(t_\alpha) \ &= \ 1 + y_q^2 y_s \ t_1^2 t_2^2 t_4 t_5 + y_q y_s \ t_1 t_2 t_3 t_4 t_5 - y_q^3 y_s^2 \ t_1^4 t_2^2 t_3 t_4^3 t_5 - y_q^2 y_s^2 \ t_1^3 t_2 t_3^2 t_4^3 t_5 \\
&\quad - y_q^3 y_s^2 \ t_1^3 t_2^3 t_3 t_4^2 t_5^2 - y_q^2 y_s^2 \ t_1^2 t_2^2 t_3^2 t_4^2 t_5^2 - y_q^3 y_s^2 \ t_1^2 t_2^4 t_3 t_4 t_5^3 - y_q^2 y_s^2 \ t_1 t_2^3 t_3^2 t_4 t_5^3 \\
&\quad + y_q^4 y_s^3 \ t_1^4 t_2^4 t_3^2 t_4^3 t_5^3 + y_q^3 y_s^3 \ t_1^3 t_2^3 t_3^3 t_4^3 t_5^3 + y_q^5 y_s^4 \ t_1^5 t_2^5 t_3^3 t_4^4 t_5^4 \ . \tag{3.11.150}
\end{aligned}
$$

The plethystic logarithm of the mesonic Hilbert series is

$$
\begin{aligned}
PL[g_1(t_\alpha, y_q, y_s; \mathcal{M}_{9a}^{mes})] &= y_s \ t_3^2 t_4 t_5 + y_q y_s \ t_1 t_2 t_3 t_4 t_5 + y_q y_s \ t_1^2 t_3 t_4^2 + y_q y_s \ t_2^2 t_3 t_5^2 \\
&\quad + y_q^2 y_s \ t_1^2 t_2^2 t_4 t_5 + y_q^2 y_s \ t_1 t_2^3 t_5^2 + y_q^2 y_s \ t_1^3 t_2 t_4^2 - 2 \ y_q^2 y_s^2 \ t_1^2 t_2^2 t_3^2 t_4^2 t_5^2 - y_q^2 y_s^2 \ t_1^3 t_2 t_3^2 t_4^3 t_5 \\
&\quad - y_q^2 y_s^2 \ t_1 t_2^3 t_3^2 t_4 t_5^3 + \dots \ . \tag{3.11.151}
\end{aligned}
$$

Consider the following fugacity map

$$f_1 = y_q^{-2/3} y_s^{1/3} \ t_1^{-2/3} t_2^{2/3} t_3^{4/3} \ , \quad f_2 = \frac{t_1 t_4}{t_2 t_5} \ , \quad \tilde{t}_1 = y_q^{1/3} y_s^{1/3} \ t_1^{1/3} t_2^{1/3} t_3^{1/3} \ , \quad \tilde{t}_2 = t_4^{1/2} t_5^{1/2} \ , \tag{3.11.152}$$

where the fugacities f_1 and f_2 count flavour charges, and the fugacities $\tilde{t}_1$ and $\tilde{t}_2$ count the R-charges R_1 and R_2 in Table 3.34 respectively. Under the fugacity map above, the plethystic logarithm becomes

$$
\begin{aligned}
PL[g_1(\tilde{t}_\alpha, f_1, f_2; \mathcal{M}_{9a}^{mes})] &= f_1 \tilde{t}_1^2 \tilde{t}_2^2 + \left(1 + f_2 + \frac{1}{f_2}\right) \tilde{t}_1^3 \tilde{t}_2^2 + \left(\frac{1}{f_1} + \frac{1}{f_1 f_2} + \frac{f_2}{f_1}\right) \tilde{t}_1^4 \tilde{t}_2^2 \\
&\quad - \left(2 + f_2 + \frac{1}{f_2}\right) \tilde{t}_1^6 \tilde{t}_2^4 + \dots \ . \tag{3.11.153}
\end{aligned}
$$

This plethystic logarithm exhibits the moduli space generators with their mesonic

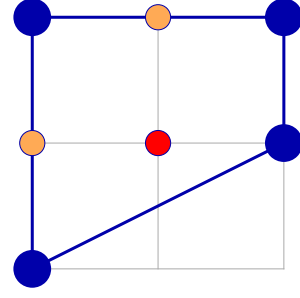| Generator	$U(1)_{f_1}$	$U(1)_{f_2}$
$p_3^2 p_4 p_5\ s$	1	0
$p_1^2 p_3 p_4^2\ q\ s$	0	1
$p_1 p_2 p_3 p_4 p_5\ q\ s$	0	0
$p_2^2 p_3 p_5^2\ q\ s$	0	-1
$p_1^3 p_2 p_4^2\ q^2\ s$	-1	1
$p_1^2 p_2^2 p_4 p_5\ q^2\ s$	-1	0
$p_1 p_2^3 p_5^2\ q^2\ s$	-1	-1
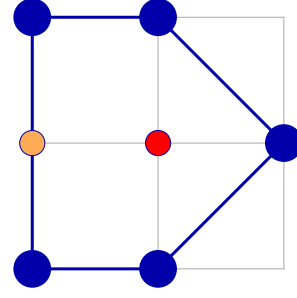
Table 3.35: The generators and lattice of generators of the mesonic moduli space of Model 9a in terms of GLSM fields with the corresponding flavor charges.

Generator	$U(1)_{f_1}$	$U(1)_{f_2}$
$X_{12}X_{21} = X_{34}X_{46}X_{65}X_{53}$	1	0
$X_{12}X_{26}X_{65}X_{51} = X_{14}X_{46}X_{65}X_{51} = X_{26}X_{65}X_{53}X_{32}$	0	1
$X_{13}X_{34}X_{46}X_{65}X_{51} = X_{26}X_{65}X_{53}X_{34}X_{42} = X_{12}X_{25}X_{51} = X_{12}X_{26}X_{61}$ $= X_{13}X_{32}X_{21} = X_{14}X_{42}X_{21} = X_{14}X_{46}X_{61} = X_{25}X_{53}X_{32}$	0	0
$X_{13}X_{34}X_{42}X_{21} = X_{13}X_{34}X_{46}X_{61} = X_{25}X_{53}X_{34}X_{42}$	0	-1
$X_{13}X_{32}X_{26}X_{65}X_{51} = X_{14}X_{42}X_{26}X_{65}X_{51}$	-1	1
$X_{13}X_{34}X_{42}X_{26}X_{65}X_{51} = X_{13}X_{32}X_{25}X_{51} = X_{13}X_{32}X_{26}X_{61} = X_{14}X_{42}X_{25}X_{51} = X_{14}X_{42}X_{26}X_{61}$	-1	0
$X_{13}X_{34}X_{42}X_{25}X_{51} = X_{13}X_{34}X_{42}X_{26}X_{61}$	-1	-1

Table 3.36: The generators in terms of bifundamental fields (Model 9a).

charges. They are summarized in Table 3.35. The generators can be presented on a charge lattice. The convex polygon formed by the generators in Table 3.35 is the dual reflexive polygon of the toric diagram of Model 9a. For the case of Model 9a, the toric diagram is self-dual, and the charge lattice of the generators forms again the toric diagram of Model 9a.

The mesonic Hilbert series and the plethystic logarithm can be re-expressed in terms of 3 fugacities

$$T_1 = \frac{t_5}{y_q^2 y_s\ t_1^4 t_4^3}\ ,\ T_2 = y_q^2 y_s\ t_1^3 t_2 t_4^2\ ,\ T_3 = y_q y_s\ t_1^2 t_3 t_4^2\ , \qquad (3.11.154)$$

such that

$$g_1(T_1, T_2, T_3; \mathcal{M}_{9a}^{mes}) =$$
$$(1 + T_1 T_2^2 + T_1 T_2 T_3 - T_1 T_2^2 T_3 - T_1 T_2 T_3^2 - T_1^2 T_2^3 T_3 - T_1^2 T_2^2 T_3^2 - T_1^3 T_2^4 T_3 - T_1^3 T_2^3 T_3^2$$
$$+ T_1^3 T_2^4 T_3^2 + T_1^3 T_2^3 T_3^3 + T_1^4 T_2^5 T_3^3)$$
$$\times \frac{1}{(1 - T_2)(1 - T_3)(1 - T_1^2 T_2^3)(1 - T_1 T_3^2)(1 - T_1^2 T_2^2 T_3)} \qquad (3.11.155)$$
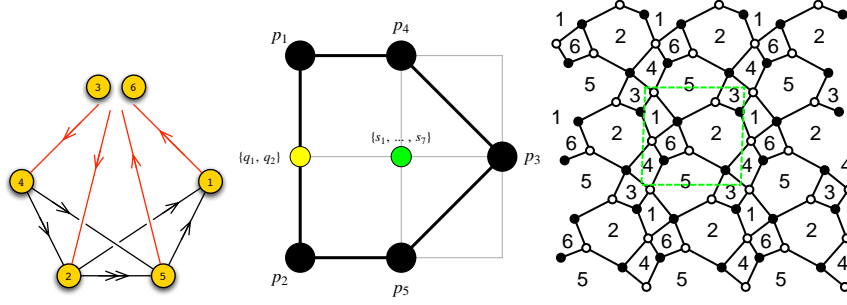
Figure 3.19: The quiver, toric diagram, and brane tiling of Model 9b. The red arrows in the quiver indicate all possible connections between blocks of nodes.

and

$$PL[g_1(T_1, T_2, T_3; \mathcal{M}_{9a}^{mes})] = T_1 T_3^2 + T_1 T_2 T_3 + T_3 + T_1^2 T_2^2 T_3 + T_1 T_2^2 + T_1^2 T_2^3 + T_2$$
$$-2T_1^2 T_2^2 T_3^2 - T_1 T_2 T_3^2 - T_1^3 T_2^3 T_3^2 + \dots . \tag{3.11.156}$$

The above Hilbert series and plethystic logarithm illustrate the conical structure of the toric Calabi-Yau 3-fold.

3.11.2 Model 9 Phase b

The superpotential is

$$\begin{aligned} W &= +X_{25}^2 X_{53} X_{32} + X_{56} X_{62} X_{25}^1 + X_{13} X_{34} X_{45} X_{51} + X_{21} X_{16} X_{64} X_{42} \\ &\quad -X_{13} X_{32} X_{21} - X_{56} X_{64} X_{45} - X_{16} X_{62} X_{25}^2 X_{51} - X_{25}^1 X_{53} X_{34} X_{42} . \end{aligned} \tag{3.11.157}$$

The perfect matching matrix is

$$P = \begin{pmatrix} \begin{array}{c|ccccc|cc|ccccccc} & p_1 & p_2 & p_3 & p_4 & p_5 & q_1 & q_2 & s_1 & s_2 & s_3 & s_4 & s_5 & s_6 & s_7 \\ \hline X_{32} & 1 & 0 & 0 & 1 & 0 & 1 & 0 & 0 & 1 & 0 & 1 & 0 & 1 & 0 \\ X_{25}^1 & 1 & 0 & 0 & 1 & 0 & 0 & 1 & 1 & 0 & 0 & 0 & 0 & 0 & 0 \\ X_{51} & 1 & 0 & 0 & 0 & 0 & 1 & 0 & 0 & 0 & 0 & 0 & 0 & 0 & 1 \\ X_{64} & 1 & 0 & 0 & 0 & 0 & 0 & 1 & 0 & 0 & 1 & 0 & 0 & 1 & 0 \\ X_{56} & 0 & 1 & 0 & 0 & 1 & 1 & 0 & 0 & 1 & 0 & 0 & 1 & 0 & 1 \\ X_{25}^2 & 0 & 1 & 0 & 0 & 1 & 0 & 1 & 1 & 0 & 0 & 0 & 0 & 0 & 0 \\ X_{42} & 0 & 1 & 0 & 0 & 0 & 1 & 0 & 0 & 0 & 0 & 1 & 0 & 0 & 0 \\ X_{13} & 0 & 1 & 0 & 0 & 0 & 0 & 1 & 0 & 0 & 1 & 0 & 1 & 0 & 0 \\ X_{45} & 0 & 0 & 1 & 1 & 0 & 0 & 0 & 1 & 0 & 0 & 1 & 0 & 0 & 0 \\ X_{21} & 0 & 0 & 1 & 0 & 1 & 0 & 0 & 1 & 0 & 0 & 0 & 0 & 0 & 1 \\ X_{62} & 0 & 0 & 1 & 0 & 0 & 0 & 0 & 0 & 0 & 1 & 1 & 0 & 1 & 0 \\ X_{53} & 0 & 0 & 1 & 0 & 0 & 0 & 0 & 0 & 0 & 1 & 0 & 1 & 0 & 1 \\ X_{16} & 0 & 0 & 0 & 1 & 0 & 0 & 0 & 0 & 1 & 0 & 0 & 1 & 0 & 0 \\ X_{34} & 0 & 0 & 0 & 0 & 1 & 0 & 0 & 0 & 1 & 0 & 0 & 0 & 1 & 0 \end{array} \end{pmatrix} . \tag{3.11.158}$$

The F-term charge matrix $Q_F = \ker(P)$ is

$$
Q_F = \left(\begin{array}{ccccc|cc|ccccccc}
p_1 & p_2 & p_3 & p_4 & p_5 & q_1 & q_2 & s_1 & s_2 & s_3 & s_4 & s_5 & s_6 & s_7 \\
1 & 1 & 0 & 0 & 0 & -1 & -1 & 0 & 0 & 0 & 0 & 0 & 0 & 0 \\
0 & 0 & 0 & 1 & 1 & 0 & 0 & -1 & -1 & 0 & 0 & 0 & 0 & 0 \\
1 & 0 & 0 & 0 & 1 & -1 & 0 & -1 & 0 & 0 & 1 & 0 & -1 & 0 \\
1 & 0 & 0 & 0 & 1 & 0 & -1 & 0 & 0 & 1 & 0 & 0 & -1 & -1 \\
0 & 1 & 1 & 1 & 0 & 0 & 0 & -1 & 0 & 0 & -1 & -1 & 0 & 0 \\
0 & 0 & 1 & 0 & 0 & 1 & 0 & 0 & 0 & 0 & -1 & 0 & 0 & -1
\end{array}\right). \tag{3.11.159}
$$

The D-term charge matrix is

$$
Q_D = \left(\begin{array}{ccccc|cc|ccccccc}
p_1 & p_2 & p_3 & p_4 & p_5 & q_1 & q_2 & s_1 & s_2 & s_3 & s_4 & s_5 & s_6 & s_7 \\
0 & 0 & 0 & 0 & 0 & 0 & 0 & 1 & -1 & 0 & 0 & 0 & 0 & 0 \\
0 & 0 & 0 & 0 & 0 & 0 & 0 & 0 & 1 & -1 & 0 & 0 & 0 & 0 \\
0 & 0 & 0 & 0 & 0 & 0 & 0 & 0 & 0 & 1 & -1 & 0 & 0 & 0 \\
0 & 0 & 0 & 0 & 0 & 0 & 0 & 0 & 0 & 0 & 1 & -1 & 0 & 0 \\
0 & 0 & 0 & 0 & 0 & 0 & 0 & 0 & 0 & 0 & 0 & 0 & 1 & -1
\end{array}\right). \tag{3.11.160}
$$

The total charge matrix Q_t does not have repeated columns. Accordingly, the global symmetry group for the Model 9b theory is $U(1)_{f_1} \times U(1)_{f_2} \times U(1)_R$. The flavour and R-charges on the extremal perfect matchings p_α are the same as for Model 9a, and are summarised in Table 3.34. They are found following the discussion in §3.2.3.

Products of non-extremal perfect matchings are expressed as

$$
q = q_1 q_2 \ , \quad s = \prod_{m=1}^{7} s_m \ . \tag{3.11.161}
$$

The fugacity counting extremal perfect matchings p_α is t_α. The fugacity y_q counts the product of non-extremal perfect matchings q above.

The mesonic Hilbert series for Model 9b is identical to the one for Model 9a. The mesonic Hilbert series is shown in (3.11.149). The corresponding plethystic logarithm in (3.11.151) indicates that the mesonic moduli space is not a complete intersection. As a summary, both Model 9a and 9b mesonic moduli spaces are identical.

The generators of the mesonic moduli space in terms of the perfect matching fields of Model 9b are presented in Table 3.35. The charge lattice of mesonic generators forms a convex polygon which is another reflexive polygon precisely being the dual of the toric diagram. The generators of the mesonic moduli space in terms of quiver fields of Model 9b are shown in Table 3.37.

Generator	$U(1)_{f_1}$	$U(1)_{f_2}$
$X_{16}X_{62}X_{21} = X_{34}X_{45}X_{53}$	1	0
$X_{25}^1 X_{53} X_{32} = X_{16} X_{62} X_{25}^1 X_{51} = X_{16} X_{64} X_{45} X_{51}$	0	1
$X_{13}X_{32}X_{21} = X_{25}^1 X_{56} X_{62} = X_{25}^2 X_{53} X_{32} = X_{45} X_{56} X_{64}$	0	0
$= X_{13}X_{34}X_{45}X_{51} = X_{16}X_{64}X_{42}X_{21} = X_{16}X_{62}X_{25}^2 X_{51} = X_{25}^1 X_{53} X_{34} X_{42}$		
$X_{25}^2 X_{56} X_{62} = X_{13} X_{34} X_{42} X_{21} = X_{25}^2 X_{53} X_{34} X_{42}$	0	-1
$X_{13} X_{32} X_{25}^1 X_{51} = X_{16} X_{64} X_{42} X_{25}^1 X_{51}$	-1	1
$X_{13} X_{32} X_{25}^2 X_{51} = X_{25}^1 X_{56} X_{64} X_{42} = X_{13} X_{34} X_{42} X_{25}^1 X_{51} = X_{16} X_{64} X_{42} X_{25}^2 X_{51}$	-1	0
$X_{25}^2 X_{56} X_{64} X_{42} = X_{13} X_{34} X_{42} X_{25}^2 X_{51}$	-1	-1

Table 3.37: The generators in terms of bifundamental fields (Model 9b).

Figure 3.20: The quiver, toric diagram, and brane tiling of Model 9c. The red arrows in the quiver indicate all possible connections between blocks of nodes.

3.11.3 Model 9 Phase c

The superpotential is

$$
\begin{aligned}
W =\ & +X_{21}X_{16}X_{62}^2 + X_{24}X_{43}X_{32}^2 + X_{25}^2 X_{53}X_{32}^1 + X_{51}X_{13}X_{35} + X_{54}X_{46}X_{62}^1 X_{25}^1 \\
& -X_{13}X_{32}^1 X_{21} - X_{24}X_{46}X_{62}^2 - X_{25}^1 X_{53}X_{32}^2 - X_{54}X_{43}X_{35} - X_{16}X_{62}^1 X_{25}^2 X_{51} \ .
\end{aligned}
$$

(3.11.162)

The perfect matching matrix is

$$
P = \left(\begin{array}{c|ccccc|cc|cccccccc}
 & p_1 & p_2 & p_3 & p_4 & p_5 & q_1 & q_2 & s_1 & s_2 & s_3 & s_4 & s_5 & s_6 & s_7 & s_8 \\ \hline
X_{25}^1 & 1 & 0 & 0 & 1 & 0 & 1 & 0 & 0 & 1 & 0 & 0 & 0 & 0 & 0 & 0 \\
X_{32}^1 & 1 & 0 & 0 & 1 & 0 & 0 & 1 & 1 & 0 & 0 & 0 & 0 & 0 & 0 & 1 \\
X_{25}^2 & 0 & 1 & 0 & 0 & 1 & 1 & 0 & 0 & 1 & 0 & 0 & 0 & 0 & 0 & 0 \\
X_{32}^2 & 0 & 1 & 0 & 0 & 1 & 0 & 1 & 1 & 0 & 0 & 0 & 0 & 0 & 0 & 1 \\
X_{43} & 1 & 0 & 0 & 0 & 0 & 1 & 0 & 0 & 0 & 1 & 1 & 0 & 1 & 0 & 0 \\
X_{51} & 1 & 0 & 0 & 0 & 0 & 0 & 1 & 0 & 0 & 0 & 0 & 0 & 1 & 1 & 0 \\
X_{13} & 0 & 1 & 0 & 0 & 0 & 1 & 0 & 0 & 0 & 1 & 1 & 1 & 0 & 0 & 0 \\
X_{54} & 0 & 1 & 0 & 0 & 0 & 0 & 1 & 0 & 0 & 0 & 0 & 1 & 0 & 1 & 0 \\
X_{53} & 0 & 0 & 1 & 0 & 0 & 0 & 0 & 0 & 0 & 1 & 1 & 1 & 1 & 1 & 0 \\
X_{62}^1 & 0 & 0 & 1 & 0 & 0 & 0 & 0 & 0 & 0 & 0 & 1 & 0 & 0 & 0 & 1 \\
X_{62}^2 & 1 & 1 & 0 & 0 & 0 & 1 & 1 & 0 & 0 & 0 & 1 & 0 & 0 & 0 & 1 \\
X_{24} & 0 & 0 & 1 & 1 & 0 & 0 & 0 & 0 & 1 & 0 & 0 & 1 & 0 & 1 & 0 \\
X_{21} & 0 & 0 & 1 & 0 & 1 & 0 & 0 & 0 & 1 & 0 & 0 & 0 & 1 & 1 & 0 \\
X_{16} & 0 & 0 & 0 & 1 & 0 & 0 & 0 & 1 & 0 & 1 & 0 & 1 & 0 & 0 & 0 \\
X_{46} & 0 & 0 & 0 & 0 & 1 & 0 & 0 & 1 & 0 & 1 & 0 & 0 & 1 & 0 & 0 \\
X_{35} & 0 & 0 & 1 & 1 & 1 & 0 & 0 & 1 & 1 & 0 & 0 & 0 & 0 & 0 & 1
\end{array}\right). \tag{3.11.163}
$$

The F-term charge matrix $Q_F = \ker(P)$ is

$$
Q_F = \left(\begin{array}{ccccc|cc|cccccccc}
p_1 & p_2 & p_3 & p_4 & p_5 & q_1 & q_2 & s_1 & s_2 & s_3 & s_4 & s_5 & s_6 & s_7 & s_8 \\ \hline
1 & 1 & 0 & 0 & 0 & -1 & -1 & 0 & 0 & 0 & 0 & 0 & 0 & 0 & 0 \\
0 & 0 & 0 & 1 & 1 & 0 & 0 & -1 & -1 & 0 & 0 & 0 & 0 & 0 & 0 \\
1 & 0 & 0 & 0 & 1 & -1 & 0 & -1 & 0 & 0 & 0 & 1 & 0 & -1 & 0 \\
1 & 0 & 0 & 0 & 1 & -1 & 0 & -1 & 0 & 1 & 0 & 0 & -1 & 0 & 0 \\
0 & 1 & 0 & 1 & 0 & -1 & 0 & -1 & 0 & 1 & 0 & -1 & 0 & 0 & 0 \\
0 & 0 & 1 & 0 & 0 & 1 & 0 & 0 & -1 & 0 & -1 & 0 & 0 & 0 & 0 \\
0 & 0 & 0 & 0 & 0 & 0 & 0 & -1 & 0 & 1 & -1 & 0 & 0 & 0 & 1
\end{array}\right). \tag{3.11.164}
$$

The D-term charge matrix is

$$
Q_D = \left(\begin{array}{ccccc|cc|cccccccc}
p_1 & p_2 & p_3 & p_4 & p_5 & q_1 & q_2 & s_1 & s_2 & s_3 & s_4 & s_5 & s_6 & s_7 & s_8 \\ \hline
0 & 0 & 0 & 0 & 0 & 0 & 0 & 0 & 1 & -1 & 0 & 0 & 0 & 0 & 0 \\
0 & 0 & 0 & 0 & 0 & 0 & 0 & 0 & 0 & 1 & -1 & 0 & 0 & 0 & 0 \\
0 & 0 & 0 & 0 & 0 & 0 & 0 & 0 & 0 & 0 & 1 & -1 & 0 & 0 & 0 \\
0 & 0 & 0 & 0 & 0 & 0 & 0 & 0 & 0 & 0 & 0 & 1 & -1 & 0 & 0 \\
0 & 0 & 0 & 0 & 0 & 0 & 0 & 0 & 0 & 0 & 0 & 0 & 0 & 1 & -1
\end{array}\right). \tag{3.11.165}
$$

The total charge matrix Q_t does not have repeated columns. Accordingly, the global symmetry of Model 9c is the same as for Model 9a and 9b above and takes the form $U(1)_{f_1} \times U(1)_{f_2} \times U(1)_R$. The mesonic charges on the extremal perfect matchings are summarised in Table 3.34.

The following products of non-extremal perfect matchings are assigned single variables

$$
q = q_1 q_2 \ , \quad s = \prod_{m=1}^{8} s_m \ . \tag{3.11.166}
$$

The extremal perfect matchings are counted by the fugacity t_α. Products of non-extremal perfect matchings such as q above are associated to fugacities of the form y_q.

The mesonic Hilbert series is identical to the mesonic Hilbert series of Model 9a and

Generator	$U(1)_{f_1}$	$U(1)_{f_2}$
$X_{35}X_{53} = X_{16}X_{62}^1 X_{21} = X_{24}X_{46}X_{62}^1$	1	0
$X_{16}X_{62}^1 X_{25}^1 X_{51} = X_{24}X_{43}X_{32}^1 = X_{25}^1 X_{53}X_{32}^1$	0	1
$X_{16}X_{62}^1 X_{25}^2 X_{51} = X_{25}^1 X_{54}X_{46}X_{62}^1 = X_{13}X_{32}^1 X_{21} = X_{13}X_{35}X_{51} =$ $X_{16}X_{62}^2 X_{21} = X_{24}X_{43}X_{32}^2 = X_{24}X_{46}X_{62}^2 = X_{25}^1 X_{53}X_{32}^2 = X_{25}^2 X_{53}X_{32}^1 = X_{35}X_{54}X_{43}$	0	0
$X_{25}^2 X_{54}X_{46}X_{62}^1 = X_{13}X_{32}^2 X_{21} = X_{25}^2 X_{53}X_{32}^2$	0	-1
$X_{13}X_{32}^1 X_{25}^1 X_{51} = X_{16}X_{62}^2 X_{25}^1 X_{51} = X_{25}^1 X_{54}X_{43}X_{32}^1$	-1	1
$X_{13}X_{32}^2 X_{25}^1 X_{51} = X_{13}X_{32}^1 X_{25}^2 X_{51} = X_{16}X_{62}^2 X_{25}^2 X_{51} = X_{25}^1 X_{54}X_{43}X_{32}^2 = X_{25}^1 X_{54}X_{46}X_{62}^2 = X_{25}^2 X_{54}X_{43}X_{32}^1$	-1	0
$X_{13}X_{32}^2 X_{25}^2 X_{51} = X_{25}^2 X_{54}X_{43}X_{32}^2 = X_{25}^2 X_{54}X_{46}X_{62}^2$	-1	-1

Table 3.38: The generators in terms of bifundamental fields (Model 9c).
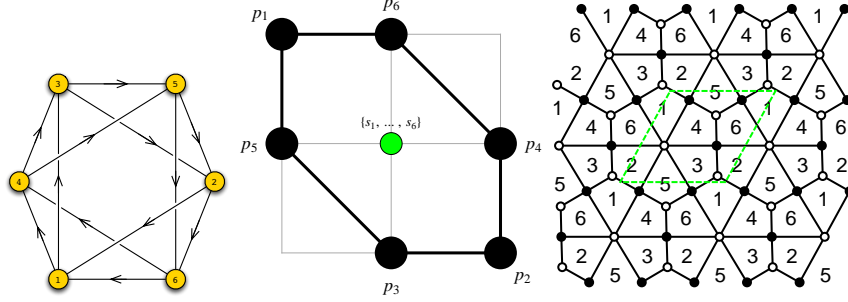
Figure 3.21: The quiver, toric diagram, and brane tiling of Model 10a.

9b. The mesonic Hilbert series is given in (3.11.149) with the corresponding plethystic logarithm in (3.11.151). The mesonic Hilbert series of Models 9a, 9b and 9c are identical and are not complete intersections.

The generators of the mesonic moduli space in terms of Model 9c GLSM fields are shown in Table 3.35. The mesonic charges of the generators correspond to lattice co-ordinates of points which form a reflexive polygon being the dual of the toric diagram. The generators in terms of quiver fields of Model 9c are shown in Table 3.38.

3.12 Model 10: dP$_3$

3.12.1 Model 10 Phase a

The superpotential is

$$
\begin{aligned}
W &= +X_{13}X_{32}X_{21} + X_{56}X_{64}X_{45} + X_{43}X_{35}X_{52}X_{26}X_{61}X_{14} \\
&\quad -X_{13}X_{35}X_{56}X_{61} - X_{14}X_{45}X_{52}X_{21} - X_{26}X_{64}X_{43}X_{32} \, . \quad (3.12.167)
\end{aligned}
$$

	$U(1)_{f_1}$	$U(1)_{f_2}$	$U(1)_R$	fugacity
p_1	-1	0	1/3	t_1
p_2	-1	1	1/3	t_2
p_3	1	0	1/3	t_3
p_4	1	-1	1/3	t_4
p_5	0	0	1/3	t_5
p_6	0	0	1/3	t_6

Table 3.39: The GLSM fields corresponding to extremal points of the toric diagram with their mesonic charges (Model 10a).

The perfect matching matrix is

$$
P = \begin{pmatrix}
 & p_1 & p_2 & p_3 & p_4 & p_5 & p_6 & s_1 & s_2 & s_3 & s_4 & s_5 & s_6 \\
\hline
X_{45} & 1 & 0 & 0 & 0 & 1 & 0 & 1 & 0 & 0 & 0 & 1 & 0 \\
X_{13} & 1 & 0 & 0 & 0 & 0 & 1 & 1 & 0 & 0 & 0 & 0 & 1 \\
X_{56} & 0 & 1 & 1 & 0 & 0 & 0 & 0 & 1 & 1 & 0 & 0 & 0 \\
X_{21} & 0 & 1 & 0 & 1 & 0 & 0 & 0 & 1 & 0 & 1 & 0 & 0 \\
X_{32} & 0 & 0 & 1 & 0 & 1 & 0 & 0 & 0 & 1 & 0 & 1 & 0 \\
X_{64} & 0 & 0 & 0 & 1 & 0 & 1 & 0 & 0 & 0 & 1 & 0 & 1 \\
X_{26} & 1 & 0 & 0 & 0 & 0 & 0 & 0 & 1 & 0 & 0 & 0 & 0 \\
X_{43} & 0 & 1 & 0 & 0 & 0 & 0 & 1 & 0 & 0 & 0 & 0 & 0 \\
X_{14} & 0 & 0 & 1 & 0 & 0 & 0 & 0 & 0 & 0 & 0 & 0 & 1 \\
X_{35} & 0 & 0 & 0 & 1 & 0 & 0 & 0 & 0 & 0 & 0 & 1 & 0 \\
X_{61} & 0 & 0 & 0 & 0 & 1 & 0 & 0 & 0 & 0 & 1 & 0 & 0 \\
X_{52} & 0 & 0 & 0 & 0 & 0 & 1 & 0 & 0 & 1 & 0 & 0 & 0
\end{pmatrix} . \tag{3.12.168}
$$

The F-term charge matrix $Q_F = \ker(P)$ is

$$
Q_F = \begin{pmatrix}
p_1 & p_2 & p_3 & p_4 & p_5 & p_6 & s_1 & s_2 & s_3 & s_4 & s_5 & s_6 \\
\hline
1 & 1 & 0 & 0 & 0 & 0 & -1 & -1 & 0 & 0 & 0 & 0 \\
0 & 0 & 0 & 1 & 1 & 0 & 0 & 0 & 0 & -1 & -1 & 0 \\
0 & 1 & 0 & 0 & 1 & 1 & -1 & 0 & -1 & -1 & 0 & 0 \\
0 & 0 & 1 & 0 & 0 & 1 & 0 & 0 & -1 & 0 & 0 & -1
\end{pmatrix} . \tag{3.12.169}
$$

The D-term charge matrix is

$$
Q_D = \begin{pmatrix}
p_1 & p_2 & p_3 & p_4 & p_5 & p_6 & s_1 & s_2 & s_3 & s_4 & s_5 & s_6 \\
\hline
0 & 0 & 0 & 0 & 0 & 0 & 1 & -1 & 0 & 0 & 0 & 0 \\
0 & 0 & 0 & 0 & 0 & 0 & 0 & 1 & -1 & 0 & 0 & 0 \\
0 & 0 & 0 & 0 & 0 & 0 & 0 & 0 & 1 & -1 & 0 & 0 \\
0 & 0 & 0 & 0 & 0 & 0 & 0 & 0 & 0 & 1 & -1 & 0 \\
0 & 0 & 0 & 0 & 0 & 0 & 0 & 0 & 0 & 0 & 1 & -1
\end{pmatrix} . \tag{3.12.170}
$$

The total charge matrix Q_t does not exhibit repeated columns. Accordingly, the global symmetry is $U(1)_{f_1} \times U(1)_{f_2} \times U(1)_R$. The mesonic charges on the GLSM fields corresponding to extremal points in the toric diagram in Figure 3.21 are found following the discussion in §3.2.3. They are presented in Table 3.39.

The product of all internal perfect matchings is labelled as follows

$$s = \prod_{m=1}^{6} s_m \ . \tag{3.12.171}$$

The fugacity counting extremal perfect matchings is t_α. The product of internal perfect matchings is associated to the fugacity y_s.

The refined mesonic Hilbert series of Model 10a is found using the Molien integral formula in (1.4.67). It is

$$g_1(t_\alpha, y_s; \mathcal{M}_{10a}^{mes}) = \frac{P(t_\alpha)}{(1 - y_s\ t_2^2 t_3^2 t_4 t_5)(1 - y_s\ t_1 t_2 t_3^2 t_5^2)(1 - y_s\ t_2^2 t_3 t_4^2 t_6)}$$
$$\times \frac{1}{(1 - y_s\ t_1^2 t_3 t_5^2 t_6)(1 - y_s\ t_1 t_2 t_4^2 t_6^2)(1 - y_s\ t_1^2 t_4 t_5 t_6^2)} \ . \tag{3.12.172}$$

The numerator is given by the polynomial

$$
\begin{aligned}
P(t_\alpha) \;=\; & 1 + y_s\ t_1 t_2 t_3 t_4 t_5 t_6 - y_s^2\ t_1 t_2^3 t_3^3 t_4^2 t_5^2 t_6 - y_s^2\ t_1^2 t_2^2 t_3^3 t_4 t_5^3 t_6 - y_s^2\ t_1 t_2^3 t_3^2 t_4^3 t_5 t_6^2 \\
& -2\ y_s^2\ t_1^2 t_2^2 t_3^2 t_4^2 t_5^2 t_6^2 - y_s^2\ t_1^3 t_2 t_3^2 t_4 t_5^3 t_6^2 + y_s^3\ t_1^2 t_2^4 t_3^4 t_4^3 t_5^3 t_6^2 + y_s^3\ t_1^3 t_2^3 t_3^4 t_4^2 t_5^4 t_6^2 \\
& - y_s^2\ t_1^2 t_2^2 t_3 t_4^3 t_5 t_6^3 - y_s^2\ t_1^3 t_2 t_3 t_4^2 t_5^2 t_6^3 + y_s^3\ t_1^2 t_2^4 t_3^3 t_4^4 t_5^2 t_6^3 + 2\ y_s^3\ t_1^3 t_2^3 t_3^3 t_4^3 t_5^3 t_6^3 \\
& + y_s^3\ t_1^4 t_2^2 t_3^3 t_4^2 t_5^4 t_6^3 + y_s^3\ t_1^3 t_2^3 t_3^2 t_4^4 t_5^2 t_6^4 + y_s^3\ t_1^4 t_2^2 t_3^2 t_4^3 t_5^3 t_6^4 - y_s^4\ t_1^4 t_2^4 t_3^4 t_4^4 t_5^4 t_6^4 \\
& - y_s^5\ t_1^5 t_2^5 t_3^5 t_4^5 t_5^5 t_6^5 \ . \tag{3.12.173}
\end{aligned}
$$

The plethystic logarithm of the mesonic Hilbert series is

$$
\begin{aligned}
PL[g_1(t_\alpha, y_s; \mathcal{M}_{10a}^{mes})] =\ & y_s\ t_1 t_2 t_3 t_4 t_5 t_6 + y_s\ t_1^2 t_3 t_5^2 t_6 + y_s\ t_2^2 t_3 t_4^2 t_6 + y_s\ t_1 t_2 t_4^2 t_6^2 \\
& + y_s\ t_1 t_2 t_3^2 t_5^2 + y_s\ t_1^2 t_4 t_5 t_6^2 + y_s\ t_2^2 t_3^2 t_4 t_5 - 3\ y_s^2\ t_1^2 t_2^2 t_3^2 t_4^2 t_5^2 t_6^2 - y_s^2\ t_1^3 t_2 t_3^2 t_4 t_5^3 t_6^2 \\
& - y_s^2\ t_1 t_2^3 t_3^2 t_4^3 t_5 t_6^2 - y_s^2\ t_1^2 t_2^2 t_3^3 t_4 t_5^3 t_6^3 - y_s^2\ t_1^2 t_2^3 t_3^3 t_4 t_5^3 t_6 - y_s^2\ t_1^3 t_2 t_3 t_4^2 t_5^2 t_6^3 \\
& - y_s^2\ t_1 t_2^3 t_3^3 t_4^2 t_5^2 t_6 + \ldots \ . \tag{3.12.174}
\end{aligned}
$$

Under the following fugacity map

$$f_1 = \frac{t_2 t_4}{t_1 t_5} \ , \quad f_2 = \frac{t_3 t_5}{t_4 t_6} \ , \quad t = y_s^{1/6}\ t_1^{1/6} t_2^{1/6} t_3^{1/6} t_4^{1/6} t_5^{1/6} t_6^{1/6} \ , \tag{3.12.175}$$

where f_1, f_2 and t are the mesonic charge fugacities, the mesonic Hilbert series and the

Generator	$U(1)_{f_1}$	$U(1)_{f_2}$
$p_2^2 p_3^2 p_4 p_5 \; s$	1	1
$p_1 p_2 p_3^2 p_5^2 \; s$	0	1
$p_2^2 p_3 p_4^2 p_6 \; s$	1	0
$p_1 p_2 p_3 p_4 p_5 p_6 \; s$	0	0
$p_1^2 p_3 p_5^2 p_6 \; s$	-1	0
$p_1 p_2 p_4^2 p_6^2 \; s$	0	-1
$p_1^2 p_4 p_5 p_6^2 \; s$	-1	-1
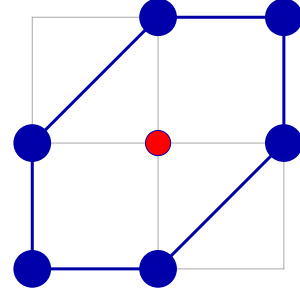
Figure 3.22: The generators and lattice of generators of the mesonic moduli space of Model 10a in terms of GLSM fields with the corresponding flavor charges.

Generator	$U(1)_{f_1}$	$U(1)_{f_2}$
$X_{14}X_{43}X_{32}X_{21} = X_{14}X_{43}X_{35}X_{56}X_{61}$	1	1
$X_{14}X_{45}X_{56}X_{61} = X_{14}X_{43}X_{32}X_{26}X_{61}$	0	1
$X_{35}X_{56}X_{64}X_{43} = X_{14}X_{43}X_{35}X_{52}X_{21}$	1	0
$X_{14}X_{43}X_{35}X_{52}X_{26}X_{61} = X_{13}X_{32}X_{21} = X_{45}X_{56}X_{64} = X_{13}X_{35}X_{56}X_{61} = X_{14}X_{45}X_{52}X_{21} = X_{26}X_{64}X_{43}X_{32}$	0	0
$X_{13}X_{32}X_{26}X_{61} = X_{14}X_{45}X_{52}X_{26}X_{61}$	-1	0
$X_{13}X_{35}X_{52}X_{21} = X_{26}X_{64}X_{43}X_{35}X_{52}$	0	-1
$X_{26}X_{64}X_{45}X_{52} = X_{13}X_{35}X_{52}X_{26}X_{61}$	-1	-1

Figure 3.23: The generators in terms of bifundamental fields (Model 10a).

plethystic logarithm are expressed as

$$
\begin{aligned}
g_1(t, f_1, f_2; \mathcal{M}_{10a}^{mes}) = &\left(1 + t^6 - \left(2 + \frac{1}{f_1} + f_1 + \frac{1}{f_2} + \frac{1}{f_1 f_2} + f_2 + f_1 f_2\right) t^{12}\right. \\
&\left. + \left(2 + \frac{1}{f_1} + f_1 + \frac{1}{f_2} + \frac{1}{f_1 f_2} + f_2 + f_1 f_2\right) t^{18} - t^{24} - t^{30}\right) \times \\
&\frac{1}{\left(1 - \frac{1}{f_1}t^6\right)\left(1 - f_1 t^6\right)\left(1 - \frac{1}{f_2}t^6\right)\left(1 - \frac{1}{f_1 f_2}t^6\right)(1 - f_2 t^6)(1 - f_1 f_2 t^6)}
\end{aligned}
$$
(3.12.176)

and

$$
\begin{aligned}
PL[g_1(t, f_1, f_2; \mathcal{M}_{10a}^{mes})] = &\left(1 + \frac{1}{f_1} + f_1 + \frac{1}{f_2} + f_2 + \frac{1}{f_1 f_2} + f_1 f_2\right)t^6 \\
&- \left(3 + \frac{1}{f_1} + f_1 + \frac{1}{f_2} + f_2 + \frac{1}{f_1 f_2} + f_1 f_2\right)t^{12} + 2\left(2 + \frac{1}{f_1} + f_1 + \frac{1}{f_2} + f_2\right. \\
&\left. + \frac{1}{f_1 f_2} + f_1 f_2\right)t^{18} + \dots \; .
\end{aligned}
$$
(3.12.177)

The above plethystic logarithm exhibits both the moduli space generators and the corresponding mesonic charges. They are summarized in Table 3.22. The generators can be presented on a charge lattice. The convex polygon formed by the generators in Table 3.22 is the dual reflexive polygon of the toric diagram of Model 10a.
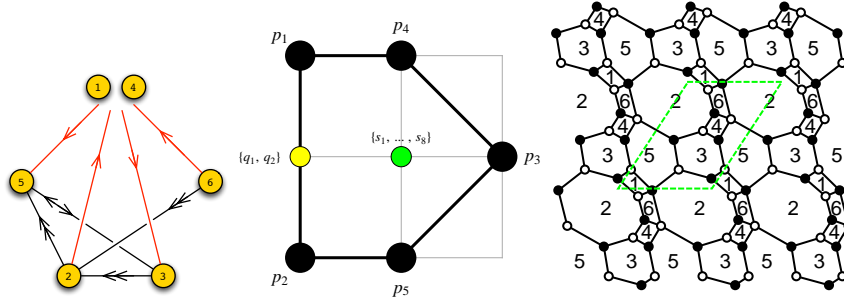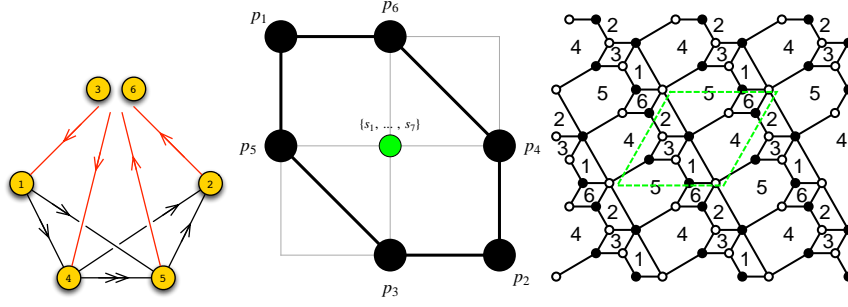
Figure 3.24: The quiver, toric diagram and brane tiling of Model 10b. The red arrows in the quiver indicate all possible connections between blocks of nodes.

Under the following fugacity map

$$T_1 = \frac{t^6}{f_1 f_2} = y_s \; t_1^2 t_4 t_5 t_6^2 \; , \; T_2 = f_1 = \frac{t_2 t_4}{t_1 t_5} \; , \; T_3 = f_2 = \frac{t_3 t_5}{t_4 t_6} \; , \tag{3.12.178}$$

the mesonic Hilbert series and the plethystic logarithm can be rewritten as

$$g_1(T_1, T_2, T_3; \mathcal{M}_{10a}^{mes}) = \big(1 + T_1 T_2 T_3 - (2T_1^2 T_2^2 T_3^2 + T_1^2 T_2 T_3^2 + T_1^2 T_2^3 T_3^2 + T_1^2 T_2^2 T_3$$
$$+ T_1^2 T_2 T_3 + T_1^2 T_2^2 T_3^3 + T_1^2 T_2^3 T_3^3) + (2T_1^3 T_2^3 T_3^3 + T_1^3 T_2^2 T_3^3 + T_1^3 T_2^4 T_3^3 + T_1^3 T_2^3 T_3^2$$
$$+ T_1^3 T_2^2 T_3^2 + T_1^3 T_2^3 T_3^4 + T_1^3 T_2^4 T_3^4) - T_1^4 T_2^4 T_3^4 - T_1^5 T_2^5 T_3^5\big) \times$$
$$\frac{1}{(1 - T_1 T_3)(1 - T_1 T_2^2 T_3)(1 - T_1 T_2)(1 - T_1)(1 - T_1 T_2 T_3^2)(1 - T_1 T_2^2 T_3^2)} \tag{3.12.179}$$

and

$$PL[g_1(t, f_1, f_2; \mathcal{M}_{10a}^{mes})] = T_1 T_2 T_3 + T_1 T_3 + T_1 T_2^2 T_3 + T_1 T_2 + T_1 T_2 T_3^2 + T_1 + T_1 T_2^2 T_3^2$$
$$- (3T_1^2 T_2^2 T_3^2 + T_1^2 T_2 T_3^2 + T_1^2 T_2^3 T_3^2 + T_1^2 T_2^2 T_3 + T_1^2 T_2^2 T_3^3 + T_1^2 T_2 T_3 + T_1^2 T_2^3 T_3^3)$$
$$+ 4T_1^3 T_2^3 T_3^3 + T_1^3 T_2^2 T_3^3 + T_1^3 T_2^4 T_3^3 + T_1^3 T_2^3 T_3^2 + T_1^3 T_2^3 T_3^4 + T_1^3 T_2^2 T_3^2 + T_1^3 T_2^4 T_3^4 + \dots$$
$$\tag{3.12.180}$$

such that the powers of the fugacities are all positive indicating the cone structure of the variety.

3.12.2 Model 10 Phase b

The superpotential is

$$
\begin{aligned}
W \;=\; & +X_{31}X_{15}X_{53} + X_{42}X_{23}X_{34} + X_{56}X_{64}X_{45}^2 + X_{52}X_{26}X_{61}X_{14}X_{45}^1 \\
& -X_{42}X_{26}X_{64} - X_{53}X_{34}X_{45}^1 - X_{56}X_{61}X_{15} - X_{14}X_{45}^2 X_{52}X_{23}X_{31} \;.
\end{aligned}
\tag{3.12.181}
$$

The perfect matching matrix is

$$
P = \left(
\begin{array}{c|cccccc|ccccccc}
 & p_1 & p_2 & p_3 & p_4 & p_5 & p_6 & s_1 & s_2 & s_3 & s_4 & s_5 & s_6 & s_7 \\
\hline
X_{45}^2 & 1 & 0 & 0 & 0 & 0 & 1 & 0 & 0 & 0 & 0 & 1 & 0 & 0 \\
X_{15} & 1 & 0 & 1 & 0 & 1 & 0 & 0 & 0 & 0 & 0 & 1 & 1 & 0 \\
X_{34} & 1 & 0 & 0 & 0 & 1 & 0 & 1 & 0 & 1 & 0 & 0 & 1 & 0 \\
X_{26} & 1 & 0 & 0 & 0 & 0 & 0 & 1 & 0 & 0 & 1 & 0 & 0 & 0 \\
X_{42} & 0 & 1 & 0 & 1 & 0 & 1 & 0 & 0 & 0 & 0 & 1 & 0 & 1 \\
X_{56} & 0 & 1 & 0 & 1 & 0 & 0 & 1 & 0 & 0 & 1 & 0 & 0 & 1 \\
X_{45}^1 & 0 & 1 & 1 & 0 & 0 & 0 & 0 & 0 & 0 & 0 & 1 & 0 & 0 \\
X_{31} & 0 & 1 & 0 & 0 & 0 & 0 & 1 & 0 & 1 & 0 & 0 & 0 & 0 \\
X_{64} & 0 & 0 & 1 & 0 & 1 & 0 & 0 & 1 & 1 & 0 & 0 & 1 & 0 \\
X_{23} & 0 & 0 & 1 & 0 & 0 & 0 & 0 & 1 & 0 & 1 & 0 & 0 & 0 \\
X_{53} & 0 & 0 & 0 & 1 & 0 & 1 & 0 & 1 & 0 & 1 & 0 & 0 & 1 \\
X_{14} & 0 & 0 & 0 & 1 & 0 & 0 & 0 & 0 & 0 & 0 & 0 & 1 & 0 \\
X_{52} & 0 & 0 & 0 & 0 & 1 & 0 & 0 & 0 & 0 & 0 & 0 & 0 & 1 \\
X_{61} & 0 & 0 & 0 & 0 & 0 & 1 & 0 & 1 & 1 & 0 & 0 & 0 & 0 \\
\end{array}
\right) .
\tag{3.12.182}
$$

The F-term charge matrix $Q_F = \ker(P)$ is

$$
Q_F = \left(
\begin{array}{cccccc|ccccccc}
p_1 & p_2 & p_3 & p_4 & p_5 & p_6 & s_1 & s_2 & s_3 & s_4 & s_5 & s_6 & s_7 \\
\hline
1 & 1 & 0 & 0 & 0 & 0 & -1 & 0 & 0 & 0 & -1 & 0 & 0 \\
1 & 0 & 1 & 0 & -1 & 0 & 0 & 0 & 0 & -1 & -1 & 0 & 1 \\
1 & 0 & 0 & 1 & 0 & -1 & -1 & 0 & 1 & 0 & 0 & -1 & 0 \\
0 & 0 & 0 & 1 & 1 & 0 & 0 & 0 & 0 & 0 & 0 & -1 & -1 \\
0 & 0 & 0 & 0 & 0 & 0 & 1 & 1 & -1 & -1 & 0 & 0 & 0 \\
\end{array}
\right) .
\tag{3.12.183}
$$

The D-term charge matrix is

$$
Q_D = \left(
\begin{array}{cccccc|ccccccc}
p_1 & p_2 & p_3 & p_4 & p_5 & p_6 & s_1 & s_2 & s_3 & s_4 & s_5 & s_6 & s_7 \\
\hline
0 & 0 & 0 & 0 & 0 & 0 & 0 & 1 & -1 & 0 & 0 & 0 & 0 \\
0 & 0 & 0 & 0 & 0 & 0 & 0 & 0 & 1 & -1 & 0 & 0 & 0 \\
0 & 0 & 0 & 0 & 0 & 0 & 0 & 0 & 0 & 1 & -1 & 0 & 0 \\
0 & 0 & 0 & 0 & 0 & 0 & 0 & 0 & 0 & 0 & 1 & -1 & 0 \\
0 & 0 & 0 & 0 & 0 & 0 & 0 & 0 & 0 & 0 & 0 & 1 & -1 \\
\end{array}
\right) .
\tag{3.12.184}
$$

The total charge matrix Q_t does not exhibit repeated columns. Accordingly, the global symmetry of Model 10b is identical to the one for Model 10a, $U(1)_{f_1} \times U(1)_{f_2} \times U(1)_R$. The flavour and R-charges on the extremal perfect matchings are found following the discussion in §3.2.3. They are identical to Model 10a, and are shown in Table 3.39.

Generator	$U(1)_{f_1}$	$U(1)_{f_2}$
$X_{15}X_{52}X_{23}X_{31} = X_{23}X_{34}X^1_{45}X_{52} = X_{26}X_{64}X^1_{45}X_{52}$	1	1
$X_{15}X_{52}X_{26}X_{61} = X_{23}X_{34}X^2_{45}X_{52} = X_{26}X_{64}X^2_{45}X_{52}$	0	1
$X^1_{45}X_{56}X_{64} = X_{14}X^1_{45}X_{52}X_{23}X_{31}$	1	0
$X_{14}X^2_{45}X_{52}X_{23}X_{31} = X_{14}X^1_{45}X_{52}X_{26}X_{61} = X_{15}X_{53}X_{31} = X_{15}X_{56}X_{61} = X_{23}X_{34}X_{42} = X_{26}X_{64}X_{42} = X_{34}X^1_{45}X_{53} = X^2_{45}X_{56}X_{64}$	0	0
$X_{34}X^2_{45}X_{53} = X_{14}X^2_{45}X_{52}X_{26}X_{61}$	-1	0
$X_{14}X_{42}X_{23}X_{31} = X_{14}X^1_{45}X_{53}X_{31} = X_{14}X^1_{45}X_{56}X_{61}$	0	-1
$X_{14}X_{42}X_{26}X_{61} = X_{14}X^2_{45}X_{53}X_{31} = X_{14}X^2_{45}X_{56}X_{61}$	-1	-1

Table 3.40: The generators in terms of bifundamental fields (Model 10b).
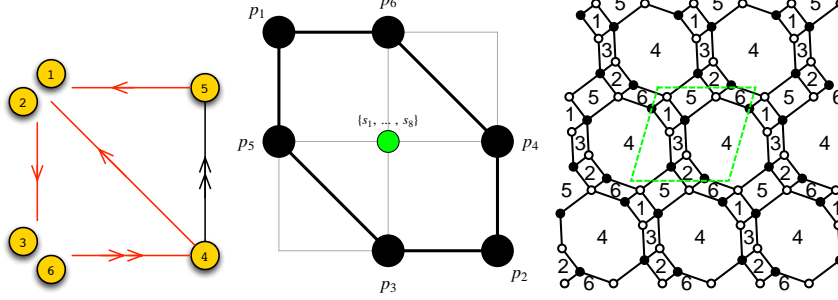
Figure 3.25: The quiver, toric diagram, and brane tiling of Model 10c. The red arrows in the quiver indicate all possible connections between blocks of nodes.

The product of all internal perfect matchings is given by the variable

$$s = \prod_{m=1}^{7} s_m \ . \tag{3.12.185}$$

The fugacity for extremal perfect matchings p_α is t_α and the fugacity for the above product of internal perfect matchings is y_s.

The mesonic Hilbert series of Model 10a and 10b are identical. They are called phases of the same toric moduli space. The Hilbert series is found in (3.12.173) with the plethystic logarithm in (3.12.174). The moduli space is not a complete intersection.

The generators of the mesonic moduli space in terms of the perfect matchings of Model 10b are shown in Table 3.22. The generators in terms of quiver fields of Model 10b are shown in Table 3.23. The charge lattice of generators is the dual reflexive polygon of the toric diagram of Model 10b.

3.12.3 Model 10 Phase c

The superpotential is

$$
\begin{aligned}
W \ = \ & +X_{41}X_{13}X^2_{34} + X_{42}X_{23}X^1_{34} + X^1_{45}X_{52}X_{26}X^2_{64} + X_{51}X_{16}X^1_{64}X^2_{45} \\
& -X_{41}X_{16}X^2_{64} - X_{42}X_{26}X^1_{64} - X^2_{45}X_{52}X_{23}X^2_{34} - X_{51}X_{13}X^1_{34}X^1_{45} \ .
\end{aligned}
$$

$$\tag{3.12.186}$$

The perfect matching matrix is

$$
P = \left(\begin{array}{c|cccccc|cccccccc}
 & p_1 & p_2 & p_3 & p_4 & p_5 & p_6 & s_1 & s_2 & s_3 & s_4 & s_5 & s_6 & s_7 & s_8 \\
\hline
X_{42} & 1 & 0 & 0 & 0 & 1 & 1 & 0 & 0 & 1 & 0 & 1 & 1 & 0 & 0 \\
X_{34}^2 & 1 & 0 & 0 & 0 & 1 & 0 & 0 & 1 & 0 & 0 & 0 & 0 & 0 & 1 \\
X_{64}^2 & 1 & 0 & 0 & 0 & 0 & 1 & 0 & 0 & 0 & 0 & 0 & 0 & 1 & 1 \\
X_{51} & 1 & 0 & 0 & 0 & 0 & 0 & 0 & 0 & 0 & 1 & 0 & 1 & 0 & 0 \\
X_{41} & 0 & 1 & 1 & 1 & 0 & 0 & 0 & 0 & 1 & 1 & 0 & 1 & 0 & 0 \\
X_{64}^1 & 0 & 1 & 1 & 0 & 0 & 0 & 0 & 0 & 0 & 0 & 0 & 0 & 1 & 1 \\
X_{34}^1 & 0 & 1 & 0 & 1 & 0 & 0 & 0 & 1 & 0 & 0 & 0 & 0 & 0 & 1 \\
X_{52} & 0 & 1 & 0 & 0 & 0 & 0 & 0 & 0 & 0 & 0 & 1 & 1 & 0 & 0 \\
X_{45}^1 & 0 & 0 & 1 & 0 & 1 & 0 & 0 & 0 & 1 & 0 & 0 & 0 & 0 & 0 \\
X_{23} & 0 & 0 & 1 & 0 & 0 & 0 & 1 & 0 & 0 & 1 & 0 & 0 & 1 & 0 \\
X_{45}^2 & 0 & 0 & 0 & 1 & 0 & 1 & 0 & 0 & 1 & 0 & 0 & 0 & 0 & 0 \\
X_{26} & 0 & 0 & 0 & 1 & 0 & 0 & 1 & 1 & 0 & 1 & 0 & 0 & 0 & 0 \\
X_{16} & 0 & 0 & 0 & 0 & 1 & 0 & 1 & 1 & 0 & 0 & 1 & 0 & 0 & 0 \\
X_{13} & 0 & 0 & 0 & 0 & 0 & 1 & 1 & 0 & 0 & 0 & 1 & 0 & 1 & 0 \\
\end{array}\right). \tag{3.12.187}
$$

The F-term charge matrix $Q_F = \ker(P)$ is

$$
Q_F = \left(\begin{array}{cccccc|cccccccc}
p_1 & p_2 & p_3 & p_4 & p_5 & p_6 & s_1 & s_2 & s_3 & s_4 & s_5 & s_6 & s_7 & s_8 \\
\hline
1 & 1 & 0 & 0 & 0 & 0 & 0 & 0 & 0 & 0 & 0 & -1 & 0 & -1 \\
1 & 0 & 0 & 1 & 0 & -1 & 0 & -1 & 0 & 0 & 1 & -1 & 0 & 0 \\
0 & 0 & 1 & 0 & 0 & 1 & 0 & 0 & -1 & 0 & 0 & 0 & -1 & 0 \\
0 & 0 & 0 & 1 & 1 & 0 & 0 & -1 & -1 & 0 & 0 & 0 & 0 & 0 \\
0 & 0 & 0 & 0 & 0 & 0 & 1 & -1 & 0 & 0 & 0 & 0 & -1 & 1 \\
0 & 0 & 0 & 0 & 0 & 0 & 1 & 0 & 0 & -1 & -1 & 1 & 0 & 0 \\
\end{array}\right). \tag{3.12.188}
$$

The D-term charge matrix is

$$
Q_D = \left(\begin{array}{cccccc|cccccccc}
p_1 & p_2 & p_3 & p_4 & p_5 & p_6 & s_1 & s_2 & s_3 & s_4 & s_5 & s_6 & s_7 & s_8 \\
\hline
0 & 0 & 0 & 0 & 0 & 0 & 0 & 0 & 1 & -1 & 0 & 0 & 0 & 0 \\
0 & 0 & 0 & 0 & 0 & 0 & 0 & 0 & 0 & 1 & -1 & 0 & 0 & 0 \\
0 & 0 & 0 & 0 & 0 & 0 & 0 & 0 & 0 & 0 & 1 & -1 & 0 & 0 \\
0 & 0 & 0 & 0 & 0 & 0 & 0 & 0 & 0 & 0 & 0 & 1 & -1 & 0 \\
0 & 0 & 0 & 0 & 0 & 0 & 0 & 0 & 0 & 0 & 0 & 0 & 1 & -1 \\
\end{array}\right). \tag{3.12.189}
$$

The global symmetry for Model 10c is identical to the global symmetries of Model 10a and Model 10b, $U(1)_{f_1} \times U(1)_{f_2} \times U(1)_R$. The mesonic charges on the extremal perfect matchings with non-zero R-charge are shown in Table 3.39.

The product of all internal perfect matchings is expressed as

$$
s = \prod_{m=1}^{8} s_m . \tag{3.12.190}
$$

The fugacity t_α counts extremal perfect matchings and the fugacity y_s counts the above product of internal perfect matchings.

The mesonic Hilbert series is identical to the Hilbert series for Models 10a and 10b in (3.12.172).

The moduli space generators in terms of all perfect matchings of Model 10c are shown in Table 3.22, with the corresponding lattice of generators being the dual reflexive

Generator	$U(1)_{f_1}$	$U(1)_{f_2}$
$X_{16}X_{64}^1 X_{41} = X_{23}X_{34}^1 X_{45}^1 X_{52} = X_{26}X_{64}^1 X_{45}^1 X_{52}$	1	1
$X_{13}X_{34}^1 X_{41} = X_{23}X_{34}^1 X_{45}^2 X_{52} = X_{26}X_{64}^1 X_{45}^2 X_{52}$	0	1
$X_{16}X_{64}^1 X_{45}^1 X_{51} = X_{23}X_{34}^2 X_{45}^1 X_{52}$	1	0
$X_{13}X_{34}^2 X_{41} = X_{16}X_{64}^2 X_{41} = X_{23}X_{34}^1 X_{42} = X_{26}X_{64}^1 X_{42}$ $= X_{13}X_{34}^1 X_{45}^1 X_{51} = X_{16}X_{64}^1 X_{45}^2 X_{51} = X_{23}X_{34}^2 X_{45}^2 X_{52} = X_{26}X_{64}^2 X_{45}^1 X_{52}$	0	0
$X_{13}X_{34}^1 X_{45}^2 X_{51} = X_{26}X_{64}^2 X_{45}^2 X_{52}$	-1	0
$X_{23}X_{34}^2 X_{42} = X_{13}X_{34}^2 X_{45}^1 X_{51} = X_{16}X_{64}^2 X_{45}^1 X_{51}$	0	-1
$X_{26}X_{64}^2 X_{42} = X_{13}X_{34}^2 X_{45}^2 X_{51} = X_{16}X_{64}^2 X_{45}^2 X_{51}$	-1	-1

Table 3.41: The generators in terms of bifundamental fields (Model 10c).
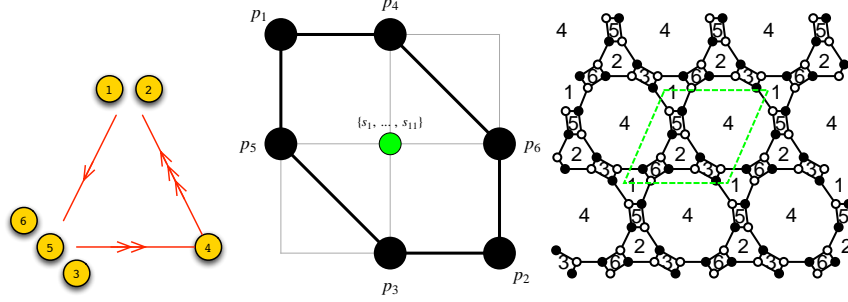
Figure 3.26: The quiver, toric diagram, and brane tiling of Model 10d. The red arrows in the quiver indicate all possible connections between blocks of nodes.

polygon of the toric diagram. The generators in terms of quiver fields of Model 10c are shown in Table 3.41.

3.12.4 Model 10 Phase d

The superpotential is

$$
\begin{aligned}
W & = +X_{15}X_{54}^1 X_{41}^2 + X_{25}X_{54}^2 X_{42}^2 + X_{26}X_{64}^2 X_{42}^3 + X_{41}^1 X_{13}X_{34}^2 \\
& \quad + X_{16}X_{64}^1 X_{41}^3 + X_{42}^1 X_{23}X_{34}^1 - X_{15}X_{54}^2 X_{41}^3 - X_{13}X_{34}^1 X_{41}^2 \\
& \quad - X_{23}X_{34}^2 X_{42}^2 - X_{25}X_{54}^1 X_{42}^3 - X_{41}^1 X_{16}X_{64}^2 - X_{42}^1 X_{26}X_{64}^1 \ .
\end{aligned}
$$

$$(3.12.191)$$

The perfect matching matrix is

$$
P = \begin{array}{c|cccccc|ccccccccccc}
 & p_1 & p_2 & p_3 & p_4 & p_5 & p_6 & s_1 & s_2 & s_3 & s_4 & s_5 & s_6 & s_7 & s_8 & s_9 & s_{10} & s_{11} \\
\hline
X_{42}^2 & 1 & 0 & 1 & 0 & 1 & 0 & 0 & 0 & 0 & 0 & 0 & 1 & 1 & 0 & 0 & 0 & 0 \\
X_{42}^3 & 1 & 0 & 0 & 1 & 0 & 1 & 0 & 0 & 0 & 0 & 0 & 1 & 1 & 0 & 0 & 0 & 0 \\
X_{41}^1 & 1 & 0 & 0 & 0 & 1 & 1 & 0 & 0 & 0 & 0 & 1 & 0 & 1 & 0 & 0 & 0 & 0 \\
X_{34} & 1 & 0 & 0 & 0 & 1 & 0 & 0 & 0 & 1 & 1 & 0 & 0 & 0 & 0 & 1 & 0 & 1 \\
X_{64} & 1 & 0 & 0 & 0 & 0 & 1 & 0 & 1 & 1 & 0 & 0 & 0 & 0 & 0 & 0 & 1 & 1 \\
X_{15} & 1 & 0 & 0 & 0 & 0 & 0 & 1 & 0 & 0 & 1 & 0 & 1 & 0 & 0 & 0 & 1 & 1 \\
X_{41}^3 & 0 & 1 & 1 & 0 & 1 & 0 & 0 & 0 & 0 & 0 & 1 & 0 & 1 & 0 & 0 & 0 & 0 \\
X_{64}^2 & 0 & 1 & 1 & 0 & 0 & 0 & 0 & 1 & 1 & 0 & 0 & 0 & 0 & 0 & 0 & 1 & 1 \\
X_{42}^1 & 0 & 1 & 1 & 1 & 0 & 0 & 0 & 0 & 0 & 0 & 0 & 1 & 1 & 0 & 0 & 0 & 0 \\
X_{41}^2 & 0 & 1 & 0 & 1 & 0 & 1 & 0 & 0 & 0 & 0 & 1 & 0 & 1 & 0 & 0 & 0 & 0 \\
X_{34}^2 & 0 & 1 & 0 & 1 & 0 & 0 & 0 & 0 & 1 & 1 & 0 & 0 & 0 & 0 & 1 & 0 & 1 \\
X_{25} & 0 & 1 & 0 & 0 & 0 & 0 & 1 & 0 & 0 & 1 & 1 & 0 & 0 & 0 & 0 & 1 & 1 \\
X_{54} & 0 & 0 & 1 & 0 & 1 & 0 & 0 & 1 & 1 & 0 & 0 & 0 & 0 & 1 & 1 & 0 & 0 \\
X_{13} & 0 & 0 & 1 & 0 & 0 & 0 & 1 & 1 & 0 & 0 & 0 & 1 & 0 & 1 & 0 & 1 & 0 \\
X_{54}^2 & 0 & 0 & 0 & 1 & 0 & 1 & 0 & 1 & 1 & 0 & 0 & 0 & 0 & 1 & 1 & 0 & 0 \\
X_{16} & 0 & 0 & 0 & 1 & 0 & 0 & 1 & 0 & 0 & 1 & 0 & 1 & 0 & 1 & 1 & 0 & 0 \\
X_{26} & 0 & 0 & 0 & 0 & 1 & 0 & 1 & 0 & 0 & 1 & 1 & 0 & 0 & 1 & 1 & 0 & 0 \\
X_{23} & 0 & 0 & 0 & 0 & 0 & 1 & 1 & 1 & 0 & 0 & 1 & 0 & 0 & 1 & 0 & 1 & 0 \\
\end{array}
\tag{3.12.192}
$$

The F-term charge matrix $Q_F = \ker(P)$ is

$$
Q_F = \begin{array}{cccccc|ccccccccccc}
p_1 & p_2 & p_3 & p_4 & p_5 & p_6 & s_1 & s_2 & s_3 & s_4 & s_5 & s_6 & s_7 & s_8 & s_9 & s_{10} & s_{11} \\
\hline
1 & 1 & 0 & -1 & -1 & 0 & 0 & 0 & 0 & 0 & 0 & 0 & 0 & 1 & 0 & -1 & 0 \\
1 & 0 & 0 & 1 & 0 & -1 & 0 & 0 & 0 & 0 & 0 & -1 & 0 & 1 & -1 & 0 & 0 \\
1 & 0 & 0 & 1 & 0 & -1 & 0 & 0 & 0 & 0 & 0 & -1 & 0 & 0 & 0 & 1 & -1 \\
0 & 1 & 0 & -1 & 0 & 1 & 0 & 0 & 0 & 1 & -1 & 0 & 0 & 0 & 0 & 0 & -1 \\
0 & 1 & 0 & -1 & 0 & 1 & 0 & 0 & 0 & 0 & 1 & -1 & 0 & 0 & -1 & 0 & 0 \\
0 & 0 & 1 & 0 & 0 & 1 & 0 & -1 & 0 & 0 & 0 & 0 & -1 & 0 & 0 & 0 & 0 \\
0 & 0 & 0 & 0 & 0 & 0 & 1 & 0 & 1 & 0 & 0 & 0 & 0 & 0 & -1 & -1 & 0 \\
0 & 0 & 0 & 0 & 0 & 0 & 0 & 1 & 0 & 1 & 0 & 0 & 0 & 0 & -1 & -1 & 0 \\
0 & 0 & 0 & 0 & 0 & 0 & 0 & 1 & -1 & 0 & 0 & 0 & 0 & 0 & 0 & -1 & 1 \\
\end{array}
\tag{3.12.193}
$$

The D-term charge matrix is

$$
Q_D = \begin{array}{cccccc|ccccccccccc}
p_1 & p_2 & p_3 & p_4 & p_5 & p_6 & s_1 & s_2 & s_3 & s_4 & s_5 & s_6 & s_7 & s_8 & s_9 & s_{10} & s_{11} \\
\hline
0 & 0 & 0 & 0 & 0 & 0 & 0 & 0 & 0 & 0 & 1 & -1 & 0 & 0 & 0 & 0 & 0 \\
0 & 0 & 0 & 0 & 0 & 0 & 0 & 0 & 0 & 0 & 0 & 1 & -1 & 0 & 0 & 0 & 0 \\
0 & 0 & 0 & 0 & 0 & 0 & 0 & 0 & 0 & 0 & 0 & 0 & 1 & -1 & 0 & 0 & 0 \\
0 & 0 & 0 & 0 & 0 & 0 & 0 & 0 & 0 & 0 & 0 & 0 & 0 & 1 & -1 & 0 & 0 \\
0 & 0 & 0 & 0 & 0 & 0 & 0 & 0 & 0 & 0 & 0 & 0 & 0 & 0 & 1 & -1 & 0 \\
\end{array}
\tag{3.12.194}
$$

The symmetry $U(1)_{f_1} \times U(1)_{f_2} \times U(1)_R$ of Model 10d is identical to Models 10a to 10c discussed above. The symmetry charges on the extremal perfect matchings with non-zero R-charges are shown in Table 3.39.

The product of all internal perfect matchings is

$$
s = \prod_{m=1}^{11} s_m \ . \tag{3.12.195}
$$

The fugacity y_s counts the above product of internal perfect matchings whereas the fugacity t_α counts the external perfect matchings p_α.

The mesonic Hilbert series of Model 10d is identical to Models 10a, 10b and 10c. This indicates that the mesonic moduli spaces are identical, and given the corresponding plethystic logarithm in (3.12.174), the mesonic moduli spaces are not complete

Generator	$U(1)_{f_1}$	$U(1)_{f_2}$
$X_{13}X_{34}^2X_{41}^3 = X_{41}^3X_{16}X_{64}^2 = X_{42}^1X_{25}X_{54}^1 = X_{42}^1X_{26}X_{64}^2$	1	1
$X_{13}X_{34}^1X_{41}^3 = X_{41}^3X_{15}X_{54}^1 = X_{42}^2X_{25}X_{54}^1 = X_{42}^2X_{26}X_{64}^2$	0	1
$X_{13}X_{34}^2X_{41}^2 = X_{41}^2X_{16}X_{64}^2 = X_{23}X_{34}^2X_{42}^1 = X_{42}^1X_{25}X_{54}^2$	1	0
$X_{13}X_{34}^1X_{41}^2 = X_{13}X_{34}^2X_{41}^1 = X_{41}^2X_{15}X_{54}^1 = X_{41}^3X_{15}X_{54}^2 = X_{41}^1X_{16}X_{64}^2 = X_{41}^3X_{16}X_{64}^1 = X_{23}X_{34}^1X_{42}^1$	0	0
$= X_{23}X_{34}^2X_{42}^2 = X_{42}^2X_{25}X_{54}^2 = X_{42}^2X_{25}X_{54}^1 = X_{42}^1X_{26}X_{64}^1 = X_{42}^3X_{26}X_{64}^2$		
$X_{13}X_{34}^1X_{41}^1 = X_{41}^1X_{15}X_{54}^1 = X_{23}X_{34}^1X_{42}^2 = X_{42}^2X_{26}X_{64}^1$	-1	0
$X_{41}^2X_{15}X_{54}^2 = X_{41}^2X_{16}X_{64}^1 = X_{23}X_{34}^2X_{42}^3 = X_{42}^3X_{25}X_{54}^2$	0	-1
$X_{41}^1X_{15}X_{54}^2 = X_{41}^1X_{16}X_{64}^1 = X_{23}X_{34}^1X_{42}^3 = X_{42}^3X_{26}X_{64}^1$	-1	-1

Figure 3.27: The generators in terms of bifundamental fields (Model 10d).
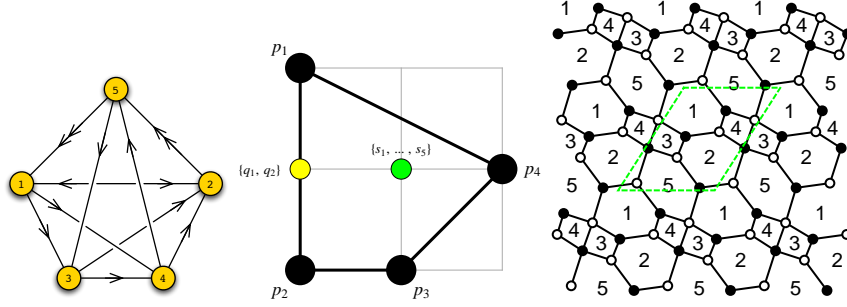
Figure 3.28: The quiver, toric diagram, and brane tiling of Model 11.

intersections.

The moduli space generators in terms of all perfect matchings of Model 10d are shown in Table 3.22 with the corresponding charge lattice of generators forming a reflexive polygon which is the dual polygon of the toric diagram. The generators in terms of quiver fields of Model 10d are shown in Table 3.27.

3.13 Model 11: PdP$_2$

The superpotential is

$$
\begin{aligned}
W &= +X_{21}X_{14}X_{42} + X_{53}X_{32}X_{25}^2 + X_{51}^2X_{12}X_{25}^1 + X_{13}X_{34}X_{45}X_{51}^1 \\
&\quad -X_{13}X_{32}X_{21} - X_{14}X_{45}X_{51}^2 - X_{51}^1X_{12}X_{25}^2 - X_{53}X_{34}X_{42}X_{25}^1 .
\end{aligned}
$$

$$(3.13.196)$$

	$U(1)_{f_1}$	$U(1)_{f_2}$	$U(1)_R$	fugacity
p_1	-1/4	-1/3	$R_1 \simeq 0.622$	t_1
p_2	-1/4	0	$R_2 \simeq 0.502$	t_2
p_3	0	2/3	$R_3 \simeq 0.306$	t_3
p_4	1/2	-1/3	$R_4 \simeq 0.570$	t_4

Table 3.42: The GLSM fields corresponding to extremal points of the toric diagram with their mesonic charges (Model 11).

The perfect matching matrix is

$$
P = \begin{pmatrix}
 & p_1 & p_2 & p_3 & p_4 & q_1 & q_2 & s_1 & s_2 & s_3 & s_4 & s_5 \\
X_{14} & 1 & 0 & 0 & 0 & 1 & 0 & 1 & 0 & 0 & 1 & 0 \\
X_{32} & 1 & 0 & 0 & 0 & 0 & 1 & 1 & 0 & 0 & 0 & 1 \\
X_{25}^1 & 1 & 0 & 0 & 0 & 1 & 0 & 0 & 1 & 0 & 0 & 0 \\
X_{25}^2 & 0 & 1 & 1 & 0 & 1 & 0 & 0 & 1 & 0 & 0 & 0 \\
X_{51}^1 & 1 & 0 & 0 & 0 & 0 & 1 & 0 & 0 & 1 & 0 & 0 \\
X_{51}^2 & 0 & 1 & 1 & 0 & 0 & 1 & 0 & 0 & 1 & 0 & 0 \\
X_{13} & 0 & 1 & 0 & 0 & 1 & 0 & 0 & 0 & 0 & 1 & 0 \\
X_{42} & 0 & 1 & 0 & 0 & 0 & 1 & 0 & 0 & 0 & 0 & 1 \\
X_{21} & 0 & 0 & 1 & 1 & 0 & 0 & 0 & 1 & 1 & 0 & 0 \\
X_{12} & 0 & 0 & 0 & 1 & 0 & 0 & 1 & 0 & 0 & 1 & 1 \\
X_{34} & 0 & 0 & 1 & 0 & 0 & 0 & 1 & 0 & 0 & 0 & 0 \\
X_{45} & 0 & 0 & 0 & 1 & 0 & 0 & 0 & 1 & 0 & 0 & 1 \\
X_{53} & 0 & 0 & 0 & 1 & 0 & 0 & 0 & 0 & 1 & 1 & 0 \\
\end{pmatrix} .
\tag{3.13.197}
$$

The F-term charge matrix $Q_F = \ker(P)$ is

$$
Q_F = \begin{pmatrix}
p_1 & p_2 & p_3 & p_4 & q_1 & q_2 & s_1 & s_2 & s_3 & s_4 & s_5 \\
1 & 1 & 0 & 0 & -1 & -1 & 0 & 0 & 0 & 0 & 0 \\
1 & 1 & 0 & 1 & -1 & 0 & 0 & 0 & -1 & 0 & -1 \\
0 & 1 & -1 & 0 & -1 & 0 & 1 & 1 & 0 & 0 & -1 \\
0 & 0 & 0 & 1 & 1 & 0 & 0 & -1 & 0 & -1 & 0 \\
\end{pmatrix} .
\tag{3.13.198}
$$

The D-term charge matrix is

$$
Q_D = \begin{pmatrix}
p_1 & p_2 & p_3 & p_4 & q_1 & q_2 & s_1 & s_2 & s_3 & s_4 & s_5 \\
0 & 0 & 0 & 0 & 0 & 0 & 1 & -1 & 0 & 0 & 0 \\
0 & 0 & 0 & 0 & 0 & 0 & 0 & 1 & -1 & 0 & 0 \\
0 & 0 & 0 & 0 & 0 & 0 & 0 & 0 & 1 & -1 & 0 \\
0 & 0 & 0 & 0 & 0 & 0 & 0 & 0 & 0 & 1 & -1 \\
\end{pmatrix} .
\tag{3.13.199}
$$

The total charge matrix Q_t does not exhibit repeated columns. Accordingly, the global symmetry is $U(1)_{f_1} \times U(1)_{f_2} \times U(1)_R$. The flavour and R-charges on the GLSM fields corresponding to extremal points in the toric diagram in Figure 3.28 are found following the discussion in §3.2.3. They are presented in Table 3.42.

Fine-tuning R-charges. The exact R-charges are expressed in terms of the root x_0 in the range $0 \leq 1 - x_0 \leq \frac{2}{3}$ of the polynomial

$$
27 - 42x - 68x^2 + 42x^3 + 9x^4 = 0,
\tag{3.13.200}
$$

where

$$
\begin{aligned}
R_1 &= 1 + \frac{1}{144}\left(-63 + 250x_0 - 422x_0^2 - 384x_0^3 + 261x_0^4 + 54x_0^5\right) \\
R_2 &= 1 + \frac{1}{72}\left(-189 + 281x_0 + 257x_0^2 - 177x_0^3 - 36x_0^4\right) \\
R_3 &= 1 + \frac{1}{288}\left(333 - 1351x_0 - 294x_0^2 + 1450x_0^3 - 327x_0^4 - 99x_0^5\right) \\
R_4 &= 1 - x_0 \ .
\end{aligned}
\tag{3.13.201}
$$

Products of non-extremal perfect matchings are assigned the following variables

$$
q = q_1 q_2 \ , \quad s = \prod_{m=1}^{5} s_m \ .
\tag{3.13.202}
$$

The fugacities y_q and y_s count respectively the above products of internal perfect matchings. The fugacity t_α counts all other extremal perfect matchings p_α.

The mesonic Hilbert series of Model 11 is found using the Molien integral formula in (1.4.67). It is

$$
\begin{aligned}
g_1(t_\alpha, y_q, y_s; \mathcal{M}_{11}^{mes}) = & (1 + y_q y_s \ t_1 t_2 t_3 t_4 + y_s^2 y_s \ t_1 t_2^3 t_3^2 + y_q^2 y_s \ t_1^2 t_2^2 t_3 - y_q^2 y_s^2 \ t_1^2 t_2^2 t_3^2 t_4^2 \\
& - y_q^2 y_s^2 \ t_1^3 t_2 t_3 t_4^2 - y_q^3 y_s^2 \ t_1^3 t_2^3 t_3^2 t_4 - y_q^3 y_s^2 \ t_1^4 t_2^2 t_3 t_4 - y_q^3 y_s^3 \ t_1^4 t_2^4 t_3^3 t_4^2 + y_q y_s \ t_2^2 t_3^2 t_4) \\
& \times \frac{1}{(1 - y_q^2 y_s \ t_1^3 t_2)(1 - y_q^2 y_s \ t_2^4 t_3^3)(1 - y_q y_s \ t_1^2 t_4)(1 - y_s \ t_3 t_4^2)} \ .
\end{aligned}
\tag{3.13.203}
$$

The plethystic logarithm of the mesonic Hilbert series is

$$
\begin{aligned}
PL[g_1(t_\alpha, y_q, y_s; \mathcal{M}_{11}^{mes})] = & \ y_q y_s \ t_1^2 t_4 + y_s \ t_3 t_4^2 + y_q^2 y_s \ t_1^3 t_2 + y_q y_s \ t_1 t_2 t_3 t_4 \\
& + y_q^2 y_s \ t_1^2 t_2^2 t_3 + y_q y_s \ t_2^2 t_3^2 t_4 + y_q^2 y_s \ t_1 t_2^3 t_3^2 + y_q^2 y_s \ t_2^4 t_3^3 - y_q^2 y_s^2 \ t_1^3 t_2 t_3 t_4^2 \\
& - y_q^3 y_s^2 \ t_1^4 t_2^2 t_3 t_4 - 2 \ y_q^2 y_s^2 \ t_1^2 t_2^2 t_3^2 t_4^2 + \dots \ .
\end{aligned}
\tag{3.13.204}
$$

Consider the following fugacity map

$$
\begin{aligned}
& f_1 = y_q^{-3/4} y_s^{1/4} \ , \quad f_2 = y_q^{-1/4} y_s^{-1/4} \ , \\
& \tilde{t}_1 = y_q^{1/4} y_s^{1/4} \ t_1 \ , \quad \tilde{t}_2 = y_q^{1/4} y_s^{1/4} \ t_2 \ , \quad \tilde{t}_3 = y_q^{1/4} y_s^{1/4} \ t_3 \ , \quad \tilde{t}_4 = y_q^{1/4} y_s^{1/4} \ t_4 \ ,
\end{aligned}
\tag{3.13.205}
$$

where the fugacities f_1 and f_2 count flavour charges, and the fugacity $\tilde{t}_i$ counts the R-charge R_i in Table 3.42.

Generator	$U(1)_{f_1}$	$U(1)_{f_2}$
$p_3 p_4^2\ s$	1	0
$p_1^2 p_4\ q\ s$	0	-1
$p_1 p_2 p_3 p_4\ q\ s$	0	0
$p_2^2 p_3^2 p_4\ q\ s$	0	1
$p_1^3 p_2\ q^2\ s$	-1	-1
$p_1^2 p_2^2 p_3\ q^2\ s$	-1	0
$p_1 p_2^3 p_3^2\ q^2\ s$	-1	1
$p_2^4 p_3^3\ q^2\ s$	-1	2
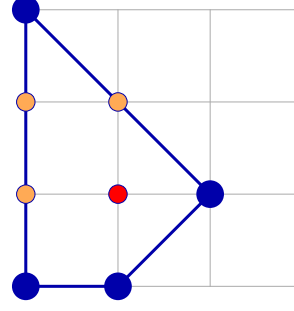
Table 3.43: The generators and lattice of generators of the mesonic moduli space of Model 11 in terms of GLSM fields with the corresponding flavor charges.

Generator	$U(1)_{f_1}$	$U(1)_{f_2}$
$X_{12}X_{21} = X_{34}X_{45}X_{53}$	1	0
$X_{12}X_{25}^1 X_{51}^1 = X_{14}X_{45}X_{51}^1 = X_{32}X_{25}^1 X_{53}$	0	-1
$X_{13}X_{34}X_{45}X_{51}^1 = X_{34}X_{25}^1 X_{53}X_{42} = X_{12}X_{25}^1 X_{51}^2 = X_{12}X_{25}^2 X_{51}^1$	0	0
$= X_{21}X_{13}X_{32} = X_{21}X_{14}X_{42} = X_{14}X_{45}X_{51}^2 = X_{32}X_{25}^2 X_{53}$		
$X_{12}X_{25}^2 X_{51}^2 = X_{21}X_{13}X_{34}X_{42} = X_{13}X_{34}X_{45}X_{51}^2 = X_{34}X_{25}^2 X_{53}X_{42}$	0	1
$X_{25}^1 X_{51}^1 X_{13}X_{32} = X_{25}^1 X_{51}^1 X_{14}X_{42}$	-1	-1
$X_{25}^1 X_{51}^1 X_{13}X_{34}X_{42} = X_{25}^2 X_{51}^1 X_{13}X_{32} = X_{25}^1 X_{51}^2 X_{13}X_{32} = X_{25}^2 X_{51}^1 X_{14}X_{42} = X_{25}^1 X_{51}^2 X_{14}X_{42}$	-1	0
$X_{25}^2 X_{51}^2 X_{13}X_{32} = X_{25}^2 X_{51}^2 X_{14}X_{42} = X_{25}^1 X_{51}^2 X_{13}X_{34}X_{42} = X_{25}^2 X_{51}^1 X_{13}X_{34}X_{42}$	-1	1
$X_{25}^2 X_{51}^2 X_{13}X_{34}X_{42}$	-1	2

Table 3.44: The generators in terms of bifundamental fields (Model 11).

Under the fugacity map above, the plethystic logarithm becomes

$$PL[g_1(\tilde{t}_\alpha, f_1, f_2; \mathcal{M}_{11}^{mes})] = \frac{1}{f_2}\tilde{t}_1^2\tilde{t}_4 + f_1\tilde{t}_3\tilde{t}_4^2 + \frac{1}{f_1 f_2}\tilde{t}_1^3\tilde{t}_2 + \tilde{t}_1\tilde{t}_2\tilde{t}_3\tilde{t}_4 + \frac{1}{f_1}\tilde{t}_1^2\tilde{t}_2^2\tilde{t}_3$$

$$+f_2\tilde{t}_2^2\tilde{t}_3^2\tilde{t}_4 + \frac{f_2}{f_1}\tilde{t}_1\tilde{t}_2^3\tilde{t}_3^2 + \frac{f_2^2}{f_1}\tilde{t}_2^4\tilde{t}_3^3 - \frac{1}{f_2}\tilde{t}_1^3\tilde{t}_2\tilde{t}_3\tilde{t}_4^2 - \frac{1}{f_1 f_2}\tilde{t}_1^4\tilde{t}_2^2\tilde{t}_3\tilde{t}_4 - 2\tilde{t}_1^2\tilde{t}_2^2\tilde{t}_3^2\tilde{t}_4^2 + \dots .$$

$$(3.13.206)$$

The plethsytic logarithm above exhibits the moduli space generators with the corresponding mesonic charges. They are summarized in Table 3.43. The generators can be presented on a charge lattice. The convex polygon formed by the generators in Table 3.43 is the dual reflexive polygon of the toric diagram of Model 11.

The mesonic Hilbert series and the plethystic logarithm can be re-expressed in terms of just 3 fugacities

$$T_1 = \frac{f_2\ \tilde{t}_2}{f_1\ \tilde{t}_1\tilde{t}_4^2} = \frac{t_2}{y_s\ t_1 t_4^2} \ , \quad T_2 = \frac{1}{f_2}\ \tilde{t}_1^2\tilde{t}_4 = y_q y_s\ t_1^2 t_4 \ , \quad T_3 = f_1\ \tilde{t}_3\tilde{t}_4^2 = y_s\ t_3 t_4^2 \ ,$$

$$(3.13.207)$$
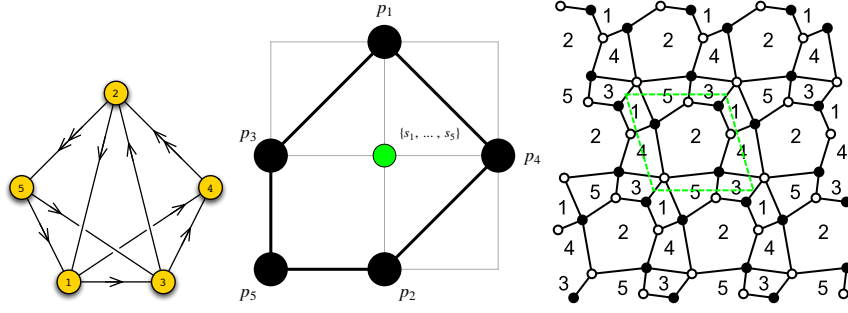
Figure 3.29: The quiver, toric diagram, and brane tiling of Model 12a.

such that

$$
g_1(T_1, T_2, T_3; \mathcal{M}_{11}^{mes}) =
$$
$$
(1 + T_1 T_2 T_3 + T_1^3 T_2^2 T_3^2 + T_1^2 T_2^2 T_3 - T_1^2 T_2^2 T_3^2 - T_1 T_2^2 T_3 - T_1^3 T_2^3 T_3^2 - T_1^2 T_2^3 T_3
$$
$$
-T_1^4 T_2^4 T_3^3 + T_1^2 T_2 T_3^2) \times \frac{1}{(1 - T_1 T_2^2)(1 - T_1^4 T_2^2 T_3^3)(1 - T_2)(1 - T_3)}
$$

$$
(3.13.208)
$$

and

$$
PL[g_1(T_1, T_2, T_3; \mathcal{M}_{11}^{mes})] = T_2 + T_3 + T_1 T_2^2 + T_1 T_2 T_3 + T_1^2 T_2^2 T_3 + T_1^2 T_2 T_3^2
$$
$$
+T_1^3 T_2^2 T_3^2 + T_1^4 T_2^2 T_3^3 - T_1^2 T_2^3 T_3 - T_1 T_2^2 T_3 + 2T_1^2 T_2^2 T_3^2 + \dots \,.
$$

$$
(3.13.209)
$$

The powers of the fugacities in the Hilbert series and plethystic logarithm above are all positive. This illustrates the conical structure of the toric Calabi-Yau 3-fold.

3.14 Model 12: dP$_2$

3.14.1 Model 12 Phase a

The superpotential is

$$
\begin{aligned}
W \;=\; & +X_{21}X_{14}X_{42}^1 + X_{25}^2 X_{53} X_{32} + X_{42}^2 X_{25}^1 X_{51} X_{13} X_{34} \\
& -X_{13} X_{32} X_{21} - X_{14} X_{42}^2 X_{25}^2 X_{51} - X_{25}^1 X_{53} X_{34} X_{42}^1 \,.
\end{aligned}
$$

$$
(3.14.210)
$$

	$U(1)_{f_1}$	$U(1)_{f_2}$	$U(1)_R$	fugacity
p_1	1/2	0	$R_1 = \frac{1}{16}\left(-21 + 5\sqrt{33}\right)$	t_1
p_2	-1/2	0	$R_2 = \frac{3}{16}\left(19 - 3\sqrt{33}\right)$	t_2
p_3	0	-1/2	$R_2 = \frac{3}{16}\left(19 - 3\sqrt{33}\right)$	t_3
p_4	0	1/2	$R_1 = \frac{1}{16}\left(-21 + 5\sqrt{33}\right)$	t_4
p_5	0	0	$R_3 = \frac{1}{2}\left(-5 + \sqrt{33}\right)$	t_5

Table 3.45: The GLSM fields corresponding to extremal points of the toric diagram with their mesonic charges (Model 12a). The R-charges are obtained using a-maximization [13].

The perfect matching matrix is

$$
P = \begin{pmatrix}
 & p_1 & p_2 & p_3 & p_4 & p_5 & s_1 & s_2 & s_3 & s_4 & s_5 \\
\hline
X_{14} & 1 & 0 & 0 & 0 & 0 & 1 & 0 & 0 & 0 & 1 \\
X_{34} & 0 & 1 & 0 & 0 & 0 & 1 & 0 & 0 & 0 & 0 \\
X_{25}^1 & 1 & 0 & 0 & 0 & 0 & 0 & 1 & 0 & 0 & 0 \\
X_{25}^2 & 0 & 1 & 0 & 0 & 1 & 0 & 1 & 0 & 0 & 0 \\
X_{42}^1 & 0 & 0 & 1 & 0 & 1 & 0 & 0 & 1 & 0 & 0 \\
X_{42}^2 & 0 & 0 & 0 & 1 & 0 & 0 & 0 & 1 & 0 & 0 \\
X_{32} & 1 & 0 & 1 & 0 & 0 & 1 & 0 & 1 & 0 & 0 \\
X_{21} & 0 & 1 & 0 & 1 & 0 & 0 & 1 & 0 & 1 & 0 \\
X_{51} & 0 & 0 & 1 & 0 & 0 & 0 & 0 & 0 & 1 & 0 \\
X_{53} & 0 & 0 & 0 & 1 & 0 & 0 & 0 & 0 & 1 & 1 \\
X_{13} & 0 & 0 & 0 & 0 & 1 & 0 & 0 & 0 & 0 & 1
\end{pmatrix} . \tag{3.14.211}
$$

The F-term charge matrix $Q_F = \ker(P)$ is

$$
Q_F = \begin{pmatrix}
p_1 & p_2 & p_3 & p_4 & p_5 & s_1 & s_2 & s_3 & s_4 & s_5 \\
\hline
1 & 1 & 0 & 0 & 0 & -1 & -1 & 0 & 0 & 0 \\
0 & 0 & 1 & 1 & 0 & 0 & 0 & -1 & -1 & 0 \\
0 & 1 & 0 & -1 & -1 & -1 & 0 & 1 & 0 & 1
\end{pmatrix} . \tag{3.14.212}
$$

The D-term charge matrix is

$$
Q_D = \begin{pmatrix}
p_1 & p_2 & p_3 & p_4 & p_5 & s_1 & s_2 & s_3 & s_4 & s_5 \\
\hline
0 & 0 & 0 & 0 & 0 & 1 & -1 & 0 & 0 & 0 \\
0 & 0 & 0 & 0 & 0 & 0 & 1 & -1 & 0 & 0 \\
0 & 0 & 0 & 0 & 0 & 0 & 0 & 1 & -1 & 0 \\
0 & 0 & 0 & 0 & 0 & 0 & 0 & 0 & 1 & -1
\end{pmatrix} . \tag{3.14.213}
$$

The total charge matrix Q_t does not exhibit repeated columns. Accordingly, the global symmetry is $U(1)_{f_1} \times U(1)_{f_2} \times U(1)_R$. The mesonic charges on the extremal perfect matchings are found following the discussion in §3.2.3. They are presented in Table 3.45.

The product of all internal perfect matchings is

$$s = \prod_{m=1}^{5} s_m \ . \tag{3.14.214}$$

The above product is counted by the fugacity y_s. The extremal perfect matchings p_α are counted by t_α.

The mesonic Hilbert series of Model 12a is calculated using the Molien integral formula in (1.4.67). It is

$$g_1(t_\alpha, y_s; \mathcal{M}_{12a}^{mes}) = \frac{P(t_\alpha)}{(1 - y_s \ t_1^2 t_3 t_4)(1 - y_s \ t_1 t_2 t_4^2)(1 - y_s \ t_1^2 t_3^2 t_5)(1 - y_s \ t_2^2 t_4^2 t_5)(1 - y_s \ t_2^2 t_3^2 t_5^3)} \ , \tag{3.14.215}$$

where the numerator is the polynomial

$$
\begin{aligned}
P(t_\alpha) \ = \ & 1 + y_s \ t_1 t_2 t_3 t_4 t_5 - y_s^2 \ t_1^3 t_2 t_3^2 t_4^2 t_5 - y_s^2 \ t_1^2 t_2^2 t_3 t_4^3 t_5 + y_s \ t_1 t_2 t_3^2 t_5^2 + y_s \ t_2^2 t_3 t_4 t_5^2 \\
& - y_s^2 \ t_1^3 t_2 t_3^3 t_4 t_5^2 - 2 \ y_s^2 \ t_1^2 t_2^2 t_3^2 t_4^2 t_5^2 - y_s^2 \ t_1 t_2^3 t_3 t_4^3 t_5^2 + y_s^3 \ t_1^4 t_2^2 t_3^3 t_4^3 t_5^2 + y_s^3 \ t_1^3 t_2^3 t_3^2 t_4^4 t_5^2 \\
& - y_s^2 \ t_1^2 t_2^2 t_3^3 t_4 t_5^3 - y_s^2 \ t_1 t_2^3 t_3^2 t_4^2 t_5^3 + y_s^3 \ t_1^3 t_2^3 t_3^3 t_4^3 t_5^3 + y_s^4 \ t_1^4 t_2^4 t_3^4 t_4^4 t_5^4 \ . \tag{3.14.216}
\end{aligned}
$$

The mesonic moduli space of Model 12a is not a complete intersection. The plethystic logarithm of the mesonic Hilbert series is

$$
\begin{aligned}
PL[g_1(t_\alpha, y_s; \mathcal{M}_{12a}^{mes})] = \ & y_s \ t_1^2 t_3 t_4 + y_s \ t_1 t_2 t_4^2 + y_s \ t_1 t_2 t_3 t_4 t_5 + y_s \ t_1^2 t_3^2 t_5 + y_s \ t_2^2 t_4^2 t_5 \\
& + y_s \ t_2^2 t_3 t_4 t_5^2 + y_s \ t_1 t_2 t_3^2 t_5^2 + y_s \ t_2^2 t_3^2 t_5^3 - y_s^2 \ t_1^3 t_2 t_3^2 t_4^2 t_5 - y_s^2 \ t_1^2 t_2^2 t_3 t_4^3 t_5 \\
& - 3 \ y_s^2 \ t_1^2 t_2^2 t_3^2 t_4^2 t_5^2 - y_s^2 \ t_1^3 t_2 t_3^3 t_4 t_5^2 - y_s^2 \ t_1 t_2^3 t_3 t_4^3 t_5^2 + \dots \ . \tag{3.14.217}
\end{aligned}
$$

Consider the following fugacity map

$$f_1 = t_3 t_4 \ , \quad f_2 = \frac{t_2 t_4^2}{t_1} \ , \quad \tilde{t}_1 = y_s^{1/4} \ t_1^{1/2} \ , \quad \tilde{t}_2 = y_s^{1/4} \ t_1^{1/2} \ , \quad \tilde{t}_3 = \frac{t_2 t_3 t_4 t_5}{t_1} \ , \tag{3.14.218}$$

where f_1 and f_2 are flavour charge fugacities, and $\tilde{t}_i$ is the fugacity for R-charge R_i in Table 3.45. Under the fugacity map above, the above plethystic logarithm becomes

$$
\begin{aligned}
PL[g_1(\tilde{t}_\alpha, f_1, f_2; \mathcal{M}_{12a}^{mes})] = \ & (f_1 + f_2) \tilde{t}_1^3 \tilde{t}_2 + \left(1 + \frac{f_1}{f_2} + \frac{f_2}{f_1}\right) \tilde{t}_1^2 \tilde{t}_2^2 \tilde{t}_3 \\
& + \left(\frac{1}{f_1} + \frac{1}{f_2}\right) \tilde{t}_1 \tilde{t}_2^3 \tilde{t}_3^2 + \frac{1}{f_1 f_2} \tilde{t}_2^4 \tilde{t}_3^3 - (f_1 + f_2) \tilde{t}_1^5 \tilde{t}_2^3 \tilde{t}_3 \\
& - \left(3 - \frac{f_1}{f_2} - \frac{f_2}{f_1}\right) \tilde{t}_1^4 \tilde{t}_2^4 \tilde{t}_3^2 + \dots \ . \tag{3.14.219}
\end{aligned}
$$

The above plethystic logarithm with its refinement exhibits all the moduli space gener-

Generator	$U(1)_{f_1}$	$U(1)_{f_2}$
$p_1^2 p_3 p_4 \ s$	1	0
$p_1 p_2 p_4^2 \ s$	0	1
$p_1^2 p_3^2 p_5 \ s$	1	-1
$p_1 p_2 p_3 p_4 p_5 \ s$	0	0
$p_2^2 p_4^2 p_5 \ s$	-1	1
$p_1 p_2 p_3^2 p_5^2 \ s$	0	-1
$p_2^2 p_3 p_4 p_5^2 \ s$	-1	0
$p_2^2 p_3^2 p_5^3 \ s$	-1	-1

Table 3.46: The generators and lattice of generators of the mesonic moduli space of Model 12a in terms of GLSM fields with the corresponding flavor charges.

Generator	$U(1)_{f_1}$	$U(1)_{f_2}$
$X_{25}^1 X_{53} X_{32} = X_{14} X_{42}^2 X_{25}^1 X_{51}$	1	0
$X_{14} X_{42}^2 X_{21} = X_{25}^1 X_{53} X_{34} X_{42}^2$	0	1
$X_{13} X_{32} X_{25}^1 X_{51} = X_{14} X_{42}^1 X_{25}^1 X_{51}$	1	-1
$X_{13} X_{34} X_{42}^2 X_{25}^1 X_{51} = X_{14} X_{42}^2 X_{25}^2 X_{51} = X_{25}^1 X_{53} X_{34} X_{42}^1 = X_{13} X_{32} X_{21} = X_{14} X_{42}^1 X_{21} = X_{25}^2 X_{53} X_{32}$	0	0
$X_{13} X_{34} X_{42}^2 X_{21} = X_{25}^2 X_{53} X_{34} X_{42}^2$	-1	1
$X_{13} X_{34} X_{42}^1 X_{25}^1 X_{51} = X_{13} X_{32} X_{25}^2 X_{51} = X_{14} X_{42}^1 X_{25}^2 X_{51}$	0	1
$X_{13} X_{34} X_{42}^2 X_{25}^2 X_{51} = X_{13} X_{34} X_{42}^1 X_{21} = X_{25}^2 X_{53} X_{34} X_{42}^1$	-1	0
$X_{13} X_{34} X_{42}^1 X_{25}^2 X_{51}$	-1	-1

Table 3.47: The generators in terms of bifundamental fields (Model 12a).

ators with their mesonic charges. They are summarized in Table 3.46. The generators can be presented on a charge lattice. The convex polygon formed by the generators in Table 3.46 is the dual reflexive polygon of the toric diagram of Model 12a.

The mesonic Hilbert series and the plethystic logarithm can be re-expressed in terms of just 3 fugacities

$$
T_1 = \frac{\tilde{t}_3}{f_1 f_2 \ \tilde{t}_1^4} = \frac{t_5}{y_s \ t_1^2 t_4^2} \ , \ T_2 = f_1 \ \tilde{t}_1^3 \tilde{t}_2 = y_s \ t_1^2 t_3 t_4 \ , \ T_3 = f_2 \ \tilde{t}_1^3 \tilde{t}_2 = y_s \ t_1 t_2 t_4^2 \ ,
$$
(3.14.220)

such that

$$
g_1(T_1, T_2, T_3; \mathcal{M}_{12a}^{mes}) =
$$
$$
(1 + T_1 T_2 T_3 - T_1 T_2^2 T_3 - T_1 T_2 T_3^2 + T_1^2 T_2^2 T_3 + T_1^2 T_2 T_3^2 - T_1^2 T_2^3 T_3 - 2T_1^2 T_2^2 T_3^2
$$
$$
- T_1^2 T_2 T_3^3 + T_1^2 T_2^3 T_3^2 + T_1^2 T_2^2 T_3^3 - T_1^3 T_2^3 T_3^2 - T_1^3 T_2^2 T_3^3 + T_1^3 T_2^3 T_3^3 + T_1^4 T_2^4 T_3^4)
$$
$$
\times \frac{1}{(1 - T_2)(1 - T_3)(1 - T_1 T_2^2)(1 - T_1 T_3^2)(1 - T_1^3 T_2^2 T_3^2)}
$$
(3.14.221)
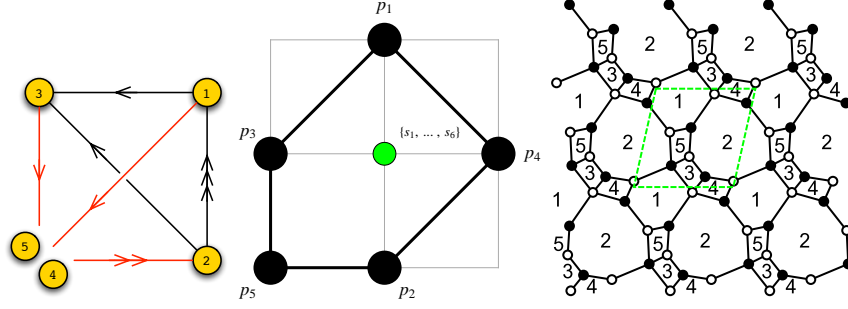
Figure 3.30: The quiver, toric diagram, and brane tiling of Model 12b. The red arrows in the quiver indicate all possible connections between blocks of nodes.

and

$$
\begin{aligned}
PL[g_1(T_1, T_2, T_3; \mathcal{M}_{12a}^{mes})] = {} & T_2 + T_3 + T_1 T_2 T_3 + T_1 T_2^2 + T_1 T_3^2 + T_1^2 T_2 T_3^2 + T_1^2 T_2^2 T_3 \\
& + T_1^3 T_2^2 T_3^2 - T_1 T_2^2 T_3 - T_1 T_2 T_3^2 - T_1^2 T_2^3 T_3 - 3 T_1^2 T_2^2 T_3^2 - T_1^2 T_2^3 T_3 - T_1^2 T_2 T_3^3 \\
& + \dots \, .
\end{aligned}
\tag{3.14.222}
$$

The above Hilbert series and plethystic logarithm illustrate the conical structure of the toric Calabi-Yau 3-fold.

3.14.2 Model 12 Phase b

The superpotential is

$$
\begin{aligned}
W = {} & + X_{15} X_{52}^2 X_{21}^2 + X_{21}^1 X_{14} X_{42}^1 + X_{35} X_{52}^1 X_{23} + X_{13} X_{34} X_{42}^2 X_{21}^3 \\
& - X_{14} X_{42}^2 X_{21}^2 - X_{15} X_{52}^1 X_{21}^3 - X_{34} X_{42}^1 X_{23} - X_{21}^1 X_{13} X_{35} X_{52}^2 \, .
\end{aligned}
\tag{3.14.223}
$$

The perfect matching matrix is

$$
P = \begin{pmatrix}
 & p_1 & p_2 & p_3 & p_4 & p_5 & s_1 & s_2 & s_3 & s_4 & s_5 & s_6 \\
\hline
X_{21}^1 & 1 & 0 & 1 & 0 & 0 & 1 & 0 & 0 & 0 & 0 & 0 \\
X_{42}^2 & 1 & 0 & 0 & 0 & 0 & 0 & 1 & 1 & 0 & 0 & 0 \\
X_{21}^2 & 0 & 1 & 1 & 0 & 1 & 1 & 0 & 0 & 0 & 0 & 0 \\
X_{21}^3 & 0 & 1 & 0 & 1 & 0 & 1 & 0 & 0 & 0 & 0 & 0 \\
X_{23} & 1 & 0 & 0 & 1 & 0 & 1 & 0 & 0 & 0 & 0 & 1 \\
X_{42}^1 & 0 & 1 & 0 & 0 & 1 & 0 & 1 & 1 & 0 & 0 & 0 \\
X_{52}^1 & 0 & 0 & 1 & 0 & 1 & 0 & 1 & 0 & 1 & 0 & 0 \\
X_{52}^2 & 0 & 0 & 0 & 1 & 0 & 0 & 1 & 0 & 1 & 0 & 0 \\
X_{15} & 1 & 0 & 0 & 0 & 0 & 0 & 0 & 1 & 0 & 1 & 1 \\
X_{35} & 0 & 1 & 0 & 0 & 0 & 0 & 0 & 1 & 0 & 1 & 0 \\
X_{34} & 0 & 0 & 1 & 0 & 0 & 0 & 0 & 0 & 1 & 1 & 0 \\
X_{14} & 0 & 0 & 0 & 1 & 0 & 0 & 0 & 0 & 1 & 1 & 1 \\
X_{13} & 0 & 0 & 0 & 0 & 1 & 0 & 0 & 0 & 0 & 0 & 1
\end{pmatrix} . \tag{3.14.224}
$$

The F-term charge matrix $Q_F = \ker(P)$ is

$$
Q_F = \begin{pmatrix}
 p_1 & p_2 & p_3 & p_4 & p_5 & s_1 & s_2 & s_3 & s_4 & s_5 & s_6 \\
\hline
 1 & 1 & 0 & 0 & 0 & -1 & 0 & -1 & 0 & 0 & 0 \\
 0 & 0 & 1 & 1 & 0 & -1 & 0 & 0 & -1 & 0 & 0 \\
 0 & 1 & 1 & 0 & -1 & -1 & 0 & 0 & 0 & -1 & 1 \\
 0 & 0 & 0 & 0 & 0 & 0 & 1 & -1 & -1 & 1 & 0
\end{pmatrix} . \tag{3.14.225}
$$

The D-term charge matrix is

$$
Q_D = \begin{pmatrix}
 p_1 & p_2 & p_3 & p_4 & p_5 & s_1 & s_2 & s_3 & s_4 & s_5 & s_6 \\
\hline
 0 & 0 & 0 & 0 & 0 & 1 & -1 & 0 & 0 & 0 & 0 \\
 0 & 0 & 0 & 0 & 0 & 0 & 0 & 1 & -1 & 0 & 0 \\
 0 & 0 & 0 & 0 & 0 & 0 & 0 & 0 & 1 & -1 & 0 \\
 0 & 0 & 0 & 0 & 0 & 0 & 0 & 0 & 0 & 1 & -1
\end{pmatrix} . \tag{3.14.226}
$$

The total charge matrix Q_t does not have repeated columns. Accordingly, the global symmetry is $U(1)_{f_1} \times U(1)_{f_2} \times U(1)_R$. The charge assignment on the extremal perfect matchings with non-zero R-charge is the the same as for Model 12a in Table 3.45.

The product of all internal perfect matchings is expressed as

$$
s = \prod_{m=1}^{6} s_m . \tag{3.14.227}
$$

The product is counted by the fugacity y_s. The remaining extremal perfect matchings p_α are counted by the fugacity t_α.

The mesonic Hilbert series and the plethystic logarithm of the Hilbert series is the same as for Model 12a. They are shown respectively in (3.14.215), (3.14.217) and (3.14.219). Accordingly, the mesonic moduli spaces of Model 12a and 12b are toric duals.

The moduli space generators in terms of perfect matching variables of Model 12b are shown in Table 3.46 with their corresponding mesonic charges. The generators in terms

Generator	$U(1)_{f_1}$	$U(1)_{f_2}$
$X_{14}X_{42}^2X_{21}^1 = X_{15}X_{52}^2X_{21}^1 = X_{23}X_{34}X_{42}^2$	1	0
$X_{14}X_{42}^2X_{21}^3 = X_{15}X_{52}^2X_{21}^3 = X_{23}X_{35}X_{52}^3$	0	1
$X_{15}X_{52}^2X_{21}^1 = X_{13}X_{34}X_{42}^2X_{21}^1$	1	-1
$X_{13}X_{35}X_{52}^2X_{21} = X_{13}X_{34}X_{42}^2X_{21} = X_{14}X_{42}^1X_{21} = X_{14}X_{42}^2X_{21} = X_{15}X_{52}^2X_{21} = X_{15}X_{52}^1X_{21} = X_{23}X_{34}X_{42}^1 = X_{23}X_{35}X_{52}^2$	0	0
$X_{14}X_{42}^1X_{21}^3 = X_{13}X_{35}X_{52}^2X_{21}^3$	-1	1
$X_{15}X_{52}^1X_{21}^2 = X_{13}X_{34}X_{42}^1X_{21}^1 = X_{13}X_{35}X_{52}^1X_{21}^1 = X_{13}X_{34}X_{42}^2X_{21}^2$	0	-1
$X_{14}X_{42}^1X_{21}^2 = X_{13}X_{35}X_{52}^2X_{21}^2 = X_{13}X_{34}X_{42}^1X_{21}^3 = X_{13}X_{35}X_{52}^1X_{21}^3$	-1	0
$X_{13}X_{34}X_{42}^1X_{21}^2 = X_{13}X_{35}X_{52}^1X_{21}^2$	-1	-1

Table 3.48: The generators in terms of bifundamental fields (Model 12b).
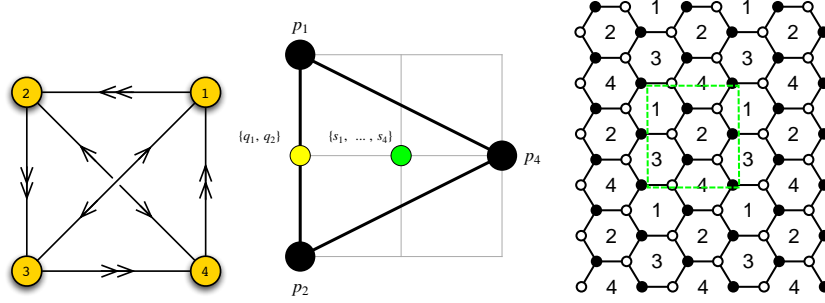
Figure 3.31: The quiver, toric diagram, and brane tiling Model 13.

of quiver fields are shown in Table 3.48.

3.15 Model 13: $\mathbb{C}^3/\mathbb{Z}_4$, $(1,1,2)$, $Y^{2,2}$

The superpotential is

$$
\begin{aligned}
W \;=\; & +X_{12}^1 X_{24} X_{41}^1 + X_{31}X_{12}^2X_{23}^2 + X_{41}^2X_{13}X_{34}^1 + X_{34}^2X_{42}X_{23}^1 \\
& -X_{12}^1X_{23}^1X_{31} - X_{13}X_{34}^2X_{41}^1 - X_{41}^2X_{12}^2X_{24} - X_{34}^1X_{42}X_{23}^2 \,.
\end{aligned}
\tag{3.15.228}
$$

The perfect matching matrix is

$$
P = \left(
\begin{array}{c|ccc|cc|cccc}
 & p_1 & p_2 & p_3 & q_1 & q_2 & s_1 & s_2 & s_3 & s_4 \\
\hline
X_{34}^1 & 1 & 0 & 0 & 1 & 0 & 1 & 0 & 0 & 0 \\
X_{34}^2 & 0 & 1 & 0 & 1 & 0 & 1 & 0 & 0 & 0 \\
X_{12}^2 & 1 & 0 & 0 & 1 & 0 & 0 & 1 & 0 & 0 \\
X_{12}^1 & 0 & 1 & 0 & 1 & 0 & 0 & 1 & 0 & 0 \\
X_{23}^1 & 1 & 0 & 0 & 0 & 1 & 0 & 0 & 1 & 0 \\
X_{23}^2 & 0 & 1 & 0 & 0 & 1 & 0 & 0 & 1 & 0 \\
X_{41}^1 & 1 & 0 & 0 & 0 & 1 & 0 & 0 & 0 & 1 \\
X_{41}^2 & 0 & 1 & 0 & 0 & 1 & 0 & 0 & 0 & 1 \\
X_{24} & 0 & 0 & 1 & 0 & 0 & 1 & 0 & 1 & 0 \\
X_{31} & 0 & 0 & 1 & 0 & 0 & 1 & 0 & 0 & 1 \\
X_{13} & 0 & 0 & 1 & 0 & 0 & 0 & 1 & 1 & 0 \\
X_{42} & 0 & 0 & 1 & 0 & 0 & 0 & 1 & 0 & 1 \\
\end{array}
\right) \,.
\tag{3.15.229}
$$

	$U(1)_f$	$SU(2)_x$	$U(1)_R$	fugacity
p_1	-1/4	1/2	2/3	t_1
p_2	-1/4	-1/2	2/3	t_2
p_3	1/2	0	2/3	t_3

Table 3.49: The GLSM fields corresponding to extremal points of the toric diagram with their mesonic charges (Model 13).

The F-term charge matrix $Q_F = \ker(P)$ is

$$
Q_F = \begin{pmatrix}
p_1 & p_2 & p_3 & q_1 & q_2 & s_1 & s_2 & s_3 & s_4 \\
1 & 1 & 0 & -1 & -1 & 0 & 0 & 0 & 0 \\
0 & 0 & 1 & 1 & 0 & -1 & -1 & 0 & 0 \\
0 & 0 & 1 & 0 & 1 & 0 & 0 & -1 & -1
\end{pmatrix} .
$$
(3.15.230)

The D-term charge matrix is

$$
Q_D = \begin{pmatrix}
p_1 & p_2 & p_3 & q_1 & q_2 & s_1 & s_2 & s_3 & s_4 \\
0 & 0 & 0 & 0 & 0 & 1 & -1 & 0 & 0 \\
0 & 0 & 0 & 0 & 0 & 0 & 1 & -1 & 0 \\
0 & 0 & 0 & 0 & 0 & 0 & 0 & 1 & -1
\end{pmatrix} .
$$
(3.15.231)

The GLSM fields p_1 and p_2 are equally charged under the F-term and D-term constraints. This is shown by the corresponding columns in the total charge matrix Q_t which are identical. Accordingly, the global symmetry is enhanced from $U(1)^3$ to $SU(2)_x \times U(1)_f \times U(1)_R$ with $U(1)_R$ being the R-symmetry. The mesonic charges on the GLSM fields corresponding to extremal points in the toric diagram in Figure 3.31 are found following the discussion in §3.2.3. They are presented in Table 3.49.

Products of non-extremal perfect matchings are expressed as follows

$$
q = q_1 q_2 \ , \quad s = \prod_{m=1}^{4} s_m \ .
$$
(3.15.232)

The fugacities counting the above products are respectively y_q and y_s. The fugacity which counts extremal perfect matchings is t_α.

The mesonic Hilbert series of Model 13 is computed using the Molien integral formula in (1.4.67). It is

$$
g_1(t_\alpha, y_q, y_s; \mathcal{M}_{13}^{mes}) =
$$
$$
\frac{1 + y_q^2 y_s\ t_1^3 t_2 + y_q^2 y_s\ t_1^2 t_2^2 + y_q^2 y_s\ t_1 t_2^3 + y_q y_s\ t_1^2 t_3 + y_q y_s\ t_1 t_2 t_3 + y_q y_s\ t_2^2 t_3 + y_q^3 y_s^2\ t_1^3 t_2^3 t_3}{(1 - y_q^2 y_s\ t_1^4)(1 - y_q^2 y_s\ t_2^4)(1 - y_s\ t_3^2)} .
$$
(3.15.233)

The mesonic moduli space of Model 13 is not a complete intersection. The plethystic

logarithm of the mesonic Hilbert series is

$$PL[g_1(t_\alpha, y_q, y_s; \mathcal{M}_{13}^{mes})] = y_s\, t_3^2 + y_q y_s\, t_1 t_2 t_3 + y_q y_s\, t_1^2 t_3 + y_q y_s\, t_2^2 t_3 + y_q^2 y_s\, t_1^4$$
$$+ y_q^2 y_s\, t_1^3 t_2 + y_q^2 y_s\, t_1^2 t_2^2 + y_q^2 y_s\, t_1 t_2^3 + y_q^2 y_s\, t_2^4 - 2\, y_q^2 y_s^2\, t_1^2 t_2^2 t_3^2 + \ldots (3.15.234)$$

Consider the following fugacity map

$$f = y_q^{-2/3} y_s^{1/3}\, t_1^{-2/3} t_2^{-2/3} t_3^{4/3}\ ,\ \ \tilde{x}^2 = x = \frac{t_1}{t_2}\ ,\ \ t = y_q^{1/3} y_s^{1/3}\, t_1^{1/3} t_2^{1/3} t_3^{1/3}\ , \ (3.15.235)$$

where the fugacities f, x and t are mesonic charge fugacities. x is the charge fugacity for the enhanced symmetry $SU(2)_x$. Using the redefinition of this fugacity to $\tilde{x} = \sqrt{x}$ and the fugacities f and t, one can rewrite the expansion of the Hilbert series in terms of characters of irreducible representations of $SU(2)$ as follows

$$g_1(t, \tilde{x}, f; \mathcal{M}_{13}^{mes}) = \sum_{m=0}^{\infty} \sum_{n=0}^{\infty} \left([2m]_{\tilde{x}} f^n t^{2n+3m} + [4(n+1) + 2m]_{\tilde{x}} f^{-(n+1)} t^{4(n+1)+3m} \right)\ .$$

$$(3.15.236)$$

The corresponding plethystic logarithm is

$$PL[g_1(t, \tilde{x}, f; \mathcal{M}_{13}^{mes})] = ft^2 + [2]_{\tilde{x}} t^3 + [4]_{\tilde{x}} \frac{1}{f} t^4 - (1 + [4]_{\tilde{x}}) t^6 - ([2]_{\tilde{x}} + [4]_{\tilde{x}}) \frac{1}{f} t^7$$
$$- (1 + [4]_{\tilde{x}}) \frac{1}{f^2} t^8 + ([2]_{\tilde{x}} + [4]_{\tilde{x}}) t^9 + (1 + 2[2]_{\tilde{x}} + 2[4]_{\tilde{x}} + [6]_{\tilde{x}}) \frac{1}{f} t^{10} + \ldots\ .$$

$$(3.15.237)$$

In terms of the mesonic charge fugacities f, x and t, the above plethystic logarithm exhibits the moduli space generators and their mesonic charges. They are summarized in Table 3.50. The flavour charges of generators are integers using f and x. They can be presented on a charge lattice. The convex polygon formed by the generators is the dual reflexive polygon of the toric diagram.

As indicated in (3.15.237), the generators fall into irreducible representation of $SU(2)$ with the characters

$$ft^2 + [2]_{\tilde{x}} t^3 + [4]_{\tilde{x}} \frac{1}{f} t^4 = ft^2 + \left(\tilde{x}^2 + 1 + \frac{1}{\tilde{x}^2} \right) t^3 + \left(\tilde{x}^4 + \tilde{x}^2 + 1 + \frac{1}{\tilde{x}^2} + \frac{1}{\tilde{x}^4} \right) \frac{1}{f} t^4\ .$$

$$(3.15.238)$$

The above three terms correspond to the three columns of points in the lattice of generators in Table 3.50. The generators in terms of quiver fields are shown in Table 3.51.

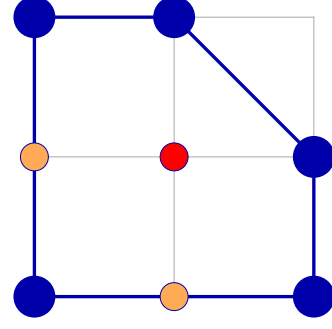| Generator	$U(1)_f$	$SU(2)_x$
$p_3^2\, s$	1	0
$p_1^2 p_3\, q\, s$	0	1
$p_1 p_2 p_3\, q\, s$	0	0
$p_2^2 p_3\, q\, s$	0	-1
$p_1^4\, q^2\, s$	-1	2
$p_1^3 p_2\, q^2\, s$	-1	1
$p_1^2 p_2^2\, q^2\, s$	-1	0
$p_1 p_2^3\, q^2\, s$	-1	-1
$p_2^4\, q^2\, s$	-1	-2
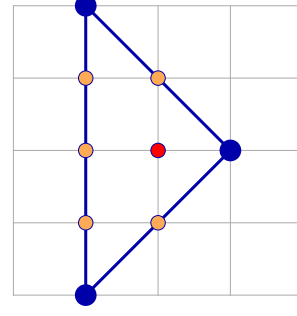
Table 3.50: The generators and lattice of generators of the mesonic moduli space of Model 13 in terms of GLSM fields with the corresponding flavor charges.

Generator	$U(1)_f$	$SU(2)_x$
$X_{13}X_{31} = X_{24}X_{42}$	1	0
$X_{12}^2 X_{23}^1 X_{31} = X_{12}^2 X_{24} X_{41}^1 = X_{13} X_{34}^1 X_{41}^1 = X_{23}^1 X_{34}^1 X_{42}$	0	1
$X_{12}^1 X_{23}^1 X_{31} = X_{12}^1 X_{24} X_{41}^1 = X_{12}^2 X_{23}^2 X_{31} = X_{12}^2 X_{24} X_{41}^2 = X_{13} X_{34}^1 X_{41}^2 = X_{13} X_{34}^2 X_{41}^1 = X_{23}^1 X_{34}^1 X_{42} = X_{23}^2 X_{34}^1 X_{42}$	0	0
$X_{12}^1 X_{23}^2 X_{31} = X_{12}^1 X_{24} X_{41}^2 = X_{13} X_{34}^2 X_{41}^2 = X_{23}^2 X_{34}^2 X_{42}$	0	-1
$X_{12}^2 X_{23}^1 X_{34}^1 X_{41}^1$	-1	2
$X_{12}^1 X_{23}^1 X_{34}^1 X_{41}^1 = X_{12}^2 X_{23}^1 X_{34}^1 X_{41}^2 = X_{12}^2 X_{23}^1 X_{34}^2 X_{41}^1 = X_{12}^2 X_{23}^2 X_{34}^1 X_{41}^1$	1	-1
$X_{12}^1 X_{23}^1 X_{34}^1 X_{41}^2 = X_{12}^1 X_{23}^1 X_{34}^2 X_{41}^1 = X_{12}^1 X_{23}^2 X_{34}^1 X_{41}^1 = X_{12}^2 X_{23}^1 X_{34}^2 X_{41}^2 = X_{12}^2 X_{23}^2 X_{34}^1 X_{41}^2 = X_{12}^2 X_{23}^2 X_{34}^2 X_{41}^1$	-1	0
$X_{12}^1 X_{23}^1 X_{34}^2 X_{41}^2 = X_{12}^1 X_{23}^2 X_{34}^1 X_{41}^2 = X_{12}^1 X_{23}^2 X_{34}^2 X_{41}^1 = X_{12}^2 X_{23}^2 X_{34}^2 X_{41}^2$	-1	-1
$X_{12}^1 X_{23}^2 X_{34}^2 X_{41}^2$	-1	-2

Table 3.51: The generators in terms of bifundamental fields (Model 13).

With the fugacity map

$$T_1 = f^{-1/4}x^{1/2}\, t = y_q^{1/2}y_s^{1/4}t_1 \ , \ T_2 = f^{-1/4}x^{-1/2}\, t = y_q^{1/2}y_s^{1/4}t_2 \ ,$$
$$T_3 = f^{1/2}\, t = y_s^{1/2}t_3 \ , \tag{3.15.239}$$

the mesonic Hilbert series takes the form

$$g_1(T_1, T_2, T_3; \mathcal{M}_{13}^{mes}) = \frac{1 + T_1^3 T_2 + T_1^2 T_2^2 + T_1 T_2^3 + T_1^2 T_3 + T_1 T_2 T_3 + T_2^2 T_3 + T_1^3 T_2^3 T_3}{(1 - T_1^4)(1 - T_2^4)(1 - T_3^2)} \ ,$$
$$\tag{3.15.240}$$

with the plethystic logarithm becoming

$$PL[g_1(T_1, T_2, T_3; \mathcal{M}_{13}^{mes})] = T_3^2 + T_1 T_2 T_3 + T_1^2 T_3 + T_2^2 T_3 + T_1^4 + T_1^3 T_2 + T_1^2 T_2^2$$
$$+ T_1 T_2^3 + T_2^4 - 2T_1^2 T_2^2 T_3^2 + \dots \ . \tag{3.15.241}$$

The above Hilbert series and plethystic logarithm is written in terms of just three fugacities with positive powers. This illustrates the conical structure of the toric Calabi-Yau 3-fold.
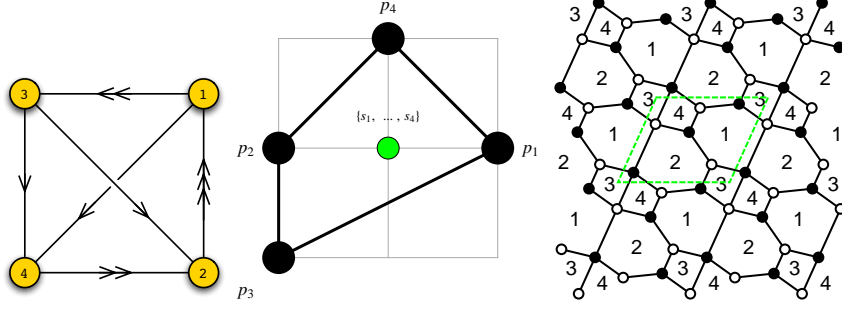
Figure 3.32: The quiver, toric diagram, and brane tiling of Model 14.

3.16 Model 14: dP_1

The superpotential is

$$
\begin{aligned}
W \;=\; & +X_{21}^1 X_{14} X_{42}^1 + X_{21}^3 X_{13}^2 X_{32} + X_{42}^2 X_{21}^2 X_{13}^1 X_{34} \\
& -X_{13}^1 X_{32} X_{21}^1 - X_{14} X_{42}^2 X_{21}^3 - X_{21}^2 X_{13}^2 X_{34} X_{42}^1 \,.
\end{aligned}
\tag{3.16.242}
$$

The perfect matching matrix is

$$
P = \left(
\begin{array}{c|cccc|cccc}
 & p_1 & p_2 & p_3 & p_4 & s_1 & s_2 & s_3 & s_4 \\
\hline
X_{21}^2 & 1 & 0 & 0 & 0 & 1 & 0 & 0 & 0 \\
X_{32} & 1 & 0 & 0 & 0 & 0 & 1 & 0 & 1 \\
X_{21}^3 & 0 & 1 & 1 & 0 & 1 & 0 & 0 & 0 \\
X_{21}^1 & 0 & 1 & 0 & 1 & 1 & 0 & 0 & 0 \\
X_{42}^1 & 0 & 0 & 1 & 0 & 0 & 1 & 0 & 0 \\
X_{42}^2 & 0 & 0 & 0 & 1 & 0 & 1 & 0 & 0 \\
X_{13}^1 & 0 & 0 & 1 & 0 & 0 & 0 & 1 & 0 \\
X_{13}^2 & 0 & 0 & 0 & 1 & 0 & 0 & 1 & 0 \\
X_{14} & 1 & 0 & 0 & 0 & 0 & 0 & 1 & 1 \\
X_{34} & 0 & 1 & 0 & 0 & 0 & 0 & 0 & 1 \\
\end{array}
\right) .
\tag{3.16.243}
$$

The F-term charge matrix $Q_F = \ker{(P)}$ is

$$
Q_F = \left(
\begin{array}{cccc|cccc}
p_1 & p_2 & p_3 & p_4 & s_1 & s_2 & s_3 & s_4 \\
\hline
1 & 1 & 0 & 0 & -1 & 0 & 0 & -1 \\
1 & 0 & 1 & 1 & -1 & -1 & -1 & 0 \\
\end{array}
\right) .
\tag{3.16.244}
$$

The D-term charge matrix is

$$
Q_D = \left(
\begin{array}{cccc|cccc}
p_1 & p_2 & p_3 & p_4 & s_1 & s_2 & s_3 & s_4 \\
\hline
0 & 0 & 0 & 0 & 1 & -1 & 0 & 0 \\
0 & 0 & 0 & 0 & 0 & 1 & -1 & 0 \\
0 & 0 & 0 & 0 & 0 & 0 & 1 & -1 \\
\end{array}
\right) .
\tag{3.16.245}
$$

The total charge matrix Q_t does not have repeated columns. Accordingly, the global symmetry is $U(1)_{f_1} \times U(1)_{f_2} \times U(1)_R$. The flavour and R-charges on the GLSM fields corresponding to extremal points in the toric diagram in Figure 3.32 are found following

211

	$U(1)_{f_1}$	$U(1)_{f_2}$	$U(1)_R$	fugacity
p_1	1	0	$R_1 = \sqrt{13} - 3$	t_1
p_2	1	1	$R_2 = (5\sqrt{13} - 17)/3$	t_2
p_3	-1	-1	$R_3 = 4(4 - \sqrt{13})/3$	t_3
p_4	-1	0	$R_3 = 4(4 - \sqrt{13})/3$	t_4

Table 3.52: The GLSM fields corresponding to extremal points of the toric diagram with their mesonic charges (Model 14). The R-charges are obtained using a-maximization [13].

the discussion in §3.2.3. They are presented in Table 3.52.

The product of all internal perfect matchings is

$$s = \prod_{m=1}^{4} s_m \ . \tag{3.16.246}$$

The fugacity counting the above product is y_s. The fugacity which counts the remaining extremal perfect matchings p_α is t_α.

The mesonic Hilbert series of Model 14 is found using the Molien integral formula in (1.4.67). It is

$$g_1(t_\alpha, y_s; \mathcal{M}_{14}^{mes}) = \frac{P(t_\alpha)}{(1 - y_s \ t_1^2 t_3)(1 - y_s \ t_2^2 t_3^3)(1 - y_s \ t_1^2 t_4)(1 - y_s \ t_2^2 t_4^3)} \ , \tag{3.16.247}$$

where the numerator is given by the polynomial

$$
\begin{aligned}
P(t_\alpha) \ = \ & 1 + y_s \ t_1 t_2 t_3^2 + y_s \ t_1 t_2 t_3 t_4 - y_s^2 \ t_1^3 t_2 t_3^2 t_4 + y_s \ t_2^2 t_3^3 t_4 - y_s^2 \ t_1^2 t_2^2 t_3^3 t_4 \\
& + y_s \ t_1 t_2 t_4^2 - y_s^2 \ t_1^3 t_2 t_3 t_4^2 + y_s \ t_2^2 t_3 t_4^2 - y_s^2 \ t_1^2 t_2^2 t_3^2 t_4^2 - y_s^2 \ t_1^2 t_2^2 t_3 t_4^3 - y_s^3 \ t_1^3 t_2^3 t_3^3 t_4^3 \ .
\end{aligned}
\tag{3.16.248}
$$

The plethystic logarithm of the mesonic Hilbert series is

$$
\begin{aligned}
PL[g_1(t_\alpha, y_s; \mathcal{M}_{14}^{mes})] = \ & y_s \ t_1^2 t_4 + y_s \ t_1^2 t_3 + y_s \ t_1 t_2 t_3 t_4 + y_s \ t_1 t_2 t_4^2 + y_s \ t_1 t_2 t_3^2 \\
& + y_s \ t_2^2 t_3^2 t_4 + y_s \ t_2^2 t_3^3 + y_s \ t_2^2 t_3 t_4^2 + y_s \ t_2^2 t_4^3 - y_s^2 \ t_1^3 t_2 t_3 t_4^2 - y_s^2 \ t_1^3 t_2 t_3^2 t_4 + \ldots \ .
\end{aligned}
\tag{3.16.249}
$$

Consider the following fugacity map

$$f_1 = t_3^{-1/2} t_4^{1/2} \ , \ \ f_2 = \frac{t_4}{t_3} \ , \ \ \tilde{t}_1 = y_s^{1/2} \ t_1 \ , \ \ \tilde{t}_2 = y_s^{1/2} \ t_2 \ , \ \ \tilde{t}_3 = t_3^{1/2} t_4^{1/2} \ , \tag{3.16.250}$$

where the fugacities f_1 and f_2 count flavour charges, and the fugacity $\tilde{t}_i$ count the

Generator	$U(1)_{f_1}$	$U(1)_{f_2}$
$p_1^2 p_3\ s$	1	-1
$p_1 p_2 p_3^2\ s$	0	-1
$p_2^2 p_3^3\ s$	-1	-1
$p_1^2 p_4\ s$	1	0
$p_1 p_2 p_3 p_4\ s$	0	0
$p_2^2 p_3^2 p_4\ s$	-1	0
$p_1 p_2 p_4^2\ s$	0	1
$p_2^2 p_3 p_4^2\ s$	-1	1
$p_2^2 p_4^3\ s$	-1	2
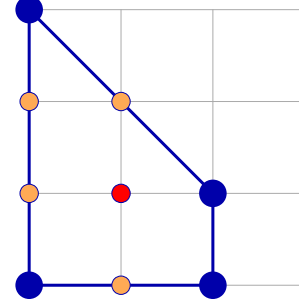
Table 3.53: The generators and lattice of generators of the mesonic moduli space of Model 14 in terms of GLSM fields with the corresponding flavor charges. The lattice of generators is the toric diagram of Model 3.

Generator	$U(1)_{f_1}$	$U(1)_{f_2}$
$X_{13}^1 X_{32} X_{21}^2 = X_{14} X_{42}^1 X_{21}^2$	1	-1
$X_{13}^1 X_{34} X_{42}^1 X_{21}^2 = X_{13}^1 X_{32} X_{21}^3 = X_{14} X_{42}^1 X_{21}^3$	0	-1
$X_{13}^1 X_{34} X_{42}^1 X_{21}^3$	-1	-1
$X_{13}^2 X_{32} X_{21}^2 = X_{14} X_{42}^2 X_{21}^2$	1	0
$X_{13}^1 X_{34} X_{42}^2 X_{21}^2 = X_{13}^2 X_{34} X_{42}^1 X_{21}^2 = X_{13}^1 X_{32} X_{21}^1 = X_{13}^2 X_{32} X_{21}^3 = X_{14} X_{42}^1 X_{21}^1 = X_{14} X_{42}^2 X_{21}^3$	0	0
$X_{13}^1 X_{34} X_{42}^1 X_{21}^1 = X_{13}^1 X_{34} X_{42}^2 X_{21}^3 = X_{13}^2 X_{34} X_{42}^1 X_{21}^3$	-1	0
$X_{13}^2 X_{34} X_{42}^2 X_{21}^2 = X_{13}^2 X_{32} X_{21}^1 = X_{14} X_{42}^2 X_{21}^1$	0	1
$X_{13}^1 X_{34} X_{42}^2 X_{21}^1 = X_{13}^2 X_{34} X_{42}^1 X_{21}^1 = X_{13}^2 X_{34} X_{42}^2 X_{21}^3$	-1	1
$X_{13}^2 X_{34} X_{42}^2 X_{21}^1$	-1	2

Table 3.54: The generators in terms of bifundamental fields (Model 14).

R-charge R_i in Table 3.52. Accordingly, the plethystic logarithm becomes

$$PL[g_1(\tilde{t}_\alpha, f_1, f_2; \mathcal{M}_{14}^{mes})] = \left(f_1 + \frac{f_1}{f_2}\right) \tilde{t}_1^2 \tilde{t}_3 + \left(1 + f_2 + \frac{1}{f_2}\right) \tilde{t}_1 \tilde{t}_2 \tilde{t}_3^2$$
$$+ \left(\frac{1}{f_1} + \frac{1}{f_1 f_2} + \frac{f_2}{f_1} + \frac{f_2^2}{f_1}\right) \tilde{t}_2^2 \tilde{t}_3^3 - \left(f_1 + \frac{f_1}{f_2}\right) \tilde{t}_1^3 \tilde{t}_2 \tilde{t}_3^3 + \dots \ . \tag{3.16.251}$$

The first positive terms in the above plethystic logarithm correspond to moduli space generators with the corresponding flavour charge counted by the fugacities f_1 and f_2. The generators and the corresponding mesonic charges are shown in Table 3.53. The generators can be presented on a charge lattice. The convex polygon formed by the generators in Table 3.53 is the dual reflexive polygon of the toric diagram of Model 14.

The mesonic Hilbert series and the plethystic logarithm can be re-expressed in terms of just 3 fugacities

$$T_1 = \frac{f_2\ \tilde{t}_2}{f_1^2\ \tilde{t}_1^3} = \frac{t_2}{y_s\ t_1^3} \ , \ T_2 = \frac{f_1}{f_2}\ \tilde{t}_1^2 \tilde{t}_3 = y_s\ t_1^2 t_3 \ , \ T_3 = f_1\ \tilde{t}_1^2 \tilde{t}_3 = y_s\ t_1^2 t_4 \ , \tag{3.16.252}$$
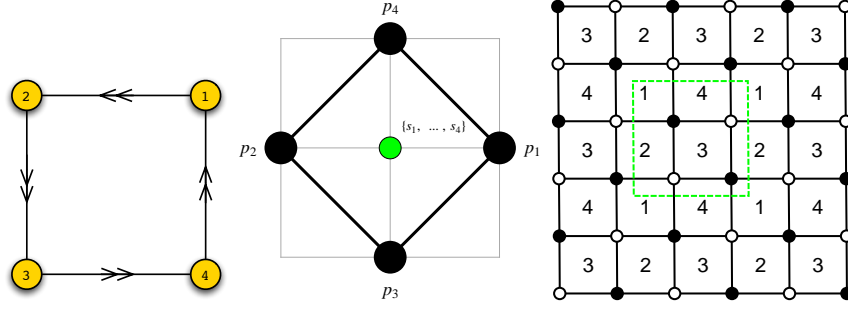
Figure 3.33: The quiver, toric diagram, and brane tiling of Model 15a.

such that

$$g_1(T_1, T_2, T_3; \mathcal{M}_{14}^{mes}) =$$
$$(1 + T_1 T_2^2 + T_1 T_2 T_3 - T_1 T_2^2 T_3 + T_1^2 T_2^2 T_3 - T_1^2 T_2^3 T_3 + T_1 T_3^2 - T_1 T_2 T_3^2 + T_1^2 T_2 T_3^2$$
$$-T_1^2 T_2^2 T_3^2 - T_1^2 T_2 T_3^3 - T_1^3 T_2^3 T_3^3) \times \frac{1}{(1 - T_2)(1 - T_1^2 T_2^3)(1 - T_3)(1 - T_1^2 T_3^3)}$$

$$(3.16.253)$$

and

$$PL[g_1(T_1, T_2, T_3; \mathcal{M}_{14}^{mes})] = T_3 + T_2 + T_1 T_2 T_3 + T_1 T_3^2 + T_1 T_2^2 + T_1^2 T_2^2 T_3 + T_1^2 T_2^3$$
$$+T_1^2 T_2 T_3^2 + T_1^2 T_3^3 - T_1 T_2 T_3^2 - T_1 T_2^2 T_3 + \dots .$$

$$(3.16.254)$$

The above Hilbert series and plethystic logarithm illustrate the conical structure of the toric Calabi-Yau 3-fold.

3.17 Model 15: $\mathcal{C}/\mathbb{Z}_2$ $(1,1,1,1)$, $\mathbb{F}_0$

3.17.1 Model 15 Phase a

The superpotential is

$$W = +X_{12}^1 X_{23}^1 X_{34}^2 X_{41}^2 + X_{12}^2 X_{23}^2 X_{34}^1 X_{41}^1 - X_{12}^1 X_{23}^2 X_{34}^2 X_{41}^1 - X_{12}^2 X_{23}^1 X_{34}^1 X_{41}^2 .$$

$$(3.17.255)$$

214

	$SU(2)_{x_1}$	$SU(2)_{x_2}$	$U(1)_R$	fugacity
p_1	1/2	0	1/2	t_1
p_2	-1/2	0	1/2	t_2
p_3	0	1/2	1/2	t_3
p_4	0	-1/2	1/2	t_4

Table 3.55: The GLSM fields corresponding to extremal points of the toric diagram with their mesonic charges (Model 15a).

The perfect matching matrix is

$$
P = \begin{pmatrix}
 & p_1 & p_2 & p_3 & p_4 & s_1 & s_2 & s_3 & s_4 \\
X_{12}^1 & 1 & 0 & 0 & 0 & 1 & 0 & 0 & 0 \\
X_{12}^2 & 0 & 1 & 0 & 0 & 1 & 0 & 0 & 0 \\
X_{34}^1 & 1 & 0 & 0 & 0 & 0 & 1 & 0 & 0 \\
X_{34}^2 & 0 & 1 & 0 & 0 & 0 & 1 & 0 & 0 \\
X_{23}^1 & 0 & 0 & 1 & 0 & 0 & 0 & 1 & 0 \\
X_{23}^2 & 0 & 0 & 0 & 1 & 0 & 0 & 1 & 0 \\
X_{41}^1 & 0 & 0 & 1 & 0 & 0 & 0 & 0 & 1 \\
X_{41}^2 & 0 & 0 & 0 & 1 & 0 & 0 & 0 & 1
\end{pmatrix} .
\tag{3.17.256}
$$

The F-term charge matrix $Q_F = \ker(P)$ is

$$
Q_F = \begin{pmatrix}
p_1 & p_2 & p_3 & p_4 & s_1 & s_2 & s_3 & s_4 \\
1 & 1 & 0 & 0 & -1 & -1 & 0 & 0 \\
0 & 0 & 1 & 1 & 0 & 0 & -1 & -1
\end{pmatrix} .
\tag{3.17.257}
$$

The D-term charge matrix is

$$
Q_D = \begin{pmatrix}
p_1 & p_2 & p_3 & p_4 & s_1 & s_2 & s_3 & s_4 \\
0 & 0 & 0 & 0 & 1 & -1 & 0 & 0 \\
0 & 0 & 0 & 0 & 0 & 1 & -1 & 0 \\
0 & 0 & 0 & 0 & 0 & 0 & 1 & -1
\end{pmatrix} .
\tag{3.17.258}
$$

The pairs of GLSM fields $\{p_1, p_2\}$ and $\{p_3, p_4\}$ have the same charge under the F-term and D-term constraints. This is shown by the identical columns in the total charge matrix Q_t. Accordingly, the global symmetry is enhanced from $U(1)^2 \times U(1)_R$ to $SU(1)_{x_1} \times SU(2)_{x_2} \times U(1)_R$. The mesonic charges on the GLSM fields corresponding to extremal points in the toric diagram in Figure 3.33 are found following the discussion in §3.2.3. They are presented in Table 3.55.

The product of all internal perfect matchings labelled by

$$
s = \prod_{m=1}^{4} s_m .
\tag{3.17.259}
$$

The above product is counted by the fugacity y_s. All remaining extremal perfect matchings p_α are counted by the fugacity t_α.

The mesonic Hilbert series of Model 15a is calculated using the Molien integral formula

in (1.4.67). It is

$$g_1(t_\alpha, y_s; \mathcal{M}_{15a}^{mes}) = \frac{P(t_\alpha)}{(1 - y_s \ t_1^2 t_3^2)(1 - y_s \ t_2^2 t_3^2)(1 - y_s \ t_1^2 t_4^2)(1 - y_s \ t_2^2 t_4^2)} \ , \ (3.17.260)$$

where the numerator is given by the polynomial

$$
\begin{aligned}
P(t_\alpha) \ = \ & 1 + y_s \ t_1 t_2 t_3^2 + y_s \ t_1^2 t_3 t_4 + y_s \ t_1 t_2 t_3 t_4 + y_s \ t_2^2 t_3 t_4 - y_s^2 \ t_1^2 t_2^2 t_3^3 t_4 \\
& + y_s \ t_1 t_2 t_4^2 - y_s^2 \ t_1^3 t_2 t_3^2 t_4^2 - y_s^2 \ t_1^2 t_2^2 t_3^2 t_4^2 - y_s^2 \ t_1 t_2^3 t_3^2 t_4^2 - y_s^2 \ t_1^2 t_2^2 t_3 t_4^3 - y_s^3 \ t_1^3 t_2^3 t_3^3 t_4^3 \ .
\end{aligned}
$$

(3.17.261)

The plethystic logarithm of the mesonic Hilbert series is

$$
\begin{aligned}
PL[g_1(t_\alpha, y_s; \mathcal{M}_{15a}^{mes})] = \ & y_s \ t_1^2 t_3^2 + y_s \ t_1 t_2 t_3^2 + y_s \ t_2^2 t_3^2 + y_s \ t_1^2 t_3 t_4 + y_s \ t_1 t_2 t_3 t_4 \\
& + y_s \ t_2^2 t_3 t_4 + y_s \ t_1^2 t_4^2 + y_s \ t_1 t_2 t_4^2 + y_s \ t_2^2 t_4^2 - y_s^2 \ t_1^2 t_2^2 t_3^4 - y_s^2 \ t_1^3 t_2 t_3^3 t_4 \\
& - 2 \ y_s^2 \ t_1^2 t_2^2 t_3^3 t_4 - y_s^2 \ t_1 t_2^3 t_3^3 t_4 - y_s^2 \ t_1^4 t_3^2 t_4^2 - 2 \ y_s^2 \ t_1^3 t_2 t_3^2 t_4^2 - 4 \ y_s^2 \ t_1^2 t_2^2 t_3^2 t_4^2 \\
& - 2 \ y_s^2 \ t_1 t_2^3 t_3^2 t_4^2 - y_s^2 \ t_2^4 t_3^2 t_4^2 - y_s^2 \ t_1^3 t_2 t_3 t_4^3 - 2 \ y_s^2 \ t_1^2 t_2^2 t_3 t_4^3 - y_s^2 \ t_1 t_2^3 t_3 t_4^3 \\
& - y_s^2 \ t_1^2 t_2^2 t_4^4 + \dots \ .
\end{aligned}
$$

(3.17.262)

From the infinite plethystic logarithm one concludes that the moduli space is not a complete intersection.

Consider the following fugacity map

$$\tilde{x}_1^2 = x_1 = \frac{t_1}{t_2} \ , \ \ \tilde{x}_2^2 = x_2 = \frac{t_3}{t_4} \ , \ \ t = y_s^{1/4} \ t_1^{1/4} t_2^{1/4} t_3^{1/4} t_4^{1/4} \ , \quad (3.17.263)$$

where x_1, x_2 and t are mesonic charge fugacities. In terms of $\tilde{x}_1$ and $\tilde{x}_2$ both the Hilbert series and the plethystic logarithm can be expressed in terms of characters of irreducible representations of $SU(2) \times SU(2)$. The Taylor expansion of the Hilbert series takes the form

$$g_1(t, \tilde{x}_1, \tilde{x}_2; \mathcal{M}_{15a}^{mes}) = \sum_{n=0}^{\infty} [2n; 2n]_{\tilde{x}_1, \tilde{x}_2} \ t^{4n} \ . \quad (3.17.264)$$

The plethystic logarithm in terms of characters of irreducible representations of $SU(2) \times$

216

Generator	$SU(2)_{x_1}$	$SU(2)_{x_2}$
$p_1^2 p_3^2\ s$	1	1
$p_1 p_2 p_3^2\ s$	0	1
$p_2^2 p_3^2\ s$	-1	1
$p_1^2 p_3 p_4\ s$	1	0
$p_1 p_2 p_3 p_4\ s$	0	0
$p_2^2 p_3 p_4\ s$	-1	0
$p_1^2 p_4^2\ s$	1	-1
$p_1 p_2 p_4^2\ s$	0	-1
$p_2^2 p_4^2\ s$	-1	-1

Table 3.56: The generators and lattice of generators of the mesonic moduli space of Model 15a in terms of GLSM fields with the corresponding flavor charges.

$SU(2)$ is

$$
\begin{aligned}
PL[g_1(t,\tilde{x}_1,\tilde{x}_2;\mathcal{M}_{15a}^{mes})] &= [2;2]_{\tilde{x}_1,\tilde{x}_2}t^4 - (1 + [4;0]_{\tilde{x}_1,\tilde{x}_2} + [2;2]_{\tilde{x}_1,\tilde{x}_2} + [0;4]_{\tilde{x}_1,\tilde{x}_2})t^8 \\
&+ ([2;0]_{\tilde{x}_1,\tilde{x}_2} + [4;0]_{\tilde{x}_1,\tilde{x}_2} + [0;2]_{\tilde{x}_1,\tilde{x}_2} + 2[2;2]_{\tilde{x}_1,\tilde{x}_2} + [4;2]_{\tilde{x}_1,\tilde{x}_2} + [0;4]_{\tilde{x}_1,\tilde{x}_2} \\
&+ [2;4]_{\tilde{x}_1,\tilde{x}_2})t^{12} - (4[2;0]_{\tilde{x}_1,\tilde{x}_2} + [4;0]_{\tilde{x}_1,\tilde{x}_2} + [6;0]_{\tilde{x}_1,\tilde{x}_2} + 4[0;2]_{\tilde{x}_1,\tilde{x}_2} + 5[2;2]_{\tilde{x}_1,\tilde{x}_2} \\
&+ 4[4;2]_{\tilde{x}_1,\tilde{x}_2} + [6;2]_{\tilde{x}_1,\tilde{x}_2} + [0;4]_{\tilde{x}_1,\tilde{x}_2} + 4[2;4]_{\tilde{x}_1,\tilde{x}_2} + [4;4]_{\tilde{x}_1,\tilde{x}_2} + [0;6]_{\tilde{x}_1,\tilde{x}_2} \\
&+ [2;6]_{\tilde{x}_1,\tilde{x}_2})t^{16} + \dots \ .
\end{aligned}
\tag{3.17.265}
$$

In terms of the fugacities x_1 and x_2 the above plethystic logarithm exhibits the moduli space generators with their mesonic charges, where the flavour charges as powers of x_1 and x_2 take integer values. They are summarized in Table 3.56. The generators can be presented on a charge lattice. The generators form a convex polygon on the charge lattice which is the dual of the toric diagram of Model 15a.

As indicated in (3.17.265), the generators fall into an irreducible representation of $SU(2) \times SU(2)$ with the character

$$
[2;2]_{\tilde{x}_1,\tilde{x}_2}t^4 = \left(\tilde{x}_1^2 + 1 + \frac{1}{\tilde{x}_1^2}\right)\left(\tilde{x}_2^2 + 1 + \frac{1}{\tilde{x}_2^2}\right) \ .
\tag{3.17.266}
$$

The generators in terms of quiver fields are shown in Table 3.57.

By introducing the fugacity map

$$
T_1 = \frac{t^4}{x_1 x_2} = y_s\ t_2^2 t_4^2\ ,\ T_2 = x_1 = \frac{t_1}{t_2}\ ,\ T_3 = x_2 = \frac{t_3}{t_4}\ ,
\tag{3.17.267}
$$

Generator	$SU(2)_{x_1}$	$SU(2)_{x_2}$
$X_{12}^1 X_{23}^1 X_{34}^1 X_{41}^1$	1	1
$X_{12}^1 X_{23}^1 X_{34}^2 X_{41}^1 = X_{12}^2 X_{23}^1 X_{34}^1 X_{41}^1$	0	1
$X_{12}^2 X_{23}^1 X_{34}^2 X_{41}^1$	-1	1
$X_{12}^1 X_{23}^1 X_{34}^1 X_{41}^2 = X_{12}^1 X_{23}^2 X_{34}^1 X_{41}^1$	1	0
$X_{12}^1 X_{23}^1 X_{34}^2 X_{41}^2 = X_{12}^1 X_{23}^2 X_{34}^2 X_{41}^1 = X_{12}^2 X_{23}^1 X_{34}^1 X_{41}^2 = X_{12}^2 X_{23}^2 X_{34}^1 X_{41}^1$	0	0
$X_{12}^2 X_{23}^1 X_{34}^2 X_{41}^2 = X_{12}^2 X_{23}^2 X_{34}^2 X_{41}^1$	-1	0
$X_{12}^1 X_{23}^2 X_{34}^1 X_{41}^2$	1	-1
$X_{12}^1 X_{23}^2 X_{34}^2 X_{41}^2 = X_{12}^2 X_{23}^2 X_{34}^1 X_{41}^2$	0	-1
$X_{12}^2 X_{23}^2 X_{34}^2 X_{41}^2$	-1	-1

Table 3.57: The generators in terms of bifundamental fields (Model 15a).
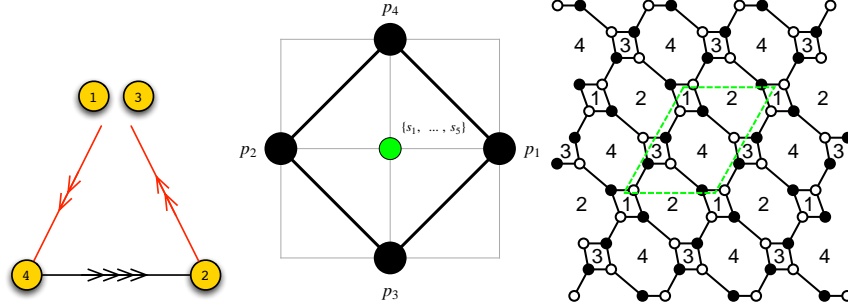
Figure 3.34: The quiver, toric diagram, and brane tiling of Model 15b. The red arrows in the quiver indicate all possible connections between blocks of nodes.

the mesonic Hilbert series can be expressed as

$$
\begin{aligned}
g_1(T_1, T_2, T_3; \mathcal{M}_{15a}^{mes}) = & \big(1 + T_1 T_2 T_3 + T_1 T_3 + T_1 T_2^2 T_3 + T_1 T_2 + T_1 T_2 T_3^2 \\
& -(T_1^2 T_2^2 T_3^2 + T_1^2 T_2 T_3^2 + T_1^2 T_2^3 T_3^2 + T_1^2 T_2^2 T_3 + T_1^2 T_2^2 T_3^3) - T_1^3 T_2^3 T_3^3 \big) \times \\
& \frac{1}{(1 - T_1)(1 - T_1 T_2^2)(1 - T_1 T_3^2)(1 - T_1 T_2^2 T_3^2)} \; .
\end{aligned}
\tag{3.17.268}
$$

The corresponding plethystic logarithm has the form

$$
\begin{aligned}
PL[g_1(T_1, T_2, T_3; \mathcal{M}_{15a}^{mes})] = & \, T_1 T_2^2 T_3^2 + T_1 T_2 T_3^2 + T_1 T_3^2 + T_1 T_2^2 T_3 + T_1 T_2 T_3 + T_1 T_3 \\
& + T_1 T_2^2 + T_1 T_2 + T_1 - T_1^2 T_2^2 - T_1^2 T_2^3 T_3^3 + \ldots \; .
\end{aligned}
\tag{3.17.269}
$$

The above Hilbert series and plethystic logarithm are in terms of three fugacities which carry only positive powers. This illustrates the conical structure of the toric Calabi-Yau 3-fold.

3.17.2 Model 15 Phase b

The superpotential is

$$
\begin{aligned}
W \;=\; & +X_{21}^1 X_{14}^1 X_{42}^1 + X_{21}^2 X_{14}^2 X_{42}^2 + X_{23}^1 X_{34}^2 X_{42}^3 + X_{23}^2 X_{34}^1 X_{42}^4 \\
& -X_{21}^1 X_{14}^2 X_{42}^3 - X_{21}^2 X_{14}^1 X_{42}^4 - X_{23}^1 X_{34}^1 X_{42}^2 - X_{23}^2 X_{34}^2 X_{42}^1 \; . \quad (3.17.270)
\end{aligned}
$$

The perfect matching matrix is

$$
P = \left(
\begin{array}{c|cccc|ccccc}
 & p_1 & p_2 & p_3 & p_4 & s_1 & s_2 & s_3 & s_4 & s_5 \\
\hline
X_{42}^2 & 1 & 0 & 1 & 0 & 0 & 0 & 1 & 0 & 0 \\
X_{42}^3 & 0 & 1 & 1 & 0 & 0 & 0 & 1 & 0 & 0 \\
X_{42}^4 & 1 & 0 & 0 & 1 & 0 & 0 & 1 & 0 & 0 \\
X_{42}^1 & 0 & 1 & 0 & 1 & 0 & 0 & 1 & 0 & 0 \\
X_{21}^1 & 1 & 0 & 0 & 0 & 1 & 0 & 0 & 1 & 0 \\
X_{21}^2 & 0 & 1 & 0 & 0 & 1 & 0 & 0 & 1 & 0 \\
X_{34}^2 & 1 & 0 & 0 & 0 & 0 & 1 & 0 & 1 & 0 \\
X_{34}^1 & 0 & 1 & 0 & 0 & 0 & 1 & 0 & 1 & 0 \\
X_{23}^2 & 0 & 0 & 1 & 0 & 1 & 0 & 0 & 0 & 1 \\
X_{23}^1 & 0 & 0 & 0 & 1 & 1 & 0 & 0 & 0 & 1 \\
X_{14}^1 & 0 & 0 & 1 & 0 & 0 & 1 & 0 & 0 & 1 \\
X_{14}^2 & 0 & 0 & 0 & 1 & 0 & 1 & 0 & 0 & 1 \\
\end{array}
\right) . \qquad (3.17.271)
$$

The F-term charge matrix $Q_F = \ker(P)$ is

$$
Q_F = \left(
\begin{array}{cccc|ccccc}
p_1 & p_2 & p_3 & p_4 & s_1 & s_2 & s_3 & s_4 & s_5 \\
\hline
1 & 1 & 0 & 0 & 0 & 0 & -1 & -1 & 0 \\
0 & 0 & 1 & 1 & 0 & 0 & -1 & 0 & -1 \\
0 & 0 & 0 & 0 & 1 & 1 & 0 & -1 & -1 \\
\end{array}
\right) . \qquad (3.17.272)
$$

The D-term charge matrix is

$$
Q_D = \left(
\begin{array}{cccc|ccccc}
p_1 & p_2 & p_3 & p_4 & s_1 & s_2 & s_3 & s_4 & s_5 \\
\hline
0 & 0 & 0 & 0 & 0 & 1 & -1 & 0 & 0 \\
0 & 0 & 0 & 0 & 0 & 0 & 1 & -1 & 0 \\
0 & 0 & 0 & 0 & 0 & 0 & 0 & 1 & -1 \\
\end{array}
\right) . \qquad (3.17.273)
$$

The total charge matrix Q_t exhibits two pairs of identical columns. Accordingly, the global symmetry is enhanced to $SU(2)_{x_1} \times SU(2)_{x_2} \times U(1)_R$. The mesonic charges on extremal perfect matchings are found following the discussion in §3.2.3. They are identical to the ones for Model 15a and are presented in Table 3.55.

The product of all internal perfect matchings is expressed as

$$
s = \prod_{m=1}^{5} s_m \; . \qquad (3.17.274)
$$

The fugacity which counts the above product is y_s. The fugacity which counts the remaining extremal perfect matchings p_α is t_α.

The mesonic Hilbert series for Model 15b is found using the Molien integral formula in (1.4.67). The mesonic Hilbert series of Model 15b is identical to the one for Model

Generator	$SU(2)_{x_1}$	$SU(2)_{x_2}$
$X_{14}^1 X_{42}^2 X_{21}^1 = X_{23}^2 X_{34}^2 X_{42}^2$	1	1
$X_{14}^1 X_{42}^3 X_{21}^1 = X_{14}^1 X_{42}^2 X_{21}^2 = X_{23}^2 X_{34}^1 X_{42}^2 = X_{23}^2 X_{34}^2 X_{42}^3$	0	1
$X_{14}^1 X_{42}^3 X_{21}^2 = X_{23}^2 X_{34}^1 X_{42}^3$	-1	1
$X_{14}^1 X_{42}^4 X_{21}^1 = X_{14}^2 X_{42}^2 X_{21}^1 = X_{23}^1 X_{34}^2 X_{42}^2 = X_{23}^2 X_{34}^2 X_{42}^4$	1	0
$X_{14}^1 X_{42}^4 X_{21}^2 = X_{14}^1 X_{42}^2 X_{21}^2 = X_{14}^2 X_{42}^3 X_{21}^1 = X_{14}^2 X_{42}^2 X_{21}^2 = X_{23}^1 X_{34}^1 X_{42}^2 = X_{23}^1 X_{34}^2 X_{42}^3 = X_{23}^2 X_{34}^1 X_{42}^4 = X_{23}^2 X_{34}^2 X_{42}^1$	0	0
$X_{14}^1 X_{42}^4 X_{21}^2 = X_{14}^2 X_{42}^3 X_{21}^2 = X_{23}^1 X_{34}^1 X_{42}^3 = X_{23}^2 X_{34}^1 X_{42}^1$	-1	0
$X_{14}^2 X_{42}^4 X_{21}^1 = X_{23}^1 X_{34}^2 X_{42}^4$	1	-1
$X_{14}^2 X_{42}^4 X_{21}^2 = X_{14}^2 X_{42}^4 X_{21}^1 = X_{23}^1 X_{34}^1 X_{42}^4 = X_{23}^1 X_{34}^2 X_{42}^1$	0	-1
$X_{14}^2 X_{42}^4 X_{21}^2 = X_{23}^1 X_{34}^1 X_{42}^1$	-1	-1

Table 3.58: The generators in terms of bifundamental fields (Model 15b).
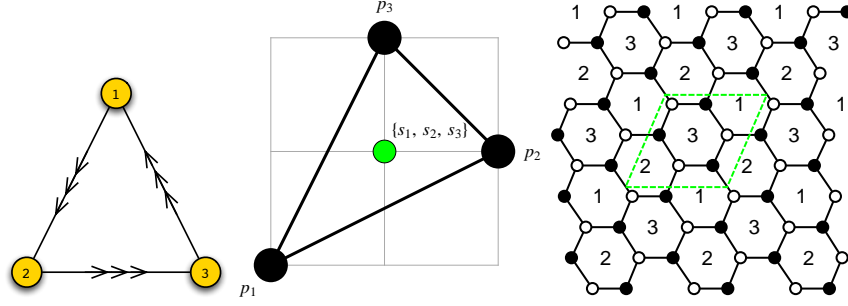
Figure 3.35: The quiver, toric diagram, and brane tiling of Model 16.

15a in (3.17.260).

The moduli space generators in terms of perfect matchings of Model 15b are shown in Table 3.56. In terms of quiver fields of Model 15b, they are presented in Table 3.58. The lattice of generators is a reflexive polygon and the dual of the toric diagram.

3.18 Model 16: $\mathbb{C}^3/\mathbb{Z}_3$ $(1,1,1)$, $\mathbf{dP_0}$

The superpotential is

$$
\begin{aligned}
W \;=\; & +X_{12}^1 X_{23}^3 X_{31}^2 + X_{12}^2 X_{23}^1 X_{31}^3 + X_{12}^3 X_{23}^2 X_{31}^1 \\
& -X_{12}^1 X_{23}^1 X_{31}^1 - X_{12}^3 X_{23}^3 X_{31}^3 - X_{12}^2 X_{23}^2 X_{31}^2
\end{aligned}
\tag{3.18.275}
$$

The perfect matching matrix is

$$
P = \left(
\begin{array}{c|ccc|ccc}
 & p_1 & p_2 & p_3 & s_1 & s_2 & s_3 \\
\hline
X_{12}^3 & 1 & 0 & 0 & 1 & 0 & 0 \\
X_{31}^2 & 1 & 0 & 0 & 0 & 1 & 0 \\
X_{23}^1 & 1 & 0 & 0 & 0 & 0 & 1 \\
X_{12}^1 & 0 & 1 & 0 & 1 & 0 & 0 \\
X_{31}^3 & 0 & 1 & 0 & 0 & 1 & 0 \\
X_{23}^2 & 0 & 1 & 0 & 0 & 0 & 1 \\
X_{12}^2 & 0 & 0 & 1 & 1 & 0 & 0 \\
X_{31}^1 & 0 & 0 & 1 & 0 & 1 & 0 \\
X_{23}^3 & 0 & 0 & 1 & 0 & 0 & 1 \\
\end{array}
\right).
\tag{3.18.276}
$$

	$SU(3)_{(x_1,x_2)}$		$U(1)_R$	fugacity
p_1	(-1/3,	-1/3)	2/3	t_1
p_2	(+2/3,	-1/3)	2/3	t_2
p_3	(-1/3,	+2/3)	2/3	t_3

Table 3.59: The GLSM fields corresponding to extremal points of the toric diagram with their mesonic charges (Model 16).

The F-term charge matrix $Q_F = \ker(P)$ is

$$Q_F = \begin{pmatrix} p_1 & p_2 & p_3 & s_1 & s_2 & s_3 \\ 1 & 1 & 1 & -1 & -1 & -1 \end{pmatrix} . \tag{3.18.277}$$

The D-term charge matrix is

$$Q_D = \begin{pmatrix} p_1 & p_2 & p_3 & s_1 & s_2 & s_3 \\ 0 & 0 & 0 & 1 & -1 & 0 \\ 0 & 0 & 0 & 0 & 1 & -1 \end{pmatrix} . \tag{3.18.278}$$

One observes that the GLSM fields corresponding to the extremal points of the toric diagram in Figure 3.35 are equally charged under the F- and D-term constraints. This is shown by three identical columns of the total charge matrix Q_t. This leads to the enhancement of the global symmetry from $U(1)^3$ to $SU(3)_{(x_1,x_2)} \times U(1)_R$. Accordingly, the mesonic charges on the GLSM fields corresponding to extremal points in the toric diagram in Figure 3.35 can be found following the discussion in §3.2.3. They are presented in Table 3.59.

The product of all internal perfect matchings expressed as

$$s = \prod_{m=1}^{3} s_m . \tag{3.18.279}$$

The above product is counted by the fugacity y_s. The remaining extremal perfect matchings p_α are counted by t_α.

The mesonic Hilbert series of Model 16 is calculated using the Molien integral formula in (1.4.67). It is

$$
g_1(t_\alpha, y_s; \mathcal{M}_{16}^{mes}) = \\
\frac{1 + y_s \, t_1^2 t_2 + y_s \, t_1 t_2^2 + y_s \, t_1^2 t_3 + y_s \, t_1 t_2 t_3 + y_s \, t_2^2 t_3 + y_s \, t_1 t_3^2 + y_s \, t_2 t_3^2 + y_s^2 \, t_1^2 t_2^2 t_3^2}{(1 - y_s \, t_1^3)(1 - y_s \, t_2^3)(1 - y_s \, t_3^3)} .
$$

$$\tag{3.18.280}$$

The plethystic logarithm of the mesonic Hilbert series is

$$
\begin{aligned}
PL[g_1(t_\alpha, y_s; \mathcal{M}_{16}^{mes})] =\; & y_s\, t_1^3 + y_s\, t_1^2 t_2 + y_s\, t_1 t_2^2 + y_s\, t_2^3 + y_s\, t_1^2 t_3 + y_s\, t_1 t_2 t_3 \\
& + y_s\, t_2^2 t_3 + y_s\, t_1 t_3^2 + y_s\, t_2 t_3^2 + y_s\, t_3^3 - y_s^2\, t_1^4 t_2^2 - y_s^2\, t_1^3 t_2^3 - y_s^2\, t_1^2 t_2^4 \\
& - y_s^2\, t_1^4 t_2 t_3 - 2\, y_s^2\, t_1^3 t_2^2 t_3 - 2\, y_s^2\, t_1^2 t_2^3 t_3 - y_s^2\, t_1 t_2^4 t_3 - y_s^2\, t_1^4 t_3^2 - 2\, y_s^2\, t_1^3 t_2 t_3^2 \\
& - 3\, y_s^2\, t_1^2 t_2^2 t_3^2 - 2\, y_s^2\, t_1 t_2^3 t_3^2 - y_s^2\, t_2^4 t_3^2 - y_s^2\, t_1^3 t_3^3 - 2\, y_s^2\, t_1^2 t_2 t_3^3 - 2\, y_s^2\, t_1 t_2^2 t_3^3 - y_s^2\, t_2^3 t_3^3 \\
& - y_s^2\, t_1^2 t_3^4 - y_s^2\, t_1 t_2 t_3^4 - y_s^2\, t_2^2 t_3^4 + \dots \; .
\end{aligned}
\tag{3.18.281}
$$

Consider the following fugacity map

$$
x_1 = \frac{t_2}{t_1} \;,\; x_2 = \frac{t_3}{t_1} \;,\; t = y_s^{1/3}\, t_1^{1/3} t_2^{1/3} t_3^{1/3} \;,
\tag{3.18.282}
$$

where x_1, x_2 and t count the mesonic charges. The fugacities x_1 and x_2 with their powers being integers count integer flavour charges. With a further redefinition of fugacities,

$$
\tilde{x}_1 = \frac{1}{x_1^{1/3} x_2^{1/3}} \;,\; \tilde{x}_2 = \frac{x_1^{1/3}}{x_2^{2/3}}
\tag{3.18.283}
$$

the Hilbert series and plethystic logarithm can be expressed in terms of characters of irreducible representations of $SU(3)$. The expansion of the Hilbert series takes the form

$$
g_1(t, \tilde{x}_1, \tilde{x}_2; \mathcal{M}_{16}^{mes}) = \sum_{n=0}^{\infty} [3n, 0]_{(\tilde{x}_1, \tilde{x}_2)}\, t^{3n} \;.
\tag{3.18.284}
$$

The plethystic logarithm is

$$
\begin{aligned}
PL[g_1(t, \tilde{x}_1, \tilde{x}_2; \mathcal{M}_{16}^{mes})] =\; & [3, 0]_{(\tilde{x}_1, \tilde{x}_2)} t^3 - [2, 2]_{(\tilde{x}_1, \tilde{x}_2)} t^6 + ([1, 1]_{(\tilde{x}_1, \tilde{x}_2)} + [1, 4]_{(\tilde{x}_1, \tilde{x}_2)} \\
& + [2, 2]_{(\tilde{x}_1, \tilde{x}_2)} + [4, 1]_{(\tilde{x}_1, \tilde{x}_2)}) t^9 - (2[0, 3]_{(\tilde{x}_1, \tilde{x}_2)} + 2[1, 1]_{(\tilde{x}_1, \tilde{x}_2)} + 2[1, 4]_{(\tilde{x}_1, \tilde{x}_2)} \\
& + 2[2, 2]_{(\tilde{x}_1, \tilde{x}_2)} + [2, 5]_{(\tilde{x}_1, \tilde{x}_2)} + 2[3, 0]_{(\tilde{x}_1, \tilde{x}_2)} + 2[3, 3]_{(\tilde{x}_1, \tilde{x}_2)} + 2[4, 1]_{(\tilde{x}_1, \tilde{x}_2)} \\
& + [5, 2]_{(\tilde{x}_1, \tilde{x}_2)}) t^{12} + \dots \; .
\end{aligned}
\tag{3.18.285}
$$

In terms of fugacities x_1 and x_2 the above plethystic logarithm exhibits the moduli space generators with their integer flavour charges and R-charges. They are summarized in Table 3.60. The generators can be presented on a charge lattice. The lattice of generators is the dual polygon of the toric diagram. As indicated in (3.18.285), the generators fall into an irreduciable representation of $SU(3)$ with the character being

$$
[3, 0]_{(\tilde{x}_1, \tilde{x}_2)} t^3 = \left(\tilde{x}_1^3 + \tilde{x}_1 \tilde{x}_2 + \frac{\tilde{x}_1^2}{\tilde{x}_2} + \frac{\tilde{x}_2^2}{\tilde{x}_1} + 1 + \frac{\tilde{x}_2^3}{\tilde{x}_1^3} + \frac{\tilde{x}_1}{\tilde{x}_2^2} + \frac{\tilde{x}_2}{\tilde{x}_1^2} + \frac{1}{\tilde{x}_1 \tilde{x}_2} + \frac{1}{\tilde{x}_2^3} \right) t^3 \;.
\tag{3.18.286}
$$

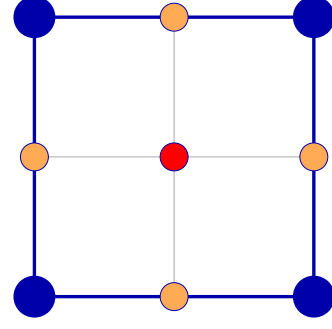| Generator	$SU(3)_{(x_1,x_2)}$
$p_1^3\,s$	(-1, -1)
$p_1^2 p_2\,s$	(0, -1)
$p_1 p_2^2\,s$	(1, -1)
$p_2^3\,s$	(2, -1)
$p_1^2 p_3\,s$	(-1, 0)
$p_1 p_2 p_3\,s$	(0, 0)
$p_2^2 p_3\,s$	(1, 0)
$p_1 p_3^2\,s$	(-1, 1)
$p_2 p_3^2\,s$	(0, 1)
$p_3^3\,s$	(-1, 2)
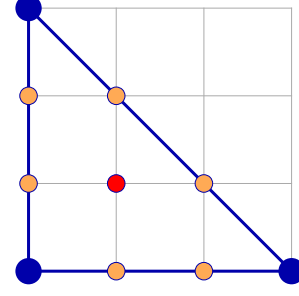
Table 3.60: The generators and lattice of generators of the mesonic moduli space of Model 16 in terms of GLSM fields with the corresponding flavor charges.

Generator	$SU(3)_{(x_1,x_2)}$
$X_{12}^3 X_{23}^1 X_{31}^2$	(-1, -1)
$X_{12}^1 X_{23}^1 X_{31}^2 = X_{12}^3 X_{23}^1 X_{31}^3 = X_{12}^3 X_{23}^2 X_{31}^2$	(0, -1)
$X_{12}^1 X_{23}^1 X_{31}^3 = X_{12}^1 X_{23}^2 X_{31}^2 = X_{12}^3 X_{23}^2 X_{31}^3$	(1, -1)
$X_{12}^1 X_{23}^2 X_{31}^3$	(2, -1)
$X_{12}^2 X_{23}^1 X_{31}^2 = X_{12}^3 X_{23}^1 X_{31}^1 = X_{12}^3 X_{23}^3 X_{31}^2$	(-1, 0)
$X_{12}^1 X_{23}^1 X_{31}^1 = X_{12}^1 X_{23}^3 X_{31}^2 = X_{12}^2 X_{23}^1 X_{31}^3 = X_{12}^2 X_{23}^2 X_{31}^2 = X_{12}^3 X_{23}^2 X_{31}^1 = X_{12}^3 X_{23}^3 X_{31}^3$	(0, 0)
$X_{12}^1 X_{23}^2 X_{31}^1 = X_{12}^1 X_{23}^3 X_{31}^3 = X_{12}^2 X_{23}^2 X_{31}^3$	(1, 0)
$X_{12}^2 X_{23}^1 X_{31}^1 = X_{12}^2 X_{23}^3 X_{31}^2 = X_{12}^3 X_{23}^3 X_{31}^1$	(-1, 1)
$X_{12}^1 X_{23}^3 X_{31}^1 = X_{12}^2 X_{23}^2 X_{31}^1 = X_{12}^2 X_{23}^3 X_{31}^3$	(0, 1)
$X_{12}^2 X_{23}^3 X_{31}^1$	(-1, 2)

Table 3.61: The generators in terms of bifundamental fields (Model 16).

The generators of the mesonic moduli space in terms of quiver fields of Model 16 are shown in Table 3.61.

With the fugacity map

$$T_1 = \frac{t}{x_1^{1/3} x_2^{1/3}} = y_s^{1/3} t_1 \ , \ T_2 = \frac{x_1^{2/3} t}{x_2^{1/3}} = y_s^{1/3} t_2 \ , \ T_3 = \frac{x_2^{2/3} t}{x_1^{1/3}} = y_s^{1/3} t_3 \ , \quad (3.18.287)$$

the mesonic Hilbert series becomes

$$g_1(T_1, T_2, T_3; \mathcal{M}_{16}^{mes}) =$$
$$\frac{1 + T_1^2 T_2 + T_1 T_2^2 + T_1^2 T_3 + T_1 T_2 T_3 + T_2^2 T_3 + T_1 T_3^2 + T_2 T_3^2 + T_1^2 T_2^2 T_3^2}{(1 - T_1^3)(1 - T_2^3)(1 - T_3^3)} \ ,$$
$$(3.18.288)$$

with the plethystic logarithm becoming

$$PL[g_1(T_1, T_2, T_3; \mathcal{M}_{16}^{mes})] = T_1^3 + T_1^2 T_2 + T_1 T_2^2 + T_2^3 + T_1^2 T_3 + T_1 T_2 T_3 + T_2^2 T_3$$
$$+ T_1 T_3^2 + T_2 T_3^2 + T_3^3 - T_1^4 T_2^2 - T_1^3 T_2^3 - T_1^2 T_2^4 - T_1^4 T_2 T_3 - 2\, T_1^3 T_2^2 T_3 - 2\, T_1^2 T_2^3 T_3$$
$$- T_1 T_2^4 T_3 - T_1^4 T_3^2 - 2\, T_1^3 T_2 T_3^2 - 3\, T_1^2 T_2^2 T_3^2 - 2\, T_1 T_2^3 T_3^2 - T_2^4 T_3^2 - T_1^3 T_3^3$$
$$- 2\, T_1^2 T_2 T_3^3 - 2\, T_1 T_2^2 T_3^3 - T_2^3 T_3^3 - T_1^2 T_3^4 - T_1 T_2 T_3^4 - T_2^2 T_3^4 + \dots \quad (3.18.289)$$

The above Hilbert series and plethystic logarithm are in terms of three fugacities with positive powers. This illustrates the conical structure of the toric Calabi-Yau 3-fold.

3.19 Seiberg Duality Trees

The above sections have identified all 30 supersymmetric gauge theories with brane tilings corresponding to the 16 reflexive polygons. 8 reflexive polygons are associated to multiple quiver gauge theories as summarized in Figure 3.36. These are called phases of the corresponding toric variety. For a given toric variety, the phases are so called *toric (Seiberg) dual* and are related under toric (Seiberg) duality as discussed in section §1.6.2. Multiple toric duality actions on various $U(n)$ gauge groups corresponding to 4-sided faces in the brane tiling create closed orbits among the phases.

In Figure 3.37 to Figure 3.44, a summary of the orbits presented as *duality trees* is shown, where nodes represent the brane tiling of the phase, and arrows are labelled with the index of the gauge group on which one acts under toric (Seiberg) duality to obtain the phase at the head of the arrow.
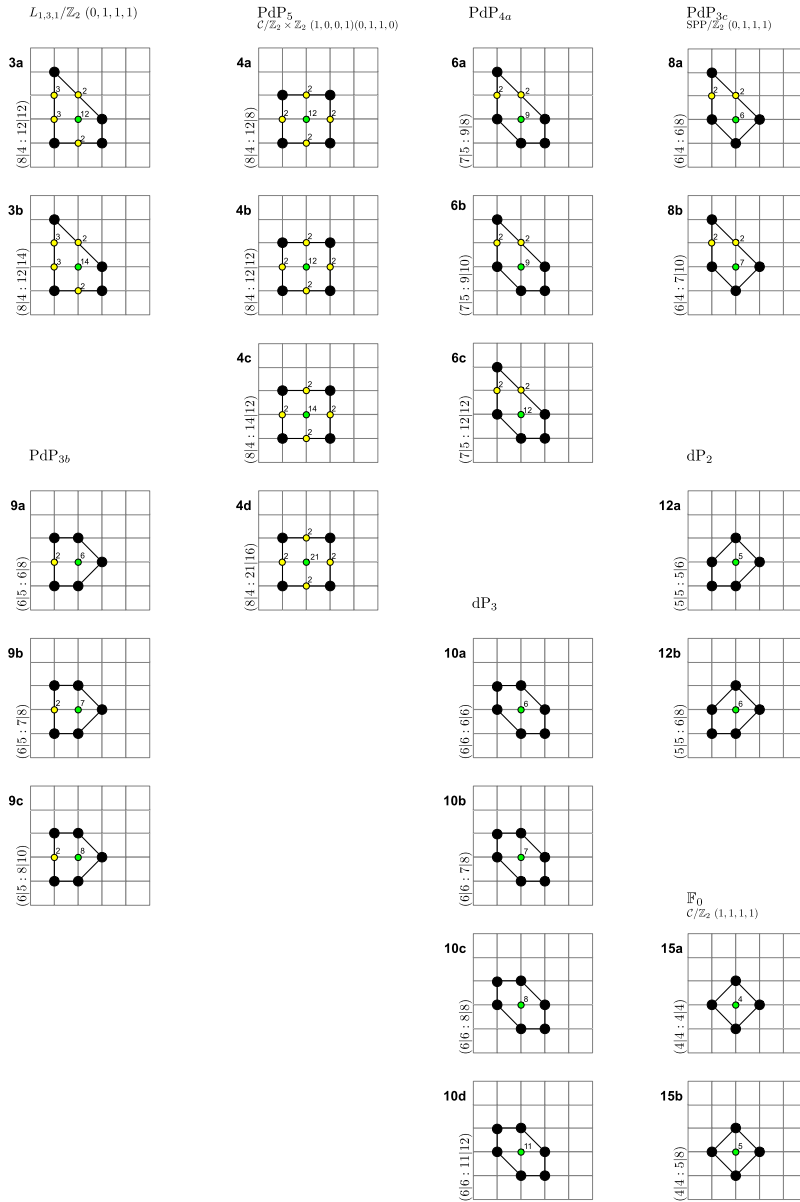
Figure 3.36: Toric Diagrams of toric (Seiberg) dual phases of quiver gauge theories with brane tilings. The label $(G|n_p : n_i|n_w)$ is used, where G, n_p, n_i and n_w are the number of $U(n)$ gauge groups, GLSM fields with non-zero R-charge, internal toric points and superpotential terms respectively.
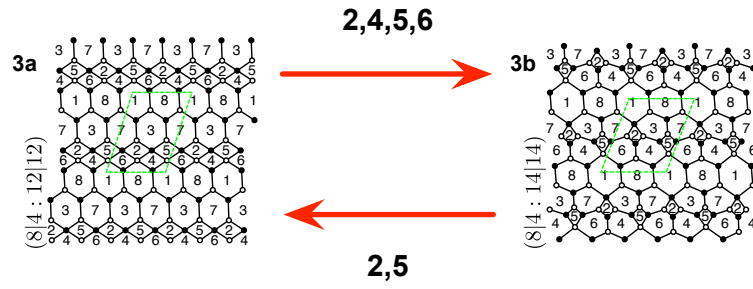
Figure 3.37: The duality tree for $L_{131}/\mathbb{Z}_2$ with orbifold action $(0,1,1,1)$ [Model 3].
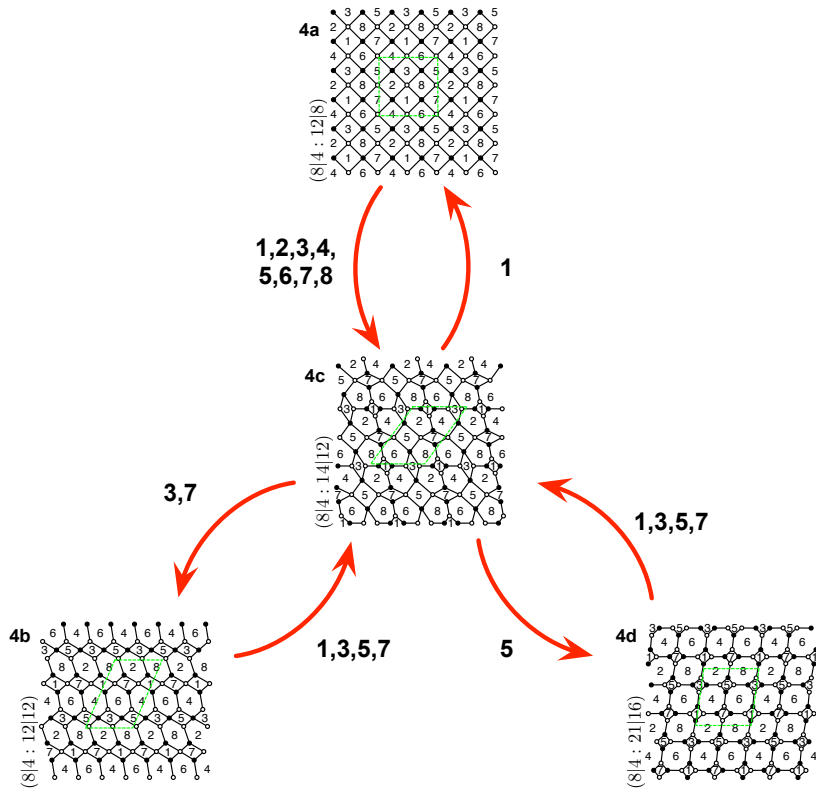
Figure 3.38: The duality tree for $\mathcal{C}/\mathbb{Z}_2 \times \mathbb{Z}_2$ with orbifold action $(0,1,1,0)(1,0,0,1)$ [Model 4].
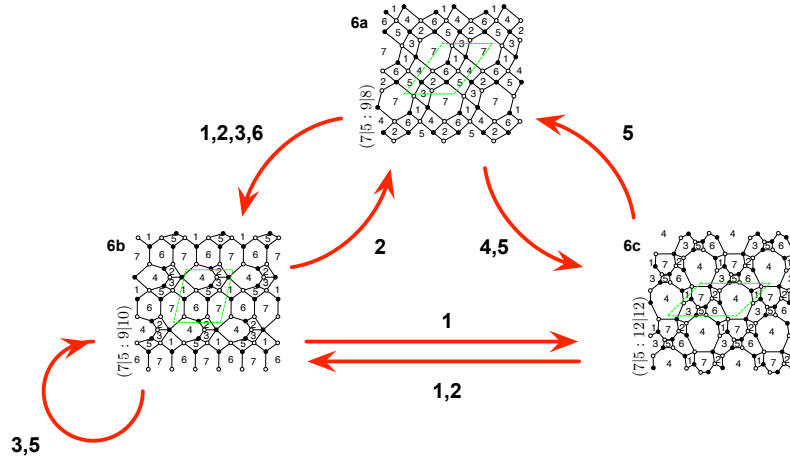
Figure 3.39: The duality tree for PdP$_{4a}$ [Model 6].
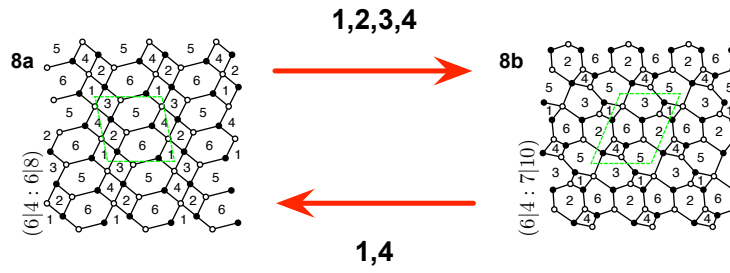
Figure 3.40: The duality tree for SPP/$\mathbb{Z}_2$ with orbifold action $(0, 1, 1, 1)$ [Model 8].
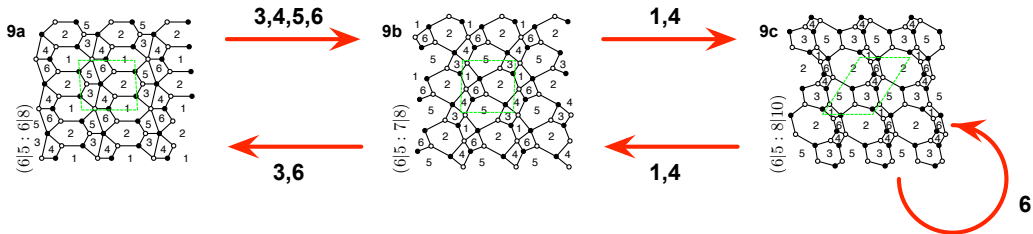
Figure 3.41: The duality tree for PdP$_{3(b)}$ [Model 9].
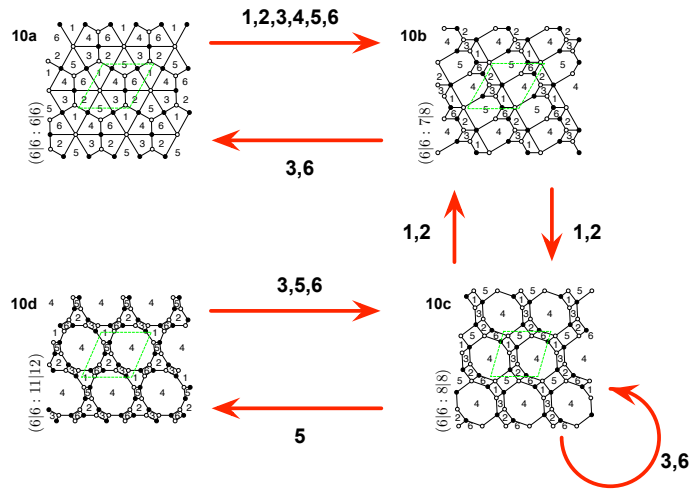
Figure 3.42: The duality tree for dP$_3$ [Model 10].
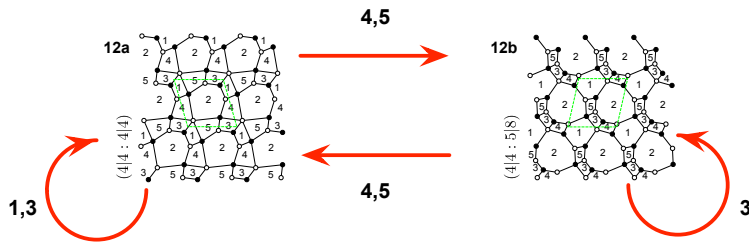
Figure 3.43: The duality tree for dP$_2$ [Model 12].
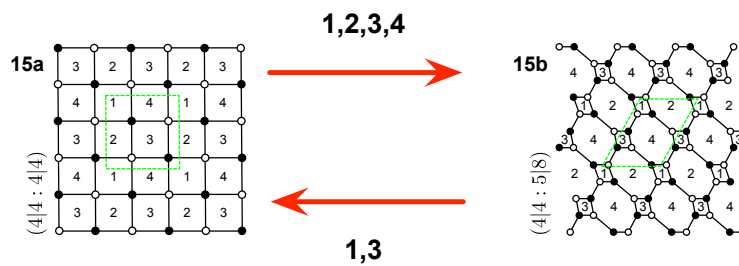
Figure 3.44: The duality tree for $\mathcal{C}/\mathbb{Z}_2$ with orbifold action $(1, 1, 1, 1)$ or the cone over F_0 [Model 15].

3.20 Specular Duality and Conclusions

The work above uses the 16 reflexive polygons in Figure 3.1 as toric diagrams of Calabi-Yau moduli spaces of $3 + 1$ dimensional $\mathcal{N} = 1$ supersymmetric gauge theories. These quiver gauge theories are represented by brane tilings. A natural question to ask from this setup is to identify all brane tilings corresponding to the 16 reflexive polygons. Motivated by this line of thought, the following comprehensive results have been presented in this chapter:

- There are exactly 30 brane tilings encoding supersymmetric quiver gauge theories whose mesonic moduli spaces are represented by reflexive polygons. All gauge theories are related by a cascade of Higgs mechanisms. In addition, toric (Seiberg) duality maps multiple gauge theories to the same reflexive polygon.

- The generating function of mesonic gauge invariant operators known as the mesonic Hilbert series is computed using the Molien integral formula for each of the 30 quiver theories. Fugacities of the Hilbert series are related both to perfect matchings and hence points in the toric diagram as well as charges under the global symmetry of the gauge theory. Hilbert series of toric dual phases have been shown to be identical.

- The generators of the mesonic moduli space of all 30 quiver gauge theories have been found both in terms of chiral fields of the gauge theory as well as the perfect matchings of the brane tiling.

- The mesonic charges on the moduli space generators have been found such that they form for each generator a point on $\mathbb{Z}^2$. The convex hull of all such points is a reflexive polygon. For all 30 quiver gauge theories, these reflexive polygons known as lattice of generators are exactly the polar duals to the toric diagrams.

The above observations made by classifying all brane tilings corresponding to reflexive polygons lead to a comprehensive overview of a special set of quiver gauge theories. This overview is the precursor to a discovery of a new duality of quiver gauge theories. This **specular duality** is best observed in the context of toric diagrams with points labelled by perfect matchings of the brane tiling. Recall that extremal perfect matchings correspond to the corner points coloured black in the toric diagrams in Figure 3.2, whereas internal perfect matchings are points lying strictly within the perimeter of the polygon. External perfect matchings are all points on the perimeter of the polygon including the extremal ones. All except extremal perfect matchings correspond to GLSM fields with zero R-charge.

The new duality we propose exchanges the internal perfect matchings with the external perfect matchings. For the set of brane tilings corresponding to reflexive polygons,

the duality map is unique by forming duality pairs between models as follows

$$1 \leftrightarrow 1$$
$$2 \leftrightarrow 4d \ , \ 3a \leftrightarrow 4c \ , \ 3b \leftrightarrow 3b \ , \ 4a \leftrightarrow 4a \ , \ 4b \leftrightarrow 4b$$
$$5 \leftrightarrow 6c \ , \ 6a \leftrightarrow 6a \ , \ 6b \leftrightarrow 6b$$
$$7 \leftrightarrow 10d \ , \ 8a \leftrightarrow 10c \ , \ 8b \leftrightarrow 9c \ , \ 9a \leftrightarrow 10b \ , \ 9b \leftrightarrow 9b \ , \ 10a \leftrightarrow 10a$$
$$11 \leftrightarrow 12b \ , \ 12a \leftrightarrow 12a$$
$$13 \leftrightarrow 15b \ , \ 14 \leftrightarrow 14 \ , \ 15a \leftrightarrow 15a$$
$$16 \leftrightarrow 16 \tag{3.20.290}$$

For instance, the dual pair $13 \leftrightarrow 15b$ in Figure 3.45 is exact under the indicated swap between external and internal perfect matchings.
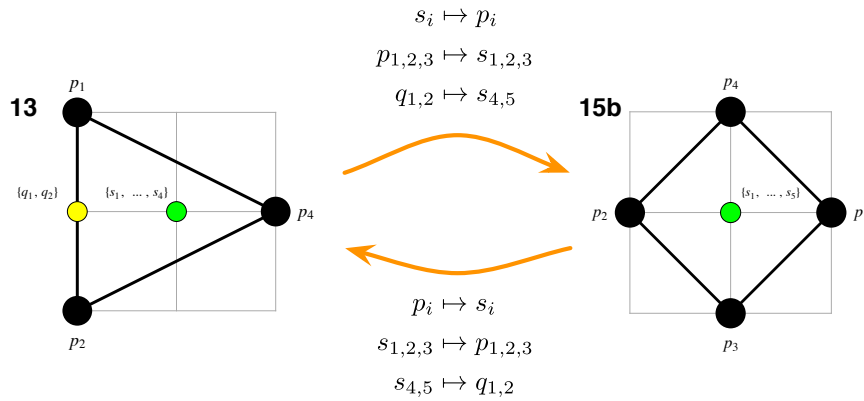
Figure 3.45: Specular duality between Model 13 ($\mathbb{C}^3/\mathbb{Z}_4(1,1,2)$) and Model 15b ($\mathbb{F}_0$, phase b). The exchange of internal and external perfect matchings map between the two models.

Accordingly, specular duality maps between brane tilings whose corresponding quiver gauge theories have different mesonic moduli spaces. In the following chapter, which is an edited version of [7], it is illustrated how specular duality maps not the mesonic moduli spaces but the master spaces [71, 73, 75, 18, 72, 74] of the dual pairs in (3.20.290). The master space is the complete moduli space including both the mesonic and baryonic branches. It is shown that the master spaces of the dual pairs in (3.20.290) are *identical* under a translation of fields given by the mapping of perfect matchings of the corresponding brane tilings. Further study of this duality is of great interest and some interpretations are given in chapter §4.

4 Brane Tilings and Specular Duality

In the previous chapter, we have classified all 30 brane tilings whose mesonic moduli space is a toric Calabi-Yau 3-fold with a reflexive toric diagram. The classification not only gave us a full understanding about the relationship between reflexive toric diagrams and lattice of mesonic generators for the brane tilings, but also led to the discovery of a new correspondence which we call specular duality. The new correspondence relates brane tilings with the same master spaces and is a direct result of the classification we have made based on reflexive polygons. This is a classic example of how classification of brane tilings can lead to a new discovery.

Furthermore, brane tiling classification highlights the viewpoint that supersymmetric theories should be handled as ensembles rather than one by one. We have already encountered ensembles of brane tilings as toric duality trees in the previous chapter in section §3.19. More tree diagrams will be given in this chapter to illustrate the relationship between brane tilings under toric duality, higgsing/unhiggsing and specular duality.

In the following chapter, we study specular duality by computing the refined Hilbert series of the master space of brane tilings with reflexive toric diagrams. The Hilbert series encodes the generators and defining relations of the combined mesonic and baryonic moduli space. The study of specular duality leads us to a new discovery of a class of yet unexplored supersymmetric quiver theories. The chapter is an edited version of [7] which is a publication in collaboration with Amihay Hanany.

4.1 Introduction

Dualities have vastly contributed towards a better understanding of string theory and beyond. A particular example is mirror symmetry [186, 148, 187, 149, 150, 151, 152, 153, 154] which identifies two Type II superstring theories compactified on Calabi-Yau 3-folds whose Hodge numbers are swapped. A similar example, although only true at low energies, is *toric (Seiberg) duality* [34, 92, 14, 33, 36, 181, 182]. It relates brane tilings with the same mesonic moduli space.

The rich combinatorial structure of brane tilings led recently to new insights beyond toric duality. For instance, certain toric diagrams have a single interior point and exhibit the special property of appearing in polar dual pairs [167, 168, 169, 170, 171, 172]. They
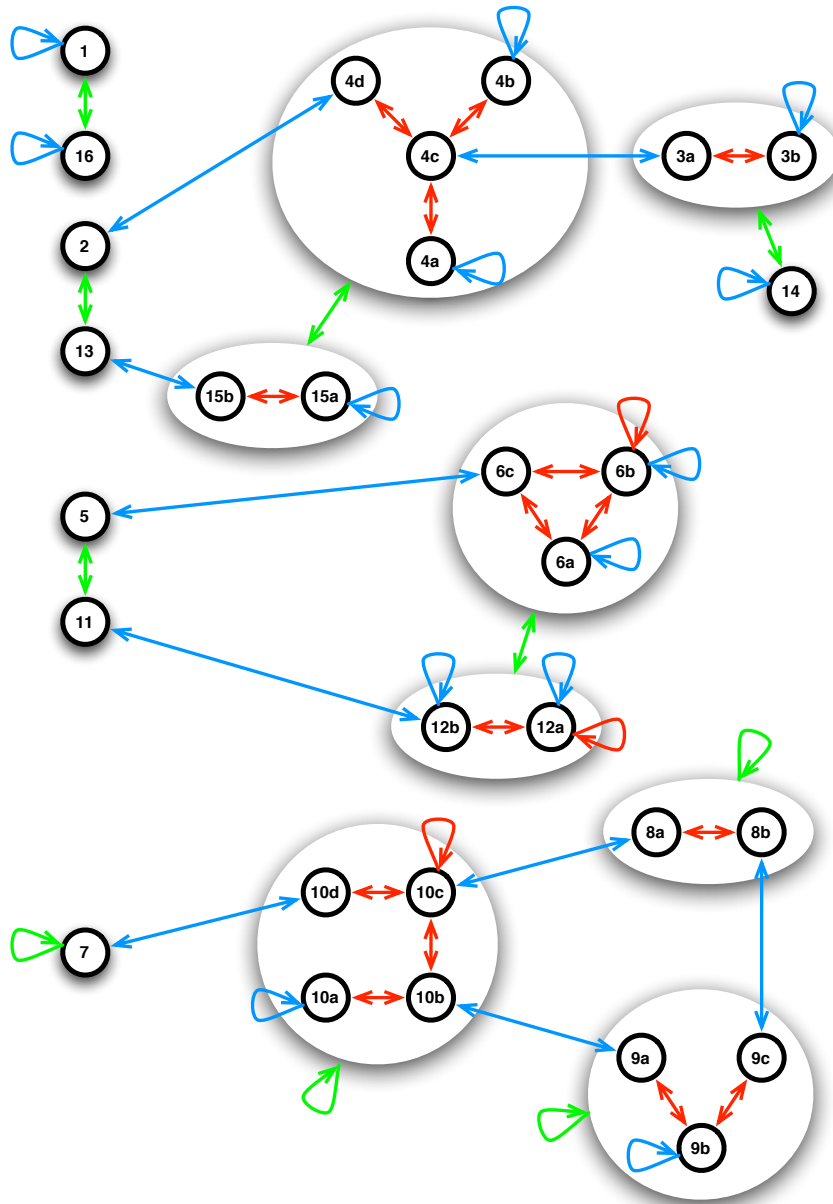
Figure 4.1: *The three dualities for Brane Tilings with Reflexive Toric Diagrams.* The arrows indicate toric duality (red), specular duality (blue), and reflexive duality (green) which is discussed in [5]. The black nodes of the duality tree represent distinct brane tilings, where the labels are taken from [5] and Figure 3.2.

are called reflexive toric diagrams and relate to a correspondence between brane tilings which was studied in [5]. Given brane tilings A and B whose reflexive toric diagrams are a dual pair, the toric diagram of brane tiling A is the lattice of generators of the mesonic moduli space of brane tiling B, and vice versa. We call this correspondence

reflexive duality.

In the following, we discuss a new correspondence that was named in [5] **specular duality**. It identifies brane tilings which have isomorphic combined mesonic and baryonic moduli spaces, also known as master spaces $\mathcal{F}^{\flat}$. The following scenarios of brane tilings apply to this new duality:

1. Dual brane tilings A and B are both on T^2. They have reflexive toric diagrams.

2. Brane tiling A is on T^2 and dual brane tiling B is not on T^2. Brane tiling A has a toric diagram which is not reflexive.

3. Both brane tilings A and B are not on T^2.

For brane tilings with reflexive toric diagrams, specular duality manifests itself not only as an isomorphism between master spaces. The additional properties are:

- The external/internal perfect matchings of brane tiling A are the internal/external perfect matchings of brane tiling B.

- The mesonic flavour symmetries of brane tiling A are the hidden or anomalous baryonic symmetries of brane tiling B, and vice versa.

The following work studies specular duality restricted to brane tilings with reflexive toric diagrams. The Hilbert series of $\mathcal{F}^{\flat}$ is computed explicitly to illustrate its invariance under the new correspondence. The swap between external and internal perfect matchings, and mesonic and baryonic symmetries is explained. Moreover, we illustrate that specular duality is a reflection of the Calabi-Yau cone of $\mathcal{F}^{\flat}$ along a hyperplane. The properties of specular duality apply to all 30 brane tilings with reflexive toric diagrams in [5].

The new correspondence extends beyond brane tilings with reflexive toric diagrams. Accordingly, specular duality can lead to brane tilings on spheres or Riemann surfaces with genus $g \geq 2$. These have no known AdS dual and have mesonic moduli spaces which are not necessarily Calabi-Yau 3-folds [54, 188, 89]. Their quiver and superpotential however admit a master space which can be traced back to a brane tiling on T^2.

Specular duality for brane tilings that are not on T^2 may lead to new insights into quiver gauge theories and Calabi-Yau moduli spaces. The work concludes with this observation and highlights the importance of future studies as well as the initial study in chapter §5.

The chapter is divided into the following sections. Section §4.2 begins with a short review on toric duality and compares its properties with the characteristics of specular duality. The new correspondence between brane tilings is explained in terms of the untwisting map [83, 81, 88] and modified shivers [52, 189, 64]. Section §4.3 studies and

summarises the transformation of the brane tiling, the exchange of perfect matchings, and the swap of mesonic and baryonic symmetries under specular duality. The concluding section gives a short introduction on how specular duality relates brane tilings on T^2 with tilings on spheres and Riemann surfaces of genus $g \geq 2$.

4.2 An introduction to Specular Duality

The following section reviews the summary on toric duality for brane tilings in section §1.6.2 and compares it with specular duality. The section illustrates how the new correspondence is related to the untwisting map [83, 81, 88] and the shiver [52, 189, 64]. We focus on the 30 brane tilings with reflexive toric diagrams.

4.2.1 Toric Duality and Specular Duality

Toric Duality. Two $4d$ quiver gauge theories with brane tilings are called toric dual [34, 92, 14, 33, 36, 181, 182] if in the UV they have different Lagrangians with a different field content and superpotential, but flow to the same universality class in the IR.

Let us summarise the properties of toric duality for brane tilings:

- The *mesonic moduli spaces* $\mathcal{M}^{mes}$ are the same, but the master spaces $^{\mathrm{Irr}}\mathcal{F}^\flat$ are not [73]. The mesonic Hilbert series are the same up to a fugacity map.

- The *toric diagrams* of $\mathcal{M}^{mes}$ are $GL(2, \mathbb{Z})$ equivalent. However, multiplicities of internal toric points with zero R-charge can differ.

- The number of *gauge groups* G remains constant.

Specular Duality. The new correspondence has the following properties for dual brane tilings:

- $^{\mathrm{Irr}}\mathcal{F}^\flat$ are isomorphic[1] and the Hilbert series are the same up to a fugacity map.

- Except for self-dual cases, $\mathcal{M}^{mes}$ are not the same.

- The number of gauge groups G remains invariant.

- The number of matter fields E remains invariant.

---

[1] Note: The master space here is the complete moduli space for one brane. Specular duality extends to the full master space $\mathcal{F}^\flat$, not just its largest irreducible component $^{\mathrm{Irr}}\mathcal{F}^\flat$. We restrict the discussion here to $^{\mathrm{Irr}}\mathcal{F}^\flat$.

d	Number of Polytopes
1	1
2	16
3	4319
4	473800776

Table 4.1: *Counting Reflexive Polytopes.* Number of distinct reflexive lattice polytopes in dimension $d \leq 4$. The number of polytopes forms a sequence which has the OEIS identifier A090045.

There are 16 reflexive toric diagrams. They are summarized in Figure 3.2 [5] and relate to 30 brane tilings. Specular duality exhibits additional properties for this set of brane tilings:

- Internal/external perfect matchings of brane tiling A become external/internal perfect matchings of the dual brane tiling B.

- The mesonic flavour symmetries of brane tiling A become the anomalous or enhanced hidden baryonic symmetries of brane tiling B.

As for toric duality, the properties of specular duality apply to the IR moduli spaces of brane tilings.

As noted above, specular duality exhibits additional properties for brane tilings with reflexive toric diagrams. Many of the 30 brane tilings which correspond to the 16 reflexive polygons are toric duals [5]. The properties of specular duality have been checked for all of the 30 brane tilings with reflexive toric diagrams.

Reflexive polytopes have the following properties:

- A **reflexive polytope** is a convex $\mathbb{Z}^d$ lattice polytope whose unique interior point is the origin $(0, \ldots, 0)$.

- A **dual (polar) polytope** exists for every reflexive polytope Δ. The dual Δ° is another lattice polytope with points

$$\Delta^\circ = \{v^\circ \in \mathbb{Z}^d \mid \langle v^\circ, v \rangle \geq -1 \ \forall v \in \Delta\} \tag{4.2.1}$$

Δ° is another reflexive polytope. There are self-dual polytopes, $\Delta = \Delta^\circ$.[2]

- A **classification of reflexive polytopes** [168, 169, 170] is available for the dimensions $d \leq 4$ as shown in Table 4.1.

---

[2]Note that this duality between reflexive polytopes does not correspond to specular duality.
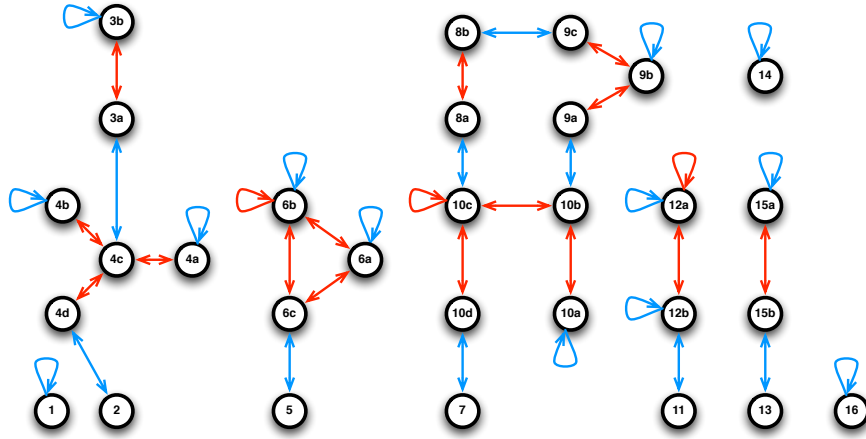
Figure 4.2: *Toric and Specular Duality.* These are the duality trees of brane tilings (nodes) with reflexive toric diagrams. The brane tiling labels are taken from [5] and Figure 3.2. Arrows indicate toric duality (red) and specular duality (blue).

Specular duality preserves the reflexivity of the toric diagram and the set of 30 brane tilings in Figure 3.2:

$$1 \leftrightarrow 1$$
$$2 \leftrightarrow 4d \ , \ 3a \leftrightarrow 4c \ , \ 3b \leftrightarrow 3b \ , \ 4a \leftrightarrow 4a \ , \ 4b \leftrightarrow 4b$$
$$5 \leftrightarrow 6c \ , \ 6a \leftrightarrow 6a \ , \ 6b \leftrightarrow 6b$$
$$7 \leftrightarrow 10d \ , \ 8a \leftrightarrow 10c \ , \ 8b \leftrightarrow 9c \ , \ 9a \leftrightarrow 10b \ , \ 9b \leftrightarrow 9b \ , \ 10a \leftrightarrow 10a$$
$$11 \leftrightarrow 12b \ , \ 12a \leftrightarrow 12a$$
$$13 \leftrightarrow 15b \ , \ 14 \leftrightarrow 14 \ , \ 15a \leftrightarrow 15a$$
$$16 \leftrightarrow 16 \qquad \qquad . \ (4.2.2)$$

All brane tilings with reflexive toric diagrams have specular duals as illustrated in Figure 4.3. The figure illustrates that dual pairs are related by a swap of internal and external perfect matchings.

Self-dual Brane Tilings. Certain brane tilings with reflexive toric diagrams are self-dual. These are:

$$1 \ , \ 3b \ , \ 4a \ , \ 4b \ , \ 6a \ , \ 6b \ , \ 9b \ , \ 10a \ , \ 12a \ , \ 14 \ , \ 15a \ , \ 16 \ , \qquad (4.2.3)$$

which are summarized in Figure 4.4. The toric diagram and brane tiling are invariant under specular duality.
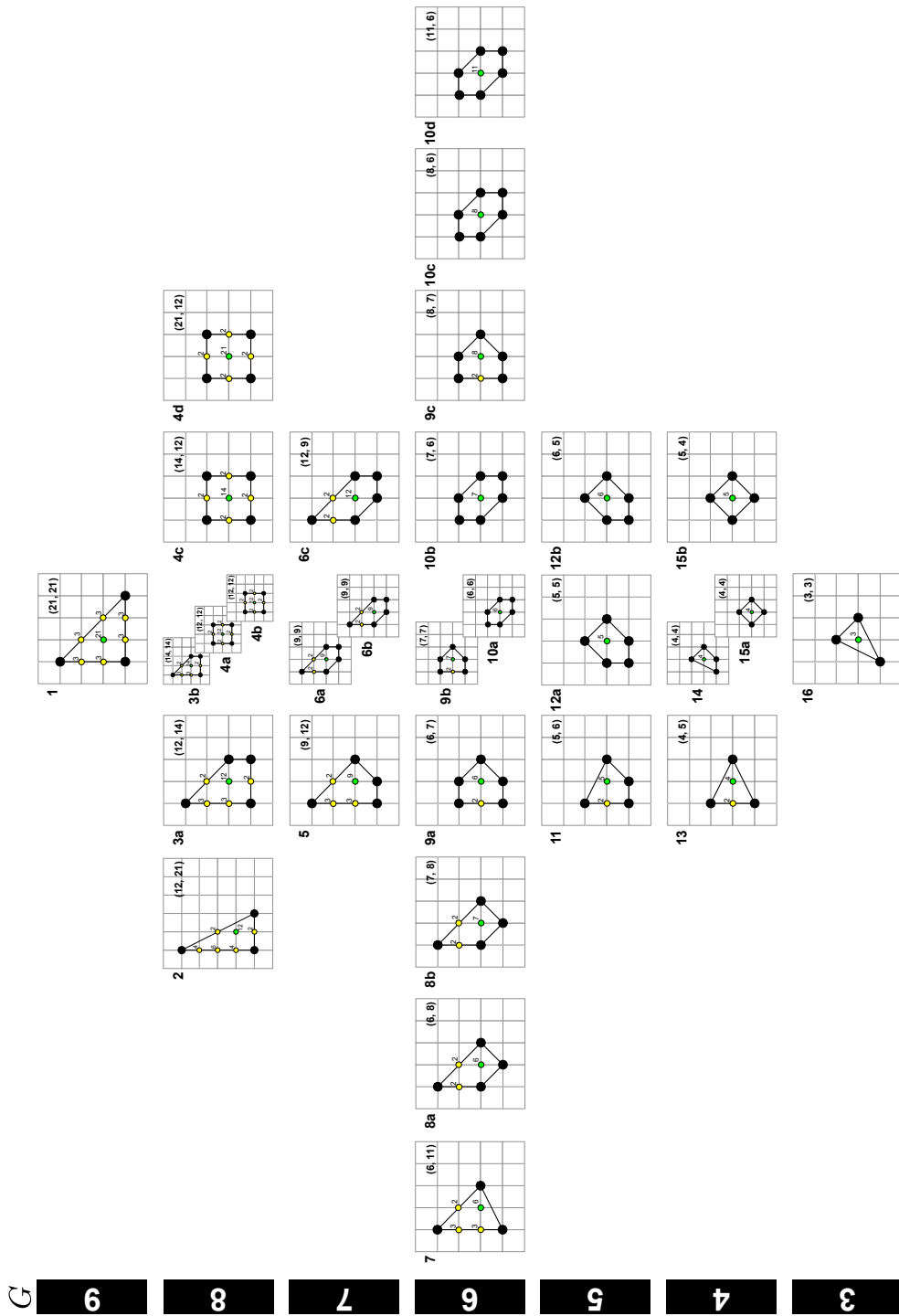
Figure 4.3: *Arbor specularis.* The 30 reflexive toric diagrams with perfect matching multiplicities. The models are labelled with (n_i, n_e), where n_i and n_e are the number of internal and external perfect matchings respectively. The y-axis is labelled by the number of gauge groups G or the area of the polygon, and the position along the x-axis relates to the difference $n_i - n_e$.
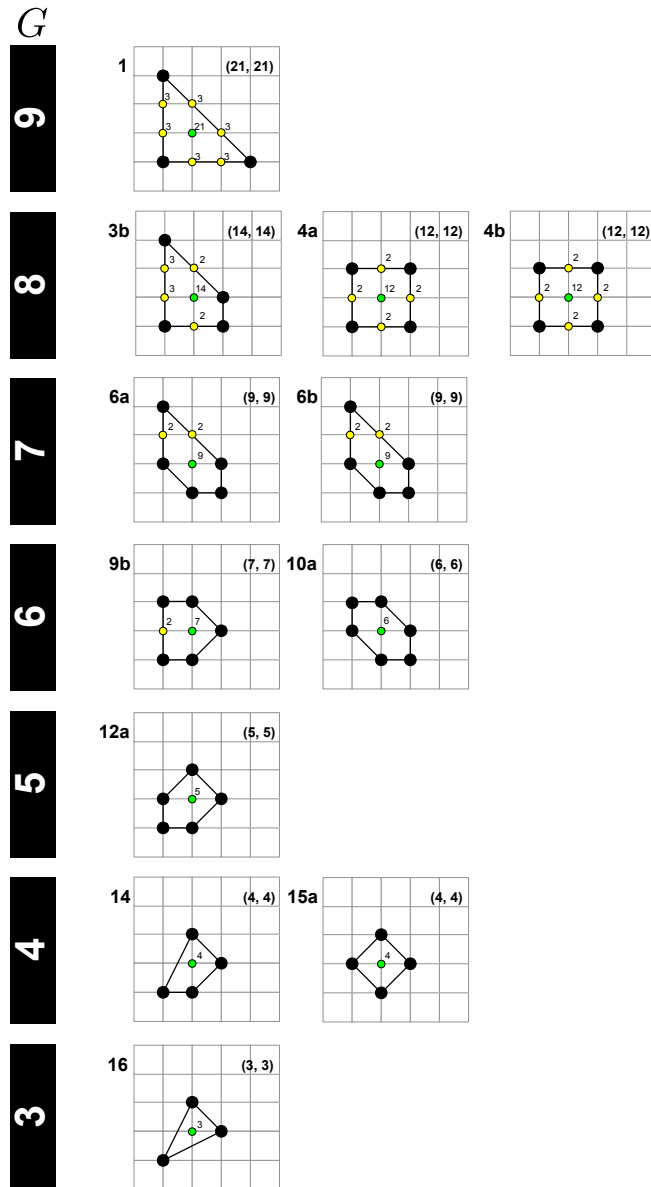
Figure 4.4: *Self-duals under Specular Duality.* These are the 12 reflexive toric diagrams which have self-dual brane tilings. The models are labelled with (n_i, n_e), where n_i and n_e are the number of internal and external perfect matchings respectively.

4.2.2 Specular Duality and 'Fixing' Shivers

As illustrated in Section §4.2.1, toric duality has a natural interpretation on the brane tiling. The following section identifies the interpretation of specular duality on the brane tiling.

A toric singularity has an associated **characteristic polynomial**, also known as the

Newton polynomial,

$$P(w,z) = \sum_{(n_1,n_2)\in\Delta} a_{n_1,n_2} w^{n_1} z^{n_2} \ , \tag{4.2.4}$$

where the sum runs over all points in the toric diagram, and a_{n_1,n_2} is a complex number. The geometric description of the **mirror manifold** [190, 191, 83] is

$$\begin{aligned} Y &= P(w,z) \ , \\ Y &= uv \ , \end{aligned} \tag{4.2.5}$$

where $w,z \in \mathbb{C}^*$ and $u,v \in \mathbb{C}$. The curve $P(w,z) - Y = 0$ describes a punctured **Riemann surface** Σ_Y with

- the genus g corresponding to the number I of internal toric points

- the number of punctures corresponding to the number E of external toric points.

The Riemann surface is fibered over each point in Y. Of particular interest to us is the Riemann surface Σ fibered over the origin $Y = 0$. It is related to the brane tiling on T^2 under the **untwisting map** ϕ_u [83, 81, 88].

A brane tiling consists of **zig-zag paths** η_i [105, 16]. These are collections of edges in the tiling that form closed non-trivial paths on T^2. Zig-zag paths maximally turn left at a black node and then maximally turn right at the next adjacent white node. The **winding numbers** (p,q) of zig-zag paths relate to the $\mathbb{Z}^2$ direction of the corresponding leg in the (p,q)-web [107]. The dual of the (p,q)-web is the toric diagram. By thickening the (p,q)-web, one obtains the punctured Riemann surface Σ.

The untwisting map ϕ_u has the following action on the brane tiling:

$$\phi_u \ : \qquad \begin{aligned} \text{brane tiling on } T^2 \ &\to \ \text{shiver on } \Sigma \\ \text{zig-zag path } \eta_i \ &\mapsto \ \text{puncture } \gamma_i \\ \text{face/gauge group } U(N)_a \ &\mapsto \ \text{zig-zag path } \tilde{\eta}_a \\ \text{node/term } w_k,\ b_k \ &\mapsto \ \text{node/term } w_k,\ b_k \\ \text{edge/field } X_{ab} \ &\mapsto \ \text{edge/field } X_{ij} \ , \end{aligned} \tag{4.2.6}$$

where a,b count $U(N)$ gauge groups/brane tiling faces, i,j count zig-zag paths on the original brane tiling on T^2, and $\tilde{\eta}_a$ are zig-zag paths of the shiver on Σ. An illustration of the untwisting map is in Figure 4.5.

The untwisted brane tiling on Σ is known as a **shiver** [52, 189, 64]. It is not associated to a quiver, a superpotential and a field theory moduli space, and therefore can be interpreted as a 'pseudo-brane tiling' on a punctured Riemann surface. An interesting

$$
\begin{array}{ccc}
\text{brane tiling on } T^2 & \overset{\phi_u}{\rightarrow} & \text{shiver on } \Sigma \\
\text{zig-zag path } \eta_i & \mapsto & \text{puncture } \gamma_i \\
\text{face/gauge group } U(N)_a & \mapsto & \text{zig-zag path } \tilde{\eta}_a \\
\text{node/term } w_k, \, b_k & \mapsto & \text{node/term } w_k, \, b_k \\
\text{edge/field } X_{ab} & \mapsto & \text{edge/field } X_{ij}
\end{array}
$$
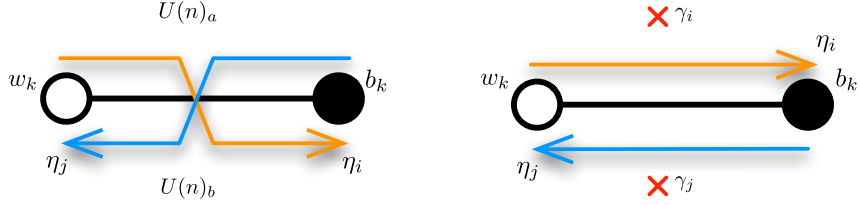
Figure 4.5: *The Untwisting Map ϕ_u*. The untwisting map relates a brane tiling on T^2 to a shiver on a punctured Riemann surface Σ.

question to ask at this point is whether a shiver can be 'fixed' by a map ϕ_f such that it becomes a consistent brane tiling.

The main obstructions are the punctures of Σ which have no interpretation in the quiver gauge theory context. Let the punctures therefore be identified with $U(N)$ gauge groups under the following definition of the **shiver fixing map**:

$$
\begin{aligned}
\phi_f \ : \qquad \text{shiver on } \Sigma &\rightarrow \text{brane tiling on } \Sigma \\
\text{puncture } \gamma_i &\mapsto \text{face/gauge group } U(N)_i \ , \qquad (4.2.7)
\end{aligned}
$$

with the zig-zag paths $\tilde{\eta}_a$, nodes w_k and b_k, and edges X_{ij} on the shiver remaining invariant.

Accordingly, using the shiver fixing map ϕ_f and the untwisting map ϕ_u, **specular duality** on brane tilings can be defined as follows

$$
\begin{aligned}
\phi_{\text{specular}} = \phi_f \circ \phi_u \ : \qquad \text{brane tiling A on } T^2 &\rightarrow \text{brane tiling B on } \Sigma \\
\text{zig-zag path } \eta_i &\mapsto \text{face/gauge group } U(N)_i \\
\text{face/gauge group } U(N)_a &\mapsto \text{zig-zag path } \tilde{\eta}_a \\
\text{node/term } w_k, \, b_k &\mapsto \text{node/term } w_k, \, b_k \\
\text{edge/field } X_{ab} &\mapsto \text{edge/field } X_{ij} \ , \qquad (4.2.8)
\end{aligned}
$$

where ϕ_{specular} is invertible. A graphical illustration of ϕ_{specular} is in Figure 4.6.

For a brane tiling to have a Calabi-Yau 3-fold as its mesonic moduli space and to have a known AdS dual [54, 188, 89], it needs to be on T^2. Brane tilings with reflexive toric diagrams have a specular dual which is always on $\Sigma = T^2$. This is because, as we recall, reflexive toric diagrams always have by definition $I = 1$ and their (p, q)-web has
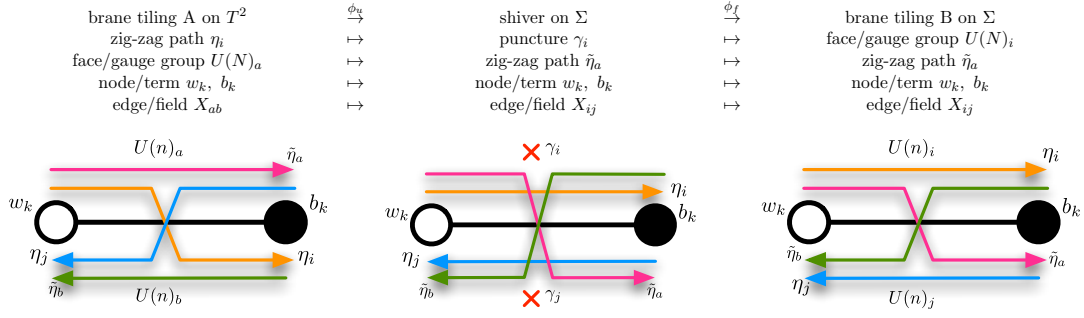
Figure 4.6: *Specular Duality on a Brane Tiling.* The map $\phi_{\text{specular}} = \phi_f \circ \phi_u$ which defines specular duality first untwists a brane tiling and then replaces punctures with $U(N)$ gauge groups.
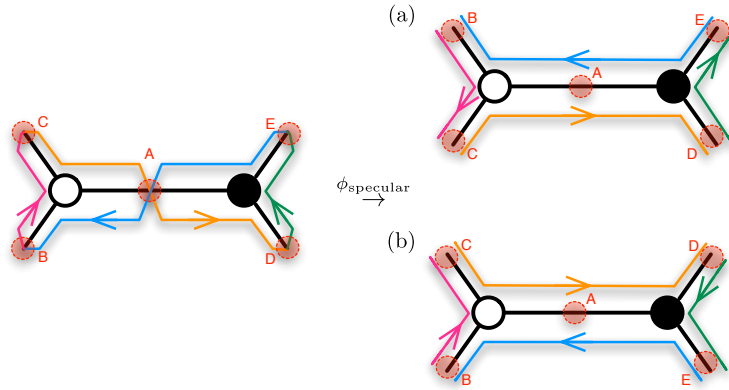
Figure 4.7: *Untwisting the Superpotential.* There are two equivalent ways of untwisting the brane tiling. The order of fields around either a white (clockwise) or black (anti-clockwise) node in the brane tiling is reversed under the untwisting. Either way results in the same brane tiling.

therefore always genus $g = 1$.

Invariance of the master space $^{\text{Irr}}\mathcal{F}^{\flat}$. Specular duality has an important effect on a brane tiling's superpotential W which can be demonstrated with the following example

$$W = \cdots + ABC - ADE + \dots \, , \tag{4.2.9}$$

where $A, \dots, E$ are quiver fields.[3] The corresponding nodes in the brane tiling are illustrated along with zig-zag paths in the left panel of Figure 4.7.

Specular duality untwists the brane tiling in such a way that the order of quiver fields around either white (clockwise) nodes or black (anti-clockwise) nodes is reversed. For

---

[3]There is an overall trace in the superpotential which is not written down for simplicity.

the example in (4.2.9), the superpotential of the dual brane tiling has either the form

$$W_{(a)} = \cdots + ACB - ADE + \ldots \tag{4.2.10}$$

or the form

$$W_{(b)} = \cdots + ABC - AED + \ldots \tag{4.2.11}$$

as illustrated in the right panel of Figure 4.7. The options of reversing the orientation around white nodes or black nodes are equivalent up to an overall swap of node colours.

For the case of single D3 brane theories with $U(1)$ gauge groups, the fields commute such that

$$W = W_{(a)} = W_{(b)} \ . \tag{4.2.12}$$

The $U(1)$ superpotential is invariant under specular duality. Since the master space $^{\mathrm{Irr}}\mathcal{F}^{\flat}$ is defined in terms of F-terms, the observation in (4.2.12) implies that it is invariant under specular duality.

No specific Quiver from an Abelian W. In order to show that the master spaces of dual one brane theories are isomorphic, it is sufficient to illustrate that the superpotentials are the same when the quiver fields commute. However, it is important to note that if the cyclic order of fields in a given superpotential is not recorded, its correspondence to a specific quiver and hence a brane tiling is not unique. A simple example would be the Abelian potential for $\mathbb{C}^3$ or the conifold $\mathcal{C}$ which is $W = 0$. In contrast to the distinct non-Abelian superpotentials, the trivial Abelian superpotential for these models encodes no information about the field content of the associated brane tilings.

Since specular duality is a well defined map between brane tilings, not just between Abelian superpotentials, we study in the following sections the new correspondence with the help of *characteristics of the mesonic moduli space*. An important observation is that specular duality exchanges internal and external perfect matchings for brane tilings with reflexive toric diagrams. The difference between internal and external perfect matchings is a property of the mesonic moduli space and its toric diagram.

Perfect matchings as GLSM fields are used for the symplectic quotient description of $^{\mathrm{Irr}}\mathcal{F}^{\flat}$. Since perfect matchings represent a choice of coordinates to identify the master space cone, one is free to introduce a new set of coordinates that correspond to the global symmetry of the field theory. In the following sections, we identify coordinate transformations that relate the exchange of internal and external perfect matchings to the exchange of mesonic flavour symmetries and hidden or anomalous baryonic symmetries. Moreover, one can find a third set of coordinates which relate to the boundaries of
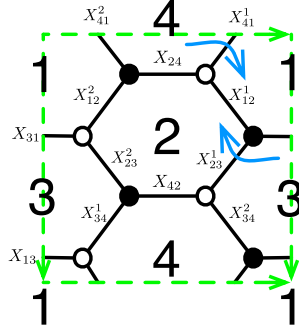
Figure 4.8: Brane Tiling of Model 13 with the edges labelled by quiver fields.

the Calabi-Yau cone and are used to illustrate how an exchange of internal and external perfect matchings leads to a reflection of the $^{\text{Irr}}\mathcal{F}^\flat$ cone along a hyperplane.

4.3 Model 13 ($Y^{2,2}$, $\mathbb{F}_2$, $\mathbb{C}^3/\mathbb{Z}_4$) and Model 15b ($Y^{2,0}$, $\mathbb{F}_0$, $\mathcal{C}/\mathbb{Z}_2$)

In the following section, we study specular duality with Model 13 which is known as $Y^{2,2}$, $\mathbb{F}_2$ or $\mathbb{C}^3/\mathbb{Z}_4$ with action $(1, 1, 2)$ in the literature, and Model 15b which is known as phase II of $Y^{2,0}$, $\mathbb{F}_0$ or $\mathcal{C}/\mathbb{Z}_2$ with action $(1, 1, 1, 1)$.

4.3.1 Brane Tilings and Superpotentials

Figure 4.9 shows how the untwisting map ϕ_u acts on the brane tiling of Model 13 to give a shiver. The fixing map ϕ_f then takes the shiver to give the brane tiling of Model 15b. Beginning with the superpotential of Model 13,

$$
\begin{aligned}
W_{13} \;=\; & +X_{12}^1 X_{24} X_{41}^1 + X_{31} X_{12}^2 X_{23}^2 + X_{41}^2 X_{13} X_{34}^1 + X_{34}^2 X_{42} X_{23}^1 \\
& -X_{12}^1 X_{23}^1 X_{31} - X_{13} X_{34}^2 X_{41}^1 - X_{41}^2 X_{12}^2 X_{24} - X_{34}^1 X_{42} X_{23}^2 \;, \quad (4.3.13)
\end{aligned}
$$

the zig-zag paths are identified as follows

$$
\begin{aligned}
\eta_1 \;=\; & \{X_{12}^1, X_{23}^1, X_{34}^2, X_{41}^1\} \;, \\
\eta_2 \;=\; & \{X_{12}^2, X_{24}, X_{41}^1, X_{13}, X_{34}^1, X_{42}, X_{23}^1, X_{31}\} \;, \\
\eta_3 \;=\; & \{X_{23}^2, X_{34}^1, X_{41}^2, X_{12}^2\} \;, \\
\eta_4 \;=\; & \{X_{13}, X_{34}^2, X_{42}, X_{23}^2, X_{31}, X_{12}^1, X_{24}, X_{41}^2\} \;. \quad (4.3.14)
\end{aligned}
$$

Figure 4.9: *Specular Duality between Models 13 and 15b.* The untwisting map ϕ_u acts on the brane tiling of Model 13 which results in a shiver. The shiver is then fixed with ϕ_f which results in the brane tiling of Model 15b.

The intersections of zig-zag paths highlighted in Figure 4.9 are

$$(A, B, C, D, E, F, G, H, I, J, K, L) =$$
$$(X_{31}, X_{13}, X_{12}^2, X_{34}^1, X_{41}^2, X_{23}^2, X_{24}, X_{42}, X_{41}^1, X_{23}^1, X_{12}^1, X_{34}^2) \quad (4.3.15)$$

Under specular duality, the intersections are mapped to the ones for zig-zag paths on the brane tiling of Model 15b.

In terms of intersections, the superpotential in (4.3.13) takes the form

$$
\begin{aligned}
W_{13} \quad = \quad & +KGI + ACF + EBD + LHJ \\
& -KJA - BLI - ECG - DHF
\end{aligned}
\quad (4.3.16)
$$

The intersections are also fields in the dual brane tiling of Model 15b. Accordingly, the

$$W_{13} \quad = \quad +X_{12}^1 X_{24} X_{41}^1 + X_{31} X_{12}^2 X_{23}^2 + X_{41}^2 X_{13} X_{34}^1 + X_{34}^2 X_{42} X_{23}^1$$
$$-X_{12}^1 X_{23}^1 X_{31} - X_{13} X_{34}^2 X_{41}^1 - X_{41}^2 X_{12}^2 X_{24} - X_{34}^1 X_{42} X_{23}^2$$

Figure 4.10: The quiver, toric diagram, brane tiling and superpotential of Model 13.

corresponding superpotential can be written as

$$\widetilde{W_{13}} = W_{15b} \quad = \quad +X_{14}^1 X_{42}^1 X_{21}^1 + X_{42}^4 X_{23}^2 X_{34}^1 + X_{34}^2 X_{42}^3 X_{23}^1 + X_{14}^2 X_{42}^2 X_{21}^2$$
$$-X_{14}^1 X_{42}^4 X_{21}^2 - X_{42}^3 X_{21}^1 X_{14}^2 - X_{34}^2 X_{42}^1 X_{23}^2 - X_{23}^1 X_{34}^1 X_{42}^2$$
$$= \quad +KGI + ACF + EBD + LHJ$$
$$-KAJ - BIL - EGC - DFH \ . \tag{4.3.17}$$

We note that the two superpotentials are the same up to a reversal of cyclic order of negative terms in (4.3.17). For the Abelian single D3 brane theory, the superpotentials and the corresponding F-terms are the same and hence lead to the same master space $^{\mathrm{Irr}}\mathcal{F}^\flat$.

4.3.2 Perfect Matchings and the Hilbert Series

In order to illustrate that specular duality exchanges internal and external perfect matchings of brane tilings, we consider the symplectic quotient description of $^{\mathrm{Irr}}\mathcal{F}^\flat$. It uses GLSM fields which relate to perfect matchings in a brane tiling. They are

$$W_{15b} \;=\; +X^1_{14}X^1_{42}X^1_{21} + X^4_{42}X^2_{23}X^1_{34} + X^2_{34}X^3_{42}X^1_{23} + X^2_{14}X^2_{42}X^2_{21}$$
$$-X^1_{14}X^4_{42}X^2_{21} - X^3_{42}X^1_{21}X^1_{14} - X^2_{34}X^1_{42}X^2_{23} - X^1_{23}X^1_{34}X^2_{42}$$

Figure 4.11: The quiver, toric diagram, brane tiling and superpotential of Model 15b.

summarized in matrices which are for Model 13 and 15b respectively

$$
P^{13} =
\left(
\begin{array}{c|ccc|cc|cccc}
 & p_1 & p_2 & p_3 & q_1 & q_2 & s_1 & s_2 & s_3 & s_4 \\
\hline
I = X^1_{41} & 1 & 0 & 0 & 1 & 0 & 1 & 0 & 0 & 0 \\
E = X^2_{41} & 0 & 1 & 0 & 1 & 0 & 1 & 0 & 0 & 0 \\
J = X^1_{23} & 1 & 0 & 0 & 1 & 0 & 0 & 1 & 0 & 0 \\
F = X^2_{23} & 0 & 1 & 0 & 1 & 0 & 0 & 1 & 0 & 0 \\
C = X^2_{12} & 1 & 0 & 0 & 0 & 1 & 0 & 0 & 1 & 0 \\
K = X^1_{12} & 0 & 1 & 0 & 0 & 1 & 0 & 0 & 1 & 0 \\
D = X^1_{34} & 1 & 0 & 0 & 0 & 1 & 0 & 0 & 0 & 1 \\
L = X^2_{34} & 0 & 1 & 0 & 0 & 1 & 0 & 0 & 0 & 1 \\
H = X_{42} & 0 & 0 & 1 & 0 & 0 & 1 & 0 & 1 & 0 \\
A = X_{31} & 0 & 0 & 1 & 0 & 0 & 1 & 0 & 0 & 1 \\
B = X_{13} & 0 & 0 & 1 & 0 & 0 & 0 & 1 & 1 & 0 \\
G = X_{24} & 0 & 0 & 1 & 0 & 0 & 0 & 1 & 0 & 1 \\
\end{array}
\right)
,\quad
P^{15b} =
\left(
\begin{array}{c|cccc|ccccc}
 & p_1 & p_2 & p_3 & p_4 & s_1 & s_2 & s_3 & s_4 & s_5 \\
\hline
I = X^1_{21} & 1 & 0 & 0 & 0 & 1 & 0 & 0 & 1 & 0 \\
E = X^2_{34} & 1 & 0 & 0 & 0 & 0 & 1 & 0 & 1 & 0 \\
J = X^2_{21} & 0 & 1 & 0 & 0 & 1 & 0 & 0 & 1 & 0 \\
F = X^1_{34} & 0 & 1 & 0 & 0 & 0 & 1 & 0 & 1 & 0 \\
C = X^2_{23} & 0 & 0 & 1 & 0 & 1 & 0 & 0 & 0 & 1 \\
K = X^1_{14} & 0 & 0 & 1 & 0 & 0 & 1 & 0 & 0 & 1 \\
D = X^1_{23} & 0 & 0 & 0 & 1 & 1 & 0 & 0 & 0 & 1 \\
L = X^2_{14} & 0 & 0 & 0 & 1 & 0 & 1 & 0 & 0 & 1 \\
H = X^2_{42} & 1 & 0 & 1 & 0 & 0 & 0 & 1 & 0 & 0 \\
A = X^4_{42} & 1 & 0 & 0 & 1 & 0 & 0 & 1 & 0 & 0 \\
B = X^3_{42} & 0 & 1 & 1 & 0 & 0 & 0 & 1 & 0 & 0 \\
G = X^1_{42} & 0 & 1 & 0 & 1 & 0 & 0 & 1 & 0 & 0 \\
\end{array}
\right).
$$
$$(4.3.18)$$

The corresponding F-term charge matrices are

$$
Q^{13}_F =
\left(
\begin{array}{ccc|cc|cccc}
p_1 & p_2 & p_3 & q_1 & q_2 & s_1 & s_2 & s_3 & s_4 \\
\hline
0 & 0 & -1 & -1 & 0 & 1 & 1 & 0 & 0 \\
0 & 0 & -1 & 0 & -1 & 0 & 0 & 1 & 1 \\
1 & 1 & 0 & -1 & -1 & 0 & 0 & 0 & 0 \\
\end{array}
\right)
,\quad
Q^{15b}_F =
\left(
\begin{array}{cccc|ccccc}
p_1 & p_2 & p_3 & p_4 & s_1 & s_2 & s_3 & s_4 & s_5 \\
\hline
1 & 1 & 0 & 0 & 0 & 0 & -1 & -1 & 0 \\
0 & 0 & 1 & 1 & 0 & 0 & -1 & 0 & -1 \\
0 & 0 & 0 & 0 & 1 & 1 & 0 & -1 & -1 \\
\end{array}
\right).
$$
$$(4.3.19)$$

From the quiver incidence matrices, one obtains the following D-term charge matrices

$$
Q^{13}_D =
\left(
\begin{array}{ccc|cc|cccc}
p_1 & p_2 & p_3 & q_1 & q_2 & s_1 & s_2 & s_3 & s_4 \\
\hline
0 & 0 & 0 & 1 & -1 & 0 & 0 & 0 & 0 \\
0 & 0 & 0 & 0 & 0 & 1 & -1 & 0 & 0 \\
0 & 0 & 0 & 0 & 0 & 0 & 0 & 1 & -1 \\
\end{array}
\right)
,\quad
Q^{15b}_D =
\left(
\begin{array}{cccc|ccccc}
p_1 & p_2 & p_3 & p_4 & s_1 & s_2 & s_3 & s_4 & s_5 \\
\hline
0 & 0 & 0 & 0 & 0 & 1 & -1 & 0 & 0 \\
0 & 0 & 0 & 0 & 0 & 0 & 1 & -1 & 0 \\
0 & 0 & 0 & 0 & 0 & 0 & 0 & 1 & -1 \\
\end{array}
\right).
$$
$$(4.3.20)$$

The kernel of the total charge matrix Q_t leads to the coordinates of points in the toric

diagram,

$$G_t^{13} = \left(\begin{array}{ccc|cc|cccc} p_1 & p_2 & p_3 & q_1 & q_2 & s_1 & s_2 & s_3 & s_4 \\ 0 & 0 & 2 & 0 & 0 & 1 & 1 & 1 & 1 \\ 2 & 0 & -1 & 1 & 1 & 0 & 0 & 0 & 0 \\ 1 & 1 & 1 & 1 & 1 & 1 & 1 & 1 & 1 \end{array} \right) , \quad G_t^{15b} = \left(\begin{array}{cccc|ccccc} p_1 & p_2 & p_3 & p_4 & s_1 & s_2 & s_3 & s_4 & s_5 \\ 2 & 0 & 2 & 0 & 1 & 1 & 1 & 1 & 1 \\ 0 & 0 & -1 & 1 & 0 & 0 & 0 & 0 & 0 \\ 1 & 1 & 1 & 1 & 1 & 1 & 1 & 1 & 1 \end{array} \right) .$$
(4.3.21)

Note that the corresponding toric diagrams in Figure 4.10 and Figure 4.11 are $GL(2, \mathbb{Z})$ transformed.

The columns in the G_t matrices indicate the coordinates of points in the toric diagram with the associated perfect matchings. Using this information, one relates columns of the matrices Q_F, Q_D and P to either external or internal perfect matchings.

Specular duality swaps external and internal perfect matchings as follows

$$(p_1, p_2, p_3, q_1, q_2, s_1, s_2, s_3, s_4)_{13} \leftrightarrow (s_1, s_2, s_3, s_4, s_5, p_1, p_2, p_3, p_4)_{15b} . \qquad (4.3.22)$$

Accordingly, the duality maps the perfect matching matrix P^{13} to P^{15b} as well as the F-term charge matrix Q_F^{13} to Q_F^{15b} by a swap of matrix columns. As a result, the following symplectic quotient descriptions of the master spaces $^{\mathrm{Irr}}\mathcal{F}^\flat$ are isomorphic

$$\begin{aligned} ^{\mathrm{Irr}}\mathcal{F}_{13}^\flat &= \mathbb{C}^9[p_1, p_2, p_3, q_1, q_2, s_1, s_2, s_3, s_4]//Q_F^{13} , \\ ^{\mathrm{Irr}}\mathcal{F}_{15b}^\flat &= \mathbb{C}^9[p_1, p_2, p_3, p_4, s_1, s_2, s_3, s_4, s_5]//Q_F^{15b} . \end{aligned} \qquad (4.3.23)$$

Specular duality can therefore be observed on the level of the Hilbert series of $^{\mathrm{Irr}}\mathcal{F}^\flat$. Starting with Model 15b, its symplectic quotient leads to the following refined Hilbert series

$$\begin{aligned} g_1(t_i, y_{s_i}; {}^{\mathrm{Irr}}\mathcal{F}_{15b}^\flat) &= \prod_{i=1}^3 \oint_{|z_i|=1} \frac{\mathrm{d}z_i}{2\pi i z_i} \frac{1}{(1 - z_1 t_1)(1 - z_1 t_2)(1 - z_2 t_3)(1 - z_2 t_4)(1 - z_3 s_1)} \\ &\qquad \times \frac{1}{(1 - z_3 s_2)(1 - \frac{1}{z_1 z_2} s_3)(1 - \frac{1}{z_1 z_3} s_4)(1 - \frac{1}{z_2 z_3} s_5)} \\ &= \frac{P(t_i, y_{s_i})}{(1 - t_1 t_2 y_{s_3})(1 - t_2 t_3 y_{s_3})(1 - t_1 t_4 y_{s_3})(1 - t_2 t_4 y_{s_3})} \\ &\qquad \times \frac{1}{(1 - t_1 s_1 y_{s_4})(1 - t_2 s_1 y_{s_4})(1 - t_1 y_{s_2} y_{s_4})(1 - t_2 y_{s_2} y_{s_4})} \\ &\qquad \times \frac{1}{(1 - t_3 y_{s_1} y_{s_5})(1 - t_4 y_{s_1} y_{s_5})(1 - t_3 y_{s_2} y_{s_5})(1 - t_4 y_{s_2} y_{s_5})} , \end{aligned}$$
(4.3.24)

where the numerator $P(t_i, y_{s_i})$ is presented in appendix §A.5. Fugacities t_i and y_{s_i} count external and internal perfect matchings p_i and s_i of Model 15b respectively. The

plethystic logarithm of the Hilbert series is

$$PL[g_1(t_i, y_{s_i}; {}^{\mathrm{Irr}}\mathcal{F}_{15b}^{\flat})] = y_{s_1}y_{s_4}t_1 + y_{s_2}y_{s_4}t_1 + y_{s_1}y_{s_4}t_2 + y_{s_2}y_{s_4}t_2 + y_{s_1}y_{s_5}t_3 + y_{s_2}y_{s_5}t_3$$
$$+ y_{s_1}y_{s_5}t_4 + y_{s_2}y_{s_5}t_4 + y_{s_3}t_1t_3 + y_{s_3}t_2t_3 + y_{s_3}t_1t_4 + y_{s_3}t_2t_4 - y_{s_1}y_{s_2}y_{s_4}y_{s_5}t_1t_3$$
$$- y_{s_1}y_{s_2}y_{s_4}y_{s_5}t_2t_3 - y_{s_1}y_{s_2}y_{s_4}y_{s_5}t_1t_4 - y_{s_1}y_{s_2}y_{s_4}y_{s_5}t_2t_4 - y_{s_1}y_{s_2}y_{s_4}^2t_1t_2 - y_{s_1}y_{s_2}y_{s_5}^2t_3t_4$$
$$- y_{s_1}y_{s_3}y_{s_4}t_1t_2t_3 - y_{s_2}y_{s_3}y_{s_4}t_1t_2t_3 - y_{s_1}y_{s_3}y_{s_4}t_1t_2t_4 - y_{s_2}y_{s_3}y_{s_4}t_1t_2t_4 - y_{s_1}y_{s_3}y_{s_5}t_1t_3t_4$$
$$- y_{s_2}y_{s_3}y_{s_5}t_1t_3t_4 - y_{s_1}y_{s_3}y_{s_5}t_2t_3t_4 - y_{s_2}y_{s_3}y_{s_5}t_2t_3t_4 - y_{s_3}^2t_1t_2t_3t_4 + \dots . \qquad (4.3.25)$$

It is not finite and therefore indicates that the master space is not a complete intersection.

By specular duality, we obtain the Hilbert series in terms of the perfect matching fugacities of Model 13. The perfect matching map in (4.3.22) translates to the fugacity map

$$(y_{s_i}, t_{1,2,3}, y_{q_{1,2}})_{13} \leftrightarrow (t_i, y_{s_{1,2,3}}, y_{s_{4,5}})_{15b} , \qquad (4.3.26)$$

where $(y_{s_i}, t_{1,2,3}, y_{q_{1,2}})$ are the fugacities for perfect matchings $(s_i, t_{1,2,3}, q_{1,2})$ of Model 13 respectively.

4.3.3 Global Symmetries and the Hilbert Series

In order to discuss global symmetries, let us introduce the notation of subscripts and superscripts on groups which refer to fugacities and model numbers respectively.

The F-term charge matrix for Model 13 indicates that the global symmetry is $SU(2)_x^{[13]} \times U(1)_f^{[13]} \times SU(2)_{h_1}^{[13]} \times SU(2)_{h_2}^{[13]} \times U(1)_b^{[13]} \times U(1)_R^{[13]}$, where $SU(2)_x^{[13]} \times U(1)_f^{[13]} \times U(1)_R^{[13]}$ represents the mesonic symmetry, $SU(2)_{h_1}^{[13]} \times SU(2)_{h_2}^{[13]}$ the hidden baryonic symmetry, and $U(1)_b^{[13]}$ the remaining baryonic symmetry. In comparison, for Model 15b, where internal and external perfect matchings are swapped under specular duality, the global symmetry is $SU(2)_x^{[15b]} \times SU(2)_y^{[15b]} \times SU(2)_{h_1}^{[15b]} \times U(1)_{h_2}^{[15b]} \times U(1)_b^{[15b]} \times U(1)_R^{[15b]}$. The mesonic symmetry is $SU(2)_x^{[15b]} \times SU(2)_y^{[15b]} \times U(1)_R^{[15b]}$, the hidden baryonic symmetry is $SU(2)_{h_1}^{[15b]} \times U(1)_{h_2}^{[15b]}$, and the remaining baryonic symmetry is $U(1)_b^{[15b]}$.

Accordingly, we observe that the swap of external and internal perfect matchings under specular duality leads to the following correspondence between global symmetries

$$
\begin{aligned}
SU(2)_x^{[13]} \times U(1)_f^{[13]} &\leftrightarrow SU(2)_{h_1}^{[15b]} \times U(1)_{h_2}^{[15b]} \\
SU(2)_{h_1}^{[13]} \times SU(2)_{h_2}^{[13]} &\leftrightarrow SU(2)_x^{[15b]} \times SU(2)_y^{[15b]} \\
U(1)_b^{[13]} &\leftrightarrow U(1)_b^{[15b]} .
\end{aligned}
\qquad (4.3.27)
$$

It is a swap between mesonic flavour and hidden baryonic symmetries.

	$SU(2)_x$	$U(1)_f$	$SU(2)_{h_1}$	$SU(2)_{h_2}$	$U(1)_b$	$U(1)_R$	fugacity
p_1	+1	+1	0	0	0	2/3	t_1
p_2	-1	+1	0	0	0	2/3	t_2
p_3	0	-2	0	0	0	2/3	t_3
q_1	0	0	0	0	+1	0	y_{q_1}
q_2	0	0	0	0	-1	0	y_{q_2}
s_1	0	0	+1	0	0	0	y_{s_1}
s_2	0	0	-1	0	0	0	y_{s_2}
s_3	0	0	0	+1	0	0	y_{s_3}
s_4	0	0	0	-1	0	0	y_{s_4}

Table 4.2: Perfect matchings of Model 13 with global charge assignment.

	$SU(2)_x$	$SU(2)_y$	$SU(2)_{h_1}$	$U(1)_{h_2}$	$U(1)_b$	$U(1)_R$	fugacity
p_1	+1	0	0	0	0	1/2	t_1
p_2	-1	0	0	0	0	1/2	t_2
p_3	0	+1	0	0	0	1/2	t_3
p_4	0	-1	0	0	0	1/2	t_4
s_1	0	0	+1	+1	0	0	y_{s_1}
s_2	0	0	-1	+1	0	0	y_{s_2}
s_3	0	0	0	-2	0	0	y_{s_3}
s_4	0	0	0	0	+1	0	y_{s_4}
s_5	0	0	0	0	-1	0	y_{s_5}

Table 4.3: Perfect matchings of Model 15b with global charge assignment.

Following the review in section §1.5.1, one can find global charges on perfect matchings such that the swap of external and internal perfect matchings corresponds to a swap of mesonic flavor and hidden baryonic symmetry charges. A choice of such perfect matching charges for Model 13 and Model 15b is in Table 4.2 and Table 4.3 respectively.

Starting from Model 15b, the following fugacity map

$$t = (y_{s_1} y_{s_2} y_{s_3} y_{s_4} y_{s_5} t_1 t_2 t_3 t_4)^{1/4} \ , \ \ x = t_1^{1/2} t_2^{-1/2} \ , \ \ y = t_3^{1/2} t_4^{-1/2} \ ,$$
$$b = (y_{s_4} y_{s_5})^{1/2} \, (t_1 t_2)^{1/4} \, (t_3 t_4)^{-1/4} \ , \ \ h_1 = y_{s_1}^{1/2} y_{s_2}^{-1/2} \ , \ \ h_2 = (y_{s_1} y_{s_2} y_{s_4} y_{s_5})^{1/4} \, y_{s_3}^{-1/4} \ ,$$

$$(4.3.28)$$

leads to the refined Hilbert series in (4.3.24) and the corresponding plethystic logarithm in (4.3.25) in terms of characters of irreducible representations of the global symmetry.

The expansion of the Hilbert series takes the form

$$g_1(t, x, y, h_i, b; {}^{\mathrm{Irr}}\mathcal{F}_{15b}^\flat) =$$
$$\sum_{n_1=0}^{\infty} \sum_{n_2=0}^{\infty} \sum_{n_3=0}^{\infty} h_2^{n_1+n_2-2n_3} b^{-n_1+n_2} \, [n_2+n_3; n_1+n_3; n_1+n_2] t^{n_1+n_2+2n_3} \,,$$

(4.3.29)

where $[n_1; n_2; n_3] \equiv [n_1]_x [n_2]_y [n_3]_{h_1}$ is the combined character of representations of $SU(2)_x \times SU(2)_y \times SU(2)_{h_1}$.[4] The corresponding plethystic logarithm is

$$\begin{aligned} PL[g_1(t, x, y, h_i, b; {}^{\mathrm{Irr}}\mathcal{F}_{15b}^\flat)] \;=\; & [1;0;1]h_2 b t + [0;1;1]h_2 b^{-1} t + [1;1;0]h_2^{-2} t^2 \\ & -[1;1;0]h_2^2 t^2 - [1;0;1]h_2^{-1} b^{-1} t^3 - [0;1;1]h_2^{-1} b t^3 \\ & -h_2^2 b^2 t^2 - h_2^2 b^{-2} t^2 - h_2^{-4} t^4 + \dots \,. \end{aligned}$$

(4.3.30)

In comparison, in terms of global charges on perfect matchings of Model 13, the fugacity map

$$\begin{aligned} t &= (y_{s_1} y_{s_2} y_{s_3} y_{s_4} y_{q_1} y_{q_2} t_1 t_2 t_3)^{1/3} \,, \quad x = t_1^{1/2} t_2^{-1/2} \,, \\ f &= (y_{s_1} y_{s_2} y_{s_3} y_{s_4})^{-1/12} \, (y_{q_1} y_{q_2} t_1 t_2)^{1/6} \, t_3^{-1/3} \,, \\ h_1 &= y_{s_1}^{1/2} y_{s_2}^{-1/2} \,, \quad h_2 = y_{s_3}^{1/2} y_{s_4}^{-1/2} \,, \\ b &= (y_{s_1} y_{s_2})^{1/4} \, (y_{s_3} y_{s_4})^{-1/4} \, y_{q_1}^{1/2} y_{q_2}^{-1/2} \,, \end{aligned}$$

(4.3.31)

leads to the following Hilbert series

$$g_1(t, x, f, h_i, b; {}^{\mathrm{Irr}}\mathcal{F}_{13}^\flat) =$$
$$\sum_{n_1=0}^{\infty} \sum_{n_2=0}^{\infty} \sum_{n_3=0}^{\infty} f^{n_1+n_2-2n_3} b^{-n_1+n_2} \, [n_1+n_2; n_2+n_3; n_1+n_3] \, t^{n_1+n_2+n_3} \,,$$

(4.3.32)

where $[n_1; n_2; n_3] \equiv [n_1]_x [n_2]_{h_1} [n_3]_{h_2}$ is the combined character of representations of $SU(2)_x \times SU(2)_{h_1} \times SU(2)_{h_2}$.

The $U(1)_R$ charges on perfect matchings of Model 15b are not mapped by specular duality to $U(1)_R$ charges on perfect matchings of Model 13. This is mainly because only extremal perfect matchings carry non-zero R-charges. In order to illustrate specular duality in terms of the refined Hilbert series, one can without loosing track of the algebraic structure of the moduli space mix the $U(1)_R$ symmetry with the remaining symmetry. This effectively modifies the charge assignment under the global symmetry.[5]

---

[4]cf. [73] with a choice of charges on fields which relates to the choice presented here. The identification $F_1 = SU(2)_x$, $F_2 = SU(2)_y$, $A_2 = SU(2)_{h_1}$, $A_1 = U(1)_{h_2}$, $B = U(1)_b$ and $R = U(1)_R$ is made.

[5]The algebraic structure of the moduli space is not lost when the orthogonality of global charges on

The modification is done via the fugacity map

$$\tilde{t} = (y_{s_1} y_{s_2} y_{s_3} y_{s_4} y_{q_1} y_{q_2} t_1 t_2 t_3)^{1/4} \ , \ \ x = t_1^{1/2} t_2^{-1/2} \ ,$$
$$\tilde{f} = (y_{q_1} y_{q_2} t_1 t_2)^{1/4} \ t_3^{-1/4} \ ,$$
$$h_1 = y_{s_1}^{1/2} y_{s_2}^{-1/2} \ , \ \ h_2 = y_{s_3}^{1/2} y_{s_4}^{-1/2} \ ,$$
$$b = (y_{s_1} y_{s_2})^{1/4} \ (y_{s_3} y_{s_4})^{-1/4} \ y_{q_1}^{1/2} y_{q_2}^{-1/2} \ , \tag{4.3.33}$$

which leads to the Hilbert series

$$g_1(\tilde{t}, x, f, h_i, b; {}^{\mathrm{Irr}}\mathcal{F}_{13}^{\flat}) =$$
$$\sum_{n_1=0}^{\infty} \sum_{n_2=0}^{\infty} \sum_{n_3=0}^{\infty} \tilde{f}^{n_1+n_2-2n_3} b^{-n_1+n_2} [n_1+n_2; n_2+n_3; n_1+n_3] \tilde{t}^{n_1+n_2+2n_3} \ ,$$
$$\tag{4.3.34}$$

where $[n_1; n_2; n_3] \equiv [n_1]_x [n_2]_{h_1} [n_3]_{h_2}$. One observes that the fugacity map equivalent to the exchange of mesonic flavour and hidden baryonic symmetries is

$$(x, \tilde{f}, \tilde{t}, h_1, h_2, b)_{13} \leftrightarrow (h_1, h_2, t, x, y, b)_{15b} \ . \tag{4.3.35}$$

It relates the Hilbert series in (4.3.29) to the one in (4.3.34).

4.3.4 Generators, the Master Space Cone and the Hilbert Series

The master space is toric Calabi-Yau and has a conical structure. Since the dimension of the master space is $G + 2 = 6$, the corresponding Hilbert series can be rewritten in terms of 6 fugacities T_i such that the exponents of T_i are positive only. This means that all elements of the ring and the corresponding integral points of the moduli space cone relate to monomials of the form $\prod_i T_i^{m_i}$ with $m_i \geq 0$ in the Hilbert series expansion. The appropriate interpretation for these monomials is that if b T_i vanish in $\prod_i T_i^{m_i}$, the associated integral point is on a codimension b cone. All points associated to monomials $\prod_i T_i^{m_i}$ with $m_i > 0$ for all i lie within the codimension 0 cone. The boundary of the codimension 0 cone is defined by monomials of the form $T_i^{m_i}$ with $m_i > 0$.

Starting with the perfect matchings of Model 15b, the fugacity map

$$T_1 = x = t_1^{1/2} t_2^{-1/2} \ , \ \ T_2 = y = t_3^{1/2} t_4^{-1/2} \ ,$$
$$T_3 = b = (y_{s_4} y_{s_5})^{1/2} \ (t_1 t_2)^{1/4} \ (t_3 t_4)^{-1/4} \ ,$$
$$T_4 = h_1 = y_{s_1}^{1/2} y_{s_2}^{-1/2} \ , \ \ T_5 = h_2 = (y_{s_1} y_{s_2} y_{s_5})^{1/4} y_{s_3}^{-1/4} \ ,$$
$$T_6 = \frac{t}{xybh_1h_2} = (y_{s_1} y_{s_2} y_{s_3} y_{s_4} y_{s_5} t_1 t_2 t_3 t_4)^{1/4} \ , \tag{4.3.36}$$

_____
perfect matchings is preserved as discussed in section §1.5.1.
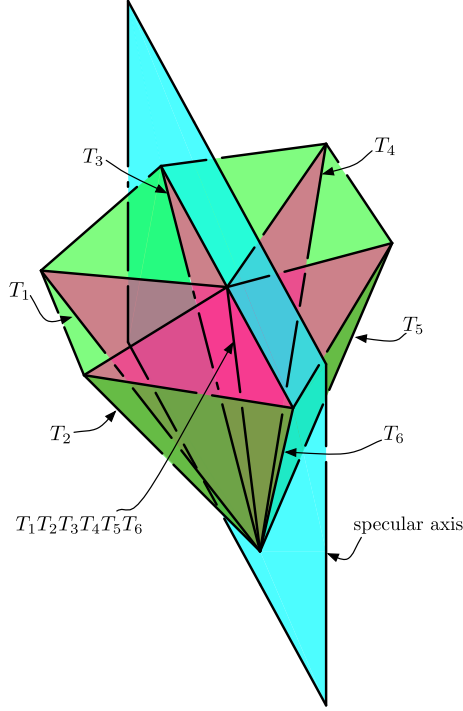
Figure 4.12: *The Specular Axis.* This is a schematic illustration of the master space cone of Models 13 and 15b. The rays corresponding to the basis of the cone are labelled with the associated fugacities T_i of the Hilbert series. The cone is symmetric along a hyperplane which we call the specular axis.

allows us to re-write the Hilbert series such that the corresponding plethystic logarithm in (4.3.25) takes the form

$$
\begin{aligned}
PL[g(T_i; {}^{\mathrm{Irr}}\mathcal{F}^{\flat}_{15b})] =\ & T_1^2 T_2 T_3^2 T_4^2 T_5^2 T_6 + T_1^2 T_2 T_3^2 T_5^2 T_6 + T_2 T_3^2 T_4^2 T_5^2 T_6 + T_2 T_3^2 T_5^2 T_6 \\
& + T_1 T_2^2 T_4^2 T_5^2 T_6 + T_1 T_2^2 T_5^2 T_6 + T_1 T_4^2 T_5^2 T_6 + T_1 T_5^2 T_6 + T_1^3 T_2^3 T_3^2 T_4^2 T_6^2 + T_1 T_2^3 T_3^2 T_4^2 T_6^2 \\
& + T_1^3 T_2 T_3^2 T_4^2 T_6^2 + T_1 T_2 T_3^2 T_4^2 T_6^2 - T_1^3 T_2^3 T_3^2 T_4^2 T_5^4 T_6^2 - T_1 T_2^3 T_3^2 T_4^2 T_5^4 T_6^2 \\
& - T_1^3 T_2 T_3^2 T_4^2 T_5^4 T_6^2 - T_1 T_2 T_3^2 T_4^2 T_5^4 T_6^2 - T_1^2 T_2^2 T_3^4 T_4^2 T_5^4 T_6^2 - T_1^2 T_2^2 T_4^2 T_5^4 T_6^2 \\
& - T_1^3 T_2^4 T_3^4 T_4^4 T_5^2 T_6^3 - T_1^3 T_2^4 T_3^2 T_4^2 T_5^2 T_6^3 - T_1^3 T_2^2 T_3^4 T_4^4 T_5^2 T_6^3 - T_1^3 T_2^2 T_3^2 T_4^2 T_5^2 T_6^3 \\
& - T_1^4 T_2^3 T_3^2 T_4^4 T_5^2 T_6^3 - T_1^4 T_2^3 T_3^2 T_4^2 T_5^2 T_6^3 - T_1^2 T_2^3 T_3^2 T_4^4 T_5^2 T_6^3 - T_1^2 T_2^3 T_3^2 T_4^2 T_5^2 T_6^3 \\
& - T_1^4 T_2^4 T_3^4 T_4^4 T_6^4 + \dots \ .
\end{aligned}
$$
(4.3.37)

As desired, the plethystic logarithm as for the Hilbert series is such that the exponents of the fugacities T_i are positive. In comparison, in relation to perfect matchings of Model 13, the fugacity map

$$
T_1 = x \ , \ T_2 = \tilde{f} \ , \ T_3 = b \ , \ T_4 = h_1 \ , \ T_5 = h_2 \ , \ T_6 = \frac{\tilde{t}}{x \tilde{f} b h_1 h_2} \ ,
$$
(4.3.38)

252

generator	fields	$SU(2)_x$	$U(1)_f$	$SU(2)_{h_1}$	$SU(2)_{h_2}$	$U(1)_b$	$U(1)_R$	fugacity
$p_3\,s_1 s_3$	X_{24}	0	-2	+1	+1	0	1/3	$T_1^2 T_3^2 T_4^3 T_5^3 T_6^2$
$p_3\,s_1 s_4$	X_{41}^1	0	-2	+1	-1	0	1/3	$T_1^2 T_3^2 T_4^3 T_5 T_6^2$
$p_3\,s_2 s_3$	X_{41}^1	0	-2	-1	+1	0	1/3	$T_1^2 T_3^2 T_4 T_5^3 T_6^2$
$p_3\,s_2 s_4$	X_{42}	0	-2	-1	-1	0	1/3	$T_1^2 T_3^2 T_4 T_5 T_6^2$
$p_1\,q_1\,s_1$	X_{13}	+1	+1	+1	0	+1	1/3	$T_1^2 T_2^2 T_3^2 T_4^2 T_5 T_6$
$p_1\,q_1\,s_2$	X_{12}^2	+1	+1	-1	0	+1	1/3	$T_1^2 T_2^2 T_3^2 T_5 T_6$
$p_2\,q_1\,s_1$	X_{34}^2	-1	+1	+1	0	+1	1/3	$T_2^2 T_3^2 T_4^2 T_5 T_6$
$p_2\,q_1\,s_2$	X_{34}^1	-1	+1	-1	0	+1	1/3	$T_2^2 T_3^2 T_5 T_6$
$p_1\,q_2\,s_3$	X_{12}^1	+1	+1	0	+1	-1	1/3	$T_1^2 T_2^2 T_4 T_5^2 T_6$
$p_1\,q_2\,s_4$	X_{31}	+1	+1	0	-1	-1	1/3	$T_1^2 T_2^2 T_4 T_6$
$p_2\,q_2\,s_3$	X_{23}^2	-1	+1	0	+1	-1	1/3	$T_2^2 T_4 T_5^2 T_6$
$p_2\,q_2\,s_4$	X_{23}^2	-1	+1	0	-1	-1	1/3	$T_2^2 T_4 T_6$

Table 4.4: The generators of the master space of Model 13 with the corresponding charges under the global symmetry.

generator	fields	$SU(2)_x$	$SU(2)_y$	$SU(2)_{h_1}$	$U(1)_{h_2}$	$U(1)_b$	$U(1)_R$	fugacity
$p_1 p_3\,s_3$	X_{42}^2	+1	+1	0	-2	0	1	$T_1^3 T_2^3 T_3^2 T_4^2 T_6^2$
$p_1 p_4\,s_3$	X_{42}^4	+1	-1	0	-2	0	1	$T_1^3 T_2 T_3^2 T_4^2 T_6^2$
$p_2 p_3\,s_3$	X_{42}^3	-1	+1	0	-2	0	1	$T_1 T_2^3 T_3^2 T_4^2 T_6^2$
$p_2 p_4\,s_3$	X_{42}^1	-1	-1	0	-2	0	1	$T_1 T_2 T_3^2 T_4^2 T_6^2$
$p_1\,s_1 s_4$	X_{21}^1	+1	0	+1	+1	+1	1/2	$T_1^2 T_2 T_3^2 T_4^2 T_5^2 T_6$
$p_2\,s_1 s_4$	X_{21}^2	-1	0	+1	+1	+1	1/2	$T_2 T_3^2 T_4^2 T_5^2 T_6$
$p_1\,s_2 s_4$	X_{34}^2	+1	0	-1	+1	+1	1/2	$T_1^2 T_2 T_3^2 T_5^2 T_6$
$p_2\,s_2 s_4$	X_{34}^1	-1	0	-1	+1	+1	1/2	$T_2 T_3^2 T_5^2 T_6$
$p_3\,s_1 s_5$	X_{23}^2	0	+1	+1	+1	-1	1/2	$T_1 T_2^2 T_4^2 T_5^2 T_6$
$p_4\,s_1 s_5$	X_{23}^1	0	-1	+1	+1	-1	1/2	$T_1 T_4^2 T_5^2 T_6$
$p_3\,s_2 s_5$	X_{14}^1	0	+1	-1	+1	-1	1/2	$T_1 T_2^2 T_5^2 T_6$
$p_4\,s_2 s_5$	X_{14}^2	0	-1	-1	+1	-1	1/2	$T_1 T_5^2 T_6$

Table 4.5: The generators of the master space of Model 15b with the corresponding charges under the global symmetry.

rewrites the Hilbert series and plethystic logarithm such that they are related to the ones from Model 15b via

$$(T_1, T_2, T_3, T_4, T_5, T_6) \leftrightarrow (T_4, T_5, T_3, T_1, T_2, T_6) \ . \tag{4.3.39}$$

Note that the above map for fugacities T_i relates to the one for global symmetry fugacities in (4.3.35).

Given that the fugacities T_i relate to the boundary of the Calabi-Yau cone, the above fugacity map can be interpreted as a reflection along a hyperplane which is associated to monomials of the form $T_3^{m_3} T_6^{m_6}$. We call the hyperplane the **specular axis**. It is schematically illustrated in Figure 4.12.

The generators of the master space in terms of perfect matchings of Model 13 and Model 15b are shown with the corresponding global symmetry charges in Table 4.4 and Table 4.5 respectively. The master space cone with a selection of generators and the specular axis are illustrated schematically in Figure 4.13. Specular duality maps generators into each other along the specular axis.
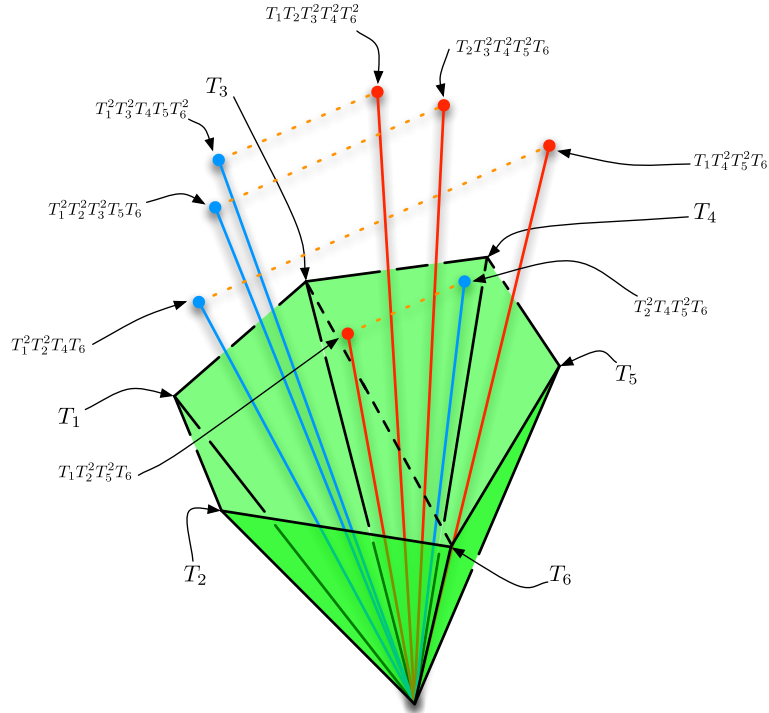
Figure 4.13: *The Specular Axis and Moduli Space Generators.* The schematic illustration shows a selection of master space generators of Model 15b and Model 13 which are highlighted in red and blue respectively. The dotted lines indicate the identifications of generators under specular duality.

4.4 Beyond the torus and Conclusions

Our work discusses specular duality between brane tilings which represent $4d$ $\mathcal{N} = 1$ supersymmetric gauge theories with toric Calabi-Yau moduli spaces.

Starting from the observations made in [5], this work identifies the following properties of specular duality for brane tilings on T^2 with reflexive toric diagrams:

- Dual brane tilings have the same master space $^{\mathrm{Irr}}\mathcal{F}^\flat$. The corresponding Hilbert series are the same up to a fugacity map.

- The new correspondence swaps internal and external perfect matchings.

- Mesonic flavor and anomalous or hidden baryonic symmetries are interchanged.

- Specular duality represents a hyperplane along which the cone of $^{\mathrm{Irr}}\mathcal{F}^\flat$ is symmetric.

The new duality is an automorphism of the set of 30 brane tilings with reflexive toric diagrams [5]. It is of great interest to identify additional properties shared by dual brane tilings.
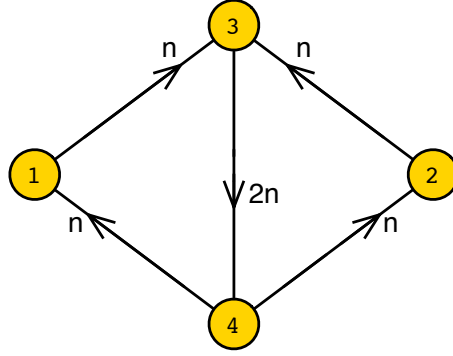
Figure 4.14: The quiver of the specular dual of the brane tiling for the Abelian orbifold of the form $\mathbb{C}^3/\mathbb{Z}_{2n}$ with orbifold action $(1, 1, -2)$.

When specular duality acts on a brane tiling whose toric diagram is not reflexive, the dual brane tiling is either on a sphere or on a Riemann surface of genus 2 or higher. Such brane tilings have no known AdS duals and their mesonic moduli spaces are not necessarily Calabi-Yau 3-folds [54, 188, 89].

In general, the number of faces G of a brane tiling relates to the number of faces $\tilde{G}$ of the dual tiling by

$$\tilde{G} = E = G - 2I + 2 . \tag{4.4.40}$$

I and E are respectively the number of internal and external toric points for the original brane tiling.

First examples of brane tilings on Riemann surfaces can be generated from Abelian orbifolds of $\mathbb{C}^3$ [126, 3, 2, 1, 4]. Consider the brane tilings which correspond to the Abelian orbifolds of the form $\mathbb{C}^3/\mathbb{Z}_{2n}$ with orbifold action $(1, 1, -2)$ and $n > 0$. The dual brane tiling is on a Riemann surface of genus $n - 1$. For the first few examples with $n = 1, 2, 3$, the superpotentials are

$$
\begin{aligned}
W_{\widetilde{\mathbb{C}^3/\mathbb{Z}_{2,(1,1,0)}}} &= X_{34}^1 X_{41} X_{13} + X_{34}^2 X_{42} X_{23} - X_{34}^2 X_{41} X_{13} - X_{34}^1 X_{42} X_{23} , \tag{4.4.41}\\
W_{\widetilde{\mathbb{C}^3/\mathbb{Z}_{4,(1,1,2)}}} &= X_{34}^1 X_{41}^1 X_{13}^1 + X_{34}^2 X_{42}^1 X_{23}^1 + X_{34}^3 X_{41}^2 X_{13}^2 + X_{34}^4 X_{42}^2 X_{23}^2 \\
&\quad - X_{34}^4 X_{41}^2 X_{13}^1 - X_{34}^1 X_{42}^2 X_{23}^1 - X_{34}^2 X_{41}^1 X_{13}^2 - X_{34}^3 X_{42}^1 X_{23}^2 \tag{4.4.42}\\
W_{\widetilde{\mathbb{C}^3/\mathbb{Z}_{6,(1,1,4)}}} &= X_{34}^1 X_{41}^1 X_{13}^1 + X_{34}^2 X_{42}^1 X_{23}^1 + X_{34}^3 X_{41}^2 X_{13}^2 + X_{34}^4 X_{42}^2 X_{23}^2 \\
&\quad + X_{34}^5 X_{41}^3 X_{13}^3 + X_{34}^6 X_{42}^3 X_{23}^3 - X_{34}^6 X_{41}^3 X_{13}^1 - X_{34}^1 X_{42}^3 X_{23}^1 \\
&\quad - X_{34}^2 X_{41}^1 X_{13}^2 - X_{34}^3 X_{42}^1 X_{23}^2 - X_{34}^4 X_{41}^2 X_{13}^3 - X_{34}^5 X_{42}^2 X_{23}^3 \tag{4.4.43}
\end{aligned}
$$

The corresponding quivers are shown in Figure 4.14. The Hilbert series of the master
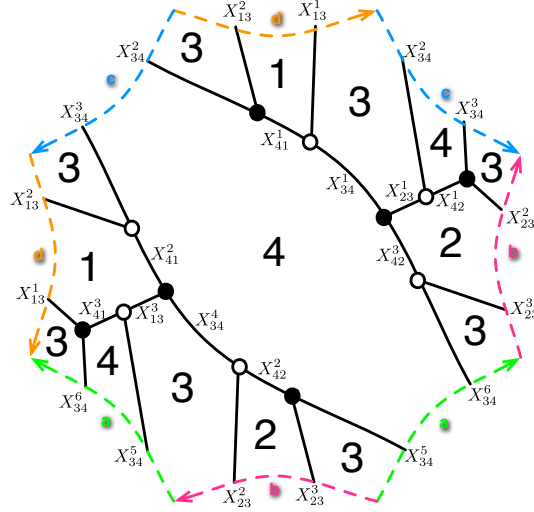
Figure 4.15: *Brane Tiling on a $g = 2$ Riemann Surface.* The figure shows the octagonal fundamental domain of the brane tiling which is the specular dual of $\mathbb{C}^3/\mathbb{Z}_6$ with action $(1, 1, 4)$.

spaces are,

$$
g_1(t; \widetilde{\mathbb{C}^3/\mathbb{Z}_{2,(1,1,0)}}) = \frac{1 - t^4}{(1 - t)(1 - t^2)^4} \ ,
$$

$$
g_1(t; \widetilde{\mathbb{C}^3/\mathbb{Z}_{4,(1,1,2)}}) = \frac{1 + 6t^3 + 6t^6 + t^9}{(1 - t^3)^6} \ ,
$$

$$
\begin{aligned}
g_1(t; \widetilde{\mathbb{C}^3/\mathbb{Z}_{6,(1,1,4)}}) = \ & (1 + 3t^2 + 7t^4 + 18t^6 + 38t^8 + 72t^{10} + 122t^{12} + 186t^{14} + 267t^{16} \\
& + 363t^{18} + 456t^{20} + 537t^{22} + 588t^{24} + 603t^{26} + 588t^{28} + 537t^{30} + 456t^{32} \\
& + 363t^{34} + 267t^{36} + 186t^{38} + 122t^{40} + 72t^{42} + 38t^{44} + 18t^{46} + 7t^{48} \\
& + 3t^{50} + t^{52}) \times \frac{(1 - t^2)^3(1 - t^4)}{(1 - t^6)^7(1 - t^8)^5} \ .
\end{aligned}
\tag{4.4.44}
$$

The fundamental domain of the brane tiling for the specular dual of $\mathbb{C}^3/\mathbb{Z}_{6,(1,1,4)}$ is in Figure 4.15. It is of great interest to study such brane tilings on higher genus Riemann surfaces. One obtains a new class of quivers and field theories via specular duality which is the subject of the following chapter.

5 Brane Tilings and Riemann Surfaces

In the previous chapter we have reviewed the new correspondence between brane tilings which we call specular duality. It opens a path for brane tilings on higher genus Riemann surfaces. These bipartite graphs on Riemann surfaces beyond the 2-torus translate to supersymmetric quiver theories using the conventional brane tiling dictionary. It is natural to ask what the moduli space of these new theories are, whether the moduli spaces are Calabi-Yau and what dimensions they have.

The first example of a brane tiling on a genus 2 Riemann surface using specular duality is the dual of the $\mathbb{C}^3/\mathbb{Z}_5$ $(1,1,3)$ brane tiling. The toric diagram of $\mathbb{C}^3/\mathbb{Z}_5$ $(1,1,3)$ is the smallest $\mathbb{Z}_2$ lattice triangle with precisely two internal points corresponding to the genus of the Riemann surface. It is now of interest whether there are genus 2 brane tilings with less quiver fields and less gauge groups than the specular dual of $\mathbb{C}^3/\mathbb{Z}_5$ $(1,1,3)$.

The following chapter introduces new technologies which we use to classify the first few brane tilings on a genus 2 Riemann surfaces. It can be seen from the classification that many brane tilings on a genus 2 Riemann surface are not specular dual to consistent torus tilings and hence cannot be easily generated by specular duality. The classification consists of 16 distinct genus 2 brane tilings with up to 8 quiver fields and 4 superpotential terms. The Higgs mechanism is used to relate the different theories. The chapter, which is an edited version of [9] under collaboration with Stefano Cremonesi and Amihay Hanany, is a pioneering step towards a wide and rich range of new supersymmetric quiver theories.

5.1 Introduction

As we have explored above, brane tilings [15, 55] provide one of the largest known classes of $4d$ $\mathcal{N} = 1$ supersymmetric gauge theories living on D3-branes which probe Calabi-Yau 3-fold singularities. As bipartite periodic graphs on the 2-torus, which encode both field theory information and geometry, brane tilings represent an epitome of the rich interface between algebraic geometry and string theory. Our work attempts to upgrade this active relationship by introducing and classifying brane tilings not confined to the traditional 2-torus.

Brane tilings have been used to classify $4d\,\mathcal{N}=1$ toric quiver gauge theories with their mesonic and baryonic moduli spaces [50, 51, 52, 192, 17, 86, 113, 183, 18, 74, 75, 72, 71], dualities [14, 92, 36, 181] and symmetries [110, 95]. With the understanding of 3d $\mathcal{N}=2$ Chern-Simons theories as worldvolume theories of M2-branes [60, 56, 57, 58, 59, 193], this tour de force of research and discovery reached new heights and led to the introduction of Chern-Simons levels on brane tilings [63, 64, 194, 137, 166, 195, 196, 197].

The work on brane boxes [68] described the construction of a prototypical brane tiling on a surface with boundaries such as a disc or cylinder. This idea recently re-emerged as bipartite graphs on discs in relation to string scattering amplitudes [198, 82]. The connection between supersymmetric gauge theories and brane tilings on surfaces with boundaries was further studied in [8].

In parallel, as explored in the previous chapters, brane tilings associated to Calabi-Yau geometries whose toric diagrams are reflexive polygons [5] were found to have the same combined mesonic and baryonic moduli spaces under a map which is known as specular duality [7]. The fascinating properties of specular duality further motivates our work.

Specular duality makes use of the untwisting map [83, 52] which relates theories with the same master space [73, 18, 74, 75, 72, 71] and generates new brane tilings that are not necessarily confined to the 2-torus. The simplest example of this capability is the $\mathbb{C}^3/\mathbb{Z}_5$ $(1,1,3)$ orbifold theory [126, 1, 3, 4, 2] whose brane tiling can be untwisted to give a dual on a $g=2$ Riemann surface. This is an important example of a brane tiling beyond the 2-torus and sheds light on a new infinite class of unexplored field theories.
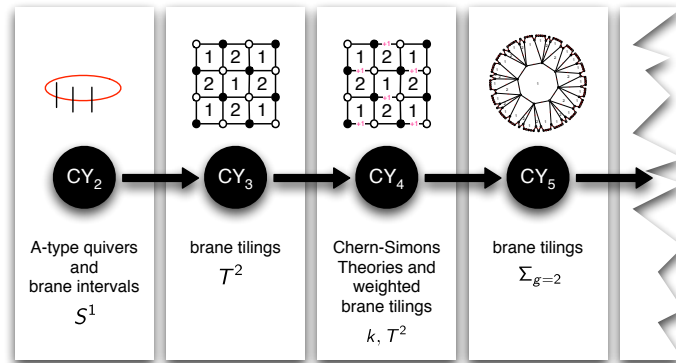
Figure 5.1: *The evolution of brane tilings.* Brane tilings have evolved from representing A-type quivers to $\mathcal{N}=1$ $4d$ supersymmetric theories and $\mathcal{N}=2$ $3d$ Chern-Simons theories. This work studies brane tilings on $g=2$ Riemann surfaces associated to Calabi-Yau 5-folds.

This work introduces a new procedure of classifying brane tilings on Riemann surfaces. We continue to call the new periodic bipartite graphs on Riemann surfaces as *brane*

tilings since they are natural generalisations of the tilings on the 2-torus. Although the brane construction for the generalisation is not yet fully understood, we believe that our classification is an important step towards a better understanding of the problem.

Despite the efficiency of generating brane tilings on $g = 2$ or higher genus Riemann surfaces with specular duality, only a subset of these new brane tilings can be identified with this method. Most other brane tilings, often with much smaller number of fields and gauge groups, can only be obtained via a direct construction on the Riemann surface.[1] The work will give the first classification of brane tilings on a $g = 2$ Riemann surface with up to 8 quiver fields and 4 superpotential terms. Our classification identifies precisely 16 distinct $g = 2$ brane tilings which can be related by a successive application of the Higgs mechanism.

The mesonic moduli space of each brane tiling in the classification is computed by imposing F-and D-term constraints. These moduli spaces are all toric Calabi-Yau 5-folds. The moduli space dimension is in general $2g + 1$ where the number of homology 1-cyles on the genus g Riemann surface is $2g$. By computing the Hilbert series, we specify the explicit algebraic structure of the moduli space and relate new geometries to classical field theories.

For generic ranks of the gauge groups, it is not clear whether the beta functions of all couplings can be set to zero.[2] Accordingly, understanding the IR behaviour of the brane tilings may be challenging. For the moment, the classification of $g = 2$ brane tilings should be considered as an important step towards a better understanding of recent lines of thought. We believe that such extensions to the field theories classified in this work along with a better understanding of the brane construction will lead to new exciting progress in the near future.

The structure of the chapter is as follows. Section §5.2 gives a first glimpse of a $g = 2$ brane tiling by untwisting the brane tiling for the $\mathbb{C}^3/\mathbb{Z}_5$ $(1, 1, 3)$ theory and then proceeds to outline an algorithm for classifying all distinct brane tilings on a $g = 2$ Riemann surface. The results are summarized in section §5.2.2. Section §5.2.3 continues with a discussion on consistency of brane tilings that plays an important role in the case of the 2-torus. The section explains that restrictions are set on $g = 2$ brane tilings to reduce the number of models in the classification even though the restrictions are not well motivated from a field theory perspective. Section §5.2.4 summarises the basic properties of the mesonic moduli spaces and continues with section §5.2.5 by explaining how the Higgs mechanism relates the theories in the classification and acts as a check of the classification. In the second part of the chapter, section §5.3 summarises the full

---

[1]These are in fact under specular duality often related to *inconsistent* brane tilings on the 2-torus. Consistency of brane tilings on the 2-torus has been studied from many perspectives [100, 16, 85, 106], and the most important properties are reviewed in this work.

[2]It is well known [16] that if the ranks of the gauge groups are all equal and none of the couplings vanish, the beta functions cannot all be zero.

classification data for $g = 2$ brane tilings, including the computation of the Hilbert series. Appendix §A.6 includes a more concise summary of the classification. In addition, $g = 2$ brane tilings with self-intersecting zig-zag paths are presented in appendix §A.7.

5.2 Brane Tilings on Riemann Surfaces

In this section we present the classification scheme which we used for the $g = 2$ brane tilings. A brief summary is given for what is meant by a $g > 1$ brane tiling, with an overview of their field theoretic and geometric properties.

5.2.1 The Construction

1	2	3	4	5	6	7	8	9	10	11	12	13	14	15
X_{51}^1	X_{14}	X_{45}^1	X_{45}^2	X_{53}	X_{34}^1	X_{34}^2	X_{42}	X_{23}^1	X_{23}^2	X_{31}	X_{12}^1	X_{12}^2	X_{25}	X_{51}^2
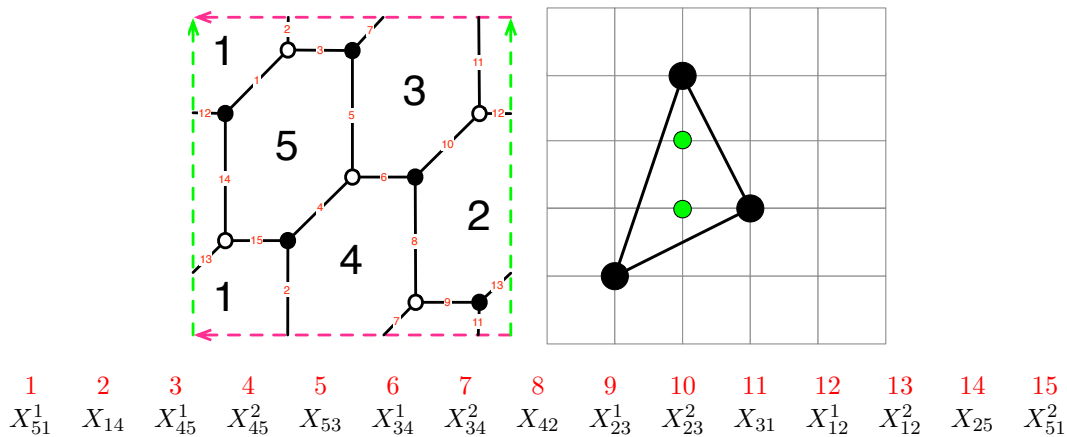
Figure 5.2: Brane tiling and toric diagram of $\mathbb{C}^3/\mathbb{Z}_5$ (1,1,3).

As seen in [7], specular duality and the untwisting map [52, 83] can be used to generate brane tilings on Riemann surfaces with genus $g > 1$. The simplest example is the brane tiling for $\mathbb{C}^3/\mathbb{Z}_5$ with orbifold action $(1, 1, 3)$, whose toric diagram is a lattice triangle with exactly two internal points. The toric diagram and the brane tiling are in Figure 5.2 with the quiver diagram in Figure 5.4. The superpotential has the form

$$
\begin{aligned}
W \;=\; & +X_{51}^1 X_{14} X_{45}^1 + X_{45}^2 X_{53} X_{34}^1 + X_{34}^2 X_{42} X_{23}^1 + X_{23}^2 X_{31} X_{12}^1 + X_{12}^2 X_{25} X_{51}^2 \\
& -X_{51}^1 X_{12}^1 X_{25} - X_{45}^2 X_{51}^2 X_{14} - X_{34}^2 X_{45}^1 X_{53} - X_{23}^2 X_{32}^1 X_{42} - X_{12}^2 X_{23}^1 X_{31} \; .
\end{aligned}
$$

$$(5.2.1)$$

Given that the superpotential has an overall trace, which is omitted for brevity, let us use the notation which replaces terms in the superpotential as a cyclic permutation of integers [199]. The integers themselves label fields with the dictionary given in
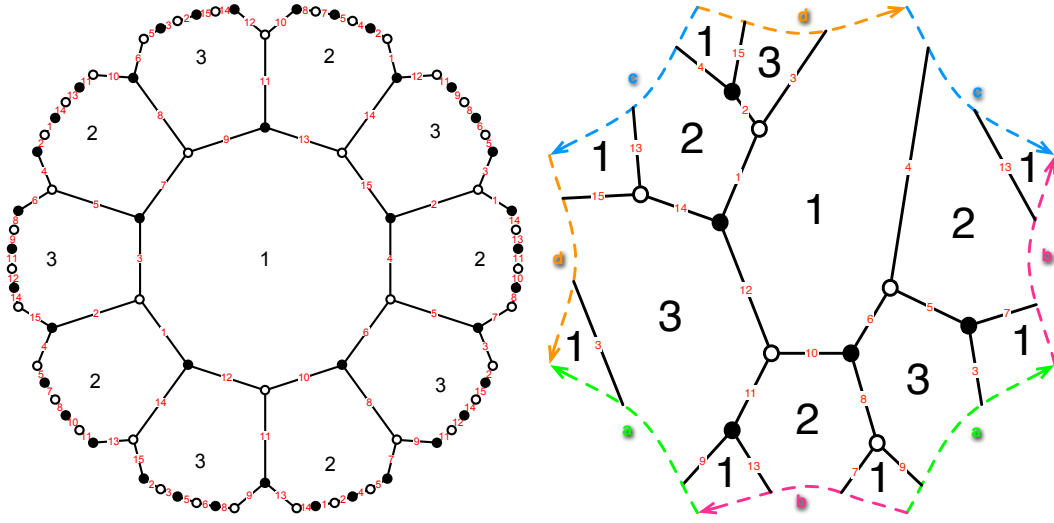
1	2	3	4	5	6	7	8	9	10	11	12	13	14	15
X_{12}^1	X_{23}^1	X_{31}^1	X_{12}^2	X_{23}^2	X_{31}^2	X_{12}^3	X_{23}^3	X_{31}^3	X_{12}^4	X_{23}^4	X_{31}^4	X_{12}^5	X_{23}^5	X_{31}^5

Figure 5.3: Specular dual brane tiling of $\mathbb{C}^3/\mathbb{Z}_5$ (1,1,3) on a $g = 2$ Riemann surface with its fundamental domain.
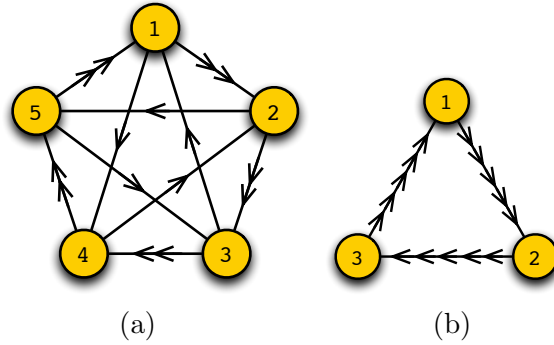
(a)   (b)

1	2	3	4	5	6	7	8	9	10	11	12	13	14	15
X_{51}^1	X_{14}	X_{45}^1	X_{45}^2	X_{53}	X_{34}^1	X_{34}^2	X_{42}	X_{23}^1	X_{23}^2	X_{31}	X_{12}^1	X_{12}^2	X_{25}	X_{51}^2
X_{12}^1	X_{23}^1	X_{31}^1	X_{12}^2	X_{23}^2	X_{31}^2	X_{12}^3	X_{23}^3	X_{31}^3	X_{12}^4	X_{23}^4	X_{31}^4	X_{12}^5	X_{23}^5	X_{31}^5

Figure 5.4: The (a) quiver of $\mathbb{C}^3/\mathbb{Z}_5$ (1,1,3) and (b) its specular dual quiver with the field map under the untwisting move.

Figure 5.2,

$$
\begin{aligned}
W \;=\;\; & +(1\ 2\ 3) + (4\ 5\ 6) + (7\ 8\ 9) + (10\ 11\ 12) + (13\ 14\ 15) \\
& -(1\ 12\ 14) - (4\ 15\ 2) - (7\ 3\ 5) - (10\ 6\ 8) - (13\ 9\ 11) \,. \qquad (5.2.2)
\end{aligned}
$$

The specular dual tiling is on a $g = 2$ Riemann surface and the corresponding su-

persymmetric field theory has a $5d$ toric Calabi-Yau mesonic moduli space. The brane tiling is shown in Figure 5.3 with the quiver in Figure 5.4. The superpotential of the specular dual is easily obtained by reversing the permutations which correspond to the negative (or equivalently the positive) terms in the original superpotential in (5.2.2).

This $g = 2$ brane tiling is the one that can be generated via specular duality with the least number of fields. In fact, there are $g = 2$ brane tilings with much fewer fields that cannot be obtained via specular duality on 2-torus tilings. In the following section, we illustrate a method of generating such tilings and give a full classification up to 8 quiver fields and 4 superpotential terms.

5.2.2 Classification of $g = 2$ Brane Tilings
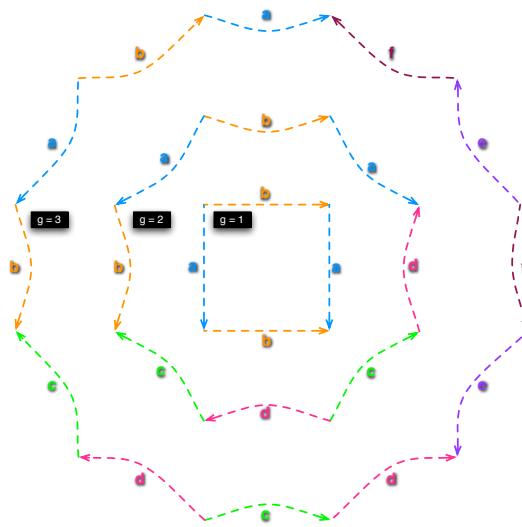
Figure 5.5: *Fundamental domains of higher genus brane tilings.* These are choices for fundamental domains for Riemann surfaces of genus $g = 1, 2, 3$.

The brane tiling as a bipartite graph satisfies the *Euler formula*,

$$F - E + V = 2 - 2g \; , \tag{5.2.3}$$

where E, V and F are respectively the number of edges, nodes and faces of the brane tiling and g is the genus of the Riemann surface. The fundamental domain of the genus g brane tiling is a $4g$-sided polygon with our identification of sides being the one shown in Figure 5.5. Accordingly, there are $2g$ fundamental cycles with every zig-zag path of the brane tiling having $2g$ winding numbers. This leads to rank $2g$ mesonic symmetry in the associated field theory [15, 89].

E	V	F	# Models
5	2	1	1
6	2	2	3
7	2	3	1
7	4	1	1
8	2	4	2
8	4	2	8

Table 5.1: *The Euler formula and the classification.* These are the numbers of distinct brane tilings on a $g = 2$ Riemann surface without self-intersecting zig-zag paths and without multi-bonded edges for specific numbers of edges E, number of vertices V and faces F.

For $g = 2$, the first few values of E, V and F satisfying the Euler formula are given in Table 5.1. By setting (E, V, F) for $g = 2$, we generate all possible permutations of E integers. From this set of permutations, all possible pairings of permutations are taken. For each permutation pair one is marked as positive and the other one as negative. We associate a pairing to a brane tiling if it satisfies the following brane tiling conditions:

- The number of cycles in the positive permutation is the same as the number of cycles in the negative permutation. This translates to the condition that there are the same number of positive and negative superpotential terms.

- Every integer precisely appears once in a positive permutation cycle and a negative permutation cycle. This translates to the *toric condition* of the brane tiling.

- The associated brane tiling has no self-intersecting zig-zag paths and no multi-bonded edges [100, 16, 85] as discussed in §5.2.3. We adopt these restrictions in the classification for $g = 2$ brane tilings to reduce the number of identified models.

Two brane tilings on any genus Riemann surface are the same if they satisfy the following *equivalence conditions*:

- The brane tilings are on the same Riemann surface with the same genus g.

- The quiver diagrams are equivalent graphs.

- The superpotential as a permutation pairing is the same partition of integers.

- The zig-zag paths [106, 109] are the same partition of integers.

- The mesonic moduli spaces $\mathcal{M}^{mes}$ [52, 5, 34] are the same.

Note that a subset of the conditions above may not be enough to identify brane tiling equivalence. An example is a pair of distinct toric dual brane tilings which are related

$$\mathcal{M}_{3,2} \equiv \mathbb{C}^5/\langle abc - de\rangle$$
$$\mathcal{M}_{3,3} \equiv \mathbb{C}^6/\langle abc - def\rangle$$
$$\mathcal{M}_{4,2} \equiv \mathbb{C}^6/\langle abcd - ef\rangle$$
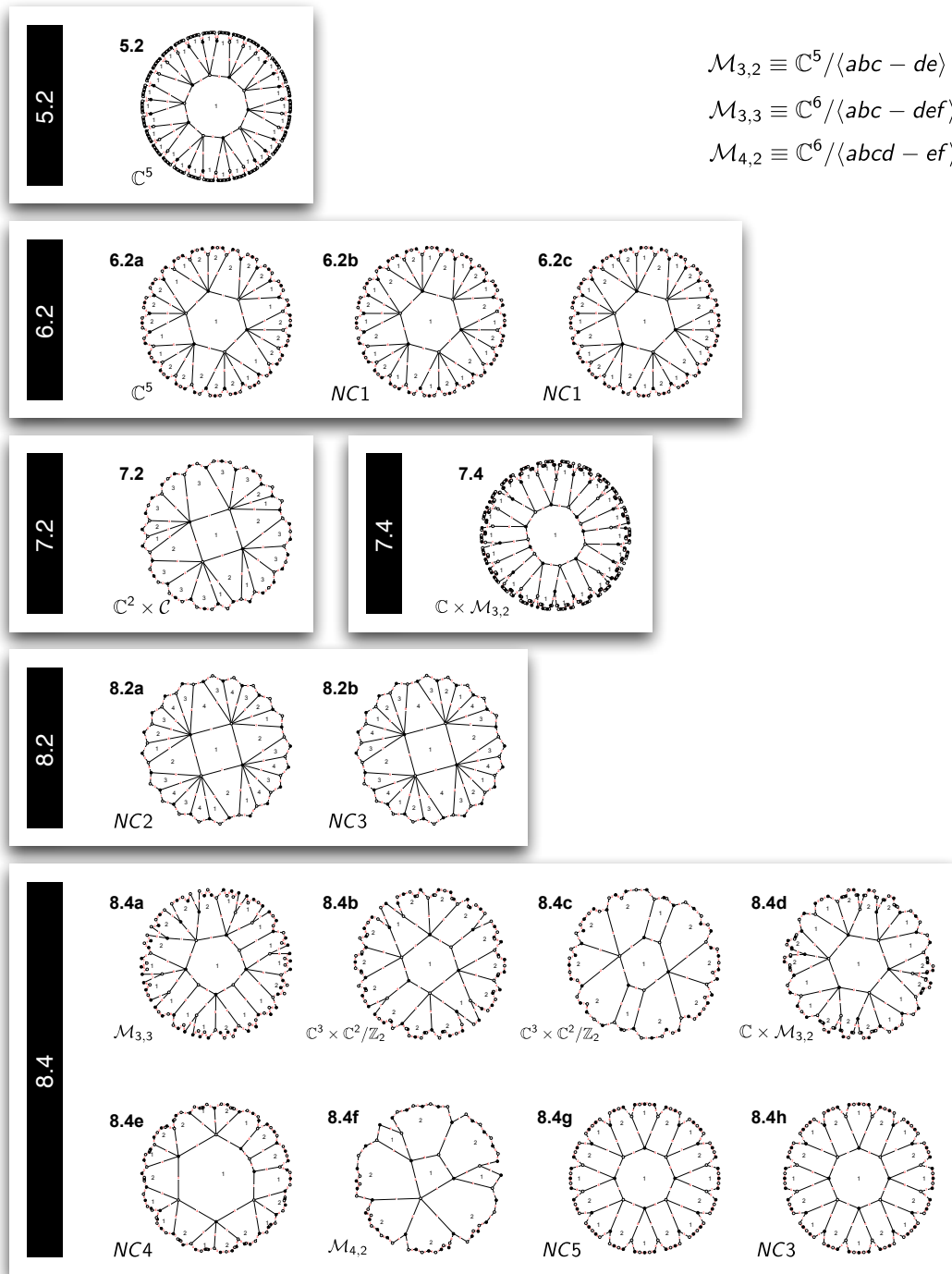
Figure 5.6: *Classification of $g = 2$ brane tilings with no self-intersecting zig-zag paths and no multi-bonded edges.* These are the first 16 brane tiling on a $g = 2$ Riemann surface with up to $E = 8$ and $V = 4$.

by the *urban renewal* move. The dual brane tilings have the same mesonic moduli space [15]. In fact, for $g > 1$ brane tilings, two distinct brane tilings which are not related by

the urban renewal move can have the same mesonic moduli space.

Following the procedure which is outlined above, we classify all distinct brane tilings on a $g = 2$ Riemann surface with up to $E = 8$ edges and $V = 4$ superpotential terms. We identify 16 distinct $g = 2$ brane tilings. They are summarized in Figure 5.6, and their mesonic moduli spaces are identified and discussed in Section §5.3. We emphasise that the 16 brane tilings are *restriced*, in other words they do not have self-intersecting zig-zag paths and no multi-bonded edges. All other tilings are not discussed in detail in this work and are subject for future studies.

5.2.3 Consistency of Brane Tilings on a 2-torus

We have reviewed in section §1.3.3 the notion of consistency of a brane tiling on the 2-torus. For a $g = 2$ or higher genus brane tiling, the physical interpretation of these consistency conditions on the 2-torus breaks down. It is of great interest to study the properties of brane tilings on higher genus Riemann surface and to reinterpret and adapt the consistency conditions on the 2-torus.

Restrictions for $g = 2$ brane tilings. For the following classification of brane tilings on a $g = 2$ Riemann surface, we restrict ourselves to brane tilings with no self-intersecting zig-zag paths and no multi-bonded edges. We call these *restricted $g = 2$ brane tilings*. We apply the restriction in order to reduce the number of brane tilings identified in the classification, even though we believe that it is of interest to study unrestricted brane tilings on $g = 2$ Riemann surfaces. We leave the study of unrestricted brane tilings for future work.

5.2.4 Mesonic Moduli Spaces

The mesonic moduli space $\mathcal{M}^{mes}$ of a brane tiling is the vacuum moduli space of the corresponding supersymmetric gauge theory under both F-and D-term constraints. The *forward algorithm* [34, 92, 14, 101, 15, 55, 103] has been used extensively in the case for brane tilings on T^2 to identify the mesonic moduli space of Abelian gauge theories with only $U(1)$ gauge groups. It is summarized in section §1.4.4.

The forward algorithm can be used to identify $\mathcal{M}^{mes}$ for supersymmetric gauge theories represented by brane tilings on Riemann surfaces of arbitrary genus. The mesonic moduli spaces of the Abelian gauge theory is a $(2g + 1)$-dimensional toric Calabi-Yau variety.

In order to compute the structure of the mesonic moduli space, we evaluate the Hilbert series of $\mathcal{M}^{mes}$. The Hilbert series is refined with fugacities which count charges

#	$\mathcal{M}^{mes}$	Global Symmetry
5.2	$\mathbb{C}^5$	$SU(5) \times U(1)_R$
6.2a	$\mathbb{C}^5$	$SU(5) \times U(1)_R$
6.2b	$NC1$	$SU(3)^2 \times U(1)_R$
6.2c	$NC1$	$SU(3)^2 \times U(1)_R$
7.2	$\mathbb{C}^2 \times \mathcal{C}$	$SU(2)^3 \times U(1) \times U(1)_R$
7.4	$\mathbb{C} \times \mathcal{M}_{3,2}$	$U(1)^4 \times U(1)_R$
8.2a	$NC2$	$SU(2)^2 \times U(1)^2 \times U(1)_R$
8.2b	$NC3$	$SU(2)^4 \times U(1)_R$
8.4a	$\mathcal{M}_{3,3}$	$U(1)^4 \times U(1)_R$
8.4b	$\mathbb{C}^3 \times \mathbb{C}^2/\mathbb{Z}_2$	$SU(3) \times SU(2) \times U(1) \times U(1)_R$
8.4c	$\mathbb{C}^3 \times \mathbb{C}^2/\mathbb{Z}_2$	$SU(3) \times SU(2) \times U(1) \times U(1)_R$
8.4d	$\mathbb{C} \times \mathcal{M}_{3,2}$	$U(1)^4 \times U(1)_R$
8.4e	$NC4$	$U(1)^4 \times U(1)_R$
8.4f	$\mathcal{M}_{4,2}$	$U(1)^4 \times U(1)_R$
8.4g	$NC5$	$U(1)^4 \times U(1)_R$
8.4h	$NC3$	$SU(2)^4 \times U(1)_R$

Table 5.2: *Mesonic moduli spaces and global symmetries.* These are the theories in the classification with their mesonic moduli spaces and global symmetries of total rank 5.

under the global symmetries. The global symmetry group has total rank $2g+1$ and can have for the case of $g = 2$ brane tilings $SU(2)$, $SU(3)$, $SU(4)$ and $SU(5)$ enhancements. Table 5.2 summarises the global symmetries which are observed in the classification.

In field theory, the superpotential is conventionally assigned R-charge 2, when the supercharges have unit R-charge. For simplicity, we rescale the R-symmetry generator: quiver fields are assigned R-charges such that every perfect matching carries a R-charge of 1. This is a notational simplification in the following sections. For the actual R-charges the reader is reminded that the charges for perfect matchings should be rescaled such that the superpotential carries R-charge 2 rather than equal to the number of perfect matchings.
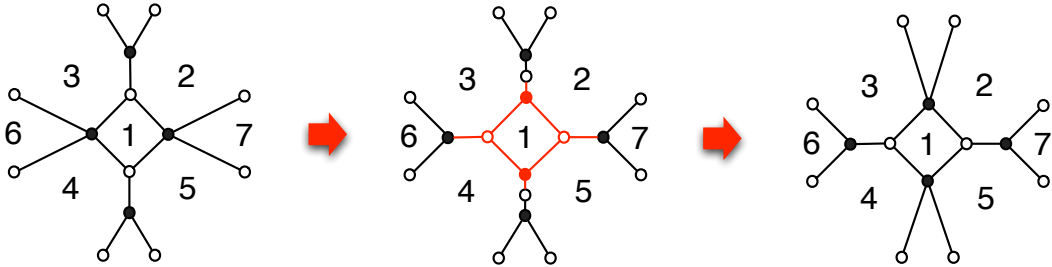
Figure 5.7: *Urban renewal move of a brane tiling.* The first step shows the urban renewal move which creates bivalent nodes. These correspond to mass terms that are integrated out and removed in the second step.

$\mathcal{M}^{mes}$	#E.T
$\mathbb{C}^5$	5.2, 6.2a
$NC1$	6.2b, 6.2c
$\mathbb{C} \times \mathcal{M}_{3,2}$	7.4, 8.4d
$NC3$	8.2b, 8.4h
$\mathbb{C}^3 \times \mathbb{C}^2/\mathbb{Z}_2$	8.4b, 8.4c

Table 5.3: Brane tilings on $g = 2$ which share the same Abelian mesonic moduli space. $NC1$ is the first non-complete intersection mesonic moduli space in the classification.

By analysing the mesonic moduli spaces of the $g = 2$ brane tilings in the classification shown in Figure 5.6, we observe interesting new phenomena. In the case of torus brane tilings, the mesonic moduli spaces of two brane tilings are the same if the brane tilings are related by an urban renewal move as depicted in Figure 5.7. Such a move seems to be still a sufficient condition for moduli space equivalence for brane tilings on higher genus Riemann surfaces. However, we observe examples of $g = 2$ brane tilings which are not related by urban renewal, but have the same mesonic moduli space. The examples identified in the classification are shown in Table 5.3.

The above classification of the mesonic moduli spaces are based on the fact that we restrict to Abelian theories with only $U(1)$ gauge groups. Whether as in the case of toric duality the supersymmetric theories share the same mesonic moduli spaces in the non-Abelian extension is unclear. It is of great interest to study this problem in future work.

5.2.5 Higgsing $g = 2$ Brane Tilings

Section §5.2.2 explained the procedure which is followed in this work to identify $g = 2$ brane tilings with up to $E = 8$ fields and $V = 4$ superpotential terms. We expect *Higgsing* [15, 101, 5] to be an exploratory way to relate the discovered brane tilings and at the same time to check the classification for consistency. Higgsing is the procedure of giving VEVs to bifundamental fields in order to solve D-term equations in the presence of FI parameters, and to integrate out mass terms in the resulting superpotential of the theory. It translates to removing edges in the brane tiling and reducing the graph such that there are no bivalent nodes. The procedure is illustrated in Figure 5.8.

Given that our classification is restricted to $g = 2$ brane tilings with no self-intersecting zig-zag paths and no multi-bonded edges, Higgsing is expected to relate them to unrestricted models. In fact, starting from the 16 restricted brane tilings in Figure 5.6, one also generates 10 unrestricted brane tilings with self-intersecting zig-zag paths which are summarized with the corresponding superpotentials and quiver diagrams in appendix §A.7. A 'Higgsing tree', which illustrates brane tilings as nodes and VEVs as arrows, is
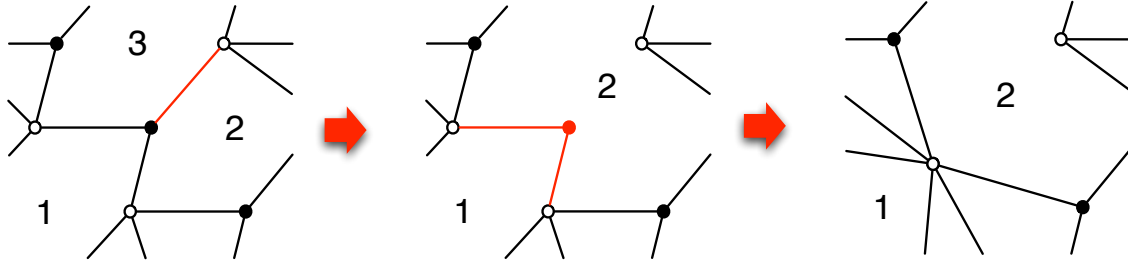
Figure 5.8: *Higgsing in a brane tiling.* The first step shows the removal of the edge which corresponds to the bifundamental field which is assigned a VEV. The Higgsing results in a bivalent node which corresponds to a mass term. This is integrated out in the second step.

shown in Figure 5.9.

5.3 A Classification of $g = 2$ Brane Tilings

This section summarizes the classification of $g = 2$ brane tilings with up to $E = 8$ fields and $V = 4$ superpotential terms. The mesonic moduli spaces are studied by computing the Hilbert series of the corresponding algebraic variety. We discover several interesting geometries which are related to the new brane tilings.

5.3.1 5 Fields, 2 Superpotential Terms, 1 Gauge Group

Model 5.2: $\mathbb{C}^5$

The first $g = 2$ brane tiling of our classification and the corresponding quiver diagram are shown in Figure 5.10 and Figure 5.11 respectively. The brane tiling is made of a single decagonal face which is the single gauge group with 5 adjoints in the quiver diagram. The superpotential is

$$W = +X_{11}^1 X_{11}^2 X_{11}^3 X_{11}^4 X_{11}^5 - X_{11}^5 X_{11}^4 X_{11}^3 X_{11}^2 X_{11}^1 . \tag{5.3.4}$$

A single adjoint on its own forms a perfect matching of the brane tiling. Accordingly,
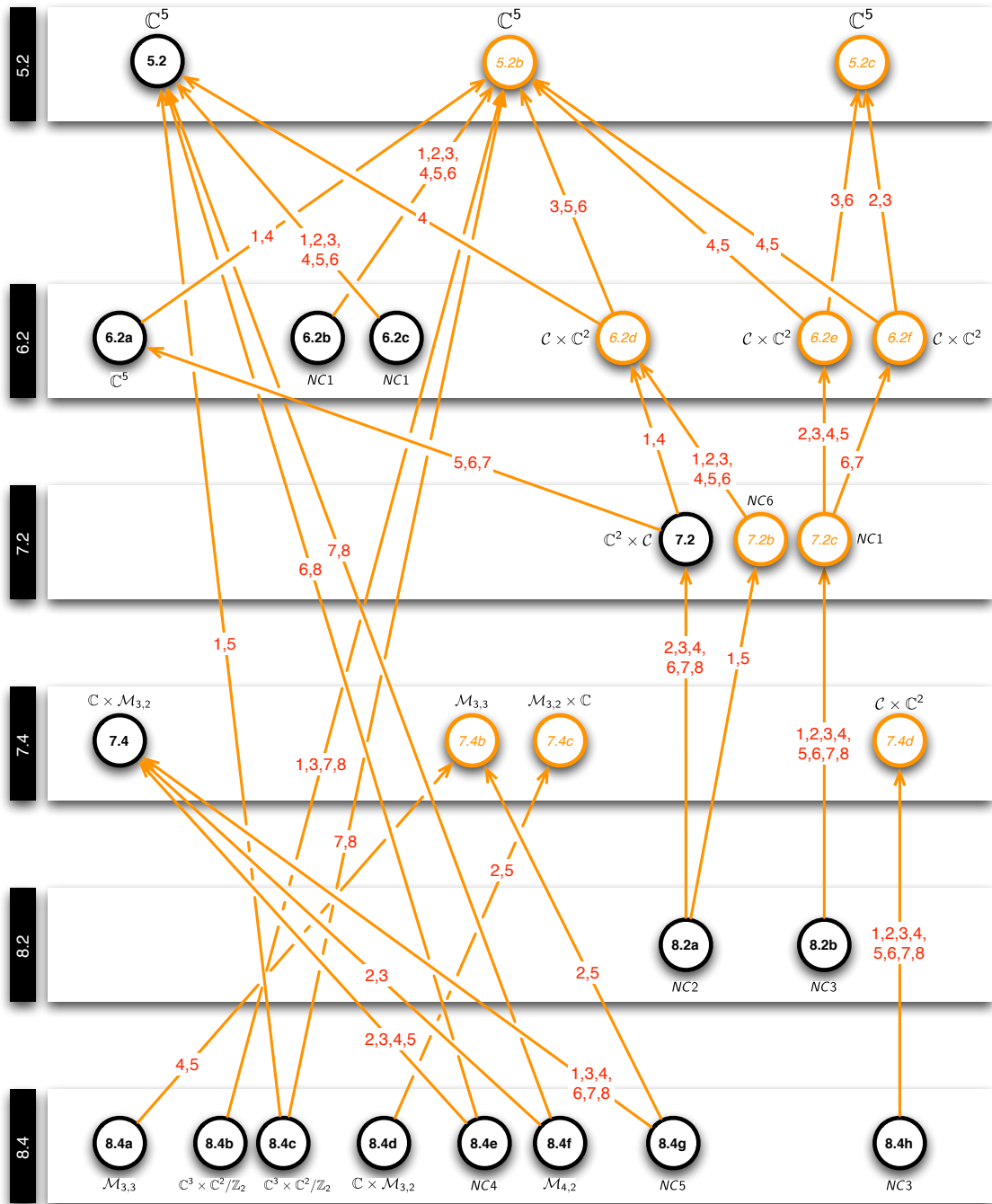
Figure 5.9: *Higgsing tree for g = 2 brane tilings with up to 8 quiver fields.* The models labeled with italics correspond to unrestricted brane tilings with self-intersecting zig-zag paths. The arrows correspond to a single field Higgsing, with the field numbers given on the arrows (see §A.6 and §A.7 for field labels).
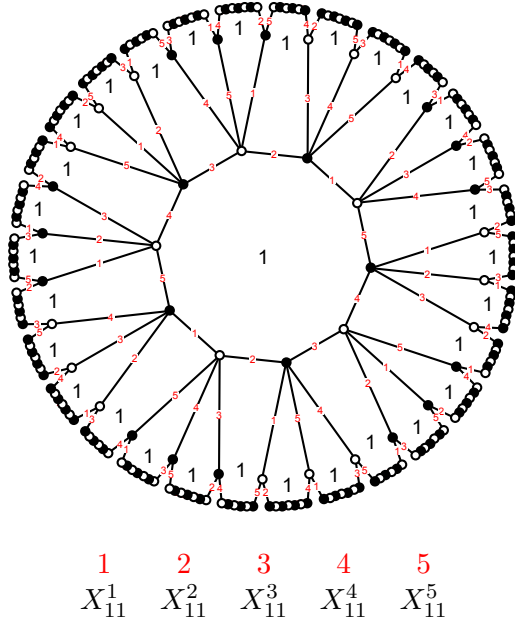
Figure 5.10: The Model 5.2 brane tiling on a $g = 2$ Riemann surface with 5 fields and 2 superpotential terms.

Figure 5.11: The quiver diagram for Model 5.2, a brane tiling on a $g = 2$ Riemann surface with 5 fields and 2 superpotential terms.

the perfect matching matrix is the identity matrix

$$
P = \begin{pmatrix}
 & a_1 & a_2 & a_3 & a_4 & a_5 \\
\hline
X_{11}^1 & 1 & 0 & 0 & 0 & 0 \\
X_{11}^2 & 0 & 1 & 0 & 0 & 0 \\
X_{11}^3 & 0 & 0 & 1 & 0 & 0 \\
X_{11}^4 & 0 & 0 & 0 & 1 & 0 \\
X_{11}^5 & 0 & 0 & 0 & 0 & 1
\end{pmatrix} . \tag{5.3.5}
$$

The perfect matching matrix is always the identity matrix for models with just 2 superpotential terms. The zig-zag paths of the brane tiling are

$$
\eta_1 = (X_{11}^1, X_{11}^2) \ , \ \eta_2 = (X_{11}^2, X_{11}^3) \ , \ \eta_3 = (X_{11}^3, X_{11}^4) \ ,
$$
$$
\eta_4 = (X_{11}^4, X_{11}^5) \ , \ \eta_5 = (X_{11}^5, X_{11}^1) \ . \tag{5.3.6}
$$

There are only trivial F- and D-terms. The mesonic moduli space is a toric Calabi-

Yau 5-fold. More specifically, Model 5.2's mesonic moduli space is $\mathbb{C}^5$ with the refined Hilbert series being

$$g_1(\alpha_i; \mathcal{M}^{mes}) \quad = \quad \frac{1}{\prod_{i=1}^{5}(1 - \alpha_i)} \ , \tag{5.3.7}$$

where the fugacities α_i count the perfect matchings a_i respectively.

Given that the mesonic moduli space is $\mathbb{C}^5$, the global symmetry group is found as $SU(5) \times U(1)_R$, where the $U(1)_R$ is the R-symmetry. The global symmetry charges assigned to perfect matchings are shown below.

	$SU(5)_{x_i}$	$U(1)_R$	fugacity
a_1	(1,0,0,0)	1	$\alpha_1 = x_1 t$
a_2	(-1,1,0,0)	1	$\alpha_2 = x_1^{-1} x_2 t$
a_3	(0,-1,1,0)	1	$\alpha_3 = x_2^{-1} x_3 t$
a_4	(0,0,-1,1)	1	$\alpha_4 = x_3^{-1} x_4 t$
a_5	(0,0,0,-1)	1	$\alpha_5 = x_4^{-1} t$

Under the above global symmetry charge assignment, the Hilbert series can be expressed in terms of characters of irreducible representations of $SU(5)$,

$$g_1(x_i, t; \mathcal{M}^{mes}) = \sum_{n=0}^{\infty} [n, 0, 0, 0]_{SU(5)} t^n \ . \tag{5.3.8}$$

The toric diagram of the mesonic moduli space is a 4 dimensional lattice polytope. The coordinates of the toric points are encoded in the matrix

$$G_t = \begin{pmatrix} a_1 & a_2 & a_3 & a_4 & a_5 \\ \hline 1 & 0 & 0 & 0 & 0 \\ 0 & 1 & 0 & 0 & 0 \\ 0 & 0 & 1 & 0 & 0 \\ 0 & 0 & 0 & 1 & 0 \\ 0 & 0 & 0 & 0 & 1 \end{pmatrix} \ . \tag{5.3.9}$$

The projected toric diagram is a unit lattice 4-simplex.
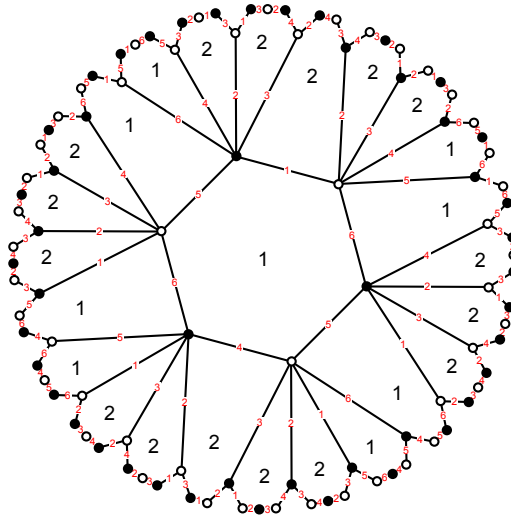
$$
\begin{array}{cccccc}
\textcolor{red}{1} & \textcolor{red}{2} & \textcolor{red}{3} & \textcolor{red}{4} & \textcolor{red}{5} & \textcolor{red}{6} \\
X_{12} & X_{22}^1 & X_{22}^2 & X_{21} & X_{11}^1 & X_{11}^2
\end{array}
$$

Figure 5.12: The Model 6.2a brane tiling on a $g = 2$ Riemann surface with 6 fields and 2 superpotential terms.
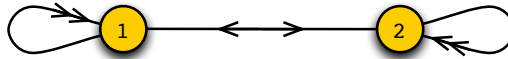
Figure 5.13: The quiver diagram for Model 6.2a, a brane tiling on a $g = 2$ Riemann surface with 6 fields and 2 superpotential terms.

5.3.2 6 Fields, 2 Superpotential Terms, 2 Gauge Groups

Model 6.2a: $\mathbb{C}^5$

The brane tiling on a $g = 2$ Riemann surface and the corresponding quiver diagram are shown in Figure 5.12 and Figure 5.13 respectively. The superpotential is

$$
W = +X_{12}X_{22}^1 X_{22}^2 X_{21} X_{11}^1 X_{11}^2 - X_{12}X_{22}^2 X_{22}^1 X_{21} X_{11}^2 X_{11}^1 \ . \tag{5.3.10}
$$

The quiver incidence matrix is

$$
d = \left(\begin{array}{c|cccccc}
 & X_{11}^1 & X_{11}^2 & X_{22}^1 & X_{22}^2 & X_{12} & X_{21} \\
\hline
 & 0 & 0 & 0 & 0 & 1 & -1 \\
 & 0 & 0 & 0 & 0 & -1 & 1
\end{array} \right) \ . \tag{5.3.11}
$$

The brane tiling has 6 perfect matchings. Since there are only 2 superpotential terms, every field on its own represents a perfect matching. The perfect matching matrix is

272

therefore the identity matrix,

$$
P = \begin{pmatrix}
 & a_1 & a_2 & a_3 & a_4 & p_1 & p_2 \\
\hline
X_{11}^1 & 1 & 0 & 0 & 0 & 0 & 0 \\
X_{11}^2 & 0 & 1 & 0 & 0 & 0 & 0 \\
X_{22}^1 & 0 & 0 & 1 & 0 & 0 & 0 \\
X_{22}^2 & 0 & 0 & 0 & 1 & 0 & 0 \\
X_{12} & 0 & 0 & 0 & 0 & 1 & 0 \\
X_{21} & 0 & 0 & 0 & 0 & 0 & 1
\end{pmatrix}
\tag{5.3.12}
$$

The zig-zag paths in the brane tiling of Model 6.2a are

$$
\eta_1 = (X_{11}^1, X_{11}^2) \ , \ \ \eta_2 = (X_{22}^1, X_{22}^2) \ ,
$$
$$
\eta_3 = (X_{12}, X_{22}^2, X_{21}, X_{11}^1) \ , \ \ \eta_4 = (X_{12}, X_{22}^2, X_{21}, X_{11}^2) \ .
\tag{5.3.13}
$$

The superpotential for a theory with only $U(1)$ gauge groups vanishes $W = 0$, and therefore the kernel of the perfect matching matrix is empty. There are no F-terms, and there are no F-term charges

$$
Q_F = 0 \ .
\tag{5.3.14}
$$

The D-term charges are encoded in the quiver incidence matrix d and are summarized in the following charge matrix,

$$
Q_D = \left(
\begin{array}{cccccc}
a_1 & a_2 & a_3 & a_4 & p_1 & p_2 \\
\hline
0 & 0 & 0 & 0 & 1 & -1
\end{array}
\right) \ .
\tag{5.3.15}
$$

Accordingly, the total charge matrix $Q_t = Q_F$, and the mesonic moduli space is given by the symplectic quotient of the form

$$
\mathcal{M}^{mes} = \mathbb{C}^6 // Q_t \ .
\tag{5.3.16}
$$

By associating the fugacities α_i, t_i to the perfect matchings a_i, p_i respectively, the fully refined Hilbert series of $\mathcal{M}^{mes}$ is given by the following Molien integral

$$
\begin{aligned}
g_1(\alpha_i, \beta_i; \mathcal{M}^{mes}) &= \frac{1}{(2\pi i)} \oint_{|z_1|=1} \frac{dz_1}{z_1} \frac{1}{\prod_{i=1}^4 (1 - \alpha_i)} \times \frac{1}{(1 - z_1 t_1)(1 - z_1^{-1} t_2)} \\
&= \frac{1}{\prod_{i=1}^4 (1 - \alpha_i)} \times \frac{1}{(1 - t_1 t_2)} \ .
\end{aligned}
\tag{5.3.17}
$$

Accordingly, the mesonic moduli space is a freely generated space, $\mathcal{M}^{mes} = \mathbb{C}^5$.

The Q_D charge matrix in (5.3.15) indicates a symmetry of $SU(4) \times U(1) \times U(1)_R$.

	$SU(4)_{x_i}$	$U(1)_b$	$U(1)_R$	fugacity
a_1	(1,0,0)	0	1	$\alpha_1 = x_1 t$
a_2	(-1,1,0)	0	1	$\alpha_2 = x_1^{-1} x_2 t$
a_3	(0,-1,1)	0	1	$\alpha_3 = x_2^{-1} x_3 t$
a_4	(0,0,-1)	0	1	$\alpha_4 = x_3^{-1} t$
p_1	(0,0,0)	1	1	$t_1 = bt$
p_2	(0,0,0)	-1	1	$t_2 = b^{-1} t$

Under the above charge assignment, the Hilbert series of $\mathcal{M}^{mes}$ can be expressed as

$$g_1(x_i, t; \mathcal{M}^{mes}) = \frac{1}{1-t^2} \sum_{n=0}^{\infty} [n,0,0]_{SU(4)} t^n . \qquad (5.3.18)$$

Since the moduli space space is $\mathbb{C}^5$, we expect a $SU(5)$ symmetry. The fully enhanced global symmetry is therefore $SU(5) \times U(1)_R$. This can be observed by modifying the global charges on the perfect matchings p_1 and p_2. A possible choice can be:

	$SU(5)_{x_i}$	$U(1)_R$	fugacity
a_1	(1,0,0,0)	1	$\alpha_1 = x_1 t$
a_2	(-1,1,0,0)	1	$\alpha_2 = x_1^{-1} x_2 t$
a_3	(0,-1,1,0)	1	$\alpha_3 = x_2^{-1} x_3 t$
a_4	(0,0,-1,1)	1	$\alpha_4 = x_4 x_3^{-1} t$
p_1	(0,0,0,-1/2)	1/2	$t_1 = x_4^{-1/2} t^{-1/2}$
p_2	(0,0,0,-1/2)	1/2	$t_2 = x_4^{-1/2} t^{-1/2}$

Under the above charge assignment, the mesonic Hilbert series can be expressed as expected in terms of characters of $SU(5)$ irreducible representations,

$$g_1(x_i, t; \mathcal{M}^{mes}) = \sum_{n=0}^{\infty} [n,0,0,0]_{SU(5)} t^n . \qquad (5.3.19)$$

The toric diagram of the mesonic moduli space is a 4 dimensional lattice polytope. The coordinates of the toric points are encoded in the matrix

$$G_t = \begin{pmatrix} a_1 & a_2 & a_3 & a_4 & p_1 & p_2 \\ \hline 1 & 0 & 0 & 0 & 0 & 0 \\ 0 & 1 & 0 & 0 & 0 & 0 \\ 0 & 0 & 1 & 0 & 0 & 0 \\ 0 & 0 & 0 & 1 & 0 & 0 \\ 0 & 0 & 0 & 0 & 1 & 1 \end{pmatrix} . \qquad (5.3.20)$$

Recall that perfect matchings correspond to toric points. We observe that the perfect

matchings p_1 and p_2 correspond to the same toric point.

Model 6.2b: $NC1$

$$\begin{array}{cccccc} \textcolor{red}{1} & \textcolor{red}{2} & \textcolor{red}{3} & \textcolor{red}{4} & \textcolor{red}{5} & \textcolor{red}{6} \\ X_{12}^1 & X_{21}^1 & X_{12}^2 & X_{21}^2 & X_{12}^3 & X_{21}^3 \end{array}$$
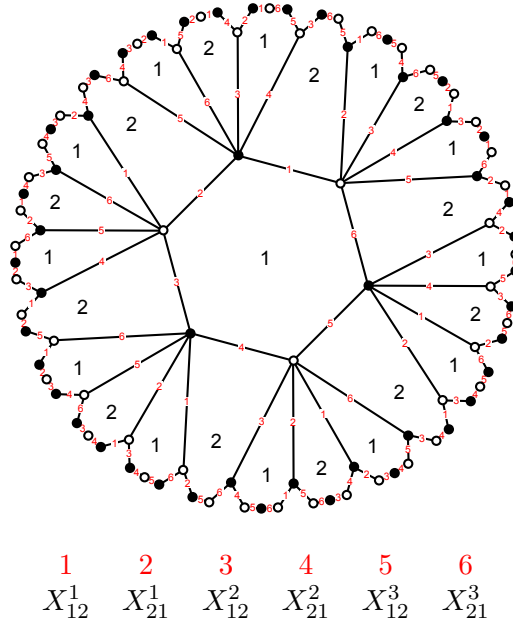
Figure 5.14: The Model 6.2b brane tiling on a $g = 2$ Riemann surface with 6 fields and 2 superpotential terms.
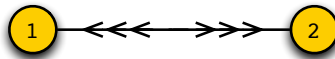
Figure 5.15: The quiver diagram for Model 6.2b, a brane tiling on a $g = 2$ Riemann surface with 6 fields and 2 superpotential terms.

The second brane tiling on a $g = 2$ Riemann surface with 2 superpotential terms with 6 fields is shown with the corresponding quiver diagram in Figure 5.14 and Figure 5.15 respectively. The superpotential is

$$W = +X_{12}^1 X_{21}^1 X_{12}^2 X_{21}^2 X_{12}^3 X_{21}^3 - X_{12}^1 X_{21}^2 X_{12}^2 X_{21}^3 X_{12}^3 X_{21}^1 \ . \tag{5.3.21}$$

The quiver incidence matrix is

$$d = \left(\begin{array}{cccccc} X_{12}^1 & X_{12}^2 & X_{12}^3 & X_{21}^1 & X_{21}^2 & X_{21}^3 \\ \hline 1 & 1 & 1 & -1 & -1 & -1 \\ -1 & -1 & -1 & 1 & 1 & 1 \end{array} \right) \ . \tag{5.3.22}$$

The brane tiling has $c = 6$ perfect matchings, each of them given by a bifundamental field. The perfect matching matrix is the identity matrix,

$$
P = \begin{pmatrix}
 & a_1 & a_2 & a_3 & b_1 & b_2 & b_3 \\
\hline
X_{12}^1 & 1 & 0 & 0 & 0 & 0 & 0 \\
X_{12}^2 & 0 & 1 & 0 & 0 & 0 & 0 \\
X_{12}^3 & 0 & 0 & 1 & 0 & 0 & 0 \\
X_{21}^1 & 0 & 0 & 0 & 1 & 0 & 0 \\
X_{21}^2 & 0 & 0 & 0 & 0 & 1 & 0 \\
X_{21}^3 & 0 & 0 & 0 & 0 & 0 & 1
\end{pmatrix}
\tag{5.3.23}
$$

The zig-zag paths of the brane tiling are

$$
\eta_1 = (X_{12}^1, X_{21}^1) \ , \quad \eta_2 = (X_{12}^2, X_{21}^2) \ , \quad \eta_3 = (X_{12}^3, X_{21}^3) \ ,
$$
$$
\eta_4 = (X_{12}^1, X_{21}^2, X_{12}^3, X_{21}^1, X_{12}^2, X_{21}^3) \ .
\tag{5.3.24}
$$

The Abelian superpotential vanishes $W = 0$, and the kernel of the perfect matching matrix is empty. There are no F-terms, therefore no F-term charges. The D-term charges are encoded in the quiver incidence matrix d:

$$
Q_D = \left(\begin{array}{cccccc}
a_1 & a_2 & a_3 & b_1 & b_2 & b_3 \\
\hline
1 & 1 & 1 & -1 & -1 & -1
\end{array} \right) \ .
\tag{5.3.25}
$$

The total charge matrix $Q_t = Q_D$, and the mesonic moduli space is the symplectic quotient

$$
\mathcal{M}^{mes} = \mathbb{C}^6 // Q_t \ .
\tag{5.3.26}
$$

By associating the fugacities α_i and β_j to the perfect matchings a_i and b_j respectively, the fully refined Hilbert series of $\mathcal{M}^{mes}$ is given by the Molien integral

$$
g_1(\alpha_i, \beta_i; \mathcal{M}^{mes}) = \oint_{|z|=1} \frac{dz}{2\pi i z} \frac{1}{\prod\limits_{i=1}^{3}(1 - z\alpha_i)(1 - z^{-1}\beta_i)} = \frac{(\prod\limits_{i=1}^{3} \alpha_i \beta_i)\, P(\alpha_i, \beta_i)}{\prod\limits_{i,j=1}^{3}(1 - \alpha_i \beta_j)} \ ,
\tag{5.3.27}
$$

where

$$
P(\alpha_i, \beta_i) = \prod_{i=1}^{3} \alpha_i^{-1}\beta_i^{-1} - \sum_{i,j=1}^{3} \alpha_i^{-1}\beta_j^{-1} + \sum_{i,j=1}^{3} (\alpha_i \alpha_j^{-1} + \beta_i \beta_j^{-1}) - 2 - \sum_{i,j=1}^{3} \alpha_i \beta_j + \prod_{i=1}^{3} \alpha_i \beta_i \ .
\tag{5.3.28}
$$

Accordingly, the mesonic moduli space is a non-complete intersection of dimension 5. By setting the fugacities $\alpha_i = \beta_i = t$, the unrefined Hilbert series is

$$g_1(t; \mathcal{M}^{mes}) = \frac{1 + 4t^2 + t^4}{(1 - t^2)^5} \ . \tag{5.3.29}$$

The palindromic numerator of the Hilbert series indicates that $\mathcal{M}^{mes}$ is a Calabi-Yau 5-fold. The plethystic logarithm of the refined Hilbert series of $\mathcal{M}^{mes}$ is of the form

$$PL[g_1(\alpha_i, \beta_i; \mathcal{M}^{mes})] \ = \ \sum_{i,j=1}^{3} \alpha_i \beta_j - \sum_{i_1 \neq i_2, j_1 \neq j_2}^{3} \alpha_{i_1} \beta_{j_1} \alpha_{i_2} \beta_{j_2} + \dots \ . \tag{5.3.30}$$

The generators of the mesonic moduli space in terms of perfect matching variables are

generator	perfect matchings
A_{ij}	$a_i b_j$

which are subject to the first order relations

$$\epsilon^{i_1 i_2 i_3} \epsilon^{j_1 j_2 j_3} A_{i_2 j_2} A_{i_3 j_3} = 0 \ . \tag{5.3.31}$$

One can assign the following enhanced $SU(3) \times SU(3) \times U(1)_R$ global charges to the perfect matching variables

	$SU(3)_x$	$SU(3)_y$	$U(1)_R$	fugacity
a_1	$(1, 0)$	0	1	$\alpha_1 = x_1 t$
a_2	$(-1, 1)$	0	1	$\alpha_2 = x_1^{-1} x_2 t$
a_3	$(0, -1)$	0	1	$\alpha_3 = x_2^{-1} t$
b_1	0	$(-1, 0)$	1	$\beta_1 = y_1^{-1} t$
b_2	0	$(1, -1)$	1	$\beta_2 = y_1 y_2^{-1} t$
b_3	0	$(0, 1)$	1	$\beta_3 = y_2 t$

Under the above charge assignment, the Hilbert series of $\mathcal{M}^{mes}$ can be expressed as

$$g_1(x_i, y_i, t; \mathcal{M}^{mes}) \ = \ \sum_{n=0}^{\infty} [n, 0; 0, n] t^{2n} \ , \tag{5.3.32}$$

where $[n, 0; 0, n] \equiv [n, 0]_{SU(3)_x} [0, n]_{SU(3)_y}$. The generators and the first order relations formed by them are encoded in the plethystics logarithm, which now takes the form

$$PL[g_1(x_i, y_i, t; \mathcal{M}^{mes})] = [1, 0; 0, 1] t^2 - [0, 1; 1, 0] t^4 + \dots \ . \tag{5.3.33}$$

The toric diagram of the mesonic moduli space is a 4 dimensional lattice polytope.

The coordinates of the toric points are encoded in the matrix

$$
G_t = \left(
\begin{array}{c|cccccc}
 & p_1 & p_2 & p_3 & p_4 & p_5 & p_6 \\
\hline
 & 1 & 0 & 0 & 0 & 0 & 1 \\
 & -1 & 0 & 0 & 0 & 1 & 0 \\
 & 1 & 0 & 0 & 1 & 0 & 0 \\
 & -1 & 0 & 1 & 0 & 0 & 0 \\
 & 1 & 1 & 1 & 1 & 1 & 1
\end{array}
\right) .
\tag{5.3.34}
$$

Note that the mesonic moduli space here is the same as the master space of $\mathbb{C}^3/\mathbb{Z}_3$ [52].

Model 6.2c: $NC1$
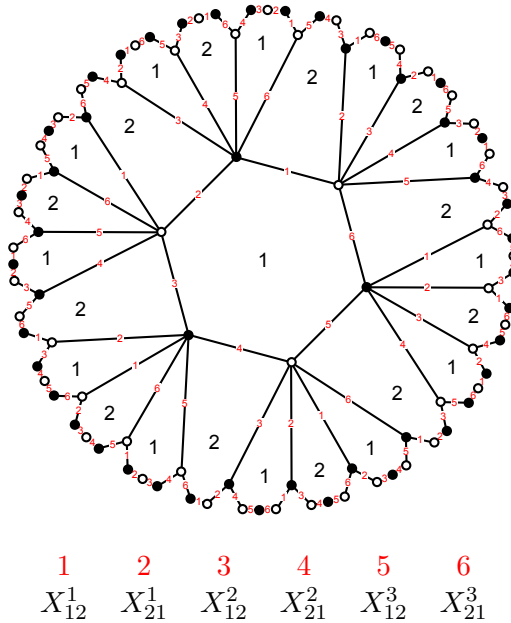
Figure 5.16: The Model 6.2c brane tiling on a $g = 2$ Riemann surface with 6 fields and 2 superpotential terms.

Figure 5.17: The quiver diagram for Model 6.2c, a brane tiling on a $g = 2$ Riemann surface with 6 fields and 2 superpotential terms.

The brane tiling and quiver for Model 6.2c are shown in Figure 5.16 and Figure 5.17

respectively. The superpotential is

$$W = +X_{12}^1 X_{21}^1 X_{12}^2 X_{21}^2 X_{12}^3 X_{21}^3 - X_{21}^3 X_{12}^3 X_{21}^2 X_{12}^2 X_{21}^1 X_{12}^1 \ . \tag{5.3.35}$$

In the Abelian gauge theory the superpotential vanishes, giving the same model as in the previous section. (The non-Abelian gauge theories differ by superpotential interactions.) There is a difference in the zig-zag paths, which now are

$$\eta_1 = (X_{21}^3, X_{12}^3) \ , \ \ \eta_2 = (X_{12}^3, X_{21}^2) \ , \ \ \eta_3 = (X_{21}^2, X_{12}^2) \ ,$$
$$\eta_4 = (X_{12}^2, X_{21}^1) \ , \ \ \eta_5 = (X_{21}^1, X_{12}^3) \ , \ \ \eta_6 = (X_{12}^3, X_{21}^2) \ . \tag{5.3.36}$$

5.3.3 7 Fields, 2 Superpotential Terms, 3 Gauge Groups

Model 7.2: $\mathbb{C}^2 \times \mathcal{C}$

1	2	3	4	5	6	7
X_{13}	X_{33}^1	X_{33}^2	X_{32}	X_{21}^1	X_{12}	X_{21}^2
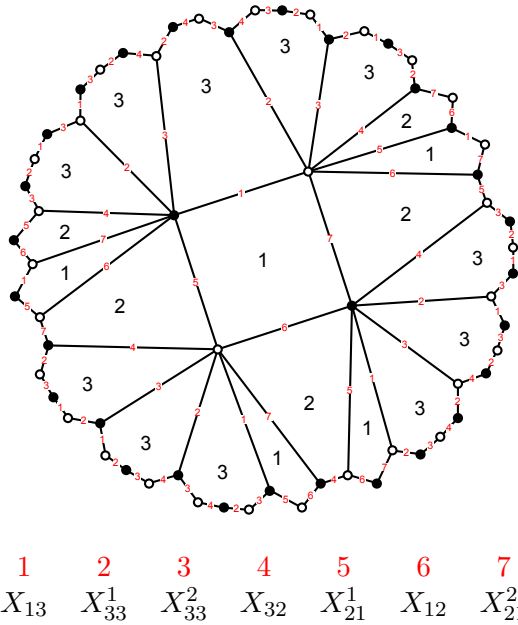
Figure 5.18: The Model 7.2 brane tiling on a $g = 2$ Riemann surface with 3 gauge groups, 7 fields and 2 superpotential terms.

The brane tiling and corresponding quiver for Model 7.2 is shown in Figure 5.18 and

Figure 5.19: The quiver diagram for Model 7.2, a brane tiling on a $g = 2$ Riemann surface with 3 gauge groups, 7 fields and 2 superpotential terms.

Figure 5.19 respectively. The superpotential is

$$W = +X_{13}X_{33}^1X_{33}^2X_{32}X_{21}^1X_{12}X_{21}^2 - X_{13}X_{33}^2X_{33}^1X_{32}X_{21}^2X_{12}X_{21}^1 \; .$$

(5.3.37)

The quiver incidence matrix is

$$d = \begin{pmatrix} X_{33}^1 & X_{33}^2 & X_{21}^1 & X_{21}^2 & X_{12} & X_{13} & X_{32} \\ \hline 0 & 0 & 1 & 1 & -1 & -1 & 0 \\ 0 & 0 & -1 & -1 & 1 & 0 & 1 \\ 0 & 0 & 0 & 0 & 0 & 1 & -1 \end{pmatrix} \; .$$

(5.3.38)

Model 7.2 has $c = 7$ perfect matchings, each made out of a single field in the quiver. The perfect matching matrix is therefore the identity matrix,

$$P = \begin{pmatrix} & a_1 & a_2 & b_1 & b_2 & p_1 & p_2 & p_3 \\ \hline X_{33}^1 & 1 & 0 & 0 & 0 & 0 & 0 & 0 \\ X_{33}^2 & 0 & 1 & 0 & 0 & 0 & 0 & 0 \\ X_{21}^1 & 0 & 0 & 1 & 0 & 0 & 0 & 0 \\ X_{21}^2 & 0 & 0 & 0 & 1 & 0 & 0 & 0 \\ X_{12} & 0 & 0 & 0 & 0 & 1 & 0 & 0 \\ X_{13} & 0 & 0 & 0 & 0 & 0 & 1 & 0 \\ X_{32} & 0 & 0 & 0 & 0 & 0 & 0 & 1 \end{pmatrix} \; .$$

(5.3.39)

The brane tiling has the following zig-zag paths,

$$\eta_1 = (X_{33}^1, X_{33}^2) \; , \quad \eta_2 = (X_{21}^1, X_{12}) \; , \quad \eta_3 = (X_{12}, X_{21}^2) \; ,$$
$$\eta_4 = (X_{13}, X_{33}^1, X_{32}, X_{21}^1) \; , \quad \eta_5 = (X_{13}, X_{33}^2, X_{32}, X_{21}^2) \; .$$

(5.3.40)

There are only trivial F-term constraints. The D-term constraints are encoded in the charge matrix

$$
Q_D = \left(\begin{array}{ccccccc}
a_1 & a_2 & b_1 & b_2 & p_1 & p_2 & p_3 \\
\hline
0 & 0 & 1 & 1 & -1 & 0 & -1 \\
0 & 0 & 0 & 0 & 0 & 1 & -1
\end{array} \right) .
\tag{5.3.41}
$$

Model 7.2's mesonic moduli space is expressed as the following symplectic quotient,

$$
\mathcal{M}^{mes} = \mathbb{C}^7 // Q_D .
\tag{5.3.42}
$$

By associating the fugacities α_i, β_i, t_i to the perfect matchings a_i, b_i, p_i respectively, the fully refined Hilbert series of $\mathcal{M}^{mes}$ is given by the following Molien integral

$$
\begin{aligned}
g_1(\alpha_i, \beta_i, t_i; \mathcal{M}^{mes}) &= \frac{1}{(2\pi i)^3} \oint_{|z_1|=1} \frac{dz_1}{z_1} \oint_{|z_2|=1} \frac{dz_2}{z_2} \oint_{|z_3|=1} \frac{dz_3}{z_3} \\
&\quad \times \frac{1}{\prod_{i=1}^2 (1-\alpha_i)(1-z_1\beta_i)} \\
&\quad \times \frac{1}{(1-z_1^{-1}t_1)(1-z_2 t_2)(1-z_1^{-1}z_2^{-1}t_3)} \\
&= \frac{1-\beta_1\beta_2 t_1 t_2 t_3}{\prod_{i=1}^2 (1-\alpha_i)(1-\beta_i t_1)(1-\beta_i t_2 t_3)} .
\end{aligned}
\tag{5.3.43}
$$

From the Hilbert series, we observe that the mesonic moduli space is a complete intersection. It is a 5-dimensional Calabi-Yau space. More specifically, the mesonic moduli space is $\mathcal{M}^{mes} = \mathbb{C}^2 \times \mathcal{C}$ where the conifold generators are

generator	perfect matchings
A_i	$b_i p_1$
B_i	$b_i p_2 p_3$

The conifold relation is

$$
\epsilon^{ij} A_i B_j = 0 .
\tag{5.3.44}
$$

The global symmetry is enhanced to $SU(2) \times SU(2) \times U(1)^2 \times U(1)_R$ according to the charge matrix in (5.3.41). One can assign the following global symmetry charges to the perfect matchings.

	$SU(2)_x$	$SU(2)_y$	$U(1)_{b_1}$	$U(1)_{b_2}$	$U(1)_R$	fugacity
a_1	+1	0	0	0	+1	$\alpha_1 = xt$
a_2	-1	0	0	0	+1	$\alpha_2 = x^{-1}t$
b_1	0	+1	0	-1	+1	$\beta_1 = yb_2^{-1}t$
b_2	0	-1	0	-1	+1	$\beta_2 = y^{-1}b_2^{-1}t$
p_1	0	0	0	+1	+1	$t_1 = b_2 t$
p_2	0	0	+1	0	+1	$t_2 = b_1 t$
p_3	0	0	-1	+1	+1	$t_3 = b_1^{-1}b_2 t$

Under the above charge assignment, the Hilbert series of $\mathcal{M}^{mes}$ can be expressed in terms of characters of irreducible representations of the global symmetry,

$$
\begin{aligned}
g_1(x,y,t;\mathcal{M}^{mes}) &= \frac{1}{(1-xt)(1-x^{-1}t)} \sum_{n_1=0}^{\infty}\sum_{n_2=0}^{\infty} [n_1+n_2]_y t^{2n_1+3n_2} \\
&= \sum_{m=0}^{\infty}\sum_{n_1=0}^{\infty}\sum_{n_2=0}^{\infty} [m]_x [n_1+n_2]_y t^{m+2n_1+3n_2} .
\end{aligned}
\tag{5.3.45}
$$

We expect however from the conifold itself two $SU(2)$ symmetries and therefore a fully enhanced symmetry of $SU(2)^3 \times U(1) \times U(1)_R$. The full symmetry can be probed by modifying the above charge assignment on perfect matchings as follows.

	$SU(2)_x$	$SU(2)_y$	$SU(2)_z$	$U(1)_b$	$U(1)_R$	fugacity
a_1	+1	0	0	0	+1	$\alpha_1 = xt$
a_2	-1	0	0	0	+1	$\alpha_2 = x^{-1}t$
b_1	0	+1	0	-1	+1	$\beta_1 = yb_2^{-1}t$
b_2	0	-1	0	-1	+1	$\beta_2 = y^{-1}b_2^{-1}t$
p_1	0	0	+1	+1	+1	$t_1 = zbt$
p_2	0	0	-1/2	+1/2	+1/2	$t_2 = z^{-1/2}b^{1/2}t^{1/2}$
p_3	0	0	-1/2	+1/2	+1/2	$t_3 = z^{-1/2}b^{1/2}t^{1/2}$

With the above refinement, the Hilbert series displays the full $SU(2)^3$ symmetry,

$$
g_1(x,y,z,t;\mathcal{M}^{mes}) = \sum_{n_1=0}^{\infty}\sum_{n_2=0}^{\infty} [n_1]_x [n_2]_y [n_2]_z t^{n_1+2n_2} .
\tag{5.3.46}
$$

The toric diagram of $\mathcal{M}^{mes}$ is given by

$$G_t = \begin{pmatrix} & a_1 & a_2 & b_1 & b_2 & p_1 & p_2 & p_3 \\ \hline & 1 & 0 & 0 & 0 & 0 & 0 & 0 \\ & 0 & 1 & 0 & 0 & 0 & 0 & 0 \\ & 0 & 0 & 1 & 0 & 1 & 0 & 0 \\ & 0 & 0 & 0 & 1 & 1 & 0 & 0 \\ & 0 & 0 & 0 & 0 & 1 & -1 & -1 \end{pmatrix} , \tag{5.3.47}$$

where we notice that the perfect matchings p_2 and p_3 relate to the same toric point.

5.3.4 7 Fields, 4 Superpotential Terms, 1 Gauge Group

**Model 7.4:** $\mathbb{C} \times \mathcal{M}_{3,2}$
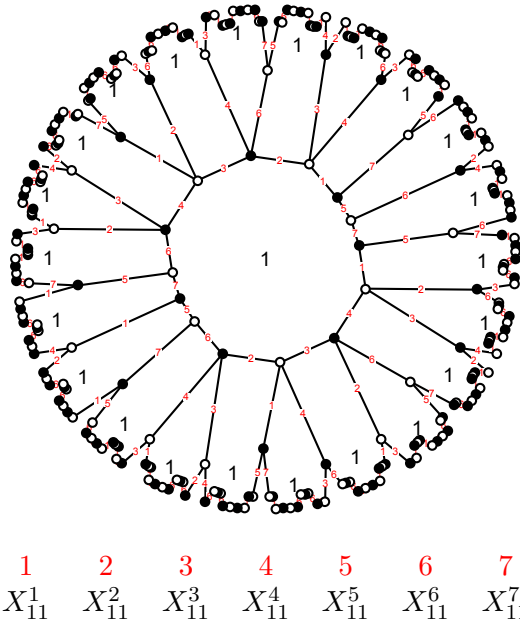
Figure 5.20: The Model 7.4 brane tiling on a $g = 2$ Riemann surface with 1 gauge group, 7 fields and 4 superpotential terms.
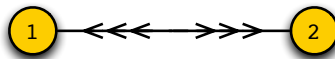

Figure 5.21: The quiver diagram for Model 7.4, a brane tiling on a $g = 2$ Riemann surface with 1 gauge group, 7 fields and 4 superpotential terms.

The brane tiling and corresponding quiver for Model 7.4 is shown in Figure 5.20 and Figure 5.21 respectively. The superpotential is

$$W = +X_{11}^1 X_{11}^2 X_{11}^3 X_{11}^4 + X_{11}^5 X_{11}^6 X_{11}^7 - X_{11}^2 X_{11}^6 X_{11}^4 X_{11}^3 - X_{11}^1 X_{11}^5 X_{11}^7 \ .$$

(5.3.48)

The brane tiling is made of a single 14-sided face with the quiver having 7 adjoints. The brane tiling has overall $c = 9$ perfect matchings,

$$P = \begin{pmatrix}
 & p_1 & p_2 & p_3 & p_4 & p_5 & p_6 & p_7 \\
\hline
X_{11}^1 & 0 & 0 & 0 & 0 & 0 & 0 & 1 \\
X_{11}^2 & 1 & 0 & 0 & 1 & 0 & 0 & 0 \\
X_{11}^3 & 0 & 1 & 0 & 0 & 1 & 0 & 0 \\
X_{11}^4 & 0 & 0 & 1 & 0 & 0 & 1 & 0 \\
X_{11}^5 & 1 & 1 & 1 & 0 & 0 & 0 & 0 \\
X_{11}^6 & 0 & 0 & 0 & 0 & 0 & 0 & 1 \\
X_{11}^7 & 0 & 0 & 0 & 1 & 1 & 1 & 0
\end{pmatrix} \ .$$

(5.3.49)

The zig-zag paths of the brane tiling are,

$$\eta_1 = (X_{11}^2, X_{11}^3) \ , \quad \eta_2 = (X_{11}^3, X_{11}^4) \ , \quad \eta_3 = (X_{11}^5, X_{11}^7) \ ,$$
$$\eta_4 = (X_{11}^1, X_{11}^2, X_{11}^6, X_{11}^7) \ , \quad \eta_5 = (X_{11}^1, X_{11}^5, X_{11}^6, X_{11}^4) \ .$$

(5.3.50)

The F-term constraints are summarized by

$$Q_F = \begin{pmatrix}
p_1 & p_2 & p_3 & p_4 & p_5 & p_6 & p_7 \\
\hline
1 & 0 & -1 & -1 & 0 & 1 & 0 \\
0 & 1 & -1 & 0 & -1 & 1 & 0
\end{pmatrix} \ .$$

(5.3.51)

There are only trivial D-term constraints.

Overall, Model 7.4's mesonic moduli space is expressed as the following symplectic quotient,

$$\mathcal{M}^{mes} = \mathbb{C}^7 //Q_F \ .$$

(5.3.52)

By associating the fugacity t_i to the perfect matching p_i, the fully refined Hilbert

series of $\mathcal{M}^{mes}$ is given by the following Molien integral

$$
\begin{aligned}
g_1(t_i; \mathcal{M}^{mes}) &= \frac{1}{(2\pi i)^2} \oint_{|z_1|=1} \frac{\mathrm{d}z_1}{z_1} \oint_{|z_2|=1} \frac{\mathrm{d}z_2}{z_2} \\
&\quad \times \frac{1}{(1 - z_1 t_1)(1 - z_2 t_2)(1 - z_1^{-1} z_2^{-1} t_3)} \\
&\quad \times \frac{1}{(1 - z_1^{-1} t_4)(1 - z_2^{-1} t_5)(1 - z_1 z_2 t_6)} \times \frac{1}{(1 - t_7)} \\
&= \frac{1}{(1 - t_7)} \times \frac{1 - t_1 t_2 t_3 t_4 t_5 t_6}{(1 - t_1 t_4)(1 - t_2 t_5)(1 - t_3 t_6)(1 - t_1 t_2 t_3)(1 - t_4 t_5 t_6)} .
\end{aligned}
$$
(5.3.53)

From the Hilbert series, we observe that the mesonic moduli space is a complete intersection. It is a 5-dimensional Calabi-Yau space. The generators of the moduli space are shown below.

generator	perfect matchings
A_1	$p_1 p_4$
A_2	$p_2 p_5$
A_3	$p_3 p_6$
B_1	$p_1 p_2 p_3$
B_2	$p_4 p_5 p_6$
C	p_7

The relation formed by the above generators is

$$A_1 A_2 A_3 = B_1 B_2 .$$
(5.3.54)

The global symmetry is $U(1)^4 \times U(1)_R$. The toric diagram of $\mathcal{M}^{mes}$ is given by

$$
G_t = \begin{pmatrix}
 & p_1 & p_2 & p_3 & p_4 & p_5 & p_6 & p_7 \\
\hline
 & 1 & 0 & 0 & 1 & 0 & 0 & 0 \\
 & 0 & 1 & 0 & 0 & 1 & 0 & 0 \\
 & 0 & 0 & 1 & 0 & 0 & 1 & 0 \\
 & 0 & 0 & 0 & 1 & 1 & 1 & 0 \\
 & 0 & 0 & 0 & 0 & 0 & 0 & 1
\end{pmatrix} .
$$
(5.3.55)
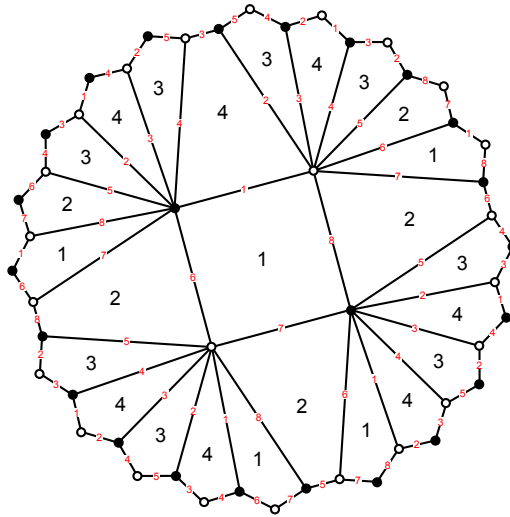
| 1	2	3	4	5	6	7	8
X_{14}	X_{43}^1	X_{34}	X_{43}^2	X_{32}	X_{21}^1	X_{12}	X_{21}^2

Figure 5.22: The Model 8.2a brane tiling on a $g = 2$ Riemann surface with 4 gauge groups, 8 fields and 2 superpotential terms.
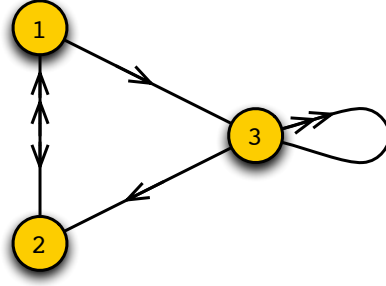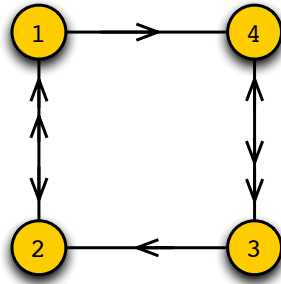

Figure 5.23: The quiver diagram for Model 8.2a, a brane tiling on a $g = 2$ Riemann surface with 4 gauge groups, 8 fields and 2 superpotential terms.

5.3.5 8 Fields, 2 Superpotential Terms, 4 Gauge Groups

Model 8.2a: $NC2$

The brane tiling and quiver of Model 8.2a are shown in Figure 5.22 and Figure 5.23 respectively. The superpotential is

$$W = +X_{14}X_{43}^1X_{34}X_{43}^2X_{32}X_{21}^1X_{12}X_{21}^2 - X_{14}X_{43}^1X_{34}X_{43}^2X_{32}X_{21}^1X_{12}X_{21}^2 \ .$$

$$(5.3.56)$$

286

The quiver incidence matrix is

$$
d = \left(
\begin{array}{c|cccccccc}
 & X_{21}^1 & X_{21}^2 & X_{43}^1 & X_{43}^2 & X_{12} & X_{14} & X_{32} & X_{34} \\
\hline
 & 1 & 1 & 0 & 0 & -1 & -1 & 0 & 0 \\
 & -1 & -1 & 0 & 0 & 1 & 0 & 1 & 0 \\
 & 0 & 0 & 1 & 1 & 0 & 0 & -1 & -1 \\
 & 0 & 0 & -1 & -1 & 0 & 1 & 0 & 1
\end{array}
\right) .
\tag{5.3.57}
$$

The brane tiling has $c = 8$ perfect matchings, each made out of a single field. The perfect matching matrix is therefore the identity matrix,

$$
P = \left(
\begin{array}{c|cccccccc}
 & a_1 & a_2 & b_1 & b_2 & p_1 & p_2 & p_3 & p_4 \\
\hline
X_{21}^1 & 1 & 0 & 0 & 0 & 0 & 0 & 0 & 0 \\
X_{21}^2 & 0 & 1 & 0 & 0 & 0 & 0 & 0 & 0 \\
X_{43}^1 & 0 & 0 & 1 & 0 & 0 & 0 & 0 & 0 \\
X_{43}^2 & 0 & 0 & 0 & 1 & 0 & 0 & 0 & 0 \\
X_{12} & 0 & 0 & 0 & 0 & 1 & 0 & 0 & 0 \\
X_{14} & 0 & 0 & 0 & 0 & 0 & 1 & 0 & 0 \\
X_{32} & 0 & 0 & 0 & 0 & 0 & 0 & 1 & 0 \\
X_{34} & 0 & 0 & 0 & 0 & 0 & 0 & 0 & 1
\end{array}
\right) .
\tag{5.3.58}
$$

The brane tiling of Model 8.2a has the following zig-zag paths

$$
\eta_1 = (X_{43}^1, X_{34}) \ , \ \ \eta_2 = (X_{34}, X_{43}^2) \ , \ \ \eta_3 = (X_{21}^1, X_{12}) \ , \ \ \eta_4 = (X_{12}, X_{21}^2) \ ,
$$
$$
\eta_5 = (X_{14}, X_{43}^1, X_{32}, X_{21}^1) \ , \ \ \eta_6 = (X_{14}, X_{43}^2, X_{32}, X_{21}^2) \ .
\tag{5.3.59}
$$

There are only trivial F-terms due to the identity perfect matching matrix. The D-term charge matrix is as follows

$$
Q_D = \left(
\begin{array}{c|cccccccc}
 & a_1 & a_2 & b_1 & b_2 & p_1 & p_2 & p_3 & p_4 \\
\hline
 & 1 & 1 & 0 & 0 & -1 & 0 & -1 & 0 \\
 & 0 & 0 & 1 & 1 & 0 & 0 & -1 & -1 \\
 & 0 & 0 & 0 & 0 & 0 & 1 & -1 & 0
\end{array}
\right) .
\tag{5.3.60}
$$

The symplectic quotient describing the mesonic moduli space is as follows,

$$
\mathcal{M}^{mes} = \mathbb{C}^8 // Q_D \ .
\tag{5.3.61}
$$

By associating the fugacities α_i, β_i, t_i to the perfect matchings a_i, b_i, p_i respectively,

the fully refined Hilbert series of $\mathcal{M}^{mes}$ is given by the following Molien integral

$$
\begin{aligned}
g_1(\alpha_i, \beta_i, t_i; \mathcal{M}^{mes}) &= \frac{1}{(2\pi i)^3} \oint_{|z_1|=1} \frac{dz_1}{z_1} \oint_{|z_2|=1} \frac{dz_2}{z_2} \oint_{|z_3|=1} \frac{dz_3}{z_3} \\
&\quad \times \frac{1}{\prod_{i=1}^{2}(1 - z_1\alpha_i)(1 - z_2\beta_i)} \\
&\quad \times \frac{1}{(1 - z_1^{-1}t_1)(1 - z_3 t_2)(1 - z_1^{-1}z_2^{-1}z_3^{-1}t_3)(1 - z_2^{-1}t_4)} \\
&= \frac{(\alpha_1\alpha_2\beta_1\beta_2 t_1 t_2 t_3 t_4) P(\alpha_i, \beta_i, t_i)}{\prod_{i=1}^{2}(1 - \alpha_i t_1)(1 - \beta_i t_4) \prod_{i,j=1}^{2}(1 - \alpha_i \beta_j t_2 t_3)} \;,
\end{aligned}
$$
(5.3.62)

where the numerator is

$$
\begin{aligned}
P(\alpha_i, \beta_i, \gamma_i) &= \alpha_1^{-1}\alpha_2^{-1}\beta_1^{-1}\beta_2^{-1}t_1^{-1}t_2^{-1}t_3^{-1}t_4^{-1} - \sum_{i=1}^{2}\alpha_i^{-1}t_1^{-1} - \sum_{i=1}^{2}\beta_i^{-1}t_4^{-1} + 1 \\
&\quad - t_1^{-1}t_2 t_3 t_4^{-1} + \sum_{i=1}^{2}\alpha_i t_2 t_3 t_4^{-1} + \sum_{i=1}^{2}\beta_i t_1^{-1}t_2 t_3 - \alpha_1\alpha_2\beta_1\beta_2 t_2^2 t_3^2 \;.
\end{aligned}
$$
(5.3.63)

By setting the fugacities $\alpha_i = \beta_i = t_i = t$, the unrefined Hilbert series is

$$
g_1(t; \mathcal{M}^{mes}) = \frac{1 - 4t^6 + 4t^{10} - t^{16}}{(1 - t^2)^4 (1 - t^4)^4} \;.
$$
(5.3.64)

The Hilbert series above indicates that the mesonic moduli space is not a complete intersection. The plethystic logarithm of the Hilbert series is,

$$
\begin{aligned}
PL[g_1(\alpha_i, \beta_i, t_i; \mathcal{M}^{mes})] &= \sum_{i=1}^{2}(\alpha_i t_1 + \beta_i t_4) + \sum_{i,j=1}^{2}\alpha_i \beta_j t_2 t_3 \\
&\quad - \sum_{i=1}^{2}(\alpha_1\alpha_2\beta_i t_1 t_2 t_3 + \alpha_i \beta_1 \beta_2 t_2 t_3 t_4) + \dots \;.
\end{aligned}
$$
(5.3.65)

The first order generators are as follows.

generator	perfect matchings
A_i	$a_i p_1$
B_j	$b_j p_4$
C_{ij}	$a_i b_j p_2 p_3$

The generators form the following first order relations

$$
\epsilon^{i_1 i_2} A_{i_1} C_{i_2 j} = 0 \;, \quad \epsilon^{j_1 j_2} B_{j_1} C_{i j_2} = 0 \;.
$$
(5.3.66)

The global symmetry is enhanced to $SU(2) \times SU(2) \times U(1)^2 \times U(1)_R$. The perfect matchings carry the following global charges.

	$SU(2)_x$	$SU(2)_y$	$U(1)_{b_1}$	$U(1)_{b_2}$	$U(1)_R$	fugacity
a_1	1	0	1	0	1	$\alpha_1 = x b_1 t$
a_2	-1	0	1	0	1	$\alpha_2 = x^{-1} b_1 t$
b_1	0	1	0	1	1	$\beta_1 = y b_2 t$
b_2	0	-1	0	1	1	$\beta_2 = y^{-1} b_2 t$
p_1	0	0	-1	0	1	$t_1 = b_1^{-1} t$
p_2	0	0	-1	0	1	$t_2 = b_1^{-1} t$
p_3	0	0	0	-1	1	$t_3 = b_2^{-1} t$
p_4	0	0	0	-1	1	$t_4 = b_2^{-1} t$

The Hilbert series of the mesonic moduli space can be expressed in terms of characters of irreducible representations of the global symmetry group. It is

$$g_1(x, y, b_i, t; \mathcal{M}^{mes}) = \sum_{n_1=0}^{\infty} \sum_{n_2=0}^{\infty} \sum_{n_3=0}^{\infty} [n_2 + n_3; n_1 + n_3] t^{2n_1 + 2n_2 + 4n_3} , \quad (5.3.67)$$

where $[n_2 + n_3; n_1 + n_3] \equiv [n_2 + n_3]_{SU(2)_x} [n_1 + n_2]_{SU(2)_y}$.

The toric diagram of $\mathcal{M}^{mes}$ is given by

$$G_t = \begin{pmatrix} \begin{array}{cccccccc} a_1 & a_2 & b_1 & b_2 & p_1 & p_2 & p_3 & p_4 \\ \hline 1 & 0 & 0 & 0 & 1 & 0 & 0 & 0 \\ 0 & 1 & 0 & 0 & 1 & 0 & 0 & 0 \\ 0 & 0 & 1 & 0 & 0 & 0 & 0 & 1 \\ 0 & 0 & 0 & 1 & 0 & 0 & 0 & 1 \\ 1 & 1 & 1 & 1 & 1 & 1 & 1 & 1 \end{array} \end{pmatrix} . \quad (5.3.68)$$

Model 8.2b: $NC3$

The brane tiling and quiver of Model 8.2b are shown in Figure 5.24 and Figure 5.25 respectively. The superpotential is

$$W = +X_{14}^1 X_{43}^1 X_{32}^1 X_{21}^1 X_{14}^2 X_{43}^2 X_{32}^2 X_{21}^2 - X_{14}^1 X_{43}^2 X_{32}^1 X_{21}^2 X_{14}^2 X_{43}^1 X_{32}^2 X_{21}^1 .$$
$$(5.3.69)$$

| 1	2	3	4	5	6	7	8
X^1_{14}	X^1_{43}	X^1_{32}	X^1_{21}	X^2_{14}	X^2_{43}	X^2_{32}	X^2_{21}

Figure 5.24: The Model 8.2b brane tiling on a $g = 2$ Riemann surface with 4 gauge groups, 8 fields and 2 superpotential terms.

Figure 5.25: The quiver diagram for Model 8.2b, a brane tiling on a $g = 2$ Riemann surface with 4 gauge groups, 8 fields and 2 superpotential terms.

The quiver incidence matrix is

$$
d = \begin{pmatrix}
X^1_{14} & X^1_{43} & X^1_{32} & X^1_{21} & X^2_{14} & X^2_{43} & X^2_{32} & X^2_{21} \\
\hline
-1 & 0 & 0 & 1 & -1 & 0 & 0 & 1 \\
0 & 0 & 1 & -1 & 0 & 0 & 1 & -1 \\
0 & 1 & -1 & 0 & 0 & 1 & -1 & 0 \\
1 & -1 & 0 & 0 & 1 & -1 & 0 & 0
\end{pmatrix} . \tag{5.3.70}
$$

The brane tiling has $c = 8$ perfect matchings, each made of a single quiver field. The

perfect matching matrix is the identity matrix,

$$
P = \begin{pmatrix}
 & a_1 & a_2 & b_1 & b_2 & c_1 & c_2 & d_1 & d_2 \\
\hline
X_{32}^1 & 1 & 0 & 0 & 0 & 0 & 0 & 0 & 0 \\
X_{32}^2 & 0 & 1 & 0 & 0 & 0 & 0 & 0 & 0 \\
X_{43}^1 & 0 & 0 & 1 & 0 & 0 & 0 & 0 & 0 \\
X_{43}^2 & 0 & 0 & 0 & 1 & 0 & 0 & 0 & 0 \\
X_{14}^1 & 0 & 0 & 0 & 0 & 1 & 0 & 0 & 0 \\
X_{14}^2 & 0 & 0 & 0 & 0 & 0 & 1 & 0 & 0 \\
X_{21}^1 & 0 & 0 & 0 & 0 & 0 & 0 & 1 & 0 \\
X_{21}^2 & 0 & 0 & 0 & 0 & 0 & 0 & 0 & 1
\end{pmatrix} . \tag{5.3.71}
$$

The zig-zag paths of the brane tiling are

$$
\begin{aligned}
\eta_1 &= (X_{14}^1, X_{43}^1, X_{32}^2, X_{21}^2, X_{14}^2, X_{43}^2, X_{32}^1, X_{21}^1) , \\
\eta_2 &= (X_{14}^1, X_{43}^2, X_{32}^2, X_{21}^1, X_{14}^2, X_{43}^1, X_{32}^1, X_{21}^2) .
\end{aligned} \tag{5.3.72}
$$

There is no F-term charge matrix. The D-term charge matrix is as follows

$$
Q_D = \begin{pmatrix}
a_1 & a_2 & b_1 & b_2 & c_1 & c_2 & d_1 & d_2 \\
\hline
1 & 1 & 0 & 0 & 0 & 0 & -1 & -1 \\
0 & 0 & 1 & 1 & 0 & 0 & -1 & -1 \\
0 & 0 & 0 & 0 & 1 & 1 & -1 & -1
\end{pmatrix} . \tag{5.3.73}
$$

The symplectic quotient describing the mesonic moduli space is

$$
\mathcal{M}^{mes} = \mathbb{C}^8 // Q_D . \tag{5.3.74}
$$

By associating the fugacity t_i to the perfect matching p_i, the fully refined Hilbert series of $\mathcal{M}^{mes}$ is given by the following Molien integral

$$
\begin{aligned}
g_1(\alpha_i, \beta_i, \gamma_i, \delta_i; \mathcal{M}^{mes}) &= \frac{1}{(2\pi i)^3} \oint_{|z_1|=1} \frac{\mathrm{d}z_1}{z_1} \oint_{|z_2|=1} \frac{\mathrm{d}z_2}{z_2} \oint_{|z_3|=1} \frac{\mathrm{d}z_3}{z_3} \\
&\quad \times \frac{1}{\prod_{i=1}^2 (1 - z_1 \alpha_i)(1 - z_2 \beta_i)(1 - z_3 \gamma_i)(1 - z_1^{-1} z_2^{-1} z_3^{-1} \delta_i)} \\
&= \frac{P(\alpha_i, \beta_i, \gamma_i, \delta_i)}{\prod_{i,j,k,l=1}^2 (1 - \alpha_i \beta_j \gamma_k \delta_l)} .
\end{aligned} \tag{5.3.75}
$$

The numerator $P(\alpha_i, \beta_i, \gamma_i, \delta_i)$ is too large to be presented here. We unrefine the above Hilbert series by setting the fugacities $\alpha_i = \beta_i = \gamma_i = \delta_i = t$. The unrefined Hilbert

series is

$$g_1(t; \mathcal{M}^{mes}) \quad = \quad \frac{1 + 11t^4 + 11t^8 + t^{12}}{(1 - t^4)^5} \ .$$
(5.3.76)

The Hilbert series above indicates that the mesonic moduli space is not a complete intersection. It is a Calabi-Yau 5-fold.

The plethystic logarithm of the refined Hilbert series is,

$$PL[g_1(\alpha_i, \beta_i, \gamma_i, \delta_i; \mathcal{M}^{mes})] = \sum_{i,j,k,l=1}^{2} \alpha_i \beta_j \gamma_k \delta_l$$

$$- \prod_{m=1}^{2} \alpha_m \beta_m \gamma_m \delta_m \left(7 + 3 \sum_{i \neq j}^{2} (\alpha_i \alpha_j^{-1} + \beta_i \beta_j^{-1} + \gamma_i \gamma_j^{-1} + \delta_i \delta_j^{-1}) \right.$$

$$+ \sum_{\substack{i \neq j \\ k \neq l}}^{2} (\alpha_i \alpha_j^{-1} \beta_k \beta_l^{-1} + \alpha_i \alpha_j^{-1} \gamma_k \gamma_l^{-1} + \alpha_i \alpha_j^{-1} \delta_k \delta_l^{-1}$$

$$\left. + \beta_i \beta_j^{-1} \gamma_k \gamma_l^{-1} + \beta_i \beta_j^{-1} \delta_k \delta_l^{-1} + \gamma_i \gamma_j^{-1} \delta_k \delta_l^{-1}) \right) + \dots \ .$$
(5.3.77)

The first order generators are shown below.

generator	perfect matchings
A_{ijkl}	$a_i b_j c_k d_l$

The generators form the following first order simplified relations

$$\epsilon^{i_1 i_2} A_{i_1 j_1 k_1 l_1} A_{i_2 j_2 k_2 l_2} = 0 \ , \ \epsilon^{j_1 j_2} A_{i_1 j_1 k_1 l_1} A_{i_2 j_2 k_2 l_2} = 0 \ ,$$

$$\epsilon^{k_1 k_2} A_{i_1 j_1 k_1 l_1} A_{i_2 j_2 k_2 l_2} = 0 \ , \ \epsilon^{l_1 l_2} A_{i_1 j_1 k_1 l_1} A_{i_2 j_2 k_2 l_2} = 0 \ .$$
(5.3.78)

The above are 112 relations which reduce to 55 independent ones in the representations $[2; 2; 0; 0]$ with permutations and $[0; 0; 0; 0]$.

The global symmetry is enhanced to $SU(2)^4 \times U(1)_R$. The perfect matchings carry the following global charges.

	$SU(2)_x$	$SU(2)_y$	$SU(2)_z$	$SU(2)_w$	$U(1)_R$	fugacity
a_1	1	0	0	0	1	$\alpha_1 = xt$
a_2	-1	0	0	0	1	$\alpha_2 = x^{-1}t$
b_1	0	1	0	0	1	$\beta_1 = yt$
b_2	0	-1	0	0	1	$\beta_2 = y^{-1}t$
c_1	0	0	1	0	1	$\gamma_1 = zt$
c_2	0	0	-1	0	1	$\gamma_2 = z^{-1}t$
d_1	0	0	0	1	1	$\delta_1 = wt$
d_2	0	0	0	-1	1	$\delta_2 = w^{-1}t$

The Hilbert series of the mesonic moduli space can be expressed in terms of characters of irreducible representations of the global symmetry group. It is

$$g_1(x, y, z, w, t; \mathcal{M}^{mes}) = \sum_{n=0}^{\infty} [n; n; n; n] t^{4n} \ , \qquad (5.3.79)$$

where $[n; n; n; n] \equiv [n]_{SU(2)_x}[n]_{SU(2)_y}[n]_{SU(2)_z}[n]_{SU(2)_w}$ is the character of the irreducible representation of $SU(2)^4$.

The toric diagram of $\mathcal{M}^{mes}$ is given by

$$G_t = \begin{pmatrix} a_1 & a_2 & b_1 & b_2 & c_1 & c_2 & d_1 & d_2 \\ \hline 1 & 0 & 1 & 0 & 1 & 0 & 1 & 0 \\ 1 & -1 & 0 & 0 & 0 & 0 & 0 & 0 \\ 0 & 0 & 1 & -1 & 0 & 0 & 0 & 0 \\ 0 & 0 & 0 & 0 & 1 & -1 & 0 & 0 \\ 0 & 0 & 0 & 0 & 0 & 0 & 1 & -1 \end{pmatrix} . \qquad (5.3.80)$$

5.3.6 8 Fields, 4 Superpotential Terms, 2 Gauge Groups

Model 8.4a: $\mathcal{M}_{3,3}$

The brane tiling on a $g = 2$ Riemann surface and the corresponding quiver are shown in Figure 5.26 and Figure 5.27 respectively. The quartic superpotential is

$$W = +X_{22}^1 X_{22}^2 X_{22}^3 X_{21} X_{12} + X_{11}^1 X_{11}^2 X_{11}^3 - X_{21} X_{11}^1 X_{11}^3 X_{11}^2 X_{12} - X_{22}^1 X_{22}^3 X_{22}^2 \ .$$

$$(5.3.81)$$
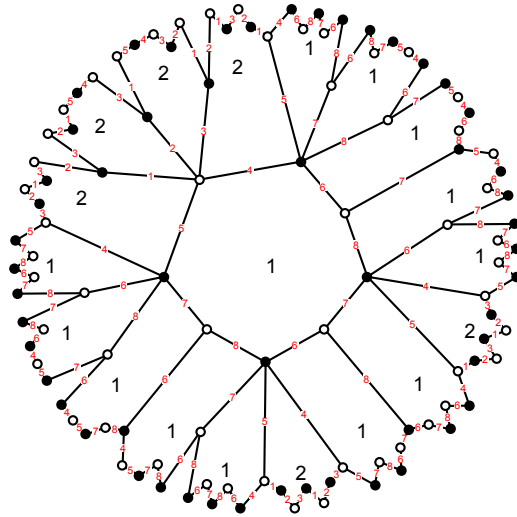
1	2	3	4	5	6	7	8
X_{22}^1	X_{22}^2	X_{22}^3	X_{21}	X_{12}	X_{11}^1	X_{11}^2	X_{11}^3

Figure 5.26: The Model 8.4a brane tiling on a $g = 2$ Riemann surface with 2 gauge groups, 8 fields and 4 superpotential terms.

Figure 5.27: The quiver diagram for Model 8.4a, a brane tiling on a $g = 2$ Riemann surface with 2 gauge groups, 8 fields and 4 superpotential terms.

The quiver incidence matrix is

$$
d = \left(\begin{array}{c|cccccccc}
 & X_{22}^1 & X_{22}^2 & X_{22}^3 & X_{21} & X_{12} & X_{11}^1 & X_{11}^2 & X_{11}^3 \\
\hline
 & 0 & 0 & 0 & 1 & -1 & 0 & 0 & 0 \\
 & 0 & 0 & 0 & -1 & 1 & 0 & 0 & 0
\end{array} \right) . \tag{5.3.82}
$$

The brane tiling has $c = 9$ perfect matchings. The perfect matchings are encoded in

the matrix

$$
P = \left(\begin{array}{c|ccccccccc}
 & p_1 & p_2 & p_3 & p_4 & p_5 & p_6 & p_7 & p_8 & p_9 \\
\hline
X_{22}^1 & 1 & 0 & 0 & 1 & 0 & 0 & 1 & 0 & 0 \\
X_{22}^2 & 0 & 1 & 0 & 0 & 1 & 0 & 0 & 1 & 0 \\
X_{22}^3 & 0 & 0 & 1 & 0 & 0 & 1 & 0 & 0 & 1 \\
X_{21} & 0 & 0 & 0 & 0 & 0 & 0 & 0 & 0 & 0 \\
X_{12} & 0 & 0 & 0 & 0 & 0 & 0 & 0 & 0 & 0 \\
X_{11}^1 & 1 & 1 & 1 & 0 & 0 & 0 & 0 & 0 & 0 \\
X_{11}^2 & 0 & 0 & 0 & 1 & 1 & 1 & 0 & 0 & 0 \\
X_{11}^3 & 0 & 0 & 0 & 0 & 0 & 0 & 1 & 1 & 1 \\
\end{array} \right) . \tag{5.3.83}
$$

The brane tiling has the following zig-zag paths,

$$
\eta_1 = (X_{22}^1, X_{22}^2) \ , \ \ \eta_2 = (X_{22}^2, X_{22}^2) \ , \ \ \eta_3 = (X_{21}, X_{12}) \ , \ \ \eta_4 = (X_{11}^1, X_{11}^3) \ ,
$$
$$
\eta_5 = (X_{11}^2, X_{11}^3) \ , \ \ \eta_6 = (X_{22}^1, X_{22}^3, X_{21}, X_{11}^1, X_{11}^2, X_{12}) \ . \tag{5.3.84}
$$

The F-term constraints can be expressed as charges carried by the perfect matchings. The charges are given by

$$
Q_F = \left(\begin{array}{ccccccccc}
p_1 & p_2 & p_3 & p_4 & p_5 & p_6 & p_7 & p_8 & p_9 \\
\hline
1 & 0 & -1 & 0 & 0 & 0 & -1 & 0 & 1 \\
0 & 1 & -1 & 0 & 0 & 0 & 0 & -1 & 1 \\
0 & 0 & 0 & 1 & 0 & -1 & -1 & 0 & 1 \\
0 & 0 & 0 & 0 & 1 & -1 & 0 & -1 & 1 \\
\end{array} \right) . \tag{5.3.85}
$$

There are no D-term constraints. The mesonic moduli space can be expressed as the symplectic quotient

$$
\mathcal{M}^{mes} = \mathbb{C}^9 // Q_F \ . \tag{5.3.86}
$$

By associating the fugacity t_i to the perfect matching p_i, the fully refined Hilbert

series of $\mathcal{M}^{mes}$ is given by the following Molien integral

$$
\begin{aligned}
g_1(t_i; \mathcal{M}^{mes}) \;=\; & \frac{1}{(2\pi i)^5} \oint_{|z_1|=1} \frac{\mathrm{d}z_1}{z_1} \oint_{|z_2|=1} \frac{\mathrm{d}z_2}{z_2} \oint_{|z_3|=1} \frac{\mathrm{d}z_3}{z_3} \oint_{|z_4|=1} \frac{\mathrm{d}z_4}{z_4} \\
& \times \frac{1}{(1 - z_1 t_1)(1 - z_2 t_2)(1 - z_1^{-1} z_2^{-1} t_3)} \\
& \times \frac{1}{(1 - z_3 t_4)(1 - z_4 t_5)(1 - z_3^{-1} z_4^{-1} t_6)} \\
& \times \frac{1}{(1 - z_1^{-1} z_3^{-1} t_7)(1 - z_2^{-1} z_4^{-1} t_8)(1 - z_1 z_2 z_3 z_4 t_9)} \\
=\; & \frac{1 - t_1 t_2 t_3 t_4 t_5 t_6 t_7 t_8 t_9}{(1 - t_1 t_2 t_3)(1 - t_4 t_5 t_6)(1 - t_7 t_8 t_9)(1 - t_1 t_4 t_7)(1 - t_2 t_5 t_8)(1 - t_3 t_6 t_9)} \; .
\end{aligned}
$$
(5.3.87)

Accordingly, the mesonic moduli space is a complete intersection of dimension 5. It is a Calabi-Yau 5-fold and its generators can be written in terms of perfect matching variables as follows:

generator	perfect matchings
A_1	$p_1 p_2 p_3$
A_2	$p_4 p_5 p_6$
A_3	$p_7 p_8 p_9$
B_1	$p_1 p_4 p_7$
B_2	$p_2 p_5 p_8$
B_3	$p_3 p_6 p_9$

The generators form a single relation of the form

$$
A_1 A_2 A_3 = B_1 B_2 B_3 \; .
$$
(5.3.88)

The global symmetry is $U(1)^4 \times U(1)_R$ and experiences no enhancement. The toric diagram of the Calabi-Yau 5-fold is given by

$$
G_t = \left(
\begin{array}{ccccccccc}
p_1 & p_2 & p_3 & p_4 & p_5 & p_6 & p_7 & p_8 & p_9 \\
\hline
1 & 0 & 0 & 1 & 0 & 0 & 1 & 0 & 0 \\
0 & 1 & 0 & 0 & 1 & 0 & 0 & 1 & 0 \\
0 & 0 & 1 & 0 & 0 & 1 & 0 & 0 & 1 \\
1 & 1 & 1 & 0 & 0 & 0 & 0 & 0 & 0 \\
0 & 0 & 0 & 1 & 1 & 1 & 0 & 0 & 0
\end{array}
\right) \; .
$$
(5.3.89)

Model 8.4b: $\mathbb{C}^3 \times \mathbb{C}^2/\mathbb{Z}_2$
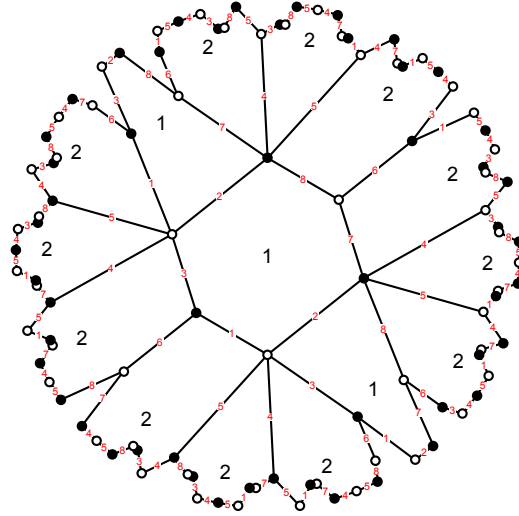
1	2	3	4	5	6	7	8
X_{21}^1	X_{11}	X_{12}^1	X_{22}^1	X_{22}^2	X_{22}^3	X_{21}^2	X_{12}^2

Figure 5.28: The Model 8.4b brane tiling on a $g = 2$ Riemann surface with 2 gauge groups, 8 fields and 4 superpotential terms.

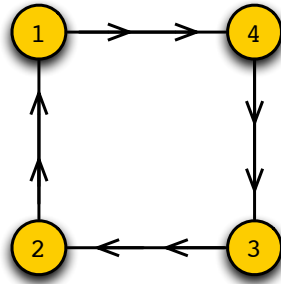Figure 5.29: The quiver diagram for Model 8.4b, a brane tiling on a $g = 2$ Riemann surface with 2 gauge groups, 8 fields and 4 superpotential terms.

For Model 8.4b, the brane tiling and corresponding quiver is shown in Figure 5.28 and Figure 5.29 respectively. The quartic superpotential is

$$W = +X_{21}^1 X_{11} X_{12}^1 X_{22}^1 X_{22}^2 + X_{22}^3 X_{21}^2 X_{12}^2 - X_{11} X_{12}^2 X_{22}^2 X_{22}^1 X_{21}^1 - X_{21}^1 X_{12}^1 X_{22}^3 \ . \tag{5.3.90}$$

The quiver incidence matrix is

$$d = \begin{pmatrix} X_{21}^1 & X_{11} & X_{12}^1 & X_{22}^1 & X_{22}^2 & X_{22}^3 & X_{21}^2 & X_{12}^2 \\ \hline 1 & 0 & -1 & 0 & 0 & 0 & 1 & -1 \\ -1 & 0 & 1 & 0 & 0 & 0 & -1 & 1 \end{pmatrix} \ . \tag{5.3.91}$$

The brane tiling has $c = 7$ perfect matchings. The perfect matchings are encoded in

the matrix

$$P = \begin{pmatrix} & a_1 & a_2 & a_3 & b_1 & b_2 & p_1 & p_2 \\ \hline X_{11} & 1 & 0 & 0 & 0 & 0 & 0 & 0 \\ X_{22}^1 & 0 & 1 & 0 & 0 & 0 & 0 & 0 \\ X_{22}^2 & 0 & 0 & 1 & 0 & 0 & 0 & 0 \\ X_{22}^3 & 1 & 1 & 1 & 0 & 0 & 0 & 0 \\ X_{12}^1 & 0 & 0 & 0 & 0 & 1 & 1 & 0 \\ X_{12}^2 & 0 & 0 & 0 & 1 & 0 & 1 & 0 \\ X_{21}^1 & 0 & 0 & 0 & 1 & 0 & 0 & 1 \\ X_{21}^2 & 0 & 0 & 0 & 0 & 1 & 0 & 1 \end{pmatrix} . \tag{5.3.92}$$

The brane tiling has the zig-zag paths,

$$\eta_1 = (X_{22}^1, X_{22}^2) \ , \quad \eta_2 = (X_{11}, X_{12}^1, X_{22}^3, X_{21}^2) \ , \quad \eta_3 = (X_{21}^1, X_{11}, X_{12}^2, X_{22}^3) \ ,$$
$$\eta_4 = (X_{21}^1, X_{12}^1, X_{22}^1, X_{21}^2, X_{12}^2, X_{22}^2) \ . \tag{5.3.93}$$

The F-term constraints can be expressed as charges carried by the perfect matchings. The charges are given by

$$Q_F = \left(\begin{array}{ccccccc} a_1 & a_2 & a_3 & b_1 & b_2 & p_1 & p_2 \\ \hline 0 & 0 & 0 & 1 & 1 & -1 & -1 \end{array} \right) . \tag{5.3.94}$$

The D-term charges are encoded in the quiver incidence matrix d and are

$$Q_D = \left(\begin{array}{ccccccc} a_1 & a_2 & a_3 & b_1 & b_2 & p_1 & p_2 \\ \hline 0 & 0 & 0 & 1 & 1 & 0 & -2 \end{array} \right) . \tag{5.3.95}$$

The combined charges can be written as

$$Q_t = \left(\begin{array}{ccccccc} a_1 & a_2 & a_3 & b_1 & b_2 & p_1 & p_2 \\ \hline 0 & 0 & 0 & 1 & 1 & -1 & -1 \\ 0 & 0 & 0 & 0 & 0 & 1 & -1 \end{array} \right) , \tag{5.3.96}$$

where the mesonic moduli space can be expressed as the symplectic quotient

$$\mathcal{M}^{mes} = \mathbb{C}^7 // Q_t . \tag{5.3.97}$$

By associating to perfect matchings a_i, b_i, p_i the fugacities α_i, β_i, t_i, the fully refined

Hilbert series of $\mathcal{M}^{mes}$ is given by the following Molien integral

$$
\begin{aligned}
g_1(\alpha_i, \beta_i, t_i; \mathcal{M}^{mes}) &= \frac{1}{(2\pi i)^5} \oint_{|z_1|=1} \frac{dz_1}{z_1} \oint_{|z_2|=1} \frac{dz_2}{z_2} \frac{1}{\prod_{i=1}^{3}(1-\alpha_i) \prod_{i=1}^{2}(1-z_1\beta_i)} \\
&\quad \times \frac{1}{(1-z_1^{-1}z_2 t_1)(1-z_1^{-1}z_2^{-1}t_2)} \\
&= \frac{1}{\prod_{i=1}^{3}(1-\alpha_i)} \times \frac{1-\prod_{i=1}^{2}\beta_i^2 t_i^2}{(1-\beta_1\beta_2 t_1 t_2) \prod_{i=1}^{2}(1-\beta_i^2 t_1 t_2)} .
\end{aligned}
$$

(5.3.98)

Accordingly, the mesonic moduli space is a complete intersection of dimension 5. It is a Calabi-Yau 5-fold and its generators can be found in terms of perfect matching variables as follows:

generator	perfect matchings
A_i	a_i
B_{ij}	$b_i b_j p_1 p_2$

A_i generate $\mathbb{C}^3$ and B_{ij} form a single relation of $\mathbb{C}^2/\mathbb{Z}_2$ which can be expressed as

$$
\det B = 0 .
$$

(5.3.99)

The global symmetry is $SU(3) \times SU(2) \times U(1) \times U(1)_R$. The perfect matchings carry the global symmetry charges as follows.

	$SU(3)_x$	$SU(2)_y$	$U(1)_h$	$U(1)_R$	fugacity
a_1	$(1,0)$	0	0	1	$\alpha_1 = x_1 t$
a_2	$(-1,1)$	0	0	1	$\alpha_2 = x_1^{-1} x_2 t$
a_3	$(0,-1)$	0	0	1	$\alpha_3 = x_2^{-1} t$
b_1	$(0,0)$	1	0	1	$\beta_1 = yt$
b_2	$(0,0)$	-1	0	1	$\beta_2 = y^{-1} t$
p_1	$(0,0)$	0	1	1	$t_1 = ht$
p_2	$(0,0)$	0	-1	1	$t_2 = h^{-1} t$

Under the above assignment of global charges the refined Hilbert series of the mesonic moduli space can be written as

$$
g_1(x_i, y, t; \mathcal{M}^{mes}) = \sum_{n_1=0}^{\infty} \sum_{n_2=0}^{\infty} [n_1, 0; n_2] t^{n_1+4n_2} ,
$$

(5.3.100)

where $[n_1, 0; n_2] \equiv [n_1, 0]_{SU(3)_x} [n_2]_{SU(2)_y}$ are characters of irreducible representations of $SU(3)_x \times SU(2)_y$.

The toric diagram is given by

$$
G_t = \left(\begin{array}{c|ccccccc}
 & a_1 & a_2 & a_3 & b_1 & b_2 & p_1 & p_2 \\
\hline
 & 1 & 0 & 0 & 0 & 0 & 0 & 0 \\
 & 0 & 1 & 0 & 0 & 0 & 0 & 0 \\
 & 0 & 0 & 1 & 0 & 0 & 0 & 0 \\
 & 0 & 0 & 0 & 1 & -1 & 0 & 0 \\
 & 0 & 0 & 0 & 0 & 2 & 1 & 1
\end{array} \right) .
\tag{5.3.101}
$$

Model 8.4c: $\mathbb{C}^3 \times \mathbb{C}^2/\mathbb{Z}_2$

1	2	3	4	5	6	7	8
X_{12}^1	X_{22}^1	X_{22}^2	X_{22}^3	X_{21}^1	X_{11}	X_{12}^2	X_{21}^2

Figure 5.30: The Model 8.4c brane tiling on a $g = 2$ Riemann surface with 2 gauge groups, 8 fields and 4 superpotential terms.
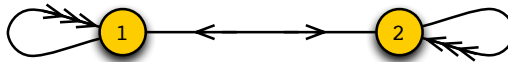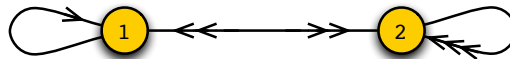

Figure 5.31: The quiver diagram for Model 8.4c, a brane tiling on a $g = 2$ Riemann surface with 2 gauge groups, 8 fields and 4 superpotential terms.

For Model 8.4c, the brane tiling and corresponding quiver is shown in Figure 5.38

and Figure 5.39 respectively. The quartic superpotential is

$$W = +X_{12}^1 X_{22}^1 X_{22}^2 X_{22}^3 X_{21}^1 + X_{11} X_{12}^2 X_{21}^2 - X_{22}^1 X_{21}^2 X_{12}^2 X_{22}^3 X_{22}^2 - X_{11} X_{12}^1 X_{21}^1 \ .$$

$$(5.3.102)$$

The quiver incidence matrix is

$$d = \left(\begin{array}{cccccccc} X_{12}^1 & X_{22}^1 & X_{22}^2 & X_{22}^3 & X_{21}^1 & X_{11} & X_{12}^2 & X_{21}^2 \\ \hline -1 & 0 & 0 & 0 & 1 & 0 & -1 & 1 \\ 1 & 0 & 0 & 0 & -1 & 0 & 1 & -1 \end{array} \right) \ . \qquad (5.3.103)$$

The brane tiling has $c = 7$ perfect matchings. The perfect matchings are encoded in the matrix

$$P = \left(\begin{array}{c|ccccccc} & a_1 & a_2 & a_3 & b_1 & b_2 & p_1 & p_2 \\ \hline X_{12}^1 & 0 & 0 & 0 & 1 & 0 & 0 & 1 \\ X_{12}^2 & 0 & 0 & 0 & 0 & 1 & 0 & 1 \\ X_{21}^1 & 0 & 0 & 0 & 0 & 1 & 1 & 0 \\ X_{21}^2 & 0 & 0 & 0 & 1 & 0 & 1 & 0 \\ X_{11} & 1 & 1 & 1 & 0 & 0 & 0 & 0 \\ X_{22}^1 & 1 & 0 & 0 & 0 & 0 & 0 & 0 \\ X_{22}^2 & 0 & 1 & 0 & 0 & 0 & 0 & 0 \\ X_{22}^3 & 0 & 0 & 1 & 0 & 0 & 0 & 0 \end{array} \right) \ . \qquad (5.3.104)$$

The zig-zag paths of the brane tiling of Model 8.4c are

$$\eta_1 = (X_{12}^1, X_{21}^1) \ , \ \ \eta_2 = (X_{22}^1, X_{22}^3) \ , \ \ \eta_3 = (X_{22}^2, X_{22}^3) \ , \ \ \eta_4 = (X_{12}^2, X_{21}^2) \ ,$$
$$\eta_5 = (X_{22}^3, X_{21}^1, X_{11}, X_{12}^2) \ , \ \ \eta_6 = (X_{12}^1, X_{22}^1, X_{21}^2, X_{11}) \ . \qquad (5.3.105)$$

As we will see below, and seen above with the quiver diagram, Model 8.4c has many similar properties as Model 8.4b in section §5.3.6. The zig-zag paths of Model 8.4c in (5.3.146) are however distinct from the ones for Model 8.4b in (5.3.93).

The F-term constraints can be expressed as charges carried by the perfect matchings. The charges are given by

$$Q_F = \left(\begin{array}{ccccccc} a_1 & a_2 & a_3 & b_1 & b_2 & p_1 & p_2 \\ \hline 0 & 0 & 0 & 1 & 1 & -1 & -1 \end{array} \right) \ . \qquad (5.3.106)$$

The D-term charges are encoded in the quiver incidence matrix d and are

$$Q_D = \left(\begin{array}{ccccccc} a_1 & a_2 & a_3 & b_1 & b_2 & p_1 & p_2 \\ \hline 0 & 0 & 0 & 1 & 1 & -2 & 0 \end{array} \right) \ . \qquad (5.3.107)$$

The charges can be combined to give

$$Q_t = \left(\begin{array}{ccccccc} a_1 & a_2 & a_3 & b_1 & b_2 & p_1 & p_2 \\ \hline 0 & 0 & 0 & 1 & 1 & -1 & -1 \\ 0 & 0 & 0 & 0 & 0 & 1 & -1 \end{array} \right) , \tag{5.3.108}$$

which is precisely the total charge matrix for Model 8.4b in §5.3.6.

Accordingly, the mesonic moduli space as the following symplectic quotient

$$\mathcal{M}^{mes} = \mathbb{C}^7 // Q_t , \tag{5.3.109}$$

is identical to the one in Model 8.4b. The mesonic moduli space is $\mathbb{C}^3 \times \mathbb{C}^2/\mathbb{Z}_2$ which is a toric Calabi-Yau 5-fold.

Model 8.4d: $\mathbb{C} \times \mathcal{M}_{3,2}$
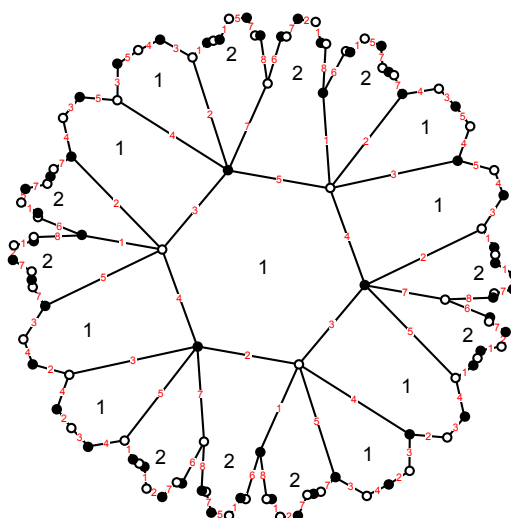
1	2	3	4	5	6	7	8
X_{22}^1	X_{21}	X_{11}^1	X_{11}^2	X_{12}	X_{22}^2	X_{22}^3	X_{22}^4

Figure 5.32: The Model 8.4d brane tiling on a $g = 2$ Riemann surface with 2 gauge groups, 8 fields and 4 superpotential terms.

The brane tiling and corresponding quiver for Model 8.4d is shown in Figure 5.32 and Figure 5.33 respectively. The superpotential is

$$W = +X_{22}^1 X_{21} X_{11}^1 X_{11}^2 X_{12} + X_{22}^2 X_{22}^3 X_{22}^4 - X_{21} X_{11}^2 X_{11}^1 X_{12} X_{22}^2 - X_{22}^1 X_{22}^2 X_{22}^4 . \tag{5.3.110}$$
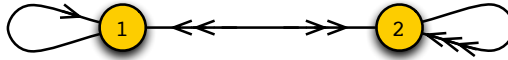
Figure 5.33: The quiver diagram for Model 8.4d, a brane tiling on a $g = 2$ Riemann surface with 2 gauge groups, 8 fields and 4 superpotential terms.

The quiver incidence matrix is

$$
d = \left(\begin{array}{c|cccccccc}
 & X_{22}^1 & X_{21} & X_{11}^1 & X_{11}^2 & X_{12} & X_{22}^2 & X_{22}^3 & X_{22}^4 \\
\hline
 & 0 & 1 & 0 & 0 & -1 & 0 & 0 & 0 \\
 & 0 & -1 & 0 & 0 & 1 & 0 & 0 & 0
\end{array} \right) . \tag{5.3.111}
$$

Model 8.4d's brane tiling has $c = 9$ perfect matchings. The perfect matchings are encoded in the matrix

$$
P = \left(\begin{array}{c|ccccccccc}
 & p_1 & p_2 & p_3 & p_4 & p_5 & p_6 & p_7 & p_8 & p_9 \\
\hline
X_{22}^1 & 0 & 0 & 0 & 0 & 1 & 0 & 0 & 0 & 0 \\
X_{21} & 1 & 0 & 0 & 0 & 0 & 1 & 0 & 0 & 0 \\
X_{11}^1 & 0 & 1 & 0 & 0 & 0 & 0 & 1 & 0 & 0 \\
X_{11}^2 & 0 & 0 & 1 & 0 & 0 & 0 & 0 & 1 & 0 \\
X_{12} & 0 & 0 & 0 & 1 & 0 & 0 & 0 & 0 & 1 \\
X_{22}^2 & 1 & 1 & 1 & 1 & 0 & 0 & 0 & 0 & 0 \\
X_{22}^3 & 0 & 0 & 0 & 0 & 1 & 0 & 0 & 0 & 0 \\
X_{22}^4 & 0 & 0 & 0 & 0 & 0 & 1 & 1 & 1 & 1
\end{array} \right) . \tag{5.3.112}
$$

The brane tiling has the following zig-zag paths,

$$
\eta_1 = (X_{11}^1, X_{11}^2) , \quad \eta_2 = (X_{22}^2, X_{22}^4) ,
$$
$$
\eta_3 = (X_{22}^1, X_{21}, X_{11}^2, X_{12}, X_{22}^3, X_{22}^4) , \quad \eta_4 = (X_{22}^1, X_{22}^2, X_{22}^3, X_{21}, X_{11}^1, X_{12}) \tag{5.3.113}
$$

The F-term charge matrix is

$$
Q_F = \left(\begin{array}{c|ccccccccc}
 & p_1 & p_2 & p_3 & p_4 & p_5 & p_6 & p_7 & p_8 & p_9 \\
\hline
 & 1 & 0 & 0 & -1 & 0 & -1 & 0 & 0 & 1 \\
 & 0 & 1 & 0 & -1 & 0 & 0 & -1 & 0 & 1 \\
 & 0 & 0 & 1 & -1 & 0 & 0 & 0 & -1 & 1
\end{array} \right) . \tag{5.3.114}
$$

The D-term charge matrix is

$$
Q_D = \left(\begin{array}{c|ccccccccc}
 & p_1 & p_2 & p_3 & p_4 & p_5 & p_6 & p_7 & p_8 & p_9 \\
\hline
 & 1 & 0 & 0 & -1 & 0 & 0 & 0 & 0 & 0
\end{array} \right) . \tag{5.3.115}
$$

The mesonic moduli space of Model 8.4d in terms of a symplectic quotient is

$$\mathcal{M}^{mes} = \mathbb{C}^9 // Q_t . \tag{5.3.116}$$

By associating the fugacity t_i to the perfect matching p_i, the fully refined Hilbert series of $\mathcal{M}^{mes}$ is given by the following Molien integral

$$
\begin{aligned}
g_1(t_i; \mathcal{M}^{mes}) &= \frac{1}{(2\pi i)^4} \oint_{|z_1|=1} \frac{\mathrm{d}z_1}{z_1} \oint_{|z_2|=1} \frac{\mathrm{d}z_2}{z_2} \oint_{|z_3|=1} \frac{\mathrm{d}z_3}{z_3} \oint_{|z_4|=1} \frac{\mathrm{d}z_4}{z_4} \\
&\times \frac{1}{(1 - z_1 z_4 t_1)(1 - z_2 t_2)(1 - z_3 t_3)(1 - z_1^{-1} z_2^{-1} z_3^{-1} z_4^{-1} t_4)} \\
&\times \frac{1}{(1 - t_5)(1 - z_1^{-1} t_6)(1 - z_2^{-1} t_7)(1 - z_3^{-1} t_8)(1 - z_1 z_2 z_3 t_9)} \\
&= \frac{1 - t_1 t_2 t_3 t_4 t_6 t_7 t_8 t_9}{(1 - t_5)(1 - t_1 t_4 t_6 t_9)(1 - t_2 t_7)(1 - t_3 t_8)(1 - t_1 t_2 t_3 t_4)(1 - t_6 t_7 t_8 t_9)} .
\end{aligned} \tag{5.3.117}
$$

From the Hilbert series, we observe that the mesonic moduli space is a complete intersection. It is a 5-dimensional Calabi-Yau space. The generators of the mesonic moduli space are:

generator	perfect matchings
A_1	$p_1 p_4 p_6 p_9$
A_2	$p_2 p_7$
A_3	$p_3 p_8$
B_1	$p_1 p_2 p_3 p_4$
B_2	$p_6 p_7 p_8 p_9$
C	p_5

The A_i, B_i generators form a single relation,

$$A_1 A_2 A_3 = B_1 B_2 . \tag{5.3.118}$$

The global symmetry is $U(1)^4 \times U(1)_R$ and has no enhancement. The toric diagram of the mesonic moduli space is given by

$$
G_t = \left(
\begin{array}{c|ccccccccc}
 & p_1 & p_2 & p_3 & p_4 & p_5 & p_6 & p_7 & p_8 & p_9 \\
\hline
 & 0 & 1 & 0 & 0 & 0 & 0 & 1 & 0 & 0 \\
 & 0 & 0 & 1 & 0 & 0 & 0 & 0 & 1 & 0 \\
 & 1 & 0 & 0 & 1 & 0 & 1 & 0 & 0 & 1 \\
 & 0 & 0 & 0 & 0 & 1 & 0 & 0 & 0 & 0 \\
 & 1 & 1 & 1 & 1 & 0 & 0 & 0 & 0 & 0
\end{array}
\right) . \tag{5.3.119}
$$

Model 8.4e: $NC4$

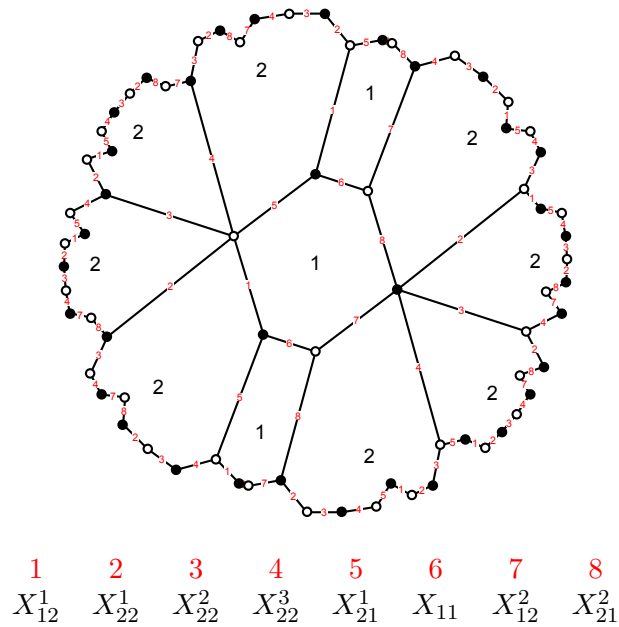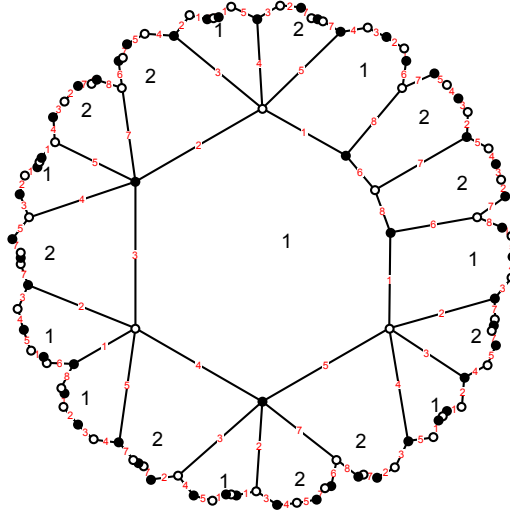| 1	2	3	4	5	6	7	8
X_{11}	X_{12}^1	X_{21}^1	X_{12}^2	X_{21}^2	X_{12}^3	X_{22}	X_{21}^3

Figure 5.34: The Model 8.4e brane tiling on a $g = 2$ Riemann surface with 2 gauge groups, 8 fields and 4 superpotential terms.

Figure 5.35: The quiver diagram for Model 8.4e, a brane tiling on a $g = 2$ Riemann surface with 2 gauge groups, 8 fields and 4 superpotential terms.

Model 8.4e's brane tiling and quiver are shown in Figure 5.34 and Figure 5.35 respectively. The superpotential is

$$W = +X_{11}X_{12}^1 X_{21}^1 X_{12}^2 X_{21}^2 + X_{12}^3 X_{22} X_{21}^3 - X_{12}^1 X_{22} X_{21}^2 X_{12}^2 X_{21}^1 - X_{11} X_{12}^3 X_{21}^3 \ . \tag{5.3.120}$$

The quiver incidence matrix is

$$d = \left(\begin{array}{c|cccccccc} & X_{11} & X_{12}^1 & X_{21}^1 & X_{12}^2 & X_{21}^2 & X_{12}^3 & X_{22} & X_{21}^3 \\ \hline 0 & -1 & 1 & -1 & 1 & -1 & 0 & 1 \\ 0 & 1 & -1 & 1 & -1 & 1 & 0 & -1 \end{array} \right) \ . \tag{5.3.121}$$

Model 8.4e has $c = 9$ perfect matchings which are

$$
P = \left(
\begin{array}{c|ccccccccc}
 & p_1 & p_2 & p_3 & p_4 & p_5 & p_6 & p_7 & p_8 & p_9 \\
\hline
X_{11} & 0 & 0 & 0 & 0 & 1 & 0 & 0 & 0 & 0 \\
X_{12}^1 & 1 & 0 & 0 & 0 & 0 & 1 & 0 & 0 & 0 \\
X_{21}^1 & 0 & 1 & 0 & 0 & 0 & 0 & 1 & 0 & 0 \\
X_{12}^2 & 0 & 0 & 1 & 0 & 0 & 0 & 0 & 1 & 0 \\
X_{21}^2 & 0 & 0 & 0 & 1 & 0 & 0 & 0 & 0 & 1 \\
X_{12}^3 & 1 & 1 & 1 & 1 & 0 & 0 & 0 & 0 & 0 \\
X_{22} & 0 & 0 & 0 & 0 & 1 & 0 & 0 & 0 & 0 \\
X_{21}^3 & 0 & 0 & 0 & 0 & 0 & 1 & 1 & 1 & 1 \\
\end{array}
\right) . \tag{5.3.122}
$$

The brane tiling has 6 zig-zag paths, which are

$$
\eta_1 = (X_{12}^1, X_{21}^1) \ , \ \ \eta_2 = (X_{12}^2, X_{21}^1) \ , \ \ \eta_3 = (X_{12}^2, X_{21}^2) \ , \ \ \eta_4 = (X_{12}^3, X_{21}^3) \ ,
$$
$$
\eta_5 = (X_{11}, X_{12}^1, X_{22}, X_{21}^3) \ , \ \ \eta_6 = (X_{11}, X_{12}^3, X_{22}, X_{21}^2) \ . \tag{5.3.123}
$$

The F-terms are encoded in the charge matrix

$$
Q_F = \left(
\begin{array}{ccccccccc}
p_1 & p_2 & p_3 & p_4 & p_5 & p_6 & p_7 & p_8 & p_9 \\
\hline
1 & 0 & 0 & -1 & 0 & -1 & 0 & 0 & 1 \\
0 & 1 & 0 & -1 & 0 & 0 & -1 & 0 & 1 \\
0 & 0 & 1 & -1 & 0 & 0 & 0 & -1 & 1 \\
\end{array}
\right) . \tag{5.3.124}
$$

The D-terms are given by the matrix

$$
Q_D = \left(
\begin{array}{c|ccccccccc}
p_1 & p_2 & p_3 & p_4 & p_5 & p_6 & p_7 & p_8 & p_9 \\
\hline
2 & -1 & 1 & -1 & 0 & -1 & 0 & 0 & 0 \\
\end{array}
\right) . \tag{5.3.125}
$$

As a symplectic quotient the mesonic moduli space is

$$
\mathcal{M}^{mes} = \mathbb{C}^9 /\!/ Q_t \ . \tag{5.3.126}
$$

By associating the fugacity t_i to the perfect matching p_i, the fully refined Hilbert

series of $\mathcal{M}^{mes}$ is given by the following Molien integral

$$
g_1(t_i; \mathcal{M}^{mes}) = \frac{1}{(2\pi i)^4} \oint_{|z_1|=1} \frac{dz_1}{z_1} \oint_{|z_2|=1} \frac{dz_2}{z_2} \oint_{|z_3|=1} \frac{dz_3}{z_3} \oint_{|z_4|=1} \frac{dz_4}{z_4}
$$

$$
\times \frac{1}{(1 - z_1 z_4^2 t_1)(1 - z_2 z_4^{-1} t_2)(1 - z_3 z_4 t_3)(1 - z_1^{-1} z_2^{-1} z_3^{-1} z_4^{-1} t_4)}
$$

$$
\times \frac{1}{(1 - t_5)(1 - z_1^{-1} z_4^{-1} t_6)(1 - z_2^{-1} t_7)(1 - z_3^{-1} t_8)(1 - z_1 z_2 z_3 t_9)}
$$

$$
= \frac{P(t_i)}{(1 - t_5)(1 - t_1 t_2 t_6 t_7)(1 - t_2 t_3 t_7 t_8)(1 - t_1 t_4 t_6 t_9)(1 - t_3 t_4 t_8 t_9)}
$$

$$
\times \frac{1}{(1 - t_1 t_2^2 t_3 t_4 t_7)(1 - t_1 t_2 t_3 t_4^2 t_9)(1 - t_1 t_6^2 t_7 t_8 t_9)(1 - t_3 t_6 t_7 t_8^2 t_9)} \,,
$$

$$(5.3.127)$$

where the numerator is

$$
\begin{aligned}
P(t_i) = \;& 1 - t_1^2 t_2^2 t_3 t_4^2 t_6 t_7 t_9 - t_1 t_2^2 t_3^2 t_4^2 t_7 t_8 t_9 - t_1 t_2 t_3 t_4 t_6 t_7 t_8 t_9 + t_1^2 t_2^3 t_3^2 t_4^2 t_6 t_7^2 t_8 t_9 - t_1^2 t_2^2 t_3 t_4 t_6^2 t_7^2 t_8 t_9 - t_1 t_2^2 t_3^2 t_4 t_6 t_7^2 t_8^2 t_9 \\
& - t_1 t_2 t_3 t_6^2 t_7^2 t_8^2 t_9 + t_1^2 t_2^3 t_3^2 t_4 t_6^2 t_7^3 t_8^2 t_9 + t_1^2 t_2^2 t_3^2 t_4 t_6 t_7 t_8 t_9^2 - t_1^2 t_2 t_3 t_4^2 t_6^2 t_7^2 t_8 t_9^2 + t_1^3 t_2^3 t_3^2 t_4^2 t_6^2 t_7^2 t_8 t_9^2 + t_1^3 t_2^2 t_3 t_4 t_6^2 t_7^2 t_8 t_9^2 \\
& - t_1 t_2 t_3 t_4^2 t_6 t_7 t_8^2 t_9^2 - t_1 t_3 t_4 t_6^2 t_7 t_8^2 t_9^2 + t_1^2 t_2^3 t_3^3 t_4 t_6 t_7^2 t_8^2 t_9^2 + 4 t_1^2 t_2^2 t_3^2 t_4^2 t_6^2 t_7^2 t_8^2 t_9^2 + t_1^2 t_2 t_3 t_4 t_6^3 t_7^2 t_8^2 t_9^2 - t_1^3 t_2^4 t_3^3 t_4^2 t_6^2 t_7^3 t_8^2 t_9^2 \\
& - t_1^3 t_2^3 t_3^2 t_4^2 t_6^3 t_7^3 t_8^2 t_9^2 + t_1^2 t_2^3 t_3^2 t_4 t_6^2 t_7^3 t_8^3 t_9^2 + t_1 t_2^2 t_3^2 t_4 t_6^2 t_7^2 t_8^3 t_9^2 - t_1^2 t_2^3 t_3^2 t_4 t_6^2 t_7^3 t_8^3 t_9^2 + t_1^2 t_2^2 t_3^2 t_4 t_6^3 t_7^3 t_8^3 t_9^2 + t_1^2 t_2 t_3^2 t_4^2 t_6 t_7 t_8^2 t_9^3 \\
& - t_1^3 t_2^3 t_3^4 t_4^2 t_6^2 t_7^2 t_8^3 t_9^3 - t_1^3 t_2^2 t_3^3 t_4^3 t_6^3 t_7^2 t_8^3 t_9^3 - t_1^2 t_2^3 t_3^4 t_4^2 t_6^2 t_7^3 t_8^3 t_9^3 + t_1 t_2 t_3^2 t_4^2 t_6^2 t_7^2 t_8^3 t_9^3 - t_1^3 t_2^3 t_3^4 t_4^2 t_6^3 t_7^3 t_8^3 t_9^3 - t_1 t_2^2 t_3^2 t_4^2 t_6^2 t_7^2 t_8^3 t_9^3 \\
& - t_1^2 t_2^2 t_3^3 t_4^2 t_6^3 t_7^2 t_8^4 t_9^3 + t_1^4 t_2^4 t_3^3 t_4^4 t_6^4 t_7^4 t_8^4 t_9^4 \,.
\end{aligned}
$$

$$(5.3.128)$$

By setting all perfect matching fugacities to $t_i = t$, the Hilbert series takes the form

$$
g_1(t; \mathcal{M}^{mes}) = \frac{1}{(1-t)} \times \frac{1 + 2t^4 + 2t^6 + 2t^8 + t^{12}}{(1 - t^4)^2 (1 - t^6)^2} \,.
$$

$$(5.3.129)$$

It can be seen that the mesonic moduli space is a Calabi-Yau 5-fold. It is not a complete intersection. The plethystic logarithm of the refined Hilbert series in (5.3.127) is

$$
\begin{aligned}
PL[g_1(t_i; \mathcal{M}^{mes})] = \;& t_5 + (t_1 t_2 t_6 t_7 + t_2 t_3 t_7 t_8 + t_1 t_4 t_6 t_9 + t_3 t_4 t_8 t_9) + (t_1 t_2^2 t_3 t_4 t_7 \\
& + t_1 t_2 t_3 t_4^2 t_9 + t_1 t_6^2 t_7 t_8 t_9 + t_3 t_6 t_7 t_8^2 t_9) - t_1 t_2 t_3 t_4 t_6 t_7 t_8 t_9 \\
& - (t_1^2 t_2^2 t_3 t_4^2 t_6 t_7 t_9 + t_1 t_2^2 t_3^2 t_4^2 t_7 t_8 t_9 + t_1 t_2 t_3 t_6^2 t_7^2 t_8^2 t_9 + t_1 t_3 t_4 t_6^2 t_7 t_8^2 t_9^2) \\
& - (t_1^2 t_2^2 t_3 t_4 t_6^2 t_7^2 t_8 t_9 + t_1 t_2^2 t_3^2 t_4 t_6 t_7^2 t_8^2 t_9 + t_1^2 t_2 t_3 t_4^2 t_6^2 t_7 t_8 t_9^2 \\
& + t_1 t_2 t_3^2 t_4^2 t_6 t_7 t_8^2 t_9^2) + \ldots
\end{aligned}
$$

$$(5.3.130)$$

The first order generators of the mesonic moduli space can be found from the above plethystic logarithm and are shown below.

generator	perfect matchings
A_1	$p_1 p_2 p_6 p_7$
A_2	$p_2 p_3 p_7 p_8$
A_3	$p_1 p_4 p_6 p_9$
A_4	$p_3 p_4 p_8 p_9$
B_1	$p_1 p_2^2 p_3 p_4 p_7$
B_2	$p_1 p_2 p_3 p_4^2 p_9$
B_3	$p_1 p_6^2 p_7 p_8 p_9$
B_4	$p_3 p_6 p_7 p_8^2 p_9$
C	p_5

The generators above form the following first order relations,

$$\{ \quad A_2 A_3 = A_1 A_4 \ , \ A_3 B_1 = A_1 B_2 \ , \ A_2 B_3 = A_1 B_4 \ , \ A_4 B_3 = A_3 B_4 \ , \ A_4 B_1 = A_2 B_2 \ ,$$
$$A_1 A_2 A_3 = B_1 B_3 \ , \ A_2 A_3 A_4 = B_2 B_4 \ , \ A_2 A_3^2 = B_2 B_3 \ , \ A_2^2 A_3 = B_1 B_4 \} \ . \quad (5.3.131)$$

The global symmetry is not enhanced and remains $U(1)^4 \times U(1)_R$. The toric diagram is given by

$$
G_t = \left(\begin{array}{c|ccccccccc}
 & p_1 & p_2 & p_3 & p_4 & p_5 & p_6 & p_7 & p_8 & p_9 \\
\hline
 & 1 & 0 & 0 & 1 & 0 & 0 & 1 & 0 & 0 \\
 & 0 & 1 & 0 & 0 & 1 & 0 & 0 & 1 & 0 \\
 & 0 & 0 & 1 & 0 & 0 & 1 & 0 & 0 & 1 \\
 & 1 & 1 & 1 & 0 & 0 & 0 & 0 & 0 & 0 \\
 & 0 & 0 & 0 & 1 & 1 & 1 & 0 & 0 & 0
\end{array} \right) \ . \qquad (5.3.132)
$$

Model 8.4f: $\mathcal{M}_{4,2}$

The brane tiling and corresponding quiver for Model 8.4f is shown in Figure 5.36 and Figure 5.37 respectively. The superpotential is

$$W = +X_{22}^1 X_{21}^1 X_{12}^1 X_{22}^2 X_{22}^3 + X_{22}^4 X_{21}^2 X_{12}^2 - X_{22}^1 X_{22}^3 X_{22}^2 X_{22}^4 - X_{21}^1 X_{12}^2 X_{21}^2 X_{12}^1 \ . \tag{5.3.133}$$

The quiver incidence matrix is

$$
d = \left(\begin{array}{c|cccccccc}
 & X_{22}^1 & X_{21}^1 & X_{12}^1 & X_{22}^2 & X_{22}^3 & X_{22}^4 & X_{21}^2 & X_{12}^2 \\
\hline
 & 0 & 1 & -1 & 0 & 0 & 0 & 1 & -1 \\
 & 0 & -1 & 1 & 0 & 0 & 0 & -1 & 1
\end{array} \right) \ . \qquad (5.3.134)
$$
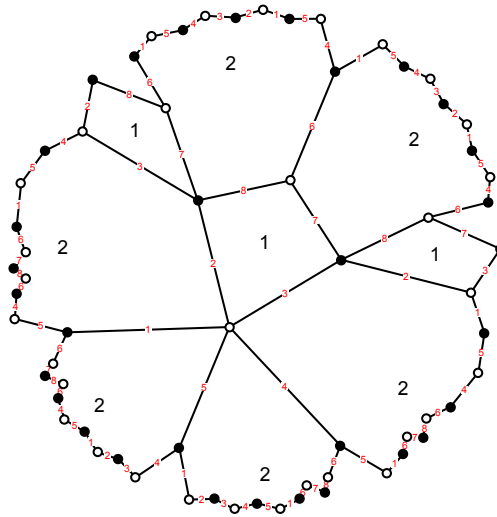
1	2	3	4	5	6	7	8
X_{22}^1	X_{21}^1	X_{12}^1	X_{22}^2	X_{22}^3	X_{22}^4	X_{21}^2	X_{12}^2

Figure 5.36: The Model 8.5f brane tiling on a $g = 2$ Riemann surface with 2 gauge groups, 8 fields and 4 superpotential terms.
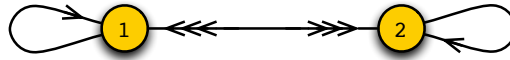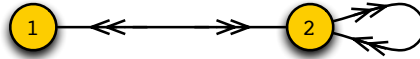

Figure 5.37: The quiver diagram for Model 8.5f, a brane tiling on a $g = 2$ Riemann surface with 2 gauge groups, 8 fields and 4 superpotential terms.

Model 8.4f's brane tiling has $c = 8$ perfect matchings. The perfect matchings are encoded in the matrix

$$P = \begin{pmatrix}
 & p_1 & p_2 & p_3 & p_4 & p_5 & p_6 & p_7 & p_8 \\
\hline
X_{12}^1 & 0 & 1 & 0 & 0 & 0 & 0 & 0 & 0 \\
X_{12}^2 & 0 & 0 & 1 & 0 & 1 & 0 & 1 & 0 \\
X_{21}^1 & 1 & 0 & 0 & 0 & 0 & 0 & 0 & 0 \\
X_{21}^2 & 0 & 0 & 0 & 1 & 0 & 1 & 0 & 1 \\
X_{22}^1 & 0 & 0 & 1 & 1 & 0 & 0 & 0 & 0 \\
X_{22}^2 & 0 & 0 & 0 & 0 & 1 & 1 & 0 & 0 \\
X_{22}^3 & 0 & 0 & 0 & 0 & 0 & 0 & 1 & 1 \\
X_{22}^4 & 1 & 1 & 0 & 0 & 0 & 0 & 0 & 0
\end{pmatrix} . \tag{5.3.135}$$

The brane tiling has 6 zig-zag paths, which are

$$\eta_1 = (X_{12}^1, X_{21}^1) \ , \ \ \eta_2 = (X_{12}^2, X_{21}^2) \ , \ \ \eta_3 = (X_{22}^1, X_{22}^3) \ , \ \ \eta_4 = (X_{22}^2, X_{22}^3) \ ,$$
$$\eta_5 = (X_{21}^1, X_{12}^2, X_{22}^4, X_{22}^1) \ , \ \ \eta_6 = (X_{21}^2, X_{12}^1, X_{22}^2, X_{22}^4) \ . \tag{5.3.136}$$

The F-term charge matrix is

$$Q_F = \left(\begin{array}{cccccccc} p_1 & p_2 & p_3 & p_4 & p_5 & p_6 & p_7 & p_8 \\ \hline 0 & 0 & 1 & -1 & 0 & 0 & -1 & 1 \\ 0 & 0 & 0 & 0 & 1 & -1 & -1 & 1 \end{array} \right) \ . \tag{5.3.137}$$

The D-terms are encoded in the matrix

$$Q_D = \left(\begin{array}{cccccccc} p_1 & p_2 & p_3 & p_4 & p_5 & p_6 & p_7 & p_8 \\ \hline 1 & -1 & -1 & 1 & 0 & 0 & 0 & 0 \end{array} \right) \ . \tag{5.3.138}$$

The symplectic quotient description of the mesonic moduli space of Model 8.4f is given in terms of the total charge matrix Q_t,

$$\mathcal{M}^{mes} = \mathbb{C}^8 // Q_t \ . \tag{5.3.139}$$

By associating the fugacity t_i to the perfect matching p_i, the fully refined Hilbert series of $\mathcal{M}^{mes}$ is given by the following Molien integral

$$
\begin{aligned}
g_1(t_i; \mathcal{M}^{mes}) &= \frac{1}{(2\pi i)^3} \oint_{|z_1|=1} \frac{\mathrm{d}z_1}{z_1} \oint_{|z_2|=1} \frac{\mathrm{d}z_2}{z_2} \oint_{|z_3|=1} \frac{\mathrm{d}z_3}{z_3} \\
&\quad \times \frac{1}{(1 - z_3 t_1)(1 - z_3^{-1} t_2)(1 - z_1 z_3^{-1} t_3)(1 - z_1^{-1} z_3 t_4)} \\
&\quad \times \frac{1}{(1 - z_2 t_5)(1 - z_2^{-1} t_6)(1 - z_1^{-1} z_2^{-1} t_7)(1 - z_1 z_2 t_8)} \\
&= \frac{1 - t_1 t_2 t_3 t_4 t_5 t_6 t_7 t_8}{(1 - t_1 t_2)(1 - t_3 t_4)(1 - t_5 t_6)(1 - t_7 t_8)(1 - t_1 t_3 t_5 t_7)(1 - t_2 t_4 t_6 t_8)} \ .
\end{aligned}
\tag{5.3.140}
$$

From the Hilbert series, we observe that the mesonic moduli space is a complete intersection. As expected for a $g = 2$ tiling, it is a 5-dimensional Calabi-Yau space. The generators of the mesonic moduli space are:

generator	perfect matchings
A_1	$p_1 p_2$
A_2	$p_3 p_4$
A_3	$p_5 p_6$
A_4	$p_7 p_8$
B_1	$p_1 p_3 p_5 p_7$
B_2	$p_2 p_4 p_6 p_8$

The generators form a single relation

$$A_1 A_2 A_3 A_4 = B_1 B_2 \ . \tag{5.3.141}$$

The global symmetry is $U(1)^4 \times U(1)_R$ and has no enhancement. The toric diagram of the Calabi-Yau 5-fold is given by

$$G_t = \left(\begin{array}{c|cccccccc}
 & p_1 & p_2 & p_3 & p_4 & p_5 & p_6 & p_7 & p_8 \\
\hline
 & 1 & 1 & 0 & 0 & 0 & 0 & 0 & 0 \\
 & 0 & 0 & 1 & 1 & 0 & 0 & 0 & 0 \\
 & 0 & 0 & 0 & 0 & 1 & 1 & 0 & 0 \\
 & 0 & 0 & 0 & 0 & 0 & 0 & 1 & 1 \\
 & 0 & 1 & 0 & 1 & 0 & 1 & 0 & 1
\end{array} \right) \ . \tag{5.3.142}$$

We further note that one can apply the urban renewal move on face 1 of the brane tiling. It can be shown that Model 8.4f is self-dual under toric duality on face 1 up to a sign of the superpotential.

Model 8.4g: $NC5$

For Model 8.4g, the brane tiling and corresponding quiver is shown in Figure 5.38 and Figure 5.39 respectively. The quartic superpotential is

$$W = +X_{21}^1 X_{12}^1 X_{21}^2 X_{12}^2 + X_{21}^3 X_{12}^3 X_{21}^4 X_{12}^4 - X_{21}^1 X_{12}^2 X_{21}^2 X_{12}^3 - X_{21}^1 X_{12}^4 X_{21}^4 X_{12}^3 \ . \tag{5.3.143}$$

The quiver incidence matrix is

$$d = \left(\begin{array}{c|cccccccc}
 & X_{21}^1 & X_{12}^1 & X_{21}^2 & X_{12}^2 & X_{21}^3 & X_{12}^3 & X_{21}^4 & X_{12}^4 \\
\hline
 & 1 & -1 & 1 & -1 & -1 & 1 & -1 & 1 \\
 & -1 & 1 & -1 & 1 & 1 & -1 & 1 & -1
\end{array} \right) \ . \tag{5.3.144}$$

The brane tiling has $c = 10$ perfect matchings. The perfect matchings are encoded
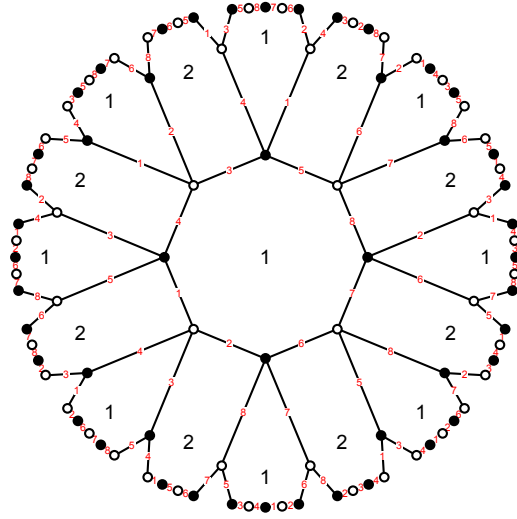
1	**2**	**3**	**4**	**5**	**6**	**7**	**8**
X^1_{21}	X^1_{12}	X^2_{21}	X^2_{12}	X^3_{21}	X^3_{12}	X^4_{21}	X^4_{12}

Figure 5.38: The Model 8.4g brane tiling on a $g = 2$ Riemann surface with 2 gauge groups, 8 fields and 4 superpotential terms.

Figure 5.39: The quiver diagram for Model 8.4g, a brane tiling on a $g = 2$ Riemann surface with 2 gauge groups, 8 fields and 4 superpotential terms.

in the matrix

$$
P = \left(
\begin{array}{c|cccccccccc}
 & p_1 & p_2 & p_3 & p_4 & p_5 & p_6 & p_7 & p_8 & p_9 & p_{10} \\
\hline
X^1_{21} & 0 & 1 & 0 & 0 & 1 & 0 & 0 & 1 & 0 & 0 \\
X^1_{12} & 1 & 0 & 0 & 0 & 0 & 0 & 0 & 0 & 0 & 0 \\
X^2_{21} & 0 & 0 & 1 & 0 & 0 & 1 & 0 & 0 & 1 & 0 \\
X^2_{12} & 0 & 0 & 0 & 1 & 0 & 0 & 1 & 0 & 0 & 1 \\
X^3_{21} & 1 & 0 & 0 & 0 & 0 & 0 & 0 & 0 & 0 & 0 \\
X^3_{12} & 0 & 1 & 1 & 1 & 0 & 0 & 0 & 0 & 0 & 0 \\
X^4_{21} & 0 & 0 & 0 & 0 & 1 & 1 & 1 & 0 & 0 & 0 \\
X^4_{12} & 0 & 0 & 0 & 0 & 0 & 0 & 0 & 1 & 1 & 1 \\
\end{array}
\right) . \tag{5.3.145}
$$

The brane tiling has 6 zig-zag paths, which are

$$
\eta_1 = (X^1_{21}, X^2_{12}) \;, \; \eta_2 = (X^2_{21}, X^2_{12}) \;, \; \eta_3 = (X^3_{21}, X^4_{12}) \;, \; \eta_4 = (X^4_{21}, X^4_{12}) \;,
$$
$$
\eta_5 = (X^1_{21}, X^1_{12}, X^4_{21}, X^3_{12}) \;, \; \eta_6 = (X^1_{12}, X^2_{21}, X^3_{12}, X^3_{21}) \;. \tag{5.3.146}
$$

The F-term constraints can be expressed as charges carried by the perfect matchings. The charges are given by

$$
Q_F = \left(\begin{array}{c|cccccccccc}
 & p_1 & p_2 & p_3 & p_4 & p_5 & p_6 & p_7 & p_8 & p_9 & p_{10} \\
\hline
 & 0 & 1 & 0 & -1 & 0 & 0 & 0 & -1 & 0 & 1 \\
 & 0 & 0 & 1 & -1 & 0 & 0 & 0 & 0 & -1 & 1 \\
 & 0 & 0 & 0 & 0 & 1 & 0 & -1 & -1 & 0 & 1 \\
 & 0 & 0 & 0 & 0 & 0 & 1 & -1 & 0 & -1 & 1
\end{array} \right) . \tag{5.3.147}
$$

The D-term charges are encoded in the quiver incidence matrix d and are

$$
Q_D = \left(\begin{array}{c|cccccccccc}
 & p_1 & p_2 & p_3 & p_4 & p_5 & p_6 & p_7 & p_8 & p_9 & p_{10} \\
\hline
 & 1 & -1 & -1 & 1 & 1 & 0 & 0 & -1 & 0 & 0
\end{array} \right) . \tag{5.3.148}
$$

Using the total charge matrix, the mesonic moduli space can be expressed as the symplectic quotient

$$
\mathcal{M}^{mes} = \mathbb{C}^{10} // Q_t . \tag{5.3.149}
$$

By associating the fugacity t_i to the perfect matching p_i, the fully refined Hilbert series of $\mathcal{M}^{mes}$ is given by the following Molien integral

$$
\begin{aligned}
g_1(t_i; \mathcal{M}^{mes}) &= \frac{1}{(2\pi i)^5} \oint_{|z_1|=1} \frac{dz_1}{z_1} \oint_{|z_2|=1} \frac{dz_2}{z_2} \oint_{|z_3|=1} \frac{dz_3}{z_3} \oint_{|z_4|=1} \frac{dz_4}{z_4} \oint_{|z_5|=1} \frac{dz_5}{z_5} \\
&\quad \times \frac{1}{(1-z_5 t_1)(1 - z_1 z_5^{-1} t_2)(1 - z_2 z_5^{-1} t_3)(1 - z_1^{-1} z_2^{-1} z_5 t_4)} \\
&\quad \times \frac{1}{(1 - z_3 z_5 t_5)(1 - z_4 t_6)(1 - z_3^{-1} z_4^{-1} t_7)(1 - z_1^{-1} z_3^{-1} z_5^{-1} t_8)} \\
&\quad \times \frac{1}{(1 - z_2^{-1} z_4^{-1} t_9)(1 - z_1 z_2 z_3 z_4 t_{10})} \\
&= \frac{P(t_i)}{(1 - t_1 t_2 t_3 t_4)(1 - t_2 t_3 t_4^2 t_7 t_{10})(1 - t_2 t_3 t_4 t_5 t_6 t_7)(1 - t_1 t_2 t_5 t_8)} \\
&\quad \times \frac{1}{(1 - t_2 t_4 t_5 t_7 t_8 t_{10})(1 - t_2 t_5^2 t_6 t_7 t_8)(1 - t_1 t_3 t_6 t_9)(1 - t_3 t_4 t_6 t_7 t_9 t_{10})} \\
&\quad \times \frac{1}{(1 - t_3 t_5 t_6^2 t_7 t_9)(1 - t_1 t_8 t_9 t_{10})(1 - t_4 t_7 t_8 t_9 t_{10}^2)(1 - t_5 t_6 t_7 t_8 t_9 t_{10})} ,
\end{aligned} \tag{5.3.150}
$$

where the numerator is

$$P(t_i) = 1 - t_1 t_2^2 t_3 t_4 t_5^2 t_6 t_7 t_8 - t_1 t_2 t_3^2 t_4 t_5 t_6^2 t_7 t_9 - t_1 t_2 t_3 t_5^2 t_6^2 t_7 t_8 t_9 + t_1^2 t_2^2 t_3^2 t_4 t_5^2 t_6^2 t_7 t_8 t_9 + t_1 t_2^2 t_3^2 t_4 t_5 t_6^3 t_7^2 t_8 t_9 - t_1 t_2^2 t_3 t_4^2 t_5 t_7 t_8 t_{10}$$

$$(5.3.151)$$

The mesonic moduli space is a non-complete intersection. The unrefined Hilbert series is

$$g_1(t; \mathcal{M}^{mes}) = \frac{(1-t^2)^3}{(1-t^4)^4 (1-t^6)^4} \times (1 + 3t^2 + 6t^4 + 14t^6 + 27t^8 + 32t^{10} + 31t^{12}$$
$$+ 32t^{14} + 27t^{16} + 14t^{18} + 6t^{20} + 3t^{22} + t^{24}) \qquad (5.3.152)$$

It is a 5-dimensional Calabi-Yau space. The plethystic logarithm of the refined Hilbert

series is

$$PL[g_1(t_i; \mathcal{M}^{mes})] = (t_1 t_2 t_3 t_4 + t_1 t_2 t_5 t_8 + t_1 t_3 t_6 t_9 + t_1 t_8 t_9 t_{10}) + (t_2 t_3 t_4 t_5 t_6 t_7 + t_2 t_5^2 t_6 t_7 t_8$$
$$+ t_3 t_5 t_6^2 t_7 t_9 + t_2 t_3 t_4^2 t_7 t_{10} + t_2 t_4 t_5 t_7 t_8 t_{10} + t_3 t_4 t_6 t_7 t_9 t_{10} + t_5 t_6 t_7 t_8 t_9 t_{10} + t_4 t_7 t_8 t_9 t_{10}^2)$$
$$- (t_1 t_2^2 t_3 t_4 t_5^2 t_6 t_7 t_8 + t_1 t_2 t_3^2 t_4 t_5 t_6^2 t_7 t_9 + t_1 t_2 t_3 t_5^2 t_6^2 t_7 t_8 t_9 + t_1 t_2^2 t_3 t_4^2 t_5 t_7 t_8 t_{10}$$
$$+ t_1 t_2 t_3^2 t_4^2 t_6 t_7 t_9 t_{10} + 3 t_1 t_2 t_3 t_4 t_5 t_6 t_7 t_8 t_9 t_{10} + t_1 t_2 t_5^2 t_6 t_7 t_8^2 t_9 t_{10} + t_1 t_3 t_5 t_6^2 t_7 t_8 t_9^2 t_{10}$$
$$+ t_1 t_2 t_3 t_4^2 t_7 t_8 t_9 t_{10}^2 + t_1 t_2 t_4 t_5 t_7 t_8^2 t_9 t_{10}^2 + t_1 t_3 t_4 t_6 t_7 t_8 t_9^2 t_{10}^2) - (t_2^2 t_3 t_4^2 t_5^2 t_6 t_7^2 t_8 t_{10}$$
$$+ t_2 t_3^2 t_4^2 t_5 t_6^2 t_7^2 t_9 t_{10} + 2 t_2 t_3 t_4 t_5^2 t_6^2 t_7^2 t_8 t_9 t_{10} + 2 t_2 t_3 t_4^2 t_5 t_6 t_7^2 t_8 t_9 t_{10}^2 + t_2 t_4 t_5^2 t_6 t_7^2 t_8 t_9 t_{10}^2$$
$$+ t_3 t_4 t_5 t_6^2 t_7^2 t_8 t_9^2 t_{10}^2) + \ldots . \tag{5.3.153}$$

We can read from the plethystic logarithm the lowest order generators of the mesonic moduli space and are

generator	perfect matchings
A_1	$p_1 p_2 p_3 p_4$
A_2	$p_1 p_2 p_5 p_8$
A_3	$p_1 p_3 p_6 p_9$
A_4	$p_1 p_8 p_9 p_{10}$
B_1	$p_2 p_3 p_4 p_5 p_6 p_7$
B_2	$p_2 p_5^2 p_6 p_7 p_8$
B_3	$p_3 p_5 p_6^2 p_7 p_9$
B_4	$p_2 p_4 p_5 p_7 p_8 p_{10}$
B_5	$p_3 p_4 p_6 p_7 p_9 p_{10}$
B_6	$p_5 p_6 p_7 p_8 p_9 p_{10}$
B_7	$p_4 p_7 p_8 p_7 p_{10}^2$

The generators form the following first order relations amongst them which correspond to the presented negative terms in the expansion of the plethystic logarithm in (5.3.153),

$$\{B_6 B_7 - B_5 B_8, \ B_4 B_7 - B_3 B_8, \ B_2 B_7 - B_1 B_8, \ B_3 B_6 - B_2 B_8, \ A_4 B_6 - A_3 B_8,$$
$$B_4 B_5 - B_2 B_8, \ B_3 B_5 - B_1 B_8, \ B_2 B_5 - B_1 B_6, \ A_4 B_5 - A_3 B_7, \ A_2 B_5 - A_1 B_8,$$
$$A_4 B_4 - A_2 B_8, \ A_3 B_4 - A_2 B_6, \ B_2 B_3 - B_1 B_4, \ A_4 B_3 - A_2 B_7, \ A_3 B_3 - A_1 B_8,$$
$$A_4 B_2 - A_1 B_8, \ A_3 B_2 - A_1 B_6, \ A_2 B_2 - A_1 B_4, \ A_4 B_1 - A_1 B_7, \ A_3 B_1 - A_1 B_5,$$
$$A_2 B_1 - A_1 B_3\} . \tag{5.3.154}$$

The global symmetry is $U(1)^4 \times U(1)_R$ and has no enhancement. The toric diagram

of the Calabi-Yau 5-fold is given by

$$
G_t = \left(
\begin{array}{cccccccccc}
p_1 & p_2 & p_3 & p_4 & p_5 & p_6 & p_7 & p_8 & p_9 & p_{10} \\
\hline
1 & 1 & 0 & 0 & 1 & 0 & 0 & 1 & 0 & 0 \\
1 & 0 & 1 & 0 & 0 & 1 & 0 & 0 & 1 & 0 \\
-1 & 0 & 0 & 1 & 0 & 0 & 1 & 0 & 0 & 1 \\
-1 & 0 & 0 & 0 & 1 & 1 & 1 & 0 & 0 & 0 \\
1 & 1 & 1 & 1 & 0 & 0 & 0 & 0 & 0 & 0
\end{array}
\right) . \tag{5.3.155}
$$

Model 8.4h: $NC3$

1	2	3	4	5	6	7	8
X_{21}^1	X_{12}^1	X_{21}^2	X_{12}^2	X_{12}^3	X_{21}^3	X_{12}^4	X_{21}^4
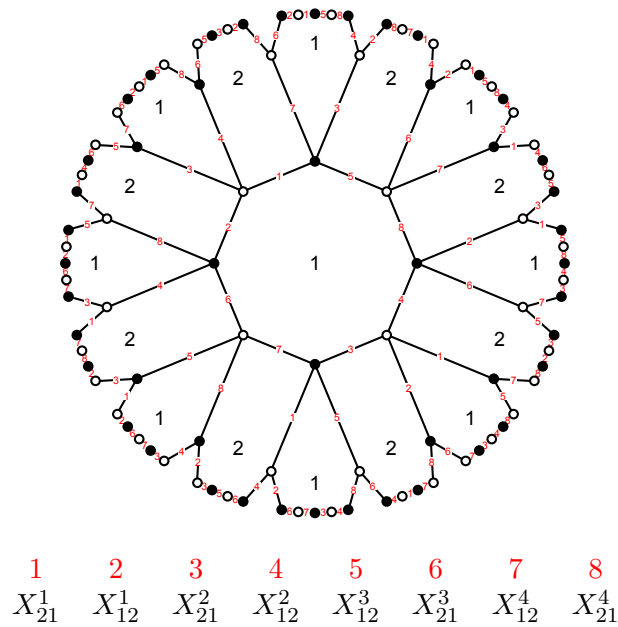
Figure 5.40: The Model 8.4h brane tiling on a $g = 2$ Riemann surface with 2 gauge groups, 8 fields and 4 superpotential terms.
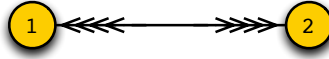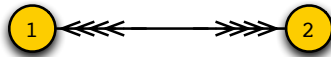

Figure 5.41: The quiver diagram for Model 8.4h, a brane tiling on a $g = 2$ Riemann surface with 2 gauge groups, 8 fields and 4 superpotential terms.

For Model 8.4h, the brane tiling and corresponding quiver is shown in Figure 5.40

and Figure 5.41 respectively. The quartic superpotential is

$$W = +X_{21}^1 X_{12}^1 X_{21}^2 X_{12}^2 + X_{12}^3 X_{21}^3 X_{12}^4 X_{21}^4 - X_{21}^1 X_{12}^3 X_{21}^2 X_{12}^4 - X_{12}^1 X_{21}^4 X_{12}^2 X_{21}^3 \ .$$

(5.3.156)

The quiver incidence matrix is

$$d = \left(\begin{array}{c|cccccccc} & X_{21}^1 & X_{12}^1 & X_{21}^2 & X_{12}^2 & X_{12}^3 & X_{21}^3 & X_{12}^4 & X_{21}^4 \\ \hline 1 & -1 & 1 & -1 & -1 & 1 & -1 & 1 \\ -1 & 1 & -1 & 1 & 1 & -1 & 1 & -1 \end{array} \right) \ .$$

(5.3.157)

The brane tiling has $c = 8$ perfect matchings. The perfect matchings are encoded in the matrix

$$P = \left(\begin{array}{c|cccccccc} & a_1 & a_2 & b_1 & b_2 & c_1 & c_2 & d_1 & d_2 \\ \hline X_{12}^1 & 0 & 0 & 0 & 0 & 1 & 0 & 0 & 1 \\ X_{12}^2 & 0 & 0 & 0 & 0 & 0 & 1 & 1 & 0 \\ X_{12}^3 & 0 & 0 & 0 & 0 & 1 & 0 & 1 & 0 \\ X_{12}^4 & 0 & 0 & 0 & 0 & 0 & 1 & 0 & 1 \\ X_{21}^1 & 1 & 0 & 0 & 1 & 0 & 0 & 0 & 0 \\ X_{21}^2 & 0 & 1 & 1 & 0 & 0 & 0 & 0 & 0 \\ X_{21}^3 & 1 & 0 & 1 & 0 & 0 & 0 & 0 & 0 \\ X_{21}^4 & 0 & 1 & 0 & 1 & 0 & 0 & 0 & 0 \end{array} \right) \ .$$

(5.3.158)

The brane tiling has the zig-zag paths,

$$\eta_1 = (X_{21}^1, X_{12}^1, X_{21}^4, X_{12}^3, X_{21}^2, X_{12}^2, X_{21}^3, X_{12}^4) \ ,$$
$$\eta_2 = (X_{21}^1, X_{12}^3, X_{21}^3, X_{12}^1, X_{21}^2, X_{12}^4, X_{21}^4, X_{12}^2) \ .$$

(5.3.159)

The F-term constraints can be expressed as charges carried by the perfect matchings. The charges are given by

$$Q_F = \left(\begin{array}{c|cccccccc} a_1 & a_2 & b_1 & b_2 & c_1 & c_2 & d_1 & d_2 \\ \hline 1 & 1 & 0 & 0 & 0 & 0 & -1 & -1 \\ 0 & 0 & -1 & -1 & 1 & 1 & 0 & 0 \end{array} \right) \ .$$

(5.3.160)

The D-term charges are encoded in the quiver incidence matrix d and are

$$Q_D = \left(\begin{array}{c|cccccccc} a_1 & a_2 & b_1 & b_2 & c_1 & c_2 & d_1 & d_2 \\ \hline 1 & 1 & -1 & -1 & 0 & 0 & 0 & 0 \end{array} \right) \ .$$

(5.3.161)

When reduced, the total charge matrix

$$Q_t = \begin{pmatrix} a_1 & a_2 & b_1 & b_2 & c_1 & c_2 & d_1 & d_2 \\ \hline 1 & 1 & 0 & 0 & 0 & 0 & -1 & -1 \\ 0 & 0 & 1 & 1 & 0 & 0 & -1 & -1 \\ 0 & 0 & 0 & 0 & 1 & 1 & -1 & -1 \end{pmatrix} . \tag{5.3.162}$$

is identical to the total charge matrix of Model 8.2b in section §5.3.5. The mesonic moduli space of Model 8.4h which can be expressed as a symplectic quotient,

$$\mathcal{M}^{mes} = \mathbb{C}^8 // Q_t , \tag{5.3.163}$$

is the same as Model 8.2b. It is a toric Calabi-Yau 5-fold and is a non-complete intersection.

5.4 Conclusions and Future Directions

We have discovered a new set of field theories with the classification of the first few brane tilings on a $g = 2$ Riemann surface. The classification identifies 16 of what we call *restricted* $g = 2$ brane tilings with up to 8 fields and 4 superpotential terms. Their mesonic moduli spaces are specified by calculating the refined Hilbert series and are shown to be toric Calabi-Yau 5-folds.

A feature that has not been highlighted so far is that although the $g = 2$ brane tilings in the classification have no self-intersecting zig-zag paths and no multi-bonded edges, some of them have multiple perfect matchings associated to extremal points in the toric diagram. This is one of a series of new observations which requires further studies in the near future. In summary, the new observations are as follows:

- For the following $g = 2$ brane tilings in the classification, more than one perfect matching is assigned to extremal toric points:

$$6.2a , 7.2 , 8.4d .$$

  These are however restricted brane tilings with no self-intersecting zig-zag paths and no multi-bonded edges. We expect that the brane tilings on a $g = 2$ Riemann surface feature graphical properties beyond zig-zag paths and multi-bonded edges that indicate the assignment of multiple GLSM fields to extremal toric points.

- Zig-zag paths that play a pivotal role in relating geometry and field theory for torus brane tilings appear to play a lesser role in $g = 2$ brane tilings. In fact, for all models in the classification, we observe that the number of zig-zag paths is less

than the number of facets of the corresponding 4-dimensional toric diagram. The only exception is Model 5.2 where the numbers are equal.

- For torus brane tilings with Calabi-Yau 3-fold mesonic moduli spaces, the area of the toric diagram corresponds to the number of gauge groups in the corresponding quiver gauge theory. The analogue of the area for the Calabi-Yau 5-fold mesonic moduli spaces for $g = 2$ brane tilings is the 4-dimensional volume of the toric diagram. For the brane tilings in our classification, the volumes of their toric diagrams are as follows:

#	Volume	Gauge Groups	#	Volume	Gauge Groups
5.2	1	1	8.4a	6	2
6.2a	1	2	8.4b	2	2
6.2b	3	2	8.4c	2	2
6.2c	3	2	8.4d	3	2
7.2	2	3	8.4e	7	2
7.4	3	1	8.4f	4	2
8.2a	4	4	8.4g	12	2
8.2b	8	4	8.4h	8	2

We observe that only Models 5.2, 8.2a, 8.4b and 8.4c have matching values for the number of gauge groups and toric diagram volumes. It is an interesting question to investigate when and why these two values match for $g = 2$ brane tilings.

On the field theory side, we observe another array of open questions from our classification of $g = 2$ brane tilings. As noted in the introduction, we have a limited understanding of the IR behaviour of these brane tilings. We hope to obtain more answers by doing the following in future studies:

- The ranks of the gauge groups can be varied, and one needs to study the IR behaviour for non-Abelian theories as well as their vacuum moduli spaces.

- Boundaries, which represent flavor groups, can be added to a brane tiling. The IR behaviour of these theories with their vacuum moduli spaces needs to be studied.

As a final note of our work, we would like to point out that the mesonic moduli spaces of brane tilings on any Riemann surface are always odd dimensional toric Calabi-Yau. The natural question given this property is to ask whether even dimensional toric Calabi-Yau spaces can be related to brane tilings on Riemann surfaces via a modification of the bipartite graphs.

As seen in the studies on Chern-Simons theories and brane tilings [63, 64, 194, 137, 166], one can assign integer weights to edges in the tiling such that they add up to

Chern-Simons levels on gauge groups. This brane tiling modification helps to represent field theories with Calabi-Yau 4-fold mesonic moduli spaces. It is clear that solving the classical moduli space for $3d$ Chern-Simons theories introduces a symplectic quotient by a further $U(1)$ action, increasing the complex dimension by 1. Therefore it appears that integer weights to edges of a brane tiling on a genus g Riemann surface with a $2g + 1$ dimensional mesonic moduli space lead to a modified brane tiling with a $2(g + 1)$ dimensional mesonic moduli space.
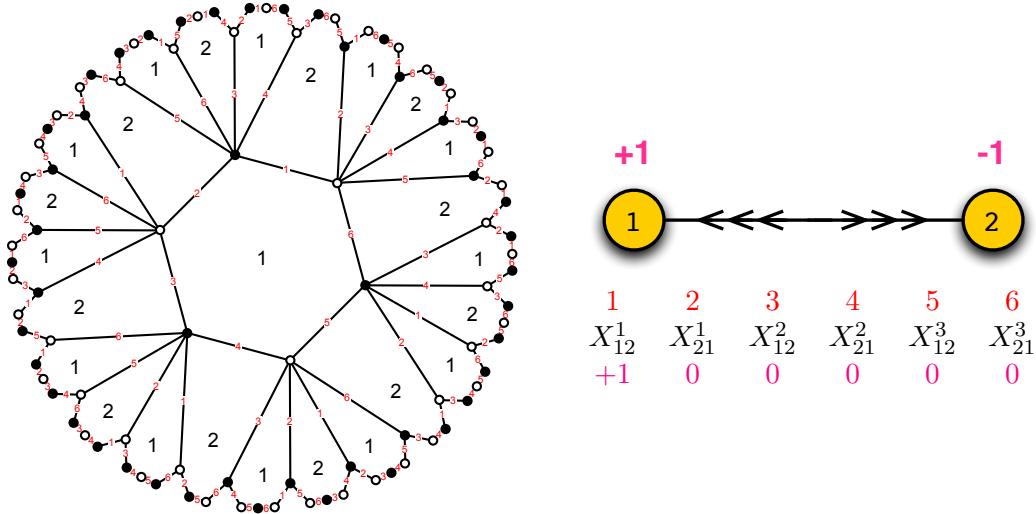
Figure 5.42: The Model 6.2b brane tiling with level assignment on the quiver and bi-fundamental fields.

Let us consider as a quick example Model 6.2b in section §5.3.2 with the mesonic moduli space being a non-complete intersection Calabi-Yau 5-fold. This model is a generalised conifold and we can assign levels ± 1 to the two gauge groups of the theory as illustrated in Figure 5.42. This for instance can be achieved by assigning the level $+1$ to the bifundamental X_{12}^1 and by assigning level 0 to all other bifundamental fields. By adopting the forward algorithm for Chern-Simons brane tilings [63, 64, 194, 137, 166][3], the level matrix C then is

$$C = \left(\begin{array}{c|cc} & U(1)_1 & U(1)_2 \\ \hline & 1 & 1 \\ & 1 & -1 \end{array} \right) , \tag{5.4.164}$$

---

[3] *cf.* forward algorithm for 4d quiver gauge theories in section §1.4.4.

and

$$d = \tilde{Q} \cdot P^t \ , \ \ Q_F = \ker(P) \ , \ \ Q_D = \ker(C) \cdot \tilde{Q} \ ,$$
$$Q_t = (Q_F \ Q_D) \rightarrow G_t = \ker(Q_t) \ . \tag{5.4.165}$$

Accordingly, with the above level assignment C, the $g = 2$ brane tiling of Model 6.2b gives the charge matrices

$$Q_F = 0 \ , \ \ \tilde{Q} = \begin{pmatrix} 1 & 1 & 1 & -1 & -1 & -1 \\ -1 & -1 & -1 & 1 & 1 & 1 \end{pmatrix} \ , \ \ Q_D = 0 \ , \tag{5.4.166}$$

and hence the toric diagram

$$G_t = \begin{pmatrix} 1 & 0 & 0 & 0 & 0 & 0 \\ 0 & 1 & 0 & 0 & 0 & 0 \\ 0 & 0 & 1 & 0 & 0 & 0 \\ 0 & 0 & 0 & 1 & 0 & 0 \\ 0 & 0 & 0 & 0 & 1 & 0 \\ 0 & 0 & 0 & 0 & 0 & 1 \end{pmatrix} \ . \tag{5.4.167}$$

This is the toric diagram for $\mathbb{C}^6$, the unit 5-simplex. We see here the precise analogue of obtaining the $\mathbb{C}^4$ mesonic moduli space by assigning Chern-Simons levels to the conifold theory.

With our classification of the first few $g = 2$ brane tilings we have paved the path for new exciting problems. Most importantly, we have obtained a new class of quiver gauge theories which exhibit interesting moduli spaces. We plan to report on more progress in the near future.

6 Overall Discussion and Future Directions

There is a plethora of problems that relate to brane tilings, and the selection of topics which are presented in this work can only be thought of as the tip of the iceberg. During the short excursion on the landscape of problems related to brane tilings, we have encountered new challenges that require ongoing investigation. Let us summarise in this final section the open problems and future challenges related to brane tilings that have been mentioned in the chapters above.

- *Counting Orbifolds beyond $\mathbb{C}^D/\Gamma$.* The counting of distinct Abelian orbifolds in chapter §2 is restricted to the case of $\mathbb{C}^3$ and more generally to $\mathbb{C}^D$. In the case for toric Calabi-Yau 3-folds where the orbifolds directly correspond to brane tilings, it is of great interest to consider and to count distinct Abelian orbifolds of various other toric Calabi-Yau 3-folds. A counting for the case of Abelian orbifolds of the conifold and SPP has been proposed in [126], and an unpublished work [146] in collaboration with Amihay Hanany aims to describe a parameterisation of such Abelian orbifolds that can be directly translated for the construction of the corresponding brane tilings. Additionally, a yet not fully investigated problem regards the finite group that needs to be used in conjunction with Polya's Enumeration Theorem in order to count distinct Abelian orbifolds of any toric Calabi-Yau 3-fold.

- *A classification beyond reflexive polygons.* Reflexive polygons are convex lattice polygons with a single interior lattice point. One can now define a convex polygon with precisely I interior points. Not only is it a problem to identify how many such distinct polygons exist for a given I, but also how many brane tilings there are which have them as toric diagrams. This is a natural generalisation of the problem solved for reflexive polygons in chapter §3. Such a general classification of brane tilings would enable us to generate via specular duality brane tilings on genus $g = I$ Riemann surfaces.

- *Specular duality and the master space for non-Abelian brane tilings.* In chapter §4, specular duality has only been studied by computing the master spaces of brane tilings with only $U(1)$ gauge groups. By computing the master spaces of

322
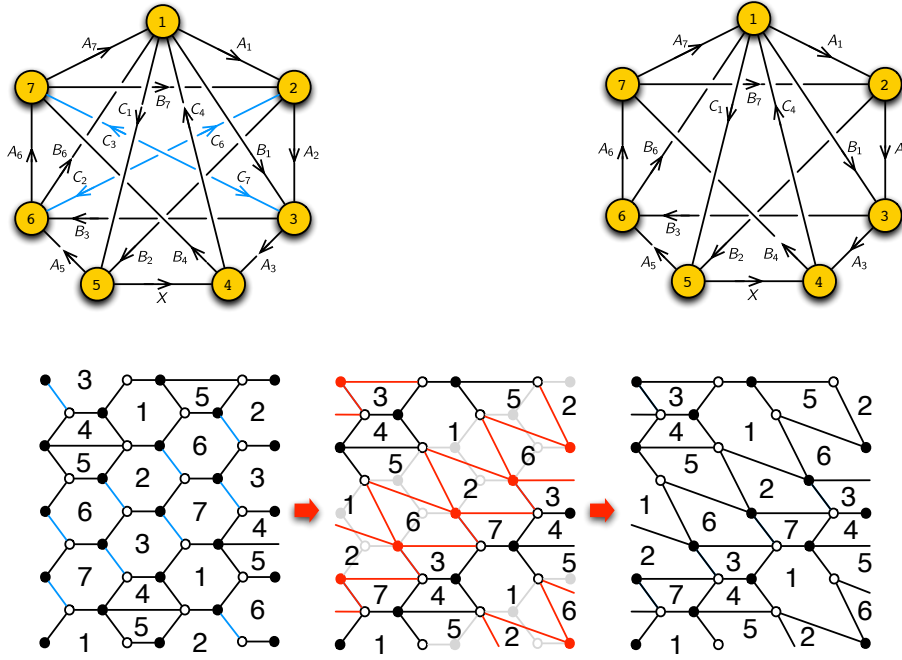
Figure 6.1: *Mass deformation.* The deformation of the brane tiling of Model 5 (PdP$_{4b}$) to Model 6a (PdP$_{4a}$). The corresponding quiver diagrams differ by a pair of bi-directional arrows corresponding to bifundamental fields between two gauge groups.

brane tilings with non-Abelian gauge groups, we hope to obtain more knowledge about this new correspondence between brane tilings. In particular, the aim is to compute the Hilbert series for non-Abelian brane tilings which correspond to reflexive polygons.

- *Open questions regarding brane tilings on Riemann surfaces.* The brane tilings on $g = 2$ Riemann surfaces that are identified in chapter §5 have been studied as supersymmetric field theories with $U(1)$ gauge groups. It is of great importance to study the field theory properties of the new brane tilings on higher genus Riemann surfaces, and furthermore to understand the underlying brane construction of these brane tilings. Interesting preliminary work has been done in [200] and it is of great interest to investigate this problem further in the near future.

This work has also omitted a range of the author's published and yet unpublished ongoing research on brane tilings. The following selection of topics gives a taste of the problems that are currently investigated:

- *Mass deformations of brane tilings.* On a closer inspection of the classification of brane tilings related to reflexive polygons in chapter §3, one notices a set of

brane tilings whose quiver diagrams contain bi-directional arrows between two vertices of the quiver. When these two bifundamental fields are removed from the quiver diagram, one obtains a new quiver diagram which intriguingly corresponds to another brane tiling with a reflexive toric diagram. In a collaboration with Massimo Bianchi, Stefano Cremonesi, Amihay Hanany, Francisco Morales and Daniel Ricci Pacifici, this new type of deformation – a mass deformation of brane tilings – is investigated [201] and will lead soon to a new publication. Figure 6.1 shows an example of a mass deformation of the brane tiling of Model 5 (PdP_{4b}) to Model 6a (PdP_{4a}).
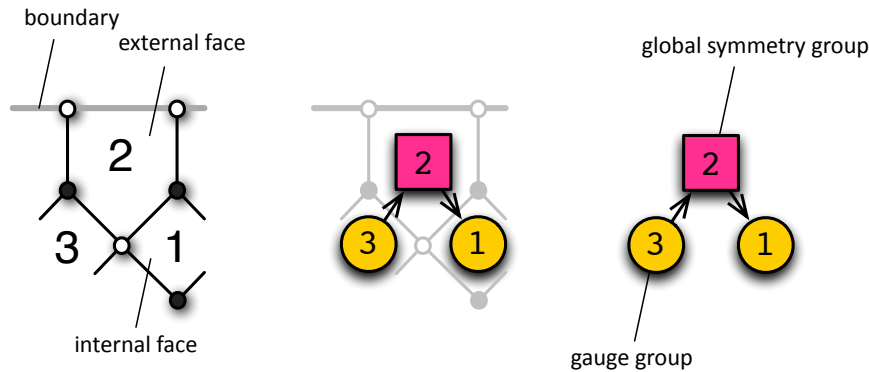
Figure 6.2: *A section of a bipartite graph and its corresponding quiver.* On the gauge theory side, internal and external faces correspond to global and gauge symmetry groups, respectively.

- *Brane tilings on Riemann surfaces with boundaries.* In chapter §5, we have classified brane tilings on $g = 2$ Riemann surfaces. In [198] as well as in a collaboration with Sebastian Franco and Daniele Galloni [8], brane tilings on Riemann surfaces with boundaries are proposed. With white and black nodes ending on the boundaries, we introduce a distinction between a face that is adjacent to a boundary and a face which is adjacent to only faces. These so called external and internal faces are interpreted in the bipartite graph respectively as global and gauge groups of the corresponding quiver theory as shown in Figure 6.2. By using the extended dictionary for these brane tilings, one generates a new class of interesting field theories which have been named bipartite field theories in [198, 8]. Their mesonic moduli spaces have been studied extensively in [8] and it is of great interest to analyse the corresponding Hilbert series in future studies. Moreover, a brane picture for these bipartite graphs on Riemann surfaces with boundaries is still under review and work in progress. We hope to report on new results in the near future.

The above list of problems and future research directions is a small selection of the new ideas generated by studying brane tilings. The interaction between physics and mathematics is a fruitful enterprise and brane tilings are at a pivotal junction for exchange of ideas between these two vast areas of research. It is of great interest to study the above problems and new results will be reported in future publications.

Appendix

A.1 $\mathbb{C}^3$ Orbifold Index

This section is an extract from [1] which was written in collaboration with John Davey and Amihay Hanany.

In the toric diagram triangles, lattice points on the edges of the triangle are colored yellow and lattice points enclosed by the triangle boundary are colored green (Tables 8-14). The column multiplicty indicates the number of Hermite Normal Forms corresponding to the particular toric diagram.

#	N	Orbifold	Orbifold Action	Toric Diagram	Multiplicity
(1.1)	1	$\mathbb{C}^3/\mathbb{Z}_1$	$\begin{pmatrix} (0,0,0) \\ (0,0,0) \end{pmatrix}$		1
(2.1)	2	$\mathbb{C}^3/\mathbb{Z}_2$	$\begin{pmatrix} (0,1,1) \\ (0,0,0) \end{pmatrix}$		3

Table A.1: Orbifold Actions and corresponding Toric Diagrams for $\mathbb{C}^3/\Gamma_N$ orbifolds with order $N = 1 \ldots 10$ **(Part 1/6)**.

#	N	Orbifold	Orbifold Action	Toric Diagram	Multiplicity
(3.1)	3	$\mathbb{C}^3/\mathbb{Z}_3$	$\begin{pmatrix} (0,1,2) \\ (0,0,0) \end{pmatrix}$		3
(3.2)	3	$\mathbb{C}^3/\mathbb{Z}_3$	$\begin{pmatrix} (1,1,1) \\ (0,0,0) \end{pmatrix}$		1
(4.1)	4	$\mathbb{C}^3/\mathbb{Z}_4$	$\begin{pmatrix} (0,1,3) \\ (0,0,0) \end{pmatrix}$		3
(4.2)	4	$\mathbb{C}^3/\mathbb{Z}_4$	$\begin{pmatrix} (1,1,2) \\ (0,0,0) \end{pmatrix}$		3
(4.3)	4	$\mathbb{C}^3/\mathbb{Z}_2 \times \mathbb{Z}_2$	$\begin{pmatrix} (1,0,1) \\ (0,1,1) \end{pmatrix}$		1
(5.1)	5	$\mathbb{C}^3/\mathbb{Z}_5$	$\begin{pmatrix} (0,1,4) \\ (0,0,0) \end{pmatrix}$		3

Table A.2: Orbifold Actions and corresponding Toric Diagrams for $\mathbb{C}^3/\Gamma_N$ orbifolds with order $N = 1 \dots 10$ **(Part 2/6)**.

#	N	Orbifold	Orbifold Action	Toric Diagram	Multiplicity
(5.2)	5	$\mathbb{C}^3/\mathbb{Z}_5$	$\begin{pmatrix} (1,1,3) \\ (0,0,0) \end{pmatrix}$		3
(6.1)	6	$\mathbb{C}^3/\mathbb{Z}_6$	$\begin{pmatrix} (0,1,5) \\ (0,0,0) \end{pmatrix}$		3
(6.2)	6	$\mathbb{C}^3/\mathbb{Z}_6$	$\begin{pmatrix} (1,1,4) \\ (0,0,0) \end{pmatrix}$		3
(6.3)	6	$\mathbb{C}^3/\mathbb{Z}_6$	$\begin{pmatrix} (1,2,3) \\ (0,0,0) \end{pmatrix}$		6
(7.1)	7	$\mathbb{C}^3/\mathbb{Z}_7$	$\begin{pmatrix} (0,1,6) \\ (0,0,0) \end{pmatrix}$		3
(7.2)	7	$\mathbb{C}^3/\mathbb{Z}_7$	$\begin{pmatrix} (1,1,5) \\ (0,0,0) \end{pmatrix}$		3

Table A.3: Orbifold Actions and corresponding Toric Diagrams for $\mathbb{C}^3/\Gamma_N$ orbifolds with order $N = 1 \ldots 10$ **(Part 3/6)**.

#	N	Orbifold	Orbifold Action	Toric Diagram	Multiplicity
(7.3)	7	$\mathbb{C}^3/\mathbb{Z}_7$	$\begin{pmatrix} (1,2,4) \\ (0,0,0) \end{pmatrix}$		2
(8.1)	8	$\mathbb{C}^3/\mathbb{Z}_8$	$\begin{pmatrix} (0,1,7) \\ (0,0,0) \end{pmatrix}$		3
(8.2)	8	$\mathbb{C}^3/\mathbb{Z}_8$	$\begin{pmatrix} (1,1,6) \\ (0,0,0) \end{pmatrix}$		3
(8.3)	8	$\mathbb{C}^3/\mathbb{Z}_8$	$\begin{pmatrix} (1,2,5) \\ (0,0,0) \end{pmatrix}$		3
(8.4)	8	$\mathbb{C}^3/\mathbb{Z}_8$	$\begin{pmatrix} (1,3,4) \\ (0,0,0) \end{pmatrix}$		3
(8.5)	8	$\mathbb{C}^3/\mathbb{Z}_4 \times \mathbb{Z}_2$	$\begin{pmatrix} (1,0,3) \\ (0,1,1) \end{pmatrix}$		3

Table A.4: Orbifold Actions and corresponding Toric Diagrams for $\mathbb{C}^3/\Gamma_N$ orbifolds with order $N = 1 \ldots 10$ **(Part 4/6)**.

#	N	Orbifold	Orbifold Action	Toric Diagram	Multiplicity
(9.1)	9	$\mathbb{C}^3/\mathbb{Z}_9$	$\begin{pmatrix} (0,1,8) \\ (0,0,0) \end{pmatrix}$		3
(9.2)	9	$\mathbb{C}^3/\mathbb{Z}_9$	$\begin{pmatrix} (1,1,7) \\ (0,0,0) \end{pmatrix}$		3
(9.3)	9	$\mathbb{C}^3/\mathbb{Z}_9$	$\begin{pmatrix} (1,2,6) \\ (0,0,0) \end{pmatrix}$		6
(9.4)	9	$\mathbb{C}^3/\mathbb{Z}_3 \times \mathbb{Z}_3$	$\begin{pmatrix} (0,1,2) \\ (1,0,2) \end{pmatrix}$		1
(10.1)	10	$\mathbb{C}^3/\mathbb{Z}_{10}$	$\begin{pmatrix} (0,1,9) \\ (0,0,0) \end{pmatrix}$		3
(10.2)	10	$\mathbb{C}^3/\mathbb{Z}_{10}$	$\begin{pmatrix} (1,1,8) \\ (0,0,0) \end{pmatrix}$		3

Table A.5: Orbifold Actions and corresponding Toric Diagrams for $\mathbb{C}^3/\Gamma_N$ orbifolds with order $N = 1 \ldots 10$ **(Part 5/6)**.

#	N	Orbifold	Orbifold Action	Toric Diagram	Multiplicity
(10.3)	10	$\mathbb{C}^3/\mathbb{Z}_{10}$	$\begin{pmatrix} (1,2,7) \\ (0,0,0) \end{pmatrix}$		6
(10.4)	10	$\mathbb{C}^3/\mathbb{Z}_{10}$	$\begin{pmatrix} (1,4,5) \\ (0,0,0) \end{pmatrix}$		6

Table A.6: Orbifold Actions and corresponding Toric Diagrams for $\mathbb{C}^3/\Gamma_N$ orbifolds with order $N = 1 \ldots 10$ **(Part 6/6)**.

A.2 $\mathbb{C}^4$ Orbifold Index

This section is an extract from [1] which was written in collaboration with John Davey and Amihay Hanany.

In the toric diagram tetrahedra, internal lattice points (I_3) are colored red, lattice points on the faces are colored green (I_2) and lattice points on edges are colored yellow (I_1) (Tables 15-24). The column multiplicty indicates the number of Hermite Normal Forms corresponding to the particular toric diagram.
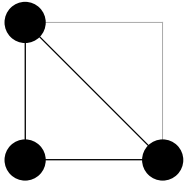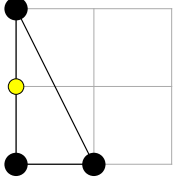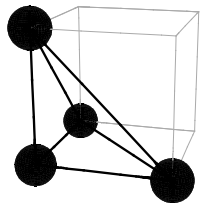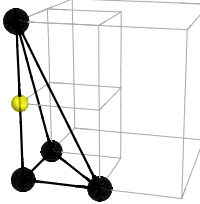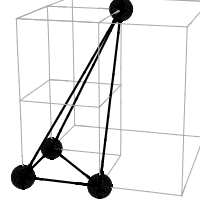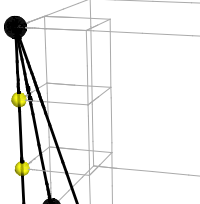
#	N	Orbifold	Orbifold Action	Toric Diagram	Multiplicity
(1.1)	1	$\mathbb{C}^4/\mathbb{Z}_1$	$\begin{pmatrix} (0,0,0,0) \\ (0,0,0,0) \\ (0,0,0,0) \end{pmatrix}$		1
(2.1)	2	$\mathbb{C}^4/\mathbb{Z}_2$	$\begin{pmatrix} (0,0,1,1) \\ (0,0,0,0) \\ (0,0,0,0) \end{pmatrix}$		6
(2.2)	2	$\mathbb{C}^4/\mathbb{Z}_2$	$\begin{pmatrix} (1,1,1,1) \\ (0,0,0,0) \\ (0,0,0,0) \end{pmatrix}$		1
(3.1)	3	$\mathbb{C}^4/\mathbb{Z}_3$	$\begin{pmatrix} (0,0,1,2) \\ (0,0,0,0) \\ (0,0,0,0) \end{pmatrix}$		6

Table A.7: Orbifold Actions and corresponding Toric Diagrams for $\mathbb{C}^4/\Gamma_N$ orbifolds with order $N = 1 \ldots 6$ (**Part 1/6**).

#	N	Orbifold	Orbifold Action	Toric Diagram	Multiplicity
(3.2)	3	$\mathbb{C}^4/\mathbb{Z}_3$	$\begin{pmatrix} (0,1,1,1) \\ (0,0,0,0) \\ (0,0,0,0) \end{pmatrix}$		4
(3.3)	3	$\mathbb{C}^4/\mathbb{Z}_3$	$\begin{pmatrix} (1,1,2,2) \\ (0,0,0,0) \\ (0,0,0,0) \end{pmatrix}$		3
(4.1)	4	$\mathbb{C}^4/\mathbb{Z}_4$	$\begin{pmatrix} (0,0,1,3) \\ (0,0,0,0) \\ (0,0,0,0) \end{pmatrix}$		6
(4.2)	4	$\mathbb{C}^4/\mathbb{Z}_4$	$\begin{pmatrix} (0,1,1,2) \\ (0,0,0,0) \\ (0,0,0,0) \end{pmatrix}$		12
(4.3)	4	$\mathbb{C}^4/\mathbb{Z}_4$	$\begin{pmatrix} (1,1,3,3) \\ (0,0,0,0) \\ (0,0,0,0) \end{pmatrix}$		3

Table A.8: Orbifold Actions and corresponding Toric Diagrams for $\mathbb{C}^4/\Gamma_N$ orbifolds with order $N = 1\ldots 6$ **(Part 2/6)**.
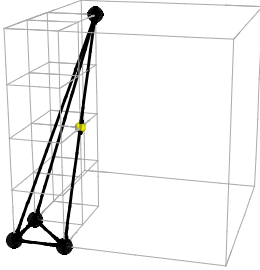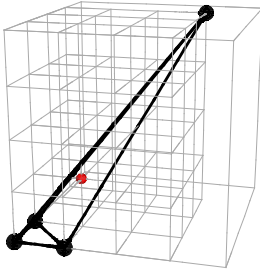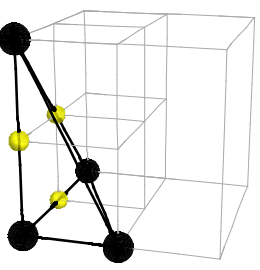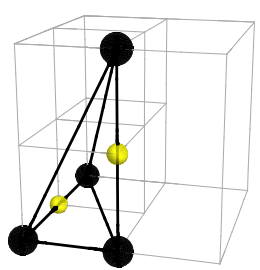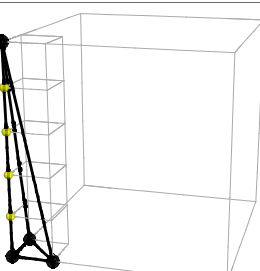
#	N	Orbifold	Orbifold Action	Toric Diagram	Multiplicity
(4.4)	4	$\mathbb{C}^4/\mathbb{Z}_4$	$\begin{pmatrix} (1,2,2,3) \\ (0,0,0,0) \\ (0,0,0,0) \end{pmatrix}$		6
(4.5)	4	$\mathbb{C}^4/\mathbb{Z}_4$	$\begin{pmatrix} (1,1,1,1) \\ (0,0,0,0) \\ (0,0,0,0) \end{pmatrix}$		1
(4.6)	4	$\mathbb{C}^4/\mathbb{Z}_2 \times \mathbb{Z}_2$	$\begin{pmatrix} (0,1,0,1) \\ (0,0,1,1) \\ (0,0,0,0) \end{pmatrix}$		4
(4.7)	4	$\mathbb{C}^4/\mathbb{Z}_2 \times \mathbb{Z}_2$	$\begin{pmatrix} (0,0,1,1) \\ (1,1,1,1) \\ (0,0,0,0) \end{pmatrix}$		3
(5.1)	5	$\mathbb{C}^4/\mathbb{Z}_5$	$\begin{pmatrix} (0,0,1,4) \\ (0,0,0,0) \\ (0,0,0,0) \end{pmatrix}$		6

Table A.9: Orbifold Actions and corresponding Toric Diagrams for $\mathbb{C}^4/\Gamma_N$ orbifolds with order $N = 1\ldots 6$ **(Part 3/6)**.
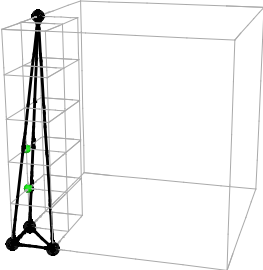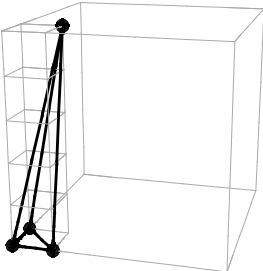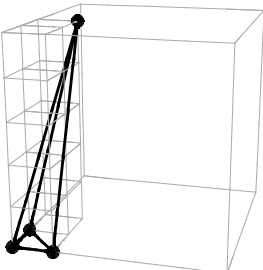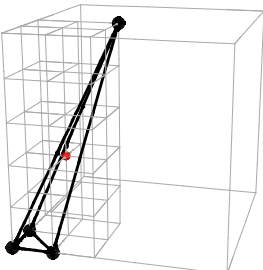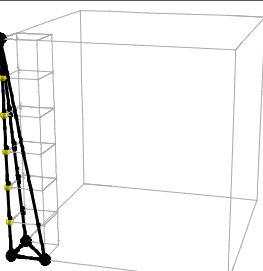
#	N	Orbifold	Orbifold Action	Toric Diagram	Multiplicity
(5.2)	5	$\mathbb{C}^4/\mathbb{Z}_5$	$\begin{pmatrix} (0,1,1,3) \\ (0,0,0,0) \\ (0,0,0,0) \end{pmatrix}$		12
(5.3)	5	$\mathbb{C}^4/\mathbb{Z}_5$	$\begin{pmatrix} (1,1,4,4) \\ (0,0,0,0) \\ (0,0,0,0) \end{pmatrix}$		3
(5.4)	5	$\mathbb{C}^4/\mathbb{Z}_5$	$\begin{pmatrix} (1,2,3,4) \\ (0,0,0,0) \\ (0,0,0,0) \end{pmatrix}$		6
(5.5)	5	$\mathbb{C}^4/\mathbb{Z}_5$	$\begin{pmatrix} (1,1,1,2) \\ (0,0,0,0) \\ (0,0,0,0) \end{pmatrix}$		4
(6.1)	6	$\mathbb{C}^4/\mathbb{Z}_6$	$\begin{pmatrix} (0,0,1,5) \\ (0,0,0,0) \\ (0,0,0,0) \end{pmatrix}$		6

Table A.10: Orbifold Actions and corresponding Toric Diagrams for $\mathbb{C}^4/\Gamma_N$ orbifolds with order $N = 1 \ldots 6$ **(Part 4/6)**.
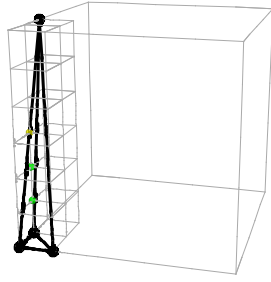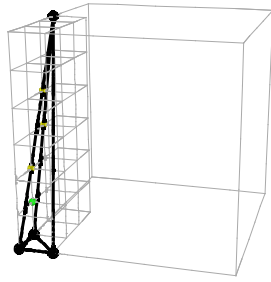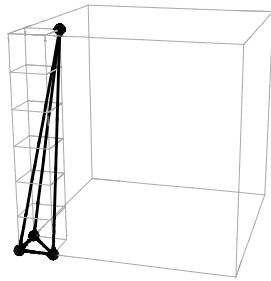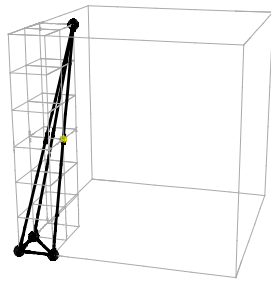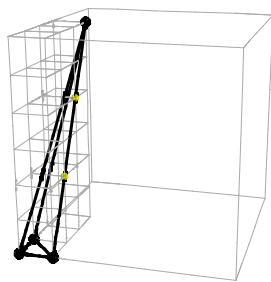
#	N	Orbifold	Orbifold Action	Toric Diagram	Multiplicity
(6.2)	6	$\mathbb{C}^4/\mathbb{Z}_6$	$\begin{pmatrix} (0,1,1,4) \\ (0,0,0,0) \\ (0,0,0,0) \end{pmatrix}$		12
(6.3)	6	$\mathbb{C}^4/\mathbb{Z}_6$	$\begin{pmatrix} (0,1,2,3) \\ (0,0,0,0) \\ (0,0,0,0) \end{pmatrix}$		24
(6.4)	6	$\mathbb{C}^4/\mathbb{Z}_6$	$\begin{pmatrix} (1,1,5,5) \\ (0,0,0,0) \\ (0,0,0,0) \end{pmatrix}$		3
(6.5)	6	$\mathbb{C}^4/\mathbb{Z}_6$	$\begin{pmatrix} (1,1,2,2) \\ (0,0,0,0) \\ (0,0,0,0) \end{pmatrix}$		12
(6.6)	6	$\mathbb{C}^4/\mathbb{Z}_6$	$\begin{pmatrix} (1,3,3,5) \\ (0,0,0,0) \\ (0,0,0,0) \end{pmatrix}$		6

Table A.11: Orbifold Actions and corresponding Toric Diagrams for $\mathbb{C}^4/\Gamma_N$ orbifolds with order $N = 1 \ldots 6$ **(Part 5/6)**.
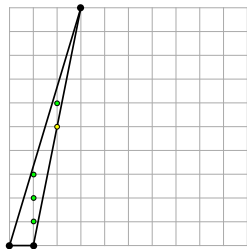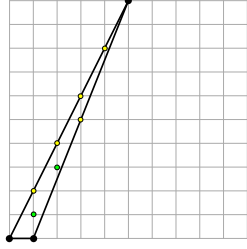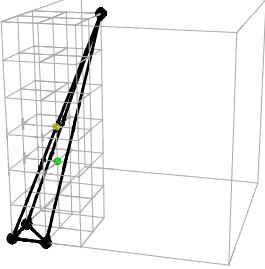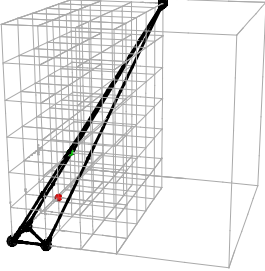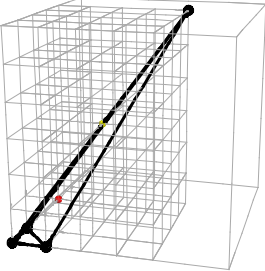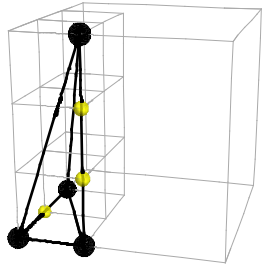
#	N	Orbifold	Orbifold Action	Toric Diagram	Multiplicity
(6.7)	6	$\mathbb{C}^4/\mathbb{Z}_6$	$\begin{pmatrix} (1,3,4,4) \\ (0,0,0,0) \\ (0,0,0,0) \end{pmatrix}$		12
(6.8)	6	$\mathbb{C}^4/\mathbb{Z}_6$	$\begin{pmatrix} (1,1,1,3) \\ (0,0,0,0) \\ (0,0,0,0) \end{pmatrix}$		4
(6.9)	6	$\mathbb{C}^4/\mathbb{Z}_6$	$\begin{pmatrix} (1,2,4,5) \\ (0,0,0,0) \\ (0,0,0,0) \end{pmatrix}$		6
(6.10)	6	$\mathbb{C}^4/\mathbb{Z}_6$	$\begin{pmatrix} (2,3,3,4) \\ (0,0,0,0) \\ (0,0,0,0) \end{pmatrix}$		6

Table A.12: Orbifold Actions and corresponding Toric Diagrams for $\mathbb{C}^4/\Gamma_N$ orbifolds with order $N = 1\ldots 6$ **(Part 6/6)**.

A.3 Examples of Identifying Symmetries using Barycentric Coordinates

This section is an extract from [2] written under collaboration with Amihay Hanany.

A.3.1 Example: Lattice Triangles corresponding to Abelian Orbifolds of $\mathbb{C}^3$

Consider the orbifold of the form $\mathbb{C}^3/\mathbb{Z}_7$ with the orbifold actions

$$A_1 = \begin{pmatrix} (1,1,5) \\ (0,0,0) \end{pmatrix}, \quad A_2 = \begin{pmatrix} (1,2,4) \\ (0,0,0) \end{pmatrix}. \qquad (A.3.1)$$

The scaled Toric Diagram. The corresponding toric 2-simplices are shown in Figure A.1 with each having $|I_2| = 3$ internal lattice points colored green in the diagram.
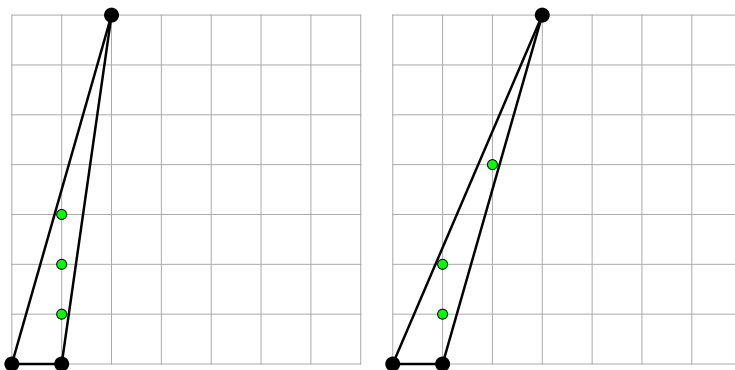
Figure A.1: Toric triangles of $\mathbb{C}^3/\mathbb{Z}_7$ with scaling $s_2 = 1$ corresponding to orbifold actions $A_1 = ((1,1,5),(0,0,0))$ and $A_2 = ((1,2,4),(0,0,0))$ respectively. Internal toric points $w_k \in I_2$ are colored green.

There are no lattice points on the edges of the toric diagrams in Figure A.1, $|I_1| = \emptyset$. To make them 'visible' for the purpose of obtaining the topological character of the toric diagram, we increase the scaling to $s_1 = 2$. This results in the toric diagrams in Figure A.2. Accordingly, the overall scaling coefficient required for the computation of the topological character is $s = \max(s_1, s_2) = \max(2, 1) = 2$.

The Topological Character. Let us call the toric triangles corresponding to the orbifold actions A_1 and A_2 as σ_1^2 and σ_2^2 respectively. The respective topological char-

338
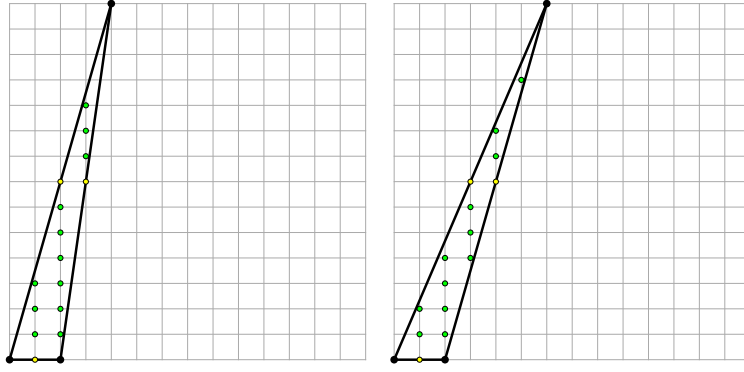
Figure A.2: Toric triangles of $\mathbb{C}^3/\mathbb{Z}_7$ with scaling $s_1 = 2$ corresponding to orbifold actions $A_1 = ((1,1,5),(0,0,0))$ and $A_2 = ((1,2,4),(0,0,0))$ respectively. Lattice points on edges are colored yellow (I_1) and internal toric points (I_2) are colored green.

acters τ_1 and τ_2 are

$$
\tau_1 = \left\{ \underbrace{(0,0,1),(0,1,0),(1,0,0),}_{I_0} \right.
$$

$$
\underbrace{\left(0,\frac{1}{2},\frac{1}{2}\right),\left(\frac{1}{2},0,\frac{1}{2}\right),\left(\frac{1}{2},\frac{1}{2},0\right),}_{I_1}
$$

$$
\underbrace{\left(\frac{1}{14},\frac{5}{14},\frac{4}{7}\right),\left(\frac{4}{7},\frac{5}{14},\frac{1}{14}\right),\left(\frac{1}{7},\frac{3}{14},\frac{9}{14}\right),\left(\frac{9}{14},\frac{3}{14},\frac{1}{7}\right),\left(\frac{3}{14},\frac{1}{14},\frac{5}{7}\right),\left(\frac{5}{7},\frac{1}{14},\frac{3}{14}\right),}_{I_2}
$$

$$
\underbrace{\left(\frac{1}{7},\frac{5}{7},\frac{1}{7}\right),\left(\frac{2}{7},\frac{3}{7},\frac{2}{7}\right),\left(\frac{3}{7},\frac{1}{7},\frac{3}{7}\right)\left(\frac{1}{14},\frac{6}{7},\frac{1}{14}\right),\left(\frac{3}{14},\frac{4}{7},\frac{3}{14}\right),\left(\frac{5}{14},\frac{2}{7},\frac{5}{14}\right)}_{I_2} \right\},
$$

$$(A.3.2)$$

339

and

$$\tau_2 = \left\{ \underbrace{(0,0,1),(0,1,0),(1,0,0),}_{I_0} \right.$$

$$\underbrace{\left(0,\frac{1}{2},\frac{1}{2}\right),\left(\frac{1}{2},0,\frac{1}{2}\right),\left(\frac{1}{2},\frac{1}{2},0\right),}_{I_1}$$

$$\underbrace{\left(\frac{1}{14},\frac{2}{7},\frac{9}{14}\right),\left(\frac{2}{7},\frac{9}{14},\frac{1}{14}\right),\left(\frac{9}{14},\frac{1}{14},\frac{2}{7}\right),\left(\frac{1}{14},\frac{11}{14},\frac{1}{7}\right),\left(\frac{1}{7},\frac{1}{14},\frac{11}{14}\right),\left(\frac{11}{14},\frac{1}{7},\frac{1}{14}\right),}_{I_2}$$

$$\left. \underbrace{\left(\frac{1}{7},\frac{4}{7},\frac{2}{7}\right),\left(\frac{4}{7},\frac{2}{7},\frac{1}{7}\right),\left(\frac{2}{7},\frac{1}{7},\frac{4}{7}\right),\left(\frac{3}{14},\frac{5}{14},\frac{3}{7}\right),\left(\frac{5}{14},\frac{3}{7},\frac{3}{14}\right),\left(\frac{3}{7},\frac{3}{14},\frac{5}{14}\right)}_{I_2} \right\}.$$

(A.3.3)

The elements of the characters above are barycentric coordinates of the topologically important points in I_0, I_1 and I_2 with an overall scaling $s = 2$.

The Symmetries. The orbifold dimension is $D = 3$. Accordingly, we consider cycles of S_3 corresponding to $C_{(1)(2)(3)}$, $C_{(1\ 2\ 3)}$, $C_{(1\ 3\ 2)}$, $C_{(2\ 3)(1)}$, $C_{(1\ 3)(2)}$ and $C_{(1\ 2)(3)}$.
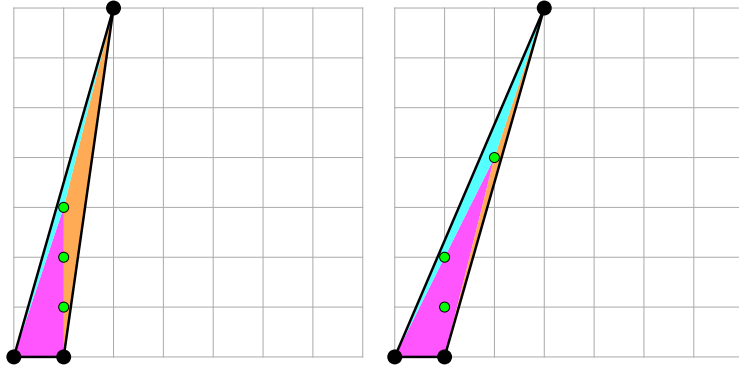
Figure A.3: Toric triangles of $\mathbb{C}^3/\mathbb{Z}_7$ with scaling $s_2 = 1$ corresponding to orbifold actions $A_1 = ((1,1,5),(0,0,0))$ and $A_2 = ((1,2,4),(0,0,0))$ respectively. For the diagram of A_1 on the left, the sub-triangles with areas proportional to the barycentric coordinates of the internal point $\left(\frac{3}{7},\frac{1}{7},\frac{3}{7}\right) \in I_2(f_{s_2=1}(\sigma_1^2))$ are colored magenta $\left(\frac{3}{7}\right)$, cyan $\left(\frac{1}{7}\right)$ and orange $\left(\frac{3}{7}\right)$. For the diagram of A_2, the sub-triangles with areas proportional to the barycentric coordinates of the internal point $\left(\frac{4}{7},\frac{2}{7},\frac{1}{7}\right) \in I_2(f_{s_2=1}(\sigma_2^2))$ are colored magenta $\left(\frac{4}{7}\right)$, cyan $\left(\frac{2}{7}\right)$ and orange $\left(\frac{1}{7}\right)$.

Picking the transformation $C_{(1\ 3)(2)}$, we observe its action on the barycentric coordinates $\left(\frac{3}{7},\frac{1}{7},\frac{3}{7}\right) \in I_2(f_{s_2=1}(\sigma_1^2))$ of an internal point from the first toric simplex σ_1^2

and the barycentric coordinates $\left(\frac{4}{7}, \frac{2}{7}, \frac{1}{7}\right) \in I_2(f_{s_2=1}(\sigma_2^2))$ of an internal point from the second toric simplex σ_2^2. As shown in Figure A.3, the chosen internal points divide the toric triangles into three sub-triangles each corresponding to one component of the barycentric coordinates.

The transformation $C_{(1\ 3)(2)}$ swaps the barycentric coordinates axes $\hat{v}_1$ and $\hat{v}_3$ such that $C_{(1\ 3)(2)} : \left(\frac{3}{7}, \frac{1}{7}, \frac{3}{7}\right) \mapsto \left(\frac{3}{7}, \frac{1}{7}, \frac{3}{7}\right)$ and $C_{(1\ 3)(2)} : \left(\frac{4}{7}, \frac{2}{7}, \frac{1}{7}\right) \mapsto \left(\frac{1}{7}, \frac{2}{7}, \frac{4}{7}\right)$. This transformation corresponds to swapping the cyan and orange colored sub-triangles in Figure A.3. $C_{(1\ 3)(2)}$ leaves the internal point $\left(\frac{3}{7}, \frac{1}{7}, \frac{3}{7}\right)$ of σ_1^2 invariant. In comparison, $C_{(1\ 3)(2)}$ maps the internal point $\left(\frac{4}{7}, \frac{2}{7}, \frac{1}{7}\right)$ to a different point $\left(\frac{1}{7}, \frac{2}{7}, \frac{4}{7}\right)$ which is in fact not an element of the original topological character of σ_2^2 in (A.3.3). Accordingly, $C_{(1\ 3)(2)}$ is not a symmetry of σ_2^2 and the corresponding orbifold with action A_2. In contrast, it turns out that τ_2 is invariant under $C_{(1\ 3)(2)}$. Accordingly, $C_{(1\ 3)(2)}$ is a symmetry of σ_1^2.

A.3.2 Example: Lattice Tetrahedra corresponding to Abelian Orbifolds of $\mathbb{C}^4$

Let us proceed with the abelian orbifold of the form $\mathbb{C}^4/\mathbb{Z}_6$ and orbifold action

$$A = \begin{pmatrix} (0,1,1,4) \\ (0,0,0,0) \\ (0,0,0,0) \end{pmatrix} . \tag{A.3.4}$$

The scaled Toric Diagram. The corresponding toric tetrahedron σ^3 for (A.3.4) is shown in Figure A.4. With unit scaling $s_1 = s_2 = 1$ there is $|I_1| = 1$ lattice point on an edge and $|I_2| = 2$ lattice points on the faces of the toric tetrahedron. For internal lattice points, we need to scale the tetrahedron with $s_3 = 2$ such that $|I_3| = 2$. Accordingly, the optimal scaling coefficient for σ^3 is $s = \max(s_1, s_2, s_3) = \max(1, 1, 2) = 2$.
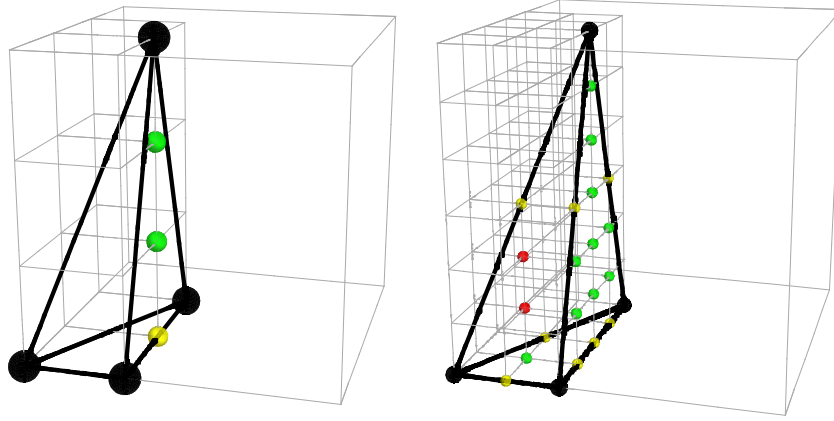
Figure A.4: Toric tetrahedra $\sigma^3 = f_1(\sigma^3)$ and $f_2(\sigma^3)$ of $\mathbb{C}^4/\mathbb{Z}_6$ corresponding to orbifold action $A = ((0,1,1,4),(0,0,0,0),(0,0,0,0))$ with optimal scaling $s_1 = s_2 = 1$ for edge $I_1(\sigma^3)$ and face $I_2(\sigma^3)$ points, and optimal scaling $s_3 = 2$ for internal points $I_3(f_2(\sigma^3))$. Internal lattice points are colored red, while edge and face points are colored yellow and green respectively.

The Topological Character. The topological character of σ^3 is

$$
\tau(\sigma^3) = \left\{ \begin{array}{l}
\underbrace{(0,0,0,1),(0,0,1,0),(0,1,0,0),(1,0,0,0),}_{I_0} \\[2mm]
\underbrace{\left(0,0,\frac{1}{2},\frac{1}{2}\right),\left(0,\frac{1}{2},\frac{1}{2},0\right),\left(\frac{1}{2},\frac{1}{2},0,0\right),\left(0,\frac{1}{2},0,\frac{1}{2}\right),}_{I_1} \\[2mm]
\underbrace{\left(\frac{1}{2},0,\frac{1}{2},0\right),\left(\frac{1}{2},0,0,\frac{1}{2}\right),\left(0,\frac{1}{4},\frac{3}{4},0\right),\left(0,\frac{3}{4},\frac{1}{4},0\right),}_{I_1} \\[2mm]
\underbrace{\left(0,\frac{1}{4},\frac{1}{4},\frac{1}{2}\right),\left(\frac{1}{2},\frac{1}{4},\frac{1}{4},0\right),\left(\frac{1}{6},\frac{1}{6},\frac{2}{3},0\right),\left(\frac{1}{6},\frac{2}{3},\frac{1}{6},0\right),}_{I_2} \\[2mm]
\underbrace{\left(\frac{2}{3},\frac{1}{6},\frac{1}{6},0\right),\left(\frac{1}{3},\frac{1}{3},\frac{1}{3},0\right),\left(\frac{1}{3},\frac{1}{12},\frac{7}{12},0\right),\left(\frac{1}{3},\frac{7}{12},\frac{1}{12},0\right),}_{I_2} \\[2mm]
\underbrace{\left(\frac{1}{6},\frac{5}{12},\frac{5}{12},0\right),\left(\frac{5}{6},\frac{1}{12},\frac{1}{12},0\right),}_{I_2}\underbrace{\left(\frac{1}{6},\frac{1}{6},\frac{1}{6},\frac{1}{2}\right),\left(\frac{1}{3},\frac{1}{12},\frac{1}{12},\frac{1}{2}\right)}_{I_3}
\end{array} \right\}.
$$

(A.3.5)

The Symmetries. Let us pick the lattice point on a face with barycentric coordinates $\left(\frac{2}{3},\frac{1}{6},\frac{1}{6},0\right) \in I_2$ as shown in Figure A.5. The face point divides the tetrahedron into four sub-tetrahedra with volumes corresponding to $\left(\frac{2}{3},\frac{1}{6},\frac{1}{6},0\right)$. One sub-tetrahedron

has zero volume, the other three have normalized volumes $\frac{2}{3}$, $\frac{1}{6}$ and $\frac{1}{6}$ colored magenta, cyan and orange respectively in Figure A.5.
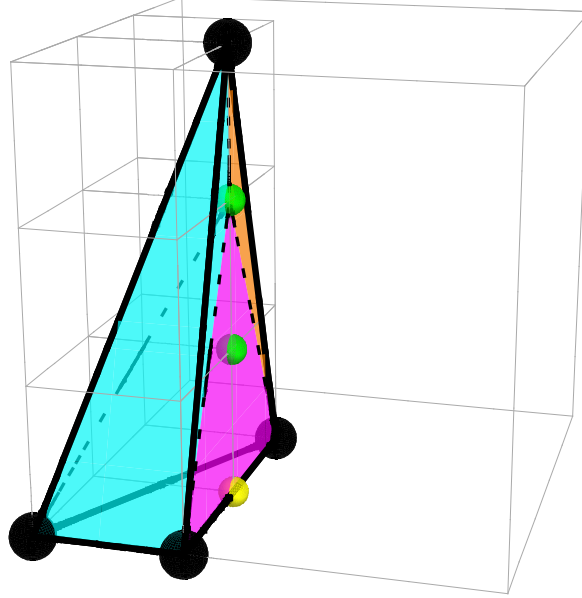
Figure A.5: Toric tetrahedra of $\mathbb{C}^4/\mathbb{Z}_6$ corresponding to orbifold action $A_3 = ((0,1,1,5),(0,0,0,0),(0,0,0,0))$ with optimal scaling $s_2 = 1$. The face point with barycentric coordinates $\left(\frac{2}{3}, \frac{1}{6}, \frac{1}{6}, 0\right)$ divides the tetrahedron into four sub-tetrahedra with one having a nil volume. The other three sub-tetrahedra have volumes $\frac{2}{3}$ (magenta), $\frac{1}{6}$ (cyan) and $\frac{1}{6}$ (orange).

Let us pick the S_4 transformation $C_{(1\ 3\ 4\ 2)}$ which acts on the barycentric coordinates axes $\{\hat{v}_1, \hat{v}_2, \hat{v}_3, \hat{v}_4\}$ as $C_{(1\ 3\ 4\ 2)} : [\hat{v}_1, \hat{v}_2, \hat{v}_3, \hat{v}_4] \mapsto [\hat{v}_3, \hat{v}_1, \hat{v}_4, \hat{v}_2]$. The transformation corresponds to a cyclic permutation of the sub-tetrahedra in Figure A.5. $C_{(1\ 3\ 4\ 2)}$ transforms the face point $\left(\frac{2}{3}, \frac{1}{6}, \frac{1}{6}, 0\right)$ into $\left(\frac{1}{6}, \frac{2}{3}, 0, \frac{1}{6}\right)$ which is not an element of the topological character $\tau(\sigma^3)$ in (A.3.5). Accordingly, the lattice simplex σ^3 and its corresponding orbifold action A are not symmetric under $C_{(3\ 1\ 2\ 4)}$.

Another transformation is $C_{(2\ 3)(1)(4)}$. It leaves the barycentric coordinates of the face point $\left(\frac{2}{3}, \frac{1}{6}, \frac{1}{6}, 0\right)$ invariant. In fact, the entire topological character $\tau(\sigma^3)$ is invariant under $C_{(2\ 3)(1)(4)}$. Accordingly, $C_{(2\ 3)(1)(4)}$ is a symmetry of the lattice simplex σ^3 and its corresponding orbifold action A.

A.4 The theory for $\mathbb{C}^3/\mathbb{Z}_4 \times \mathbb{Z}_4$ $(1,0,3)(0,1,3)$

This section is an extract from [5] written under collaboration with Amihay Hanany.
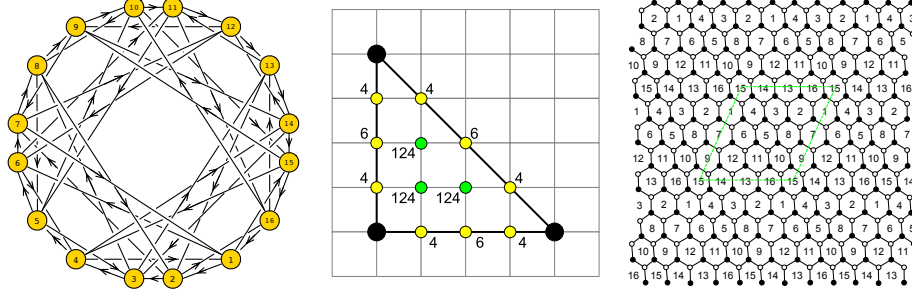
Figure A.6: The quiver, toric diagram, and brane tiling of the abelian orbifold of the form $\mathbb{C}^3/\mathbb{Z}_4 \times \mathbb{Z}_4$ with orbifold action $(1,0,3)(0,1,3)$.

The quiver, toric diagram and brane tiling of $\mathbb{C}^3/\mathbb{Z}_4 \times \mathbb{Z}_4$ $(1,0,3)(0,1,3)$ theory are shown in Figure A.6 with the superpotential[1] having the form

$$
\begin{aligned}
W \quad = \quad & +X_{7\,8}\,X_{8\,2}\,X_{2\,7} + X_{12\,9}\,X_{9\,7}\,X_{7\,12} + X_{13\,14}\,X_{14\,12}\,X_{12\,13} + X_{2\,3}\,X_{3\,13}\,X_{13\,2} \\
& +X_{8\,5}\,X_{5\,3}\,X_{3\,8} + X_{9\,10}\,X_{10\,8}\,X_{8\,9} + X_{14\,15}\,X_{15\,9}\,X_{9\,14} + X_{3\,4}\,X_{4\,14}\,X_{14\,3} \\
& +X_{5\,6}\,X_{6\,4}\,X_{4\,5} + X_{10\,11}\,X_{11\,5}\,X_{5\,10} + X_{15\,16}\,X_{16\,10}\,X_{10\,15} + X_{4\,1}\,X_{1\,15}\,X_{15\,4} \\
& +X_{6\,7}\,X_{7\,1}\,X_{1\,6} + X_{11\,12}\,X_{12\,6}\,X_{6\,11} + X_{16\,13}\,X_{13\,11}\,X_{11\,16} + X_{1\,2}\,X_{2\,16}\,X_{16\,1} \\
& -X_{7\,8}\,X_{8\,9}\,X_{9\,7} - X_{12\,9}\,X_{9\,14}\,X_{14\,12} - X_{13\,14}\,X_{14\,3}\,X_{3\,13} - X_{2\,3}\,X_{3\,8}\,X_{8\,2} \\
& -X_{8\,5}\,X_{5\,10}\,X_{10\,8} - X_{9\,10}\,X_{10\,15}\,X_{15\,9} - X_{14\,15}\,X_{15\,4}\,X_{4\,14} - X_{3\,4}\,X_{4\,5}\,X_{5\,3} \\
& -X_{5\,6}\,X_{6\,11}\,X_{11\,5} - X_{10\,11}\,X_{11\,16}\,X_{16\,10} - X_{15\,16}\,X_{16\,1}\,X_{1\,15} - X_{4\,1}\,X_{1\,6}\,X_{6\,4} \\
& -X_{6\,7}\,X_{7\,12}\,X_{12\,6} - X_{11\,12}\,X_{12\,13}\,X_{13\,11} - X_{16\,13}\,X_{13\,2}\,X_{2\,16} - X_{1\,2}\,X_{2\,7}\,X_{7\,1}\ .
\end{aligned}
$$

$$\text{(A.4.6)}$$

A.5 Hilbert series of $^{\mathrm{Irr}}\mathcal{F}^\flat$ for Models 13 and 15b

This section is an extract from [5] written under collaboration with Amihay Hanany.

The refined Hilbert series of the master space of Model 15b, and by specular duality

---

[1]Note: The superpotential features an overall trace which is not explicitly written down in the following discussion.

of the master space of Model 13, is of the form

$$g_1(t_i, y_{s_i}; {}^{\mathrm{Irr}}\mathcal{F}_{15b}^{\flat}) = \frac{P(t_i, y_{s_i})}{(1 - t_1 t_2 y_{s_3})(1 - t_2 t_3 y_{s_3})(1 - t_1 t_4 y_{s_3})(1 - t_2 t_4 y_{s_3})}$$
$$\times \frac{1}{(1 - t_1 s_1 y_{s_4})(1 - t_2 s_1 y_{s_4})(1 - t_1 y_{s_2} y_{s_4})(1 - t_2 y_{s_2} y_{s_4})}$$
$$\times \frac{1}{(1 - t_3 y_{s_1} y_{s_5})(1 - t_4 y_{s_1} y_{s_5})(1 - t_3 y_{s_2} y_{s_5})(1 - t_4 y_{s_2} y_{s_5})} ,$$

$$(\text{A.5.7})$$

where the numerator is

$P(t_i, s_i) =$

$1 - t_1 t_2 t_3 t_4 y_{s_3}^2 - t_1 t_2 t_3 y_{s_1} y_{s_3} y_{s_4} - t_1 t_2 t_4 y_{s_1} y_{s_3} y_{s_4} - t_1 t_2 t_3 y_{s_2} y_{s_3} y_{s_4} - t_1 t_2 t_4 y_{s_2} y_{s_3} y_{s_4}$

$+ t_1^2 t_2 t_3 t_4 y_{s_1} y_{s_3}^2 y_{s_4} + t_1 t_2^2 t_3 t_4 y_{s_1} y_{s_3}^2 y_{s_4} + t_1^2 t_2 t_3 t_4 y_{s_2} y_{s_3}^2 y_{s_4} + t_1 t_2^2 t_3 t_4 y_{s_2} y_{s_3}^2 y_{s_4} - t_1 t_2 y_{s_1} y_{s_2} y_{s_4}^2$

$+ t_1^2 t_2 t_3 y_{s_1} y_{s_2} y_{s_3} y_{s_4}^2 + t_1 t_2^2 t_3 y_{s_1} y_{s_2} y_{s_3} y_{s_4}^2 + t_1^2 t_2 t_4 y_{s_1} y_{s_2} y_{s_3} y_{s_4}^2 + t_1 t_2^2 t_4 y_{s_1} y_{s_2} y_{s_3} y_{s_4}^2 - t_1^3 t_2 t_3 t_4 y_{s_1} y_{s_2} y_{s_3}^2 y_{s_4}^2$

$- t_1^2 t_2^2 t_3 t_4 y_{s_1} y_{s_2} y_{s_3}^2 y_{s_4}^2 - t_1 t_2^3 t_3 t_4 y_{s_1} y_{s_2} y_{s_3}^2 y_{s_4}^2 - t_1 t_3 t_4 y_{s_1} y_{s_3} y_{s_5} - t_2 t_3 t_4 y_{s_1} y_{s_3} y_{s_5} - t_1 t_3 t_4 y_{s_2} y_{s_3} y_{s_5}$

$- t_2 t_3 t_4 y_{s_2} y_{s_3} y_{s_5} + t_1 t_2 t_3^2 t_4 y_{s_1} y_{s_3}^2 y_{s_5} + t_1 t_2 t_3 t_4^2 y_{s_1} y_{s_3}^2 y_{s_5} + t_1 t_2 t_3^2 t_4 y_{s_2} y_{s_3}^2 y_{s_5} + t_1 t_2 t_3 t_4^2 y_{s_2} y_{s_3}^2 y_{s_5}$

$- t_1 t_3 y_{s_1} y_{s_2} y_{s_4} y_{s_5} - t_2 t_3 y_{s_1} y_{s_2} y_{s_4} y_{s_5} - t_1 t_4 y_{s_1} y_{s_2} y_{s_4} y_{s_5} - t_2 t_4 y_{s_1} y_{s_2} y_{s_4} y_{s_5} + t_1 t_2 t_3 t_4 y_{s_1}^2 y_{s_3} y_{s_4} y_{s_5}$

$+ t_1 t_2 t_3^2 y_{s_1} y_{s_2} y_{s_3} y_{s_4} y_{s_5} + t_1^2 t_3 t_4 y_{s_1} y_{s_2} y_{s_3} y_{s_4} y_{s_5} + 5 t_1 t_2 t_3 t_4 y_{s_1} y_{s_2} y_{s_3} y_{s_4} y_{s_5} + t_2^2 t_3 t_4 y_{s_1} y_{s_2} y_{s_3} y_{s_4} y_{s_5}$

$+ t_1 t_2 t_4^2 y_{s_1} y_{s_2} y_{s_3} y_{s_4} y_{s_5} + t_1 t_2 t_3 t_4 y_{s_2}^2 y_{s_3} y_{s_4} y_{s_5} - t_1^2 t_2 t_3^2 t_4 y_{s_1} y_{s_2} y_{s_3}^2 y_{s_4} y_{s_5} - t_1 t_2^2 t_3^2 t_4 y_{s_1} y_{s_2} y_{s_3}^2 y_{s_4} y_{s_5}$

$- t_1^2 t_2 t_3 t_4^2 y_{s_1} y_{s_2} y_{s_3}^2 y_{s_4} y_{s_5} - t_1 t_2^2 t_3 t_4^2 y_{s_1} y_{s_2} y_{s_3}^2 y_{s_4} y_{s_5} - t_1^2 t_2^2 t_3 t_4 y_{s_1}^2 y_{s_3}^3 y_{s_4} y_{s_5} - t_1^2 t_2^2 t_3 t_4 y_{s_1} y_{s_2} y_{s_3}^3 y_{s_4} y_{s_5}$

$- t_1^2 t_2^2 t_3 t_4 y_{s_2}^2 y_{s_3}^3 y_{s_4} y_{s_5} + t_1 t_2 t_3 y_{s_1}^2 y_{s_2} y_{s_4}^2 y_{s_5} + t_1 t_2 t_4 y_{s_1}^2 y_{s_2} y_{s_4}^2 y_{s_5} + t_1 t_2 t_3 y_{s_1} y_{s_2}^2 y_{s_4}^2 y_{s_5}$

$+ t_1 t_2 t_4 y_{s_1} y_{s_2}^2 y_{s_4}^2 y_{s_5} - t_1^2 t_2 t_3 t_4 y_{s_1}^2 y_{s_2} y_{s_3} y_{s_4}^2 y_{s_5} - t_1 t_2^2 t_3 t_4 y_{s_1}^2 y_{s_2} y_{s_3} y_{s_4}^2 y_{s_5} - t_1^2 t_2 t_3 t_4 y_{s_1} y_{s_2}^2 y_{s_3} y_{s_4}^2 y_{s_5}$

$- t_1 t_2^2 t_3 t_4 y_{s_1} y_{s_2}^2 y_{s_3} y_{s_4}^2 y_{s_5} - t_1^2 t_2^2 t_3 t_4 y_{s_1}^2 y_{s_2} y_{s_3}^2 y_{s_4}^2 y_{s_5} - t_1^2 t_2^2 t_3 t_4 y_{s_1} y_{s_2}^2 y_{s_3}^2 y_{s_4}^2 y_{s_5} - t_1^2 t_2^2 t_3 t_4 y_{s_1} y_{s_2}^2 y_{s_3}^2 y_{s_4}^2 y_{s_5}$

$- t_1^2 t_2^2 t_3 t_4 y_{s_1} y_{s_2}^2 y_{s_3}^2 y_{s_4}^2 y_{s_5} + t_1^3 t_2^2 t_3^2 t_4 y_{s_1}^2 y_{s_2} y_{s_3}^3 y_{s_4}^2 y_{s_5} + t_1^2 t_2^3 t_3^2 t_4 y_{s_1}^2 y_{s_2} y_{s_3}^3 y_{s_4}^2 y_{s_5} + t_1^3 t_2^2 t_3^2 t_4 y_{s_1} y_{s_2}^2 y_{s_3}^3 y_{s_4}^2 y_{s_5}$

$+ t_1^2 t_2^3 t_3^2 t_4 y_{s_1} y_{s_2}^2 y_{s_3}^3 y_{s_4}^2 y_{s_5} - t_1^2 t_2^3 y_{s_1}^2 y_{s_2}^2 y_{s_3} y_{s_4}^3 y_{s_5} - t_1^2 t_2 t_3 t_4 y_{s_1}^2 y_{s_2}^2 y_{s_3} y_{s_4}^3 y_{s_5} - t_1^2 t_2^4 y_{s_1}^2 y_{s_2}^2 y_{s_3} y_{s_4}^3 y_{s_5}$

$+ t_1^3 t_2^2 t_3 t_4 y_{s_1}^2 y_{s_2}^2 y_{s_3}^2 y_{s_4}^3 y_{s_5} + t_1^3 t_2^2 t_3 t_4 y_{s_1} y_{s_2}^2 y_{s_3}^2 y_{s_4}^3 y_{s_5} + t_1^3 t_2^2 t_3 t_4 y_{s_1} y_{s_2}^2 y_{s_3}^2 y_{s_4}^3 y_{s_5} + t_1^3 t_2^2 t_3 t_4 y_{s_1} y_{s_2}^2 y_{s_3}^2 y_{s_4}^3 y_{s_5}$

$- t_1^2 t_2^3 t_3^2 t_4 y_{s_1} y_{s_2}^2 y_{s_3}^2 y_{s_4}^3 y_{s_5} - t_3 t_4 y_{s_1} y_{s_2} y_{s_5}^2 + t_1 t_3^3 t_4 y_{s_1} y_{s_2} y_{s_3} y_{s_5}^2 + t_2 t_3^3 t_4 y_{s_1} y_{s_2} y_{s_3} y_{s_5}^2$

$+ t_1 t_3 t_4^2 y_{s_1} y_{s_2} y_{s_3} y_{s_5}^2 + t_2 t_3 t_4^2 y_{s_1} y_{s_2} y_{s_3} y_{s_5}^2 - t_1 t_2 t_3^3 t_4 y_{s_1} y_{s_2} y_{s_3}^2 y_{s_5}^2 - t_1 t_2 t_3^2 t_4^2 y_{s_1} y_{s_2} y_{s_3}^2 y_{s_5}^2$

$- t_1 t_2 t_3 t_4^3 y_{s_1} y_{s_2} y_{s_3}^2 y_{s_5}^2 + t_1 t_3 t_4 y_{s_1}^2 y_{s_2} y_{s_4} y_{s_5}^2 + t_2 t_3 t_4 y_{s_1}^2 y_{s_2} y_{s_4} y_{s_5}^2 + t_1 t_3 t_4 y_{s_1} y_{s_2}^2 y_{s_4} y_{s_5}^2$

$+ t_2 t_3 t_4 y_{s_1} y_{s_2}^2 y_{s_4} y_{s_5}^2 - t_1 t_2 t_3^2 t_4 y_{s_1}^2 y_{s_2} y_{s_3} y_{s_4} y_{s_5}^2 - t_1 t_2 t_3 t_4^2 y_{s_1}^2 y_{s_2} y_{s_3} y_{s_4} y_{s_5}^2 - t_1 t_2 t_3^2 t_4 y_{s_1} y_{s_2}^2 y_{s_3} y_{s_4} y_{s_5}^2$

$- t_1 t_2 t_3 t_4^2 y_{s_1} y_{s_2}^2 y_{s_3} y_{s_4} y_{s_5}^2 - t_1^2 t_2^3 t_4^2 y_{s_1} y_{s_2}^2 y_{s_3}^2 y_{s_4} y_{s_5}^2 - t_1 t_2 t_3^2 t_4^2 y_{s_1} y_{s_2}^2 y_{s_3}^2 y_{s_4} y_{s_5}^2 - t_1^2 t_2 t_3^2 t_4 y_{s_1} y_{s_2}^2 y_{s_3}^2 y_{s_4} y_{s_5}^2$

$+ t_1^2 t_2^2 t_3^2 t_4 y_{s_1} y_{s_2}^2 y_{s_3}^2 y_{s_4} y_{s_5}^2 - t_1 t_2 t_3 t_4 y_{s_1}^3 y_{s_2} y_{s_4}^2 y_{s_5}^2 - t_1 t_2 t_3 t_4 y_{s_1}^2 y_{s_2}^2 y_{s_4}^2 y_{s_5}^2 - t_1 t_2 t_3 t_4 y_{s_1} y_{s_2}^3 y_{s_4}^2 y_{s_5}^2$

$- t_1^2 t_2 t_3 t_4 y_{s_1}^2 y_{s_2}^2 y_{s_3} y_{s_4}^2 y_{s_5}^2 - t_1 t_2^2 t_3 t_4 y_{s_1}^2 y_{s_2}^2 y_{s_3} y_{s_4}^2 y_{s_5}^2 - t_1^2 t_2 t_3 t_4 y_{s_1} y_{s_2}^2 y_{s_3} y_{s_4}^2 y_{s_5}^2 - t_1 t_2^2 t_3 t_4 y_{s_1} y_{s_2}^2 y_{s_3} y_{s_4}^2 y_{s_5}^2$

$+ t_1^2 t_2^2 t_3^2 t_4 y_{s_1}^3 y_{s_2} y_{s_3}^2 y_{s_4}^2 y_{s_5}^2 + t_1^2 t_2^3 t_4 y_{s_1}^2 y_{s_2}^2 y_{s_3}^2 y_{s_4}^2 y_{s_5}^2 + t_1^3 t_2 t_3 t_4 y_{s_1}^2 y_{s_2}^2 y_{s_3}^2 y_{s_4}^2 y_{s_5}^2 + 5 t_1^2 t_2^2 t_3 t_4 y_{s_1}^2 y_{s_2}^2 y_{s_3}^2 y_{s_4}^2 y_{s_5}^2$

$+ t_1 t_2^3 t_3 t_4 y_{s_1}^2 y_{s_2}^2 y_{s_3}^2 y_{s_4}^2 y_{s_5}^2 + t_1^2 t_2^3 t_4 y_{s_1} y_{s_2}^3 y_{s_3}^2 y_{s_4}^2 y_{s_5}^2 + t_1^2 t_2^2 t_3 t_4 y_{s_1} y_{s_2}^3 y_{s_3}^2 y_{s_4}^2 y_{s_5}^2 - t_1^3 t_2^3 t_3^2 t_4 y_{s_1}^2 y_{s_2}^2 y_{s_3}^3 y_{s_4}^2 y_{s_5}^2$

$- t_1^3 t_2^3 t_3^2 t_4 y_{s_1}^2 y_{s_2}^2 y_{s_3}^3 y_{s_4}^2 y_{s_5}^2 - t_1^3 t_2^3 t_3^2 t_4 y_{s_1}^2 y_{s_2}^2 y_{s_3}^3 y_{s_4}^2 y_{s_5}^2 - t_1^3 t_2^3 t_3^2 t_4 y_{s_1}^2 y_{s_2}^2 y_{s_3}^3 y_{s_4}^2 y_{s_5}^2 + t_1^2 t_2^3 t_4 y_{s_1}^3 y_{s_2}^2 y_{s_3} y_{s_4}^3 y_{s_5}^2$

$+ t_1^2 t_2^3 t_4 y_{s_1}^3 y_{s_2}^2 y_{s_3} y_{s_4}^3 y_{s_5}^2 + t_1^2 t_2^3 t_4 y_{s_1}^2 y_{s_2}^3 y_{s_3} y_{s_4}^3 y_{s_5}^2 + t_1^2 t_2^3 t_3 t_4 y_{s_1}^2 y_{s_2}^3 y_{s_3} y_{s_4}^3 y_{s_5}^2 - t_1^3 t_2^2 t_3^2 t_4 y_{s_1}^2 y_{s_2}^2 y_{s_3}^3 y_{s_4}^3 y_{s_5}^2$

$- t_1^2 t_3^2 t_3^2 t_4 y_{s_1}^3 y_{s_2}^2 y_{s_3}^3 y_{s_4}^2 y_{s_5}^2 - t_1^2 t_2^3 t_3^2 t_4 y_{s_1}^2 y_{s_2}^3 y_{s_3}^3 y_{s_4}^2 y_{s_5}^2 - t_1^3 t_2^3 t_3^2 t_4 y_{s_1}^2 y_{s_2}^2 y_{s_3}^3 y_{s_4}^3 y_{s_5}^2 - t_1^2 t_2^3 t_3^2 t_4 y_{s_1}^3 y_{s_2}^2 y_{s_3} y_{s_4}^3 y_{s_5}^2$

$$-t_1t_2t_3^2t_4^2y_{s_1}^2y_{s_2}^2y_{s_3}y_{s_4}y_{s_5}^3 - t_2^2t_3^2t_4^2y_{s_1}^2y_{s_2}^2y_{s_3}y_{s_4}y_{s_5}^3 + t_1^2t_2t_3^3t_4^2y_{s_1}^2y_{s_2}^2y_{s_3}^2y_{s_4}y_{s_5}^3 + t_1t_2t_3^3t_4^2y_{s_1}^2y_{s_2}^2y_{s_3}^2y_{s_4}y_{s_5}^3$$
$$+t_1^2t_2t_3^3t_4^2y_{s_1}^2y_{s_2}^2y_{s_3}^2y_{s_4}y_{s_5}^3 + t_1t_2^2t_3^3t_4^2y_{s_1}^2y_{s_2}^2y_{s_3}^2y_{s_4}y_{s_5}^3 - t_1^2t_2^2t_3^3t_4^2y_{s_1}^2y_{s_2}^2y_{s_3}^3y_{s_4}y_{s_5}^3 + t_1^2t_2t_3^2t_4^2y_{s_1}^3y_{s_2}^2y_{s_3}y_{s_4}^2y_{s_5}^3$$
$$+t_1t_2^2t_3^2t_4^2y_{s_1}^3y_{s_2}^2y_{s_3}y_{s_4}^2y_{s_5}^3 + t_1^2t_2t_3^2t_4^2y_{s_1}^3y_{s_2}^2y_{s_3}y_{s_4}^2y_{s_5}^3 + t_1t_2^2t_3^2t_4^2y_{s_1}^3y_{s_2}^2y_{s_3}y_{s_4}^2y_{s_5}^3 - t_1^2t_2^2t_3^3t_4^2y_{s_1}^3y_{s_2}^2y_{s_3}^2y_{s_4}^2y_{s_5}^3$$
$$-t_1^2t_2^2t_3^3t_4^2y_{s_1}^3y_{s_2}^2y_{s_3}^2y_{s_4}^2y_{s_5}^3 - t_1^2t_2^2t_3^3t_4^2y_{s_1}^3y_{s_2}^2y_{s_3}^2y_{s_4}^2y_{s_5}^3 - t_1^2t_2^2t_3^3t_4^2y_{s_1}^3y_{s_2}^2y_{s_3}^2y_{s_4}^2y_{s_5}^3 - t_1^2t_2^2t_3^3t_4^2y_{s_1}^3y_{s_2}^2y_{s_3}^3y_{s_4}^3y_{s_5}^3$$
$$+t_1^3t_2^3t_3^3t_4^3y_{s_1}^3y_{s_2}^3y_{s_3}^3y_{s_4}^3y_{s_5}^3 \; .$$

$$\text{(A.5.8)}$$

A.6 Summary of restricted $g = 2$ Brane Tilings

This section is an extract from [9] written under collaboration with Stefano Cremonesi and Amihay Hanany.

E.T#	Brane Tiling	Quiver & Superpotential & $\mathcal{M}^{mes}$
5.2		 $W = (1\,2\,3\,4\,5) - (5\,4\,3\,2\,1)$ $\mathcal{M}^{mes} = \mathbb{C}^5$ $\eta_i = ((5\,4),(4\,3),(3\,2),(2\,1),(1\,5))$
6.2a		 $W = (1\,2\,3\,4\,5\,6) - (2\,4\,6\,5\,1\,3)$ $\mathcal{M}^{mes} = \mathbb{C}^5$ $\eta_i = ((6\,5),(3\,2),(5\,1\,2\,4),(4\,6\,1\,3))$
6.2b		 $W = (1\,2\,3\,4\,5\,6) - (2\,1\,4\,3\,6\,5)$ $\mathcal{M}^{mes} = NC1$ $\eta_i = ((6\,5),(4\,3),(2\,1),(5\,2\,3\,6\,1\,4))$
6.2c		 $W = (1\,2\,3\,4\,5\,6) - (6\,5\,4\,3\,2\,1)$ $\mathcal{M}^{mes} = NC1$ $\eta_i = ((6\,5),(5\,4),(4\,3),(3\,2),(2\,1),(1\,6))$

Table A.13: Restricted $g = 2$ brane tilings **(1/4)**.

E.T#	Brane Tiling	Quiver & Superpotential & $\mathcal{M}^{mes}$
7.2		$W = (1\ 2\ 3\ 4\ 5\ 6\ 7) - (1\ 3\ 2\ 4\ 7\ 6\ 5)$ $\mathcal{M}^{mes} = \mathbb{C}^2 \times \mathcal{C}$ $\eta_i = ((7\ 6),(6\ 5),(3\ 2),(5\ 1\ 2\ 4),(4\ 7\ 1\ 3))$
7.4		$W = (1\ 2\ 3\ 4) + (5\ 6\ 7)$ $\quad -(1\ 5\ 7) - (2\ 6\ 4\ 3)$ $\mathcal{M}^{mes} = \mathbb{C} \times \mathcal{M}_{3,2}$ $\eta_i = ((5\ 7),(4\ 3),(3\ 2),(7\ 1\ 2\ 6),(6\ 4\ 1\ 5))$
8.2a		$W = (1\ 2\ 3\ 4\ 5\ 6\ 7\ 8) - (1\ 4\ 3\ 2\ 5\ 8\ 7\ 6)$ $\mathcal{M}^{mes} = NC2$ $\eta_i = ((8\ 7),(7\ 6),(4\ 3),(3\ 2),$ $\quad (6\ 1\ 2\ 5),(5\ 8\ 1\ 4))$
8.2b		$W = (1\ 2\ 3\ 4\ 5\ 6\ 7\ 8) - (1\ 6\ 3\ 8\ 5\ 2\ 7\ 4)$ $\mathcal{M}^{mes} = NC3$ $\eta_i = ((8\ 5\ 6\ 3\ 4\ 1\ 2\ 7),(7\ 4\ 5\ 2\ 3\ 8\ 1\ 6))$
8.4a		$W = (1\ 2\ 3\ 4\ 5) + (6\ 7\ 8)$ $\quad -(1\ 3\ 2) - (4\ 6\ 8\ 7\ 5)$ $\mathcal{M}^{mes} = \mathcal{M}_{3,3}$ $\eta_i = ((8,7),(6\ 8),(5\ 4),(3\ 2),(2\ 1),$ $\quad (7\ 5\ 1\ 3\ 4\ 6))$

Table A.14: Restricted $g = 2$ brane tilings **(2/4)**.

E.T#	Brane Tiling	Quiver & Superpotential & $\mathcal{M}^{mes}$
8.4b		$W = (1\ 2\ 3\ 4\ 5) + (6\ 7\ 8)$ $\quad - (1\ 3\ 6) - (2\ 8\ 5\ 4\ 7)$ $\mathcal{M}^{mes} = \mathbb{C}^3 \times \mathbb{C}^2/\mathbb{Z}_2$ $\eta_i = ((5\ 4), (7\ 2\ 3\ 6), (6\ 1\ 2\ 8),$ $\quad (8\ 5\ 1\ 3\ 4\ 7))$
8.4c		$W = (1\ 2\ 3\ 4\ 5) + (6\ 7\ 8)$ $\quad - (1\ 5\ 6) - (2\ 8\ 7\ 4\ 3)$ $\mathcal{M}^{mes} = \mathbb{C}^3 \times \mathbb{C}^2/\mathbb{Z}_2$ $\eta_i = ((8\ 7), (4\ 3), (3\ 2), (1\ 5),$ $\quad (7\ 4\ 5\ 6), (6\ 1\ 2\ 8))$
8.4d		$W = (1\ 2\ 3\ 4\ 5) + (6\ 7\ 8)$ $\quad - (1\ 6\ 8) - (2\ 4\ 3\ 5\ 7)$ $\mathcal{M}^{mes} = \mathbb{C} \times \mathcal{M}_{3,2}$ $\eta_i = ((6\ 8), (4\ 3), (8\ 1\ 2\ 4\ 5\ 7),$ $\quad (7\ 2\ 3\ 5\ 1\ 6))$
8.4e		$W = (1\ 2\ 3\ 4\ 5) + (6\ 7\ 8)$ $\quad - (1\ 6\ 8) - (2\ 7\ 5\ 4\ 3)$ $\mathcal{M}^{mes} = NC4$ $\eta_i = ((8\ 1\ 5\ 4\ 3\ 2\ 1\ 6), (7\ 5\ 4\ 3\ 2\ 7\ 6\ 8))$
8.4f		$W = (1\ 2\ 3\ 4\ 5) + (6\ 7\ 8)$ $\quad - (1\ 5\ 4\ 6) - (2\ 8\ 7\ 3)$ $\mathcal{M}^{mes} = \mathcal{M}_{4,2}$ $\eta_i = ((8\ 7), (5\ 4), (3\ 2), (1\ 5),$ $\quad (7\ 3\ 4\ 6), (6\ 1\ 2\ 8))$

Table A.15: Restricted $g = 2$ brane tilings **(3/4)**.

E.T#	Brane Tiling	Quiver & Superpotential & $\mathcal{M}^{mes}$
8.4g		$W = (1\ 2\ 3\ 4) + (5\ 6\ 7\ 8)$ $\quad - (1\ 4\ 3\ 5) - (2\ 8\ 7\ 6)$ $\mathcal{M}^{mes} = NC5$ $\eta_i = ((8\ 7),(7\ 6),(4\ 3),(1\ 4),$ $\qquad (6\ 2\ 3\ 5),(5\ 1\ 2\ 8))$
8.4h		$W = (1\ 2\ 3\ 4) + (5\ 6\ 7\ 8)$ $\quad - (1\ 5\ 3\ 7) - (2\ 8\ 4\ 6)$ $\mathcal{M}^{mes} = NC4$ $\eta_i = ((8\ 4\ 1\ 5\ 6\ 2\ 3\ 7),(7\ 1\ 2\ 8\ 5\ 3\ 4\ 6))$

Table A.16: Restricted $g = 2$ brane tilings **(4/4)**.

A.7 Unrestricted Brane Tilings from Higgsing

This section is an extract from [9] written under collaboration with Stefano Cremonesi and Amihay Hanany.

E.T#	Brane Tiling	Quiver & Superpotential & $\mathcal{M}^{mes}$
5.2b*		$W = (1\ 4\ 5\ 3\ 2) - (1\ 2\ 5\ 4\ 3)$ $\mathcal{M}^{mes} = \mathbb{C}^5$ $\eta_i = ((5\ 4),(1\ 2),(4\ 3\ 2\ 5\ 3\ 1))$
5.2c*		$W = (1\ 2\ 3\ 5\ 4) - (1\ 3\ 4\ 2\ 5)$ $\mathcal{M}^{mes} = \mathbb{C}^5$ $\eta_i = ((5\ 1\ 2\ 5\ 4\ 2\ 3\ 4\ 1\ 3))$

Table A.17: Unrestricted $g = 2$ brane tilings from Higgsing **(1/3)**.

E.T#	Brane Tiling	Quiver & Superpotential & $\mathcal{M}^{mes}$
6.2d*		$W = (1\ 2\ 4\ 5\ 3\ 6) - (1\ 4\ 6\ 3\ 5\ 2)$ $\mathcal{M}^{mes} = \mathcal{C} \times \mathbb{C}^2$ $\eta_i = ((6\ 3), (3\ 5), (2\ 1), (5\ 2\ 4\ 6\ 1\ 4))$
6.2e*		$W = (1\ 2\ 4\ 6\ 3\ 5) - (1\ 4\ 5\ 2\ 3\ 6)$ $\mathcal{M}^{mes} = \mathcal{C} \times \mathbb{C}^2$ $\eta_i = ((3\ 6), (6\ 1\ 2\ 3\ 5\ 2\ 4\ 5\ 1\ 4))$
6.2f*		$W = (1\ 3\ 6\ 5\ 2\ 4) - (1\ 2\ 6\ 4\ 3\ 5)$ $\mathcal{M}^{mes} = \mathcal{C} \times \mathbb{C}^2$ $\eta_i = ((6\ 4\ 1\ 2\ 4\ 3), (5\ 1\ 3\ 5\ 2\ 6))$
7.2b*		$W = (1\ 5\ 2\ 6\ 3\ 7\ 4) - (1\ 4\ 3\ 6\ 2\ 7\ 5)$ $\mathcal{M}^{mes} = NC6$ $\eta_i = ((6\ 2), (5\ 1), (3\ 6), (1\ 4), (7\ 5\ 2\ 7\ 4\ 3))$
7.2c*		$W = (1\ 3\ 7\ 5\ 2\ 6\ 4) - (1\ 2\ 7\ 4\ 3\ 6\ 5)$ $\mathcal{M}^{mes} = NC1$ $\eta_i = ((7\ 4\ 1\ 2\ 6\ 5\ 2\ 7\ 5\ 1\ 3\ 6\ 4\ 3))$

Table A.18: Unrestricted $g = 2$ brane tilings from Higgsing **(2/3)**.
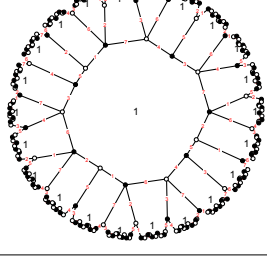
E.T#	Brane Tiling	Quiver & Superpotential & $\mathcal{M}^{mes}$
7.4b*		$W = (1\ 2\ 3) + (5\ 6\ 7\ 4)$ $\qquad - (5\ 7\ 6) - (1\ 3\ 2\ 4)$ $\mathcal{M}^{mes} = \mathcal{M}_{3,3}$ $\eta_i = ((7\ 6), (6\ 5), (3\ 2), (1\ 3), (5\ 7\ 4\ 1\ 2\ 4))$
7.4c*		$W = (1\ 2\ 3\ 4) + (5\ 6\ 7)$ $\qquad - (1\ 3\ 6\ 2) - (4\ 5\ 7)$ $\mathcal{M}^{mes} = \mathcal{M}_{3,2} \times \mathbb{C}$ $\eta_i = ((5\ 7), (2\ 1), (7\ 4\ 1\ 3\ 4\ 5\ 6\ 2\ 3\ 6))$
7.4d*		$W = (1\ 5\ 2) + (3\ 6\ 4\ 7)$ $\qquad - (3\ 5\ 4) - (1\ 7\ 2\ 6)$ $\mathcal{M}^{mes} = \mathcal{C} \times \mathbb{C}^2$ $\eta_i = ((7\ 2\ 1\ 7\ 3\ 5\ 2\ 6\ 4\ 3\ 6\ 1\ 5\ 4))$

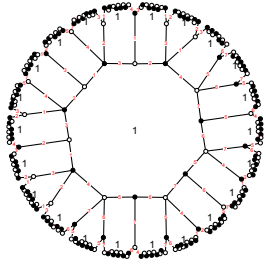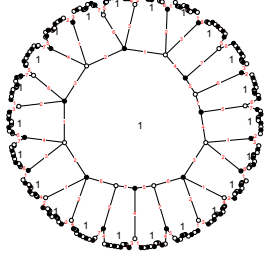Table A.19: Unrestricted $g = 2$ brane tilings from Higgsing **(3/3)**.

Bibliography

[1] J. Davey, A. Hanany, and R.-K. Seong, *Counting Orbifolds*, *JHEP* **06** (2010) 010, [arXiv:1002.3609].

[2] A. Hanany and R.-K. Seong, *Symmetries of Abelian Orbifolds*, *JHEP* **01** (2011) 027, [arXiv:1009.3017].

[3] J. Davey, A. Hanany, and R.-K. Seong, *An Introduction to Counting Orbifolds*, *Fortsch. Phys.* **59** (2011) 677–682, [arXiv:1102.0015].

[4] A. Hanany, V. Jejjala, S. Ramgoolam, and R.-K. Seong, *Calabi-Yau Orbifolds and Torus Coverings*, *JHEP* **09** (2011) 116, [arXiv:1105.3471].

[5] A. Hanany and R.-K. Seong, *Brane Tilings and Reflexive Polygons*, *Fortsch.Phys.* **60** (2012) 695–803, [arXiv:1201.2614].

[6] K. Hosomichi, R.-K. Seong, and S. Terashima, *Supersymmetric Gauge Theories on the Five-Sphere*, *Nucl.Phys.* **B865** (2012) 376–396, [arXiv:1203.0371].

[7] A. Hanany and R.-K. Seong, *Brane Tilings and Specular Duality*, *JHEP* **1208** (2012) 107, [arXiv:1206.2386].

[8] S. Franco, D. Galloni, and R.-K. Seong, *New Directions in Bipartite Field Theories*, arXiv:1211.5139.

[9] S. Cremonesi, A. Hanany, and R.-K. Seong, *Double Handled Brane Tilings*, arXiv:1305.3607.

[10] R.-K. Seong and D. D. Vvedensky, *Statistical thermodynamics and weighted topology of radial networks*, *ArXiv e-prints* (May, 2010) [arXiv:1005.3019].

[11] R.-K. Seong, C. M. Salafia, and D. D. Vvedensky, *Statistical topology of radial networks: a case study of tree leaves*, *Philosophical Magazine* **92** (2012), no. 1-3 230–245, [http://www.tandfonline.com/doi/pdf/10.1080/14786435.2011.614965].

[12] R.-K. Seong, P. Getreuer, Y. Li, T. Girardi, C. Salafia, and D. Vvedensky, *Statistical geometry and topology of the human placenta*, in *Advances in Applied Mathematics, Modeling, and Computational Science* (R. Melnik and I. S.

Kotsireas, eds.), vol. 66 of *Fields Institute Communications*, pp. 187–208. Springer US, 2013.

[13] M. Bertolini, F. Bigazzi, and A. Cotrone, *New checks and subtleties for AdS/CFT and a-maximization*, *JHEP* **0412** (2004) 024, [`hep-th/0411249`].

[14] B. Feng, S. Franco, A. Hanany, and Y.-H. He, *Symmetries of toric duality*, *JHEP* **12** (2002) 076, [`hep-th/0205144`].

[15] A. Hanany and K. D. Kennaway, *Dimer models and toric diagrams*, `hep-th/0503149`.

[16] A. Hanany and D. Vegh, *Quivers, tilings, branes and rhombi*, *JHEP* **10** (2007) 029, [`hep-th/0511063`].

[17] J. Davey, A. Hanany, and J. Pasukonis, *On the Classification of Brane Tilings*, *JHEP* **01** (2010) 078, [`arXiv:0909.2868`].

[18] A. Hanany and A. Zaffaroni, *The master space of supersymmetric gauge theories*, *Adv.High Energy Phys.* **2010** (2010) 427891.

[19] J. Polchinski, *String theory*, vol. 1,2. Cambridge university press, 1998.

[20] M. E. Peskin and D. V. Schroeder, *Quantum field theory*, *The Advanced Book Program, Perseus Books (Reading, Massachusetts* (1995).

[21] K. Becker, M. Becker, and J. H. Schwarz, *String theory and M-theory*. Cambridge University Press Cambridge, 2006.

[22] J. Terning, *Modern supersymmetry: Dynamics and duality*, vol. 132. Oxford University Press, 2006.

[23] A. Uranga, *Introduction to string theory*, *Graduate Course in String Theory. http://www. ift. uam. es/paginaspersonales/angeluranga/Lect. pdf* (1982).

[24] M. Kaku, *Quantum field theory: a modern introduction*, vol. 5. Oxford University Press New York, Oxford, 1993.

[25] M. Green, J. Schwarz, and E. Witten, *Superstring theory, vols i and ii*, 1987.

[26] A. Zee, *Quantum field theory in a nutshell*. Universities Press, 2005.

[27] D. Tong, *Lectures on string theory*, *arXiv preprint arXiv:0908.0333* (2009).

[28] O. Aharony, S. S. Gubser, J. M. Maldacena, H. Ooguri, and Y. Oz, *Large N field theories, string theory and gravity*, *Phys.Rept.* **323** (2000) 183–386, [`hep-th/9905111`].

[29] A. Sen, *An Introduction to nonperturbative string theory*, `hep-th/9802051`.

[30] A. Hanany and E. Witten, *Type IIB superstrings, BPS monopoles, and three-dimensional gauge dynamics*, *Nucl.Phys.* **B492** (1997) 152–190, [`hep-th/9611230`].

[31] S. Elitzur, A. Giveon, and D. Kutasov, *Branes and N=1 duality in string theory*, *Phys.Lett.* **B400** (1997) 269–274, [`hep-th/9702014`].

[32] A. Giveon and D. Kutasov, *Brane dynamics and gauge theory*, *Rev.Mod.Phys.* **71** (1999) 983–1084, [`hep-th/9802067`].

[33] N. Seiberg, *Electric - magnetic duality in supersymmetric nonAbelian gauge theories*, *Nucl.Phys.* **B435** (1995) 129–146, [`hep-th/9411149`].

[34] B. Feng, A. Hanany, and Y.-H. He, *D-brane gauge theories from toric singularities and toric duality*, *Nucl. Phys.* **B595** (2001) 165–200, [`hep-th/0003085`].

[35] C. E. Beasley and M. R. Plesser, *Toric duality is Seiberg duality*, *JHEP* **0112** (2001) 001, [`hep-th/0109053`].

[36] B. Feng, A. Hanany, Y.-H. He, and A. M. Uranga, *Toric duality as Seiberg duality and brane diamonds*, *JHEP* **12** (2001) 035, [`hep-th/0109063`].

[37] F. Cachazo, B. Fiol, K. A. Intriligator, S. Katz, and C. Vafa, *A Geometric unification of dualities*, *Nucl.Phys.* **B628** (2002) 3–78, [`hep-th/0110028`].

[38] J. M. Maldacena, *The large N limit of superconformal field theories and supergravity*, *Adv. Theor. Math. Phys.* **2** (1998) 231–252, [`hep-th/9711200`].

[39] S. Gubser, I. R. Klebanov, and A. M. Polyakov, *Gauge theory correlators from noncritical string theory*, *Phys.Lett.* **B428** (1998) 105–114, [`hep-th/9802109`].

[40] E. Witten, *Anti-de Sitter space and holography*, *Adv.Theor.Math.Phys.* **2** (1998) 253–291, [`hep-th/9802150`].

[41] M. R. Douglas, B. R. Greene, and D. R. Morrison, *Orbifold resolution by D-branes*, *Nucl.Phys.* **B506** (1997) 84–106, [`hep-th/9704151`].

[42] D. R. Morrison and M. R. Plesser, *Nonspherical horizons. 1.*, *Adv.Theor.Math.Phys.* **3** (1999) 1–81, [`hep-th/9810201`].

[43] C. Beasley, B. R. Greene, C. Lazaroiu, and M. Plesser, *D3-branes on partial resolutions of Abelian quotient singularities of Calabi-Yau threefolds*, *Nucl.Phys.* **B566** (2000) 599–640, [`hep-th/9907186`].

[44] M. R. Douglas and G. W. Moore, *D-branes, Quivers, and ALE Instantons*, hep-th/9603167.

[45] I. R. Klebanov and E. Witten, *Superconformal field theory on three-branes at a Calabi-Yau singularity*, *Nucl.Phys.* **B536** (1998) 199–218, [hep-th/9807080].

[46] A. M. Uranga, *Brane configurations for branes at conifolds*, *JHEP* **9901** (1999) 022, [hep-th/9811004].

[47] O. Aharony and A. Hanany, *Branes, superpotentials and superconformal fixed points*, *Nucl.Phys.* **B504** (1997) 239–271, [hep-th/9704170].

[48] R. P. Stanley, *Hilbert functions of graded algebras*, *Adv. Math* **28** (1978), no. 1 57–83.

[49] J. Harris, *Algebraic geometry: a first course*, vol. 133. Springer Verlag, 1992.

[50] S. Benvenuti, B. Feng, A. Hanany, and Y.-H. He, *Counting BPS operators in gauge theories: Quivers, syzygies and plethystics*, *JHEP* **11** (2007) 050, [hep-th/0608050].

[51] B. Feng, A. Hanany, and Y.-H. He, *Counting Gauge Invariants: the Plethystic Program*, *JHEP* **03** (2007) 090, [hep-th/0701063].

[52] A. Butti, D. Forcella, A. Hanany, D. Vegh, and A. Zaffaroni, *Counting Chiral Operators in Quiver Gauge Theories*, *JHEP* **11** (2007) 092, [arXiv:0705.2771].

[53] B. S. Acharya, J. M. Figueroa-O'Farrill, C. M. Hull, and B. J. Spence, *Branes at conical singularities and holography*, *Adv. Theor. Math. Phys.* **2** (1999) 1249–1286, [hep-th/9808014].

[54] S. Benvenuti and A. Hanany, *New results on superconformal quivers*, *JHEP* **0604** (2006) 032, [hep-th/0411262].

[55] S. Franco, A. Hanany, K. D. Kennaway, D. Vegh, and B. Wecht, *Brane Dimers and Quiver Gauge Theories*, *JHEP* **01** (2006) 096, [hep-th/0504110].

[56] J. Bagger and N. Lambert, *Modeling Multiple M2's*, *Phys.Rev.* **D75** (2007) 045020, [hep-th/0611108].

[57] J. Bagger and N. Lambert, *Gauge symmetry and supersymmetry of multiple M2-branes*, *Phys.Rev.* **D77** (2008) 065008, [arXiv:0711.0955].

[58] J. Bagger and N. Lambert, *Comments on multiple M2-branes*, *JHEP* **0802** (2008) 105, [arXiv:0712.3738].

[59] A. Gustavsson, *Algebraic structures on parallel M2-branes*, *Nucl.Phys.* **B811** (2009) 66–76, [arXiv:0709.1260].

[60] O. Aharony, O. Bergman, D. L. Jafferis, and J. Maldacena, *N=6 superconformal Chern-Simons-matter theories, M2-branes and their gravity duals*, *JHEP* **0810** (2008) 091, [arXiv:0806.1218].

[61] I. R. Klebanov and G. Torri, *M2-branes and AdS/CFT*, *Int.J.Mod.Phys.* **A25** (2010) 332–350, [arXiv:0909.1580].

[62] D. Martelli and J. Sparks, *Moduli spaces of Chern-Simons quiver gauge theories and AdS(4)/CFT(3)*, *Phys.Rev.* **D78** (2008) 126005, [arXiv:0808.0912].

[63] A. Hanany and A. Zaffaroni, *Tilings, Chern-Simons Theories and M2 Branes*, *JHEP* **0810** (2008) 111, [arXiv:0808.1244].

[64] A. Hanany, D. Vegh, and A. Zaffaroni, *Brane Tilings and M2 Branes*, *JHEP* **0903** (2009) 012, [arXiv:0809.1440].

[65] S. Franco, A. Hanany, J. Park, and D. Rodriguez-Gomez, *Towards M2-brane Theories for Generic Toric Singularities*, *JHEP* **0812** (2008) 110, [arXiv:0809.3237].

[66] P. Kasteleyn, *The statistics of dimers on a lattice: I. the number of dimer arrangements on a quadratic lattice*, *Physica* **27** (1961), no. 12 1209 – 1225.

[67] P. W. Kasteleyn, *Graph theory and crystal physics*, *Graph theory and theoretical physics* **1** (1967) 43–110.

[68] A. Hanany and A. Zaffaroni, *On the realization of chiral four-dimensional gauge theories using branes*, *JHEP* **9805** (1998) 001, [hep-th/9801134].

[69] R. Kenyon, *Local statistics of lattice dimers*, in *Annales de l'Institut Henri Poincare (B) Probability and Statistics*, vol. 33.

[70] R. Kenyon, *Conformal invariance of domino tiling*, *Annals of probability* (2000) 759–795.

[71] D. Forcella, A. Hanany, Y.-H. He, and A. Zaffaroni, *The Master Space of N=1 Gauge Theories*, *JHEP* **0808** (2008) 012, [arXiv:0801.1585].

[72] D. Forcella, A. Hanany, Y.-H. He, and A. Zaffaroni, *Mastering the Master Space*, *Lett.Math.Phys.* **85** (2008) 163–171, [arXiv:0801.3477].

[73] D. Forcella, A. Hanany, and A. Zaffaroni, *Master Space, Hilbert Series and Seiberg Duality*, *JHEP* **0907** (2009) 018, [arXiv:0810.4519].

[74] A. Zaffaroni, *The master space of N=1 quiver gauge theories: Counting BPS operators*, . Prepared for 8th Workshop on Continuous Advances in QCD (CAQCD-08), Minneapolis, Minnesota, 15-18 May 2008.

[75] D. Forcella, *Master Space and Hilbert Series for N=1 Field Theories*, `arXiv:0902.2109`.

[76] S. Krippendorf, M. J. Dolan, A. Maharana, and F. Quevedo, *D-branes at Toric Singularities: Model Building, Yukawa Couplings and Flavour Physics*, JHEP **1006** (2010) 092, [`arXiv:1002.1790`].

[77] M. Yamazaki, *Geometry and Combinatorics of Crystal Melting*, ArXiv e-prints (Feb., 2011) [`arXiv:1102.0776`].

[78] M. Yamazaki, *Crystal Melting and Wall Crossing Phenomena*, Int.J.Mod.Phys. **A26** (2011) 1097–1228, [`arXiv:1002.1709`].

[79] M. Yamazaki, *Quivers, YBE and 3-manifolds*, JHEP **1205** (2012) 147, [`arXiv:1203.5784`].

[80] A. B. Goncharov and R. Kenyon, *Dimers and cluster integrable systems*, ArXiv e-prints (July, 2011) [`arXiv:1107.5588`].

[81] S. Franco, *Dimer Models, Integrable Systems and Quantum Teichmuller Space*, JHEP **1109** (2011) 057, [`arXiv:1105.1777`].

[82] N. Arkani-Hamed, J. L. Bourjaily, F. Cachazo, A. B. Goncharov, A. Postnikov, et. al., *Scattering Amplitudes and the Positive Grassmannian*, `arXiv:1212.5605`.

[83] B. Feng, Y.-H. He, K. D. Kennaway, and C. Vafa, *Dimer models from mirror symmetry and quivering amoebae*, Adv.Theor.Math.Phys. **12** (2008) 3, [`hep-th/0511287`].

[84] G. Mikhalkin, *Amoebas of algebraic varieties and tropical geometry*, ArXiv Mathematics e-prints (Feb., 2004) [`math/0403`].

[85] N. Broomhead, *Dimer models and Calabi-Yau algebras*, `arXiv:0901.4662`.

[86] A. Ishii and K. Ueda, *On moduli spaces of quiver representations associated with dimer models*, ArXiv e-prints (Oct., 2007) [`arXiv:0710.1898`].

[87] A. Ishii and K. Ueda, *Dimer models and the special McKay correspondence*, ArXiv e-prints (May, 2009) [`arXiv:0905.0059`].

[88] J. Stienstra, *Hypergeometric Systems in two Variables, Quivers, Dimers and Dessins d'Enfants*, `arXiv:0711.0464`.

[89] K. D. Kennaway, *Brane Tilings*, *Int. J. Mod. Phys.* **A22** (2007) 2977–3038, [`arXiv:0706.1660`].

[90] M. Yamazaki, *Brane Tilings and Their Applications*, *Fortsch. Phys.* **56** (2008) 555–686, [`arXiv:0803.4474`].

[91] H. Derksen, J. Weyman, and A. Zelevinsky, *Quivers with potentials and their representations I: Mutations*, *ArXiv e-prints* (Apr., 2007) [`arXiv:0704.0649`].

[92] B. Feng, A. Hanany, and Y.-H. He, *Phase structure of D-brane gauge theories and toric duality*, *JHEP* **08** (2001) 040, [`hep-th/0104259`].

[93] B. Feng, Y.-H. He, and F. Lam, *On correspondences between toric singularities and (p,q) webs*, *Nucl.Phys.* **B701** (2004) 334–356, [`hep-th/0403133`].

[94] B. V. Karpov and D. Y. Nogin, *Three-block exceptional collections over Del Pezzo surfaces*, `alg-geom/9703027`.

[95] S. Franco, A. Hanany, and P. Kazakopoulos, *Hidden exceptional global symmetries in 4d CFTs*, *JHEP* **07** (2004) 060, [`hep-th/0404065`].

[96] R. Kenyon, *An introduction to the dimer model*, *ArXiv Mathematics e-prints* (Oct., 2003) [`math/0310`].

[97] R. Kenyon and A. Okounkov, *Planar dimers and Harnack curves*, `math/0311062`.

[98] R. Kenyon, A. Okounkov, and S. Sheffield, *Dimers and amoebae*, `math-ph/0311005`.

[99] R. Bocklandt, *Calabi Yau algebras and weighted quiver polyhedra*, `arXiv:0905.0232`.

[100] S. Franco *et. al.*, *Gauge theories from toric geometry and brane tilings*, *JHEP* **01** (2006) 128, [`hep-th/0505211`].

[101] B. Feng, S. Franco, A. Hanany, and Y.-H. He, *Unhiggsing the del Pezzo*, *JHEP* **08** (2003) 058, [`hep-th/0209228`].

[102] A. Hanany, P. Kazakopoulos, and B. Wecht, *A new infinite class of quiver gauge theories*, *JHEP* **08** (2005) 054, [`hep-th/0503177`].

[103] S. Franco and D. Vegh, *Moduli spaces of gauge theories from dimer models: Proof of the correspondence*, *JHEP* **0611** (2006) 054, [`hep-th/0601063`].

[104] E. Witten, *Phases of N = 2 theories in two dimensions*, *Nucl. Phys.* **B403** (1993) 159–222, [`hep-th/9301042`].

[105] R. Kenyon and J.-M. Schlenker, *Rhombic embeddings of planar graphs with faces of degree 4*, *ArXiv Mathematical Physics e-prints* (May, 2003) [`math-ph/0`].

[106] D. R. Gulotta, *Properly ordered dimers, R-charges, and an efficient inverse algorithm*, *JHEP* **10** (2008) 014, [`arXiv:0807.3012`].

[107] O. Aharony, A. Hanany, and B. Kol, *Webs of (p,q) 5-branes, five dimensional field theories and grid diagrams*, *JHEP* **01** (1998) 002, [`hep-th/9710116`].

[108] A. Hanany and A. Iqbal, *Quiver theories from D6 branes via mirror symmetry*, *JHEP* **0204** (2002) 009, [`hep-th/0108137`].

[109] A. Butti and A. Zaffaroni, *From toric geometry to quiver gauge theory: The Equivalence of a-maximization and Z-minimization*, *Fortsch.Phys.* **54** (2006) 309–316, [`hep-th/0512240`].

[110] A. Butti and A. Zaffaroni, *R-charges from toric diagrams and the equivalence of a- maximization and Z-minimization*, *JHEP* **11** (2005) 019, [`hep-th/0506232`].

[111] D. Martelli, J. Sparks, and S.-T. Yau, *The Geometric dual of a-maximisation for Toric Sasaki-Einstein manifolds*, *Commun.Math.Phys.* **268** (2006) 39–65, [`hep-th/0503183`].

[112] A. Hanany and C. Romelsberger, *Counting BPS operators in the chiral ring of N = 2 supersymmetric gauge theories or N = 2 braine surgery*, *Adv. Theor. Math. Phys.* **11** (2007) 1091–1112, [`hep-th/0611346`].

[113] D. Forcella, *Operators and vacua of N=1 field theories*, *Nuovo Cim.* **B125** (2010) 905–914, [`arXiv:0912.3444`].

[114] D. R. Grayson and M. E. Stillman, "Macaulay2, a software system for research in algebraic geometry." Available at http://www.math.uiuc.edu/Macaulay2/.

[115] W. Fulton and J. Harris, *Representation theory: a first course*. Graduate Texts in Mathematics / Readings in Mathematics Series. Springer London, Limited, 1991.

[116] J. P. Gauntlett, D. Martelli, J. Sparks, and D. Waldram, *Supersymmetric AdS(5) solutions of M-theory*, *Class. Quant. Grav.* **21** (2004) 4335–4366, [`hep-th/0402153`].

[117] J. P. Gauntlett, D. Martelli, J. Sparks, and D. Waldram, *Sasaki-Einstein metrics on S(2) x S(3)*, *Adv. Theor. Math. Phys.* **8** (2004) 711–734, [`hep-th/0403002`].

[118] S. Benvenuti, A. Hanany, and P. Kazakopoulos, *The toric phases of the Y(p,q) quivers*, *JHEP* **07** (2005) 021, [`hep-th/0412279`].

[119] S. Benvenuti, S. Franco, A. Hanany, D. Martelli, and J. Sparks, *An infinite family of superconformal quiver gauge theories with Sasaki-Einstein duals*, *JHEP* **06** (2005) 064, [`hep-th/0411264`].

[120] D. Martelli and J. Sparks, *Toric geometry, Sasaki-Einstein manifolds and a new infinite class of AdS/CFT duals*, *Commun. Math. Phys.* **262** (2006) 51–89, [`hep-th/0411238`].

[121] V. Novikov, M. A. Shifman, A. Vainshtein, and V. I. Zakharov, *Exact gell-mann-low function of supersymmetric yang-mills theories from instanton calculus*, *Nuclear Physics B* **229** (1983), no. 2 381–393.

[122] D. Martelli, J. Sparks, and S.-T. Yau, *Sasaki-Einstein manifolds and volume minimisation*, *Commun. Math. Phys.* **280** (2008) 611–673, [`hep-th/0603021`].

[123] R. Eager, *Equivalence of A-Maximization and Volume Minimization*, `arXiv:1011.1809`.

[124] S. Fomin and A. Zelevinsky, *Cluster algebras i: foundations*, *Journal of the American Mathematical Society* **15** (2002), no. 2 497–529.

[125] R. Marsh, M. Reineke, and A. Zelevinsky, *Generalized associahedra via quiver representations*, *Transactions of the American Mathematical Society* **355** (2003), no. 10 4171–4186.

[126] A. Hanany, D. Orlando, and S. Reffert, *Sublattice Counting and Orbifolds*, *JHEP* **06** (2010) 051, [`arXiv:1002.2981`].

[127] M. R. Douglas and B. R. Greene, *Metrics on d-brane orbifolds*, *Adv.Theor.Math.Phys.* **1** (1998) 184–196, [`hep-th/9707214`].

[128] T. Muto, *D-branes on orbifolds and topology change*, *Nucl.Phys.* **B521** (1998) 183–201, [`hep-th/9711090`].

[129] S. Kachru and E. Silverstein, *4-D conformal theories and strings on orbifolds*, *Phys.Rev.Lett.* **80** (1998) 4855–4858, [`hep-th/9802183`].

[130] A. E. Lawrence, N. Nekrasov, and C. Vafa, *On conformal field theories in four-dimensions*, *Nucl.Phys.* **B533** (1998) 199–209, [`hep-th/9803015`].

[131] M. Bershadsky, Z. Kakushadze, and C. Vafa, *String expansion as large N expansion of gauge theories*, *Nucl.Phys.* **B523** (1998) 59–72, [`hep-th/9803076`].

[132] A. Hanany and Y.-H. He, *NonAbelian finite gauge theories*, *JHEP* **9902** (1999) 013, [`hep-th/9811183`].

[133] A. M. Uranga, *From quiver diagrams to particle physics*, `hep-th/0007173`.

[134] B. Feng, A. Hanany, Y. H. He, and A. Iqbal, *Quiver theories, soliton spectra and Picard-Lefschetz transformations*, *JHEP* **0302** (2003) 056, [`hep-th/0206152`].

[135] A. Hanany and Y.-H. He, *M2-Branes and Quiver Chern-Simons: A Taxonomic Study*, `arXiv:0811.4044`.

[136] J. Davey, A. Hanany, N. Mekareeya, and G. Torri, *Phases of M2-brane Theories*, *JHEP* **0906** (2009) 025, [`arXiv:0903.3234`].

[137] J. Davey, A. Hanany, N. Mekareeya, and G. Torri, *Higgsing M2-brane Theories*, *JHEP* **11** (2009) 028, [`arXiv:0908.4033`].

[138] J. Davey, A. Hanany, N. Mekareeya, and G. Torri, *Brane Tilings, M2-branes and Chern-Simons Theories*, `arXiv:0910.4962`.

[139] S. Lee, *Superconformal field theories from crystal lattices*, *Phys.Rev.* **D75** (2007) 101901, [`hep-th/0610204`].

[140] S. Lee, S. Lee, and J. Park, *Toric AdS4/CFT3 duals and M-theory Crystals*, *JHEP* **0705** (2007) 004, [`hep-th/0702120`].

[141] M. Taki, *M2-branes Theories without 3+1 Dimensional Parents via Un-Higgsing*, `arXiv:0910.0370`.

[142] A. Hanany, M. J. Strassler, and A. M. Uranga, *Finite theories and marginal operators on the brane*, *JHEP* **9806** (1998) 011, [`hep-th/9803086`].

[143] A. Hanany and A. M. Uranga, *Brane boxes and branes on singularities*, *JHEP* **9805** (1998) 013, [`hep-th/9805139`].

[144] W. Fulton, *Introduction to Toric Varieties. (Am-131)*. Annals of Mathematics Studies. Princeton University Press, 1993.

[145] Y.-H. He, *On Fields over Fields*, `arXiv:1003.2986`.

[146] A. Hanany and R.-K. Seong, *An étude on abelian orbifold harmonics (unpublished)*, .

[147] N. C. Leung and C. Vafa, *Branes and Toric Geometry*, *ArXiv High Energy Physics - Theory e-prints* (Nov., 1997) [`hep-th/9711013`].

[148] P. Candelas, M. Lynker, and R. Schimmrigk, *Calabi-Yau Manifolds in Weighted P(4)*, *Nucl. Phys.* **B341** (1990) 383–402.

[149] D. R. Morrison, *Mirror symmetry and rational curves on quintic threefolds: a guide for mathematicians*, *J.AMER.MATH.SOC.* **6** (1993) 223.

[150] V. V. Batyrev, *Dual polyhedra and mirror symmetry for Calabi-Yau hypersurfaces in toric varieties*, *J. Alg. Geom.* **3** (1994) 493–545.

[151] V. Batyrev and D. Dais, *Strong McKay correspondence, string theoretic Hodge numbers and mirror symmetry*, `alg-geom/9410001`.

[152] V. V. Batyrev and L. A. Borisov, *Dual cones and mirror symmetry for generalized Calabi-Yau manifolds*, . In *Greene, B. (ed.): Yau, S.T. (ed.): Mirror symmetry II* 71-86.

[153] D. Cox and S. Katz, *Mirror symmetry and algebraic geometry*. Mathematical surveys and monographs. American Mathematical Society, 1999.

[154] K. Hori, S. Katz, A. Klemm, R. Pandharipande, R. Thomas, C. Vafa, R. Vakil, and E. Zaslow, *Mirror symmetry*, vol. 1 of *Clay mathematics monographs*. American Mathematical Society, Providence, RI, 2003.

[155] H. Verlinde and M. Wijnholt, *Building the standard model on a D3-brane*, *JHEP* **0701** (2007) 106, [`hep-th/0508089`].

[156] V. A. Iskovskih, *Fano 3-folds. i*, *Mathematics of the USSR-Izvestiya* **11** (1977), no. 3 485.

[157] V. A. Iskovskih, *Fano 3-folds. ii*, *Mathematics of the USSR-Izvestiya* **12** (1978), no. 3 469.

[158] G. Ellingsrud, *Complex projective geometry*. London Mathematical Society lecture note series. Cambridge University Press, 1992.

[159] S. Mori and S. Mukai, *Classification of fano 3-folds with b2 ≥ 2*, *manuscripta mathematica* **36** (1981) 147–162. 10.1007/BF01170131.

[160] J. Murre, *Classification of fano threefolds according to fano and iskovskih*, . 10.1007/BFb0093585.

[161] S. D. Cutkosky, *On fano 3-folds*, *manuscripta mathematica* **64** (1989) 189–204. 10.1007/BF01160118.

[162] V. V. Batyrev, *Toroidal fano 3-folds*, *Mathematics of the USSR-Izvestiya* **19** (1982), no. 1 13.

[163] V. V. Batyrev, *On the Classification of Toric Fano 4-folds*, *ArXiv Mathematics e-prints* (Jan., 1998) [`math/9801107`].

[164] M. Kreuzer and B. Nill, *Classification of toric Fano 5-folds*, *ArXiv Mathematics e-prints* (Feb., 2007) [`math/0702890`].

[165] M. Øbro, *An algorithm for the classification of smooth Fano polytopes*, *ArXiv e-prints* (Apr., 2007) [`arXiv:0704.0049`].

[166] J. Davey, A. Hanany, N. Mekareeya, and G. Torri, *M2-Branes and Fano 3-folds*, *J.Phys.* **A44** (2011) 405401, [`arXiv:1103.0553`].

[167] M. Kreuzer and H. Skarke, *On the Classification of Reflexive Polyhedra*, *Communications in Mathematical Physics* **185** (1997) 495–508, [`hep-th/9512204`].

[168] M. Kreuzer and H. Skarke, *Classification of Reflexive Polyhedra in Three Dimensions*, *Adv. Theor. Math. Phys.* **2** (1998) 847–864, [`hep-th/9805190`].

[169] M. Kreuzer and H. Skarke, *Reflexive polyhedra, weights and toric Calabi-Yau fibrations*, *Rev. Math. Phys.* **14** (2002) 343–374, [`math/0001106`].

[170] M. Kreuzer and H. Skarke, *Complete classification of reflexive polyhedra in four dimensions*, *Adv. Theor. Math. Phys.* **4** (2002) 1209–1230, [`hep-th/0002240`].

[171] V. Batyrev and M. Kreuzer, *Constructing new Calabi-Yau 3-folds and their mirrors via conifold transitions*, *ArXiv e-prints* (Feb., 2008) [`arXiv:0802.3376`].

[172] P. Candelas and R. Davies, *New Calabi-Yau Manifolds with Small Hodge Numbers*, *ArXiv e-prints* (Sept., 2008) [`arXiv:0809.4681`].

[173] P. Candelas and A. Font, *Duality between the webs of heterotic and type II vacua*, *Nuclear Physics B* **511** (Feb., 1998) 295–325, [`hep-th/9603170`].

[174] Y.-H. He, S.-J. Lee, and A. Lukas, *Heterotic Models from Vector Bundles on Toric Calabi-Yau Manifolds*, *JHEP* **1005** (2010) 071, [`arXiv:0911.0865`].

[175] Y.-H. He, *An Algorithmic Approach to String Phenomenology*, *Modern Physics Letters A* **25** (2010) 79–90, [`arXiv:1001.2419`].

[176] P. Candelas, E. Perevalov, and G. Rajesh, *F-theory duals of non-perturbative heterotic $E_8 \times E_8$ vacua in six dimensions*, *Nuclear Physics B* **502** (Feb., 1997) 613–628, [`hep-th/9606133`].

[177] P. Candelas and H. Skarke, *F-theory, SO(32) and toric geometry*, *Physics Letters B* **413** (Nov., 1997) 63–69, [`hep-th/9706226`].

[178] H. Skarke, *Reflexive polyhedra and their applications in string and F-theory*, `hep-th/0002246`.

[179] J. Knapp, M. Kreuzer, C. Mayrhofer, and N.-O. Walliser, *Toric Construction of Global F-Theory GUTs*, *JHEP* **1103** (2011) 138, [`arXiv:1101.4908`].

[180] A. Hanany, C. P. Herzog, and D. Vegh, *Brane tilings and exceptional collections*, *JHEP* **07** (2006) 001, [`hep-th/0602041`].

[181] C. E. Beasley and M. Ronen Plesser, *Toric duality is Seiberg duality*, *Journal of High Energy Physics* **12** (Dec., 2001) 1–+, [`hep-th/0109053`].

[182] S. Franco, A. Hanany, and Y.-H. He, *A trio of dualities: Walls, trees and cascades*, *Fortsch. Phys.* **52** (2004) 540–547, [`hep-th/0312222`].

[183] A. Hanany, *Counting BPS operators in the chiral ring: The plethystic story*, *AIP Conf.Proc.* **939** (2007) 165–175.

[184] A. Butti, *Deformations of toric singularities and fractional branes*, *JHEP* **10** (2006) 080, [`hep-th/0603253`].

[185] S. Pinansky, *Quantum deformations from toric geometry*, *JHEP* **03** (2006) 055, [`hep-th/0511027`].

[186] W. Lerche, C. Vafa, and N. P. Warner, *Chiral Rings in N=2 Superconformal Theories*, *Nucl.Phys.* **B324** (1989) 427.

[187] B. R. Greene and M. Plesser, *DUALITY IN CALABI-YAU MODULI SPACE*, *Nucl.Phys.* **B338** (1990) 15–37.

[188] S. Benvenuti and A. Hanany, *Conformal manifolds for the conifold and other toric field theories*, *JHEP* **0508** (2005) 024, [`hep-th/0502043`].

[189] S. Franco, A. Hanany, D. Krefl, J. Park, A. M. Uranga, *et. al.*, *Dimers and orientifolds*, *JHEP* **0709** (2007) 075, [`arXiv:0707.0298`].

[190] K. Hori and C. Vafa, *Mirror symmetry*, `hep-th/0002222`.

[191] K. Hori, A. Iqbal, and C. Vafa, *D-branes and mirror symmetry*, `hep-th/0005247`.

[192] L. Grant and K. Narayan, *Mesonic chiral rings in Calabi-Yau cones from field theory*, *Class. Quant. Grav.* **25** (2008) 045010, [`hep-th/0701189`].

[193] A. Gustavsson, *Selfdual strings and loop space Nahm equations*, *JHEP* **0804** (2008) 083, [`arXiv:0802.3456`].

[194] K. Ueda and M. Yamazaki, *Toric Calabi-Yau four-folds dual to Chern-Simons-matter theories*, *JHEP* **0812** (2008) 045, [`arXiv:0808.3768`].

[195] F. Benini, C. Closset, and S. Cremonesi, *Chiral flavors and M2-branes at toric CY4 singularities*, *JHEP* **1002** (2010) 036, [`arXiv:0911.4127`].

[196] F. Benini, C. Closset, and S. Cremonesi, *Quantum moduli space of Chern-Simons quivers, wrapped D6-branes and AdS4/CFT3*, *JHEP* **1109** (2011) 005, [`arXiv:1105.2299`].

[197] C. Closset and S. Cremonesi, *Toric Fano varieties and Chern-Simons quivers*, *JHEP* **1205** (2012) 060, [`arXiv:1201.2431`].

[198] S. Franco, *Bipartite Field Theories: from D-Brane Probes to Scattering Amplitudes*, `arXiv:1207.0807`.

[199] V. Jejjala, S. Ramgoolam, and D. Rodriguez-Gomez, *Toric CFTs, Permutation Triples and Belyi Pairs*, *JHEP* **1103** (2011) 065, [`arXiv:1012.2351`].

[200] J. J. Heckman, C. Vafa, D. Xie, and M. Yamazaki, *String Theory Origin of Bipartite SCFTs*, `arXiv:1211.4587`.

[201] M. Bianchi, S. Cremonesi, A. Hanany, F. Morales, D. Ricci Pacific, and R.-K. Seong, *Double Handled Brane Tilings (unpublished)*, `arXiv:1305.xxxx`.

[202] A. Kehagias, *New type IIB vacua and their F-theory interpretation*, *Phys. Lett.* **B435** (1998) 337–342, [`hep-th/9805131`].